CO_2-RESPONSIVE SURFACES

by

Kyle James Boniface

A thesis submitted to the Department of Chemistry

In conformity with the requirements for

the degree of Doctor of Philosophy

Queen's University

Kingston, Ontario, Canada

January 2018

Abstract

Green chemistry and green engineering are ideals to which a great many modern chemists and engineers subscribe. The engagement of chemists and engineers worldwide in the application of green chemistry and engineering principles is one of the largest and most promising collective efforts of our time. The core message of green chemistry and green engineering is to pursue chemical and technical advances that benefit society and the economy, whilst minimizing or avoiding human and environmental hazards.

Designing smart materials with green chemistry in mind is a common theme throughout this thesis. Smart surfaces, i.e. a surface that can perform multiple tasks as a function of an external stimulus, have the potential to reduce waste by simplifying processes, reducing solvent use, and extending the lifetime of materials through simple regenerative procedures.

The work presented in this thesis focuses on the development of CO_2-responsive smart surfaces for green applications. CO_2-responsive smart surfaces have been used as desiccants for the removal of water from organic solvents. For the first time, CO_2-responsive smart desiccants were able to remove more water and were regenerated at a lower energy cost than traditional recyclable desiccants such as molecular sieves. Additionally, CO_2-responsive smart surfaces were demonstrated to be smart supports for heterogeneous catalysis with ruthenium nanoparticles by allowing reversible changes in catalyst selectivity for the hydrogenation of furfural. In both applications, the CO_2-responsive smart materials were recycled multiple times with little to no loss in performance. CO_2-responsive smart materials were demonstrated to selectively capture and release hydrophobic liquids and dyes without loss of performance over time.

A variety of substrates were evaluated as CO_2-switchable surfaces using both single-unit and polymeric modifiers. A robust and user-friendly method for "surface-initiated activators generated by electron transfer atom transfer radical polymerization" (SI-AGET-ATRP) is described. The SI-AGET-ATRP technique is compatible with various CO_2-responsive polymers and will allow future work to study topics of interest such as the relationships between grafting density, molecular weight, and material performance.

Acknowledgements

I offer my sincerest thanks to the following people: my supervisors Prof. Philip Jessop and Prof. Michael Cunningham, for their support, encouragement, mentorship, and for always letting me figure it out on my own. I hope that one day I will be able to truly appreciate the full scope of your influence; to the members of both the Jessop and Cunningham research groups for their helpful discussions, general comradery, and willingness to fix the GC or brave the weather to run a GPC sample across campus; to the various collaborators and research institutions that I have had the privilege of working with; to the National Sciences and Engineering Research Council for funding this research; to Queen's University and the Province of Ontario for partially funding my studies; to the faculty and support staff of the Department of Chemistry at Queen's University that have served as mentors, collaborators, readers, and supervisory committee members; to the colleagues who became close friends, Brandon Moore, Kyle Bachus, Andrew Fraser, Kevin Fowler, Tamara de Winter, and Alexandre Dunlop-Brière among others, it has been a pleasure to work and play alongside you all; to my family, whose support has been endless and unwavering, you are the giants upon whose shoulders I stand.

Statement of Originality

I hereby certify that all of the work described within this thesis is the original work of the author. The work described within this thesis was conducted in the Department of Chemistry at Queen's University under the supervision of Prof. Philip Jessop and Prof. Michael Cunningham. Any published (or unpublished) ideas and/or techniques from the work of others are fully acknowledged in accordance with the standard referencing practices. Any and all contributions from collaborators are clearly noted below.

In Chapter 2, Dr. Ryan Dykeman and Dr. Hong-Bo Wang synthesized and tested the porous polymer particles. In addition, they did the calculations regarding the energy consumption of porous polymer particles in comparison to molecular sieves.

In Chapter 3, Mr. Sami El Sayed, under the supervision of Dr. Kylie Luska and Prof. Walter Leitner, synthesized the active catalysts from our CO_2-responsive particles and conducted subsequent hydrogenation studies.

All X-ray photoelectron spectroscopy studies were conducted by Dr. Rana Sodhi of the University of Toronto or by Dr. Gabriele. Schatte of Queen's University; their respective contributions are noted where appropriate. Mass spectrometry was conducted by Dr. Randy Whittal of The University of Alberta or by Mr. David Mcleod of Queen's University; their respective contributions are noted where appropriate. Additionally, all solid-state nuclear magnetic resonance studies were conducted by Dr. Franoçise. Sauriol of Queen's University.

Portions of this thesis have been published previously:

Chapter 2	K. J. Boniface, R. R. Dykeman, A. Cormier, H. Wang, S. M. Mercer, G. Liu, M. Cunningham and P. G. Jessop, *Green Chem*., 2016, **18**, 208-213. Reproduced with permission of the Royal Society of Chemistry.
Chapter 5	K. J. Boniface, T. J. Clark, M. F. Cunningham, P. G. Jessop, B. E. Mariampillai, S. M. Mercer, R. Resendes, T. Robert, WO. Pat., 039 247, 2015.
Chapter 6	P. Champagne, P. G. Jessop, K. J. Boniface, M. F. Cunningham, H. Wang, O. Garcia-Valdez, A. Cormier, S. Ge, J. Arrendondo-Luna, WO. Pat., 149 815, 2016.

Kyle James Boniface

January, 2018

Table of Contents

List of Figures

List of Tables

List of Schemes

List of Abbreviations

AA	Ascorbic acid
AIBN	Azobisisobutyronitrile
API	1-(3-Aminopropyl)imidazole
APTES	(3-Aminopropyl)triethoxysilane
AGET	Activators generated by electron transfer
ARGET	Activators regenerated by electron transfer
aq	Aqueous
ATR	Attenuated Total Reflectance
ATRP	Atom transfer radical polymerization
BE	Binding energy
BET	Brunauer-Emmett-Teller
BHT	Butylated hydroxytoluene
BIBB	2-Bromo-2-methylpropionyl bromide
BMA	Butyl methacrylate
CA	Contact angle
ca.	Circa
CAE	Constant analyser energy
CAH	Contact angle hysteresis
CDI	1,1'-Carbonyldiimidazole
CMC	Carboxymethylchitosan
CNC	Cellulose nanocrystals
cod	1,5-Cyclooctadiene
conv.	Conversion
CP-MAS	Cross polarization-magic angle spinning
DA	Drying agent
DCC	N,N'-Dicyclohexylcarbodiimide
DCM	Dichloromethane
DEAEMA	2-(Diethylamino)ethyl methacrylate
DEAPA	3-(Diethylamino)propylamine
DHB	Dihydroxybenzoic acid
DI	Deionized
DIPEA	Diisopropylethylamine
DIpAEMA	2-(Diisopropylamino)ethyl methacrylate
DMAc	Dimethylacetamide
DMAEA	2-(Dimethylamino)ethyl acrylate
DMAEIB	2-(Dimethylamino)ethyl isobutyrate
DMAEMA	2-(Dimethylamino)ethyl methacrylate
DMAE-A	3-(Dimethylamino)-1-propylamine
DMAE-OH	2-(Dimethylamino)ethanol
DMAP	4-(Dimethylamino)pyridine
DMAP-OH	2-(Dimethylamino)propanol
DMAPMAm	N-[3-(Dimethylamino)propyl]methacrylamide
DMA-S	Dimethylamino-functionalised silica particles

DMC	Dimethyl carbonate
DMF	Dimethylformamide
DMSO	Dimethylsulfoxide
DNA	Deoxyribonucleic acid
DP	Degree of polymerisation
DRIFT	Diffuse Reflectance Infrared Fourier Transform
DSC	Differential scanning calorimetry
DTT	1,4-Dithiothreitol
EA	Elemental analysis
eATRP	Electrochemically mediated atom transfer radical polymerization
EBIB	Ethyl 2-bromo-2-methylpropionate
ECF	Ethylchloroformate
EDC	1-Ethyl-3-(3-dimethylaminopropyl)carbodiimide
EDTA	Ethylenediaminetetraacetic acid
EH	Ethyl hexanoate
eq.	Equivalent
FA	4-(Furan-2-yl)butan-2-ol
FcBARF	Ferrocenium tetrakis[3,5-bis(trifluoromethyl)phenyl]borate
FFA	Furfural acetone
FK	4-(Furan-2-yl)butan-2-one
FP	Free polymer
FRP	Free radical polymerisation
FT	Fourier transform
FTIR	Fourier transform infrared
GC	Gas chromatography
GP	Grafted polymer
GPC	Gel permeation chromatography
HAADF-STEM	High angle annular dark field scanning transmission electron microscopy
HATU	N-[(Dimethylamino)-1H-1,2,3-triazolo-[4,5-b]pyridin-1-ylmethylene]-N-methylmethanaminium hexafluorophosphate N-oxide
HCA	Hexadecane contact angle
HCl	Hydrochloric acid
HEBIB	2-Hydroxyethyl-2-bromoisobutyrate
HF	Hydrofluoric acid
HMDS	1,1,1,3,3,3–Hexamethyldisilazane
HSQC	Heteronuclear single quantum correlation
HQ	Hydroquinone
ImHCl	Imidazole hydrochloride
IR	Infrared
MAC	Methacryloyl chloride
MALDI-TOF	Matrix assisted laser desorption/ionization time of flight
MCC	Microcrystalline cellulose
MCF	Methylchloroformate
MEHQ	Hydro-quinone monomethyl ether
MeOH	Methanol
MHV	Molar hydration value

MOF	Metal organic framework
MS	Mass spectrometry
n-BuLi	n-Butyllithium
$NaBH_4$	Sodium borohydride
NaH	Sodium hydride
NaOH	Sodium hydroxide
NFK	Nanofabrication Kingston
NP	Nanoparticle
NP@RP	Nanoparticle deposited on CO_2-responsive particle
NMP	Nitroxide mediated polymerisation
NMR	Nuclear magnetic resonance
P-1	Porous polymer particles
PAA·Na	Sodium polyacrylate
PDEAEMA	Poly(2-(diethylamino)ethyl methacrylate)
PDiPAEMA	Poly(2-(diisopropylamino)ethyl methacrylate)
PDMAEA	Poly(2-(dimethylamino)ethyl acrylate)
PDMAEMA	Poly(2-(dimethylamino)ethyl methacrylate)
PDMAPMAm	Poly(N-[3-(dimethylamino)propyl]methacrylamide)
PGC	Polymer-grafted cotton
PGFP	Polymer-grafted filter paper
PGS	Polymer-grafted silica
pH	Negative logarithm of the concentration of hydronium ions
pH_i	Negative logarithm of the initial concentration of hydronium ions
PIM	Polymers of intrinsic microporosity
pK_a	Negative logarithm of the acid dissociation constant
pK_{aH}	Negative logarithm of the conjugate acid dissociation constant
pK_{app}	Negative logarithm of the apparent acid dissociation constant
PMDETA	N,N,N′,N″,N″-Pentamethyldiethylenetriamine
PMMA	Poly(methyl methacrylate)
PNIPAAm	Poly(N-isopropylacrylamide)
POP	Porous organic polymers
ppm	Parts per million
PS	Polystyrene
PT	Proton transfer
PTFE	Polytetrafluoroethylene
RA	Reducing agent
RAFT	Reversible addition-fragmentation chain transfer
RBF	Round bottom flask
RDRP	Reversible-deactivation radical polymerisation
ROP	Ring opening polymerization
RP	CO_2-responsive particle
RPM	Revolutions per minute
rt	Room temperature
Ru	Ruthenium
RuNP@SP	Ruthenium nanoparticle deposited on a switchable particle
SA	Surface area

SAM	Self-assembled monolayer
SEM	Scanning electron microscopy
SFRP	Stable free radical polymerisation
SI	Surface-initiated
SSA	Spherical sector analyser
TBAEM	2-(*tert*-Butylamino)ethyl methacrylate
TBC	4-*tert*-Butylcatechol
TCD	Thermal conductivity detector
tBuOK	Potassium *tert*-butoxide
TEA	Triethylamine
TEOS	Tetraethyl orthosilicate
TGA	Thermogravimetric analysis
THF	Tetrahydrofuran
THFA	4-(Tetrahydrofuran-2-yl)butan-2-ol
THFK	4-(Tetrahydrofuran-2-yl)butan-2-one
TMA	Tetramethylammonium
TMCS	Trimethylchlorosilane
TMG	1,1,3,3-Tetramethylguanidine
TPMA	Tris(2-pyridylmethyl)amine
UPLC	Ultra performance liquid chromatography
VA-061	2,2'-Azobis[2-(2-imidazolin-2-yl)propane]
VBC	4-Vinylbenzyl chloride
WCA	Water contact angle
XPS	X-ray photoelectron spectroscopy

List of Symbols and Units

@	At
Å	Angstrom
Al	Aluminium
Ar	Argon
atm	Atmosphere (unit)
At%	Atomic percentage
Au	Gold
B	Boron
b	Length of repeat unit
$\mathscr{b}$	Broad
bar	Bar (unit)
Br	Bromine
Br3d	Bromine 3d orbital
℃	Celsius
^{13}C	Carbon-13 isotope
C	Carbon
C	Concentration
C1s	Carbon 1s orbital
Cl	Chlorine
cm	Centimeter
CO_2	Carbon dioxide
[Cu]	Molar concentration of Copper
Cu	Copper
Cu^{I}	Copper (I)
Cu^{II}	Copper (II)
Cu(I)Br	Copper (I) bromide
Cu(II)Br_2	Copper (II) bromide
Cu(I)Cl	Copper (I) chloride
Cu(II)Cl_2	Copper (II) chloride
Δ	Delta
D	Distribution coefficient
δ	NMR chemical shift
Đ	Dispersity
eV	Electronvolt
F	Fluorine
fs	Femtosecond
γ_{LV}	Surface tension of the liquid-vapour interface
γ_{SL}	Surface tension of the solid-liquid interface
γ_{SV}	Surface tension of the solid-vapour interface
(g)	Gas
g	Gram
^{1}H	Hydrogen-1 isotope
H	Hydrogen

H_2	Elemental Hydrogen
h	Hour
H_2O	Water
I	Iodine
$I_{solution}$	Initiator dissolved in solution
$I_{substrate}$	Initiator bound to a substrate
I_{total}	Total amount of initiator
J	Joule
K	Potassium
°K	Kelvin
K_α	K-alpha emission
k_{act}	Rate constant of activation
kDa	Kilodalton
k_{Deact}	Rate constant of deactivation
K_H	Henrys law constant
kHz	Kilohertz
kJ	Kilojoule
k_{obs}	Observed rate constant
k_p	Rate constant of propagation
k_t	Rate constant of termination
kPa	Kilopascal
kV	Kilovolt
L	Litre
L_P	Length of polymer
L	Ligand
l	Bond length
Log	Logarithm
M	Molar
m	Metre
m	Mass
$\mathcal{m}$	Medium
mbar	Millibar
Mg	Magnesium
mg	Milligram
min	Minute
mJ	Millijoule
mL	Millilitre
mM	Millimolar
mm	Millimeter
mmol	Millimole
$mmol_{AA}$	Millimole of accessible amines
$mmol_W$	Millimole of water
mN	Millinewton
ms	Millisecond
M_n	Number average molecular weight
MΩ	Megaohm

mW	Milliwatt
M_w	Weight average molecular weight
mol	Mole
N_2	Elemental Nitrogen
N	Nitrogen
N	Number of bonds
n	Number of repeat units
n	Mole
n	Narrow
N1s	Nitrogen 1s orbital
Na	Sodium
nm	Nanometer
O_2	Elemental Oxygen
O	Oxygen
O1s	Oxygen 1s orbital
P	Phosphorus
p	Partial pressure
$\mathcal{P}$	Partition coefficient
p	Probability
%	Percentage
ϕ_s	Fraction of a surface that is in contact with a probe liquid
1 - ϕ_s	Fraction of a surface that is in contact with air
pm	Picometre
$\propto_{OH}$	Kiselev-Zhuravlev constant
ps	Picosecond
R	Roughness factor
R_g	Radius of gyration
σ	Standard deviation
S	Sulfur
s	Second
s	Strong
Se	Selenium
sh	Sharp
^{29}Si	Silicon-29 isotope
Si	Silicon
Si2p	Silicon 2p orbital
Sn	Tin
$Sn(EH)_2$	Tin (II) ethyl hexanoate
sp	Hybrid orbital containing s and p_x orbitals
sp^2	Hybrid orbital containing s, p_x, and p_y orbitals
sp^3	Hybrid orbital containing s, p_x, p_y, and p_z orbitals
T	Temperature
T_g	Glass transition temperature
θ	True contact angle
θ^*	Measured contact angle
θ_A	Advancing contact angle

θ_{CA}	Static contact angle
θ_R	Receding contact angle
θ_{SA}	Sliding angle
θ_{SHA}	Shedding angle
μm	Micrometre
μL	Microlitre
V	Volts
v	Volume
v_t	Total volume
W	Watt
w	Weight fraction
w	Weak
wt%	Percentage by weight

List of Numbered Compounds

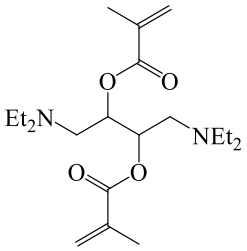

1,4-Bis(diethylamino)-2,3-butanediol

2-1

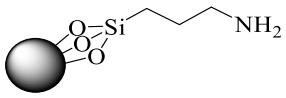

(3-Aminopropyl)triethoxysilane-grafted silica particles

4-1

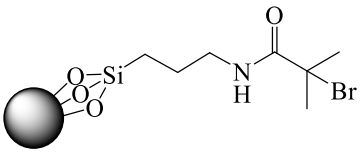

2-Bromo-2-methylpropionyl-grafted silica particles

4-2

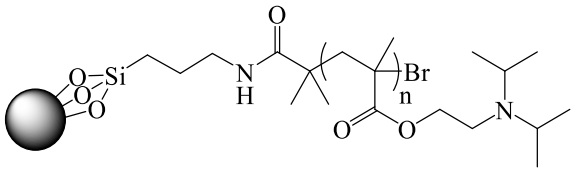

Poly(2-(diisopropylamino)ethyl methacrylate)-grafted silica particles

4-3

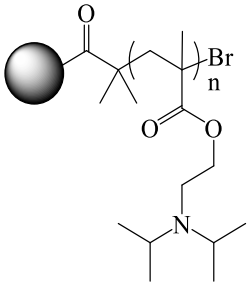

Poly(2-(diisopropylamino)ethyl methacrylate)-grafted silica particles

4-3*a*

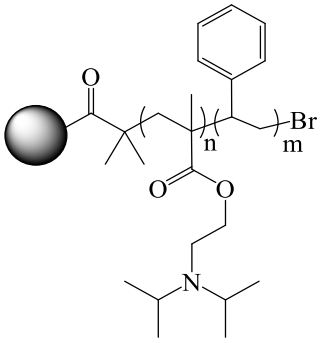

[Poly(2-(diisopropylamino)ethyl methacrylate)-block-polystyrene]-grafted silica particles

4-4*b*

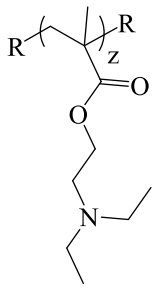

Poly(2-(diethylamino)ethyl methacrylate)

5-1

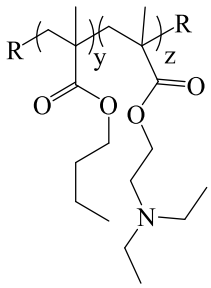

Poly[2-(diethylamino)ethyl methacrylate-co-butyl methacrylate)

5-2

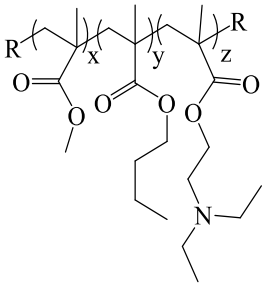

Poly[2-(diethylamino)ethyl methacrylate-co-butyl methacrylate-co-methyl methacrylate)

5-3

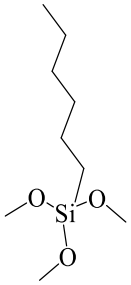

n-Hexyltrimethoxysilane

S1

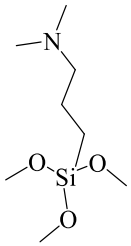

(N,N-Dimethylaminopropyl)trimethoxysilane

S2

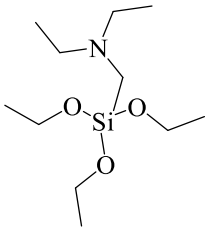

(Diethylaminomethyl)trimethoxysilane

S3

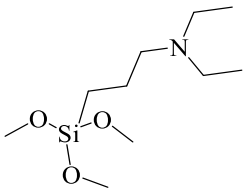

[3-(Diethylamino)propyl]-trimethoxysilane

S4

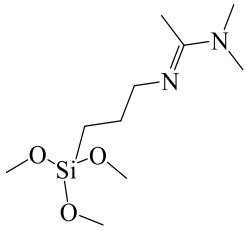

N,N-Dimethyl-N’-(3-(trimethoxysilyl)propyl)acetimidamide

S5

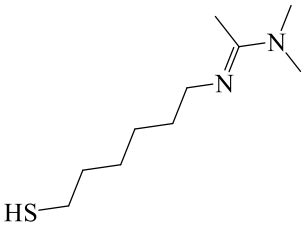

N’-(6-Mercaptohexyl)-N,N-dimethylacetimidamide

S6

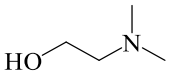

2-Dimethylaminoethanol

S7

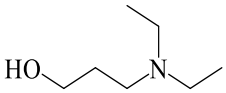

3-Diethylamino-1-propanol

S8

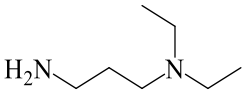

3-(Diethylamino)propylamine

S9

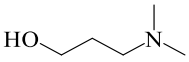

3-Dimethylamino-1-propanol

S10

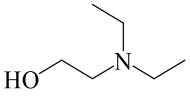

2-(Diethylamino)ethanol

S11

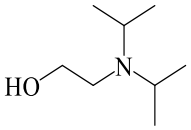

2-(Diisopropylamino)ethanol

S12

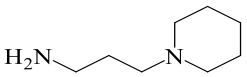

N-(3-Aminopropyl)piperidine

S13

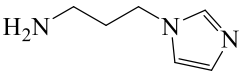

1-(3-Aminopropyl)imidazole

S14

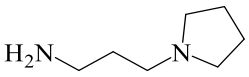

1-(3-Aminopropyl)pyrrolidine

S15

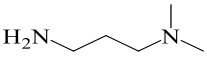

3-(Dimethylamino)propylamine

A1

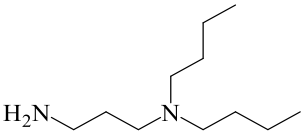

3-(Dibutylamino)-1-propylamine

A2

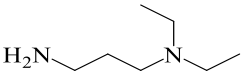

3-(Diethylamino)propylamine

A3

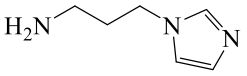

1-(3-aminopropyl)imidazole

A4

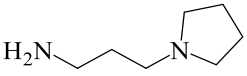

N-(3-Aminopropyl)piperidine

A5

[a]Alternative depiction of 4-3 in which the silane surface-linker has been compressed for clarity.
[b]Silane surface-linker has been compressed for clarity.

Chapter 1

Introduction

1.1 CO_2-switchable chemistry

The dissolution of CO_2 in water affords a series of acid/base equilibria. The dissolution of CO_2 into water is dictated by Henry's Law (Equation 1.1) where the concentration of dissolved CO_2 (C) is proportional to the CO_2 partial pressure (p) and inversely proportional to the Henry's Law constant (K_H). The Henry's law constant for CO_2 in water at 298 K is 29.41 L·atm·mol^{-1}.

$$C = \frac{p}{K_H} \tag{1.1}$$

The reaction of dissolved CO_2 with water then generates carbonic acid, H_2CO_3, a weak acid with an apparent pK_a of 6.4.[1–7] Aqueous H_2CO_3 is understood to dissociate by a proton-relay mechanism that uses several catalysing water molecules. For this reason, direct observation of aqueous H_2CO_3 has proven to be challenging.[8] Thus, the apparent pK_a (pK_{app}, Equation 1.5) reflects the combination of the CO_2 hydration equilibria (Equation 1.2) and the first dissociation of H_2CO_3 (Equation 1.3).

$$CO_{2\,(g)} \underset{}{\overset{K_H,\ pCO_2}{\rightleftharpoons}} CO_{2\,(aq)} \tag{1.2}$$

Where $CO_{2(aq)}$ is a mixture of hydrated CO_2 ($CO_2{\cdot}H_2O$) and carbonic acid (H_2CO_3).

$$H_2CO_{3(aq)} + H_2O \xrightleftharpoons{K_{a1}} H_3O^+_{(aq)} + HCO_3^-{}_{(aq)} \quad (1.3)$$

$$HCO_3^-{}_{(aq)} + H_2O \xrightleftharpoons{K_{a2}} H_3O^+_{(aq)} + CO_3^{2-}{}_{(aq)} \quad (1.4)$$

$$CO_{2\,(aq)} + 2H_2O \xrightleftharpoons{K_{app}} H_3O^+_{(aq)} + HCO_3^-{}_{(aq)} \quad (1.5)$$

$$K_{app} = \frac{[H_3O^+]_{aq}[HCO_3^-]_{aq}}{[CO_2]_{aq}} \quad (1.6)$$

Where:

$$[CO_2]_{aq} = [CO_2 \cdot H_2O]_{aq} + [H_2CO_3]_{aq} \quad (1.7)$$

Carbonic acid is a polyprotic acid; its two actual dissociation values have been measured, they are pK_{a1}=3.8[7,8] and pK_{a2}=10.3[9]. The extent of dissociation and therefore the concentration of each species, H_2CO_3, HCO_3^-, and CO_3^{2-}, is pH dependent (Figure 1.1).

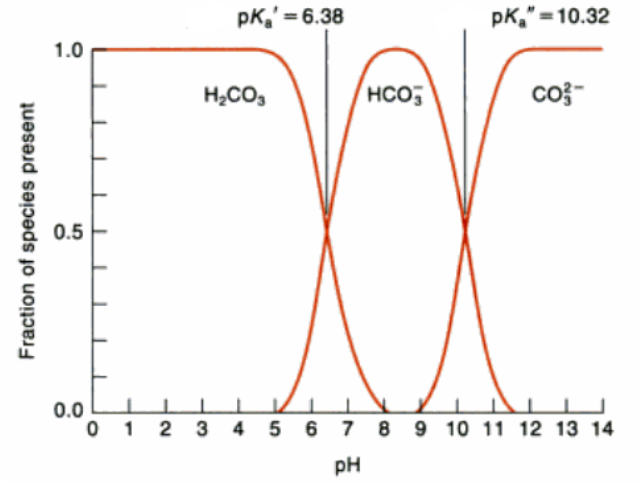

Figure 1.1. A distribution plot of carbonic acid and the subsequent dissociated species based on pH.[9] K_{app} (Equations 1.5 and 1.6) is used in place of both the hydrated CO_2 equilibrium (Equations 1.2 and 1.7) and the first dissociation of $H_2CO_{3(aq)}$ (Equation 1.3).

Removal of CO_2 from an aqueous solution is predominately governed by equilibrium kinetics. However, the removal of $CO_{2\,(aq)}$ from solution can be accelerated by adding heat, thus reducing the solubility of CO_2 in water, or by sparging with an inert gas which effectively increases the rate at which CO_2 is removed from solution (Equation 1.2). The combination of mild heating (ca. 50 °C) and sparging with Ar has successfully removed CO_2 from a variety of CO_2-responsive materials when in an aqueous solution.[10,11]

In recent years, CO_2-triggered switchable solvents,[12] surfactants,[13] latex particles,[14] and heterogeneous surfaces,[10,11,15–23] that are switchable in polarity or hydrophilicity have been developed.[24–26] In general, CO_2-switchable functional groups are those that switch from neutral to cationic, anionic or carbamate salts. CO_2-switchable functional groups that switch from neutral to cationic rely on the protonation of a nitrogenous base when CO_2 is dissolved in an aqueous solution. CO_2, H_2O, and a nitrogenous base have multiple pathways by which they can react with one another. A tertiary amine, bulky secondary or primary amine, guanidine, or amidine, when in the presence of CO_2 and H_2O will react to preferentially form a bicarbonate salt (Equation 1.8). CO_2 can also form carbamic acids with primary and secondary amines, or amidines and guanidines containing N-H bonds. The formation of carbamic acid happens quickly and preferentially, often leading to carbamate salt formation when a second equivalent of an amine is available[27] (Equation 1.9). When possible and when water is present, the formation of carbamic acid and carbamate salts is often in addition to and in competition with the formation of bicarbonate salts.

$$R_3N + H_2O + CO_2 \rightleftharpoons [R_3NH]^+[HCO_3]^- \qquad (1.8)$$

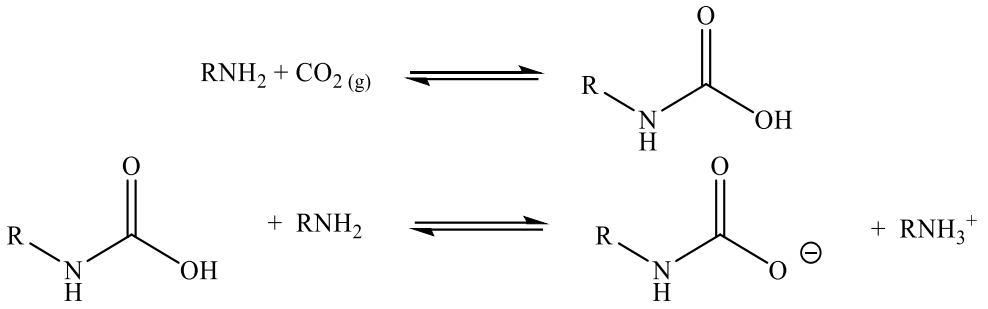

(1.9)

The work presented herein has been limited to the study of CO_2-switchable functional groups that do not contain N-H bonds and switch from neutral to cationic. With these limitations, the bicarbonate salt is the only product of the reaction pathway when the functional group is mixed with CO_2 in H_2O. Additionally, the work presented herein has focused on reactions of tertiary amines with CO_2 in H_2O.

Most tertiary amines are moderately basic; because of this, their pK_a values are quite high and not accessible to acid-base chemistry that occurs in an aqueous solution. Thus, it is prudent to discuss tertiary amines and other similar basic species in terms of their pK_{aH} value, which describes the ability of the protonated species to lose the proton. Most tertiary amines have pK_{aH} values ranging from ~9-11. Polymers containing tertiary amines typically have pK_{aH} values ranging from ~6-9. The switch from neutral to cationic relies on the protonation of the tertiary amine with carbonic acid (pK_{app} 6.4). The more basic the tertiary amine is, the more favourable the cationic state becomes. Switching the tertiary amine back to neutral requires deprotonation of the tertiary amine and removal of CO_2 from solution. Deprotonation is an endothermic process; heat is generally required to facilitate the deprotonation reaction (Table 1.1).

Table 1.1. The enthalpy of protonation of CO_2-switchable surfactants and estimated pK_{aH} values for selected bases. Reproduced from reference 28 with permission from the RSC.

Molecule	Enthalpy of protonation ($kJ \cdot mol^{-1}$)	pK_{aH} (H_2O scale)
N'-Heptyl-N,N-dimethylethanimidamide 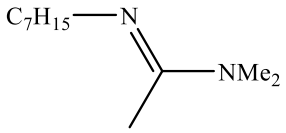	86 ± 0.2	13.8
N'-Octyl-N,N-dimethylethanimidamide 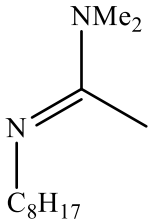	71 ± 1	12.2
1-Methyl-2-octylimidazoline 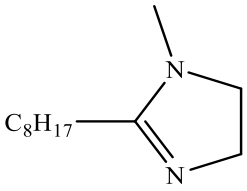	54 ± 0.7	11.0
4,5-Dihydro-2-octyl-1H-imidazole 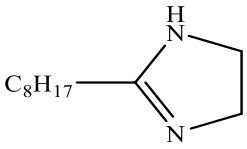	47 ± 0.8	11.1
1-(Dimethylamino)octane $C_8H_{17}NMe_2$	53 ± 0.5	10.0
N-(4-Heptylphenyl)-N,N-dimethylethanimidamide 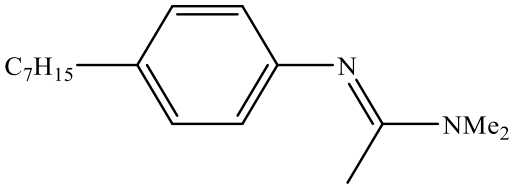	48 ± 0.3	10.8

Note: pK_{aH} values are estimates based upon the measure pK_{aH} values of structurally similar compounds.[28]

The greater the protonation enthalpy, the more heat must be supplied to switch the compound back to its neutral form. Polymers that contain very basic sites (e.g. those with pK_{aH} values above 13) are usually not preferred because, in most aqueous solutions, these basic sites would be largely protonated by water even in the absence of an acid stimulus.

Tertiary amines and imidazolines have a low enthalpy of protonation. Thus, the reverse reaction requires less energy input than that of amidines or guanidines, which have a higher enthalpy of protonation. Additionally, tertiary amines are synthetically more accessible and commercially more available than imidazolines. When all factors are considered, tertiary amines make favourable CO_2-switchable functionalities that facilitate the synthesis and study of CO_2-responsive materials for near-room temperature applications.

1.2 CO_2-responsive materials

A CO_2-switchable material is one where the application or removal of CO_2 from a material causes a physical or chemical change in the material. The stimulus used to trigger the change strongly affects the cost, environmental impact, and ease of switching. In comparison with other triggers such as acids/bases, oxidants/reductants, salts, and light, CO_2 is an attractive choice as it is easily-removed, does not accumulate in a system, and is functional for non-transparent systems (e.g. oil pipelines or steel reactor vessels).[10] CO_2 is an abundant, non-toxic gas and being a key metabolite in cells, it also possesses good biocompatibility and membrane permeability.[29] Therefore, CO_2 has been recently exploited as a "green" trigger for artificial smart systems.[11,18,24–26]

To achieve switchability, the application or removal of CO_2 often exploits the inherent acid/base reactivity of a substrate to enact the change between two sets of chemical and/or physical properties. Previous materials which have been explicitly labelled as CO_2-switchable include surfactants, solvents, latexes, solutes, polymers, particles, and surfaces.[24–26]

As demonstrated in Figure 1.2, the number of publications in the field of CO_2-switchable chemistry has proliferated over the past decade, with over ten times as many publications in 2016, than in 2006.

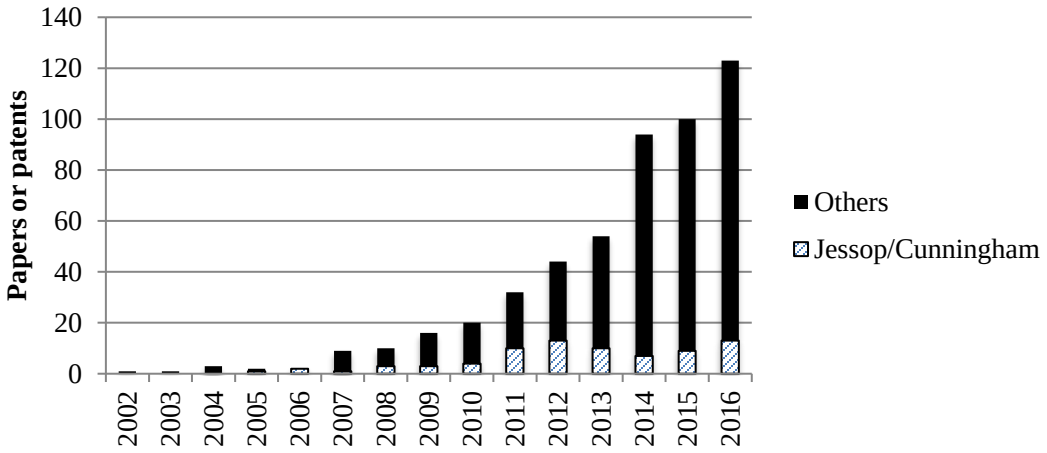

Figure 1.2. Increasing trend of scientific publications containing "CO_2-switchable" chemistry as a topic of discussion in various journals from 2002-2016. Publications from the Jessop and Cunningham groups are highlighted with diagonal lines for illustrative purposes.

To the best of our knowledge, literature examples of CO_2-responsive surfaces have been limited to silicon wafers[15,30] and gold particles.[21,22] These examples are discussed in detail where relevant throughout this thesis. The introduction of CO_2-responsive molecules on substrates to form dynamic surfaces has rarely been investigated and is highly-desirable.

The work presented here has seen CO_2-responsive surfaces expanded to include new examples of silicon surfaces, silica particles, gold surfaces, and polysaccharide surfaces such as filter paper and woven cotton textiles.[10,11,18] The envisioned uses of CO_2-responsive surfaces are currently limited only by one's imagination. However, we have demonstrated potential for applicability as drying agents, functional supports for catalysis, chromatographic packing materials, solid-phase extraction mediums, and as functional filters for analyte capture or oil-water separation.[10,11,18,31]

1.3 Stimuli-responsive materials

Stimuli-responsive or "smart" surfaces that undergo a reversible transition of surface properties in response to environmental changes have attracted considerable interest due to their promising applications in diverse fields, such as bioengineering, switchable wettability, controlled lithography, and drug delivery. External stimuli typically include electrical potential,[32] pH,[33] solvent,[34] counterions,[35] light,[36] temperature,[37] and redox triggers.[38] Several reviews, which highlight the breadth of available stimuli, have been published recently.[39–42]

Smart surfaces with stimuli-responsive changes in wettability, especially switching between superhydrophobicity and superhydrophilicity, are of interest for the development of, for example, micro- and nanofluidic devices, self-cleaning and anti-fog surfaces, and sensor devices.[43,44] Artificial surfaces with superhydrophobicity and superoleophobicity are commonly fabricated via two kinds of approaches: creating micro-/nanostructures on hydrophobic substrates, or chemically modifying a micro-/nanostructured surface with

materials of low surface free energy. Superhydrophilic and superoleophilic surfaces have also been fabricated via increasing both the surface roughness and the surface free energy.[39] In some cases, the surface chemical composition or geometrical structure of a rough surface can be tuned dynamically. Since the wettability of a solid substrate is governed by the surface free energy and surface geometrical structure, dynamically altering one of these two properties can be used to modulate the surface wettability.[39–42]

A variety of inorganic oxide films and organic materials are used as stimuli-responsive materials. In general, inorganic oxides offer clear advantages over organic molecules; they are structurally and photochemically more stable, they have lower toxicity and remarkably larger wettability changes. However, compared with inorganic metal oxides, organic compounds are more varied, ranging from photosensitive materials and thermoresponsive films to pH-responsive polymers. Furthermore, organic polymers have been shown to undergo conformational reorientations when exposed to various stimuli because of phase transitions between a well solvated and a poorly solvated state.[33,45–47] Stimuli-responsive polymers, in some cases, have the potential advantage of being able to simultaneously control the surface energy and topography of a material. Moreover, the sophisticated design of organic films provides a versatile platform for introducing appropriate chemical functionalities to satisfy various practical demands.[48]

The majority of smart surfaces described to date are responsive to only one kind of external stimulus at a time, such as light, temperature, or solvent. Additionally, the stimulus must be held constant to achieve the desired state, e.g. light must be consistently applied to azobenzene-derived smart surfaces to favour the hydrophilic cis-configuration.[36] To work in the complex conditions of a real environment, the next generation of intelligent

materials will have surface wettability that can be tuned by dual or multiple external stimuli, such as a combination of temperature and solvent, light and temperature, solvent and light, electrical potential, magnetic fields, and so on.

The work presented in this thesis describes the development of a variety of CO_2-responsive and dual-responsive smart surfaces using surface-initiated reversible-deactivation radical polymerisation techniques to graft stimuli-responsive polymer chains to both organic and inorganic substrates.

1.4 Reversible-deactivation radical polymerization

Free radical polymerisation (FRP) is one of the most common and practical techniques for producing commodity polymers. FRP exhibits a high compatibility with a wide range of vinyl monomers making it a very robust and cost-effective process that accounts for a significant portion of polymer production. FRP, when thermally initiated, can be divided into three basic steps: initiator decomposition and chain initiation; propagation; and termination, by either combination or disproportionation (Scheme 1.1).

Initiator dissociation	$I \xrightarrow{k_d} 2R\cdot$
Initiation	$R\cdot + M \xrightarrow{k_i} P_1\cdot$
Propagation	$P_n\cdot + M \xrightarrow{k_p} P_{n+1}\cdot$
Termination by combination	$P_n\cdot + P_m\cdot \xrightarrow{k_{tc}} D_{n+m}$
Termination by disproportionation	$P_n\cdot + P_m\cdot \xrightarrow{k_{td}} D_n + D_m$

Scheme 1.1. A general mechanism for free radical polymerisation.[49]

Due to the high reactivity of transient radical species, polymer chain lifetimes are short (~0.1-1 s) with unavoidable termination and transfer reactions that yield a broad molecular weight distribution with statistical polymer architecture. This makes it difficult to generate more complex and defined structures which are required for advanced applications.[49]

In the last 20 years, several methods of reversible-deactivation radical polymerisation (RDRP), frequently known by the term 'living' or 'controlled' radical polymerisation, have led to a paradigm shift in the synthesis of macromolecular structures and soft matter materials.[50] The most studied methods of RDRP are stable free radical polymerisation/nitroxide mediated polymerisation (SFRP/NMP),[51,52] reversible addition-fragmentation chain transfer (RAFT) polymerisation,[53–55] and atom transfer radical polymerisation (ATRP).[56–59] The central principle shared by all forms of RDRP is to suppress bimolecular termination by providing a route for reversibly deactivating propagating chains, and typically involves maintaining a low radical concentration throughout the polymerisation. This is accomplished through an equilibrium between dormant polymer chains, capped by a mediating species, and active polymer chains, which are free to undergo propagation and other FRP mechanisms. The equilibrium must favour the formation of dormant chains and the formation of a dormant chain should be fast to suppress irreversible termination reactions. The general mechanism for ATRP, a form of RDRP, is shown in Scheme 1.2.

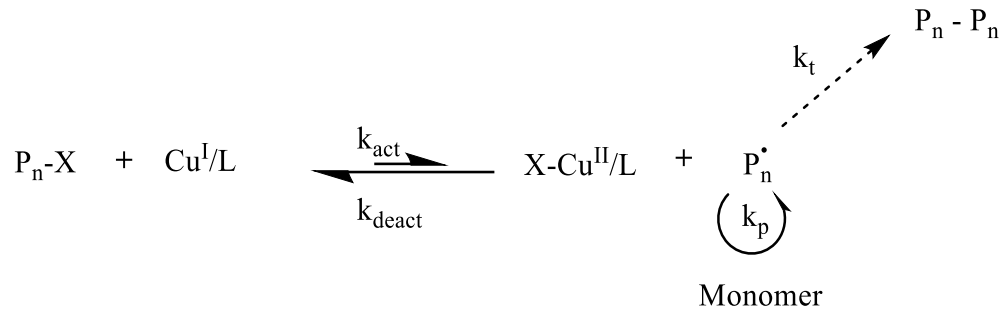

Scheme 1.2. A simplified version of ATRP kinetics.

ATRP has been used almost exclusively in this thesis. The pioneering work on ATRP was conducted independently by two groups in 1995. Kato et al. demonstrated the polymerisation of MMA using a ruthenium-based complex,[56] while at the same time Wang and Matyjaszewski showed the polymerization of styrene using a copper-based mediator.[57] Since then, an immense amount of literature has been published on ATRP and its various incarnations, mostly using copper bound to a nitrogen-based ligand as the mediating species due to its low cost and versatility compared to other transition metals.[10,49,58–61]

Interest in the development of new hybrid materials has grown exponentially in the last decade.[60] Such materials are commonly obtained by the graft modification of surfaces with polymer brushes via RDRP. The generation of polymer brushes by surface-initiated (SI) RDRP techniques, such as SI-RAFT,[62] SI-NMP,[63] and SI-ATRP,[64] has become a powerful approach to developing new hybrid materials with the ability to tailor chemical and physical properties of interfaces. In the most general sense, polymer brushes can be thought of as ultrathin polymer coatings consisting of polymer chains that are tethered by one chain end to an interface, which is commonly a solid substrate.

Depending on the grafting density, a given polymer brush can adopt various conformations. At high grafting densities, i.e. when the distance between neighbouring grafting points is small, steric repulsion leads to chain stretching and a brush-type conformation of the surface-tethered chains. At lower grafting densities, surface-tethered polymer chains can adopt various other conformations, which are referred to as mushroom or pancake.

Polymer brushes are commonly prepared following two main strategies: (i) the *grafting to* and (ii) the *grafting from* strategies (Figure 1.3).

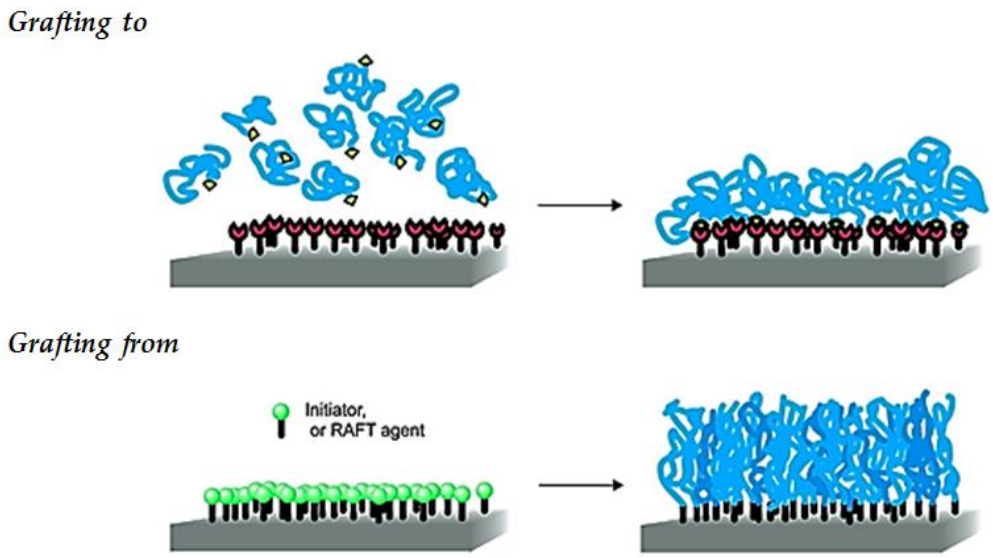

Figure 1.3. Chemisorption via reaction of appropriately end-functionalized polymers with corresponding functional groups on the substrate surface (*grafting to* approach). Polymer brushes are grown via the surface-initiated polymerisation technique (*grafting from* approach). Image adapted from Barbey et al.[65]

The *grafting to* strategy involves the attachment of prefabricated polymers via covalent bond formation with a surface. Since the polymer is prefabricated before it is attached to the surface, it can be characterised directly thus allowing for an exact

determination of polymer loading and grafting density on the polymer-grafted substrate. Although experimentally very straightforward, the *grafting to* strategy suffers from several limitations, which make it difficult to produce dense polymer brushes. Steric repulsions between polymer chains hamper the formation of dense polymer brushes since bound polymer chains inhibit neighbouring attachment sites.[66] Furthermore, with increasing polymer molecular weight, the reaction between the polymer end-group and the corresponding group on the substrate surface becomes less efficient.

An additional consideration when using the *grafting to* approach is the compatibility of the surface attachment site, the attachment moiety on the polymer, and the functional groups on the polymer since the functional groups of the polymer can compete with the attachment moieties for surface attachment sites (Figure 1.4).

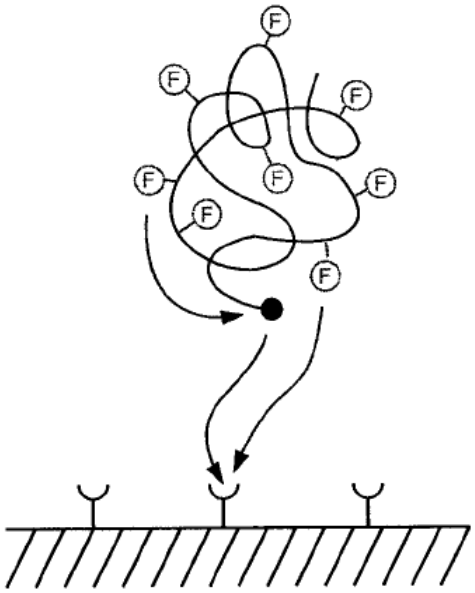

Figure 1.4. The depiction of the chemisorption of polymer molecules with functional groups (F) to solid surfaces through the anchor group (black dot). Image adapted from Rühe and Knoll.[66]

Competition between the anchor and the functional groups has been observed, for example, in the case of the attachment of a low molecular weight alkoxysilane containing amine groups to a silicon oxide surface.[66] In this system, interactions between the (basic) amine groups of the silane and the (acidic) silanol groups of the silicon oxide substrate can strongly compete with the chemisorption reaction of the alkoxysilyl moiety with the substrate silanol groups. As a result, a layer was obtained where both strong physisorption due to acid-base interactions and chemisorption occurred. This problem is self-correcting for "monomeric" amino-silanes since competitive adsorption leads to rearrangement and then chemisorption, specifically at low concentration.[67] However, given a polymeric amine, the competitive adsorption would be more efficient and more likely, whereas rearrangement is much less efficient owing to the steric bulk of the polymeric amine. When considering CO_2-responsive surfaces, the *grafting to* method should be avoided for substrates that interact strongly with CO_2-responsive polymers, which contain amines. Substrates like silicon or silica are better suited for the *grafting from* method (Chapters 2-5),[10,11] whereas substrates such as polysaccharides can be treated with either the *grafting from* (Chapter 6) or the *grafting to* methods.[18,19,23]

In the *grafting from* approach, the polymerisation is directly initiated from initiator-functionalized surfaces. "Living" polymerisation techniques are particularly attractive for the preparation of polymer brushes following the *grafting from* strategy, as they allow accurate control over brush thickness, composition, and architecture.[60,65,68–72] Examples include anionic polymerisation,[73–75] cationic polymerisation,[75–78] ring-opening polymerizations,[79–84] and ring-opening metathesis polymerization.[83,85–89] Conventional

free radical polymerisation has also found widespread use for the synthesis of polymer brushes.[66,90–97] Most of the polymer brushes produced by the *grafting from* approach, however, are prepared using SI-RDRP.[60]

1.5 Surface wettability

Surface wetting involves the interaction between a liquid, the surrounding environment, and a solid surface. The characterization of the surface energy, or the wettability, of a given surface is commonly achieved through calculations using a combination of static and dynamic contact angle measurements.

For a liquid drop resting on a horizontal solid surface, the contact angle (θ_{CA}) is defined as the angle formed by the intersection of the lines tangent to the solid-liquid interface and the liquid-vapour interface (Figure 1.5.). Generally, a surface is considered hydrophilic when θ_{CA}<90° and hydrophobic when θ_{CA}>90°. Specifically, a surface with θ_{CA}>150° and a sliding angle θ_{SA}<10° is deemed superhydrophobic or super-repellant.

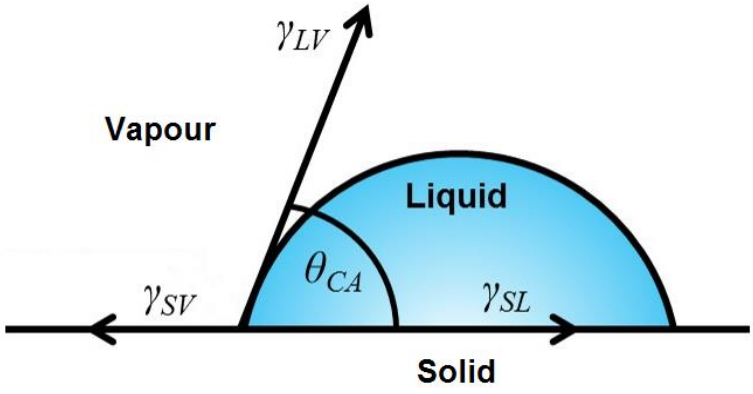

Figure 1.5. The contact angle (CA) of a given liquid on a solid surface. The contact angle is measured between the lines tangential to the solid-liquid and liquid-vapour-interface.

The θ_{CA} of the drop is related to the interfacial energies acting between the solid-liquid (γ_{SL}), solid-vapour (γ_{SV}), and liquid-vapour (γ_{LV}) interfaces. The θ_{CA} was first described by Thomas Young, over 200 years ago, with an equation now known as Young's equation (Equation 1.12).[98]

$$\cos(\theta_{CA}) = \frac{\gamma_{SL} - \gamma_{SV}}{\gamma_{LV}} \tag{1.12}$$

Young's equation is a simplification as it is strictly valid for an ideal surface that is chemically homogeneous, atomically smooth, and does not change characteristics due to the interaction with the probing liquid or by any other outside force. Notably, there is no such ideal surface in the real world.[99] Any real surface will exhibit two contact angles, an advancing (θ_A) and a receding (θ_R) contact angle (Figure 1.6). The difference between the two angles, commonly referred to as the contact angle hysteresis (CAH), is a measure of the surfaces' deviation from ideality. CAH has important implications regarding the adhesive nature of a given surface; the larger the CAH the more adhesive a surface will be to the respective probe liquid. An additional indication of the adhesive nature of a surface is provided by measurement of the "tilt angle". The tilt angle refers to the critical angle between the substrate and the horizontal surface, at which the droplet starts to slide or roll. Tilt angle measurements are described differently for smooth and rough surfaces. The sliding angle (θ_{SA}) is used for macroscopically flat surfaces and the shedding angle (θ_{SHA}) is used for macroscopically rough surfaces, such as cotton fabrics and wools (Figure 1.6).[100,101]

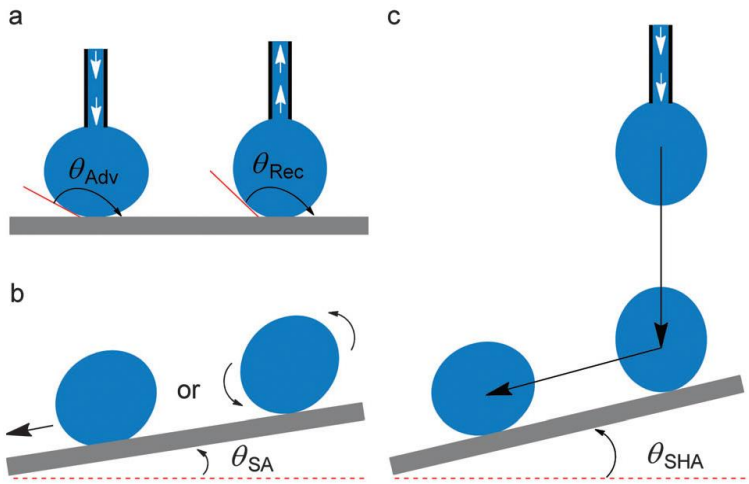

Figure 1.6. An illustration of the techniques for the determination of contact angle hysteresis: (a) advancing (θ_A) and receding contact angle (θ_R); (b) tilt angle, i.e. the so-called roll off angle or sliding angle (θ_{SA}); (c) the shedding angle (θ_{SHA}). Reproduced from Reference 100 with permission from The Royal Society of Chemistry.

To describe non-ideal surfaces two different wetting models, in which a droplet is said to be in either a Wenzel regime[102] or a Cassie–Baxter regime,[103] were developed to explain the wetting behaviour on a rough surface (Figure 1.7).

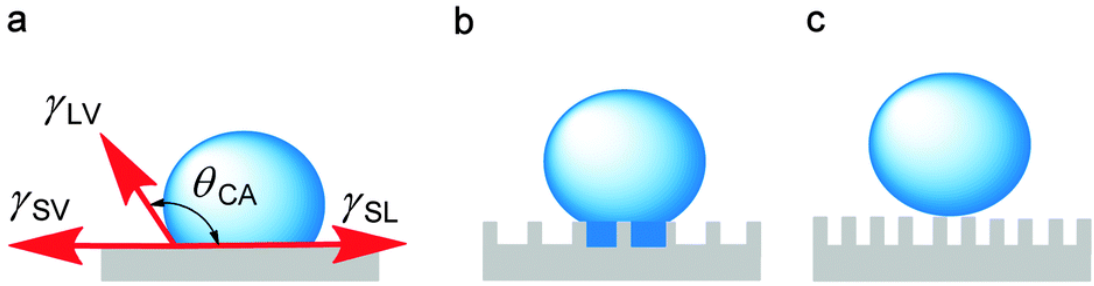

Figure 1.7. Illustration of a droplet placed onto a flat substrate (a) and rough substrates (b) and (c). Depending on the roughness of the surface, the droplet is either in the so-called Wenzel regime (b) or the Cassie–Baxter regime (c). Reproduced from Reference 100 with permission from The Royal Society of Chemistry.

The two wetting regimes can be distinguished by surface roughness. In the Wenzel wetting regime, the liquid wets the surface, but the measured contact angle (θ^*) differs from the contact angle (θ_{CA}) as described by Young's equation by a roughness factor, R (Equation 1.13).

$$\cos(\theta^*) = R \bullet \cos(\theta_{CA}) = R \bullet \frac{\gamma_{SL} - \gamma_{SV}}{\gamma_{LV}} \tag{1.13}$$

In equation 1.13, R is the ratio between the actual surface area of the rough surface and the projected (apparent) area.[99] The roughness factor (R) promotes either wettability (θ<90°) or non-wettability (θ>90°), depending on the nature of the substrate. In simple terms, the Wenzel wetting regime is one in which the liquid-surface interface is not interrupted by surface roughness (Figure 1.7 b). When the surface is made of small protrusions, which cannot be filled by the liquid and are thus filled with air, the surface wettability is described by the Cassie-Baxter wetting regime (Equation 1.14).

$$\begin{aligned} \cos(\theta^*) &= -1 + \phi_s[\cos(\theta_{CA}) + 1] \\ &= -1 + \phi_s\left[\frac{\gamma_{SL} - \gamma_{SV}}{\gamma_{LV}} + 1\right] \end{aligned} \tag{1.14}$$

In Equation 1.14, ϕ_s is the fraction of the surface that is in contact with the liquid; the remaining fraction ($1 - \phi_s$) is in contact with the air (Figure 1.7 c). It is important to note that Equation 1.14 applies to cases were the liquid touches just the top of the surface; if partial penetration of the surface grooves by the liquid occurs, a more complex version of Equation 1.14 is required.[100]

Consider a rough surface that follows the Cassie-Baxter wetting regime when in air, using water as a probe liquid. The pores of the rough surface are filled with air, which is hydrophobic. Thus, the contact angle of the rough surface will always increase relative to that of a flat substrate having identical chemical composition, under the same conditions. Hence, surface topography has a profound effect on a materials wettability.

Notably, the largest water contact angle for a flat surface has been predicted to occur on a surface with close-packed trifluoromethyl groups, having a surface energy of ~6.0 $mJ \cdot m^{-2}$.[104] Nishino et al. reported water contact angles of 119°, where the surface energy was determined to be ~6.7 $mJ \cdot m^{-2}$, on a flat surface comprising hexagonally packed $-CF_3$ groups.[105] In comparison, fractal roughness was reported to induce a water contact angle of 174°.[106]

Recent work in the field of wettability includes the identification of natural examples with superwettability, the fabrication of superhydrophobic surfaces, superhydrophilic surfaces, stimuli-responsive surfaces with switchable wettability, adhesion controlled liquid/solid surfaces, superoleophobic surfaces, and lastly, superomniphobic materials which are repellant to liquids of the lowest known surface tension (10 $mN \cdot m^{-1}$).[107]

1.6 Silicon and silica surface chemistry

Silicon substrates were used extensively throughout this thesis. Silicon substrates are relatively robust, commercially available, and compatible with a wide variety of analytical techniques including X-ray photoelectron spectroscopy (XPS). Chemical modification of silicon wafers and silica particles allowed for the creation and study of CO_2-responsive surfaces.

Silicon wafers are commonly manufactured by the Czochralski process. During the manufacture of silicon single crystals, donor impurity atoms such as boron or phosphorus can be added to the molten silicon in precise amounts to dope the silicon crystal, thus changing it into n-type or p-type extrinsic semiconductor. When using XPS, the semiconducting properties of the silicon wafer helps to reduce instrumental error that is a result of charge buildup. Silicon wafers used throughout this work were purchases as oxides; the wafers were thermally oxidised such that the surface layer was comprised of silicon oxide.

Silica particles are commonly synthesised by the Ströber method, in which tetraethyl orthosilicate (TEOS) undergoes a self-condensation polymerisation to form spherical colloidal particles that are terminated in silanol groups. Upon drying, the hydrogel yields a xerogel, the final product, which retains some or all of the silanol groups on its surface. The surface silicon atoms tend to have a complete tetrahedral configuration, and in an aqueous medium, their free valence becomes saturated with hydroxyl groups.[108] The surface properties of silica depend on the type and concentration of various surface silanol groups. These silanol groups act as centres for molecular adsorption by partaking in donor-acceptor interactions, often in the form of hydrogen bonds. Multiple types of

silanol species are present on the surface of the silica particle at any given time including free silanols, siloxane bridges, geminal silanols, and vicinal silanols (Figure 1.8).

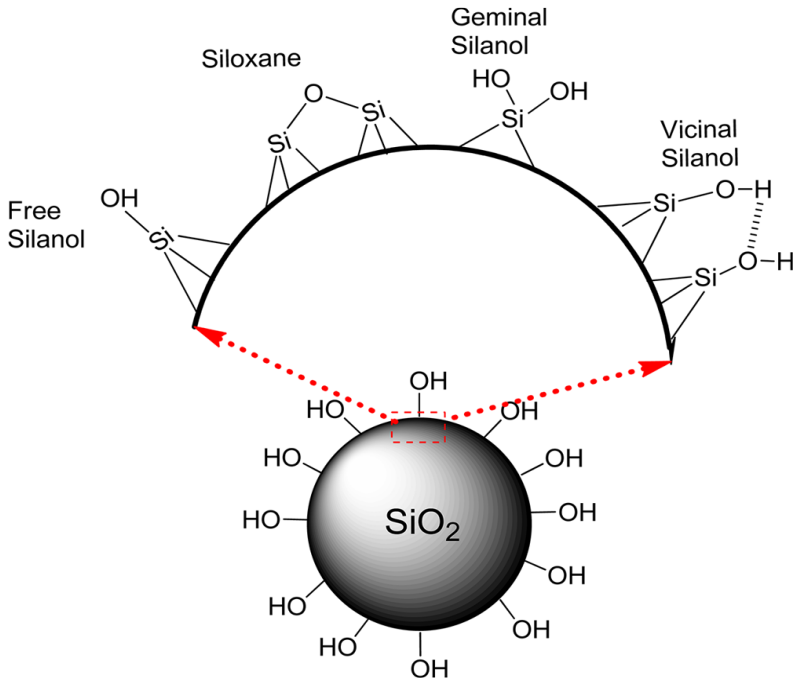

Figure 1.8. Surface silanol species present on a silicon oxide surface, shown here as a spherical silica particle. Reprinted with permission from S. Cerveny et al., *J. Phys. Chem. C,* 2012, **116**, 24340-24349. Copyright (2017) American Chemical Society.

Different types of silica are widely used as efficient adsorbents and selective absorbents, active phase carriers in catalysis, fillers for polymeric systems, adsorbents and supports for gas and liquid chromatography, thickeners for dispersion mediums, binding agents for moulding materials, reinforcing fibres, and so forth.[108]

Chemical modification of the silica surface allows researchers to tailor the adsorption properties and technological characteristics of composite materials. The acid-base activity of the various silanol species has been studied experimentally[109] and computationally.[110] Generally, these studies agree that there are two types of acidic silanol species, those with pK_a=4.5 and those with pK_a=8.5, which correlate to the free silanols

and the geminal silanols, respectively. The various protonated silanol species ($SiOH_2^+$) have pK_a values estimated to be lower than -2.5,[110] implying that protonation of the silanols is unlikely to occur within the common pH range. Additionally, computational results estimate that the second geminal silanol (i.e. $Si(O^-)(OH)$) has a pK_a>11,[110] suggesting that it is unlikely to be deprotonated within the common pH range.

In addition to their acid-base reactivity, silanol species are known to condense via silane coupling, react as nucleophiles when in the presence of a strong electrophile, and react as electrophiles in the presence of a fluoride source. These reactivity trends are exploited throughout this thesis and will be highlighted where appropriate.

1.7 Research objectives

The focus of this thesis is to incorporate CO_2-switchability into new functional materials. CO_2-switchable materials, also called CO_2-responsive materials, are materials in which the physical properties of the material can be reversibly changed by the addition or removal of CO_2. This research program has two central themes, the development of CO_2-responsive materials and the application of CO_2-responsive materials.

The first objective was to develop flat or rough surfaces that are thermally and chemically stable and that have repeatable and reversible CO_2-responsive behaviour. This involved the evaluation of different switchable groups, substrates, and attachment strategies for the creation of CO_2-responsive surfaces. The goals were to understand the factors that make the most responsive and yet chemically and thermally stable surfaces. These factors include the rate of switching, the method of attachment of CO_2-responsive

functional groups, the loading or grafting density of CO_2-responsive functional groups, and the structure of the CO_2-responsive functional group that is required to give the greatest change in surface hydrophilicity.

The second objective was to evaluate those surfaces in a variety of applications. Flat and rough CO_2-responsive surfaces have been evaluated and compared using contact angle goniometry. This research has pushed the boundaries of knowledge regarding the chemistry of interfaces; specifically looking at "switchable" nano-structures on larger micro-structures and how we can tailor surface properties such as superhydrophobicity and superhydrophilicity. These developments have led to the evaluation of CO_2-responsive surfaces as filters for the selective capture and release of organic dyes and as filters for the separation of oil from water. CO_2-responsive particles have been evaluated as drying agents for the removal of water from recycled organic solvents. Additionally, multiple collaborative efforts have seen CO_2-responsive particles evaluated as packing materials for chromatographic columns, as packing materials for solid-phase extraction columns, and as functional supports for heterogeneous catalysis.

Chapter 2 focuses on the development of CO_2-responsive polymer-grafted silica particles and their application as CO_2-switchable drying agents for wet organic solvents. Chapter 3 demonstrates how CO_2-responsive silica particles can be used to create switchable bifunctional catalysts. In Chapter 4, the development of a novel and robust method for the creation of CO_2-responsive surfaces with improved performance, substrate scope, and ease of characterisation is presented. Chapter 5 outlines the evolution of CO_2-responsive surfaces on flat and rough inorganic substrates. Chapter 6 outlines the

evolution of CO_2-responsive surfaces on a variety of polysaccharide substrates including particulate and woven substrates.

1.8 References

1 A. C. Walker, U. B. Bray and J. Johnston, *J. Am. Chem. Soc.*, 1927, **49**, 1235–1256.

2. T. Shedlovsky and D. A. MacInnes, *J. Am. Chem. Soc.*, 1935, **57**, 1705–1710.

3. D. A. MacInnes and D. Belcher, *J. Am. Chem. Soc.*, 1933, **55**, 2630–2646.

4. D. A. MacInnes and D. Belcher, *J. Am. Chem. Soc.*, 1935, **57**, 1683–1685.

5. H. S. Harned and R. Davis, *J. Am. Chem. Soc.*, 1943, **65**, 2030–2037.

6. J. Kendall, *J. Am. Chem. Soc.*, 1916, **38**, 1480–1497.

7. T. Loerting and J. Bernard, *ChemPhysChem*, 2010, **11**, 2305–2309.

8. K. Adamczyk, M. Prémont-Schwarz, D. Pines, E. Pines and E. T. J. Nibbering, *Science*, 2009, **326**, 1690–1694.

9. R. Chang, *Physical Chemistry for the Biosciences*, University Science Books, Sansalito, California, 2005.

10. K. J. Boniface, R. R. Dykeman, A. Cormier, H.-B. Wang, S. M. Mercer, G. Liu, M. F. Cunningham and P. G. Jessop, *Green Chem.*, 2015, **18**, 208–213.

11. K. J. Boniface, T. J. Clark, M. F. Cunningham, P. G. Jessop, B. E. Mariampillai, S. M. Mercer, R. Resendes, T. Robert, WO. Pat., 039 247, 2015.

12. P. G. Jessop, D. J. Heldebrant, X. Li, C. A. Eckert and C. L. Liotta, *Nature*, 2005, **436**, 1102–1102.

13. Y. Liu, P. G. Jessop, M. Cunningham, C. A. Eckert and C. L. Liotta, *Science*, 2006, **313**, 958–960.

14. X. Su, P. G. Jessop and M. F. Cunningham, *Macromolecules*, 2012, **45**, 666–670.

15. E. Stratakis, A. Mateescu, M. Barberoglou, M. Vamvakaki, C. Fotakis and S. H. Anastasiadis, *Chem. Commun.*, 2010, **46**, 4136–4138.

16. H.-D. Wang, P. G. Jessop, J. Bouchard, P. Champagne and M. F. Cunningham, *Cellulose*, 2015, **22**, 3105–3116.

17. F. S. Mohammed, S. Wuttigul and C. L. Kitchens, *Ind. Eng. Chem. Res.*, 2011, **50**, 8034–8041.

18. P. Champange, P. G. Jessop, K. J. Boniface, M. F. Cunningham, H. -B. Wang, O. Garcia-Valdez, A. Cormier, S. Ge, J. Arredondo-Luna, WO. Pat., 149 815, 2016.

19. O. Garcia-Valdez, T. Brescacin, J. Arredondo, J. Bouchard, P. G. Jessop, P. Champagne and M. F. Cunningham, *Polym. Chem.*, 2017, **8**, 4124–4131.

20. J. Arredondo, P. G. Jessop, P. Champagne, J. Bouchard and M. F. Cunningham, *Green Chem.*, 2017, **19**, 4141–4152.

21. N. Li, L. Thia and X. Wang, *Chem. Commun.*, 2014, **50**, 4003–4006.

22. J. Zhang, D. Han, H. Zhang, M. Chaker, Y. Zhao and D. Ma, *Chem. Commun.*, 2012, **48**, 11510–11512.

23. J. Glasing, J. Bouchard, P. G. Jessop, P. Champagne and M. F. Cunningham, Polym. Chem., in press, DOI:10.1039/C7PY01258F.

24. A. Darabi, P. G. Jessop and M. F. Cunningham, *Chem. Soc. Rev.*, 2016, **45**, 4391–4436.

25. S. Lin and P. Theato, *Macromol. Rapid Commun.*, 2013, **34**, 1118–1133.

26. P. G. Jessop, S. M. Mercer and D. J. Heldebrant, *Energy Environ. Sci.*, 2012, **5**, 7240–7253.

27. L. Phan, J. R. Andreatta, L. K. Horvey, C. F. Edie, A.-L. Luco, A. Mirchandani, D. J. Darensbourg and P. G. Jessop, *J. Org. Chem.*, 2008, **73**, 127–132.

28. L. M. Scott, T. Robert, J. R. Harjani and P. G. Jessop, *RSC Adv.*, 2012, **2**, 4925–4931.

29. Q. Yan, R. Zhou, C. Fu, H. Zhang, Y. Yin and J. Yuan, *Angew. Chem. Int. Ed.*, 2011, **50**, 4923–4927.

30. S. Kumar, X. Tong, Y. L. Dory, M. Lepage and Y. Zhao, *Chem. Commun.*, 2012, **49**, 90–92.

31. X. Yuan, E. G. Kim, C. A. Sanders, B. E. Richter, M. F. Cunningham, P. G. Jessop and R. D. Oleschuk, *Green Chem.*, 2017, **19**, 1757–1765.

32. J. Lahann, S. Mitragotri, T.-N. Tran, H. Kaido, J. Sundaram, I. S. Choi, S. Hoffer, G. A. Somorjai and R. Langer, *Science*, 2003, **299**, 371–374.

33. M. D. Wilson and G. M. Whitesides, *J. Am. Chem. Soc.*, 1988, **110**, 8718–8719.

34. H. Mori, A. Hirao, S. Nakahama and K. Senshu, *Macromolecules*, 1994, **27**, 4093–4100.

35. O. Azzaroni, A. A. Brown and W. T. S. Huck, *Adv. Mater.*, 2007, **19**, 151–154.

36. S. Wang, Y. Song and L. Jiang, *J. Photochem. Photobiol. C Photochem. Rev.*, 2007, **8**, 18–29.

37. T. Sun, G. Wang, L. Feng, B. Liu, Y. Ma, L. Jiang and D. Zhu, *Angew. Chem. Int. Ed.*, 2004, **43**, 357–360.

38. N. L. Abbott and G. M. Whitesides, *Langmuir*, 1994, **10**, 1493–1497.

39. X. J. Feng and L. Jiang, *Adv. Mater.*, 2006, **18**, 3063–3078.

40. S. L. Gras, T. Mahmud, G. Rosengarten, A. Mitchell and K. Kalantar-zadeh, *ChemPhysChem*, 2007, **8**, 2036–2050.

41. P. M Mendes, *Chem. Soc. Rev.*, 2008, **37**, 2512–2529.

42. B. Xin and J. Hao, *Chem. Soc. Rev.*, 2010, **39**, 769–782.

43. J. A. Howarter and J. P. Youngblood, *Adv. Mater.*, 2007, **19**, 3838–3843.

44. R. Blossey, *Nat. Mater.*, 2003, **2**, 301–306.

45. G. de Crevoisier, P. Fabre, J.-M. Corpart and L. Leibler, *Science*, 1999, **285**, 1246–1249.

46. Y. G. Takei, T. Aoki, K. Sanui, N. Ogata, Y. Sakurai and T. Okano, *Macromolecules*, 1994, **27**, 6163–6166.

47. T. Thavanesan, C. Herbert and F. A. Plamper, *Langmuir*, 2014, **30**, 5609–5619.

48. J. O. Zoppe, N. C. Ataman, P. Mocny, J. Wang, J. Moraes and H.-A. Klok, *Chem. Rev.*, 2017, **117**, 1105–1318.

49. N. Chan, PhD thesis, Queen's University, 2012.

50. A. D. Jenkins, R. G. Jones and G. Moad, *Pure Appl. Chem.*, 2009, **82**, 483–491.

51. M. K. Georges, R. P. N. Veregin, P. M. Kazmaier and G. K. Hamer, *Macromolecules*, 1993, **26**, 2987–2988.

52. C. J. Hawker, A. W. Bosman and E. Harth, *Chem. Rev.*, 2001, **101**, 3661–3688.

53. R. T. A. Mayadunne, E. Rizzardo, J. Chiefari, Y. K. Chong, G. Moad and S. H. Thang, *Macromolecules*, 1999, **32**, 6977–6980.

54. J. Chiefari, Y. K. (Bill) Chong, F. Ercole, J. Krstina, J. Jeffery, T. P. T. Le, R. T. A. Mayadunne, G. F. Meijs, C. L. Moad, G. Moad, E. Rizzardo and S. H. Thang, *Macromolecules*, 1998, **31**, 5559–5562.

55. G. Moad, *Polym. Chem.*, 2017, **8**, 177–219.

56. M. Kato, M. Kamigaito, M. Sawamoto and T. Higashimura, *Macromolecules*, 1995, **28**, 1721–1723.

57. J.-S. Wang and K. Matyjaszewski, *J. Am. Chem. Soc.*, 1995, **117**, 5614–5615.

58. K. Matyjaszewski and J. Xia, *Chem. Rev.*, 2001, **101**, 2921–2990.

59. K. Matyjaszewski and N. V. Tsarevsky, *Nat. Chem.*, 2009, **1**, 276–288.

60. J. O. Zoppe, N. C. Ataman, P. Mocny, J. Wang, J. Moraes and H.-A. Klok, *Chem. Rev.*, 2017, **117**, 1105–1318.

61. M. Ouchi, T. Terashima and M. Sawamoto, *Chem. Rev.*, 2009, **109**, 4963–5050.

62. M. Baum and W. J. Brittain, *Macromolecules*, 2002, **35**, 610–615.

63. M. Husseman, E. E. Malmström, M. McNamara, M. Mate, D. Mecerreyes, D. G. Benoit, J. L. Hedrick, P. Mansky, E. Huang, T. P. Russell and C. J. Hawker, *Macromolecules*, 1999, **32**, 1424–1431.

64. X. Huang and M. J. Wirth, *Anal. Chem.*, 1997, **69**, 4577–4580.

65. R. Barbey, L. Lavanant, D. Paripovic, N. Schüwer, C. Sugnaux, S. Tugulu and H.-A. Klok, *Chem. Rev.*, 2009, **109**, 5437–5527.

66. J. Rühe and W. Knoll, *J. Macromol. Sci. Part C*, 2002, **42**, 91–138.

67. N. R. E. N. Impens, P. van der Voort and E. F. Vansant, *Microporous Mesoporous Mater.*, 1999, **28**, 217–232.

68. S. Edmondson, V. L. Osborne and W. T. S. Huck, *Chem. Soc. Rev.*, 2004, **33**, 14–22.

69. S. Edmondson, C.-D. Vo, S. P. Armes and G.-F. Unali, *Macromolecules*, 2007, **40**, 5271–5278.

70. Y. Tsujii, K. Ohno, S. Yamamoto, A. Goto and T. Fukuda, *SpringerLink*, 1–45.

71. J. Pyun, T. Kowalewski and K. Matyjaszewski, *Macromol. Rapid Commun.*, 2003, **24**, 1043–1059.

72. J. Pyun and K. Matyjaszewski, *Chem. Mater.*, 2001, **13**, 3436–3448.

73. R. Advincula, Q. Zhou, M. Park, S. Wang, J. Mays, G. Sakellariou, S. Pispas and N. Hadjichristidis, *Langmuir*, 2002, **18**, 8672–8684.

74. R. Jordan, A. Ulman, J. F. Kang, M. H. Rafailovich and J. Sokolov, *J. Am. Chem. Soc.*, 1999, **121**, 1016–1022.

75. R. Advincula, in *Surface-Initiated Polymerization I*, ed. R. Jordan, Springer Berlin Heidelberg, Berlin, Heidelberg, 2006, pp. 107–136.

76. R. Jordan and A. Ulman, *J. Am. Chem. Soc.*, 1998, **120**, 243–247.

77. B. Zhao and W. J. Brittain, *J. Am. Chem. Soc.*, 1999, **121**, 3557–3558.

78. B. Zhao and W. J. Brittain, *Macromolecules*, 2000, **33**, 342–348.

79. I. S. Choi and R. Langer, *Macromolecules*, 2001, **34**, 5361–5363.

80. R. H. Wieringa, E. A. Siesling, P. F. M. Geurts, P. J. Werkman, E. J. Vorenkamp, V. Erb, M. Stamm and A. J. Schouten, *Langmuir*, 2001, **17**, 6477–6484.

81. Y. Wang and Y.-C. Chang, *Langmuir*, 2002, **18**, 9859–9866.

82. K. R. Yoon, Y.-W. Lee, J. K. Lee and I. S. Choi, *Macromol. Rapid Commun.*, 2004, **25**, 1510–1513.

83. H.-L. Zeng, C. Gao and D.-Y. Yan, *Adv. Funct. Mater.*, 2006, **16**, 812–818.

84. T. Jaworek, D. Neher, G. Wegner, R. H. Wieringa and A. J. Schouten, *Science*, 1998, **279**, 57–60.

85. M. Weck, J. J. Jackiw, R. R. Rossi, P. S. Weiss and R. H. Grubbs, *J. Am. Chem. Soc.*, 1999, **121**, 4088–4089.

86. N. Y. Kim, N. L. Jeon, I. S. Choi, S. Takami, Y. Harada, K. R. Finnie, G. S. Girolami, R. G. Nuzzo, G. M. Whitesides and P. E. Laibinis, *Macromolecules*, 2000, **33**, 2793–2795.

87. B. Kong, J. K. Lee and I. S. Choi, *Langmuir*, 2007, **23**, 6761–6765.

88. A. Juang, O. A. Scherman, R. H. Grubbs and N. S. Lewis, *Langmuir*, 2001, **17**, 1321–1323.

89. Y. Harada, G. S. Girolami and R. G. Nuzzo, *Langmuir*, 2003, **19**, 5104–5114.

90. O. Prucker and J. Rühe, *Macromolecules*, 1998, **31**, 602–613.

91. O. Prucker and J. Rühe, *Macromolecules*, 1998, **31**, 592–601.

92. O. Prucker and J. Rühe, *Langmuir*, 1998, **14**, 6893–6898.

93. N. Tsubokawa, A. Kogure, K. Maruyama, Y. Sone and M. Shimomura, *Polym. J.*, 1990, **22**, 827–833.

94. M. Suzuki, A. Kishida, H. Iwata and Y. Ikada, *Macromolecules*, 1986, **19**, 1804–1808.

95. B. Peng, D. Johannsmann and J. Rühe, *Macromolecules*, 1999, **32**, 6759–6766.

96. W. Huang, Skanth, G. L. Baker and M. L. Bruening, *Langmuir*, 2001, **17**, 1731–1736.

97. M. Biesalski and J. Rühe, *Macromolecules*, 1999, **32**, 2309–2316.

98. T. Young, *Philos. Trans. R. Soc. Lond.*, 1805, **95**, 65–87.

99. J. Genzer and K. Efimenko, *Biofouling*, 2006, **22**, 339–360.

100. Z. Chu and S. Seeger, *Chem. Soc. Rev.*, 2014, **43**, 2784–2798.

101. G. R. J. Artus, S. Jung, J. Zimmermann, H.-P. Gautschi, K. Marquardt and S. Seeger, *Adv. Mater.*, 2006, **18**, 2758–2762.

102. R. N. Wenzel, *Ind. Eng. Chem.*, 1936, **28**, 988–994.

103. A. B. D. Cassie and S. Baxter, *Trans. Faraday Soc.*, 1944, **40**, 546–551.

104. E. F. Hare, E. G. Shafrin and W. A. Zisman, *J. Phys. Chem.*, 1954, **58**, 236–239.

105. T. Nishino, M. Meguro, K. Nakamae, M. Matsushita and Y. Ueda, *Langmuir*, 1999, **15**, 4321–4323.

106. T. Onda, S. Shibuichi, N. Satoh and K. Tsujii, *Langmuir*, 1996, **12**, 2125–2127.

107. S. Wang, K. Liu, X. Yao and L. Jiang, *Chem. Rev.*, 2015, **115**, 8230–8293.

108. L. T. Zhuravlev, *Colloids Surf. Physicochem. Eng. Asp.*, 2000, **173**, 1–38.

109. S. Ong, X. Zhao and K. B. Eisenthal, *Chem. Phys. Lett.*, 1992, **191**, 327–335.

110. X. Liu, J. Cheng, X. Lu and R. Wang, *Phys. Chem. Chem. Phys.*, 2014, **16**, 26909–26916.

Chapter 2

CO_2-Switchable Silica Particles

2.1 Preface

The development of synthetic methodologies for the synthesis of CO_2-responsive silicon surfaces (Chapter 5) was challenging owing to the difficulty of the characterization of silicon surfaces. Fourier transform infrared (FTIR) spectroscopy analysis is often destructive to a silicon wafer; X-ray photoelectron spectroscopy (XPS) analysis is a lengthy pursuit that requires a high degree of technical knowledge to interpret and process the data. Common techniques such as nuclear magnetic resonance spectroscopy (NMR) and elemental analysis (EA) do not work with large, semi-fragile substrates such as silicon wafers. The most accessible way to determine whether a synthesis on a wafer was successful was by water contact angle (WCA) analysis. WCA analysis is a useful indicator of the surface energy of a material. Comparison of WCAs before and after the application of a stimulus can indicate whether a change in surface energy has occurred, but it does not indicate why that surface energy has changed. Qualitative assessments of synthetic methodologies for the development of CO_2-responsive surfaces did not provide enough information to move the project forward. The synthetic methods that will be outlined in Chapter 5 were producing CO_2-responsive surfaces that would switch (i.e. application of a stimulus would change the surface energy) for a cycle or two. However, subsequent cycles failed to exhibit a change in surface energy. Better methods that allowed for the characterization of the CO_2-responsive materials were needed. It became apparent that a

more robust substrate that allowed for faster characterization by less knowledge intensive methods was necessary.

Experimentation herein, with the functionalisation of silica particles, began as a necessity, not as an intellectual pursuit. Silica particles, which have the same surface chemistry as a silicon wafer, are more robust and are conducive to analysis by various IR (Infrared) techniques, EA, solid-state NMR, Brunauer-Emmett-Teller (BET) analysis, as well as XPS. With the use of silica particles as the preferred substrate, the development of methodologies for the synthesis of CO_2-responsive surfaces progressed rapidly. This simple choice led to multiple new avenues of research, which in its entirety has included multiple collaborators at various academic institutions, professional research institutions, privately held for-profit companies, and government funded research centres.

2.1.1 Abstract

Herein the synthesis and evaluation of CO_2-switchable drying agents in the drying of isobutanol are described. The conditions for use and regeneration are explored, and it is shown that CO_2-switchable amine-containing particles can remove water from isobutanol and are easily recycled several times under very mild conditions. Specifically, CO_2-switchable drying agents were created for the first time and evaluated in the drying of wet isobutanol. Through the application of CO_2 to suspensions of drying agent (DA), the water content of the isobutanol could be reduced by 490 $mg \cdot gDA^{-1}$. This value exceeds the values obtained for commercial drying agents such as silica, alumina, and molecular sieves. All of the CO_2-switchable drying agents were superior to unfunctionalised silica and alumina with respect to the quantity of water removed per g of drying agent. The synthesised CO_2-switchable drying agents were superior to the commercially available amine-functionalised silica with respect to drying ability and hydrolytic stability at low pH. The polymer-grafted silica drying agents (PGS-1 & PGS-2) capture ~10 times more water per amine ($mmol_W/mmol_{AA}$) than the other amine-containing CO_2-switchable drying agents. Additionally, a new method for the measurement of the accessible amine content on surfaces is reported.

2.1.2 Introduction

Drying organic liquids (i.e. removing water from them) is an important task in many fields of chemistry as well as several industrial processes such as solvent recycling and the production of ethanol and biodiesel. Many industries use large volumes of organic solvents; solvent recycling helps to save money and the environment. Used solvent is usually contaminated with water, rendering it useless for the industrial process for which it was intended. Ethanol, when it is manufactured by fermentation, is also contaminated with water.[1] The presence of water in fuel grade ethanol reduces the heat of fuel combustion and causes phase separation in ethanol-petroleum blends.[2] The removal of water from ethanol, as well as many other solvents, is complicated by the formation of azeotropes. Azeotrope formation necessitates the use of additional means beyond distillation to reduce the water content; desiccants are a commonly employed agent to address this issue.

Desiccants can be broken down into two categories: single use desiccants like sodium hydride and sodium sulphate; and reusable desiccants such as molecular sieves. The desiccants in both categories pose economic and environmental concerns. All single-use desiccants result in the generation of solid waste and therefore disposal issues and recurring costs. Further, highly reactive single use desiccants such as sodium hydride pose safety concerns and require significant energy consumption during manufacture. Although molecular sieves have the advantage of being reusable, they require significant amounts of energy for regeneration.[3] Therefore, it would be advantageous, both economically and environmentally, to have a reusable desiccant (i.e. drying agent) that is easily regenerated.

The criteria for the ideal drying agent can be defined as follows: able to bind water strongly during the capture stage; able to release water easily during regeneration; robust enough to be recycled; inert to the solvent of interest; and possessing a high water binding capacity. To meet the first two of these requirements, the drying agent would have to be 'switchable' in response to an external trigger; its affinity for water would be different depending on whether it is in capture mode or regeneration mode.

The choice of external trigger strongly affects the cost, environmental impact, and ease of switching. In comparison with other triggers such as acids/bases, oxidants/reductants, salts and light, CO_2 is an attractive choice as it is easily-removed, does not accumulate in a system, and is functional for non-transparent systems.[4]

In recent years, CO_2-triggered switchable solvents,[5] surfactants,[6] and latex particles[7] that are switchable in polarity or hydrophilicity have been developed. In general, CO_2-switchable materials rely on the protonation of amine- or amidine-containing molecules when CO_2 is dissolved in an aqueous solution (Equation 2.1).

$$R_3N + CO_2 + H_2O \rightleftharpoons [R_3NH]^+[HCO_3]^- \qquad (2.1)$$

The fact that this reaction both consumes an equivalent of water and simultaneously increases the hydrophilicity of the charged species suggests that there is the possibility of capturing more than one water molecule per nitrogen atom through waters of hydration when in an organic solvent.

Fundamentally, a CO_2-responsive drying agent must be robust enough to be recycled many times in order to be effective. CO_2-responsive functionalities have been incorporated into homogenous materials such as porous polymer particles and they have been grafted from inorganic substrates such as silica. Porous polymer particles are a viable option as long as the polymer particle can withstand the conditions outlined in the drying and regeneration steps. Since polymers are not bioavailable, there should be no concern regarding toxicity. Polymer grafting methods have allowed for a wide variety of silica based stimuli-responsive materials.[8] Silica is an attractive candidate for an inorganic support for CO_2-responsive functionalities owing to the fact that it has a high surface area and is physically robust. One of the ways polymer grafting can be achieved is through surface-initiated atom transfer radical polymerisation (SI-ATRP). SI-ATRP has been used to synthesise a CO_2-responsive surface previously.[9]

Herein the synthesis and evaluation of CO_2-switchable drying agents are described. The conditions for use and regeneration are explored, and it is shown that the tertiary amine-containing particles can remove water from various organic solvents and are easily recycled several times under very mild conditions (Figure 2.1).

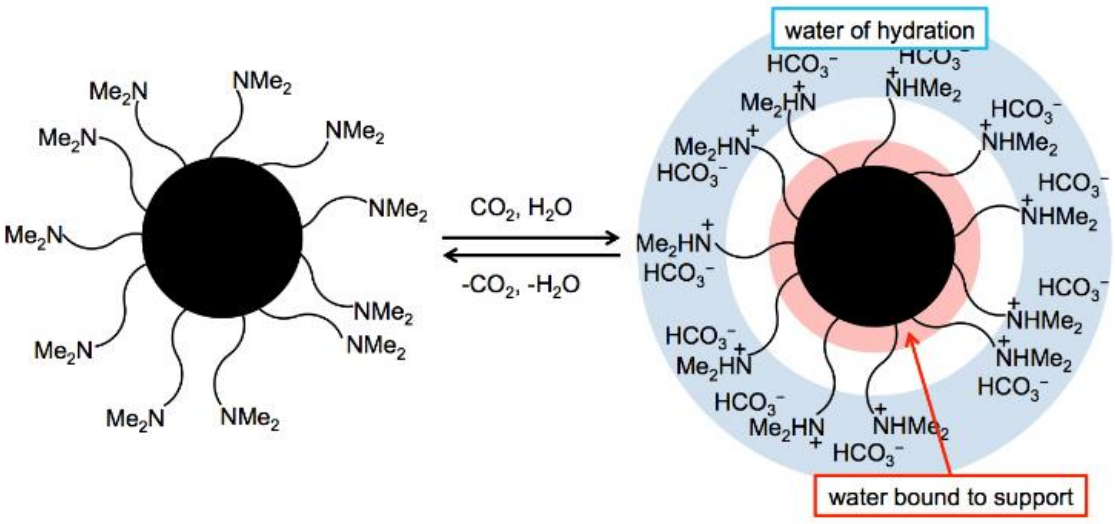

Figure 2.1. A CO_2-switchable drying agent to which water could bind in three ways: a) by reacting with the amine and CO_2 to form the bicarbonate salt b) by adsportion to the support (shown as a pink band), and c) as waters of hydration of the salt ions (shown as a blue band). Reproduced from reference 10 with permission from The Royal Society of Chemistry.

2.2 Results and discussion

2.2.1 Synthesis of porous polymer particles

Porous polymer particles (P-1) were the first incarnation of a CO_2-responsive particle. A detailed account of their synthesis and characterization was published previously.[10] Briefly, P-1 was synthesised because it was believed that the high nitrogen content of monomer 2-1 (5.4 mmol of nitrogen atoms per g of material), would translate into a high accessible nitrogen content in the resulting porous particles. Monomer 2-1 was synthesised in two steps from commercially available 2,3-dibromo-1,4-butanediol (Scheme 2.1), which was converted to 1,4-bis(diethylamino)-2,3-butanediol under basic conditions via an epoxide intermediate,[11,12] which reacted in situ with diethylamine. The methacrylate moiety was introduced under basic conditions in dimethyl carbonate (DMC)

with methacryloyl chloride (MAC). Benign solvents were used in both steps, and neither step required chromatographic techniques for product purification.

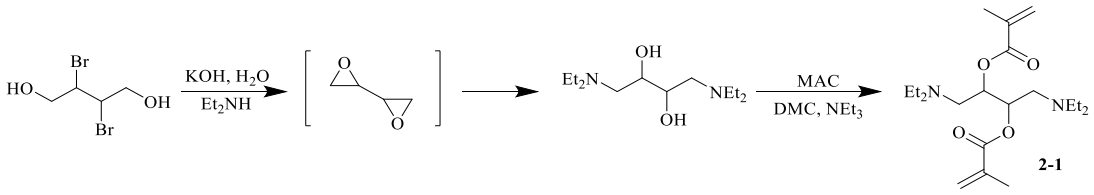

Scheme 2.1. Synthesis of monomer 2-1, for porous CO_2-switchable polymer particles. Reproduced from reference 10 with permission from The Royal Society of Chemistry.

The porous polymer particles were prepared using suspension polymerisation of 2-1 in a water and toluene mixture. The particles were determined to have a mean particle size of 220 μm through diffractive light scattering measurements. Scanning electron microscopy (SEM) images of the particles show a surface with many deep pores (Figure 2.2), indicating that the polymer particles are highly porous. The porosity of the polymer particles was confirmed through $N_{2(g)}$ sorption experiments through which the BET surface area was found to be 40 $m^2 \cdot g^{-1}$. Finally, the particles were shown to be thermally stable up to 300 °C by thermogravimetric analysis (TGA).

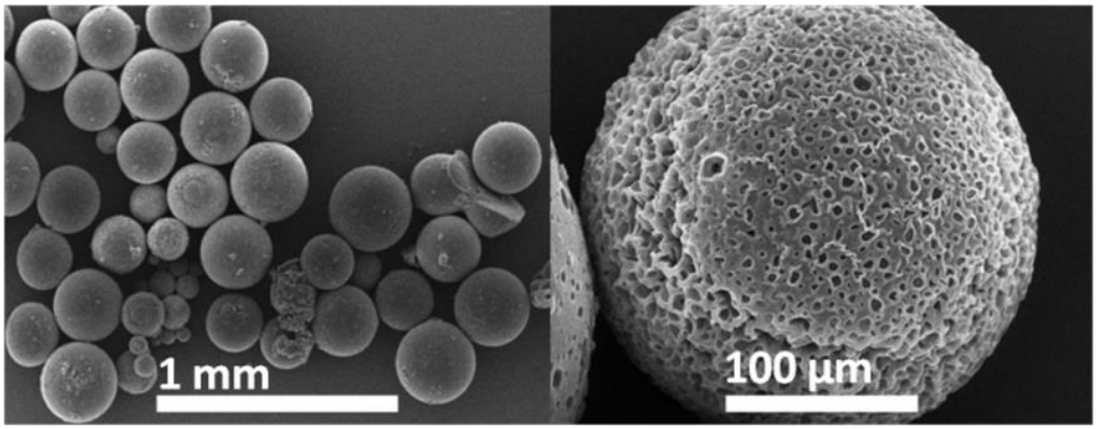

Figure 2.2. SEM images of porous polymer particles synthesised from monomer 2-1. Reproduced from reference 10 with permission from The Royal Society of Chemistry.

P-1 was used to establish the regeneration conditions for CO_2-responsive particles. The regeneration conditions outlined by experimentation with P-1 were used as the standard regeneration conditions for all future tests involving CO_2-responsive particles. After the drying process was performed for isobutanol using the polymer particles, TGA was performed on the used polymer particles; they were heated isothermally at 50 °C for 4 h and subsequently heated to 120 °C (Figure. 2.3). The mass of the 'wet' particles continues to drop as CO_2 and water are lost at 50 °C. However, no further weight loss was observed upon subsequent heating to 120 °C. Therefore, the regeneration conditions were set as heating to 50 °C for 4 h.

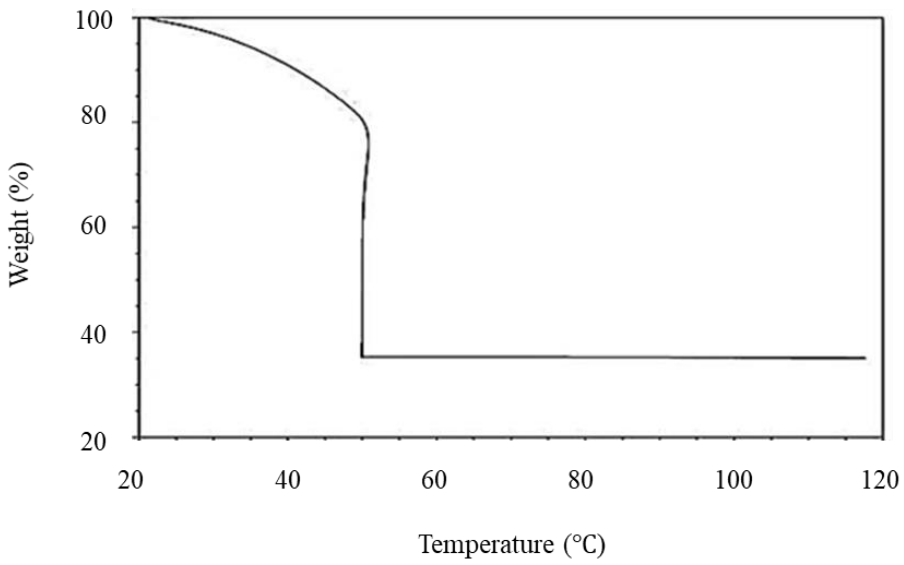

Figure 2.3. Thermogravimetric analysis of wet porous polymer particles (P-1) after the drying process was applied for the drying of wet isobutanol. Reproduced from reference 10 with permission from The Royal Society of Chemistry.

2.2.2 Synthesis of polymer-grafted silica particles: determination of initiator content

An ideal surface-initiated atom transfer radical polymerisation (SI-ATRP) is one in which polymer is grafted to the substrate surface and the grafted polymer has a low molecular weight dispersity. To achieve good control, the initiator content in the system must be high enough such that the persistent radical effect is achieved, yet low enough that the probability of irreversible termination is not significantly increased. Typically, chain concentrations of $\sim 10^{-2}$ M facilitate controlled polymerizations in solution. Comparatively, surface-initiated systems have a smaller surface area, resulting in lower initiator content and therefore lower chain concentration. To remedy this issue, free initiator is often added in solution to surface-initiated polymerizations. Thus, to understand

and execute a surface-initiated polymerization, both the free initiator and the bound initiator content should be known.

Initiator loading (i.e. bound initiator) is often reported as a $mmol \cdot g^{-1}$ value because this value does not rely on surface area. As such, the $mmol \cdot g^{-1}$ value is substrate independent; not all substrates (e.g. filter paper) are conducive to precise measurements of surface area owing to their rough surface texture.

Commonly, researchers approximate the initiator loading by estimating the number of grafted chains and dividing it by the initiation efficiency. The number of grafted chains can be estimated using the number average molecular weight (M_n) and the percentage by weight (wt%) of grafted polymer on the surface. The M_n of the grafted polymer is commonly determined by destructive etching techniques that can be ineffective and non-selective. Thus, this approach often results in poor confidence associated with number of grafted chains and subsequently the initiator loading. Alternatively, if free polymer was produced in situ, it can be characterised to determine M_n in place of the grafted polymers.[14–16] This alternative, while widely practiced, remains somewhat controversial.[17]

In one instance, the initiator loading of silica nanoparticles was reported to be in the region of 0.07 to 0.25 $mmol \cdot g^{-1}$.[14] Alternatively, another instance resulted in the conclusive determination of initiator loading. Hansson et al. used a disulphide-containing initiator immobilised on the surface of a cellulosic substrate (Whatman no.1 filter paper).[15] From that surface, poly(methyl methacrylate) (PMMA) was grown using SI-ARGET-ATRP. The polymer grafts were cleaved from the surface of cellulose using

1,4-dithiothreitol (DTT). The remaining thiol moieties present on the surface after cleavage were utilised to assess the initiator loading. Ellman's reagent was employed and the initiator loading was determined to be 0.021 mmol·g^{-1}. Additionally, the authors reported good agreement between the free polymer (FP) produced in situ (FP M_n: 20.9 kDa, Đ: 1.14) and the grafted polymer (GP) (GP M_n: 19.0 kDa, Đ: 1.21) that was cleaved from the substrate post reaction. The initiator loading value reported by Hansson et al. is lower than the others; plausibly because Whatman no.1 filter paper is a low surface area substrate. When this approach was applied to a high surface area substrate, microcrystalline cellulose (MCC), having a diameter 20 μm, the initiator loading was found to be twice as high.[15] In summary, the initiator loading values were found to be dependent on the surface area of the substrate. Reports of initiator loading values range from 0.02 mmol·g^{-1} to 0.25 mmol·g^{-1}.

Throughout this research, two initiator types were studied. The first initiator, 2-bromo-2-methylpropionyl bromide (BIBB) was chosen for two reasons; firstly, the reactive acyl bromide facilitates the substitution reactions necessary for coupling with a substrate. Secondly, the tertiary bromide functionality is well known as a suitable initiating group for ATRP.[13] The BIBB initiator is, therefore, suitable for SI-ATRP using the *grafting from* technique. Methacryloyl chloride (MAC) was the second initiator studied. It was chosen in part for the same reasons as BIBB; the reactive acyl chloride facilitates the substitution reactions necessary for coupling with a substrate. MAC is suitable for SI-ATRP using the *grafting to* or the *grafting through* techniques, due to its accessible double bond. Initial attempts at the functionalisation of silica particles via direct acyl substitution proved fruitful, as the subsequent polymerisations were determined to have

grafted polymer on the substrate surface. Thus, the conclusion is that the initiator must have been present on the surface of the material, otherwise, the polymer would not have been present. The polymer-grafted silica particles were washed and sonicated in good solvents, (tetrahydrofuran or toluene) for the respective polymers, multiple times to ensure that the polymer detected by TGA or NMR was a result of covalently bound grafted-polymer and not physisorbed free polymer.

A series of experiments were undertaken, in which various initiators and conditions were screened, to identify the grafting density of the initiator functionality on the silica particle. The general reaction scheme in which silica particles were functionalised with an initiator (e.g. BIBB), in the presence of an auxiliary base such as diisopropylethylamine (DIPEA) to yield initiator-functionalised silica particles is shown in Scheme 2.2.

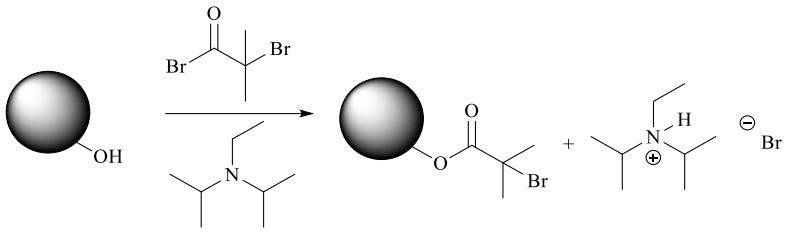

Scheme 2.2. The preparation of BIBB-functionalised silica particles (denoted by black circles). Reproduced from reference 10 with permission from The Royal Society of Chemistry.

The initiator-functionalised silica particles were characterised by EA and solid-state NMR (Appendix I). Determining the amount of bound initiator proved difficult due to low grafting densities. For instance, the %C of initiator-grafted silica particles, as determined by EA, was found to be within the experimental error of ±0.4%. Additionally,

the use of triethylamine as an auxiliary base is not recommended due to it's propensity to stick to the surface of the silica particles (Appendix I). A representative synthesis is presented in the section 2.4.2, with the remaining methods appearing in Appendix I.

2.2.3 Synthesis of polymer-grafted silica particles: initiator content as determined by the Kiselev-Zhuravlev constant

The initiator content remained an important value to which a reliable method for its determination was still needed. The initiator reacts with free surface silanol groups in a nucleophilic acyl substitution reaction. Initially, the methodology needed to calculate the amount of free surface silanols on a silica particle substrate was unknown. The amount of free surface silanols that were available to react with the initiator had to be approximated to standardise the reactions conditions. Early estimates postulated that the free surface silanol concentration would be approximately 1 $mmol \cdot g^{-1}$. To achieve high initiator loadings on silica particles, the equivalence of free surface silanols on silica particles was set as 2 $mmol \cdot g^{-1}$. In hindsight, this was an over estimation that resulted in the production of significant amounts of free polymer in addition to the polymer-grafted materials. Thus, a better understanding of the nature of the silica particle was required.

To better understand the nature of the silica particle, the concentration of various silanol species, and to reduce wastefulness, the scientific literature was searched for information regarding the surface chemistry of silica particles. An enlightening publication and suggested reading for those working with silica particles is "The surface chemistry of amorphous silica. Zhuravlev model."[18] A physio-chemical model is presented for the

determination of the concentration and distribution of various types of surface silanols and to characterise the energetic heterogeneity of the silica surface as a function of the pretreatment temperature of SiO_2 samples. The magnitude of the silanol number, i.e. the number of OH groups per unit surface area, $\propto_{OH}$, when the surface is hydroxylated to the maximum degree, is considered to be a physio-chemical constant.[18] The Kiselev-Zhuravlev constant, $\propto_{OH,}$ is reported to be 4.9 $OH \cdot nm^{-2}$. In tandem with this constant, the surface area (SA) as determined by the BET method can be used to calculate the amount of moles of the surface silanol species, and their relative distribution, at a specific temperature, for amorphous silica particles.

Two temperature regimes are of interest; between 180 ℃ and 200 ℃ the number of OH groups per unit surface area is 4.9 $OH \cdot nm^{-2}$, at 400 ℃ the number of OH groups per unit surface area is ca. 2.35 $OH \cdot nm^{-2}$. If a high degree of functionalisation can be achieved, a thermal pretreatment could be used to influence the grafting density of grafted polymer. A thermal pretreatment between 180 ℃ and 200 ℃ would result in a high grafting density and a thermal pretreatment at 400 ℃ would result in a lower grafting density. In either case, 2 h is recommended and the silica particles must be added to the reaction mixture immediately after being removed from the oven. The calculation of the maximum amount of free surface silanols ($mmol_{OH} \cdot g^{-1}$), when pre-treated between 180 ℃ and 200 ℃ for 2 h, can be simplified to 0.00814 $OH \cdot (m^2\ mmol)^{-1} \cdot SA$, where SA is the surface area as measured by the BET method, reported in m^2/g. When pre-treated at 400 ℃, the calculation simplifies to 0.00814 $OH \cdot (m^2\ mmol)^{-1} \cdot SA$. Since the only variable is the surface area of the substrate, the free surface silanol concentration will vary for different types of silica particles (Table 2.1).

Table 2.1. The amount of free surface silanols for silica particles as determined by BET analysis using the Kiselev-Zhuravlev constant.

Particle Designation	Particle Type	Pore Size (Å)	BET Surface Area	$mmol_{OH} \cdot g^{-1}$ @ 200 °C[a]	$mmol_{OH} \cdot g^{-1}$ @ 400 °C[b]
SiO_2 #1	Spherical	100	426	3.47	1.66
SiO_2 #2	Amorphous	60	285	2.32	1.11

[a]Calculated using the Kiselev-Zhuravlev constant, $\propto_{OH}$=4.9 $OH \cdot nm^{-2}$
[b]Calculated using Kiselev-Zhuravlev constant, $\propto_{OH}$=2.35 $OH \cdot nm^{-2}$

The Kiselev-Zhuravlev constant was declared a physio-chemical constant because the number of moles of surface silanols was shown to be independent of the origin and structural characteristics of amorphous silica.[18] Spherical silica particles have a surface area larger than that of amorphous particles owing to their porous nature. Thus, the number of moles of surface silanols (Table 2.1, SiO_2 #1) for spherical silica particles will be higher than that of amorphous silica particles (Table 2.1, SiO_2 #2). A considerable amount of the surface area reported for a spherical particle will be internal. If the pore size is small enough that it sterically disfavours functionalisation of the internal surface silanols, the resultant magnitude of accessible surface silanols will be more akin to that of an amorphous counterpart.

The internal surface area thus has implications in the grafting densities that can be achieved based on the molecular weight of the polymer and grafting technique in which the polymer chains are bound to a silica particle. For example, a 30 kDA PDiPAEMA chain has a maximum length of ~250 Å (maximum extension 430 Å) and a 7.0 kDa PDiPAEMA chain has a maximum length of ~60 Å (maximum extension ca. 102 Å); sample calculations are provided in Appendix II. If a *grafting to* approach were applied, polymers larger than 7.0 kDa would be much too big to covalently bind inside the pores,

assuming that the chain must be in an extended state, such that the reactive end group is accessible and binding to the substrate can occur. Polymer chains in solution are unlikely to be found in a fully extended state unless they are in an ideal solvent, at a low concentration. Their shape in solution is best described by the random walk model, which proposes that the polymers size can be approximated by its radius of gyration. For example, the radius of gyration for a 30 kDa freely jointed chain of PDiPAEMA is ~10.5 Å (Appendix II). Thus, a freely jointed chain could penetrate into the pores of the silica particles, but the likelihood of a given polymer achieving an extended conformation within a pore is low. For *grafting to* techniques to be successful, the end group that is capable of reacting further must be accessible. The reactive end group will be most accessible when the polymer chain is in an extended conformation and not collapsed upon itself. Thus, the size of the pore, in which reactive groups reside, will play a major factor in whether a polymer chain will successfully bind using the *grafting to* approach. If the polymer chain cannot fully extend within the pore, it is unlikely that the reactive group on the terminus of the polymer will be accessible. However, if a *grafting from* approach were applied, the polymers could grow inside the pore until they become sterically hindered to the point that they cease growing. Therefore, using the molar amount of free surface silanols to determine grafting density will result in significant error. The error will reach a maximum for porous materials using higher molecular weight polymers and a *grafting to* approach.

Theoretical calculations using the Kiselev-Zhuravlev constant have allowed for the approximation of the maximum number of free surface silanols that are present on a silica particle. Elemental analysis of initiator-functionalised silica particles concluded that the maximum initiator loading that could have been achieved was 0.2 $mmol \cdot g^{-1}$. Accordingly,

ca. 6.6% of the free surface silanols of SiliaFlash P60 (SiO_2 #5) have been functionalised by the initiator-grafting methods presented in this chapter. Additionally, a great deal of care should be used when relying on EA or the Kiselev-Zhuravlev constant when estimating the grafting density of grafted polymer chains.

2.2.4 Hydrolysis of CO_2-responsive materials

The CO_2-responsive system, as described, fundamentally requires the presence of water, whether as a solvent or an additive. In the majority of the systems being studied, water is the solvent. Thus, the hydrolytic stability of CO_2-responsive polymers and the subsequent CO_2-responsive materials must be taken into consideration. The degradation pathway that is expected to be the most prevalent for CO_2-responsive polymers, which have been grafted on silicon or polysaccharide substrates, is hydrolysis catalyzed by either acid or base.

Van de Wetering et al. studied the hydrolysis of poly(2-(dimethylamino)ethyl methacrylate) (PDMAEMA) and various monomeric analogues and their respective degradation products.[19] Compounds of interest, the majority of which were studied by Van de Wetering et al., are presented in Figure 2.4. The compounds of interest are 2-(dimethylamino)ethyl methacrylate (DMAEMA, A), 2-(dimethylamino)ethyl isobutyrate (DMAEIB, B), 2-(dimethylamino)propyl methacrylate (DMAPMA, C), 2-(dimethylamino)ethyl acrylate (DMAEA, D), 2-(dimethylamino)ethanol (DMAE-OH, E), 2-(dimethylamino)propanol (DMAP-OH, F), N-[3-(dimethylamino)propyl]methacrylamide (DMAPMAm, G),

3-(dimethylamino)-1-propylamine (DMAP-A, H), and lastly, for descriptive purposes, a generic CO_2-responsive monomer (I).

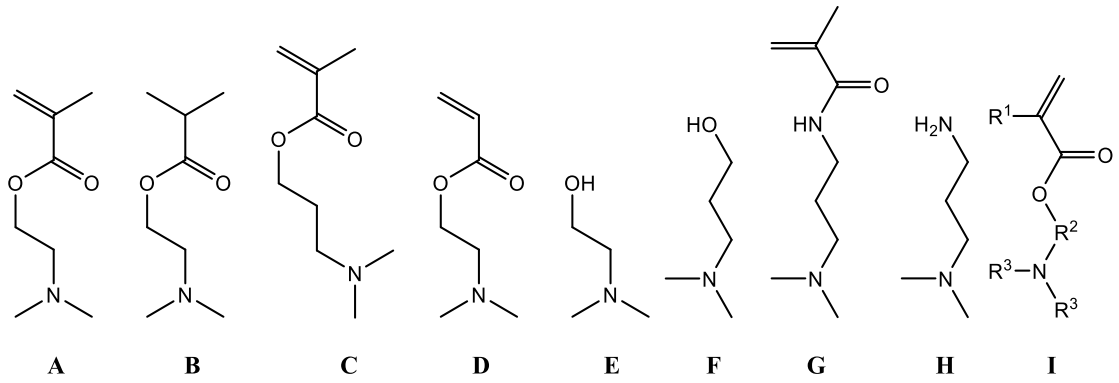

Figure 2.4. A select group of CO_2-responsive, tertiary amine-containing compounds and their respective amine-containing degradation products. DMAEMA (A), DMAEIB (B), DMAPMA (C), DMAEA (D), DMAE-OH (E), DMAP-OH (F), DMAPMAm (G), DMAP-A (H), Generic CO_2-responsive monomer (I), where R^1= H, methyl; R^2= ethylene, propylene; R^3= alkyl group.

Of initial interest from the study is that the pK_{aH} of PDMAEMA decreases as molecular weight increases, from 7.8 at 4.0 kDa to 7.4 at 550 kDa.[19] The variation in pK_{aH} values for PDMAEMA, as reported by Van de Wetering, is in good agreement with other reports.[19–22] The pK_{aH} was determined by a titration method in which solutions of 2-3 mg/mL of polymer were prepared in 0.15 M NaCl, acidified with 0.1 M HCl, and titrated with 0.1 M NaOH. One of the factors presented by Van de Wetering is of particular importance to the mechanism of protonation and hydrolysis; as demonstrated in Figure 2.5, DMAEMA is capable of adopting a cyclic conformation in addition to its commonly depicted stretched conformation.

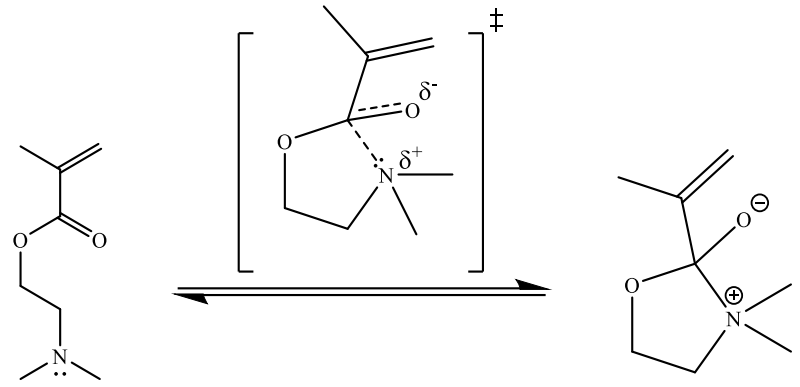

Figure 2.5. The cyclic conformation of DMAEMA (A).

When DMAEMA adopts the cyclic conformation, the free electron pair of the amino group is delocalized by interaction with the carbonyl carbon, thus becoming less accessible for protonation, therefore resulting in a lower pK_{aH}.[23] Similarly, when the amino group is protonated, the molecule can adopt a 7-membered cyclic conformation through hydrogen bonding to the carbonyl oxygen (Figure 2.6).

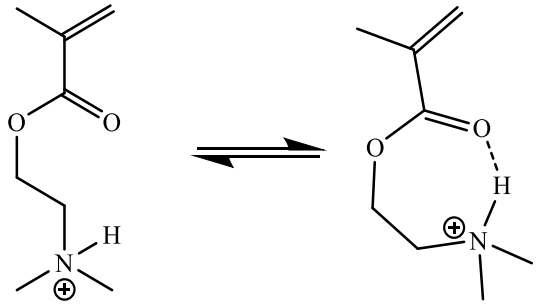

Figure 2.6. The cyclic conformation of DMAEMA-H^+.

Coordination of the protonated amino group to the carbonyl oxygen via hydrogen bonding renders the carbonyl carbon more electropositive, thus more susceptible to nucleophilic attack. Interestingly, within a pH range of 4-8, the observed rate of hydrolysis for

compound C was smaller than those of compounds A and B, thus compound C is more stable towards hydrolysis within that pH range. A possible explanation is that the additional -CH_2- group in the propylene linker of C disfavors the formation of a cyclic conformation that would lead to destabilisation of the carbonyl carbon (R^2, compound I, Figure 2.4). The cyclic conformation of C, when protonated, would be an eight-member ring, whereas the cyclic conformations for A and B, when protonated, would be seven-member rings. Additionally, when not protonated, the cyclic conformation for C is a six-member ring, where as those for A and B are five-member rings. Six-member ring conformations minimise ring strain and are thus the most stable ring size. As ring size increases or decreases from six, the ring strain increases and formation of that ring becomes less likely. The increased ring size of the hydrogen-bonded conformation of compound C, when protonated, decreases the likelihood of the formation of the ring conformation, and thus subsequent destabilisation of the carbonyl carbon is reduced. The reduced tendency to form the cyclic conformation that leads to carbonyl destabalisaztion is the likely cause for the increased stability towards hydrolysis of compound C in comparison to compounds A and B. In support of this theory, Van de Wetering et al. postulated, on the basis of FTIR spectral analysis, that intramolecular interactions are indeed more pronounced in DMAEMA-H^+ (A) than those in DMAPMA-H^+ (C).[19]

Another consideration that must be addressed when considering the hydrolytic stability of these compounds is the substitution of the backbone of the subsequent polymer chain. Alkylation of the backbone resulted in a significant improvement in the stability of PDMAEMA over poly(2-(dimethylamino)ethyl acrylate) (PDMAEA) towards hydrolysis. PDMAEMA was shown to be resistant to hydrolysis at 80 ℃, with a k_{obs} of 1×10^{-8} at pH

1.3, and 7×10^{-8} at pH 7.0. Whereas, PDMAEA was shown to be quite susceptible to hydrolysis at 80 ℃, with a k_{obs} of 1×10^{-5} at pH 1.3 and 7×10^{-6} at pH 7.0.

A logical extension of this work is that when the size of the alkyl substituents on the amino group increase (R^3, compound I, Figure 2.4), the steric effects would result in further destabilisation of the hydrolysis-promoting ring conformation. Thus the more hydrophobic the amino group is, the less likely hydrolysis of the compound becomes. Additionally, if the carbonyl carbon were to be more stable, the rate of hydrolysis could be decreased. Thus, amide bonding in the carbonyl moiety (G, Figure 2.4) increases resistance to hydrolysis in comparison to ester bonding in the carbonyl moiety (C, Figure 2.4). With all factors considered, the CO_2-responsive monomers that are most resistant to hydrolysis would be those that contained a methacrylamide, a linker of 3 or more carbons (R^2, I, Figure 2.7), and significant hydrophobicity surrounding the amino group (R^3, I, Figure 2.4). DMAPMAm (G, Figure 2.4) was selected as a suitable monomer to be used in the synthesis of CO_2-responsive silica particles owing to its commercial availability, relative affordability and fit to the criteria previously mentioned.

2.2.5 Synthesis of CO_2-responsive polymer-grafted silica particles

Experiments were undertaken to determine what effect the uncertainty regarding the amount of initiator on the initiator grafted-silica particles would have in the SI-ATRP polymerisation of CO_2-responsive silica particles. The synthesis of CO_2-responsive silica particles in the presence of initiator-grafted silica particles was approached in two ways. The first way considered each reactant individually and accounted for the initiator loading on the initiator-grafted silica particles. The second way involved running an ATRP reaction in the presence of the initiator-grafted silica particles, where the initiator loading on the silica particles was not accounted for and its equivalency was ignored. In this approach, the initiator BIBB was added in solution, similar to what would be done in a normal ATRP.

The first approach was used for the majority of the reactions presented in this chapter. The initiator loading on the silica particles, using the best approximations at the time, was standardised as 1 equivalent (eq.), and the remaining reactants and reagents were calculated relative to the initiator content. This approach was utilised in making polymer-grafted silica particles (PGS): PGS-1 and PGS-2. The silica particles resulting from these reactions exhibited a hydrogel-like behavior in response to CO_2, therefore, the reactions were deemed successful, in that polymer had been grafted to the silica particle.

As the experimentation evolved, more information was required for the characterization of the CO_2-responsive materials (i.e. the M_n of grafted polymer). The first approach did not allow for the production of free polymer in addition to the CO_2-responsive material (i.e. PGS) during the polymerisation. Therefore, the only method to characterise

the CO_2-responsive polymer was a destructive technique in which fluoride ions are used to cleave the polymer from silica surface of the silica particle.

The second approach, which mirrors that of Hansson et al., provided free polymer from which the M_n of the grafted-polymer could be approximated.[15] This approach was applied to the synthesis of PGS-3, and PGS-6. In both cases, the initiator (i.e. BIBB) was added to the polymerisation in addition to the initiator-grafted silica particles. The relative amounts of free initiator in solution (mmol $I_{solution}$) and initiator grafted to the silica particles (mmol $I_{substrate}$) can be calculated and compared. For PGS-3: $I_{solution}$: 0.05 mmol, $I_{substrate}$: 0.459 mmol. Thus, the total amount of initiator in the polymerisation was I_{total}: 0.509 mmol, where $I_{solution}$: 10% and $I_{substrate}$: 90%. In the case of PGS-6, the total amount of initiator in the polymerisation was I_{total}: 1.038 mmol, where $I_{solution}$: 6% and $I_{substrate}$: 94%. It should be noted that surface bound initiating groups often suffer from low initiation efficiencies, typically ~10-30%.[14,24,25] The lower efficiency of initiation from colloidal surfaces may be explained by steric congestion of the initiation sites (i.e. the surface-bound 2-bromoisobutyrate groups).[24] In all cases, the resultant polymer-grafted silica particles (PGS-1 to PGS-6) were CO_2-responsive.

The polymer that was collected from each experiment, whether by destructive or nondestructive means, was subjected to analysis by gel permeation chromatography (GPC), mass spectrometry (MS), NMR, and FTIR. The identity of the polymer (PDMAPMAm) was confirmed by NMR, FTIR, and MS. The M_n of the polymers could not be determined, by MS or GPC, with certainty. Due to solvent incompatibilities, the PDMAPMAm samples could not be analysed by GPC. Additionally, NMR was not sensitive enough to determine the M_n of the PDMAPMAm samples, which suggests that

the M_n > ~3.0 kDa.[26] Extensive analysis by mass spectrometry provided inconclusive data and thus failed to elucidate the molecular weight of the grafted polymer.

In retrospect, adding BIBB to the reaction solution as the free initiator species was a mistake. The reactive acyl bromide of BIBB, when in the presence of a variety of nucleophilic species such as tertiary amines or protic solvents, will participate in a variety of unwanted side reactions. Therefore, a less reactive analogue should be used, such that unwanted side reactions are minimised. The suggested analogue is ethyl 2-bromo-2-methylpropionate (EBIB). EBIB was used for all subsequent polymerisations.

2.2.6 Characterization of surface CO_2-responsive groups

To provide a comparison to the porous polymer particles (P-1) and the polymer-grafted silica particles (PGS), commercially available silica, alumina, and silica functionalised with 3-(dimethylamino)propyl groups were characterised and evaluated as drying agents for wet isobutanol.

Commercially available amine-functionalised silica particles are characterised by the loading of the amine on the solid support, in units of $mmol \cdot g^{-1}$. Amine loading refers to the amount of amine in a given sample, whereas accessible amine content refers to the number of reactive amine groups and does not include amine groups that are physically buried and therefore unreactive.

Commonly, amine loading values are determined by EA, however, to differentiate between the overall loading of amines and the accessible amines, a titration with a strong

acid such as HCl is recommended. Ojo et al. highlighted the difference between EA values and titration values. In one example, only 85% of the amines reported by EA are reported accessible by titration to low pH (ca. 2) with HCl.[27] The titration method used by Ojo et al. is an effective method for amine-containing particles that have only one protonatable species. In the case of the polymer particles (P-1), every protonatable site is an amine. Therefore titration to low pH (ca. 2) with HCl is an appropriate method for determining the accessible amine content. Elemental analysis of P-1 would determine amine loading but would be ineffective for determining accessible amine content because it would account for all amines, including physically buried amines that would not participate in chemical reactions under normal circumstances.

Another problem arises when the material in question has two or more protonatable species, as is the case with commercially available amine-functionalised silica particles (DMA-S) and the polymer-grafted silica particles (PGS-1 & PGS-2). High grafting densities are not easily achieved with silica based materials; as a result, some surface silanol groups remain active. A full titration of these particles reveals two equivalents points (ca. pH 7 and ca. pH 3). This phenomenon can be attributed to both the amine functionalities ($pK_{aH} \leq 9.3$) and the unfunctionalised surface silanols ($pK_a = 4.5$).[28] The pK_{aH} of PDMAPMAm in solution is 8.8.[19] To accurately report accessible amine content the titration is stopped at pH 4, assuming that at pH 4 all of the amines are protonated and none of the surface silanols have been protonated. Centrifugation allows for the separation of material from supernatant. Back titration of the supernatant allows for the extrapolation of an accessible amine value that can be fully attributed to the reactive amine functional groups. This assumption is supported by the data shown in Table 2.2.

Table 2.2. Determination of accessible amine content ($mmol \cdot g^{-1}$) in various drying agents. Reproduced from reference 10 with permission from The Royal Society of Chemistry.

Drying Agent	Reported Commercially	Protonatable Sites ($mmol \cdot g^{-1}$)		Accessible Amine ($mmol \cdot g^{-1}$)
		pH_i to pH 4[a]	pH_i to pH 2[a]	
DMA-S	1.51	1.1	0.70[b]	1.1
P-1	-	2.6	2.6	2.6
PGS-1	-	0.30	0.50	0.30
PGS-2	-	0.40	0.50	0.40
Silica	0	0	0.80	0

[a] Samples were titrated from the initial pH to the pH indicated.
[b]Loss in protonatable sites is due to cleavage of amine functionalities from the silica particle.

When titrated to pH 4, the silica sample shows no interaction with HCl. However, when titrated to pH 2, the silica sample shows an interaction with HCl analogous to a protonatable site content of 0.8 $mmol \cdot g^{-1}$. Furthermore, when the silica-based polymer-grafted samples (PGS-1 & PGS-2) are titrated to pH 2 they show an increase in the accessible amine content, an increase that can be confidently attributed to the silica and not the amine functionalities.

Interestingly, when the silica-based DMA-S samples were titrated to pH 2 they showed a decrease in the accessible amine content. Silanes are known to hydrolyze from a silica support at low pH.[29] The reduced accessible amine content when titrated to pH 2 is a result of the Si-O-Si bond being hydrolyzed and the subsequent cleavage of the amino-silanes from the silica support.

In contrast, PGS-1 and PGS-2 show no signs of hydrolysis at low pH. The increased hydrolytic stability of PGS-1 and PGS-2 is of great importance because the hydrolytic stability of the polymer was planned. The amide bonds in PDMAPMAm resist hydrolysis at low pH, whereas the ester linkages in the more commonly used monomers

such as DMAEMA, DEAEMA, and DiPAEMA hydrolyze at ca. pH 3.[19]

Regardless of the increased stability of the polymer, the stability of the link between the silica support and the polymer chain was still in question. The stability of the Si-O-C(=O) in comparison to the commonly used Si-O-Si bond was unknown. Since no loss in accessible amine content was detected at low pH for PGS-1 and PGS-2, it can be concluded that the Si-O-C(=O) remains stable at low pH (Table 2.2). The polymer might also contribute to the overall stability of the Si-O-C(=O) bond through steric hindrance, partly by blocking the cyclic conformation and partly due to its large hydrodynamic volume.

2.2.7 Evaluation of CO_2-responsive particles as drying agents for wet isobutanol

The solvent chosen to compare the various drying agents was isobutanol, which was doped with 5 wt% water. The drying agent (5 wt%) was added to the 'wet' isobutanol solution, and $CO_{2(g)}$ was bubbled through the solution for 1 h. The vial was then sealed and stirred for 15 h. Silica and alumina were activated before use by heating the absorbents to 250 ℃ for 24 h before being added to the wet isobutanol solution. The same procedure was then followed as described above but in the absence of CO_2. The water content of the solvent after filtration was determined by gas chromatography, using a thermal conductivity detector (GC-TCD). Calibration curves were prepared to determine the wt% water of each sample before and after the drying experiment. The drying abilities of multiple drying agents are compared in Table 2.3. The response of the GC-TCD to water and isobutanol was monitored over the course of 2 years by running multiple calibration curves. The response of the GC-TCD was found to be highly consistent.

Table 2.3. Table detailing the recycling of various drying agents to remove water from isobutanol solutions. Reproduced from reference 10 with permission from The Royal Society of Chemistry.

Drying Agent	Accessible Amine ($mmol \cdot g^{-1}$)	Particle Size (μm)	Water Removed[b] ($mg \cdot g^{-1}$) Cycle			
			1	2	3	4
DMA-S	1.1	20	180	140	160	140
P-1	2.6	220	300	220	200	160
P-1	2.6	220	380[c]	520[c]	400[c]	400[c]
PGS-1	0.30	60-100	490	480	480	470
PGS-2	0.40	60-100	540	440	430	430
PGS-1	0.30	60-100	520[d]	580[d]	-	-
PGS-2	0.40	60-100	580[d]	580[d]	-	-
Molecular sieves	0	4000	380	40	60	-
Silica	0	74-177	150	150	140	140
Alumina	0	37-63	40	80	70	80

[a]Reaction conditions: 10 g isobutanol with water at a concentration of 5 wt%, 0.5 g drying agent added, 1 h mixing with CO_2 bubbling through solution then continued mixing in a sealed vial for 15 h, water content analysed by GC-TCD. Drying agent regeneration was performed at 50 °C for 4 h. [b]Water removed with respect to drying agent used. [c]An increased bubbling time of 3 h and continued mixing under 1 atm of $CO_{2(g)}$ was employed. [d]An increased reaction time of 18 h was employed. For each cycle, a new solution of isobutanol containing 5 wt% water was used.

The synthesised porous polymer particles (P-1) and polymer-grafted silica (PGS-1 & PGS-2) showed the greatest ability to capture water (rows 2-5). The efficacy of most drying agents decreases slightly with continued recycling, with the exception being the silica-based drying agents. With an increased CO_2 bubbling time of 3 h, the polymer particles removed more water per g of drying agent and maintained their drying ability through 4 cycles (row 3). Upon increasing the reaction time from 15 to 18 h, the polymer-grafted silica particles removed more water per g of drying agent than they did previously (rows 6 and 7). Thus, drying performance is a function of CO_2 exposure and time.

The porous polymer particles (P-1) were compared to molecular sieves, an industrial standard for reusable drying agents, in an attempt to understand the relative

energy costs associated with regenerating each drying agent. As seen in Table 2.3, both P-1 and the molecular sieves are effective drying agents for one cycle, but only P-1 is effective after regeneration at 50 °C. A possible explanation for the reduced recyclability of the molecular sieves is that not enough thermal energy was supplied during the regeneration step for the release of water to occur. Differential scanning calorimetry (DSC) was used to compare the energy required to release water from the two drying agents after one cycle. Heating P-1 to the regeneration temperature of 50 °C requires ca. 36 $J \cdot g^{-1}$ g of particles compared to 325 °C and 219 $J \cdot g^{-1}$ for the molecular sieves. Once at the regeneration temperature, P-1 requires 16 $J \cdot g^{-1}$ of particles to desorb the water, according to the DSC measurement, compared to 30 $J \cdot g^{-1}$ for the molecular sieves. Thus, the lower regeneration temperature and lower desorption enthalpy result in significant energy savings when P-1, rather than molecular sieves, are used. Although this comparison is an approximation and not for optimised systems, it highlights the advantage of using CO_2-switchable drying agents regarding the lower energy required for regeneration.

Two further experiments were performed using isobutanol doped with less water to evaluate the ability of these agents to dry isobutanol having a lower initial water content. P-1 was able to reduce the water content of solutions containing 1 wt% H_2O, to a value of 0.8 wt%, but could not remove water from solutions containing only 0.5 wt% H_2O. The lower limit for the P-1 to dry isobutanol is therefore slightly less than 1 wt% H_2O but not as low as 0.5 wt% H_2O. Presumably, increasing the basicity of the functional group, such as by using amidine groups, would increase the efficacy of the drying agent to dry solvents to a lower level of residual water.

2.2.8 Determination of the molar hydration value for CO_2-responsive drying agents

An important internal measure of performance for a switchable drying agent is the amount of water ($mmol_w$) removed per accessible amine ($mmol_{aa}$). Therefore, the concept of a molar hydration value ($mmol_w/mmol_{aa}$) was introduced. The molar hydration value (MHV) allows for a quantitative determination of the amount of water captured per protonatable site. The molar hydration value of the drying agents varied greatly depending on the synthetic strategy employed (Table 2.4).

Table 2.4. Quantitative determination of the Molar Hydration Value for each CO_2-switchable drying agent.

Drying Agent	Accessible Amine ($mmol \cdot g^{-1}$)	Water Removed[a] ($mg \cdot g^{-1}$)	Molar Hydration Value ($mmol_W/mmol_{AA}$)[b]
DMA-S	1.1	180	9.1
P-1	2.6	300	6.4
PGS-1	0.30	490	91
PGS-2	0.40	540	75

[a]Refer to Table 2.3. [b]mmol of water removed per mmol of amine, refer to Appendix II.

The commercially available amine-functionalised silica particles (DMA-S), as well as the synthesised polymer particles (P-1), behave predictably. Their molar hydration values can be attributed to the previously proposed three ways in which water can bind to a CO_2-switchable drying agent (Figure 2.1). However, the polymer-grafted silica drying agents have molar hydration values that are an order of magnitude greater than P-1 or the commercially available amine-functionalised silica. The hydration model proposed in Figure 2.1 does not adequately account for the molar hydration values of the polymer-grafted silica drying agents (PGS-1 & PGS-2), suggesting that the polymeric nature of the

amine functionalities plays a crucial role in the hydration of the particle.

In one example of polymeric hydration, thermo-responsive poly(N-isopropylacrylamide) (PNIPAAm) and pH-responsive poly(N,N'-diethylaminoethyl methacrylate) (PDEAEMA) polymers were grafted to carboxymethylchitosan (CMC) to form highly water-swellable hydrogels with dual responsive properties.[30] The hydrogels showed an enhanced water-swellability when grafted with PDEAEMA. The increase in the bulk hydrophilicity of the hydrogel was attributed to the presence of tertiary amino groups in the DEAEMA unit. Thus, the polymeric amines in (PDMAPMAm) would increase the hydrophilicity of the silica particle by behaving as a hydrogel, therefore capturing more water.

The water content of the hydrated polymeric hydrogel can be estimated. PGS-1 was determined to be 7.5 wt% polymer by thermogravimetric analysis. Accounting for the consistent water uptake of silica (150 $mg \cdot g^{-1}$) and removing it from the equation, 340 $mg \cdot g^{-1}$ of water uptake can be attributed to the polymer. The polymer is, therefore, able to absorb 82 wt% water. If PGS-1 is looked at as a single entity, it can absorb 33 wt% water. In contrast, the CMC grafted P(DEAEMA-co-NIPAAm) copolymer absorbed 79 wt.% water.[30] In another study, various free polymers were tested via a comparable method yielding water uptake values ranging from 0.06 wt% for neutral PMMA, to 88 wt% for sodium polyacrylate (PAA·Na).[31]

With all factors considered, these values indicate hydrogel behaviour on the part of the polymer-grafted silica drying agents. This behaviour would adequately explain why polymer-grafted silica drying agents have molar hydration values that are an order of magnitude greater than P-1 or the commercially-available amine-functionalised silica. The

hydrogel-like nature, and therefore the performance of the polymer-grafted silica drying agents could be improved by increasing the molecular weight of the grafted polymer, thereby increasing the polymer to silica weight ratio.

2.2.9 Evaluation of CO_2-responsive particles as drying agents for wet organic Solvents other than isobutanol

The CO_2-responsive polymer-grafted silica particles (PGS-3) were tested as drying agents for a variety of wet solvents. Solvents that are immiscible with water or have a miscibility of less than 5 wt% with water are incompatible with the GC-TCD method of analysis. Future experiments can be designed with an alternative method of analysis to determine drying efficiency in solvents such as hexanes, dichloromethane, or toluene. For suitable solvents, CO_2 was introduced at 5 kPa (gauge pressure) via a needle into a vented vial containing a stir bar rotating at 400 RPM. (Table 2.5).

Table 2.5. Removal of water from a variety of solvents using PGS-3, a CO_2-switchable drying agent. Reproduced from reference 10 with permission from The Royal Society of Chemistry.

Solvent	Water Removed[b] ($mg \cdot g^{-1}$)	
	Cycle 1	Cycle 2
Isobutanol	560	520
Acetonitrile	380	380
Ethanol	220	280
Ethylene Glycol	380	<70
Hexanes	Incompatible	

[a]Reaction conditions: 10 g solvent with water at a concentration of 5 wt%, 0.5 g drying agent added, 1 h mixing with CO_2 bubbling through solution then continued mixing in a sealed vial for 15 h, water content analysed by GC-TCD. Drying agent regeneration was performed at 50 ℃ for 4 h. [b]Water removed with respect to drying agent used. For each cycle, a new solution of isobutanol containing 5 wt% water was used.

The combination of stirring and CO_2 bubbling causes significant solvent loss with solvents having boiling points lower than that of ethanol (78 ℃). For example, THF has a boiling point of 65-67 ℃ and within 30 min of bubbling CO_2 into THF over half of the THF had evaporated. Solvent evaporation is a problem for this experiment; if the solvent is lost during the experiment, then the end ratio of water to solvent will be artificially higher than it should have been if no solvent was lost, resulting in the perception of lower performance by the drying agent.

The data suggests that some solvent loss had occurred when drying ethanol (Table 2.6, cycle 1, 220 $mg \cdot g^{-1}$). To test this theory, a round bottom flask connected to a reflux condenser was used in place of a common vial. The additional solvent retention measures resulted in an increase in drying performance and therefore a more accurate representation of the drying ability of PGS-3 in ethanol (Table 2.6, cycle 2, 280 $mg \cdot g^{-1}$).

Each solvent brings different challenges to the removal of water; ethylene glycol, for instance, is more viscous and has a significantly higher boiling point (197 ℃) than the other solvents tested. Retention of ethylene glycol during the particle regeneration step is significant, resulting in the complete loss of drying performance in subsequent steps. The drying process would have to be optimised for each solvent individually to provide a truly green solution to the removal of water from organic solvents.

Following the publication of these results, a partnership with Fielding Chemical saw that the drying agents were tested in a real world scenario, using recycled solvents. Fielding Chemical was interested in whether recycled isobutanol and recycled ethylene glycol could be dried using the PGS series of CO_2-responsive materials. PGS-6 was synthesised and evaluated as a drying agent for recycled isobutanol (Table 2.6).

Table 2.6. Removal of water from recycled isobutanol using PGS-6, a CO_2-switchable drying agent.

Isobutanol Water Content (wt%)						
As Received	Cycle 1	Cycle 2	Cycle 3	Cycle 4	Cycle 5	Cycle 6
19.5	14.7	12.1	9.7	4.6	0.9	0.7

The same sample of isobutanol (50 g) was used throughout the experiment. PGS-6 (2.5 g) was regenerated before each cycle in an oven at to 50 ℃ for 4 h. Recycled isobutanol was provided by Fielding Chemical Inc.

The isobutanol sample supplied by Fielding Chemical was determined to be 19.5 wt% water. The isobutanol was off coloured and heavily contaminated with particulate matter. The recycled isobutanol was filtered through a 0.2 µm polytetrafluoroethylene (PTFE) syringe filter to remove the particulate matter before use in the drying experiment; the colour remained unchanged after filtration. Filtration was done as a preventative measure to avoid clogging of the GC injector port and was not done out of concern for the drying process. PGS-6 (2.5 g) was added to 50 g of recycled solvent (isobutanol, 19.5 wt% water). CO_2 was introduced at 34 kPa (gauge pressure) via a needle into a vented round bottom flask containing the recycled isobutanol, PGS-6, and a stir bar rotating at 400 RPM. The round bottom flask was fitted with a reflux condenser to help prevent solvent loss during the addition of $CO_{2(g)}$. The round bottom flask was then sealed and mixed for an additional 15 h. The drying agent was separated from the solvent by vacuum filtration and the solvent was collected and stored for the next cycle. The drying agent was regenerated in a vacuum oven at 50 ℃ for 4 h. Efforts were made to reuse as much of the solvent as possible from cycle to cycle; at no point was fresh solvent added. The water content of the solvent was analysed by GC-TCD. Utilising PGS-6, the water content of recycled isobutanol was reduced from 19.5 wt% to less than 1 wt% over 5 cycles. The application of a 6^{th} cycle did little to further reduce the wt% of water in the isobutanol (Table 2.6).

In addition to removing water from isobutanol, various unknown contaminants were removed by PGS-6. Since the contaminants did not show up in subsequent cycles, and the amount of water removed per cycle remained consistent, it is hypothesised that the unknown contaminants were removed from PGS-6 during the regeneration step. However, if adsorbed contaminants were harder to remove from PGS-6 than water during regeneration, it is plausible that their presence on PGS-6 could explain for the apparent dip in performance in cycles 2 and 3. The average drying performance of PGS-6 for recycled isobutanol as received from Fielding Chemical was 3.7 $\pm$1.23 wt% (740 $\pm$ 240 mg·g^{-1}) water per cycle, for 5 cycles. The 6th cycle was not included in the calculation of average performance because CO_2-responsive drying agents lose efficiency below 1 wt% water, as was shown by earlier experiments with the porous polymer particles (P-1).

2.3 Conclusions

CO_2-switchable drying agents have been created for the first time and were evaluated in the drying of wet isobutanol. Through the application of CO_2 to suspensions of drying agent, the water content of the isobutanol could be reduced by 490 mg per g of drying agent. This value exceeds the values obtained for commercial drying agents such as silica or alumina. The closest commercial competitor was molecular sieves at 380 mg of water removed per g of drying agent; however, the molecular sieves could not be regenerated under the very mild conditions employed for the CO_2-switchable materials. Nonetheless, molecular sieves are superior in terms of their ability to dry wet solvent to very low concentrations of water. All of the CO_2-switchable drying agents were superior

to normal silica and alumina regarding the quantity of water removed per g of drying agent. The synthesised CO_2-switchable drying agents (P-1, PGS-1, PGS-2) were superior to the commercial amine-functionalised silica (DMA-S) regarding drying ability and hydrolytic stability at low pH.

The concept of molar hydration value has been introduced; molar hydration values have been used to quantify the magnitude of water adsorption per accessible amine. The polymer-grafted silica drying agents (PGS-1 & PGS-2) capture 10 times more water per amine ($mmol_W/mmol_{AA}$) than the other amine-containing CO_2-switchable drying agents. Additionally, a new method for the measurement of accessible amine content on surfaces has been reported.

The efforts of various Jessop and Cunningham group members have aided in the understanding of CO_2-responsive materials and their behaviour as drying agents. Currently, the performance of the CO_2-responsive materials is understood to be highly dependant on the amount of CO_2 delivered into the system. Adequate CO_2 exposure is essential to maximising the response of the CO_2-responsive material. Subsequently, drying of organic solvents is best done in series, where the solvent is exposed sequentially to multiple small "plugs" of drying agent in a closed system. Using gaseous CO_2 as the propellant ensures that each successive plug is adequately exposed to CO_2.

2.4 Experimental methods

2.4.1 Materials

All aqueous solutions were prepared with deionized water (DIW) unless stated otherwise. All silica particles were purchased from SiliCycle Inc. The following chemicals were used as received unless otherwise stated: sulfuric acid (Fisher, ACS reagent grade, 95-98%), ammonium hydroxide (Aldrich, ACS reagent grade, 28-30% NH_3 basis), water (Millipore, type 1, 18.2 MΩ·cm @ 25 ℃), hydrogen peroxide (Aldrich, 30 wt% in H_2O), 2-bromo-2-methylpropionyl bromide (BIBB, Aldrich, 98%), methacryloyl chloride (MAC, Aldrich, >97%), diisopropylethylamine (DIPEA, Aldrich, ≥99%), 4-(dimethylamino)pyridine (DMAP, Aldrich, ≥99%), dichloromethane (DCM, EMD Millipore, anhydrous, ≥98.5%), tetrahydrofuran (THF, Aldrich, anhydrous, contains 250 ppm BHT as inhibitor, ≥99.9%), methanol (MeOH, EMD Millipore, anhydrous), copper(I) bromide (Aldrich, 99.999% trace metals basis), N-[3-(dimethylamino)propyl]methacrylamide (DMAPMAm, Aldrich, contains MEHQ as inhibitor, 99%), N,N,N`,N``,N``-pentamethyldiethylenetriamine (PMDETA, Aldrich, 99%), ethylenediaminetetraacetic acid (EDTA, Aldrich, purified grade, ≥98.5%), sodium hydroxide (NaOH, Aldrich, ACS reagent, ≥97%), aluminium oxide (Aldrich, activated, basic, Brockmann I).

Piranha solutions were used to clean silica substrates. Acidic piranha solution consists of a 7:3 (v/v) mixture of concentrated sulfuric acid and 30% hydrogen peroxide solution, commonly heated to 85 ℃. Basic piranha solution consists of a 5:1:1 (v/v/v)

mixture of Millipore water, 30% hydrogen peroxide solution, and 40% ammonium hydroxide solution, commonly heated to 70 ℃.

Warning: Piranha solution is highly dangerous and its use requires considerable care. Piranha solution is either strongly acidic or basic and a strong oxidizer. The mixing of piranha solution is very exothermic and should be done slowly; if the reagents are mixed too quickly the temperature can easily exceed 100 ℃, which will result in boiling and splashing of the piranha solution. Piranha solution will react violently with organic compounds; therefore, it should be used in a fume hood clear of organic solvents and waste. Make only as much Piranha solution as needed; when disposing of excess or used piranha solution do NOT cap the bottle. It commonly takes a day or two for the reagent to neutralize fully, during this time oxygen gas is produced. Refer to your institution's standard operating procedures before attempting to use or dispose of piranha solutions.

Silica particles for all experiments presented here were cleaned and hydroxylated using Piranha solutions. An example is as follows:

Spherical silica particles (SiO_2 #1, Silicycle, 200-500 μm particle size, 100 Å pore size, 30 g) were subjected to a three-part treatment to remove organic contaminants and promote a hydroxyl-rich surface. Firstly, the particles were stirred in acidic piranha solution for 1 h at 85 ℃, followed by rinsing three times with Millipore water. Secondly, the particles were stirred in basic piranha solution for 20 min at 70 ℃, followed by rinsing three times with Millipore water. Lastly, the particles were vacuum filtered and dried in an oven overnight at 100 ℃. The clean and hydroxyl-rich particles were stored in a sealed vessel under Ar until further use.

2.4.2 Initiator grafting on silica particles

Various experimental conditions were tested to determine a suitable method for grafting the initiating species on to a silica particle. These methods are outlined in detail in Appendix I. The following method produced the most reliable results with the least amount of particle contamination from amine-containing auxiliary bases or catalysts.

Clean and hydroxyl-rich silica particles (2 g) were added to a 250 mL round bottom flask and flame dried under vacuum. Reactants were added using Schlenk techniques for inert conditions; diisopropylethylamine (1 eq., 4.09 mmol) and 150 mL of anhydrous dichloromethane were added to the round bottom flask. The round bottom flask was cooled in an ice bath for approximately 30 min, after which the initiator, 2-bromo-2-methylpropionyl bromide (BIBB, 1 eq., 4.04 mmol), was added dropwise via syringe. The mixture was stirred for 20 min, the ice bath removed, and the mixture was allowed to warm to room temperature (ca. 27 ℃). The reaction was stirred vigorously (via magnetic stir bar) overnight for approximately 16 h. The silica particles were recovered by vacuum filtration and washed thoroughly with methanol, followed by multiple washings with distilled water. The washed particles were dried at 110 ℃ for 20 min, then stored under Ar until further use.

2.4.3 Synthesis of polymer-grafted silica-1 (PGS-1)

Initiator grafting (KB-B4-PG58):

Clean and hydroxyl-rich silica particles (SiO_2 #5, SiliaFlash P60, 40-63 μm, 100 Å pore size, 5 g, 1 eq., assumption 3.6 mmol·g^{-1}) were added to a 100 mL round bottom flask containing solution of potassium carbonate (4.6 mmol) in 50 mL of acetone. To that mixture, the initiator, 2-bromo-2-methylpropionyl bromide (BIBB, 18 mmol), was added dropwise at room temperature (ca. 27 ℃). The contents of the round bottom flask were heated at a continuous reflux for 12 h. The silica particles were recovered by vacuum filtration and washed thoroughly with ethanol, followed by multiple washings with distilled water. The washed particles were dried at 110 ℃ for 20 min, then stored under Ar until further use.

SI-AGET-ATRP of PDMAPMAm from silica, PGS-1 (KB-B4-PG63):

Initiator-functionalised silica particles (SiO_2 #5, SiliaFlash P60, 40-63 μm, 100 Å pore size, 2.5 g) were added to a 100 mL 3-neck round bottom flask containing 40 mL of anhydrous methanol. The mixture was sparged with Ar for 1 h. The monomer, N-[3-(dimethylamino)propyl]methacrylamide (DMAPMAm 90 mmol, 10 eq.) was passed through a basic alumina column and sparged with Ar for 30 min. The catalyst was prepared by mixing copper(I) bromide (9 mmol, 1 eq.) with N,N,N′,N″,N″-pentamethyldiethylenetriamine (PMDETA, 18 mmol, 2 eq.) in 10 mL anhydrous methanol. The mixture was sparged with Ar for 1 h. The sparged components were added to the 3-neck flask under Ar and heated to 45 ℃ overnight. The polymer-grafted silica was

recovered via vacuum filtration and washed thoroughly with an aqueous solution of ethylenediaminetetraacetic acid (EDTA), followed by multiple washings with distilled water. The particles were dried at 110 °C overnight, then stored under Ar until further use.

2.4.4 Synthesis of polymer-grafted silica-2 (PGS-2)

Initiator grafting (KB-B4-PG62):

Clean and hydroxyl-rich silica particles (SiO_2 #5, SiliaFlash P60, 40-63 μm, 100 Å pore size, 5 g) were added to a 100 mL round bottom flask containing solution of triethylamine (80.9 mmol) in 50 mL of tetrahydrofuran. The mixture was continuously stirred while being cooled to 0 ℃. After 1 h, the initiator, 2-bromo-2-methylpropionyl bromide (BIBB, 18 mmol), was added dropwise to the cooled mixture. The mixture was warmed to room temperature (ca. 27 ℃) and allowed to react for 12 h. The silica particles were recovered by vacuum filtration and washed thoroughly with ethanol, followed by multiple washings with distilled water. The washed particles were dried at 110 ℃ for 20 min, then stored under Ar until further use.

SI-AGET-ATRP of PDMAPMAm from silica, PGS-2 (KB-B4-PG63):

Initiator-functionalised silica particles (SiO_2 #5, SiliaFlash P60, 40-63 μm, 100 Å pore size, 2.5 g) were added to a 100 mL 3-neck round bottom flask containing 40 mL of anhydrous methanol. The mixture was sparged with Ar for 1 h. The monomer, N-[3-(dimethylamino)propyl]methacrylamide (DMAPMAm 90 mmol, 10 eq.) was passed

through a basic alumina column and sparged with Ar for 30 min. The catalyst was prepared by mixing copper(I) bromide (9 mmol, 1 eq.) with N,N,N′,N″,N″-pentamethyldiethylenetriamine (PMDETA, 18 mmol, 2 eq.) in 10 mL anhydrous methanol. The mixture was sparged with Ar for 1 h. The sparged components were added to the 3-neck flask under Ar and heated to 45 ℃ overnight. The polymer-grafted silica was recovered via vacuum filtration and washed thoroughly with an aqueous solution of ethylenediaminetetraacetic acid (EDTA), followed by multiple washings with distilled water. The particles were dried at 110 °C overnight, then stored under Ar until further use.

2.4.5 Synthesis of polymer-grafted silica-3 (PGS-3)

Initiator grafting (KB-B5-PG61):

Clean and hydroxyl-rich silica particles (SiO_2 #5, SiliaFlash P60, 40-63 μm, 100 Å pore size, 6.5 g, 1 eq. assumption 1.72 $mmol \cdot g^{-1}$) were added to a 250 mL round bottom flask containing solution of diisopropylethylamine (1 eq., 11.0 mmol), in 125 mL of anhydrous dichloromethane (DCM). The mixture was continuously stirred while being cooled to 0 ℃. After 1 h, the initiator, 2-bromo-2-methylpropionyl bromide (BIBB, 1 eq., 11 mmol), was added dropwise to the cooled mixture. The mixture was warmed to room temperature (ca. 27 ℃) and allowed to react for 12 h. The silica particles were recovered by vacuum filtration and washed thoroughly with ethanol, followed by multiple washings with Millipore water. The washed particles were dried at 110 ℃ for 20 min, then stored under Ar until further use.

SI-AGET-ATRP of PDMAPMAm from silica, PGS-3 (KB-B5-PG68):

Initiator-functionalised silica particles (SiO_2 #5, SiliaFlash P60, 40-63 μm, 100 Å pore size,3 g, 1 eq., assumption 1.72 mmol·g^{-1}) were added to a 250 mL 3-neck round bottom flask containing 100 mL of anhydrous methanol. The mixture was sparged with Ar for 1 h. The monomer, N-[3-(dimethylamino)propyl]methacrylamide (DMAPMAm 158 mmol, 30 eq.) was passed through a basic alumina column and sparged with Ar for 30 min. The monomer and sacrificial free initiator 2-bromo-2-methylpropionyl bromide (BIBB, 0.01 eq., 0.05 mmol) were added to the reaction flask containing sparged anhydrous methanol. The catalyst was prepared by mixing copper(I) bromide (9 mmol, 1 eq.) with N,N,N′,N″,N″-pentamethyldiethylenetriamine (PMDETA, 18 mmol, 2 eq.) in 50 mL anhydrous methanol. The mixture was sparged with Ar for 1 h. The sparged components were added to the 3-neck flask under Ar and heated to 45 ℃ overnight. The polymer-grafted silica particles were recovered via vacuum filtration and washed thoroughly with an aqueous solution of ethylenediaminetetraacetic acid (EDTA), followed by multiple washings with distilled water. The particles were dried at 110 ℃ overnight, then stored under Ar until further use.

2.4.6 Synthesis of polymer-grafted silica-6 (PGS-6)

Initiator grafting (KB-B6-PG23):

Clean and hydroxyl-rich silica particles (SiliaFlash P60, 45-60 μm, 100 Å pore size, 10.2 g, 1 eq. assumption 2 mmol·g^{-1})) were added to a 250 mL flame dried round bottom flask, to which a condenser was fixed. Reactants were added using Schlenk techniques for inert conditions; diisopropylethylamine (1.1 eq., 22.0 mmol), 4-(dimethylamino)pyridine (DMAP, 0.015 eq., 0.29 mmol) and 150 mL of anhydrous dichloromethane (DCM) were added to the round bottom flask. The round bottom flask was cooled in an ice bath for approximately 30 min, after which the 2-bromo-2-methylpropionyl bromide (BIBB, 1.1 eq., 22 mmol) was added dropwise via syringe. The mixture was stirred via a magnetic stir bar (1200 RPM) for 20 min before the ice bath was removed and the mixture was allowed to warm to room temperature (ca. 27 ℃) and allowed to react overnight. The BIBB-grafted silica particles were then collected by vacuum filtration and washed multiple times with DCM. The washed particles were dried at 110 ℃ for 20 min, then stored under Ar until further use.

SI-AGET-ATRP of PDMAPMAm from silica, PGS-6 (KB-B6-PG25):

Initiator-functionalised silica particles (SiliaFlash P60, 45-60 μm, 100 Å pore size, 6.5 g) were added to a 500 mL 3-neck round bottom flask containing 150 mL of anhydrous methanol. The mixture was sparged with Ar for 1 h. The monomer, N-[3-(dimethylamino)propyl]methacrylamide (DMAPMAm 1.2 mol, 100 eq.) was passed through a basic alumina column and sparged with Ar for 30 min. The monomer and

sacrificial free initiator 2-bromo-2-methylpropionyl bromide (BIBB, 0.005 eq., 0.06 mmol) were added to the reaction flask containing the sparged anhydrous methanol. The catalyst was prepared by mixing copper(I) bromide (12 mmol, 1 eq.) with N,N,N′,N″,N″-pentamethyldiethylenetriamine (PMDETA, 24 mmol, 2 eq.) in 25 mL anhydrous methanol. The mixture was sparged with Ar for 1 h. The sparged components were added to the 3-neck flask under Ar and heated to 50 ℃ and stirred via magnetic stir bar (900 RPM) overnight. The polymer-grafted silica particles were recovered via vacuum filtration and washed thoroughly with an aqueous solution of ethylenediaminetetraacetic acid (EDTA), followed by multiple washings with distilled water. The particles were dried at 110 ℃ overnight, then stored under Ar until further use.

2.4.7 Mass spectroscopy of polymer-grafted silica particles

Matrix-assisted laser desorption/ionisation time of flight mass spectrometry (MALDI-TOF-MS) was conducted on PGS-3 using an Applied Biosystems DE-Pro MALDI-TOF mass spectrometer by Mr. David Mcleod of Queen's University. Additionally, MALDI-TOF MS was conducted on PGS-6 using a Bruker Ultraflextreme MALDI-TOF mass spectrometer by Dr. Randy Whittal of The University of Alberta. Several matrices were tested and both dithranol and 2,5-dihydroxybenzoic acid (DHB) did not produce fragments but appeared to provide molecular ions, whereas other matrices gave fragment ions. The data presented herein were collected using DHB as the matrix. Samples were dissolved in DHB in acetone, mixed, and then spotted on the MALDI target. Some of the PDMAPMAm samples did not completely dissolve in acetone, but the samples

dissolved at sufficiently high concentration to provide an adequate MALDI signal. The data provided is in reflectron mode on the MALDI instrument to provide the best resolution. The samples were checked in linear mode as the molecular weight (MW) was expected to be high. However, this does not appear to be the case; if high mass materials were present, they were not detected. Analysis of the spacing between prominent peaks in both spectrums yields the MW of DMAPMAm, 170.25 m/z, thus confirming that PDMAPMAm was formed (Figures 2.7, 2.8, 2.9, 2.10).

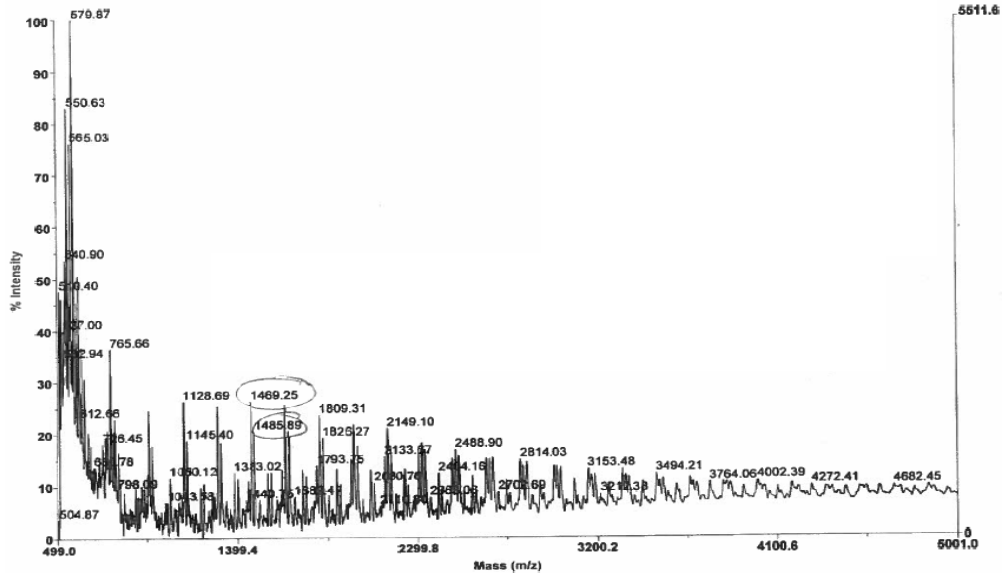

Figure 2.7. MALDI-TOF-MS spectrum of PDMAPMAm free polymer collected from the synthesis of PGS-3.

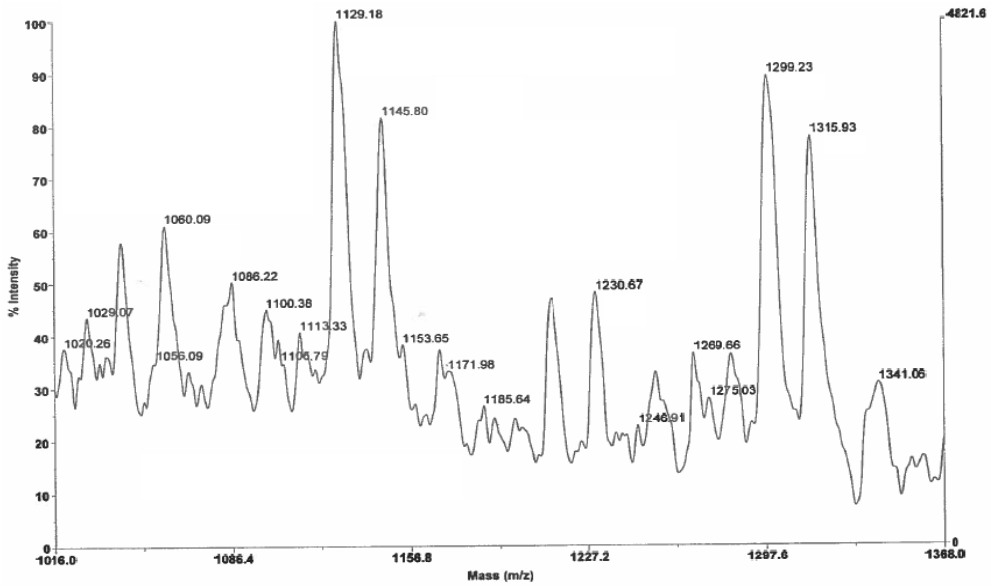

Figure 2.8. A portion of the MALDI-TOF-MS spectrum of PDMAPMAm free polymer collected from the synthesis of PGS-3.

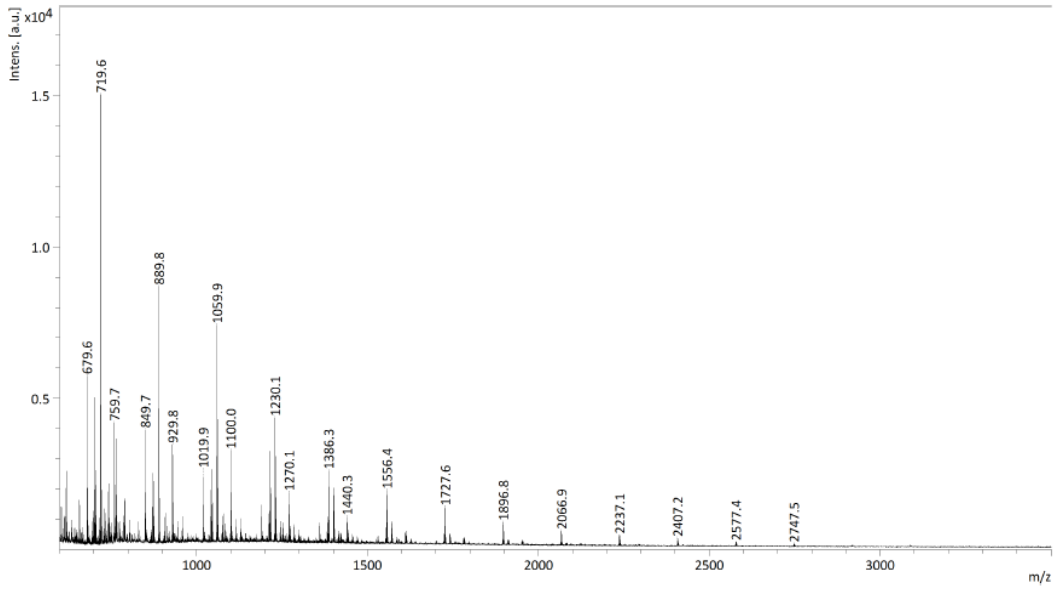

Figure 2.9. MALDI-TOF-MS spectrum of PDMAPMAm free polymer collected from the synthesis of PGS-6.

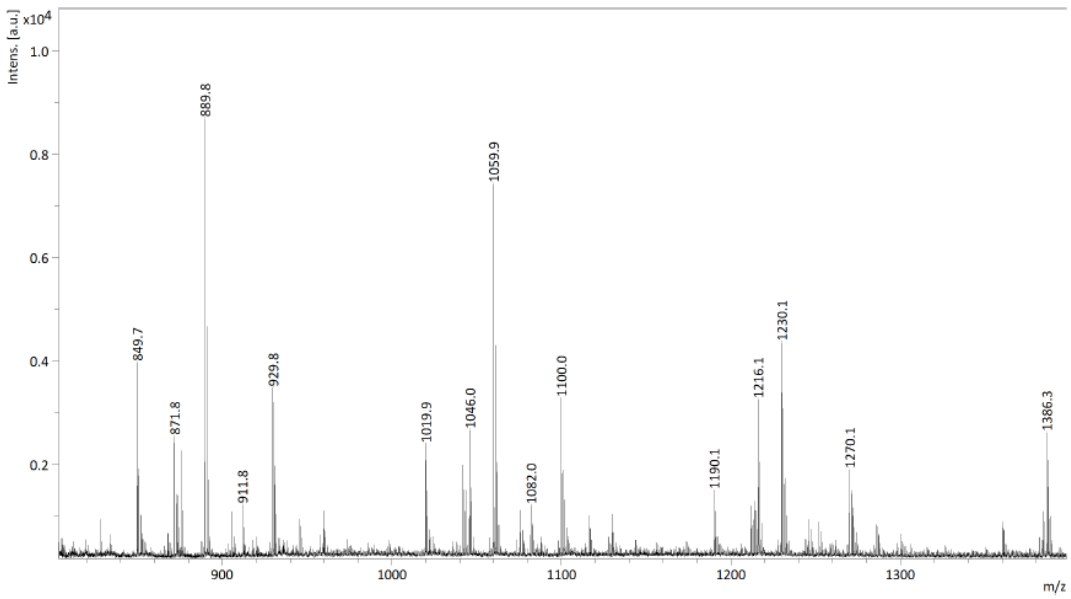

Figure 2.10. A portion of the MALDI-TOF-MS spectrum of PDMAPMAm free polymer collected from the synthesis of PGS-6.

2.4.8 Thermogravimetric analysis of polymer-grafted silica particles

Thermogravimetric analysis (TGA) was performed using a TA Instruments Q500 TGA analyzer by heating the sample using the following ramp: 10 °C min^{-1} from 30 to 120 ℃, held for 20 min and 120 ℃, followed by 10 ℃ min^{-1} to 900 ℃. The initial isothermal hold at 120 ℃ is to remove bulk solvents and adsorbed liquids such as moisture from the atmosphere. The organic content of the polymer-grafted silica particles was calculated from the point at which mass loss begins to occur, after the initial isothermal hold, until the point at which mass loss stops.

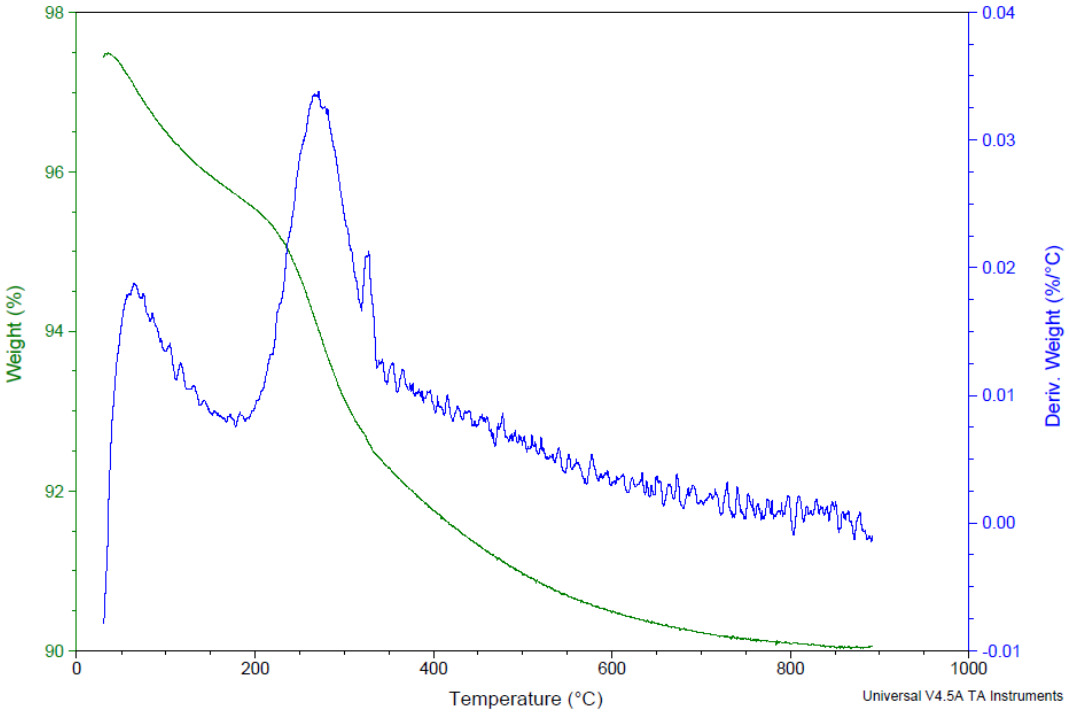

Figure 2.11. TGA of dried PGS-1 heated at a rate of 10 °C min^{-1} to 900 °C.

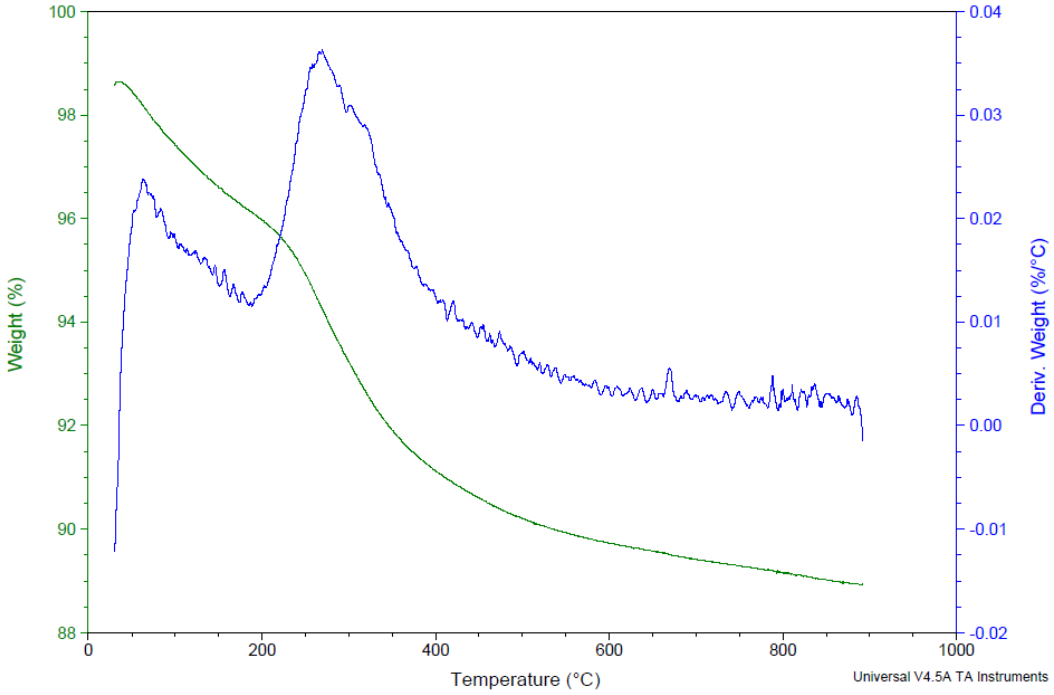

Figure 2.12. TGA of dried PGS-2 heated at a rate of 10 °C min^{-1} to 900 °C.

2.4.9 Water content analysis by gas chromatography

Quantitative gas chromatography (GC) using a thermal conductivity detector (TCD) was performed on a PerkinElmer Clarus 680 gas chromatograph instrument equipped with a CP-Volamine (30 m x 0.32 mm i.d.). Calibration curves were collected multiple times over the course of these experiments (Figure 2.13). Little to no change in the calibration curve was noted over time.

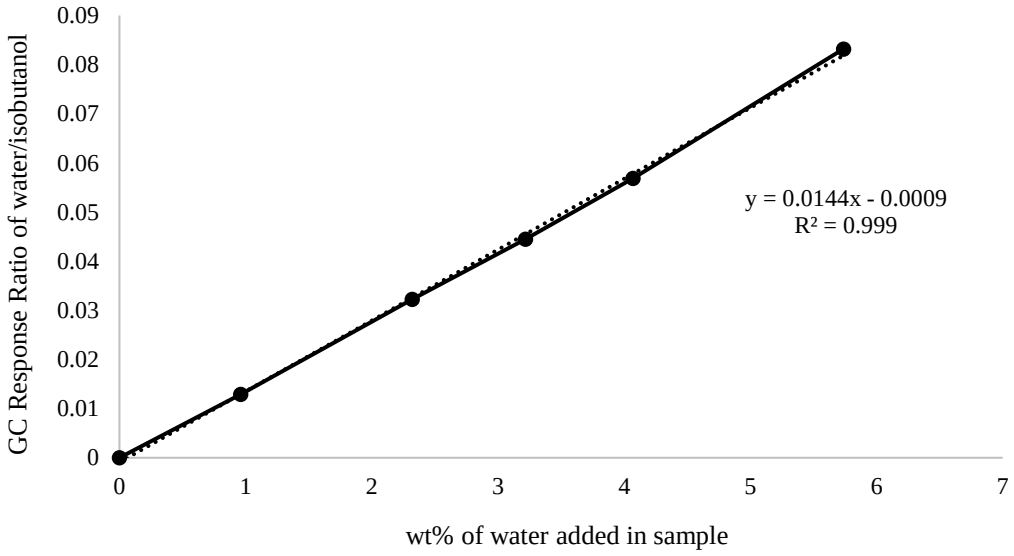

Figure 2.13. GC-TCD calibration curve for water in isobutanol (wt%).

2.5 References

1. J. E. Logsdon, Isopropyl Alcohol, in Kirk-Othmer Encyclopedia of Chemical Technology, John Wiley & Sons, Inc., 2000.

2. R. French and P. Malone, *Fluid Phase Equilibria*, 2005, **228**, 27–40.

3. W. L. F. Armarego and C. L. L. Chai, Purification of Laboratory Chemicals, Butterworth-Heinemann, New York, 2003.

4. P. G. Jessop, S. M. Mercer and D. J. Heldebrant, *Energy Environ. Sci*., 2012, **5**, 7240–7253.

5. P. G. Jessop, D. J. Heldebrant, X. Li, C. A. Eckert and C. L. Liotta, *Nature*, 2005, **436**, 1102–1102.

6. Y. Liu, P. G. Jessop, M. Cunningham, C. A. Eckert and C. L. Liotta, *Science*, 2006, **313**, 958–960.

7. X. Su, P. G. Jessop and M. F. Cunningham, *Macromolecules*, 2012, **45**, 666–670.

8. R. Barbey, L. Lavanant, D. Paripovic, N. Schüwer, C. Sugnaux, S. Tugulu and H.-A. Klok, *Chem. Rev*., 2009, **109**, 5437–5527.

9. S. Kumar, X. Tong, Y. L. Dory, M. Lepage and Y. Zhao, *Chem. Commun*., 2012, **49**, 90–92.

10. K. J. Boniface, R. R. Dykeman, A. Cormier, H.-B. Wang, S. M. Mercer, G. Liu, M. F. Cunningham and P. G. Jessop, *Green Chem*., 2015, **18**, 208–213.

11. W. F. Beech, *J. Chem. Soc. Resumed*, 1951, **0**, 2483–2487.

12. V. F. Kalasinsky, S. Subramaniam, C.-F. Su and R. L. Cook, *J. Mol. Struct.*, 2000, **550**, 521–530.

13. K. Matyjaszewski, *Macromolecules*, 2012, **45**, 4015–4039.

14. T. von Werne and T. E. Patten, *J. Am. Chem. Soc.*, 2001, **123**, 7497–7505.

15. S. Hansson, P. Antoni, H. Bergenudd and E. Malmström, *Polym. Chem.*, 2011, **2**, 556–558.

16. M. Barsbay, O. Güven, M. H. Stenzel, T. P. Davis, C. Barner-Kowollik and L. Barner, *Macromolecules*, 2007, **40**, 7140–7147.

17. J. O. Zoppe, Y. Habibi, O. J. Rojas, R. A. Venditti, L.-S. Johansson, K. Efimenko, M. Österberg and J. Laine, *Biomacromolecules*, 2010, **11**, 2683–2691.

18. L. T. Zhuravlev, Colloids Surf. *Physicochem. Eng. Asp.*, 2000, **173**, 1–38.

19. P. van de Wetering, E. E. Moret, N. M. E. Schuurmans-Nieuwenbroek, M. J. van Steenbergen and W. E. Hennink, *Bioconjug. Chem.*, 1999, **10**, 589–597.

20. V. Bütün, S. P. Armes and N. C. Billingham, *Polymer*, 2001, **42**, 5993–6008.

21. N. G. Hoogeveen, M. A. C. Stuart, G. J. Fleer, W. Frank and M. Arnold, *Macromol. Chem. Phys.*, 1996, **197**, 2553–2564.

22. F. A. Plamper, M. Ruppel, A. Schmalz, O. Borisov, M. Ballauff and A. H. E. Müller, *Macromolecules*, 2007, **40**, 8361–8366.

23. M. Přádný and S. Ševčík, *Makromol. Chem.*, 1985, **186**, 111–121.

24. J. Pyun, S. Jia, T. Kowalewski, G. D. Patterson and K. Matyjaszewski, *Macromolecules*, 2003, **36**, 5094–5104.

25. A. Heise, S. Diamanti, J. L. Hedrick, C. W. Frank and R. D. Miller, *Macromolecules*, 2001, **34**, 3798–3801.

26. Molecular self-assembly, http://www.sigmaaldrich.com/content/dam/sigma-aldrich/materials-science/material-matters/material_matters_v1n2.pdf, (accessed November 2017).

27. K. O. Ojo, L. V. Golovko, Y. P. Gomza and A. N. Vasiliev, *Silicon*, 2012, **4**, 189–195.

28. S. Ong, X. Zhao and K. B. Eisenthal, *Chem. Phys. Lett.*, 1992, **191**, 327–335.

29. J. J. Kirkland, J. L. Glajch and R. D. Farlee, *Anal. Chem.*, 1989, **61**, 2–11.

30. N. Rodkate, B. Rutnakornpituk, U. Wichai, G. Ross and M. Rutnakornpituk, *J. Appl. Polym. Sci.*, 2015, **132**, 41505.

31. H. M. L. Thijs, C. R. Becer, C. Guerrero-Sanchez, D. Fournier, R. Hoogenboom and U. S. Schubert, *J. Mater. Chem.*, 2007, **17**, 4864–4871.

Chapter 3

CO_2-Responsive Heterogeneous Catalysis

3.1 Preface

Spurred by the publication of the CO_2-switchable drying agents paper, multiple collaborative efforts began. One of those efforts involved Prof. Walter Leitner and his research group at Rheinisch-Westfälische Technische Hochschule (RWTH) Aachen, Germany. The research undertaken sought to establish whether CO_2-responsive silica particles could serve as an effective, smart support for heterogeneous catalysis. The collaboration involved shipping out materials, which were made in-house, overseas for experimentation and validation. The collaboration is an ongoing effort; state of the art CO_2-responsive silica particles are currently being investigated by Prof. Leitner and his research group.

3.1.1 Abstract

CO_2-switchable polymers (PDMAPMAm) were grafted from silica particles to create CO_2-responsive particles (RP, PGS-7). Ruthenium complexes were reduced in a suspension of those particles to place ruthenium nanoparticles (NP) on the surface of the RP (NP@RP). The NP@RP were examined for catalytic activity, selectivity, and air sensitivity in the presence and absence of CO_2. In collaboration with Sami El Sayed, supervised by Dr. Kylie Luska and Prof. Walter Leitner at RWTH Aachen, Germany, preliminary results utilising PGS-7 show that the hydrogenation of furfural acetone (FFA) as catalysed by RuNP@RP, reduces the C=C and C=O bonds in the absence of CO_2 but is selective for just C=C bonds in the presence of CO_2.[74]

This work is proof of concept that not only can a smart material influence heterogeneous catalysis but the smart material can utilize CO_2 as an effective stimulus. The forward stimulus is the application of CO_2 in the presence of the smart material, causing the smart material to become hydrophilic. The reverse stimulus is the application of moderate heating, which causes the removal of CO_2 from the smart material. The removal of CO_2 from the smart material returns it to its original hydrophobic state.

3.1.2 Introduction

Catalysis is often a necessary component for the effective transformation of readily available building blocks into high-value materials. Research in this field has largely focused on the development of new catalytically active species and their study. The aim is to optimise performance to achieve high conversions and/or selectivities.[1] Inspired by nature, chemists have begun to investigate 'bio-like' catalytic systems in which a catalyst responds to an external stimulus. These systems work in much the same way as the activity of an enzyme, via modulation through feedback loops and various external stimuli.[2,3]

The incorporation of stimuli-responsive functionalities into catalytically active systems could enable these systems to perform difficult or impossible transformations that are currently out of the reach of modern catalysis. Switchable catalysts have been used to speed up or slow down the rate of reaction or change the stereochemical outcome of a reaction given the presence or absence of a specific external stimulus. Recent developments include a catalytic system that selectively promotes a single reaction from a one-pot mixture of building blocks. Williams et al. developed a chemoselective CO_2-switchable homogenous dizinc catalyst which when under an N_2 atmosphere catalyses the ring-opening polymerization (ROP) of lactones, and when under a CO_2 atmosphere catalyses the ROP of epoxides. By altering between these two conditions, the authors achieved the selective preparation of poly(carbonate-block-ester) copolymers.[4]

A variety of stimuli can be used, and the modern chemist is only limited by their imagination. Recent years have demonstrated both heterogeneous and homogeneous switchable catalytic systems that respond to a variety of stimuli such as pH,[5-10] light,[11-25], temperature,[26-30] redox,[31-47] solvent,[48-55] addition or removal of analytes,[56-59] and

mechanical forces.[60-66] The stimulus commonly causes steric effects, electronic effects, supramolecular aggregation or dissociation, or coordination effects.

Diaconescu et al. demonstrated a redox-switchable homogeneous catalyst based on a Ce(III)-salen complex, wherein oxidation of the complex resulted in the deactivation of the catalyst and subsequent reduction activated the catalyst.[35] The Ce(III)-salen complex was catalytically active in the ROP of L-lactide, achieving 85% conversion in over 2 h. The addition of ferrocenium tetrakis[3,5-bis(trifluoromethyl)phenyl]borate (FcBARF) oxidised the Ce(III) complex; the oxidised Ce (IV) complex showed no catalytic activity towards ROP. The system could be switched in situ by reduction of the Ce(IV) complex with cobaltocene. The re-activated complex showed no loss of catalytic activity. The drawback to this approach is that given enough cycles, the salt will accumulate in the system eventually requiring removal. Also, the chosen stimuli are complex reagents, resulting in a significant financial investment over time.

A different approach to a redox system was reported by Matyjaszewski.[39] Dynamic modulations of atom transfer radical polymerization (ATRP) rates were achieved through electrochemical switching of the oxidation state of the copper catalyst. The application of a potential of -0.68 V (vs. Ag^+/Ag) reduces the inactive Cu(II) species to the active Cu(I) species. Application of a more positive potential (-0.40 V) shifted the equilibrium back towards the catalytically inactive Cu(II) species. Varying the applied potential between -0.69 V and -0.40 V switches the polymerization “on” or “off”, respectively.

Switchable functionalities can be utilised to address multiple aspects of a catalytic system. Switchable functionalities can directly affect catalyst behaviour or they can influence the broader reaction conditions, subsequently facilitating the separation of the

catalyst from the product. For example, switchable phase transfer ligands have been developed to shuttle a catalyst between phases in biphasic mixtures. Thus, the catalyst can be recovered and reused after the reaction has gone to completion.[9,67] Similarly, an ionic liquid catalyst has been designed to phase separate as the reaction goes to completion, since it is not miscible with one of more of the products.[56] In 2007, Hamamoto et al. published a novel solid-phase reaction system in water which is switchable with temperature. A thermomorphic catalyst was created in which the affinity for an organic substrate increased with higher temperature. This allowed for efficient catalyst activity, driving the solid inner-phase oxidative cyclisation of pent-4-en-1-ol to tetrahydropyran-2-methanol. Lower temperatures reduced the affinity for the organic substrate causing loss of activity and phase separation, thereby allowing for easy catalyst-product separation.[30]

Modern catalysts have overcome many challenges; often allowing for high conversions, high turnover frequencies and high regio- or chemo-selectivities. A challenging yet crucial component of the catalytic system that remains to be addressed is the recovery and reuse of the catalyst. Precious metals and synthetically complex ligands are often used to achieve high regio- or chemo-selectivities. As such, their recovery is paramount because the loss of even a small percentage of catalyst over time results in significant financial losses and may eventually lead to a strain on global resources. The main problems causing catalyst losses are either related to the catalyst stability in air or moisture and the task of protecting it during product separation, or the leaching of catalytic material into the product phase. To facilitate catalyst-product separation and minimise financial loss, researchers have investigated supported catalyst systems in which a homogenous catalyst is tethered to an organic polymeric support, an inorganic support, or

a hybrid support.[58] In addition to a solid support, a variety of modern materials have been developed where the material can encapsulate and protect a catalytically active species during product separation. These materials include but are not limited to polymers of intrinsic microporosity (PIMs),[68] stimuli-responsive polymers,[69] porous organic polymers (POPs),[70-72] and metal-organic frameworks (MOFs).[73]

Kong et al. recently reported a smart heterogeneous catalyst for the enantioselective tandem reduction-lactonization of ethyl 2-acylarylcarboxylates.[26] By taking advantage of the thermoresponsive behaviour of poly(ethene-co-acrylamide-co-acrylonitrile) in water and the confined feature of silica nanoparticles, they prepared a silica material with chiral rhodium/diamine functionality on SiO_2 nanospheres coated with a water-soluble thermoresponsive polymer. At 40 ℃ the polymer coating is in an extended form, allowing the asymmetric reaction to proceed with high catalytic efficiency owing to the homogenous-like catalytic environment. At 15 ℃ the polymer coating is in a collapsed state, completely stopping the catalytic activity and thus allowing efficient catalyst-product separation and recycling. Interestingly, the catalyst displayed enhanced performance and comparable enantioselectivity relative to its homogeneous counterpart. The authors attribute this to the water-soluble polymer coating and the confined chiral rhodium/diamine catalyst. The authors showed that the catalyst could be recycled at least eight times without loss of its enantioselectivity.

Future research efforts will seek to expand on current catalyst capabilities in hopes of developing multi-responsive switchable catalysts that can control multiple catalytic processes by applying stimuli in a specific order. Further advances can be made by incorporating stimuli-responsive catalysts with an inert support that facilities effective

catalyst separation, or by incorporating stimuli-responsive catalysts with a stimuli-responsive support that facilitates multiple reactions pathways as well as effective catalyst separation and protection. In this sense, one can envision a support that responds to a different stimulus than the catalyst, therefore protecting it during separation and subsequently exposing it during a reaction, in which the catalyst can then be activated towards chemo- or regio-selective responses via additional stimuli.

In this chapter, traditional ATRP was utilised to create CO_2-responsive supports (i.e. polymer-grafted silica particles) for catalytically active nanoparticles. The combination of functional support and catalyst was investigated for a specific catalytic response as a function of the state of the CO_2-responsive support. These heterogeneous catalysts have the potential to switch from active to inactive or from one selectivity to another upon application or removal of CO_2. CO_2-responsive technology has the potential to increase the lifetime of heterogeneous catalysts, as well as the potential to expand the range of applications for which these catalysts can be used.

3.2 Results and discussion

3.2.1 Synthesis of CO_2-responsive polymer-grafted silica particles

The CO_2-responsive smart material was created using the *grafting from* method previously outlined in Chapter 2. PDMAPMAm was *grafted from* the surface of silica particles to create PGS-7. The irregular silica particles had an average particle size in the range of 40-63 μm. PGS-7 was determined to be 17 wt% polymer by thermogravimetric analysis (TGA) and ca. 6 wt% nitrogen by X-ray photoelectron spectroscopy (XPS). This batch of particles was synthesized without the addition of free initiator to the polymerization solution. Additionally, the primary purpose of this batch was to initiate collaborative experimentation in hopes of determining whether a CO_2-responsive smart material could serve as a smart support for heterogeneous catalysis. For this chapter, PGS-7 will be referred to directly or as a responsive particle (RP).

3.2.2 Ruthenium nanoparticles stabilised on CO_2-responsive polymer-grafted silica particles

In collaboration with Sami El Sayed, supervised by Dr. Kylie Luska and Prof. Walter Leitner at RWTH Aachen, Germany, RPs were examined as functional supports for ruthenium nanoparticles. Metal complexes were reduced in a suspension of RPs to place metal nanoparticles (NP) on the surface of the RP (NP@RP). The NP@RP were examined for catalytic activity, selectivity, and air sensitivity in the presence and absence of CO_2. Preliminary results show that the hydrogenation of furfural acetone (FFA) catalysed by

RuNP@RP reduces the C=C and C=O bonds in the absence of CO_2 but is selective for just C=C bonds in the presence of CO_2.[74]

The synthesis of RuNP@RP was accomplished by wet impregnation of the PGS-7 support with [Ru(2-methylallyl)$_2$(cod)] followed by subsequent reduction under $H_{2(g)}$ (Scheme 3.1). The PGS-7 based material was characterized by N_2 sorption using the Brunauer-Emmett-Teller (BET) method, revealing a surface area of 233 m^2g^{-1} and a pore size diameter of 80 Å. Analysis of the RuNP@PGS-7 using high angle annular dark field scanning transmission electron microscopy (HAADF-STEM) revealed the formation of RuNPs with a particle size between 1-4 nm.[74]

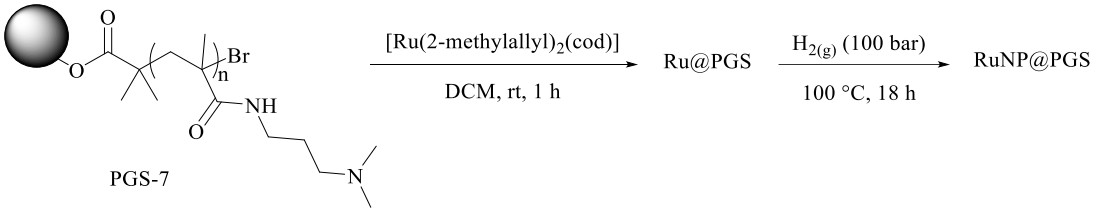

Scheme 3.1. Preparation of RuNP@PGS-7 from PGS-7 as reported by El Sayed et al.

3.2.3 Hydrogenation of furfuralacetone with ruthenium nanoparticles stabilized on CO_2-responsive polymer-grafted silica particles

Furfuralacetone (FFA) was chosen as a model substrate to study the influence of PGS on the catalytic behaviour of supported RuNP catalysts. The hydrogenation reaction of FFA involves multiple steps, the first being the hydrogenation of the C=C bond to form 4-(furan-2-yl)butan-2-one (FK). From FK there are two possible routes to the fully hydrogenated product 4-(tetrahydrofuran-2-yl)butan-2-ol (THFA) (Scheme 3.2):

1. C=O hydrogenation to 4-(furan-2-yl)butan-2-ol (FA), followed by aromatic hydrogenation.
2. Aromatic hydrogenation to 4-(tetrahydrofuran-2-yl)butan-2-one (THFK), followed by C=O hydrogenation.

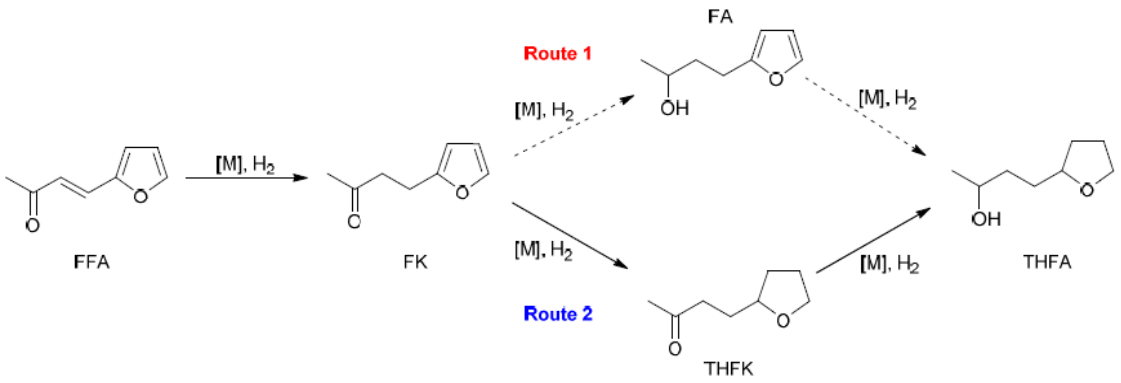

Scheme 3.2. The reaction mechanism for the hydrogenation of FFA as reported by El Sayed et al.

PGS-7 was able to influence the selectivity of the RuNP when CO_2 was present. The hydrogenation of FFA with RuNP@PGS-7, in the presence of CO_2 provided mostly aromatic ketone (FK: 17%) and saturated ketone (THFK: 71%). In contrast, the hydrogenation of FFA with RuNP@PGS-7, in the absence of CO_2 provided exclusively saturated alcohol (THFA: 100%). In another experiment, the hydrogenation of FFA was carried out with RuNP immobilised on non-functionalized silica (RuNP@SiO_2) and compared to RuNP@PGS-7. The results are as follows: RuNP@SiO_2 (THFK: 43%, THFA: 50%) and RuNP@PGS-7 (THFK: 76%, THFA: 16%). The data indicates that the CO_2-responsive silica particles provided selectivity towards THFK due to the presence of the amine functionality and its interaction with CO_2. Additionally, the data indicates that the hydrogenation of the alkene and aromatic moieties was facile, while the hydrogenation of the C=O bond was hindered in the presence of CO_2. Thus, the combination of RuNP@PGS-7 and an atmosphere of CO_2 could be employed to control the product selectivity in this reaction.[74]

The product selectivity towards THFK provided by RuNP@PGS-7 in the presence of CO_2 was achieved by hindering the catalyst's ability to hydrogenate C=O functional groups. Investigations are currently underway to elucidate the exact mechanism causing this selectivity. However, it is suspected that the formation of the bicarbonate salt of the nitrogenous polymer is responsible for hindering the hydrogenation of the C=O (Scheme 3.3). It is important to note that while water was not added to the hydrogenation reactions, the solvents used were not anhydrous or dried by any additional means. Additionally, the reagents were exposed to the lab atmosphere, from which moisture could have been absorbed or adsorbed. Since the hydrogenations were carried out with a small loading of

RuNP@PGS-7 (75 mg), it stands to reason that enough water could be present in the reaction to facilitate significant bicarbonate formation. Thus, formation of the bicarbonate ion could be responsible for the increased selectivity towards THFK in the presence of CO_2.

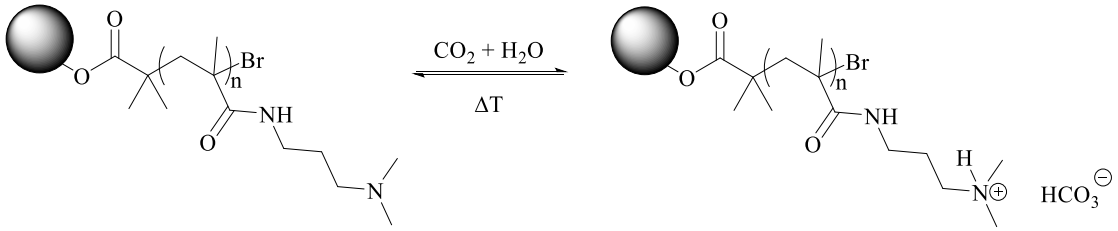

Scheme 3.3. The formation of the bicarbonate salt of PGS-7 (PDMAPMAm) in the presence of CO_2 and H_2O.

In order to determine the lifetime of RuNP@PGS-7, a variety of recycling experiments were conducted. Initial testing revealed that the product selectivity of RuNP@PGS-7 was inconsistent, as the yield of THFK decreased from 52 to 39% over four cycles.[74] The drop in selectivity was attributed to the loss of catalyst (ca. 30 wt%) between the first and fourth cycles. Further recycling experiments were performed using physical agitation instead of magnetic stirring in an effort to reduce the mechanical degradation and loss of RuNP@PGS-7. Under shaking conditions, the catalytic activity and selectivity of RuNP@PGS-7 remained consistent over the two cycles that were conducted. The yield of THFK was between 46-48% after 16 h.[74] It is possible that the reduced mass transport that is achieved using physical agitation may be responsible for the lower activity observed for RuNP@PGS-7 under these conditions. It was therefore demonstrated that RuNP@PGS-7

could be efficiently cycled and recovered using physical agitation as a method to induce mass transport within the reactor.[74]

3.2.4 Considerations of functional response and its influence on catalytic activity

Various particle sizes and morphologies of silica particles are being explored in attempts to improve the catalytic properties of the RuNP@RP. New methods have been developed and implemented for the synthesis of 2nd generation CO_2-responsive particles (i.e. PGS-15 and PGS-17). The method development will be outlined in Chapter 4; however, due to the relevance of the purpose of the material (i.e. catalytic support), both PGS-15 and PGS-17 will be discussed here. Catalyst activity is dependent on variations in the particle surfaces; including zeta potential, size, local pH, the degree of protonation, and local polarity. It is important to note that the polymer brush conformation depends heavily on a combination of solvent effects,[75] grafting density,[76,77] and the degree of protonation achieved by introducing CO_2 into the solvent.[78] For this discussion, it is assumed that both the CO_2 and water concentrations are in excess and the solvent choice is ideal.

It is worth noting that the size fluctuation of an individual particle due to the polymer brush extending or collapsing is negligible. However, either state could trigger aggregation or flocculation.[79,80] The 1st generation CO_2-responsive particles (i.e. PGS-7) lacked the ability to be characterised via traditional methods, thus the molecular weight and dispersity of the grafted polymer is unknown. This oversight was corrected in the development of the 2nd generation CO_2-responsive particles. Consequently, the 2nd generation CO_2-responsive particles (i.e. PGS-15 and PGS-17), which are currently being

tested, will be utilized for detailed discussion. For example, PGS-17 was poly-(diisopropylamino)ethyl methacrylate (PDiPAEMA) grafted from 200-500 μm spherical silica particles. The M_n of PDiPAEMA was determined to be ca. 30 kDa, therefore consisting of ca. 140 repeat units of DIpAEMA. The repeat unit in PDiPAEMA contains two carbon–carbon bond equivalents, which are each ca. 154 pm in length. The polymer in its extended state would then reach ca. 25,000 pm (0.025 μm) off the surface of the silica particle. If the smallest PGS-17 particle were to be considered, having a diameter of 200 μm, the polymer brush would equate to ca. 0.01% of the diameter of the particle. Similarly, the M_n of PDiPAEMA grafted from PGS-15 was determined to be ca. 43 kDa and the smallest particle size to consider is 40 μm. Therefore, the maximum extension of PDiPAEMA off the surface of the particle is ca. 0.036 μm, which equates to ca. 0.09% of the diameter of the particle. At best, one should discuss these materials as hairy particles, as is commonly done in literature, and not as core-shell particles in which the core is smaller or equal to the size of the shell.

The particle size will remain effectively unchanged as a result of the extension or collapse of the polymer brush. However, these conformational changes will have a large effect on the considerably smaller metal nanoparticles deposited on the surface of the silica. As discussed previously, the RuNPs were determined to be 1-4 nm in diameter.[74] Comparing the size of the RuNP (1-4 nm) to the size of the CO_2-switchable polymer brushes (25-36 nm when fully extended), a clearer image of how the brush might influence catalytic activity begins to form. The brushes, if fully extended, would be ca. 6-36 times larger than the RuNPs. It makes sense then that the brush could effectively dictate the local environment surrounding the RuNP. Changing this local environment is one mechanism

in which catalytic activity is thought to be influenced. The introduction of either carbamate or bicarbonate ions in proximity to the RuNP is another. The particle size, however, is hypothesised to do little to change the local environment, and thus will influence the catalytic activity in a negligible way.

3.3 Conclusions

Heterogeneous catalysts are industrially preferred over homogeneous catalysts but could be even more useful if they had the ability to catalyse one reaction and then another, to catalyse a reaction and then protect themselves during separations, or to change their selectivity from one product to another on demand. In collaboration with Prof. Walter Leitner at RWTH Aachen, Germany, preliminary results have demonstrated that CO_2-responsive particles, when used as a functional support for ruthenium nanoparticles, can influence the selectivity of the hydrogenation of furfuralacetone in the presence of CO_2. The hydrogenation of furfuralacetone (FFA) catalysed by RuNP@PGS-7 reduces the C=C and C=O bonds in the absence of CO_2 but is selective for just C=C bonds in the presence of CO_2.

The hydrogenation results obtained with RuNP@PGS-7 were reproducible when shaken, not stirred. When combined alongside experimental observations that were collected in-house it was determined that spherical silica particles are too fragile to withstand the repeated abuse of a mechanical stirring via a stirbar.

Owing to the small size of the active metal site (1-4 nm) and the maximum extension of the polymer brush (30 kDa to 43 kDa equating to 25-36 nm) it stands to reason

that there may be a limit to the amount of polymer needed to influence the catalytic properties of the active metal site. It also stands to reason that too much polymer may inhibit mass transfer to the active metal site and reduce the effectiveness of the catalyst.

This collaboration has aided in the identification of shortcomings that exist with the 1st generation of CO_2-responsive polymer-grafted silica particles and the method utilised to synthesise them. Consequently, this collaboration has driven the development of a 2nd generation of CO_2-responsive polymer-grafted silica particles, which will be discussed in detail in chapter 4. In summary, 2nd generation CO_2-responsive polymer-grafted silica particles using PDiPAEMA are currently being tested as a new CO_2-responsive supports for RuNP and the effects of molecular weight and grafting density are being explored. PDiPAEMA has been grafted to irregular silica (PGS-15) and spherical silica (PGS-17) and will thus allow properties such as surface area and particle size to be examined.

Further experimentation is required to optimize reaction conditions with RuNP@PGS-7; however, from the experiments conducted with RuNP@PGS-7, it can be concluded that the molecular weight of the grafted polymer must be determined. This work demonstrates the need for a method of synthesizing CO_2-responsive polymer-grafted materials that can provide reliable insight into the molecular weight of the grafted polymer in a nondestructive manner.

3.4 Experimental methods

Experimental conditions outlined below are those that the author, Kyle J. Boniface, has undertaken, demonstrated, and/or developed of his own accord. Experimental conditions relevant to the work done by the collaborators was mentioned in the discussion or can be found in the master's thesis of Sami El Sayed.[74]

3.4.1 Materials

All aqueous solutions were prepared with deionized water (DIW) unless stated otherwise. All silica particles were purchased from Silicycle. The following chemicals were used as received unless otherwise stated: sulfuric acid (Fisher, ACS reagent grade, 95-98%), ammonium hydroxide (Aldrich, ACS reagent grade, 28-30% NH_3 basis), water (Millipore, type 1, 18.2 MΩ·cm @ 25 ℃), hydrogen peroxide (Aldrich, 30 wt% in H_2O), 2-bromo-2-methylpropionyl bromide (BIBB, Aldrich, 98%), ethyl 2-bromo-2-methylpropionate (EBIB, Aldrich, 98%), diisopropylethylamine (DIPEA, Aldrich, ≥99%), 4-(dimethylamino)pyridine (DMAP, Aldrich, ≥99%), dichloromethane (DCM, EMD Millipore, anhydrous, ≥98.5%), methanol (MeOH, EMD Millipore, anhydrous), copper(I) bromide (Aldrich, 99.999% trace metals basis), N-[3-(dimethylamino)propyl]methacrylamide (DMAPMAm, Aldrich, contains MEHQ as inhibitor, 99%), N,N,N`,N``,N``-pentamethyldiethylenetriamine (PMDETA, Aldrich, 99%), ethylenediaminetetraacetic acid (EDTA, Aldrich, purified grade, ≥98.5%), sodium hydroxide (NaOH, Aldrich, ACS reagent, ≥97%), aluminium oxide (Aldrich, activated, basic, Brockmann I).

Piranha solutions were used to clean silica substrates. Acidic piranha solution consists of a 7:3 (v/v) mixture of concentrated sulfuric acid and 30% hydrogen peroxide solution, commonly heated to 85 ℃. Basic piranha solution consists of a 5:1:1 (v/v/v) mixture of Millipore water, 30% hydrogen peroxide solution, and 40% ammonium hydroxide solution, commonly heated to 70 ℃.

Warning: Piranha solution is highly dangerous and its use requires considerable care. Piranha solution is either strongly acidic or basic and a strong oxidizer. The mixing of piranha solution is very exothermic and should be done slowly; if the reagents are mixed too quickly the temperature can easily exceed 100 ℃, which will result in boiling and splashing of the piranha solution. Piranha solution will react violently with organic compounds; therefore, it should be used in a fume hood clear of organic solvents and waste. Make only as much Piranha solution as needed; when disposing of excess or used piranha solution do NOT cap the bottle. It commonly takes a day or two for the reagent to neutralize fully, during this time oxygen gas is produced. Refer to your institution's standard operating procedures before attempting to use or dispose of piranha solutions.

3.4.2 Synthesis of polymer-grafted silica-7 (PGS-7)

Cleaning and hydroxylation of silica particles:

Silica particles (SiO_2 #5, SiliaFlash P60, 40-63 μm, 100 Å pore size) were subjected to a three-part treatment to remove organic contaminants and promote a hydroxyl-rich surface. Firstly, the particles were stirred in acidic piranha solution for 1 h at 85 ℃, followed by rinsing three times with Millipore water. Secondly, the particles were stirred in basic piranha solution for 20 min at 70 ℃, followed by rinsing three times with Millipore water. Lastly, the particles were vacuum filtered and dried in an oven overnight at 110 ℃. The clean and hydroxyl-rich particles were stored in a sealed vessel under Ar until further use.

Warning: Piranha solution is very dangerous. Refer to Materials section

Initiator grafting method (PGS-7, KB-B6-PG32):

Clean and hydroxyl-rich silica particles (SiO_2 #5, SiliaFlash P60, 40-63 μm, 100 Å pore size, 15 g, 1 eq. assumption 2 $mmol \cdot g^{-1}$) were added to a 250 mL flame dried round bottom flask, to which a condenser was fixed. Reactants were added using Schlenk techniques for inert conditions; diisopropylethylamine (DIPEA, 1.1 eq., 33.0 mmol), 4-(dimethylamino)pyridine (DMAP, 0.013 eq., 0.39 mmol) and 150 mL of anhydrous dichloromethane (DCM) were added to the round bottom flask. The round bottom flask was cooled in an ice bath for approximately 30 min, after which the initiator, 2-bromo-2-methylpropionyl bromide, (BIBB, 1.1 eq., 33.0 mmol) was added dropwise via syringe. The mixture was stirred via a magnetic stir bar (1200 RPM) for 20 min before the

ice bath was removed and the mixture was allowed to warm to room temperature, ca. 27 ℃ and allowed to react overnight. The BIBB-grafted silica was then collected by vacuum filtration and washed multiple times with DCM. The washed particles were dried at 110 ℃ for 20 min, then stored under Ar until further use.

SI-AGET-ATRP PDMAPMAm from silica, PGS-7:

Initiator-functionalized silica particles (SiO_2 #5, SiliaFlash P60, 40-63 μm, 100 Å pore size, 6.2 g) were added to a 500 mL 3-neck round bottom flask containing 150 mL of anhydrous methanol. The mixture was sparged with Ar via needle for 1 h. The monomer, N-[3-(dimethylamino)propyl]methacrylamide (DMAPMAm 1.2 mol, 80 eq.) passed through a basic alumina column and sparged with Ar via needle for 30 min. The catalyst was prepared by mixing copper(I) bromide (12.9 mmol, 1 eq.) with N,N,N`,N``,N``-pentamethyldiethylenetriamine (PMDETA, 26 mmol, 2 eq.) in 25 mL anhydrous methanol. The mixture was sparged with Ar via needle for 1 h. The sparged solutions were added to the 3-neck flask under Ar, heated to 50 ℃, and stirred via magnetic stir bar (900 RPM) overnight. The polymer-grafted silica particles were recovered via vacuum filtration and washed thoroughly with an aqueous solution of ethylenediaminetetraacetic acid (EDTA), followed by multiple washings with distilled water. The particles were dried at 110 °C overnight, then stored under Ar until further use.

3.4.3 Thermogravimetric analysis of PGS-7

Thermogravimetric analysis (TGA) was performed using a TA Instruments Q500 TGA analyzer by heating the sample using the following ramp: 10 °C min^{-1} from 30 to 120 ℃, held for 20 min and 120 ℃, followed by 10 °C min^{-1} to 900 ℃. The initial isothermal hold at 120 ℃ was to remove bulk solvents and adsorbed liquids such as moisture from the atmosphere. The organic content of PGS-7 was determined from the mass lost after the initial isothermal hold, from 97.5 wt% to 80.5 wt%. PGS-7 was determined to be 17% PDMAPMAm by weight.

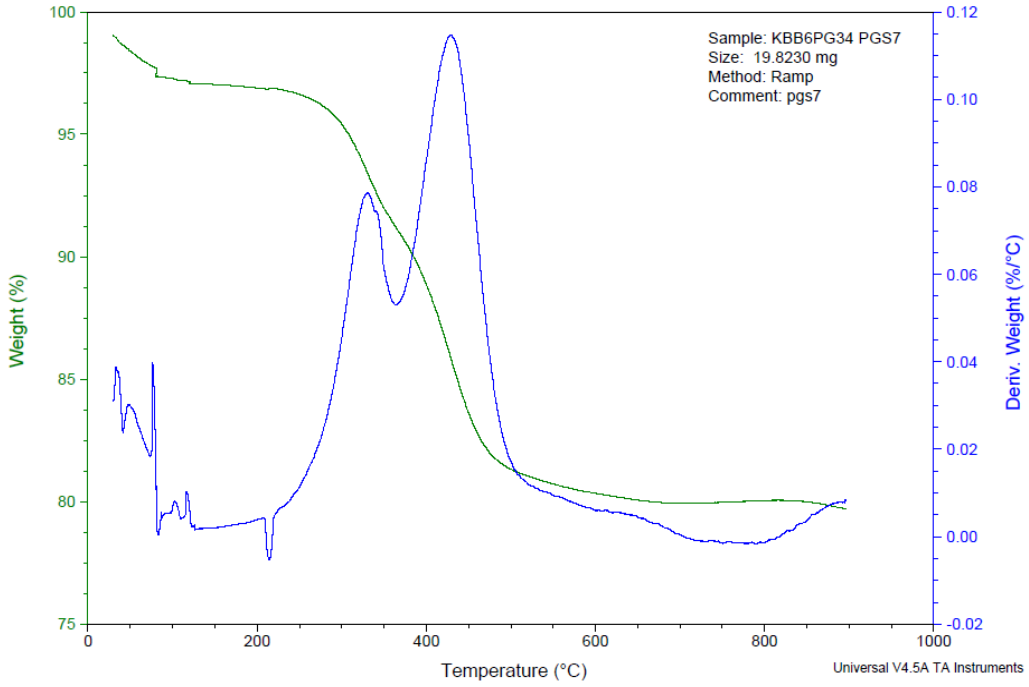

Figure 3.1. Thermogravimetric analysis of PGS-7. Ramp profile: 10 ℃ min^{-1} from 30 ℃ to 120 ℃, held for 20 min and 120 ℃, followed by 10 ℃ min^{-1} to 900 ℃.

3.4.4 Nuclear magnetic resonance spectroscopy of PGS-7

Solid-state NMR (^{13}C and ^{29}Si) spectra were recorded by Dr. Francoise Sauriol on a Bruker Avance 600 FT-NMR spectrometer operating at 150.91 MHz using a Bruker 5 mm cross polarization magic angle spinning (CP-MAS) probe. The spinning rate was 12 kHz with a cross-polarization contact time of 3 ms and a repetition delay of 2 s. Various contact times and repetition delays were explored in efforts to improve the signal to noise ratio. In some instances, longer contact times (i.e. 5 or 7 ms) resulted in a better spectrum for silica samples with low organic content. For polymer-grafted silica samples, which have a high organic content, a contact time of 3 ms with a delay of 2 s is recommended.

PGS-7 ^{13}C CP-MAS NMR (Figure 3.2):	177 ppm, 56 ppm, 47 ppm, 43 ppm, 23 ppm, 16 ppm.
PGS-7 ^{29}Si CP-MAS NMR (Figure 3.3):	-105 ppm, -106 ppm, -117 ppm.

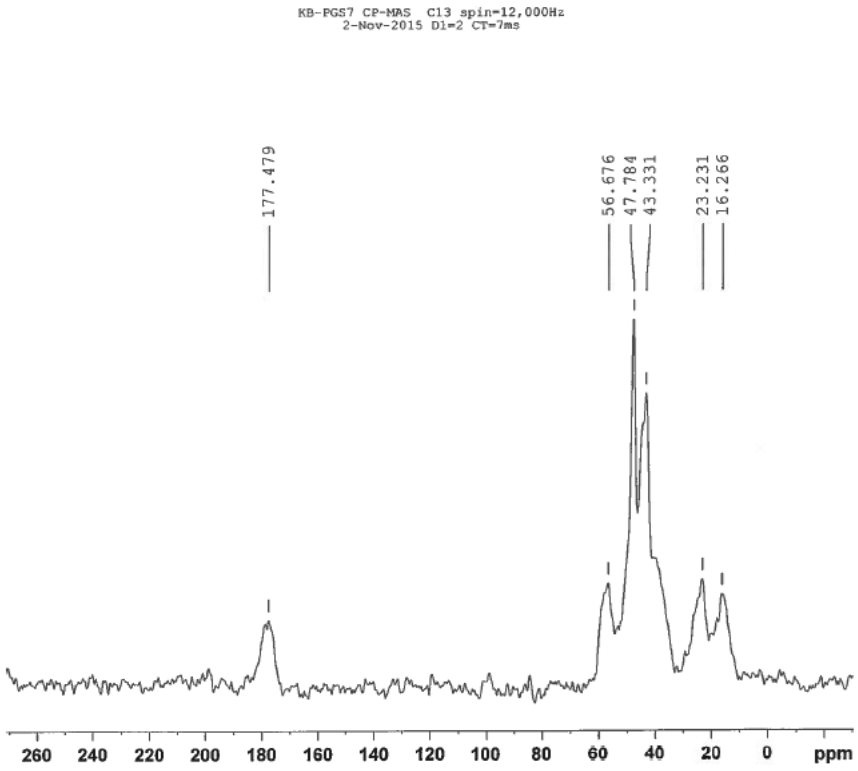

Figure 3.2. ^{13}C CP-MAS NMR spectrum of PGS-7.

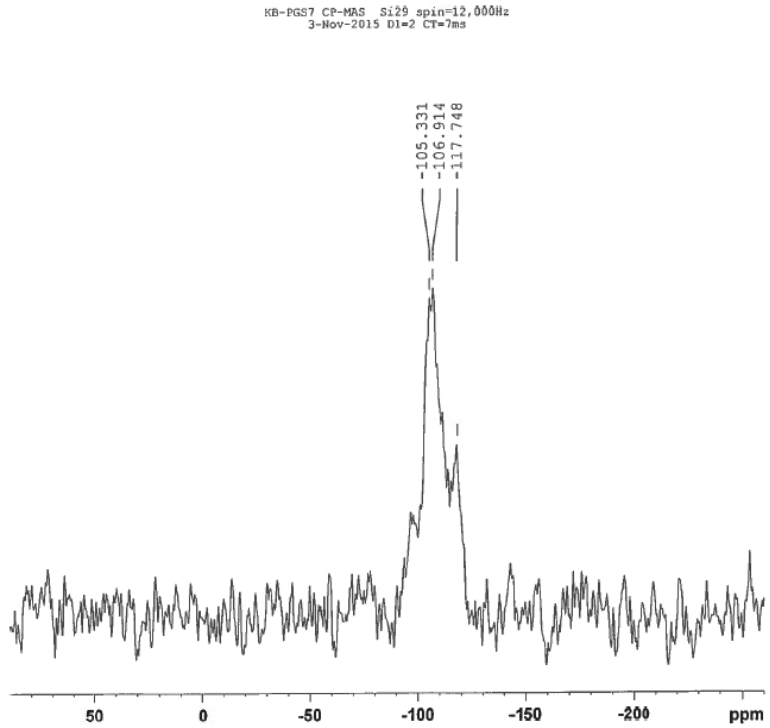

Figure 3.3. ^{29}Si CP-MAS NMR spectrum of PGS-7.

3.4.5 X-ray photoelectron spectroscopy of PGS-7

XPS measurements were conducted and interpreted by Dr. Gabriele Schatte of Queen's University, Kingston, Ontario, Canada. The XPS spectra were measured on a Microlab 310-F spectrometer equipped with an XR-4 twin anode (Al/Mg). The manufacturer of this system is VG Scientific. The samples were mounted on a stub-type stainless steel holder using double-sided adhesive Cu tape and kept under high vacuum (10^{-8} mbar) overnight inside the preparation chamber before they were transferred into the analysis chamber (10^{-9} mbar) of the spectrometer. The XPS data were collected using MgK_{α} radiation at 1253.6 eV (280 W, 14 kV) and a spherical sector analyser (SSA) operating in CAE (constant analyser energy) mode. Binding energies are referenced to the C1s peak at 285 eV. Survey spectra were recorded from -5 to 1000 eV at a pass energy of 40 eV (number of scans: 5) using an energy step size of 2 eV. High-resolution spectra were measured for C1s, O1s, N1s and Br3d in the appropriate region at a pass energy of 20 eV and an energy step size of 0.05 eV. The analysed area on the specimens is about 5×2 mm^2.

XPS analysis of PGS-7 identified significant amounts of carbon and nitrogen on the silica substrate. The atomic composition was determined by comparative analysis of peak heights, and is as follows: 37.19% carbon, 5.89% nitrogen, 56.91% oxygen, No bromine was detected. The carbon to nitrogen ratio for PDMAPMAm is 6.31 to 1 (experimental), and 4.5 to 1 (theoretical). The M_n of the polymer is unknown, so grafting density cannot be estimated for PGS-7. However, the carbon to nitrogen ratio reported by XPS is within acceptable limits for PDMAPMAm, when considerations are given for initiating groups and low-level contaminants such as adsorbed carbon dioxide. Analysis

for bromine failed to detect a signal; this is likely due to the low amount of bromine relative to the total organic content of the sample, which is only 17% organic. Additionally, early chain termination events could account for a loss of bromine in the grafted polymer. Such events are unwanted but would likely have occurred due to the high concentration of catalyst used in the 1st generation CO_2-responsive particle synthesis.

Table 3.1. XPS peak analysis for PGS-7, atomic percent reported as a function of peak area.

Name	Start BE	Peak BE	End BE	Area (normalised)	Atom %
C1s	291.4	285	282.15	31.76	7.72
C1s A	291.4	286.36	282.15	60.79	14.77
C1s B	291.4	287.54	282.15	44.07	10.71
C1s C	291.4	289.05	282.15	16.44	3.99
O1s	537.95	532.21	529.5	31.9	7.75
O1s A	537.95	533.67	529.5	142.4	34.61
O1s B	537.95	534.8	529.5	59.87	14.55
N1s	403.88	400.71	397.63	15.42	3.75
N1s A	403.88	401.55	397.63	8.79	2.14

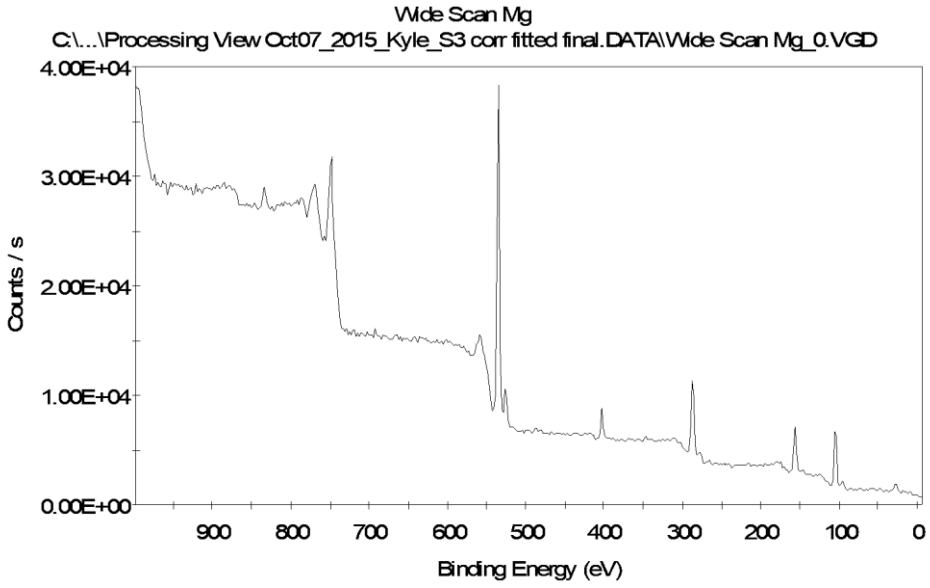

Figure 3.4. Survey spectrum of PGS-7.

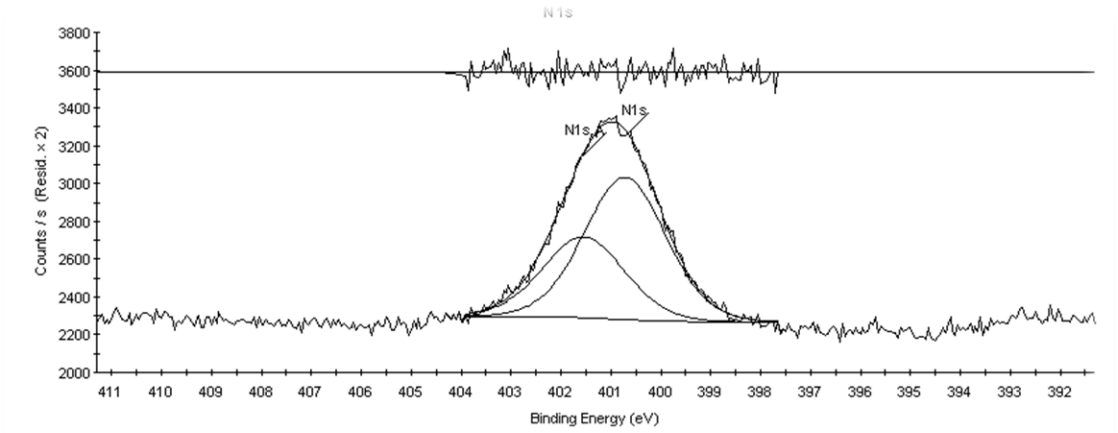

Figure 3.5. High-resolution N1s core-level spectrum of PGS-7.

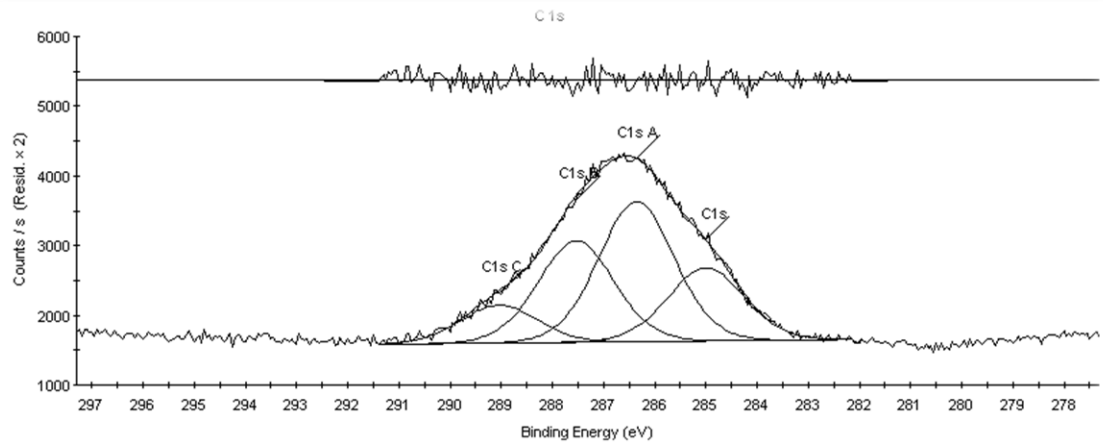

Figure 3.6. High-resolution C1s core-level spectrum of PGS-7.

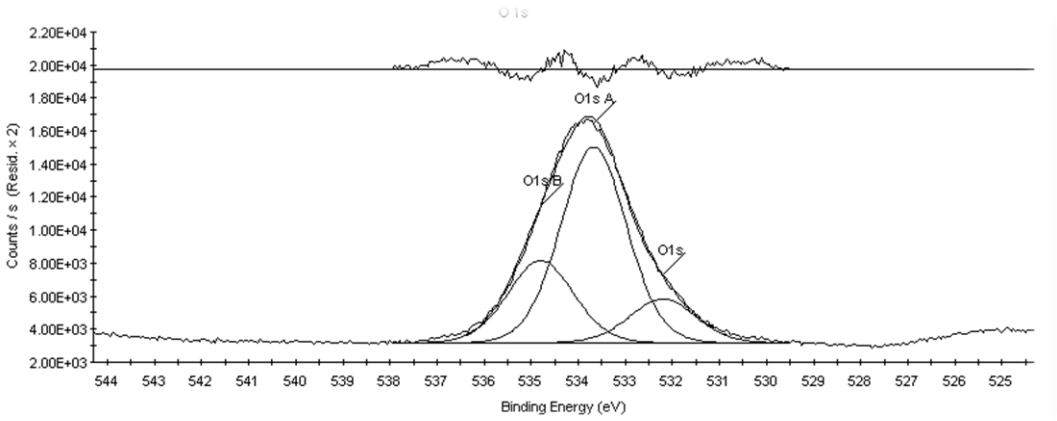

Figure 3.7. High-resolution O1s core-level spectrum of PGS-7.

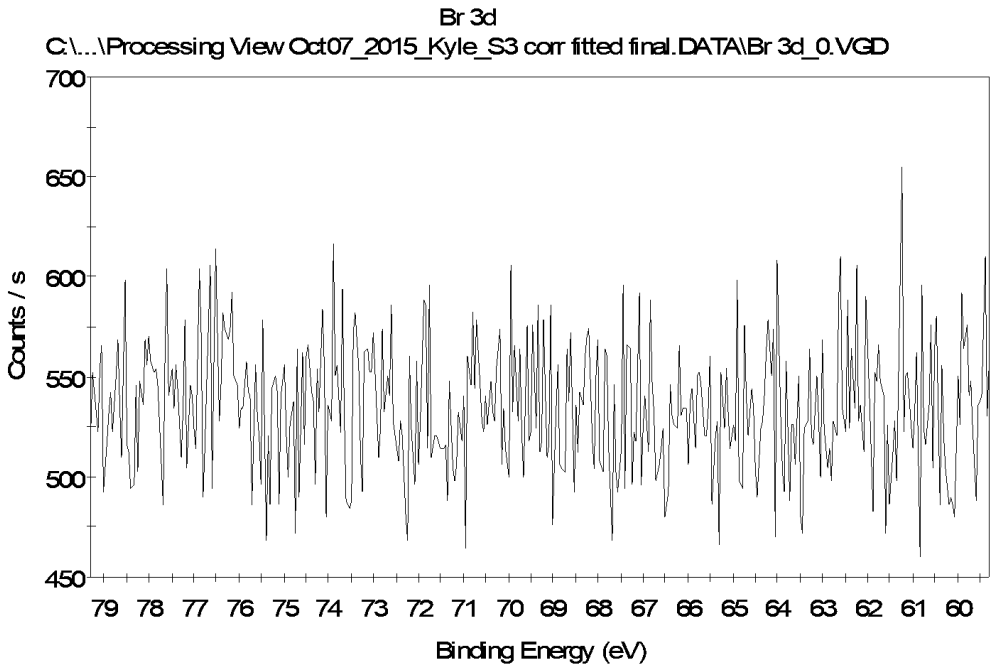

Figure 3.8. High-resolution Br3d core-level XPS spectrum of PGS-7.

3.5 References

1. V. Blanco, D. A. Leigh and V. Marcos, *Chem. Soc. Rev*., 2015, **44**, 5341-5370.

2. T. Traut, Enzyme Activity: Allosteric Regulation, in eLS, John Wiley & Sons, 2001.

3. T. Traut, Allosteric Regulatory Enzymes, Springer, New York, 2008.

4. C. Romain and C. K. Williams, *Angew. Chem. Int. Ed.*, 2014, **53**, 1607-1610.

5. S. L. Balof, S. J. P'Pool, N. J. Berger, E. J. Valente, A.M. Shiller and H.-J. Schanz, *Dalton Trans*., 2008, **0**, 5791-5799.

6. S. L. Balof, B. Yu, A. B. Lowe, Y. Ling, Y. Zhang and H.-J. Schanz, *Eur. J. Inorg. Chem*., 2009, 1717-1722.

7. L. H. Peeck, S. Leuthausser and H. Plenio, *Organometallics*, 2010, **29**, 4339-4345.

8. M. Akbarzadeh, Z. Moosavi-Movahedi, A. Shockravi, R. Jafari, K. Nazari, N. Sheibani and A. A. Moosavi-Movahedi, *J. Mol. Catal., A: Chem.*, 2016, **424**, 181-193.

9. S. L. Desset and D. J. Cole-Hamilton, *Angew. Chem. Int. Ed*., 2009, **48**, 1472-1474.

10. D. A. Leigh, V. Marcos and M. R. Wilson, *ACS Catal*., 2014, **4**, 4490-4497.

11. F. Würthner and J. Rebek, *Angew. Chem., Int. Ed. Engl*., 1995, **34**, 446-448.

12. F. Würthner and J. Rebek, *J. Chem. Soc., Perkin Trans., 2*, 1995, 1727-1734.

13. R. Cacciapaglia, S. Di Stefano and L. Mandolini, *J. Am. Chem. Soc*., 2003, **125**, 2224-2227.

14. M. Samanta, V. S. Rama Krishna and S. Bandyopadhyay, *Chem. Commun*., 2014, **50**, 10577-10579.

15. A. Ueno, K. Takahashi and T. Osa, *J. Chem. Soc., Chem. Commun*., 1980, 837-838; A. Ueno, K. Takahashi and T. Osa, *J. Chem. Soc., Chem. Commun*., 1981, 93-94.

16. W.-S. Lee and A. Ueno, *Macromol. Rapid Commun*., 2001, **22**, 448-450.

17. L. Zhu, H. Yan, C. Y. Ang, K. T. Nguyen, M. Li and Y. Zhao, *Chem. Eur. J*., 2012, **18**, 13979-13983.

18. M. Osaki, Y. Takashima, H. Yamaguchi and A. Harada, *Org. Biomol. Chem*., 2009, **7**, 1646-1651.

19. O. B. Berryman, A. C. Sather, A. Lledo and J. Rebek, *Angew. Chem., Int. Ed*., 2011, **50**, 9400-9403.

20. D. Wilson and N. R. Branda, *Angew. Chem., Int. Ed*., 2012, **51**, 5431-5434.

21. B. M. Neilson and C. W. Bielawski, *Organometallics*, 2013, **32**, 3121-3128.

22. T. Niazov, B. Shlyahovsky and I. Willner, *J. Am. Chem. Soc*., 2007, **129**, 6374-6375.

23. Y. Wei, S. Han, J. Kim, S. Soh and B. A. Grzybowski, *J. Am. Chem. Soc*., 2010, **132**, 11018-11020.

24. A. Nojiri, N. Kumagai and M. Shibasaki, *Chem. Commun*., 2013, **49**, 4628-4630.

25. R. Beniazza, R. Lamber, L. Harmand, F. Molton, C. Duboc, S. Denisov, G. Jonusauskas, N D. McClenaghan, D. Lastecoueres and J. Vincent. *Chem. Eur. J.,* 2014, **20**, 13181-13187.

26. L. Kong, J. Zhao, T. Cheng, J. Lin and G. Liu, *ACS Catal*., 2016, **6**, 2244-2249.

27. S. Sun, X. Yu, Y. Guo, L. Chen, X. Wang and Z. Jiang, *Catal. Surv. Asia*, 2016, **20**, 98-108.

28. Y. M, S. Qing, L. Wang, N. Islam, S. Guan, Z. Gao, X. Mamat, H. Li, W. Eli and T. Wang, *RSC Adv*., 2015, **5**, 47377-47383.

29. G. Storch and O. Trapp, *Angew. Chem., Int. Ed*., 2015, **54**, 3580-3586.

30. H. Hamamoto, Y. Suzuki, H. Takahashi and S. Ikegami, *Adv. Synth. Catal*., 2007, **349**, 2685-2689.

31. S. Cobo, J. Heidkamp, P. Jacques, J. Fize, V. Fourmond, L. Guetaz, B. Jousselme, V. Ivanona, H. Dau, S. Palacin, M. Fontecave and V. Artero, *Nat. Mater*., 2012, **11**, 802-807.

32. I. M. Lorkovic, R. R. Duff and M. S. Wrighton, *J. Am. Chem. Soc*., 1995, **117**, 3617-3618.

33. C. S. Slone, C. A. Mirkin, G. P. A. Yap, I. A. Guzei and A. L. Rheingold, *J. Am. Chem. Soc*., 1997, **119**, 10743-10753.

34. C. K. A. Gregson, V. C. Gibson, N. J. Long, E. L. Marshall, P. J. Oxford and A. J. P. White, *J. Am. Chem. Soc*., 2006, **128**, 7410-7411.

35. E. M. Broderick, N. Guo, C. S. Vogel, C. Xu, J. Sutter, J. T. Miller, K. Meyer, P. Mehrkhodavandi and P. L. Diaconescu, *J. Am. Chem. Soc*., 2011, **133**, 9278-9281.

36. K. Arumugam, C. D. Varnado, S. Sproules, V. M. Lynch and C. W. Bielawski, *Chem. Eur. J*., 2013, **19**, 10866-10875.

37. M. Süßner and H. Plenio, *Angew. Chem., Int. Ed*., 2005, **44**, 6885-6888.

38. P. Neumann, H. Dib, A.-M. Caminade and E. Hey-Hawkins, *Angew. Chem., Int. Ed*., 2015, **54**, 311-314.

39. A. J. D. Magenau, N. C. Strandwitz, A. Gennaro and K. Matyjaszewski, *Science*, 2011, **332**, 81-84.

40. E. M. Broderick, N. Guo, T. Wu, C. S. Vogel, C. Xu, J. Sutter J. T. Miller, K. Meyer, T. Cantat and P. L. Diaconescu, *Chem. Commun*., 2011, **47**, 9897-9899.

41. A. Sauer, J.-C. Buffet, T. P. Spaniol, H. Nagae, K. Mashima and J. Okuda, *ChemCatChem*, 2013, **5**, 1088-1091.

42. Y.-Y. Fang, W.-J. Gong, X.-J. Shang, H.-X. Li, J. Gao, J.-P. Lang, *Dalton Trans*., 2014, **43**, 8282-8289.

43. S. Mortezaei, N. R. Catarineu and J. W. Canary, *J. Am. Chem. Soc*., 2012, **134**, 8054-8057.

44. X. Wang, A. Thevenon, J. L. Brosmer, I. Yu, S. I. Khan, P. Mehrkhodavandi and P. L. Diaconescu, *J. Am. Chem. Soc*., 2014, **136**, 11264-11267.

45. Q. Zhang, X. Cui, L. Zhang, S. Luo, H. Wang and Y. Wu, *Angew. Chem., Int. Ed*., 2015, **54**, 5210-5213.

46. M. Fujiwara, S. Terashima, Y. Endo, K. Shiokawa and H. Ohue, *Chem. Commun*., 2006, **0**, 4635-4637.

47. A. G. Tennyson, V. M. Lynch and C. W. Bielawski, *J. Am. Chem. Soc*., 2010, **132**, 9420-9429.

48. S. Chavan, G. Bishwa Bidita Varadwaj, K. M. Parida and B. M. Bhanage, *ChemCatChem*, 2016, **8**, 2649-2658.

49. Y. Sohtome, S. Tanaka, K. Takada, T. Yamaguchi and K. Nagasawa, *Angew. Chem. Int. Ed*., 2010, **49**, 9254-9257.

50. X. Tian, C. Cassani, Y. Liu, A. Moran, A. Urakawa,P. Galzerano, E. Arceo and P. Melchiorre, *J. Am. Chem.Soc*., 2011, **133**, 17934-17941.

51. S. Arseniyadis, A. Valleix, A. Wagner and C. Mioskowski, *Angew. Chem., Int. Ed*., 2004, **43**, 3314-3371.

52. A. B. Northrup and D. W. C. MacMillan, *Science*, 2004, **305**, 1752-1755.

53. T. Yamamoto, T. Yamada, Y. Nagata and M. Suginome, *J. Am. Chem. Soc*., 2010, **132**, 7899-7901.

54. M. Messerer and H. Wennemers, *Synlett*, 2011, 499-502.

55. R. J. Chew, X.-R. Li, Y. Li, S. A. Pullarkat and P.H. Leung, *Chem. Eur. J*., 2015, **21**, 4800-4804.

56. Y. Leng, J. Wang, D. Zhu, X. Ren, H. Ge and L. Shen, *Angew. Chem. Int. Ed*., 2009, **48**, 168-171.

57. O. Coulembier, S. Moins, R. Todd and P. Dubois, *Macromolecules*, 2014, **47**, 486-491.

58. A. J. Sandee, J. N. Reek, P. C. J. Kamer and P. W. N. M. van Leeuwan, *J. Am. Chem. Soc.*, 2001, **123**, 8468-8476.

59. S. Karabulut, B. Sariaslan and B. O. Öztürk, *Catal. Commun.*, 2013, **41**, 12-16.

60. R. Groote, R. T. M. Jakobs and R. P. Sijbesma, *Polym. Chem*., 2013, **4**, 4846-4859.

61. S. Karthikeyan, S. L. Potisek, A. Piermattei and R. P. Sijbesma, *J. Am. Chem. Soc*., 2008, **130**, 14968-14969.

62. A. Piermattei, S. Karthikeyan and R. P. Sijbesma, *Nat. Chem*., 2009, **1**, 133-137.

63. R. Groote, L. van Haandel and R. P. Sijbesma, *J. Polym. Sci., Part A: Polym. Chem*., 2012, **50**, 4929-4935.

64. R. Groote, R. T. M. Jakobs and R. P. Sijbesma, *ACS Macro Lett*., 2012, **1**, 1012-1015.

65. R. T. M. Jakobs and R. P. Sijbesma, *Organometallics*, 2012, **31**, 2476-2481.

66. R. T. M. Jakobs and S. Ma, R. P. Sijbesma, *ACS Macro Lett*., 2013, **2**, 613-616.

67. D. J. Cole-Hamilton, S. L. Desset, D. B. Williams, M. Mokhadinyana, WO. Pat., 013 525, 2009.

68. N. B. McKeown and P. M. Budd, *Chem. Soc. Rev*., 2006, **35**, 675-683.

69. D. D. Diaz, D. Kühbeck and R. J. Koopmans, *Chem. Soc. Rev*., 2011, **40**, 427-448.

70. P. Kaur, J. T. Hupp and S. T. Nguyen, *ACS Catal*., 2011, **1**, 819-835.

71. Y. Zhang and S. N. Riduan, *Chem. Soc. Rev*., 2012, **41**, 2083-2094.

72. D. Wu, F. Xu, B. Sun, R. Fu, H. He and K. Matyjaszewski, *Chem. Rev.,* 2012, **112**, 3959-4015.

73. H. Zhou and S. Kitagawa, *Chem. Soc. Rev*., 2014, **43**, 5415-5418.

74. S. El Sayed, MSc thesis, RWTH Aachen University, 2016.

75. J. D. Willott, T. J. Murdoch, B. A. Humphreys, S. Edmondson, E. J. Wanless and G. B. Webber, *Langmuir*, 2015, **31**, 3707-3717.

76. H. Yim, M. S. Kent, S. Mendez, G. P. Lopez, S. Satija and Y. Seo, *Macromolecules*, 2006, **39**, 3420-3426.

77. B. Zuo, S. Zhang, C. Niu, H. Zhou, S. Sun and X. Wang, *Soft Matter*, 2017, **13**, 2426-2436.

78. A. K. Alshamrani, J.R. Vanderveen and P.G. Jessop, *Phys. Chem. Chem. Phys.,* 2016, **18**, 19276-19288.

79. P. Champange, P. G. Jessop, K. J. Boniface, M. F. Cunningham, H. Wang, O. Garcia-Valdez, A. Cormier, S. Ge, J. Arrendondo-Luna, WO. Pat., 149 815, 2016.

80. S. Ge, P. Champagne, H. Wang, P. G. Jessop and M. F. Cunningham, *Environ. Sci. Technol. Lett.,* 2016, **50**, 7896-7903.

Chapter 4

Method Development for the Synthesis of CO_2-Responsive Surfaces

4.1 Preface

As the CO_2-switchable drying agent project evolved, the synthetic methodology also evolved. Shortcomings of traditional ATRP methods were identified and resolved by the use of special equipment, new monomers, and a novel "surface-initiated activators generated by electron transfer atom transfer radical polymerisation" (SI-AGET-ATRP) method. In this chapter, newly designed polymer grafting methods are described. A robust, user and substrate friendly SI-AGET-ATRP method was developed specifically for problematic tertiary amine-containing monomers. The SI-AGET-ATRP method has facilitated the creation of a variety of CO_2-responsive surfaces. The work in this Chapter is currently being prepared for publication.

4.1.1 Abstract

The controlled radical polymerisation of PDiPAEMA from a surface has been achieved with levels of control not previously reported in the literature.[1–3] ARGET-ATRP and AGET-ATRP methodologies were utilised to create CO_2-responsive smart materials. Using AGET-ATRP, high molecular weight and low dispersity PDiPAEMA can be produced as a homopolymer (>100 kDa, Đ: 1.17) or grown from a surface (>40 kDa, Đ: 1.17). When $[M]_0$:$[I]_0$:$[Cu]_0$:$[L]_0$:[RA] is [253]:[1]:[0.66]:[3.3]:[10], and [M] is ca. 4 M, the surface-initiated polymerisation proceeds to high conversion (>90% in 12 h), yielding narrowly distributed PDiPAEMA-grafted surfaces. PDiPAEMA has been grafted from silica particles, silicon wafers, and cotton fabric with good control. The SI-AGET-ATRP method presented herein allows for the nondestructive approximation of the molecular weight of the grafted polymer chains. Thus, the relationship between molecular weight and stimuli-responsiveness can be studied in greater detail.

A 2nd generation of CO_2-responsive particles, created using the SI-AGET-ATRP method, removed twice as much water per g of material (1053 mg H_2O/g DA) than the 1st generation of CO_2-responsive particles (490 mg H_2O/g DA) when removing water from wet isobutanol.

4.2 Introduction

4.2.1 CO_2-responsive monomers

In the research described in this chapter, the previously utilised monomer, DMAPMAm (N-[3-(dimethylamino)propyl]methacrylamide) was replaced by DiPAEMA (2-(diisopropylamino)ethyl methacrylate). The characterisation of PDMAPMAm was challenging. At the time, the research facility was unequipped to handle the analysis of PDMAPMAm by GPC due to a lack of solvent compatibility. PDMAPMAm requires an aqueous mobile phase with an acidic modifier to dissolve the sample, whereas the equipment was setup to use organic mobile phases. Additionally, NMR was not sensitive enough to distinguish PDMAPMAm peaks from ATRP initiator peaks at the molecular weights that were being investigated (>2 kDa). Furthermore, matrix assisted laser desorption/ionisation time of flight (MALDI-TOF) mass spectrometry proved unsuccessful at identifying molecular weights >5 kDa.

The first generation of CO_2-responsive silica particles was successful in that they exhibited a response to CO_2 and that response could be quantified in terms of the number of water molecules of hydration. The next logical step was to determine the amount of polymer-grafted on the silica particles and how it related to waters of hydration. At this point, questions that were critical to the future progress of CO_2-responsive particles were raised. Did more polymer allow for a larger volume of water to be captured? Was there a limit to the amount of polymer that could be loaded on the substrate? Did water capture reach a local or global maximum at a specific molecular weight? The molecular weight of the grafted polymer must be known or at least approximated with a high degree of certainty

to answer these questions. Because the molecular weight of PDMAPMAm could not be determined, PDMAPMAm had to be replaced to move the project forward.

The foundation of this body of work is that the response to CO_2 is a direct consequence of the formation of a bicarbonate ion. CO_2, H_2O, and a nitrogenous base have multiple pathways in which they can react with one another. This work focuses on one pathway in particular and that is bicarbonate formation. Tertiary amines interact with CO_2 in water to form a bicarbonate ion. Thus, only monomers containing tertiary amine functional groups were studied. The following monomers were considered as a replacement for DMAPMAm: 2-(dimethylamino)ethyl methacrylate (DMAEMA), 2-(diethylamino)ethyl methacrylate (DEAEMA), and 2-(diisopropylamino)ethyl methacrylate (DiPAEMA).

DiPAEMA was chosen to replace DMAPMAm; monomer choice was weighed against multiple factors, but the decision to choose DiPAEMA came down to only two. Firstly, in comparison to DMAEMA and DEAEMA, there are considerably fewer studies using DiPAEMA and the instances of controlled polymerisation of PDiPAEMA are rare.[1] Thus, any work using DiPAEMA will have intrinsic value and will most certainly add to the relatively small body of published studies in the scientific community. Secondly, the dual pH- and thermo-responsive properties of PDiPAEMA in an aqueous solution present a unique opportunity for a CO_2-responsive system.[4,5] The pH and temperature of a system can be controlled independently of one another and either stimulus can be applied independently to favour either the charged or neutral state of PDiPAEMA in solution.

The CO_2-responsive system, as described here, is one in which a water-insoluble polyamine is suspended in water. The polyamine, when suspended in water, is mostly

neutral and thus hydrophobic and water-insoluble. The polyamine may or may not be bound to a surface. Upon addition of CO_2, carbonic acid is formed; through an acid-base reaction with carbonic acid, the polyamine becomes cationic and thus hydrophilic and water-soluble. The removal of CO_2 from the aqueous solution forces the equilibrium towards the neutral, hydrophobic, and water-insoluble state of the polyamine. Removal of CO_2 is achieved by the application of an inert gas to the aqueous solution or by application of heat to the aqueous solution. Currently, reaction vessels are pressurised to atmospheric pressure with CO_2. At atmospheric pressure and 25 °C, the pH range accessible with CO_2 in water is ca. 4–7.

Both the thermo-responsive behaviour and the pH-responsive behaviour of polyamines can be utilised to decrease the time it takes to switch the polyamine from its charged, water-soluble state to its neutral, water-insoluble state. The water-soluble to water-insoluble phase transition for polyamines is pH is dependent, given that the neutral state is hydrophobic enough to be water-insoluble. The pH-responsive, water-soluble to water-insoluble, phase transition is dependent on the pK_{aH} of the polyamine. The pK_{aH} of linear PDMAEMA has been reported as 7.4,[6] 7.0,[4,7], and 7.8.[8] The pK_{aH} for star-shaped PDMAEMA, at various molecular weights, was reported to range from 7.9-8.2.[8] The pK_{aH} for PDEAEMA has been reported as 7.5,[6] 7.3,[4] and 6.7.[9] The pK_{aH} for PDiPAEMA has been reported as 6.2.[4] For the three polyamines in question, PDMAEMA, PDEAEMA, and PDiPAEMA, their pK_{aH} values are ca. 7.

While the pH-response of PDEAEMA and PDiPAEMA have been reported and studied, their respective thermo-responsive behaviour is just becoming understood. A recent study by Thavanesan et al. involved fluorescent dyes to probe the aqueous behaviour

of PDMAEMA, PDEAEMA, and PDiPAEMA as a function of pH and temperature. Their findings concluded that PDMAEMA showed little thermo-responsive behaviour across the pH range of 6.9–8.9. PDEAEMA showed a pronounced response to temperature as pH decreases, notably a sharp phase transition from water-soluble to water-insoluble occurs at 60 °C (pH 6.9) and a broad phase transition from water-soluble to water-insoluble occurs across a range of 20 to 40 °C, at pH 7.7. PDiPAEMA exhibited a drastic response to temperature across the pH range of 5.2-6.6. Most notably with PDiPAEMA, a sharp phase transition from water-soluble to water-insoluble occured at ca. 28 °C, at pH 6.6.[5]

The polyamines PDEAEMA and PDiPAEMA are therefore of greater value to a CO_2-responsive system than PDMAEMA since their dual pH- and thermo-responsive properties occur in aqueous solutions, within a pH range that is accessible with CO_2-responsive systems. The polyamine which exhibits this tandem behaviour to the greatest extent is PDiPAEMA.[5] Thus, with all factors considered equal, PDiPAEMA would exhibit the fastest and most pronounced switch from a charged and water-soluble species, when CO_2 is present, to a neutral and water-insoluble species when CO_2 is removed. Additionally, the temperature required to aid the transition from charged and water-soluble with CO_2, to neutral and water-insoluble without CO_2, is only 28 °C. For the applications studied in this work, in which the charged and water-soluble state is required at room temperature and an atmospheric pressure of CO_2, PDiPAEMA is the most attractive of the three polyamines to study. PDiPAEMA is both pH- and thermo-responsive within the pH and temperature ranges that are accessible to the CO_2 responsive system and the solubility of PDiPAEMA in water is governed by the combination of both pH and temperature.[5]

Whether the thermo-responsive behaviour of polyamines is an advantage depends on the end use and the temperature range in which the material is expected to perform. Additionally, the CO_2 and water equilibria are influenced enthalpically. Added heat drives the reaction in reverse, disfavoring the formation of dissolved CO_2, carbonic acid, and its various dissociated species. The enthalpic influence on the concentration of CO_2 in solution will hinder the ability of the polyamine to stay water-soluble at higher temperatures. However, this could be addressed by increasing the pressure of CO_2 in the system. Future applications will need to consider both the thermo-responsive properties of the polyamines as well as the effects of temperature on the concentration of CO_2, carbonic acid, and its various dissolved forms in solution.

4.2.2 SI-ATRP as a tool for the synthesis of CO_2-responsive polymer-grafted silica particles

The 1st generation of CO_2-responsive silica particles was synthesised by SI-ATRP utilising Cu(I)Br as the copper source. Utilising Cu^I metal sources, commonly Cu(I)Br or Cu(I)Cl, as a precursor for the active catalyst is indicative of traditional ATRP methods.[10–13] These metals are air sensitive and much care is required to prepare the catalyst. Any oxygen in the reaction will rapidly oxidise the Cu^I species to the Cu^{II} oxide. Removal of oxygen, thus reducing the amount of Cu^I lost to the formation of Cu^{II} oxide, is important because the ATRP rate is sensitive to the amount of Cu^I in the system (Scheme 4.1). Any deviations from the planned amount of Cu^I in solution will henceforth alter the rate of propagation and the controlled nature of the propagation, leading to variable conversions and a broad molecular weight dispersity in the final polymer.[14]

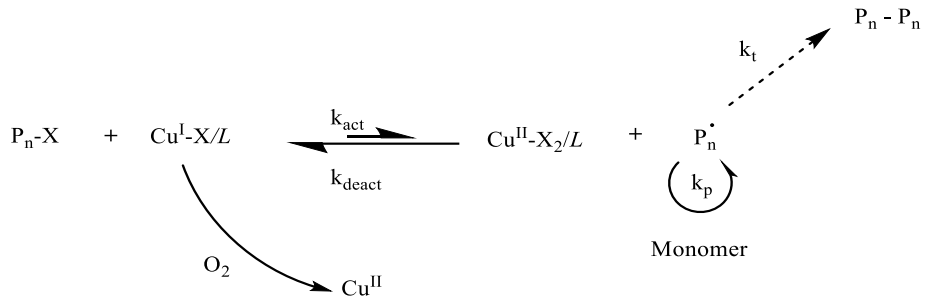

Scheme 4.1. A simplified version of ATRP kinetics highlighting the negative effect of oxygen in the system. Where the ligand is represented by *L*.

Polymer-grafted materials are challenging to create and reproduce using traditional ATRP methods. Larger substrates, such as silicon wafers, complicate the necessary deoxygenation steps since they require larger reaction vessels that are not conducive to Schlenk techniques. Dissolved oxygen resultant from inadequate deoxygenation is a critical issue for traditional ATRP. Since dissolved oxygen is always present to some extent and its concentration inconsistent, the proper amount of Cu(I)Br could not be added or determined once in solution. If polymerisation occurs, the results would be difficult to replicate. As these problems became more apparent and more limiting, specifically in surface-initiated applications, the scientific community engaged in an effort to find alternatives to traditional ATRP methods. The effort has produced multiple elegant solutions to traditional ATRP, the most applicable to this project being AGET-ATRP[15] and ARGET-ATRP.[16–18]

The defining characteristic of AGET or ARGET ATRP is that a mechanism exists for the reduction of a Cu^{II} to a Cu^{I} species. Commonly, an external reducing agent such as ascorbic acid, Cu^0, glucose or tin(II) 2-ethylhexanoate is responsible for this process.[14] However, amine-containing monomers and ligands can also facilitate the reduction

process.[19,20] The major distinction between AGET- and ARGET-ATRP is the concentration of copper in the polymerisation reaction. AGET commonly consists of higher concentrations of copper, typically from ~100 to ~1000 ppm. On the other hand, ARGET was developed in the pursuit of lowering copper concentration below ~100 ppm; Using ARGET-ATRP, Dong et al. successfully polymerised DEAEMA using 100 ppm $Cu(II)Cl_2$.[19] In this thesis, literature methods were modified and ARGET-ATRP of DiPAEMA was successfully carried out with copper concentrations less than 17 ppm (Chapter 4, KBB8PG37, M_n: 10.7 kDa, Đ: 1.33). AGET-ATRP has been successfully carried out, with consistent results, with copper concentrations of ca. 1300 ppm (Chapter 4, KBB9PG8, PDiPAEMA, M_n: 111 kDa, Đ: 1.17; Chapter 5, KBB9PG82, PDiPAEMA SI-AGET-ATRP, silicon wafer, M_n: 39.6 kDa, Đ: 1.17; Chapter 4, KBB9PG14, PDiPAEMA, SI-AGET-ATRP, silica particles, M_n: 42.8 kDa, Đ: 1.27).

In general, the AGET/ARGET process begins with the catalyst metal precursor in its oxidatively more stable state; for Cu-based systems, this is Cu^{II}. The less stable Cu^{I} species is then generated in situ via reduction with an external reducing agent such as ascorbic acid or tin(II) 2-ethylhexanoate, or via reduction with an internal reducing agent such as a nitrogenous-monomer or -ligand[14,19,20] (Scheme 4.2 and 4.3).

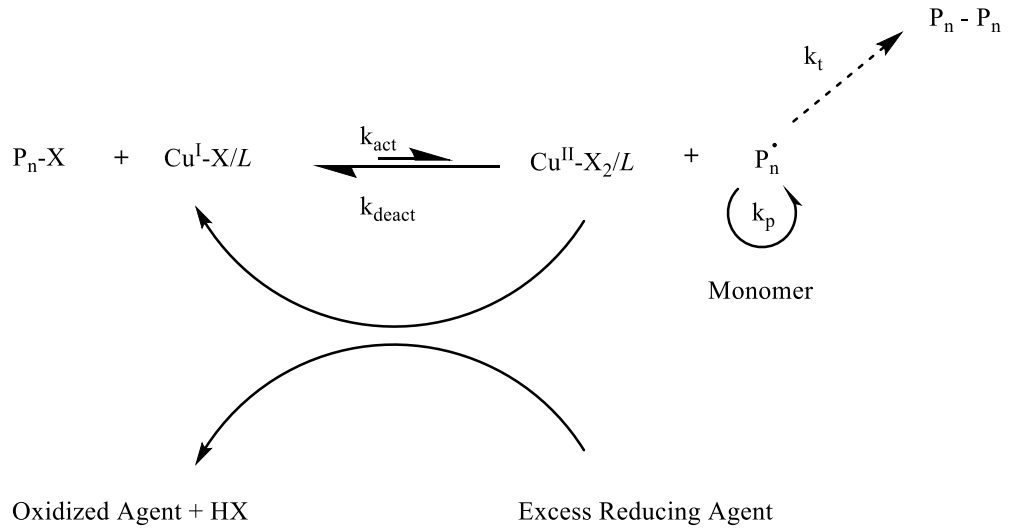

Scheme 4.2. Simplified mechanism for AGET and ARGET ATRP. HX is a byproduct when ascorbic acid is used as a reducing agent.

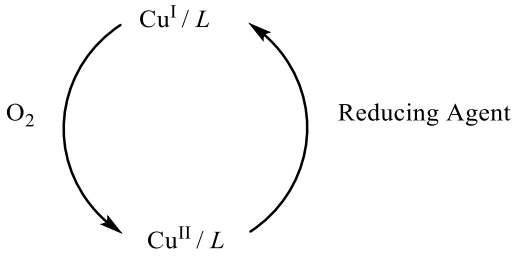

Scheme 4.3. The fundamental purpose of the reducing agent in ARGET or AGET ATRP. Whether by ATRP mechanisms or by oxidation from oxygen, the catalyst is shuffled between the two oxidation states. The presence of excess reducing agent returns Cu^{II} to the Cu^I state.

Externally reduced AGET or ARGET-ATRP systems have been extensively reported for monomers such as styrene, methyl methacrylate, poly(ethylene glycol) methacrylate and poly(N-isopropyl acrylamide).[1] In contrast, considerably fewer instances of controlled AGET or ARGET ATRP methods have been reported for tertiary amine-containing monomers relevant to this project, such as DMAEMA, DEAEMA, DMAPMAM, and DiPAEMA. Even fewer instances of *grafting from* or *grafting to* a

surface, using these techniques, have been reported.[1] Additionally, amine-containing monomers such as DMAEMA or DMAPMAm are a more difficult class of monomer to polymerise in a controlled manner due to their propensity for either competitive complexation with the catalyst[21] (Scheme 4.4), or their ability to react as internal reducing agents (Scheme 4.5).[19]

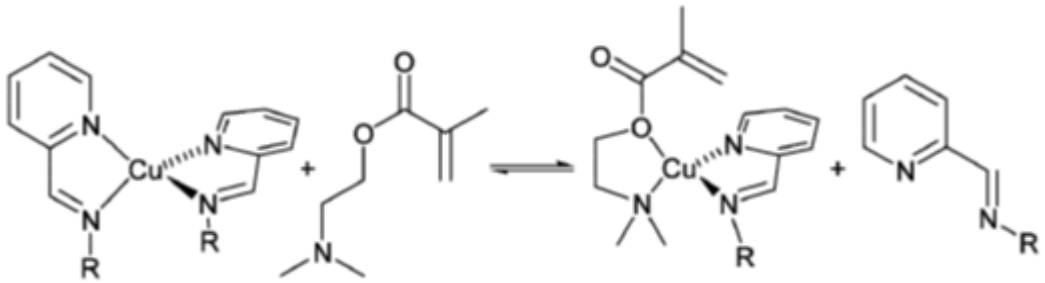

Scheme 4.4. The proposed equilibrium involving DMAEMA and N-propyl- 2-pyridylmethanimine/copper complexes where R is an alkyl group. Reproduced from reference 21 with permission from The Royal Society of Chemistry.

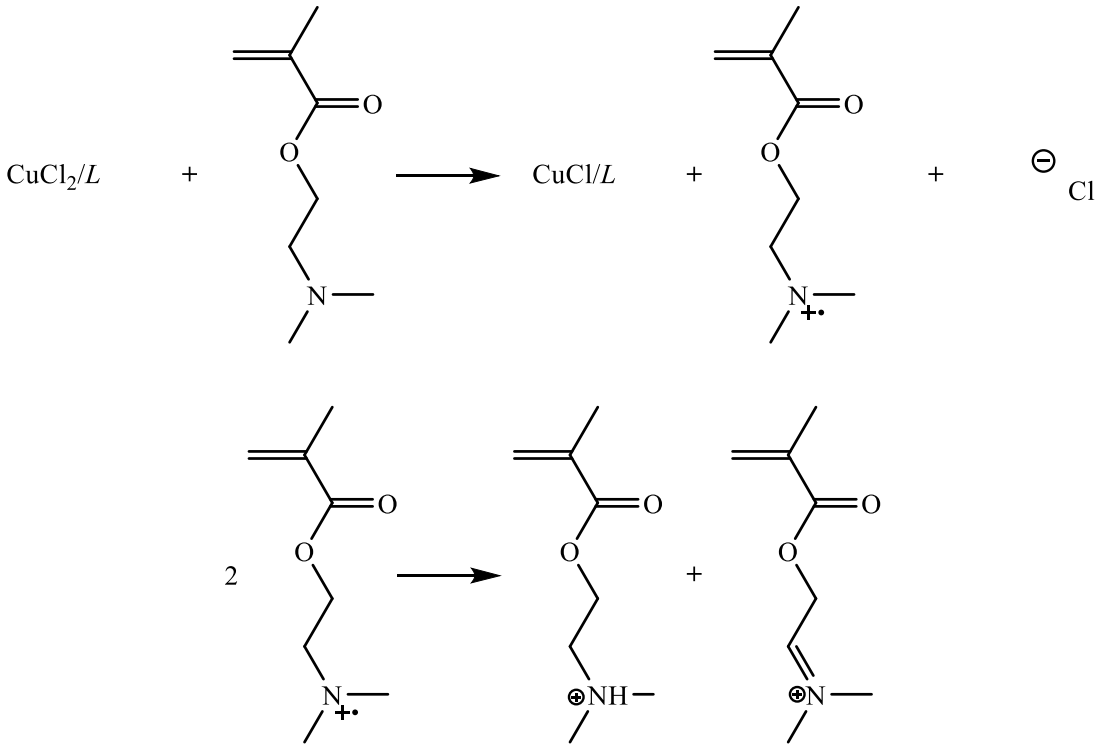

Scheme 4.5. Proposed mechanism of reduction of Cu(II)Cl_2/TPMA with DMAEMA. Adapted with permission from H. Dong and K. Matyjaszewski, *Macromolecules*, 2008, **41**, 6868–6870. Copyright (2017) American Chemical Society.

The amount of ligand in the system is an important consideration for AGET or ARGET polymerisations, specifically when utilising monomers that compete for binding sites on the catalyst. Traditional ATRP is typically carried out with 1 or 2 eq. of ligand relative to copper. AGET and ARGET on the other hand commonly use 5 or more eq. of ligand.[20,22] Excess ligand serves multiple purposes; firstly, to facilitate a higher rate of complexation to the catalyst and thus a higher concentration of active catalyst in solution. Therefore, the excess ligand helps to negate the effects of competitive complexation to the catalyst by the nitrogenous monomer.[21] Secondly, excess ligand must be added to account for ligand lost to protonation via HBr, which is produced as a byproduct of the reduction of Cu(II)Br_2 with ascorbic acid.[18] Thirdly, the excess ligand can serve as a sacrificial

reductant much the way that ascorbic acid does. Thus, the presence of excess ligand aids in scavenging oxygen from the polymerisation reaction. However, too much ligand can be detrimental to the controlled nature of polymerisation. If excess ligand reduces too much Cu^{II} to Cu^{I} the rate of polymerisation will be too high, resulting in a loss of control. The right balance of ligand, copper, and external reducing agent must be identified experimentally.

Herein, AGET and ARGET methods for ATRP of DiPAEMA were developed in pursuit of synthesising CO_2-responsive surfaces. The molecular weight and dispersity of the grafted-polymer was approximated by characterising free polymer that was produced in situ during *grafting from* reactions. Reagent ratios that provided narrowly distributed molecular weights with high conversion were identified. Tris(2-pyridylmethyl)amine (TPMA), an ATRP ligand, and $Sn(EH)_2$, a commonly used reducing agent, were determined to be incompatible with silica particles. CO_2-responsive surfaces were created using newly developed AGET ATRP conditions and evaluated for the drying of wet isobutanol.

4.3 Results and discussion

4.3.1 CO_2-responsive polymers on spherical silica particles: investigation of particle size and morphology

In Chapter 3, CO_2-responsive polymer-grafted silica particles (RP) were demonstrated to be suitable supports for ruthenium nanoparticles (RuNP). The smart catalyst (RuNP@RP) responded to CO_2 as a stimulus, altering the selectivity of the catalytic hydrogenation of furfural.

It is plausible that the selectivity could be improved if the stimuli-response was more pronounced. Additionally, the lifetime and reusability of the smart catalyst could be improved by changing the size and morphology of the silica particle.

The particle size and morphology of the silica substrate are essential parts of the overall picture when designing a functional support for heterogeneous catalysts. The particle size can directly influence the polymer grafting density,[23] the amount of polymer-grafted, the application in which the material is best suited, the ease of use, the ease of recovery, and the lifetime of the material. Various particle sizes and morphologies were investigated as a means of improving the performance of the CO_2-responsive polymer-grafted silica particles.

The first generation polymer-grafted silica particles were difficult to handle and difficult to characterise because the silica particles accumulated static charge. The ease of use of these materials was poor and attempts to rectify that were undertaken. Initial *grafting from* experiments utilised the most readily available silica source available at the time, which was SiliaFlashP60. SiliaFlashP60 is an irregular silica particle that varies in

size from 40-63 μm (60 Å pore size); PGS-7, and by extension, RuNP@RP were created from SiliaFlashP60. During experimentation, the RuNP@RP material was consistently lost during mass transfer steps such as catalyst loading and subsequent recovery post reaction. It was observed that the smaller the silica particles are, the more prone they are to accumulating static charge.

The accumulation of static charge on the material not only causes mass loss during transfer steps but it causes difficulties with more advanced characterisation techniques such as XPS and SEM. The static charge that builds up on the surface of the material decreases the amount of incident electrons landing on the specimen, thereby decreasing the amount of secondary electrons that are emitted by the sample and available for detection. Deteriorating the signal in this manner often results in a poor quality image and low-resolution spectra.

A larger spherical particle was employed to avoid static charging. For PGS-17, spherical silica particles (SiO_2 #3, Silicycle, 200-500 μm particle size, 500 Å pore size) were utilised as the support for the CO_2-responsive polymer. It was observed that when the particles are wet, they are easily transferred and collected. However, when dry, the particles are still prone to static charging and mass loss during transfer and collection becomes unavoidable. Therefore, we can conclude that static charging is reduced but not eliminated by using larger spherical particles.

The switch to spherical particles did not completely solve the static charging problem, but it did offer another variable to experiment with: the pore size. Spherical particles are available in a variety of particle and pore sizes, whereas early experiments

with irregular silica had one pore size (100 Å). Future experimentation will allow various particle sizes to be explored and characterised via BET N_2 sorption analysis.

The switch to spherical particles, while intrinsically valuable with regards to being able to vary the particle specifications, came with a variety of challenges. Firstly, the spherical particles are not robust enough to withstand the mechanical forces generated by impact with a magnetic stir bar. Although it was unknown at the time, this was an inherent advantage of using SiliaFlashP60 (PGS-1 to PGS-7). The particles, being irregular in shape and having a solid core, are resistant to further degradation from mechanical forces, such as the impact force generated from a stir bar at 800 revolutions per minute (RPM). Initial attempts at using CO_2-switchable spherical particles (PGS-8 & PGS-9) resulted in poor results when employed in the same fashion as PGS-7 in the RuNP@RP experiment; the spherical particles failed to change the selectively of the catalyst (unpublished work). The synthesis of the spherical RP and the RuNP@RP experiment both mechanically degraded the spherical silica particle. Degradation of the silica particle resulted in a sporadic deposition of RuNPs, thus reducing polymer to RuNP contact. The resultant material performed similar to RuNP on silica. The RuNP@RP experiment can be easily done via shaking, thus avoiding the issue of mechanical degradation via impact with the magnetic stir bar (Chapter 3, Table 3.3).

The polymer-grafting step is not as forgiving and it is essential to have adequate mixing to achieve a controlled ATRP. A variety of SI-AGET-ATRP experiments have been run with various substrates including cellulose particles, silica particles, silicon wafers, and cotton fabric; the minimum recommended stir rate varies with the substrate. For example, all AGET-ATRP homopolymerisations were carried out with a minimum stir

rate of 800 RPM using a magnetic stir bar (Chapter 4, KBB9PG8, PDiPAEMA, M_n: 111 kDa, Đ: 1.17). Adequate mixing for an SI-AGET-ATRP from a silicon wafer is achieved at roughly 600 RPM (Chapter 5, KBB9PG82, M_n: 39.6 kDa, Đ: 1.17); higher RPM often results in a damaged substrate. In contrast, adequate mixing for silica particles is much higher; commonly 900 RPM is necessary to keep the silica particles dispersed throughout the solution (Chapter 4, KBB9PG14, M_n: 42.8 kDa, Đ: 1.27). Interestingly, a recent report suggested that stirring, when conducting a SI-ATRP from a silicon wafer, results in early chain termination for surface bound chains.[24] The study found that when the polymerization was not stirred, the grafted-polymer layer was thicker than when the polymerization was stirred. Additionally, the study concluded that this observation was not applicable to particle/colloidal substrates, owing to the fact that constant stirring is required to keep the substrate dispersed in solution. Inadequate mixing in an SI-ATRP leads to lower grafting densities on the material and a greater disparity between the free polymer and the grafted polymer. At the suggestion of the industrial partner on this project, Bruce Richter of Agilent Technologies, overhead stirring replaced mechanical stirring for all subsequent SI-ATRP reactions utilizing particulate substrates (Figure 4.1).

Figure 4.1. Experimental setup, utilising the overhead stirring device, for SI-AGET-ATRP for the synthesis of CO_2-responsive polymer-grafted spherical silica particles.

Kunqiang Jiong, also of Agilent Technologies, suggested that the Piranha solution pretreatment (cleaning and hydroxylation of silica particle) may be too aggressive for spherical silica and the particle integrity is likely being damaged by subsequent treatments of acid and base piranha solutions. In place of piranha solutions, the following pretreatment method was suggested: stir silica particles in 1 M hydrochloric acid, 50 °C, 4 h. Adjust solution back to neutral pH with ammonium hydroxide, collect silica via filtration, and wash with water multiple times (henceforth referred to as "Agilent method").

To ensure that particles were not being degraded via either mechanical or chemical means, the particle pore size was monitored by collecting N_2 sorption isotherms at various stages during material synthesis and use. The BET method is commonly used to determine the surface area and pore size of a porous material.[25–27] With this information, the particle

integrity can be monitored at various points during a synthesis to evaluate whether significant degradation has occurred. To determine changes in particle integrity, both the N_2 adsorption/desorption isotherms (Figure 4.2) and the pore size distributions (Figure 4.3) were collected and monitored for change. SiO_2 #1 (Silicycle, 200-500 μm particle size, 100 Å pore size) was tested "as is" from the manufacturer (S1-1) and plotted against SiO_2 #1 pretreated with Agilent method (S1-2), and SiO_2 #1 that was pretreated by Agilent method and grafted with the ATRP initiator 2-bromo-2-methylpropionyl bromide (S1-3). The BET specific surface area of each sample was determined to be 303 m^2g^{-1} (S1-1), 285 m^2g^{-1} (S1-2), and 287 m^2g^{-1} (S1-3).

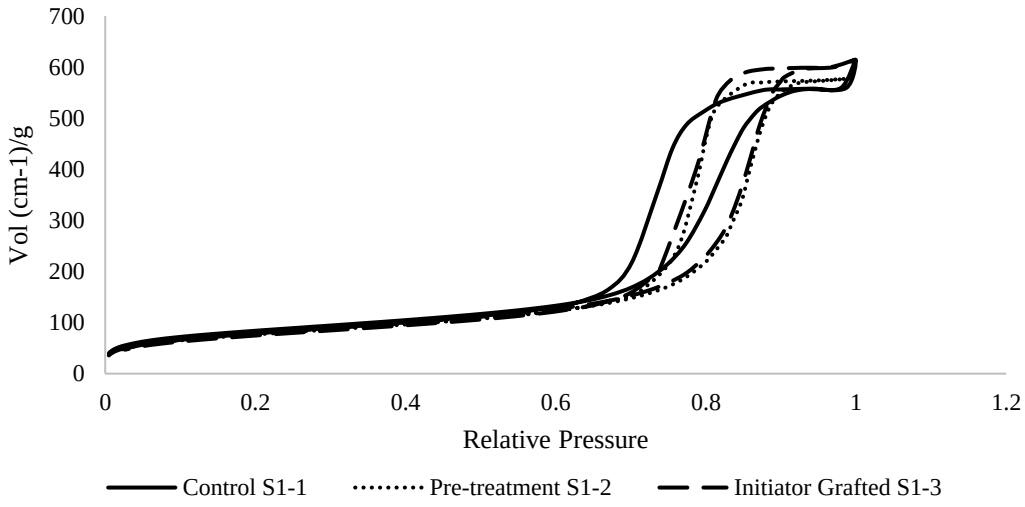

Figure 4.2. Combined N_2 adsorption/desorption isotherms of spherical silica (200-500 μm, 100 Å, SiO_2 #1).

The pore size distributions reached a maximum value at 100 Å (S1-1), 138 Å (S1-2), and 138 Å (S1-3).

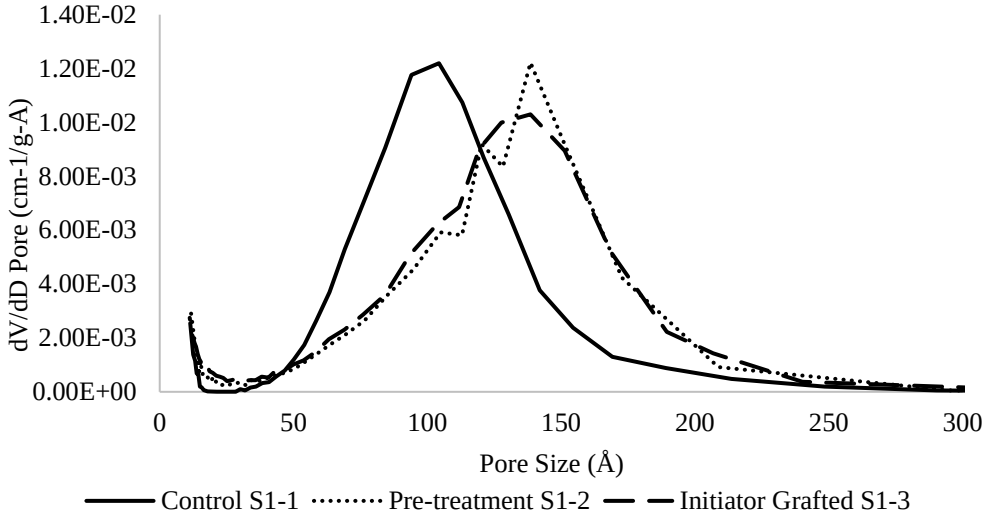

Figure 4.3. Combined pore size distributions for spherical silica, 200-500 μm, 100 Å (SiO_2 #1), as determined by N_2 adsorption/desorption isotherms.

As a result of the pretreatment, the pore size got larger by ca. 38% and the BET specific surface area got smaller by ca. 6%. Acidic or basic treatments are expected to increase pore size via silanol hydrolysis. As the pore size increases, a decrease in BET specific surface area is also expected. Subsequent grafting of the initiator did not change the pore size or BET surface area significantly. The results of the pretreatment method were expected; since they are minor deviations, they are of little cause for concern. Subsequent experimentation, as shown by the initiator-grafting step, causes no significant change in either the pore size distribution or the BET specific surface area. Particle integrity was maintained within reasonable expectations. The Agilent recommended pretreatment and the experimental setup utilising the overhead stirring device are therefore

suitable for the synthesis of CO_2-responsive particles; they were used exclusively for the reaming experiments with grafting PDiPAEMA from silica particles.

4.3.2 CO_2-responsive polymers on spherical silica particles: investigations of AGET and ARGET for O_2 tolerance

The overhead stirring method was determined to be mechanically sound and with its use, the destruction of particles was avoided. However, the reagents and solvents must be added to the reaction flask before the stir shaft is lowered into place. Thus, the reaction flask contained a significant amount of oxygen, whether gaseous or dissolved. Henceforth, traditional ATRP methods and overhead stirring were deemed incompatible with the resources at hand.

The inspiration for traditional ATRP methodology came from literature,[2] lab expertise, and past successes.[30] As mentioned previously, one of the challenges of using DMAPMAm was that the polymer properties (M_n and Đ), as well as reaction conversions, were not able to be determined with the available equipment. Switching to DiPAEMA solved all of the characterisation challenges and Table 4.1 represents the first instance in which conversion and molecular weight were successfully measured for CO_2-responsive polymer-grafted materials using traditional ATRP, and the first experiments with ARGET-ATRP of DiPAEMA.

Table 4.1. Various reagent combinations explored for ATRP of DiPAEMA.

	ATRP Type	Reducing Agent	Catalyst	[Cu] ppm	% Conv.	Time (h)	M_n[c] (kDa)	Đ
1	Traditional KBB8PG7	-	Cu(I)Br PMDETA	1600	53	18	-	-
2	SI-Traditional PGFP-5 (Ch.6)	-	Cu(I)Br PMDETA	560	-	51	42.5	1.38
3	ARGET KBB8PG15	ascorbic acid	$Cu(II)Cl_2$ TPMA	17	-	96	15.3[a] 9.4[b]	1.19[a] 5.64[b]
4	ARGET KBB8PG37	ascorbic acid	$Cu(II)Cl_2$ TPMA	17	-	-	10.7	1.34

[a]Indicates these values are associated with each other. [b]Indicates these values are associated with each other. [c]Determined by GPC in tetrahydrofuran (THF), based on poly(methylmethacrylate) (PMMA) equivalents. All reactions were carried out at a constant temperature [ascorbic aicd]:[Cu] was 15:1.

Entry 1 represents a typical result that was observed with the polymerisation of DiPAEMA using traditional ATRP: 53% conversion in 18 h. Entry 2 is the first instance of grafting DiPAEMA from a surface; in this case, it was a cellulosic substrate (Whatman type 1 filter paper, 42.5 mm, PGFP-5, Ch.6). Surface-initiated polymerisations usually require a significantly greater volume of solvent than the corresponding homopolymerisation; this is attributed to the need to submerge the substrate in the polymerisation solution. Thus, the [Cu] of entry 2 is significantly lower than that of entry 1, despite the equivalents of all reagents other than the solvent being the same. Methanol is routinely used in literature as a solvent for ATRP of DiPAEMA.[2,3] However, it was observed that significant amounts of PDiPAEMA precipitate out methanol when M_n>15 kDa. Since the goal is to graft narrowly distributed PDiPAEMA onto a substrate, the polymer absolutely must remain soluble at all molecular weights. Thus, methanol is not a suitable solvent and was replaced with anisole (Appendix III).

Drawing inspiration from literature,[19] ARGET-ATRP was applied to DiPAEMA in anisole. (Table 4.2).

Table 4.2. Various reagent combinations explored for ARGET ATRP of DiPAEMA.

	ATRP Type	Reducing Agent	Catalyst	[Cu] ppm	% Conv.	Time (h)	M_n[b] (kDa)	Đ
1	ARGET KBB8PG45-1	$Sn(EH)_2$	$Cu(II)Cl_2$ TPMA	120	89	19	10.3	1.99
2[a]	ARGET KBB8PG45-2	d-Toluene $Sn(EH)_2$	$Cu(II)Cl_2$ TPMA	130	93	26	-	-
3	ARGET KBB8PG49	$Sn(EH)_2$	$Cu(II)Cl_2$ TPMA	80	40	46	-	-
4	SI-ARGET PGS-10	$Sn(EH)_2$	$Cu(II)Cl_2$ TPMA	80	61	72	19.3	2.5
5	SI-ARGET PGS-11	$Sn(EH)_2$	$Cu(II)Cl_2$ TPMA	120	65	67	20.7	2.59

[a] Reaction carried out in d-tolune at 40 °C, all other reactions were carried out at a constant temperature of 40 °C in anisole. [b]Determined by GPC in tetrahydrofuran (THF), based on poly(methylmethacrylate) (PMMA) equivalents. Conversion determined by ^{1}H NMR spectroscopy. Where $[Sn(EH)_2]$:[Cu] was 100:1.

When the reducing agent to copper ratio was reduced to 100:1; almost identical conversion was achieved with PDiPAEMA (entry 1) as was reported for PDMAEMA (90% conv., 18 h, M_n: 61.5 kDa, Đ: 1.35).[19] However, the molecular weight and dispersity for PDiPAEMA (entry 1) were considerably less impressive than that reported for PDMAEMA.

The development of an ARGET method for DiPAEMA was particularly challenging owing to the very small amount of reagents that are called for when running small scale test reactions. To further complicate the process, the full amount of copper in an ARGET-ATRP process is not fully dissolved at any one time; this makes the use of a stock solution of catalyst cumbersome and likely to lead to irreproducible results. Catalyst

stock solutions were used for NMR monitoring experiments (Figure 4.4) and the results were successful, but challenging to reproduce (Table 4.2. entry 2).

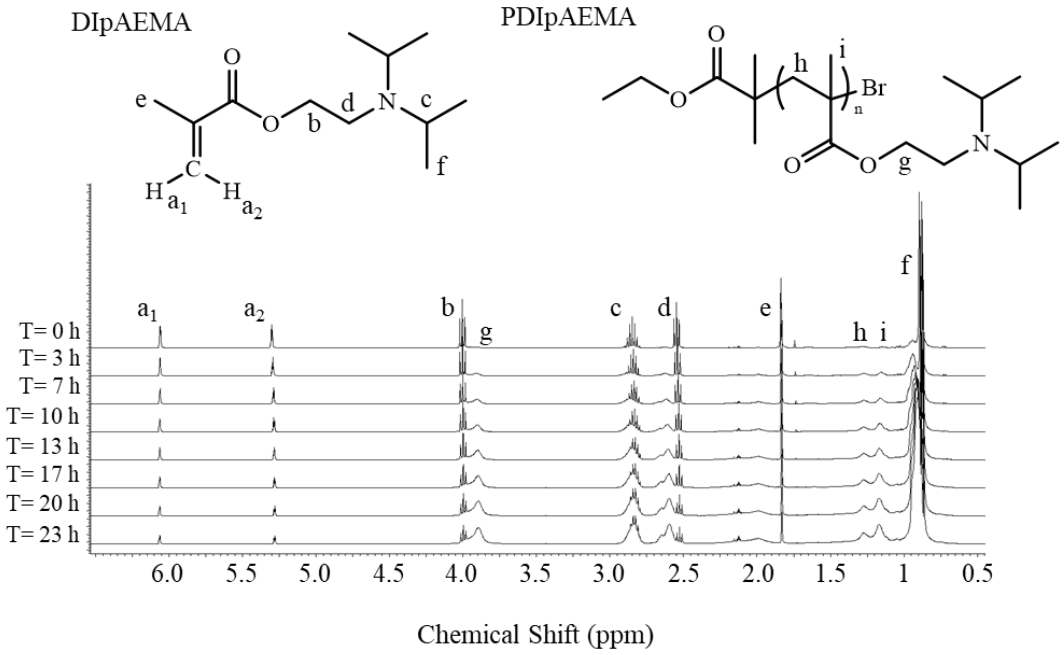

Figure 4.4 ^{1}H NMR monitoring of an ARGET-ATRP of DiPAEMA, KBB8PG45-2 (entry 2, Table 4.2).

As seen in Figure 4.4, it takes ca. 3 h before an appreciable polymer signal appears in the ^{1}H NMR spectrum. The peak at 4.0 ppm is the ester –CH_2- of the monomer (peak b); as the monomer is polymerised, this -CH_2- peak shifts slightly upfield and broadens considerably (peak g). By comparing the integration of the vinyl peaks (peak a_1 and a_2, ca. 6.16 or 5.27 ppm) to the combined ester –CH_2- peaks (peaks b and g, ca. 3.8 to 4.2 ppm) the monomer conversion can be approximated.

Further modification of ARGET reaction conditions led to variable but acceptable results and a surface-initiated grafting reaction was attempted on silica particles. PGS-10

and PGS-11 (Table 4.2, entries 4 and 5) reached modest conversions with almost identical molecular weight and dispersity despite PGS-11 using half of the solvent that PGS-10 did.

However, after considerable investigation it was determined that the ligand (TPMA) was selectively binding to the silica particles (Appendix III). XPS analysis of each sample of PGS-11, showed a bimodal distribution for the peak area in the high-resolution N1s core-level spectrum. In their study of maghemite nanoparticles, Prado et al. attributed a 404 eV peak in the N1s core-level spectrum to a tetramethylammonium (TMA^+) cation.[31] Similarly, the XPS results for PGS-11 could be explained by a cationic TPMA-H^+, with the silica substrate (Si-O^-) forming the anion. Thus, TPMA was replaced as the ligand of choice for further studies.

TPMA is considered to be a highly active ligand for ATRP, as such, it is commonly paired with Cu(II)Cl_2. Cu(II)Cl_2 is a less active copper source owing to the strength of the copper chloride bond. Upon replacing TPMA with PMDETA, which is less active than TPMA, the copper metal source was changed to Cu(II)Br_2. The halide bond in Cu(II)Br_2 is more labile than that of Cu(II)Cl_2 and therefore more reactive in ATRP. The increased reactivity of Cu(II)Br_2 serves to accommodate the use of a less active ligand.[28] Moving forward with reaction screening, the choice was made to switch from ARGET (low levels of Cu) to AGET (500+ ppm of Cu) in hopes of decreasing reaction time by incorporating more catalyst. A shown in Table 4.3, the switch to AGET ATRP produced immediate results as the rate of polymerisation increased drastically.

Table 4.3. Various reagent combinations explored for AGET ATRP and SI-AGET ATRP of DiPAEMA using $Sn(EH)_2$ as a reducing agent.

Entry	ATRP Type	Reducing Agent	Catalyst	[Cu] ppm	% Conv.	Time (h)	M_n[e] kDa	Đ
1	AGET KBB8PG67	$Sn(EH)_2$	$Cu(II)Br_2$ PMDETA	1100	68[a] 77[b]	1.5[a] 5.0[b]	-	-
2	AGET KBB8PG71-R1	$Sn(EH)_2$	$Cu(II)Br_2$ PMDETA	1100	82	18	15.8	1.79
3	AGET KBB8PG71-R2	$Sn(EH)_2$	$Cu(II)Br_2$ PMDETA	490	67	18	-	-
4	AGET KBB8PG75	$Sn(EH)_2$	$Cu(II)Br_2$ PMDETA	1100	64[c] 66[d]	4.0[c] 21[d]	16.3	1.75
5	AGET PGS-12	$Sn(EH)_2$	$Cu(II)Br_2$ PMDETA	1100	-	24	9.4	1.34
6	SI-AGET PGS-13	$Sn(EH)_2$	$Cu(II)Br_2$ PMDETA	1100	61	20	9.8	2.20

[a]Indicates these values are associated with each other. [b]Indicates these values are associated with each other. [c]Indicates these values are associated with each other. [d]Indicates these values are associated with each other. [e]Determined by GPC in tetrahydrofuran (THF), based on poly(methylmethacrylate) (PMMA) equivalents. All reactions were carried out a constant temperature of 40 °C in Anisole. Conversion determined by ^1H NMR spectroscopy. Where $[Sn(EH)_2]$:[Cu] was 100:1.

Various solvent volumes were tested to determine the effect that the volume of solvent had on conversion and whether increasing solvent volume would still facilitate a moderately successful polymer-grafting reaction to a silica particle substrate. From the analysis of entries 1-3, it is clear that the higher [Cu], >1000 ppm, facilitated high conversions in under 5 h. This marked a significant improvement over previous experiments in which the polymerisation took days to reach comparable conversions. Entry 5 (PGS-12) was run as a control reaction to probe whether the presence of silica particles was detrimental to the polymerisation, similar to that which occurred with TPMA in PGS-10 and PGS-11. The PDiPAEMA sample collected from entry 5 agreed well with theoretical M_n predictions and exhibited an acceptable M_n dispersity of 1.35. It is fair to say the silica particles did not

interact significantly with any of the reagents in the AGET-ATRP, at least not to the extent such that the interaction was detrimental to the controlled nature of the polymerisation.

Complications were observed in SI-AGET-ATRP reactions (Table 4.3, entry 6, PGS-13) that were not observed during the AGET-ATRP of PDiPAEMA homopolymers. After precipitation, a close examination of the remaining solids from PGS-13 revealed two material types, the polymer-grafted silica particles and another white solid. After IR analysis, the unknown solid is believed to be the reducing agent $Sn(EH)_2$ in its various oxidised states. To resolve the possible confusion and to avoid issues with the characterisation of the polymer-grafted particles, $Sn(EH)_2$ was replaced with L-ascorbic acid for future experimentation. The switch to L-ascorbic acid (Table 4.4 entry 1) yielded the best results reported as of this date, with PDiPAEMA homopolymer having a M_n of 111 kDa and a Đ of 1.17.

Table 4.4. Various reagent combinations explored for AGET ATRP and SI-AGET ATRP of DiPAEMA using L-ascorbic acid as a reducing agent.

Entry	ATRP Type	Reducing Agent	Catalyst	[Cu] ppm	% Conv.	Time (h)	M_n[a] kDa	Đ
1	AGET	ascorbic acid	$Cu(II)Br_2$ PMDETA	1300	-	16	111	1.17
2	SI-AGET PGS-15	ascorbic acid	$Cu(II)Br_2$ PMDETA	1300	-	16	42.9	1.27
3	SI-AGET PGS-16	ascorbic acid	$Cu(II)Br_2$ PMDETA	1300	-	16	51.7	2.20
4	SI-AGET PGS-17	ascorbic acid	$Cu(II)Br_2$ PMDETA	1300	-	16	29.4	1.77

[a]Determined by GPC in tetrahydrofuran (THF), based on poly(methylmethacrylate) (PMMA) equivalents. All reactions were carried out a constant temperature of 40 °C in Anisole. Conversion determined by ^1H NMR spectroscopy. Where [ascorbic acid]:[Cu] was 15:1.

The GPC traces from various SI-AGET-ATRP *grafting from* reactions are shown in Figure 4.5. PGS-15 was grafted from irregular silica particles, whereas the rest were grafted from spherical silica particles. PGS-16 suffered from material degradation owing to poor placement of the stirring shaft during synthesis. These GPC traces serve to highlight the improvements in molecular weight dispersity as the SI-AGET-ATRP methodology evolved. The molecular weight dispersity is narrower when *grafting from* irregular particles (PGS-15, Đ: 1.27) than it is from spherical particles (PGS-17, Đ: 1.77).

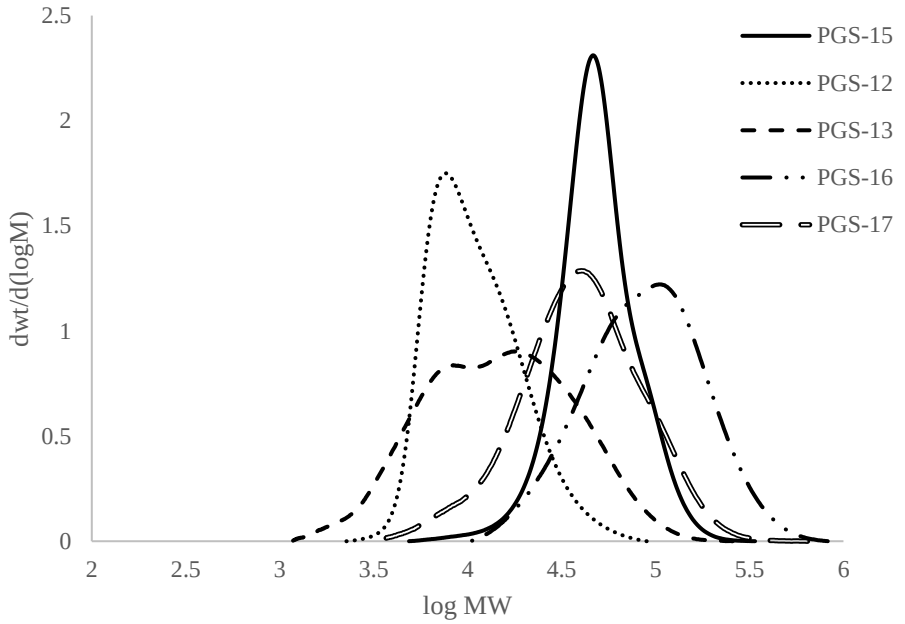

Figure 4.5. GPC traces of PDiPAEMA homopolymers produced in situ during surface-initiated polymerization from various types of silica particles.

Further experimentation sought to build on the success of experiment AA-1 (DiPAEMA homopolymerisation, Table 4.4, entry 1) by grafting PDiPAEMA from various substrates in a controlled manner (Figure 4.6). Those substrates included irregular silica particles (PGS-15, Đ: 1.27, M_n: 42.8 kDa, Table 4.4, entry 3), spherical silica particles (PGS-17, Đ: 1.77, M_n: 29.4 kDa, Table 4.4, entry 4), silicon wafers (SiO_2-S18, Đ:

1.17, M_n: 39.6 kDa, Chapter 5), and cotton fabric (PGC-1, Đ: 1.25, M_n: 55.6 kDa, Chapter 6). PGS-15 and PGS-17 were sent to our collaborators, Mr. Sami El Sayed, supervised by Dr. Kylie Luska and Prof. Walter Leitner at RWTH Aachen, Germany, to further investigate CO_2-responsive polymer-grafted silica particles and their applicability as supports for RuNP in the next generation RuNP@RP.

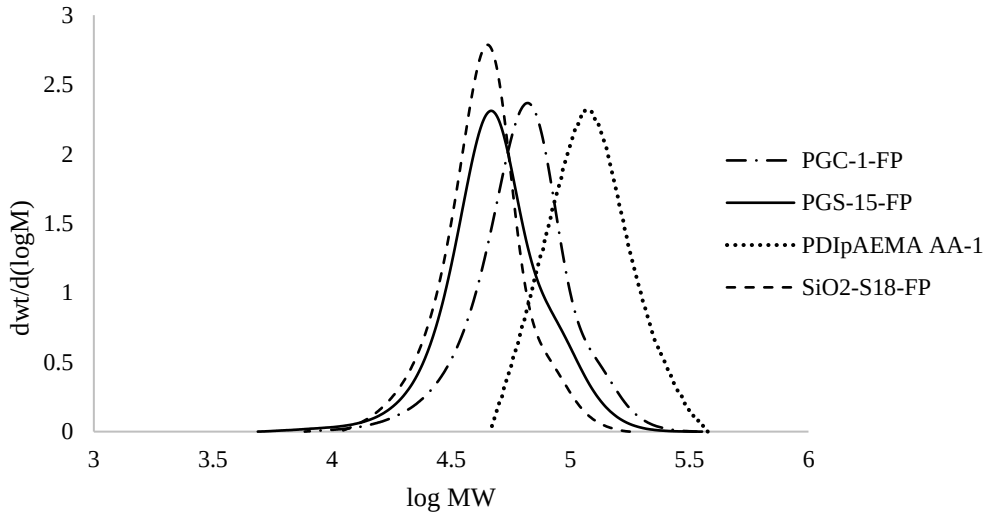

Figure 4.6. GPC traces of PDiPAEMA as polymerised: PGC-1-FP (cotton fabric), PGS-15-FP (irregular silica particles), AA-1 (homopolymer), SiO_2-S18 (silicon wafer).

4.3.3 Activation of SI-AGET/ARGET ATRP

Controlling the initial activation and the final deactivation of the polymerisation is a challenging and often futile pursuit for AGET or ARGET ATRP, owing to the multitude of equilibria that are dependent on the Cu^I to Cu^{II} ratio in solution. Advanced ATRP methods such as eATRP have elegantly addressed this challenge using an electric current. Applied current either forces the metal to an active or an inactive state, thus providing absolute control over the polymerisation.[14] AGET and ARGET ATRP will, in theory,

remain dormant until the external reducing agent is added. Once the reducing agent is added there is a period, often an hour or two, in which the inactive metal oxides are reduced in situ and the dissolved or gaseous oxygen is removed. Not much can be done to control the length of time it takes for the oxygen to be removed and the polymerisation to become fully active since the concentration of dissolved or gaseous oxygen is variable. Thus, precise monitoring of a SI-ARGET or SI-AGET ATRP is challenging and was not achieved in this work.

While experimenting with ARGET-ATRP and various reagent ratios, a chance mistake led to an interesting observation. The goal of the experiment was to determine the effect that different ligands have on the polymerisation. N,N,N′,N″,N″-pentamethyldiethylenetriamine (PMDETA) and tris(2-pyridylmethyl)amine (TPMA) were selected because they are commonly used for traditional ATRP; their differences are well studied and have been reported previously.[28,29] In this instance, two reactions, where all thing being equal except the ligand, were to be started and monitored in unison. The two reactions were prepared and started at the same time by simultaneous injection of the reducing agent to both reaction flasks. However, an oversight occurred and the ligand (PMDETA) was not added to reaction 1 until 12 h after the reactions had been started. Interestingly, no conversion was noted during that 12 h period and it was not until after PMDETA was added that the polymerisation in reaction 1 began. In contrast, reaction 2 was at 61% conversion by the 12 h mark (Table 4.1). This observation implies that the reaction can, in fact, be "started" when intended, without the ambiguity associated with the dormant period where dissolved and gaseous oxygen are slowly being removed by the reducing agent. Therefore, the addition of ligand, if added

after a period in which dissolved and gaseous oxygen are removed, can be used to precisely control the activation of the polymerisation.

Table 4.5. Ligand effects on ARGET-ATRP of DiPAEMA.

KBB8PG66	Ligand	Conv.% (12 h)	Conv.% (15 h)	Conv.% (21 h)
Reaction 1	PMDETA (0.35 eq.)[a]	0.0[b]	74	78
Reaction 2	TPMA (0.25 eq.)[a]	61	62	-

[a]Conditions: DiPAEMA/EBIB/$Cu(II)Br_2$/Ligand/Anisole/$Sn(EH)_2$: 117/1/0.05/L/270/5, 40 °C. [b]PMDETA was added to reaction 1 after 12 h had passed. Conversion determined by ^1H NMR spectroscopy.

The data in Table 4.5 might be misleading if not interpreted correctly; one interpretation of the data might lead to the conclusion that the reaction with PMDETA is considerably faster (74% conv., 3 h) than the reaction with TPMA (61% conv., 12 h). This interpretation is incorrect; the reaction with PMDETA is not faster than the reaction with TPMA. Table 4.5 provides inadequate information to compare reaction rates. However, it is known that TPMA gives a higher rate of activation than PMDETA.[28] What the table fails to address are the underlying equilibria that must occur before the polymerisation begins, such as the complex set of equilibria that are responsible for the complexation of dissolved and gaseous oxygen to the external reducing agent. Another interpretation of this data is that reaction 1 appears to reach a high conversion quickly because dissolved and gaseous oxygen has been removed. Thus, all the system required was the ligand to form the active catalyst such that the polymerisation could begin. A third interpretation of this data is that both reaction 1 and reaction 2 are fast and that the sampling intervals did not occur early enough to monitor the polymerisation. While the last interpretation is most likely, it is hard to say with certainty which is correct. Future work can exploit this finding

to enable precise monitoring of the polymerization by ensuring that oxygen is scavenged from the reaction before the ligand is added, thus allowing the activation of the polymerization at the users descretion.

4.3.4 CO_2-responsive polymers on spherical silica particles: investigation of active chain ends

Polymers prepared by ATRP have active chain-ends that can be used for chain extension or further functionalisation, thus allowing for the preparation of copolymers, supramolecular architectures, and bioconjugates.[1,14,32] Not only are active chain-ends necessary for further functionalisation but they are an important measure of the success of the polymerisation. A polymerisation that results in a low fraction of active chain-ends would likely have a broad molecular weight distribution owing in large part to early termination events causing significant amounts of dead polymer chains. For reasons mentioned previously, broad molecular weight distributions are unwanted and can be considered an indicator of a poorly controlled polymerisation. A polymerisation with a high fraction of active chain-ends would likely have a narrow molecular weight distribution.

To probe the degree of chain-end functionality that remains present on polymer-grafted silica particles, a batch of PDiPAEMA-grafted silica particles (Scheme 4.6, PGS-15, 4-3) was subjected to subsequent SI-AGET-ATRP with styrene (Scheme 4.7). In this experiment, the PDiPAEMA-grafted silica particles act as a large macroinitiator from which styrene will polymerise, or with which free polystyrene (PS) will combine via radical termination or radical disproportionation.

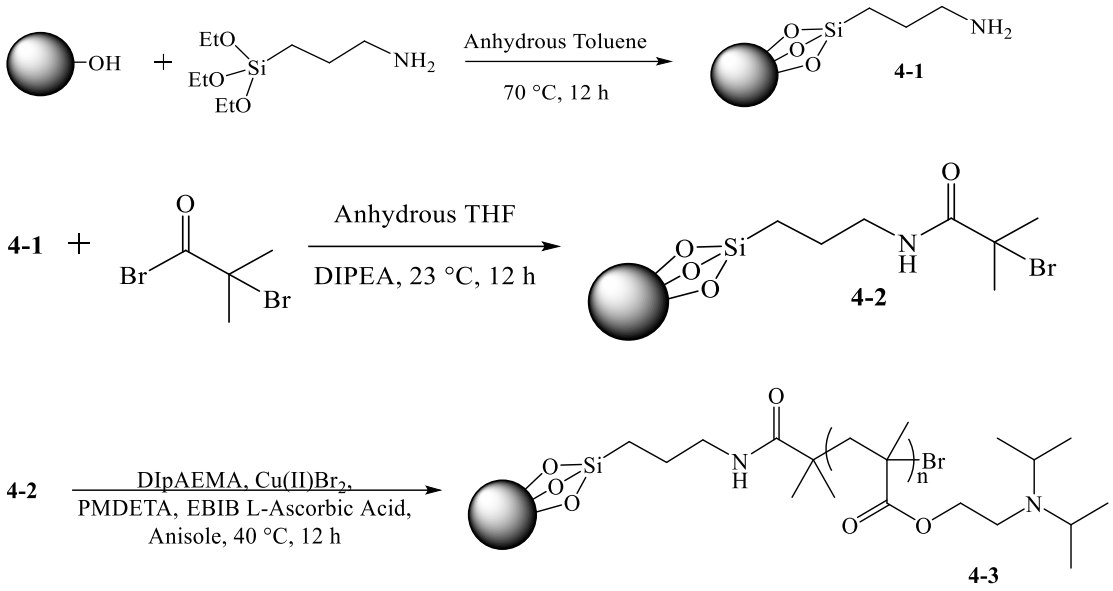

Scheme 4.6. The synthesis of PGS-15 (4-3**)**.

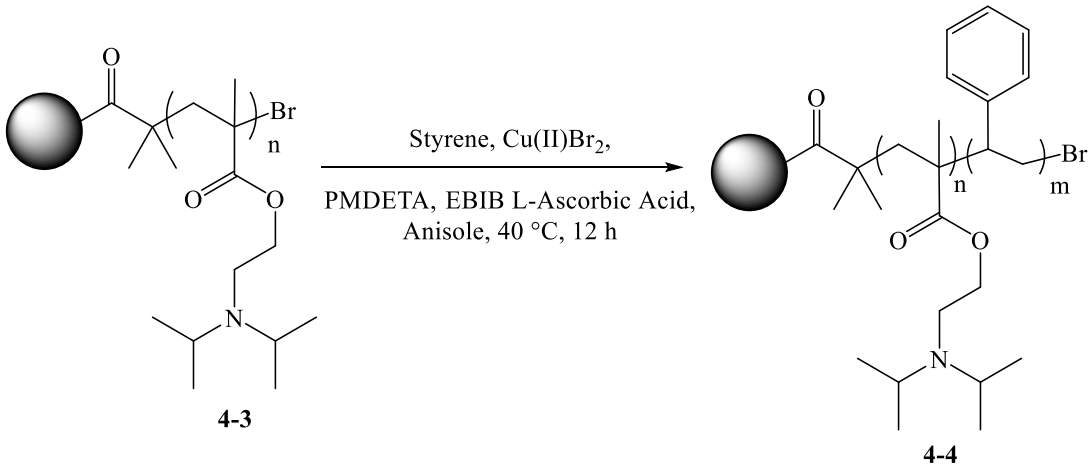

Scheme 4.7. Chain extension of PGS-15 (4-3) with PS to yield PGS-15-EXT-PS (4-4).

^{13}C CP-MAS NMR spectroscopy was used to identify whether PS had been grafted to PGS-15. In Figure 4.7 (PGS-15) the strong carbonyl shift of PDiPAEMA is visible at 176 ppm and there are no noticeable shifts between 100-170 ppm. In Figure 4.8 (PGS-15-EXT-PS) the strong carbonyl shift of PDiPAEMA is visible, as are multiple aromatic peaks at 145 ppm and 127 ppm, henceforth attributed to PS. Since PGS-15-EXT-PS contains PS, the grafted polymer must be a block copolymer of PDiPAEMA-co-PS. Therefore, PGS-15 must have contained active chain-end functionalities. No meaningful changes were observed between the ^{29}Si CP-MAS NMR spectra of PGS-15 and PGS-15-EXT-PS, which further bolsters the evidence for the successful SI-AGET-ATRP of PDiPAEMA on silica particles.

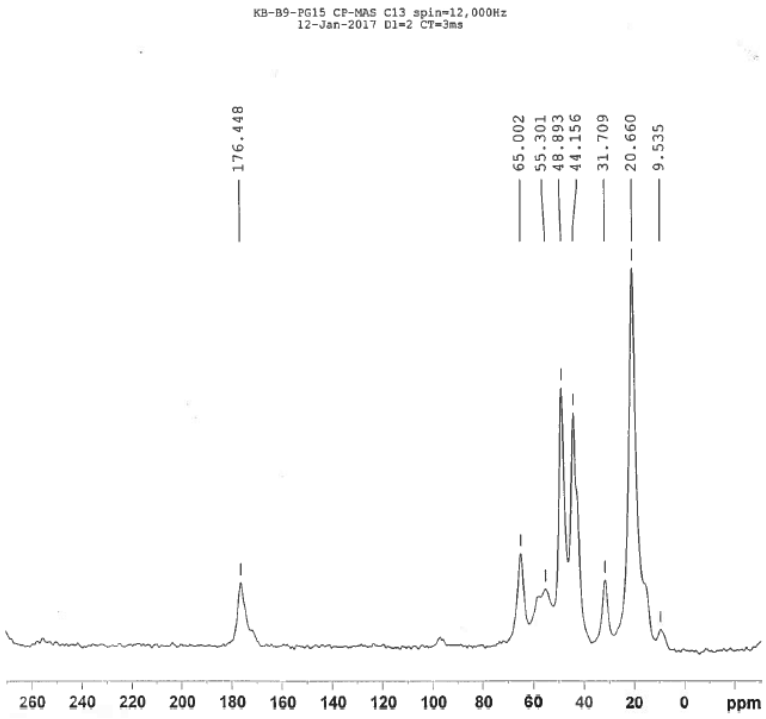

Figure 4.7. ^{13}C CP-MAS NMR spectrum of PGS-15 (4-3).

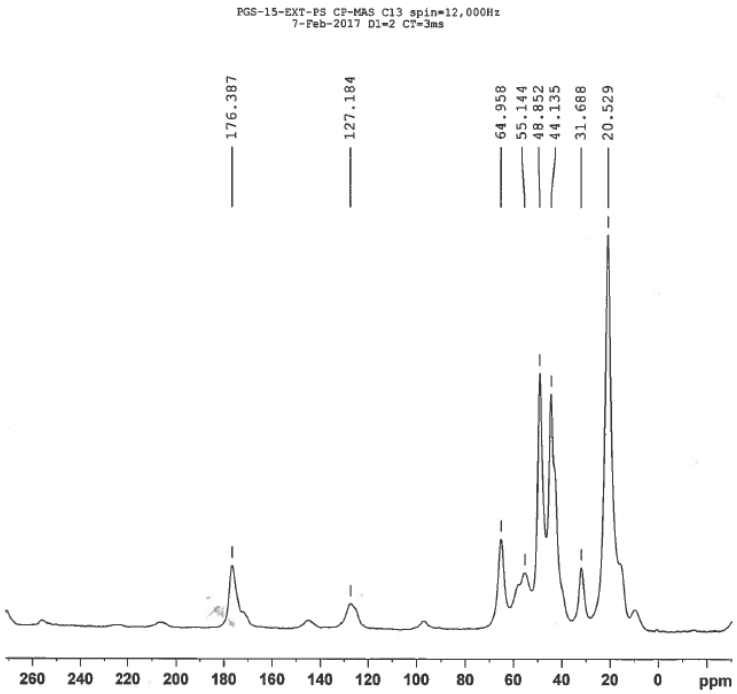

Figure 4.8. ^{13}C CP-MAS NMR spectrum of PGS-15-EXT-PS (4-4).

4.3.5 SI-AGET-ATRP for CO_2-responsive polymers: the workup

The method for the separation and isolation of the free polymer and the polymer-grafted substrate varied considerably over the course of this research. The variations will be evident from the experimental section, in which each experiment is documented in detail. The workup procedure depended on whether a substrate was present as well as the nature of that substrate. In *grafting from* reactions on solid substrates such as a silicon wafer or a cotton swatch, the isolation of the substrate from the free polymer is as simple as physically removing the substrate and treating the substrate and the reaction solution as two separate entities, to which each receives further treatment. However, care must be taken when *grafting from* silica particles when $Sn(EH)_2$ is being used as a reducing agent. The particles must be separated from the reaction solution before being introduced to a precipitation solvent. Otherwise the reducing agent and its various oxidised forms

might be mistaken for silica particles, since tin precipitates are indistinguishable from silica particles by eye. Alternatively, if ascorbic acid is being used a reducing agent, no special care is needed for silica particles because ascorbic acid is soluble in the precipitation solution, as described in the following workup for PGS-17.

The recommended workup for PDiPAEMA-grafted silica particles involves two precipitations, the pH for either precipitation solution is $9<pH<11$. In both cases, the pH must be above the pK_{aH} of the polymer such that the polymer is not protonated and is therefore insoluble in water. In the first precipitation, the higher pH is necessary to ensure full solvation of ethylenediaminetetraacetic acid (EDTA). EDTA is necessary to remove any remaining copper from the polymer and or the polymer-grafted substrate.

The recommended workup procedure for CO_2-responsive silica particles is as follows: The reaction setup is dismantled and the contents are poured over a 600 mL glass frit vacuum funnel. The polymer-grafted silica particles are separated from the reaction solution using the vacuum funnel. In cases where the reaction solution is particularly viscous and the separation is proceeding slowly, a small amount of good solvent can be added to speed up the process. THF is recommended as it can be reduced in volume under vacuum much more easily than other good solvents, such as anisole or toluene. The side-arm flask containing the filtrate (i.e. the reaction solution) is removed and stored until it is time to add it to the precipitation solvent.

The polymer-grafted silica particles, which remain in the vacuum funnel, are washed repeatedly with THF, followed by sonication in THF (10 min, three times) to remove any physisorbed polymer. The washed polymer-grafted silica particles are then stirred gently for 1 h in an aqueous solution of EDTA (0.1 M), pH>9, adjusted with NaOH.

The polymer-grafted silica particles are collected via vacuum filtration and washed with distilled water multiple times. The particles are then washed with THF, collected, and dried under reduced pressure at 60 ℃ overnight. The dry particles are then stored under Ar until further use.

If the side-arm flask containing the filtrate (i.e. the reaction solution) has additional THF in it, the solution can be reduced in volume in-vacuo as much as possible before the first precipitation. To produce a pure polymer, two rounds of precipitation are required. Each precipitation serves a specific purpose. The first precipitation solution was chosen to solubilize all parts of the reaction medium except PDiPAEMA. The precipitation solution is a 0.1 M EDTA solution, adjusted to a pH>9 with NaOH. With vigorous stirring and slow addition, approximately 200 mL of the bulk polymer solution is added to 3.5 L of precipitation solution. The solution is left stirring overnight to yield a semi-solid off-white/yellow polymer. The precipitated polymer is collected, pressed dry with a paper towel, and then dissolved in THF. The second precipitation solvent is water adjusted to a pH>9 with NaOH. With very slow stirring and slow addition, approximately 100 mL of the polymer solution is added to 3.5 L of precipitation solvent. The polymer solution precipitates immediately to yield a white solid, which is easily collected from the precipitation solution by hand. The solid polymer is pressed dry with paper towel and then dissolved in THF. THF is removed from the polymer solution in-vacuo to yield a dry PDiPAEMA sample, which is then characterised and stored as needed.

The precipitation events were carried out in 4 L beakers, commonly with large stir bars to provide the mixing. If one has access to an overhead stirring device, its use is highly recommended. The vigorous stir rate achieved with an overhead stirring device

significantly reduces the overall time it takes for the first precipitation event to occur. With the use of an overhead stirring device, the total time for the workup to occur can be reduced from a full day to 2 h.

This workup procedure can be applied to PDMAEMA, PDEAEMA, and PDMAPMAm since each polymer is insoluble in basic water (pH 9 is recommended).

4.3.6 The application of PGS-17 as a CO_2-responsive drying agent for the removal of water from isobutanol

CO_2-responsive materials created with the SI-AGET-ATRP described in this chapter were applied to an industrially relevant scenario. PGS-17 was utilised as a CO_2-responsive drying agent (DA) for the removal of water from wet isobutanol. The removal of water from organic solvents such as isobutanol has previously been shown to be of importance to the chemical industry.[30] The experiments presented here follow the same experimental procedure that was discussed in detail in Chapter 2. Table 4.6 shows that when CO_2 is applied to a solution of wet isobutanol, 170 mg of water is lost (entry 1). Additionally, when CO_2 is not present, PGS-17 fails to remove a statistically significant amount of water from the wet isobutanol solution (0.02 wt% water, entry 2). When PGS-17 and CO_2 were both added, 1053 mg H_2O/g DA was removed from the wet isobutanol solution. PGS-17 was collected and regenerated at 100 ℃ for 1 h, then used again in cycle 2, where it removed 1034 mg H_2O/g DA (entry 4). In both cycles utilising PGS-17 and CO_2, ca. 50% of the water content was removed from the wet isobutanol solution (4 wt%

water total). This result is a stark improvement over the previous generation of CO_2-responsive drying agents in which PGS-2 was able to remove 490 mg H_2O/g DA.

Table 4.6. Application of PGS-17 as a CO_2-responsive drying agent for the removal of water from wet isobutanol.

	Entry	Water (g)	Isobutanol (g)	PGS-17 (g)	CO_2	H_2O Removed (mg)	H_2O removed (mg H_2O/g DA)
1	Control 1	2.17	41.50	0	Yes	170	-
2	Control 2	2.11	41.67	1.2	No	9	7.5
3	PGS-17 Cycle 1	2.51	60.02	1.25	Yes	1317	1053
4	PGS-17 Cycle 2	2.50	60.02	1.20	Yes	1241	1034

[a]Reaction conditions: 1 h mixing with CO_2 (when indicated). CO_2 was bubbled through solution at ca. 34 kPa. After CO_2 bubbling, the vial was sealed and left standing for 15 h. The water content was analysed by GC-TCD. PGS-17 regeneration was performed at 100 °C for 1 h. For each cycle, a new solution of isobutanol containing 5 wt% water was used.

4.4 Conclusions

To date, studies evaluating CO_2-switchable technology on surfaces do not report the molecular weight of the grafted polymer.[2,30] In the best cases, ellipsometry is used to measure the thickness of the growing polymer surface, from which grafting density may be approximated. The molecular weight is not reported because a reliable and nondestructive method does not exist. Additionally, studies have used polymerisation solvents, such as methanol, that are not conducive to polymerising controlled PDiPAEMA at molecular weights greater than 10 kDa, owing to the tendency of PDiPAEMA to precipitate from polar solvents.

This work presents a method that can produce high molecular weight PDiPAEMA, with low dispersity, as a homopolymer (M_n>100 kDa, Đ: 1.17) or from a surface (M_n>40

kDa, Đ: 1.17). The control provided by this method adds confidence to the overall characterization of the CO_2-responsive material. The drying of wet isobutanol with PGS-17 (1043 mg H_2O/g DA) was a significant improvement over PGS-2 (490 mg H_2O/g DA).

The combination of a newly found confidence in the control of the polymerisation and the improved performance of the 2nd generation of CO_2-responsive particles in a industrially applicable scenario, validates the use of the SI-AGET-ATRP method presented here, as well as the use of CO_2-responsive technology to address challenges in the chemical industries.

The SI-AGET-ATRP method developed in this work is a powerful tool that can be used to answer the question: how much polymer is enough? The M_n of the system is a statistical distribution; therefore, a precise answer of exactly which M_n strikes the perfect balance between material performance and polymer loading will not be achieved, but a reasonable approximation can be determined. By varying reaction time, temperature and equivalents of monomer, the molecular weight to response relationship can be elucidated. The SI-AGET-ATRP method presented in this chapter is a robust and powerful tool for that endeavour.

4.5 Experimental methods

4.5.1 Materials

All aqueous solutions were prepared with deionized water (DIW) unless stated otherwise. All silica particles were purchased from Silicycle. The following chemicals were used as received unless otherwise stated: sulfuric acid (Fisher, ACS reagent grade, 95-98%), ammonium hydroxide (Aldrich, ACS reagent grade, 28-30% NH_3 basis), water (Millipore, type 1, 18.2 MΩ·cm @ 25 ℃), hydrogen peroxide (Aldrich, 30 wt% in H_2O), 2-bromo-2-methylpropionyl bromide (BIBB, Aldrich, 98%), ethyl 2-bromo-2-methylpropionate (EBIB, Aldrich, 98%), diisopropylethylamine (DIPEA, Aldrich, ≥99%), 4-(dimethylamino)pyridine (DMAP, Aldrich, ≥99%), dichloromethane (DCM, EMD Millipore, anhydrous, ≥98.5%), methanol (MeOH, EMD Millipore, anhydrous), dimethylformamide (DMF, Aldrich, 98%), anisole (Aldrich, anhydrous, 99.7%), toluene (Aldrich, anhydrous), toluene-d_8 (Aldrich, 99 atom % D) , tetrahydrofuran (Aldrich, anhydrous, contains 250 ppm BHT as inhibitor, ≥99.9%), copper(I) bromide (Aldrich, 99.999% trace metals basis), copper(II) bromide (Aldrich, 99.999% trace metals basis), copper(II) chloride (Aldrich, 99.999% trace metals basis), N-[3-(dimethylamino)propyl]methacrylamide (DMAPMAm, Aldrich, contains MEHQ as inhibitor, 99%), 2-(diisopropylamino)ethyl methacrylate (DiPAEMA, Aldrich, 97%, contains ~100 ppm monomethyl ether hydroquinone as inhibitor), N,N,N`,N``,N```-pentamethyldiethylenetriamine (PMDETA, Aldrich, 99%), tris(2-pyridylmethyl)amine (TPMA, Aldrich, 98%), ethylenediaminetetraacetic acid (EDTA, Aldrich, purified grade, ≥98.5%), sodium hydroxide (NaOH, Aldrich, ACS reagent, ≥97%), aluminium oxide (Aldrich, activated, basic, Brockmann I),

(3-aminopropyl)triethoxysilane (APTES, Aldrich, 99%), L-ascorbic acid (AA, Aldrich, reagent grade), tin(II) 2-ethylhexanoate ($Sn(EH)_2$, Aldrich, 92.5 – 100%).

Piranha solutions were used to clean silica substrates. Acidic piranha solution consists of a 7:3 (v/v) mixture of concentrated sulfuric acid and 30% hydrogen peroxide solution, commonly heated to 85 ℃. Basic piranha solution consists of a 5:1:1 (v/v/v) mixture of Millipore water, 30% hydrogen peroxide solution, and 40% ammonium hydroxide solution, commonly heated to 70 ℃.

Warning: Piranha solution is highly dangerous and its use requires considerable care. Piranha solution is either strongly acidic or basic and a strong oxidizer. The mixing of piranha solution is very exothermic and should be done slowly; if the reagents are mixed too quickly the temperature can easily exceed 100 ℃, which will result in boiling and splashing of the piranha solution. Piranha solution will react violently with organic compounds; therefore, it should be used in a fume hood clear of organic solvents and waste. Make only as much Piranha solution as needed; when disposing of excess or used piranha solution do NOT cap the bottle. It commonly takes a day or two for the reagent to neutralize fully, during this time oxygen gas is produced. Refer to your institution's standard operating procedures before attempting to use or dispose of piranha solutions.

Silica particles for experiments PGS-8 to PGS-11 were cleaned and hydroxylated using Piranha solutions. An example is as follows:

Spherical silica particles (SiO_2 #1, Silicycle, 200-500 μm particle size, 100 Å pore size, 30 g) were subjected to a three-part treatment to remove organic contaminants and promote a hydroxyl-rich surface. Firstly, the particles were stirred in acidic piranha solution heated to 85 ℃ for 1 h. The particles were collected via vacuum filtration and washed thoroughly with Millipore water. Secondly, the particles were stirred in basic piranha solution heated to 70 ℃ for 30 min. The particles were collected via vacuum filtration and washed thoroughly with Millipore water. Lastly, the particles were vacuum filtered and dried in an oven overnight at 100 ℃. The clean and hydroxyl-rich particles were stored in a sealed vessel under Ar until further use.

Silica particles for experiments PGS-12 to PGS-17 were cleaned and hydroxylated using the method suggested by Agilent technologies. An example is as follows:

Silica particles (SiO_2 #5, SiliaFlash P60, 40-63 μm, 100 Å pore size, 10 g) were subjected to a two-part treatment to remove organic contaminants and promote a hydroxyl-rich surface. Firstly, the particles were stirred with an overhead stirrer in an acidic solution, consisting of 1 M $HCl_{(aq)}$ for 4 h at 50 ℃. The silica particles were collected by vacuum filtration and rinsed three times with Millipore water. Secondly, the particles were added to 1 L of Millipore water and stirred vigorously with an overhead stirrer. Small volumes of ammonium hydroxide were added until the pH of the solution reached pH 7. Lastly, the neutral particles were collected by vacuum filtration and dried in an oven at 200 ℃ for a minimum of 2 h. The clean and hydroxyl-rich particles were used immediately upon removal from the oven.

For illustrative purposes, the full synthesis and characterization of PGS-15 and PGS-17 are presented here. The remaining experimental data can be found in Appendix IV.

4.5.2 Synthesis of polymer-grafted silica-15 (PGS-15)

Initiator grafting method part 1, (KBB9PG1):

Clean, hydroxyl-rich silica particles (SiO_2 #5, SiliaFlash P60, 40-63 μm, 100 Å pore size, 2 g) were added to a 500 mL glass reaction vessel. The glass reaction vessel was equipped with an overhead stirrer and an ethylene glycol heating unit. The vessel was kept at a constant temperature of 70 ℃. The atmosphere in the reaction vessel was removed under vacuum and replaced with Ar. To the sealed reaction vessel, 500 mL of anhydrous toluene was added via cannula transfer. After vigorous stirring, 5 mL of (3-aminopropyl)triethoxysilane (APTES) was added via syringe. The reaction was left stirring at 70 ℃ overnight. The APTES-grafted silica was collected by vacuum filtration and washed multiple times with ethanol before being stored under Ar until further use.

Initiator grafting method part 2, (KBB9PG2):

APTES-functionalised silica particles (SiO_2 #5, SiliaFlash P60, 40-63 μm, 100 Å pore size 2 g) were added to a flame dried 250 mL round bottom flask which was equipped with an overhead stirrer. Reactants were added using Schlenk techniques for inert conditions; diisopropylethylamine (1 eq., 4.0 mmol) and 200 mL of anhydrous

tetrahydrofuran (THF) were added to the round bottom flask. The round bottom flask was cooled in an ice bath for approximately 30 min, after which the initiator, 2-bromo-2-methylpropionyl bromide (BIBB, 1 eq., 4.04 mmol), was added dropwise via syringe. The mixture was stirred for 20 min before the ice bath was removed and the mixture was allowed to warm to room temperature (ca. 27 ℃) and to react overnight. The BIBB-grafted silica was then collected by vacuum filtration and washed multiple times with THF before being stored under Ar until further use.

SI-AGET-ATRP PDiPAEMA from silica, PGS-15 (KBB9PG14):

Initiator-functionalised silica particles (SiO_2 #5, SiliaFlash P60, 40-63 μm, 100 Å pore size, 10.5 g) were added to a 250 mL round bottom flask equipped with an overhead stirring device. 2-(Diisopropylamino)ethyl methacrylate (DiPAEMA, 235 eq., 401 mmol) was passed through an inhibitor remover column [Sigma-Aldrich, removing hydroquinone (HQ) or hydroquinone monomethyl ether (MEHQ, 4-methoxyphenol), or 4-*tert*-butylcatechol (TBC)] and charged to the 250 mL round bottom flask containing the initiator-functionalised silica. Anisole (100 mL), Cu(II)Br_2 (0.66 eq., 1.1 mmol), N,N,N′,N″,N″-pentamethyldiethylenetriamine (PMDETA, 3.29 eq., 5.6 mmol) and ethyl 2-bromo-2-methylpropionate (EBIB, 1 eq., 1.7 mmol) were added to the round bottom flask and the mixture was stirred vigorously while slowly heating to 40 ℃. Once the mixture reached the desired temperature, L-ascorbic acid (10 eq., 16.7 mmol) was added to the round bottom flask; which was promptly sealed. No additional techniques were used to remove atmospheric or dissolved oxygen. The polymerisation solution

changed colour from blue (oxidized copper) to colourless (ca. 2 h on average) and then to yellow/orange over the course of 16 h.

Isolation of free polymer and polymer-grafted silica:

Refer to Section 4.3.5.

4.5.3 Synthesis of polymer-grafted silica-17 (PGS-17)

Initiator grafting method part 1, (KBB9PG23):

Clean, hydroxyl-rich silica particles (SiO_2 #3, Silicycle, 200-500 μm particle size, 500 Å pore size, 20 g) were added to a 500 mL glass reaction vessel. The glass reaction vessel was equipped with an overhead stirrer and an ethylene glycol heating unit. The vessel was kept at a constant temperature of 70 ℃. The atmosphere in the reaction vessel was removed under vacuum and replaced with Ar. To the sealed reaction vessel, 500 mL of anhydrous toluene was added via cannula transfer. After vigorous stirring, 5 mL of (3-aminopropyl)triethoxysilane (APTES) was added via syringe. The reaction was left stirring at 70 ℃ overnight. The APTES-grafted silica was collected by vacuum filtration and washed multiple times with ethanol before being stored under Ar until further use.

Initiator grafting method part 2, (KBB9PG23):

APTES-functionalised silica particles (SiO_2 #3, Silicycle, 200-500 μm particle size, 500 Å pore size, 20 g) were added to a flame dried 250 mL round bottom flask. The round bottom flask was equipped with an overhead stirring device. Reactants were added using Schlenk techniques for inert conditions; diisopropylethylamine (1 eq., 4.0 mmol) and 200 mL of anhydrous tetrahydrofuran (THF) were added to the round bottom flask. The round bottom flask was cooled in an ice bath for approximately 30 min, after which the initiator, 2-bromo-2-methylpropionyl bromide (BIBB, 1 eq., 4.04 mmol), was added dropwise via syringe. The mixture was stirred for 20 min before the ice bath was removed and the mixture was allowed to warm to room temperature (ca. 27 ℃) and to react overnight. The BIBB-grafted silica was then collected by vacuum filtration and washed multiple times with THF before being stored under Ar until further use.

SI-AGET-ATRP of PDiPAEMA from silica, PGS-17, (KBB9PG23):

Initiator-functionalised silica particles (SiO_2 #3, Silicycle, 200-500 μm particle size, 500 Å pore size, 23 g) were added to a 250 mL round bottom flask equipped with an overhead stirring device. 2-(Diisopropylamino)ethyl methacrylate (DiPAEMA, 258 eq., 439 mmol) was passed through an inhibitor remover column [Sigma-Aldrich, removing hydroquinone (HQ) or hydroquinone monomethyl ether (MEHQ, 4-methoxyphenol), or 4-*tert*-butylcatechol (TBC)] and charged to the 250 mL round bottom flask containing the initiator-functionalised silica. Anisole (100 mL), Cu(II)Br2 (0.68 eq., 1.2 mmol), N,N,N′,N″,N″-pentamethyldiethylenetriamine (PMDETA, 3.26 eq., 5.5 mmol) and

ethyl 2-bromo-2-methylpropionate (EBIB, 1 eq., 1.7 mmol) were added to the round bottom flask. The mixture was stirred vigorously while being slowly heated to 40 ℃. Once the mixture reached the desired temperature, L-ascorbic acid (10 eq., 17 mmol) was added to the round bottom flask, which was promptly sealed. No additional techniques were used to remove atmospheric or dissolved oxygen. The polymerisation solution changed colour from blue (oxidised copper) to colourless (ca. 2 h on average) and then to yellow/orange over the course of 16 h.

Isolation of free polymer and polymer-grafted silica:

Refer to Section 4.3.5.

4.5.4 Infrared spectroscopy of polymer-grafted silica particles

Fourier Transform Infrared (FTIR) spectroscopy analysis was conducted on a Bruker Alpha spectrometer using a Diffuse Reflectance Infrared Fourier Transform (DRIFT) accessory. The spectrometer was referenced using a gold disk. PGS samples (10 mg) were dispersed in KBr (100 mg). Samples were mixed thoroughly using a mortar and pestle prior to analysis. Particle samples will typically contain water as extensive drying procedures were not conducted prior to analysis. In addition, fluctuations in the baseline that occur between 2200 cm^{-1} and 2500 cm^{-1} can be attributed to user error, specifically to exhalation. Caution should therefore be exercised when assessing the spectra. The presence of bound CO_2, which is likely, should not be inferred by these experiments. It should be noted that various forms of Infrared (IR) analysis were conducted over the course

of this research project. DRIFT-FTIR spectroscopy vastly outperforms Attenuated Total Reflectance (ATR) and traditional Fourier Transform (FT) IR spectroscopy when it comes to the analysis of silica particles and silicon wafers. DRIFT-FTIR spectroscopy is non-destructive; using DRIFT-FTIR spectroscopy, better resolution was achieved in comparison to ATR-FTIR when detecting grafted-polymers on silicon wafers.

For illustrative purposes a select few spectra and been processed and re-graphed into Figures 4.9 and 4.10. Additional spectra can be found in Appendix IV. Since each spectrum is recorded relative to a background scan, the peak heights tends to vary between experiments. To facilitate visual comparison the y-axis has been normalised to a value of 1. Figure 4.9 illustrates a typical spectrum that is recorded for a polymer-grafted silica sample, juxtaposed to a control spectrum. PGS-17 consists of spherical silica particles that have been grafted with PDiPAEMA. The control sample is the same spherical silica particles used for PGS-17 but without chemical modification of any means. Comparison of these two spectra allows for the identification of target regions in which one looks to determine whether a given sample of silica contains polymer. The regions between 1300 cm^{-1} to 2000 cm^{-1} and 2800 cm^{-1} to 3000 cm^{-1} are the target regions in which the presence of peaks are indicative of functionalisation with PDiPAEMA.

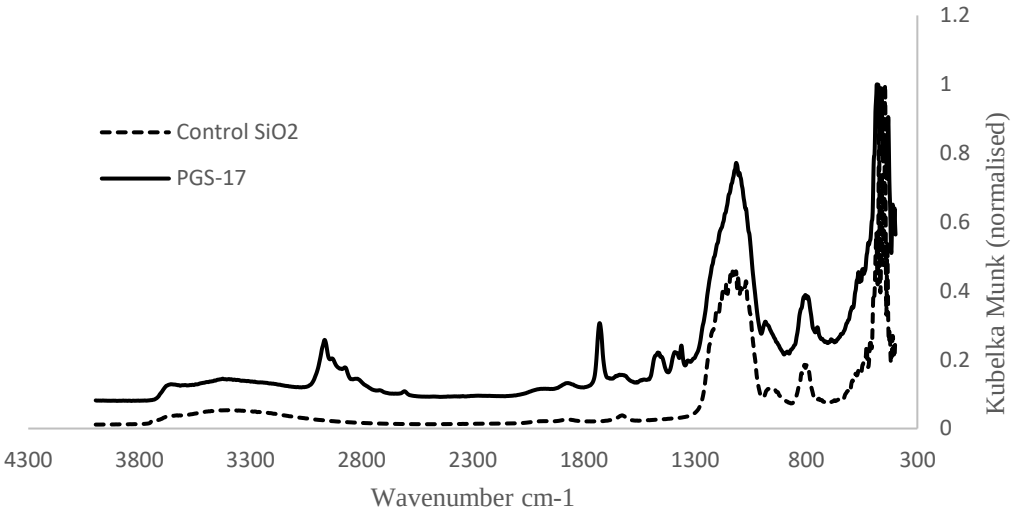

Figure 4.9. DRIFT spectrum of clean SiO_2 #3 (control) superimposed against polymer-grafted silica (PGS-17).

Figure 4.10 illustrates the same PGS-17 sample that was shown in Figure 4.9 juxtaposed against a spectrum collected from a sample of PDiPAEMA homopolymer. The homopolymer was precipitated twice; the ^{1}H NMR spectrum of the twice precipitated polymer did not show signs of residual monomer. Figure 4.10 clearly indicates that the target regions identified from analysis of Figure 4.19 (1300 cm^{-1} to 2000 cm^{-1} and 2800 cm^{-1} to 3000 cm^{-1}) are resultant from PDiPAEMA and not from an impurity. All SI-AGET-ATRP and SI-ARGET-ATRP reactions listed in this section contain indications of PDiPAEMA. The best agreement between peaks that are characteristic of functionalisation with PDiPAEMA are 1727 $\pm$2 cm^{-1} and 2874 $\pm$1 cm^{-1}. Therefore, the SI-AGET-ATRP experiments that can conclusively be declared as to have successfully grafted PDiPAEMA to silica particles are PGS-15 and PGS-17.

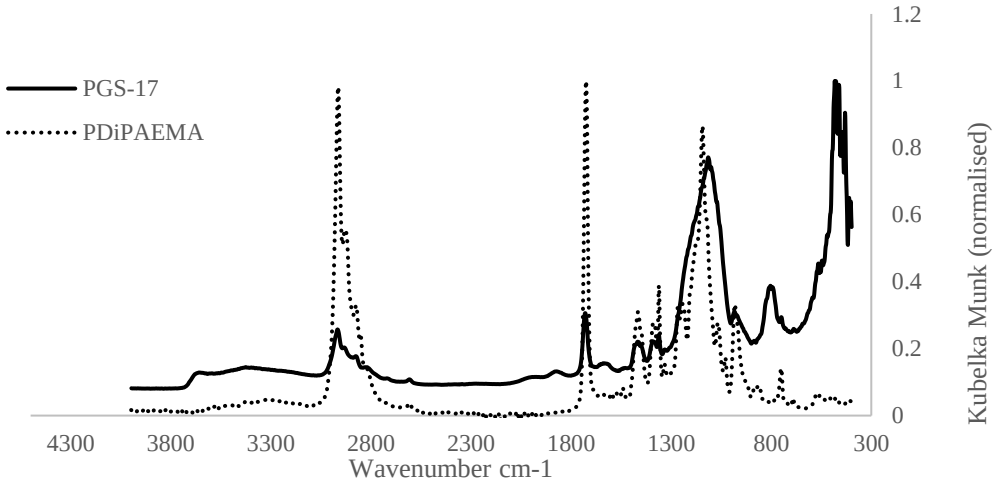

Figure 4.10. DRIFT spectrum of PDiPAEMA superimposed against polymer-grafted silica (PGS-17).

4.5.5 Thermogravimetric analysis of polymer-grafted silica particles

Thermogravimetric analysis (TGA) was performed using a TA Instruments Q500 TGA analyzer by heating the sample using the following ramp: 10 °C min^{-1} from 30 to 120 °C, held for 20 min and 120 °C, followed by 10 °C min^{-1} to 900 °C. The initial isothermal hold at 120 °C is to remove bulk solvents and adsorbed liquids such as moisture from the atmosphere. The organic content of the polymer-grafted silica particles was calculated from the point at which mass loss begins to occur, after the initial isothermal hold, until the point at which mass loss stops.

Figure 4.11 shows that the onset of mass loss for a sample of PDiPAEMA homopolymer occurs at ca. 300 °C. Figures 4.12 and 4.13 demonstrate close agreement with Figure 4.11, the onset of major mass loss for the polymer-grafted silica samples containing PDiPAEMA begins at ca. 300 °C. From analysis of the Figure 4.12 it is

concluded that PGS-15 was 45 wt% polymer. From the analysis of Figure 4.13, PGS-17 was determined to be 35 wt% polymer.

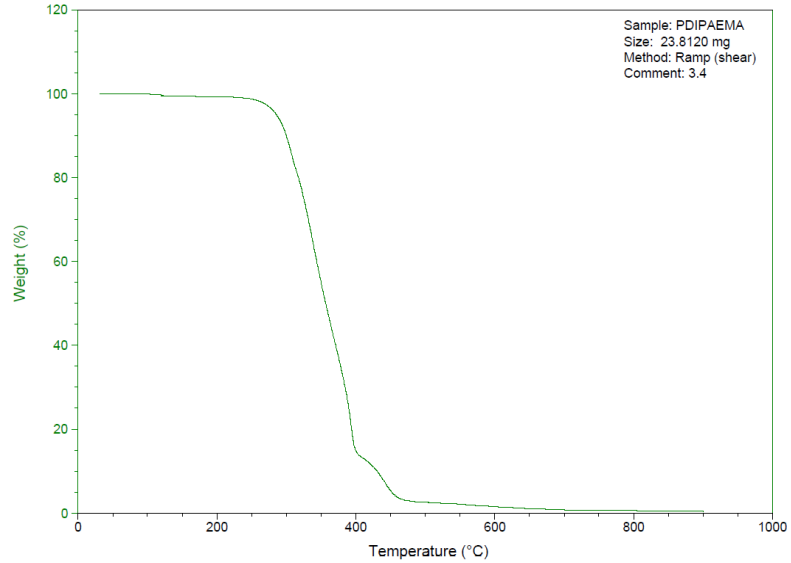

Figure 4.11. The thermogravimetric analysis of PDiPAEMA homopolymer.

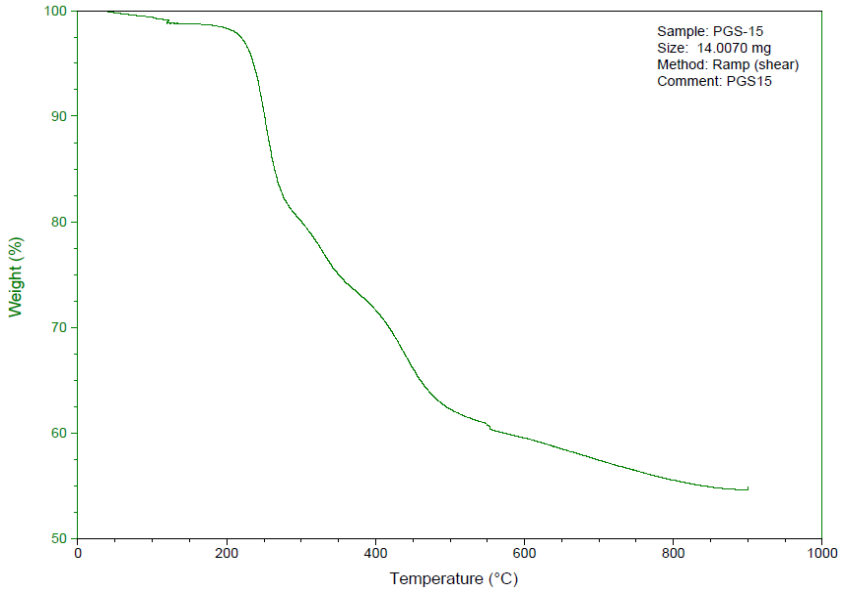

Figure 4.12. The thermogravimetric analysis of PGS-15.

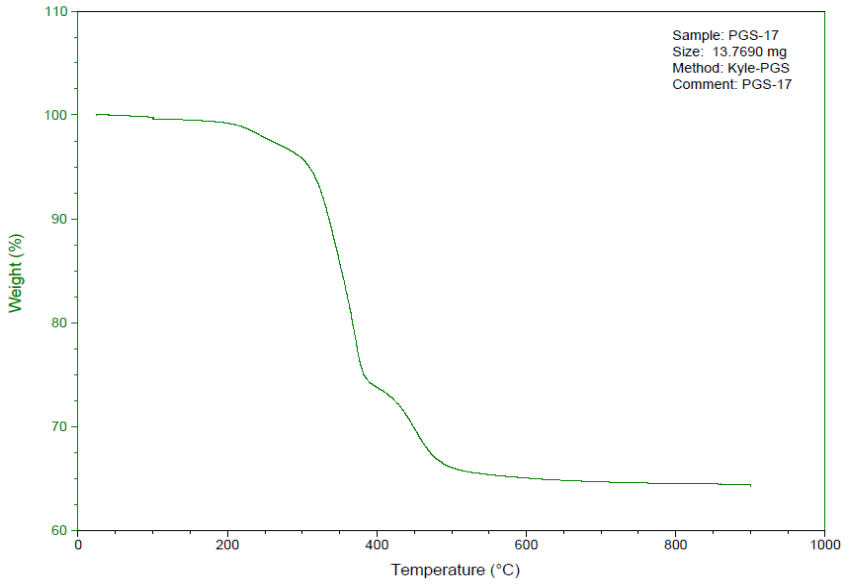

Figure 4.13. The thermogravimetric analysis of PGS-17.

4.5.6 Nuclear magnetic resonance spectroscopy of polymer-grafted silica particles

CP-MAS NMR (^{13}C and ^{29}Si) spectra were recorded by Dr. Francoise Sauriol on a Bruker Avance 600 FT-NMR spectrometer operating at 150.91 MHz using a Bruker 5 mm CP-MAS probe. The spinning rate was 12 kHz with a cross-polarization contact time of 3 ms and a repetition delay of 2 s. Various contact times and repetition delays were explored in efforts to improve the signal to noise ratio. In some instances, longer contact times (i.e. 5 or 7 ms) resulted in a better spectrum for silica samples with low organic content. For polymer-grafted silica samples, which have a high organic content, a contact time of 3 ms with a delay of 2 s is recommended.

Selected spectra have been provided for illustrative purposes. Additional CP-MAS-NMR data for PGS samples can be found in Appendix IV. The following figures are high-quality examples of the solid-state CP-MAS NMR spectra obtained from silica-based materials. ^{13}C and ^{29}Si spectra for spherical silica (SiO_2 #3) and irregular silica (SiO_2

#5), at the various stages of functionalisation, are provided. The wt% polymer for PGS-15 was ca. 45% and for PGS-17 it was ca. 35%. The spectra for SiO_2 #3 are in good agreement with the spectra collected for SiO_2 #5.

The exception to the agreement can be seen by comparing Figures 4.15 to 4.22, in which the ^{29}Si spectra are given for APTES-functionalised SiO_2 #3 and SiO_2 #5 respectively. Figure 4.15 shows two peaks closely associated, whereas Figure 4.22 shows two very distinct peaks. For functionalisation with a silane derivative such as APTES, two separate peaks in the ^{29}Si spectrum are expected. This can be seen in Figure 4.22, with one peak for the Si-O bond, and one peak for the Si-C bond. Similar spectra have been independently validated by colleagues and are well reported in literature. It is unclear why there is a discrepancy, especially considering that the ^{13}C spectra for both silica samples are in good agreement at each stage of functionalisation.

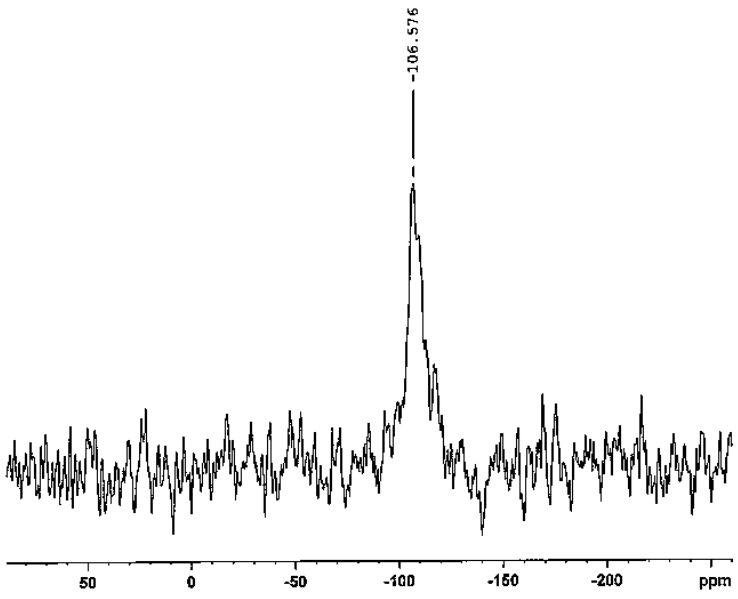

Figure 4.14. ^{29}Si CP-MAS NMR spectrum of SiO_2 #3 cleaned using the Agilent method.

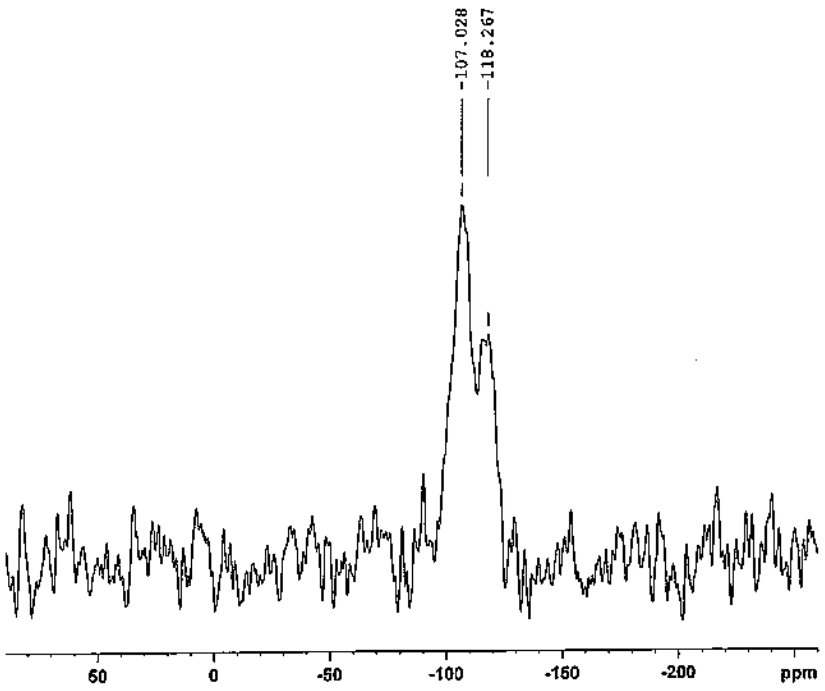

Figure 4.15. ^{29}Si CP-MAS NMR spectrum of SiO_2 #3 treated with APTES.

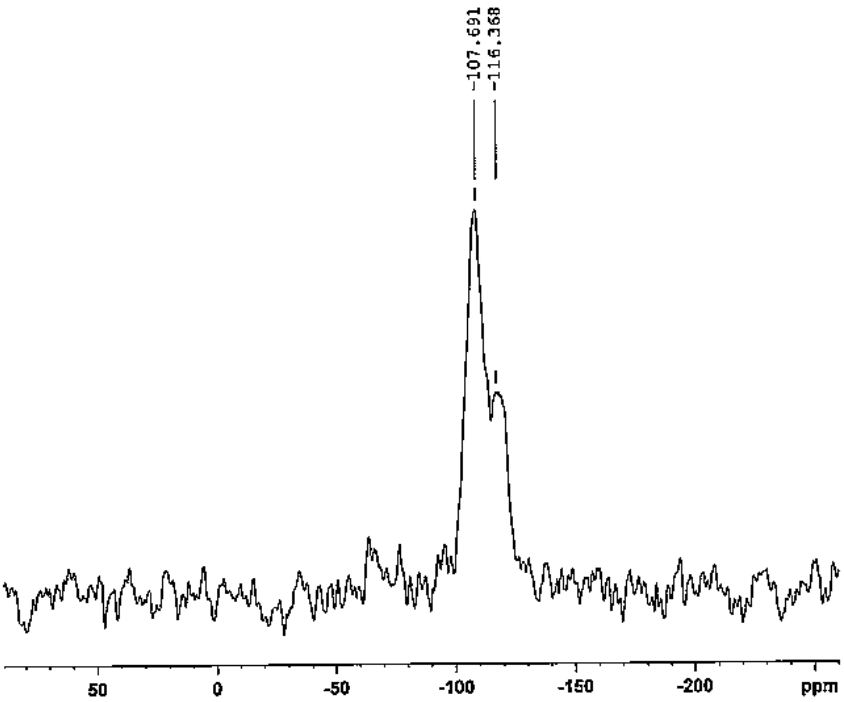

Figure 4.16. ^{29}Si CP-MAS NMR spectrum of SiO_2 #3 treated with APTES and BIBB.

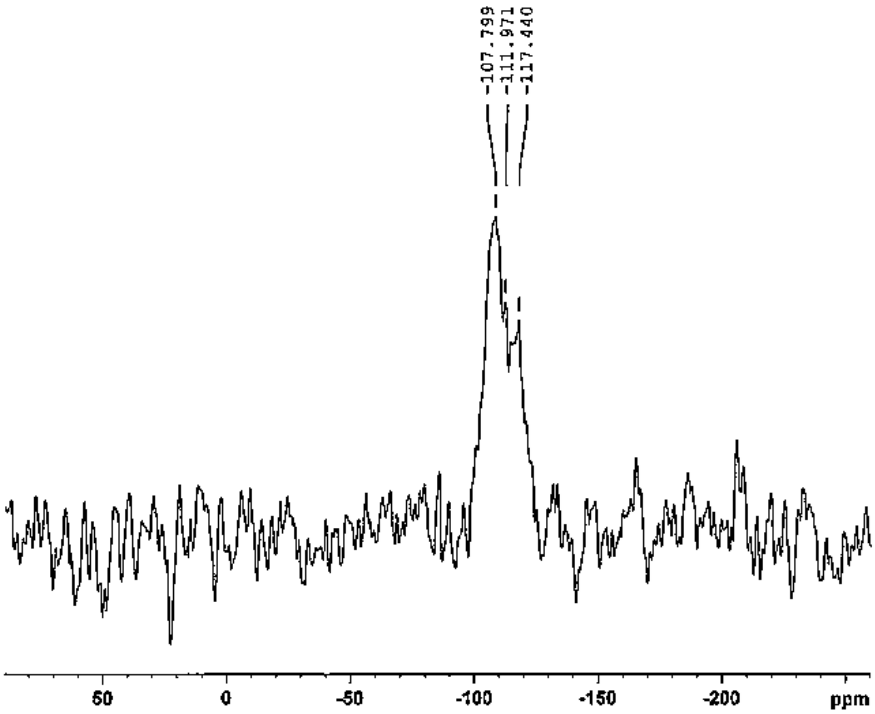

Figure 4.17. ^{29}Si CP-MAS NMR spectrum of PGS-17.

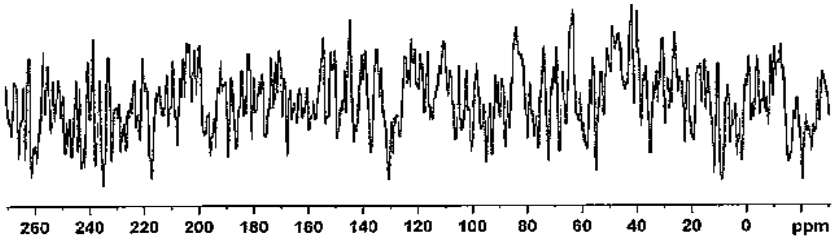

Figure 4.18. ^{13}C CP-MAS NMR spectrum of SiO_2 #3 cleaned using the Agilent method. The same spectrum was obtained regardless of silica type.

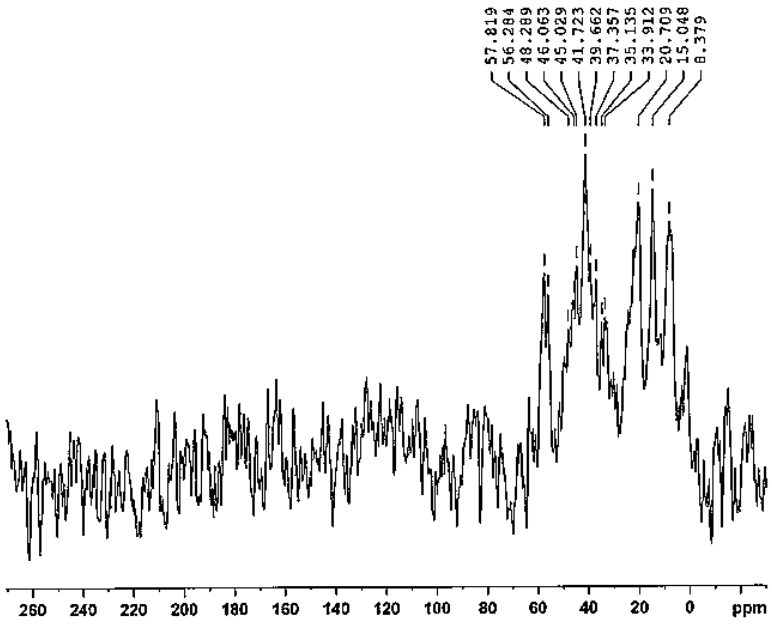

Figure 4.19. ^{13}C CP-MAS NMR spectrum of SiO_2 #3 treated with APTES.

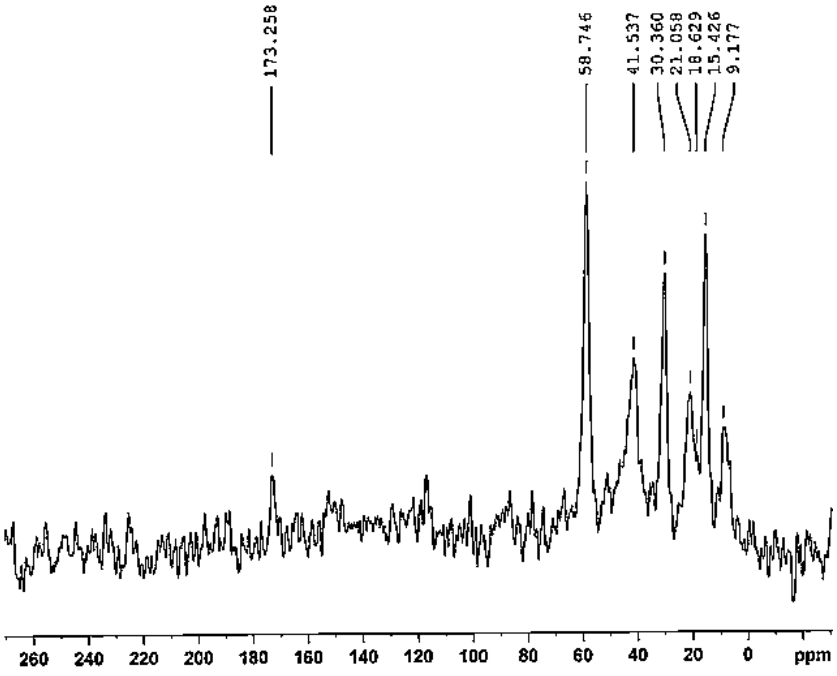

Figure 4.20. ^{13}C CP-MAS NMR spectrum of SiO_2 #3 treated with APTES and BIBB.

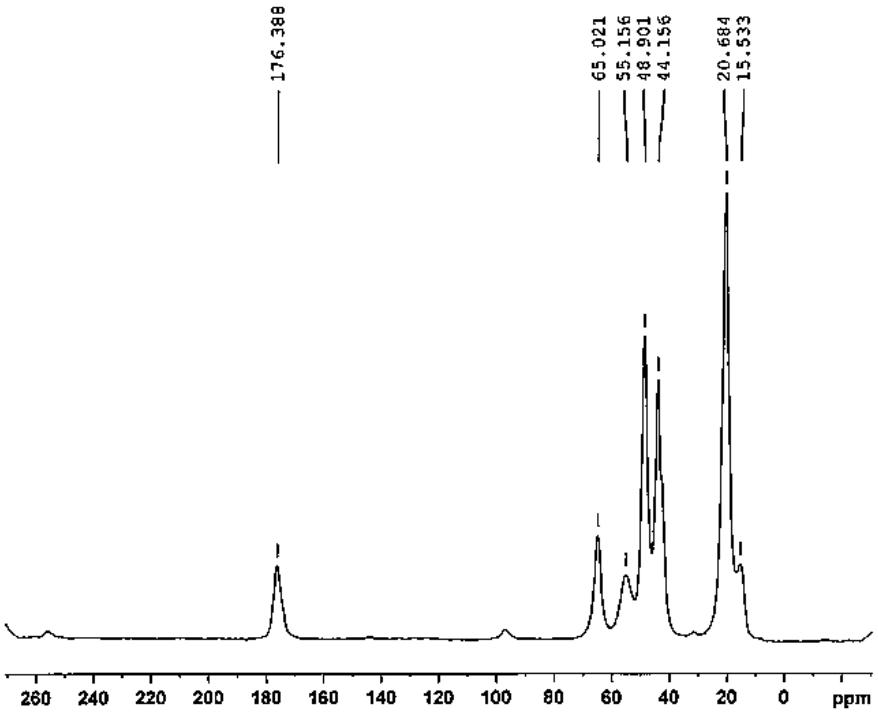

Figure 4.21. ^{13}C CP-MAS NMR spectrum of PGS-17.

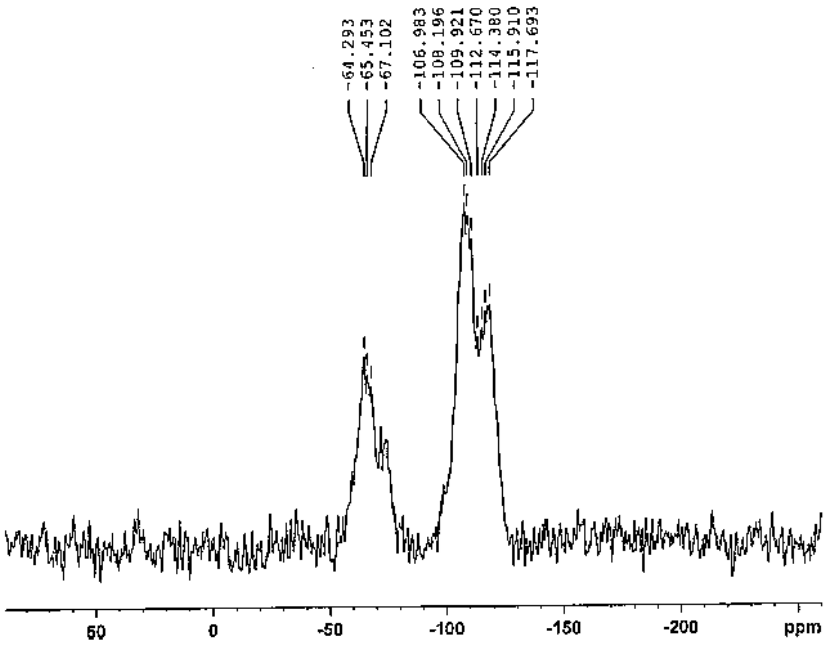

Figure 4.22. ^{29}Si CP-MAS NMR spectrum of SiO_2 #5 with APTES.

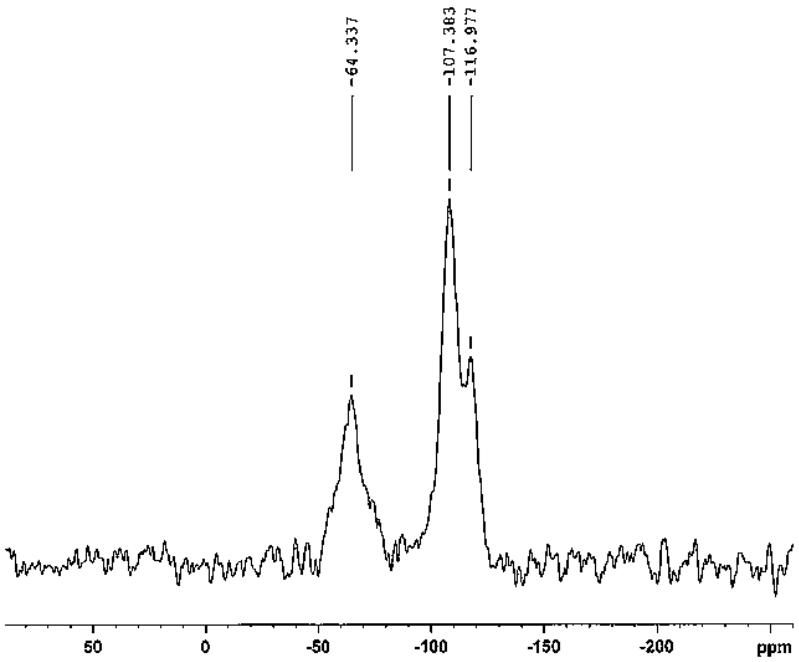

Figure 4.23. ^{29}Si CP-MAS NMR spectrum of SiO_2 #5 treated with APTES and BIBB.

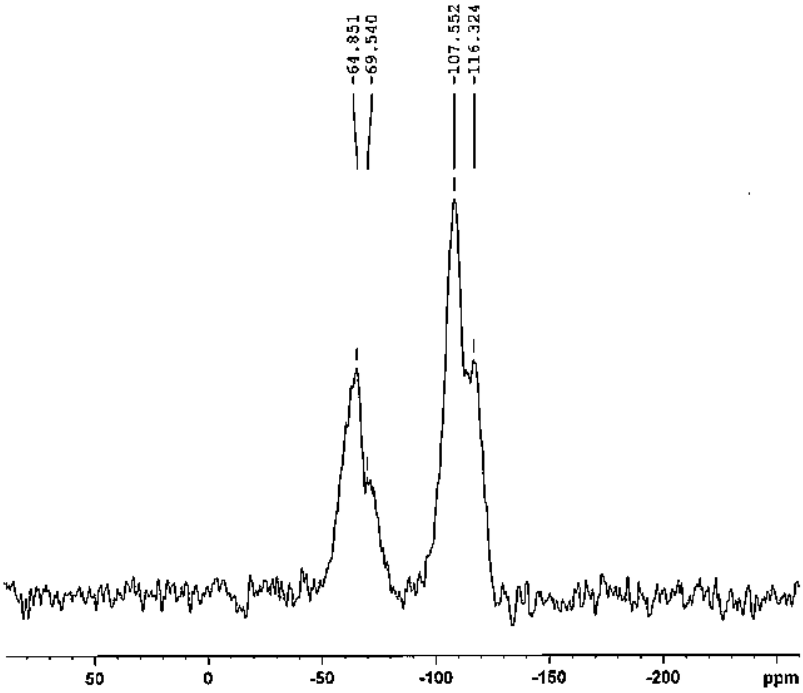

Figure 4.24. ^{29}Si CP-MAS NMR spectrum of PGS-15.

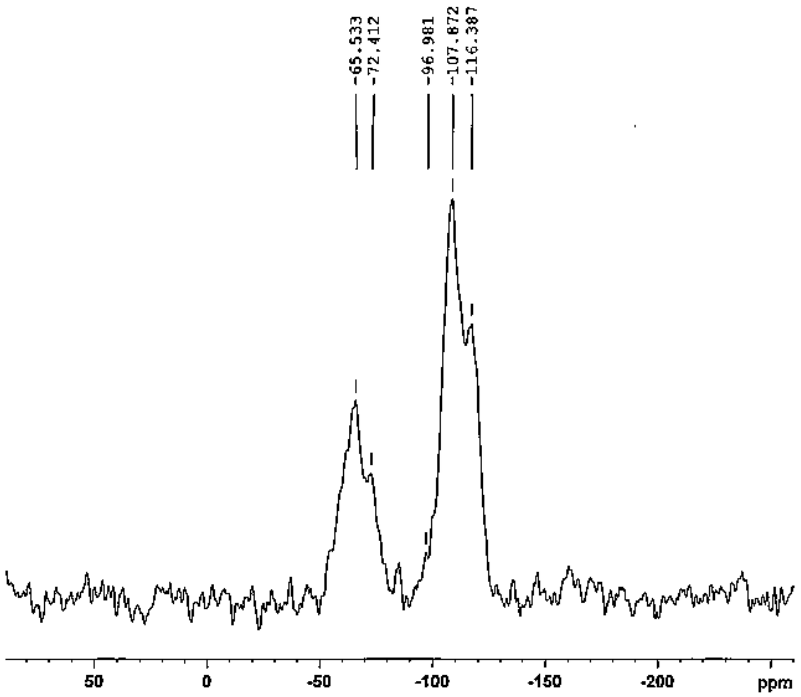

Figure 4.25. ^{29}Si CP-MAS NMR spectrum of PGS-15-EXT-PS.

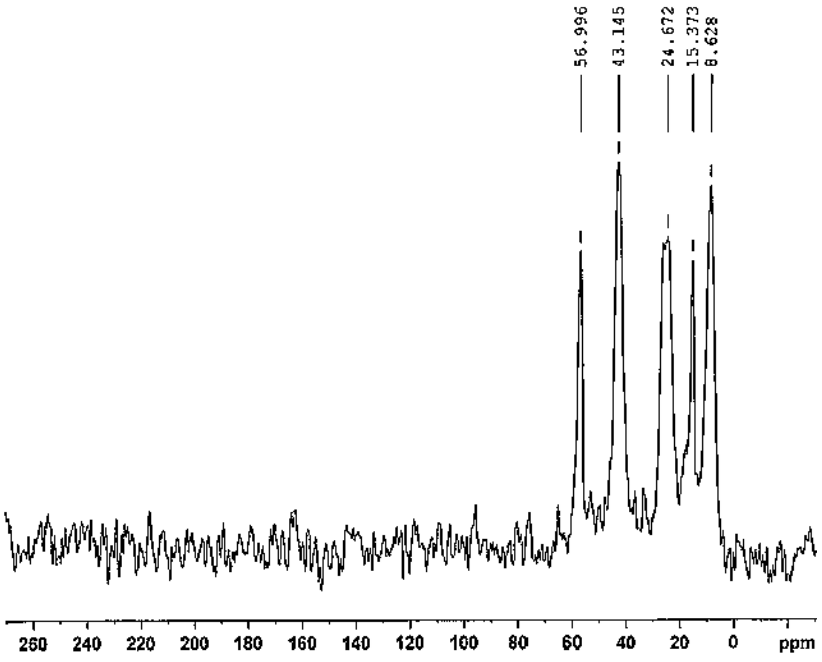

Figure 4.26. ^{13}C CP-MAS NMR spectrum of SiO_2 #5 with APTES.

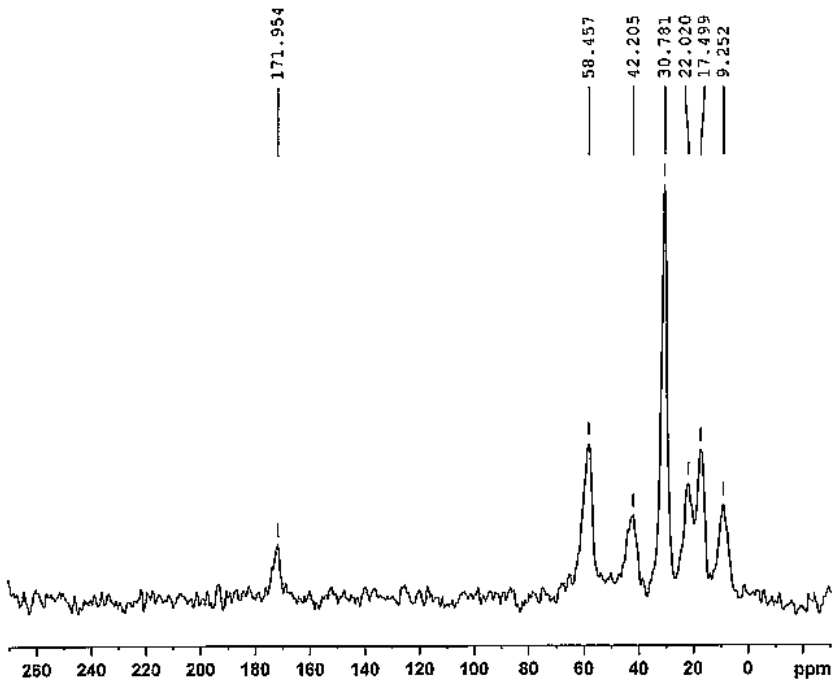

Figure 4.27. ^{13}C CP-MAS NMR spectrum of SiO_2 #5 with APTES and BIBB.

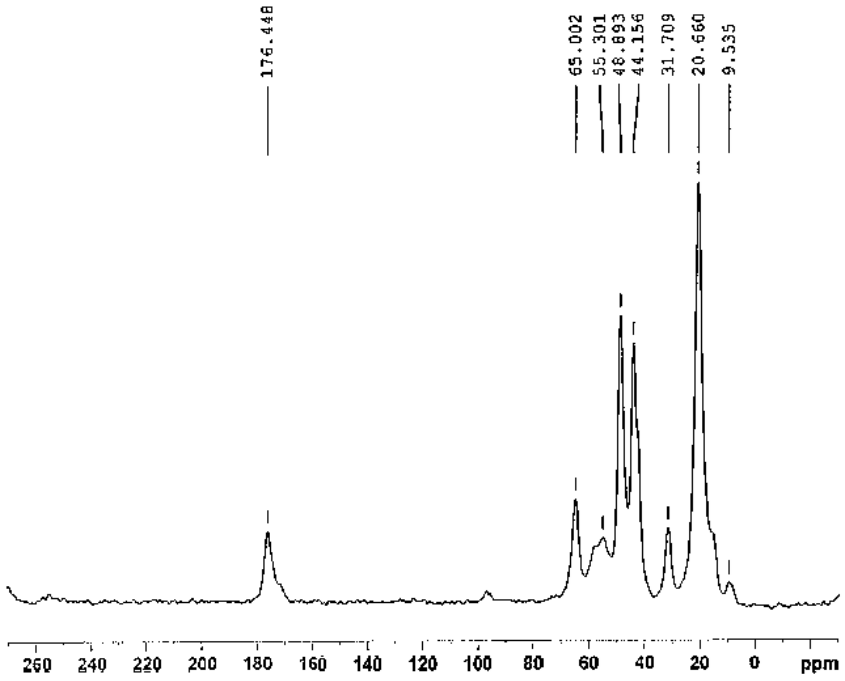

Figure 4.28. ^{13}C CP-MAS NMR spectrum of PGS-15.

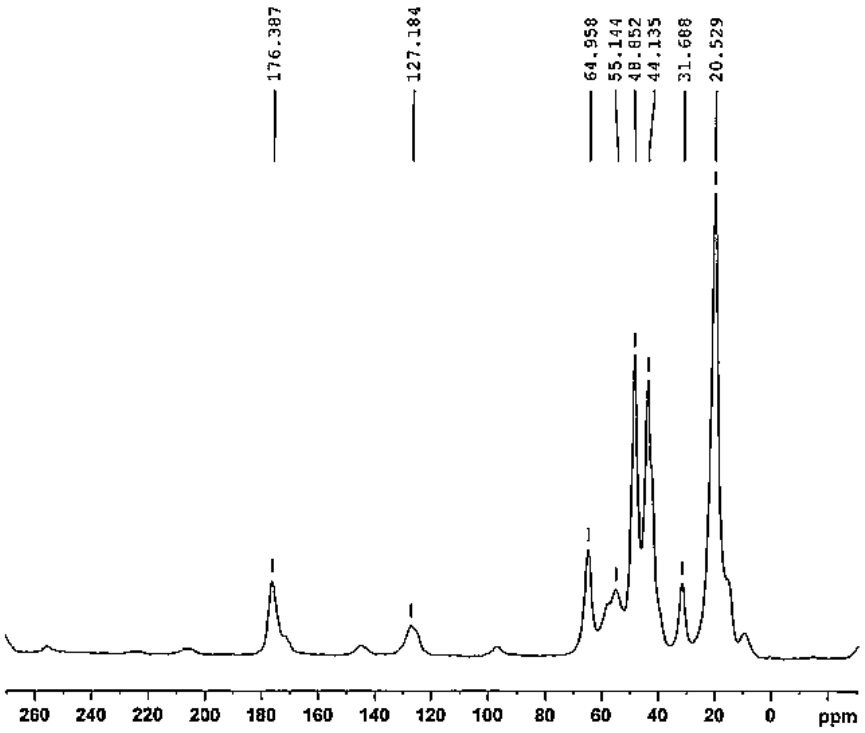

Figure 4.29. ^{13}C CP-MAS NMR spectrum of PGS-15-EXT-PS.

4.5.7 Gel permeation chromatography

Gel Permeation Chromatography (GPC) was performed with a Waters 2690 Separation Module and Waters 410 Differential Refractometer with THF as the eluent. The column bank consisted of Waters Styragel HR (4.6x300 mm) 4, 3, 1, and 0.5 separation columns operating at 40°C and 0.3 mL min^{-1}. GPC data are reported as poly(methylmethacrylate) (PMMA) equivalents, based on a calibration curve of narrow molecular weight distribution PMMA standards purchased from Polymer Standards.

4.6 References

1. J. O. Zoppe, N. C. Ataman, P. Mocny, J. Wang, J. Moraes and H.-A. Klok, *Chem. Rev.*, 2017, **117**, 1105–1318.

2. S. Kumar, X. Tong, Y. L. Dory, M. Lepage and Y. Zhao, *Chem. Commun.*, 2013, **49**, 90–92.

3. E. Stratakis, A. Mateescu, M. Barberoglou, M. Vamvakaki, C. Fotakis and S. H. Anastasiadis, *Chem. Commun.*, 2010, **46**, 4136–4138.

4. V. Bütün, S. P. Armes and N. C. Billingham, *Polymer*, 2001, **42**, 5993–6008.

5. T. Thavanesan, C. Herbert and F. A. Plamper, *Langmuir*, 2014, **30**, 5609–5619.

6. P. van de Wetering, E. E. Moret, N. M. E. Schuurmans-Nieuwenbroek, M. J. van Steenbergen and W. E. Hennink, *Bioconjug. Chem.*, 1999, **10**, 589–597.

7. N. G. Hoogeveen, M. A. C. Stuart, G. J. Fleer, W. Frank and M. Arnold, *Macromol. Chem. Phys.*, 1996, **197**, 2553–2564.

8. F. A. Plamper, M. Ruppel, A. Schmalz, O. Borisov, M. Ballauff and A. H. E. Müller, *Macromolecules*, 2007, **40**, 8361–8366.

9. A. Schmalz, M. Hanisch, H. Schmalz and A. H. E. Müller, *Polymer*, 2010, **51**, 1213–1217.

10. J.-S. Wang and K. Matyjaszewski, *J. Am. Chem. Soc.*, 1995, **117**, 5614–5615.

11. K. Matyjaszewski and J. Xia, *Chem. Rev.*, 2001, **101**, 2921–2990.

12. N. V. Tsarevsky and K. Matyjaszewski, *Chem. Rev.*, 2007, **107**, 2270–2299.

13. K. Matyjaszewski and N. V. Tsarevsky, *Nat. Chem.*, 2009, **1**, 276–288.

14. K. Matyjaszewski, *Macromolecules*, 2012, **45**, 4015–4039.

15. W. Jakubowski and K. Matyjaszewski, *Macromolecules*, 2005, **38**, 4139–4146.

16. W. Jakubowski and K. Matyjaszewski, *Angew. Chem.*, 2006, **118**, 4594–4598.

17. W. Jakubowski, K. Min and K. Matyjaszewski, *Macromolecules*, 2006, **39**, 39–45.

18. K. Matyjaszewski, W. Jakubowski, K. Min, W. Tang, J. Huang, W. A. Braunecker and N. V. Tsarevsky, *Proc. Natl. Acad. Sci.*, 2006, **103**, 15309–15314.

19. H. Dong and K. Matyjaszewski, *Macromolecules*, 2008, **41**, 6868–6870.

20. Y. Kwak and K. Matyjaszewski, *Polym. Int.*, 2009, **58**, 242–247.

21. J. Lad, S. Harrisson, G. Mantovani and D. M. Haddleton, *Dalton Trans.*, 2003, **0**, 4175–4180.

22. J. D. Willott, T. J. Murdoch, B. A. Humphreys, S. Edmondson, E. J. Wanless and G. B. Webber, *Langmuir*, 2015, **31**, 3707–3717.

23. C. D. Walkey, J. B. Olsen, H. Guo, A. Emili and W. C. W. Chan, *J. Am. Chem. Soc*., 2012, **134**, 2139–2147.

24. B. T. Cheesman, A. J. G. Neilson, J. D. Willott, G. B. Webber, S. Edmondson and E. J. Wanless, *Langmuir*, 2013, **29**, 6131–6140.

25. S. Brunauer, P. H. Emmett and E. Teller, *J. Am. Chem. Soc*., 1938, **60**, 309–319.

26. K. S. Walton and R. Q. Snurr, *J. Am. Chem. Soc*., 2007, **129**, 8552–8556.

27. L. T. Zhuravlev, *Colloids Surf. Physicochem. Eng. Asp.*, 2000, **173**, 1–38.

28. W. Tang, Y. Kwak, W. Braunecker, N. V. Tsarevsky, M. L. Coote and K. Matyjaszewski, *J. Am. Chem. Soc.*, 2008, **130**, 10702–10713.

29. H. Tang, N. Arulsamy, M. Radosz, Y. Shen, N. V. Tsarevsky, W. A. Braunecker, W. Tang and K. Matyjaszewski, *J. Am. Chem. Soc.*, 2006, **128**, 16277–16285.

30. K. J. Boniface, R. R. Dykeman, A. Cormier, H.-B. Wang, S. M. Mercer, G. Liu, M. F. Cunningham and P. G. Jessop, *Green Chem.*, 2015, **18**, 208–213.

31. Y. Prado, N. Daffé, A. Michel, T. Georgelin, N. Yaacoub, J.-M. Grenèche, F. Choueikani, E. Otero, P. Ohresser, M.-A. Arrio, C. Cartier-dit-Moulin, P. Sainctavit, B. Fleury, V. Dupuis, L. Lisnard and J. Fresnais, *Nat. Commun.*, 2015, **6**, 10139.

32. P. V. Mendonca, S. E. Averick, D. Konkolewicz, A. C. Serra, A. V. Popov, T. Guliashvili, K. Matyjaszewski and J. F. J. Coelho, *Macromolecules*, 2014, **47**,4615–4621.

Chapter 5

CO_2-Responsive Inorganic Surfaces

5.1 Preface

This chapter is unique in the sense that the work presented herein, in part, predates the previous chapters. Much of the early work on inorganic surfaces such as glass or silicon wafers was unsuccessful. As previously discussed, the work in Chapter 2 began with the intent of solving the larger problems that were plaguing the synthetic efforts focused on inorganic flat surfaces. The methods developed throughout Chapters 2, 3, and 4 were then applied to the synthesis of CO_2-responsive silicon surfaces, thus bringing the project full circle.

The development of CO_2-responsive inorganic flat surfaces is perhaps the most challenging pursuit undertaken to date. The scientific field in which this research is applicable has multiple broad goals. However, one in particular that receives consistent attention is the creation of robust, superhydrophobic self-cleaning surfaces. Innovations in this field often find harmony between fragile nanoscale architectures and larger more robust, micro-, and macro-scale structures. The unity of structural design and chemical response, at all scales, holds the greatest hope for the attainment of these goals. The work presented herein represents curiosity-driven science in pursuit of the relationship between simple structures and the chemical responses governed by CO_2-responsive chemistry.

5.1.1 Abstract

Synthetic methods for the synthesis of CO_2-responsive silicon surfaces are presented. CO_2-responsive surfaces have been evaluated using single-unit functionalisation techniques such as self-assembled monolayers (SAM) and direct functionalisation techniques, which use acyl transfer reagents to mediate the coupling of CO_2-responsive functional groups to a silicon substrate. Polymeric functionalisation of silicon substrates was achieved using a *grafting from* approach with surface-initiated ATRP (SI-ATRP). Poly(2-(diisopropylamino)ethyl methacrylate) (PDiPAEMA) was grown from various silicon wafers and a reproducible response to CO_2 was documented with no losses in performance after 10 cycles. Techniques to induce microscale and nanoscale roughness onto the silicon surface will be presented and discussed.

5.1.2 Introduction

Switchable surfaces can be used as smart materials for many applications, some of which have potential to be applied in an industrial setting. One envisioned industrial application aims to address the need for cleaning reaction vessels and/or pipelines that have otherwise become less efficient and/or hinder reactions due to chemical residue build-up. If a reaction vessel and/or pipeline were coated with a switchable surface, the vessel/pipeline could be effectively cleaned by simply applying an external stimulus.[1] We have demonstrated that a CO_2-responsive surface can switch between a hydrophobic and a hydrophilic form.[1–4] Only molecules with like properties will adhere to the vessel/pipeline's walls; for example, only hydrophobic molecules (e.g. oil residues or tar, in which CO_2 is soluble) stick to a vessel/pipeline wall when the switchable surface is in its hydrophobic form. With the application of the appropriate stimulus, the surface switches from its hydrophobic form to its hydrophilic form and all hydrophobic molecules that were previously adhered to the wall are forced off. Once clean, the surface can be switched back to its hydrophobic form and reactions/transportation of materials can continue.[3,5]

During the past few decades, many different synthesis strategies have been developed to fabricate functional surfaces with superwettability, i.e. superhydrophilic, superhydrophobic, and superoleophobic surfaces.[6] Applications of surfaces with superwettability include water harvesting, anti-corrosion, anti-icing, anti-fogging, oil-water separations, drug release, printing, textiles, drag-reduction, microfluidics, and self-cleaning.[6]

Surfaces with superwettability can be adapted for use as switchable surfaces. For example, superhydrophobic materials can become less effective due to contamination from oils and other hydrophobic materials. If these superhydrophobic materials could switch their properties between a superhydrophobic/superoleophilic surface to a superhydrophilic/superoleophobic surface, then surface contaminants would be readily removed or washed away. Once clean, the surface could be switched back to its superhydrophobic/superoleophilic surface for further use. For example, the switchable surface could respond to CO_2, to a flushing inert gas, and/or to heat (ca. 50 °C) as external stimuli. In an industrial application of such a switchable surface, both CO_2 and heat could be captured from waste streams of other processes, allowing a repurposing of the waste heat and CO_2.

Other smart materials that use light or pH to switch, instead of CO_2, can be used industrially, but would require retrofitting reaction vessels to facilitate light exposure, or would generate excessive amounts of waste for controlling pH. Additionally, the accumulation of salt in a closed system from the use of pH modifiers such as NaOH and HCl has been shown to significantly reduce the performance of a pH-responsive smart material.[7] The use of CO_2 as an external stimulus is distinct from other methods of achieving a pH change (addition of acids/bases) since the pH change can be readily reversed by removal of CO_2, rather than by addition of a counteracting base. Thus, material performance will not degrade over time due to the accumulation of salt in the system.

The wetting characteristics of a surface can be greatly enhanced by physical modification of the surface (i.e. creating surface roughness) or by chemical modification by means of modifying a surface (rough or smooth) with hydrophobic coatings.[8] Various

methods for both chemical modification of a surface with CO_2-responsive functional groups and physical modification of inorganic substrates have been investigated for the development of CO_2-responsive smart surfaces with superwettability.

5.1.3 Chemical modification of surfaces

An initial assessment of switchable materials yielded multiple pathways in which chemical modification techniques could be used to create a CO_2-responsive smart surface. In the broadest of terms, the CO_2-functionalities could be physisorbed or chemisorbed to a surface. Physisorbed CO_2-responsive surfaces can be created by spin coating thin films of a CO_2-responsive functionality/polymer onto an inorganic surface such as a silicon wafer or a glass microscope slide.

Of the chemisorbed pathways assessed, self-assembly stood out as a relatively simple and well-studied method for creating a smart surface. Molecular self-assembly is the assembly of molecules without the control of an outside influence. Self-assembly occurs spontaneously throughout nature, the most prominent example being the double helix of deoxyribonucleic acid (DNA). Of the diverse approaches for molecular self-assembly, two strategies have received the most attention; electrostatic self-assembly (layer-by-layer assembly), and self-assembled monolayers (SAMs).[9]

Electrostatic self-assembly involves anionic and cationic interactions to assemble layers atop of one another. Typically, one layer acts as a binding layer for another, leaving the top layer to become the active surface layer. The chemistry of a CO_2-switchable system involves the formation of ions (an ammonium hydrogen carbonate species) to change the

ionic strength of a solution; incorporate this into surface chemistry, and the ions play a role in wettability. Since electrostatic self-assembly involves both cations and anions—and not always a perfectly balanced amount of either, because successful binding does not depend on a perfect ratio—this process could potentially hinder the effects of an ammonium hydrogen carbonate species on wettability.

The better alternative for self-assembled materials is the approach consisting of the formation self-assembled monolayers. The SAM approach involves the spontaneous assembly of synthetically accessible constituent molecules such as thiols and silanes onto an appropriate substrate. In the 1980's, scientists discovered that alkanethiols spontaneously assemble on noble metals. This discovery opened up the doors to a simple and effective method for creating new surfaces. They found that, by placing a gold surface into a millimolar solution of an alkanethiol, virtually any desired surface chemistry could be achieved. The resulting crystalline-like monolayers on the metal surface were then termed self-assembled monolayers.[10]

Thiol and dithiol SAMs on metals, particularly on Au, have attracted considerable attention due to their easy preparation from gas phase or from solution and their relatively high stability mediated by the strength of the S–Au bond and by van der Waals interactions.[9]

The sulfur-gold affinity is one of the driving forces for self-assembly, but it has little to no influence on the arrangement of each molecule on the surface. Surface packing is chiefly controlled by the hydrophobic van der Waals interactions that occur between the methylene carbons on the neighbouring alkane chains. These hydrophobic interactions cause alkanethiol chains to tilt in order to maximise chain-chain interactions, effectively

lowering the overall surface energy of the SAM. When chain length exceeds ten carbon atoms, the hydrophobic chain-chain interactions are strong enough such that they overcome the molecule's rotational degrees of freedom.[11,12]

A typical alkanethiol is broken down into three parts: the terminal sulphur group, which forms a strong, covalent bond with the substrate; the hydrocarbon chain (of variable length), which stabilizes the SAM through van der Waals interactions; and the head group, which can have different functionalities. The head group provides a platform to tailor the surface chemistry of the material through further functionalisation. By simply changing the head group, a surface can be designed to be: hydrophobic (alkyl); hydrophilic (carboxyl, amino, etc.); protein resistant (ethylene glycol); or chemically reactive (azide, sulfur, alkene, carboxyl, primary amine, etc...).[9] Due to the wide variety of surface properties that are readily available, the gold-thiol SAM system is a very attractive methodology for the creation of smart materials.

An alternative to the gold-thiol methodology for SAM creation is the silicon-silane method. Silane coupling agents are a family of organosilicon monomers, represented by the general structure R-SiX_3, where R is a functional group bound to silicon in a hydrolytically stable manner. Silane compounds are commonly available, with functionalities such as amino (-NH_2, -NR_2), vinyl (-$CH{=}CH_2$), alkyl (-CH_3), and mercapto (-SH). The X term is most commonly a methoxy (-OCH_3) or ethoxy (-OCH_2CH_3) group. These groups undergo hydrolysis in the presence of minute quantities of water to form a reactive silanol species. After hydrolysis, the reactive silanol species will undergo either self-condensation, which is not desired, or condensation with the substrate, which is desired.

Silane hydrolysis and condensation (silane-silane or silane-substrate) reactions transpire at the same time, for most silanes both reactions happen rather rapidly. Silane self-condensation reactions need to be minimised in order to form well-ordered SAMs. Prolonging the lifetime of the reactive silanol species in solution will increase the chances of silane-substrate condensation and reduce the chances of silane-silane self-condensation. Slightly acidified water, pH 3-6, has been shown to slow the condensation process.[13] For most silanes, an acidic solution is preferred. To further avoid self-condensation, silane concentrations should not exceed 1 to 10% v/v; commonly, 10 mM silane in an anhydrous solvent is used.

Silanes with basic functionalities (i.e. an amine) are susceptible to potentially problematic acid-base interactions, such as protonation of the amine when low pH-aqueous deposition solutions are used. Protonation of the amine can hinder silane-substrate condensation, thus reducing monolayer formation. Additionally, protonation of the amine functionalities at low pH will reduce the number of amine functional groups that are capable of binding CO_2, thus require additional workup steps to yield a fully functional CO_2-responsive surface. It is therefore recommended that silanes with basic functionalities, such as amino ($-NH_2$, $-NR_2$) groups, be deposited onto substrates in basic or anhydrous solutions. Basic solutions with pH values upwards of pH 11 are recommended; triethylamine is commonly used as the additive to increase pH.[14]

Most commercial silanes have limited solubility in common solvents. The most versatile solvents for silane compounds are ethanol and toluene.[15,16] While both solvents are effective deposition solutions, the higher boiling point of toluene allows for higher temperatures that can drive off the alcoholic byproducts of silane hydrolysis and

condensation, thus driving the surface functionalisation forwards. Multiple depositions were screened throughout this thesis. However, the use of anhydrous toluene as the deposition solvent resulted in the most reproducible results.

Further chemical modification of a silicon surface, whether at the silicon interface or from a tethered functionality, can be achieved through standard peptide coupling and acyl transfer methods. The reaction of nucleophiles with acyl transfer reagents, such as acid chlorides, is one of the most important classes of functionalisation reactions used in organic synthesis.[17,18] Fundamentally, acyl transfer reactions allow for the linking of two nucleophilic species. Thus, acyl transfer reagents provide a powerful tool for building molecules or functional materials, such as CO_2-responsive surfaces. Commonly, the corresponding transfer of an electrophilic carbamoyl species ($R^1R^2NC=O$) is used in the formation of ureas, carbamates and thiocarbamates.[17]

One of the more prominent acyl transfer groups that has recently received attention in the literature is 1,1'-carbonyldiimidazole (CDI). The intermediate imidazolides obtained upon the reaction of CDI with a nucleophilic species possess reactivity comparable to acid chlorides. However, they are more easily handled and may be isolated if required.[19] In addition to the ease of use, CDI is relatively inexpensive and the byproducts of the reaction are CO_2 and imidazole. In most regards, the use of CDI and CDI-mediated coupling is an example of green chemistry. As such, CDI-mediated coupling is an attractive alternative to traditional carbodiimide-based reagents that are commonly employed in peptide coupling reactions such as N,N'-dicyclohexylcarbodiimide (DCC), 1-ethyl-3-(3-dimethylaminopropyl)carbodiimide

(EDC), and N-[(dimethylamino)-1H-1,2,3-triazolo-[4,5-b]pyridin-1-ylmethylene]-N-methylmethanaminium hexafluorophosphate N-oxide (HATU).

Polymer grafting methods, such as SI-ATRP, are powerful tools for the modification and manipulation of surface properties.[20] In the broadest sense, polymeric grafts can be thought of as a thin film of polymer that is covalently linked to a substrate. Covalent bonding imparts a durability to the polymer thin film that is not easily achieved with physisorbed methods. SI-AGET-ATRP methods developed in Chapter 4 will be discussed here as they are applied to silicon surfaces. Additionally, two literature examples of CO_2-responsive polymer grafts on a silicon surface will be presented and reviewed critically.[7,21]

5.1.4 Physical modification of surfaces

The wetting characteristics of a surface can be enhanced by creating a rough surface on a hydrophobic material or by modifying a rough surface with a hydrophobic coating. Consequently, the pursuit and study of superhydrophobic surfaces often involves the physical modification of silicon surfaces. Surface roughening or patterning is often achieved through photolithography, nanocasting, vertically alinged carbon nanotubes, wet etching, and electron-beam lithography.[8] Despite their excellent performance, these methods suffer from shortcomings, such as involving multiple complex steps that require expensive clean room facilities and the need for expensive lithographic masks.[22]

In comparison to these methods, direct laser processing of the silicon substrate has emerged as a dominant novel approach for the modification of surface wettability.

Numerous examples of hierarchical structures consisting of micro- and nanoscale features have been created using laser patterning. Laser patterning systems do not require clean room facilities and experiments can be conducted in a vacuum or gaseous atmospheres such as air and SF_6.[22] Laser patterning is particularly useful for the creation of biomimetic surfaces in which complex surface patterns are required. There have been several laser-assisted techniques applied to the fabrication of biomimetic surfaces. In a recent review, Chen et al. compiled a comprehensive study of laser microfabrication on biomimetic wettability; techniques such as direct laser writing, laser interference lithography, pulsed laser deposition, and laser-textured templating are discussed.[22]

Traditional nanosecond (ns) laser systems have an apparent drawback of photothermal ablation, which brings about a significant amount of molten material and produces a "corona" around the ablated hole.[23] Progress in technology has given birth to a new femtosecond (fs) laser system with an ultrashort pulse of <1 picosecond (ps). A comparison between the structures created with the ns and fs lasers demonstrates that fs laser micromachining can tremendously increase the precision associated with microstructuring. The increase in precision can be associated with the very rapid creation of vapour and plasma phases, negligible heat conduction, and an absence of a liquid phase.[22]

Despite being in its infancy, laser microfabrication techniques are gaining attention as reports of their use proliferate rapidly. The first reported example of a CO_2-responsive superhydrophobic/superhydrophilic surface was reported by Stratakis et al. using dual-length-scale roughened silicon wafers that were fabricated using fs laser patterning techniques.

5.2 Results and discussions

5.2.1 CO_2-responsive polymer thin films

CO_2-responsive polymeric thin films were evaluated as smart materials. The smart surface comprises a silicon wafer, or a glass slide, onto which a polymer thin film has been spun. PDEAEMA has been studied within the Jessop and Cunningham research groups and has been shown to be a CO_2-switchable polymer.[4] PDEAEMA and PDEAEMA-co-polymers were synthesised using conventional free radical polymerization using VA-061 as a thermal initiator (Figure 5.1).

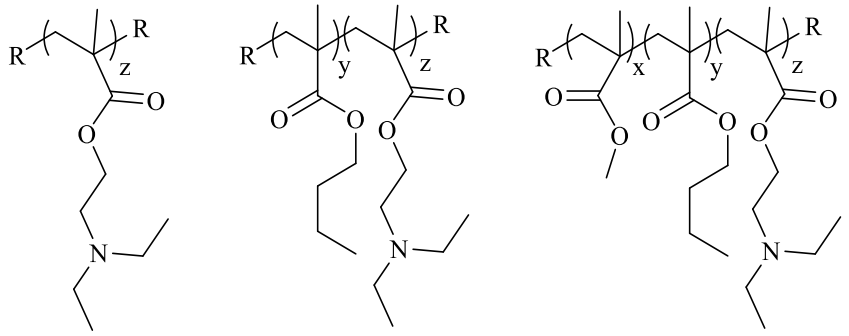

5-1 **5-2** **5-3**

Figure 5.1. PDEAEMA (5-1), P(BMA-co-DEAEMA) (5-2), P(MMA-co-BMA-co-DEAEMA) (5-3).

Thin films of ~50.0 kDA poly(diethylamino)ethylmethacrylate (PDEAEMA) polymers and copolymers were spun onto clean glass microscope slides. Solutions of PDEAEMA in methanol having a concentration of 2 mg/mL were spun at 5000 RPM. Coated slides were oven cured at 110 ℃ for 10 min. CO_2-responsive behaviour of the thin films was examined using WCA (water contact angle) analysis. WCA analysis was

conducted before and after CO_2 exposure; CO_2 was introduced to, and removed from the thin films by the following protocol:

1. $CO_{2(g)}$ was bubbled through a gas dispersion tube into a glass beaker of Millipore water (pH 8.2) until pH was <4. The solution was at room temperature, which was ca. 22 °C.
2. Glass slide supported thin films were placed into the low pH solution for a total of 30 min. $CO_{2(g)}$ was continually bubbled during that 30 min exposure time.
3. After 30 min, the glass slide-supported thin films were removed and characterised by WCA analysis.
4. Ar was sparged through the glass beaker of Millipore water, which was heated to 60 ˚C.
5. The hydrophilic forms of glass slide-supported thin films were placed into the Millipore water for a total of 30 min. Ar was continually bubbled during that 30 min exposure time and a constant temperature of 60 °C was maintained.
6. After 30 min, the glass slide-supported thin films were removed and characterised by WCA analysis.

Initial characterization of the PDEAEMA thin films proved difficult; PDEAEMA (5-1) has a low glass transition temperature (T_g) of ca. 20 °C.[24,25] Below its T_g, a polymer will be glassy, hard, and brittle. Above its T_g, a polymer will be in a molten or rubbery state, making it difficult to manipulate and weigh precisely, which is the case for PDEAEMA at room temperature. The T_g of amorphous mixtures and random copolymers were estimated using the Fox equation; where w_A is the mass fraction of component A, and T_{gA} is the glass transition temperature for homopolymer A, etc… (Equation 5.1).[26]

$$T_{gCopolymer}^{-1} = w_A T_{gA}^{-1} + w_B T_{gB}^{-1} + w_C T_{gC}^{-1} \quad (5.1)$$

Once the PDEAEMA thin film was exposed to CO_2 in water, the polymer film separated from the glass slide and partially dissolved in solution. Desorption of the polymer thin film was hypothesised to be due to the polymer's high solubility in water when exposed to CO_2.

To decrease PDEAEMA's water solubility, a hydrophobic monomer was added. Butyl methacrylate (BMA) has a predicted logD of 2.63, whereas DEAEMA has a predicted logD of 1.03 at pH=8 and logD of -1.41 at pH=4.6.[27] BMA was copolymerised with DEAEMA at various ratios to lower the water solubility of the resultant copolymer (5-2). The resultant P(BMA-co-DEAEMA) polymers were not soluble in water at room temperature. However, the P(BMA-co-DEAEMA) polymers had a T_g of approximately 17 ºC, thus the P(BMA-co-DEAEMA) polymers were difficult to work with at room temperature. The P(BMA-co-DEAEMA) polymers were spun onto glass slides and despite having a decreased solubility in water, they separated from the glass slide upon exposure to CO_2 and water.

Poly(methyl methacrylate) (PMMA) has a T_g of 104 ºC.[28] Thus, PMMA was considered a suitable candidate to raise a copolymer's overall T_g. DEAEMA, BMA, and methyl methacrylate (MMA) were copolymerised at a 1:1:1 molar ratio to yield a terpolymer (5-3) with an adequate T_g (45 ºC) and a sufficiently low water solubility. Unfortunately, the resultant terpolymer still failed to remain attached to the glass slide upon exposure to CO_2 in water. Generation of the terpolymer's hydrophilic form, a salt complex

with a bicarbonate anion, raised the terpolymer's water solubility such that it peeled away from the glass slide (Figure 5.2).

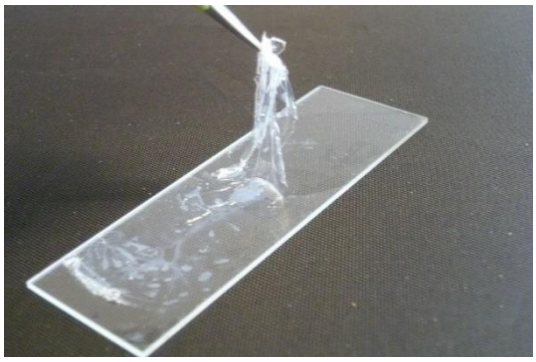

Figure 5.2. A CO_2-responsive polymer thin film of P(MMA-co-BMA-co-DEAEMA) terpolymer (5-3) desorbing from the glass slide. The image was captured shortly after exposure to CO_2 in water.

It was concluded that CO_2-responsive polymer thin films failed to show any promise in applications that would be of current use. Additionally, owing to the fact that a CO_2-responsive polymer becomes increasingly soluble in water when CO_2 is present, the CO_2-responsive polymer would need to be covalently bound to the substrate to prevent desorption of the CO_2-responsive functionality from the surface.

5.2.2 CO_2-responsive amino-silane self-assembled monolayers

The problems associated with the materials prepared by coating a surface with a CO_2-responsive thin film (i.e. desorption) were addressed by functionalising the surface of a solid material by covalently attaching a switchable moiety. Covalently attached CO_2-responsive surfaces were achieved by the direct functionalisation of a silicon wafer or glass slide using silanes bearing a CO_2-responsive moiety (Scheme 5.1).

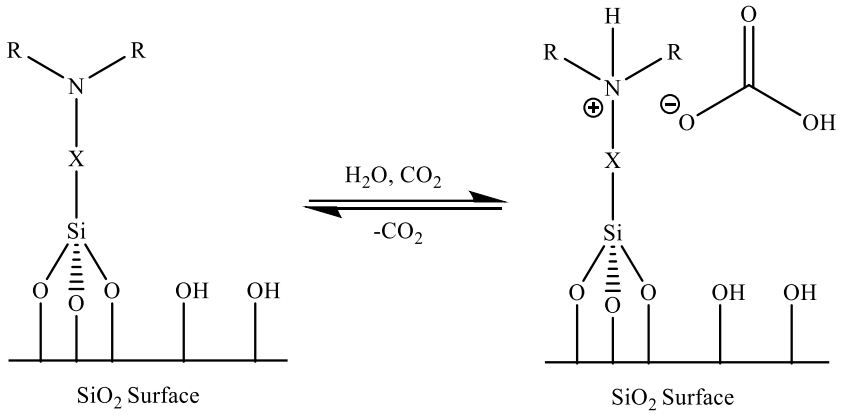

Scheme 5.1. A generic depiction of a CO_2-responsive silane-functionalised surface, where X: ethylene or propylene and R: methyl or ethyl.

Glass microscope slides were cleaned by exposure to acidic piranha solution at 85 °C for 1 h, followed by basic piranha solution at 70 °C, for 20 min.[29,30] The cleaned surfaces were functionalised immediately after the pretreatment process to minimise unwanted surface contamination. Cleaned surfaces were immersed in a 1% v/v solution of silane in anhydrous toluene, at 70 °C, overnight. Silane-functionalised surfaces were washed thoroughly and sonicated in toluene three times to ensure that any physisorbed silane was washed away from the substrate. Silane-functionalised surfaces were evaluated by WCA before and after CO_2 exposure, the results of which are summarised in Table 5.1.

Table 5.1. Water contact angles of glass slides coated with various silanes.

Silane	Water Contact Angle			σ	Switch
	Initial	Exposed to CO_2	CO_2 Removed		
n-Hexyltrimethoxysilane (S1)	101°	103°	101°	3°	2°
(N,N-Dimethylaminopropyl)trimethoxysilane (S2)	87°	57°	-	6°	30°
(Diethylaminomethyl)trimethoxysilane (S3)	84°	48°	-	6°	36°
[3-(Diethylamino)propyl]-trimethoxysilane (S4)	94°	20°	91°	9°	74°
N,N-dimethyl-N'-(3-(trimethoxysilyl)propyl)acetimidamide (S5)	69°	42°	-	9°	27°

The molecular structures for the silanes tested are shown in Figure 5.3. Silanes S1-S4 were purchased from commercial sources, and S5 was synthesised from 3-(aminopropyl)triethoxysilane (APTES) and N,N-dimethylacetamide dimethyl acetal.

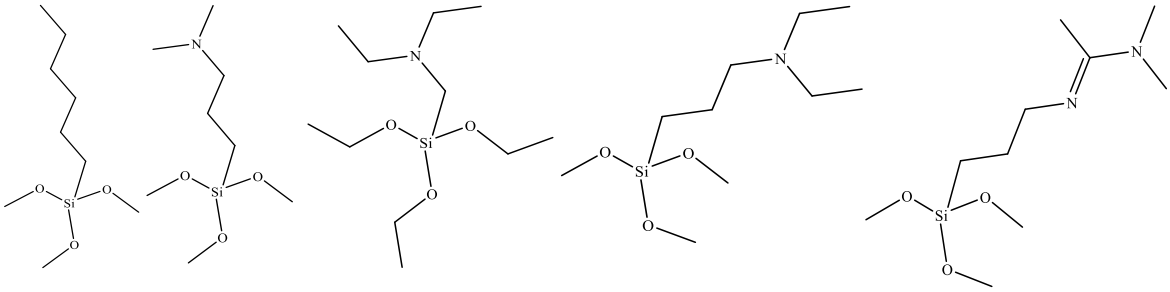

Figure 5.3. Various amino-silanes used for the functionalisation of glass and silicon substrates. The corresponding names of each compound can be found in Table 5.1.

An alkyl-silane, hexyltrimethoxysilane (S1), was first used to functionalise the silicon or glass surfaces to establish whether direct bond formation between the surface and silane would be robust enough to withstand the CO_2 switching processes. S1 was

chosen as a test compound because it was structurally similar to silanes bearing CO_2-responsive functional groups but it did not contain a CO_2-responsive functional group; thus, the stability of the silane linkage to the surface could be isolated and probed directly. The surface of a glass microscope slide functionalised with S1 remained hydrophobic before CO_2 exposure, after CO_2 exposure, and after CO_2-removal (Table 5.1). Thus, it was concluded that the Si-O-Si bond was strong enough to withstand the switching process.

A variety of amine or amidine-containing silanes were tested by WCA analysis for CO_2-responsive behaviour (Table 5.1). A detailed description of WCA analysis for CO_2-responsive behaviour is outlined in Section 5.4.10. [3-(Diethylamino)propyl]-trimethoxysilane (S4) offered the largest change in water contact angle upon switching between its hydrophilic form and its hydrophobic form. Consequently, S4 was selected for further testing. Glass surfaces functionalised with S4 were successfully switched from a hydrophobic form to a hydrophilic form by exposure to CO_2 in water. The addition of Ar and heat (~60 °C) resulted in the switch of the material back to its hydrophobic form, but the material was not readily switched back to its hydrophilic form with subsequent exposure to CO_2 in water. The material(s) persisted in a hydrophobic state. XPS analysis of the silane-functionalised surface before and after CO_2 exposure indicated no change in the nitrogen content; therefore, the loss of CO_2-responsive functionalities from the substrate surface was not the cause of the persistent hydrophobic state. The persistent hydrophobic nature of the surface was hypothesised to be due to interactions between the amino-functional group and nonfunctionalised surface silanols on the silicon substrate (Figure 5.4).

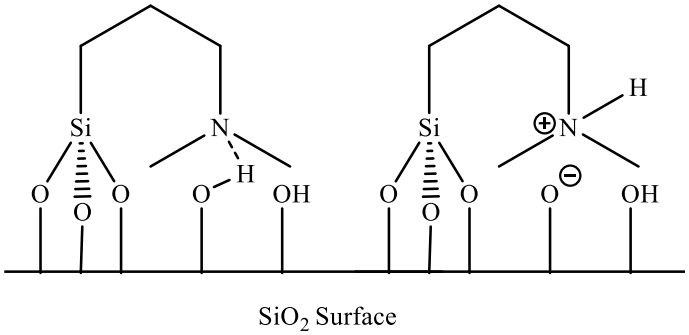

Figure 5.4. A graphic depiction of two possible interactions between a CO_2-responsive silane and the free surface silanols on a CO_2-responsive silane-functionalised surface.

Two strategies were envisioned to prevent unwanted amine-silanol interactions. Firstly, amino-silane surfaces were prepared. Once prepared, the functionalised surfaces were treated with 1,1,1,3,3,3–hexamethyldisilazane + trimethylchlorosilane (HMDS + TMCS) to functionalise any remaining free surface silanols (Scheme 5.2). This process is known as end-capping and is quite common with siloxane based materials;[15,16,31–37] the reaction is known to work in the presence of amines.[37]

$$R_3Si\text{-}OH \xrightarrow[\text{Base, rt}]{\text{TMSCl}} R_3Si\text{-}O\text{-}Si(CH_3)_3 + \text{Base}\cdot HCl \quad (5.2)$$

$$2\ R_3Si\text{-}OH \xrightarrow[\text{rt}]{\text{HMDS}} 2\ R_3Si\text{-}O\text{-}Si(CH_3)_3 + NH_3 \quad (5.3)$$

$$5\ R_3Si\text{-}OH \xrightarrow[\text{1\% TMSCl, rt}]{\text{HMDS}} 5\ R_3Si\text{-}O\text{-}Si(CH_3)_3 + NH_4^+Cl^- + NH_3 \quad (5.4)$$

Scheme 5.2. Reactions of common silylating agents used for silanol end-capping. Adapted from Anwander et al.[31]

Typical hydrophobic states, with contact angles of 90-95° were observed for glass slides treated with S4 and subsequently end-capped (Equation 5.4). Upon exposure to CO_2 for 30 min, no change in the WCA was noticed. Additional exposure for a total time of 2 h yielded a minimal, arguably negligible, variation in the WCA of approximately 10°.

A final treatment with glycolic acid was conducted to ensure full protonation of the amine functionalities. Protonation with glycolic acid should induce a hydrophilic state, even if for some reason carbonic acid had failed. Glycolic acid is a stronger acid, having a pK_a of 3.83, whereas carbonic acid has an apparent pK_{app} of 6.36. Exposure of the end-capped amino-functionalised surfaces to glycolic acid failed to induce a hydrophilic state; the surface was slightly more hydrophilic with a measured WCA of ca. 85°. Thus, both carbonic acid and glycolic acid failed to make a significant difference in the overall hydrophilicity of the material. It is hypothesised that either: a) the TMS capping group must be blocking the pathway for protonation by steric hindrance; or b) through hydrophobic contributions to the surface, TMS counteracts the hydrophilic effects of the protonated amine species.

It was postulated that creating a raised "effective surface" by introducing longer and/or larger monovalent or divalent moieties to the switchable moiety may put enough distance between the CO_2-responsive domain and the non-switchable silanol or capped-silanol groups to create a surface in which the top domain is CO_2-responsive. Having two distinct domains may be sufficient enough to allow the surface to exhibit CO_2-responsive behaviour. However, long chain amino-silanes that would distance the CO_2-responsive group from the substrate surface were not readily available.

It was thus determined that switchable silane moieties attached to silicon surfaces via Si-O-Si linkages that constain alkyl linkers of ethylene or propylene chains (Figure 5.3) were not a readily viable means for accessing a switchable surface of current use. Nevertheless, amidines and tertiary amine functionalities containing methyl and ethyl alkyl groups were demonstrated to be CO_2-responsive and the Si-O-Si linkages were determined to be stable over the range of conditions employed in CO_2 switching processes.

5.2.3 CO_2-responsive gold-thiol self-assembled monolayers

A CO_2-responsive self-assembled monolayer (SAM) on a gold surface was studied as an alternative in which potential acid-base interactions between free surface silanols and CO_2-responsive moieties would be non-existent. Additionally, the covalent gold-thiol bond circumvents earlier concerns regarding the physical desorption of the CO_2-responsive functionalities. A self-assembled monolayer created using N'-(6-mercaptohexyl)-N,N-dimethylacetimidamide was evaluated for CO_2-responsive behaviour (Scheme.5.3).

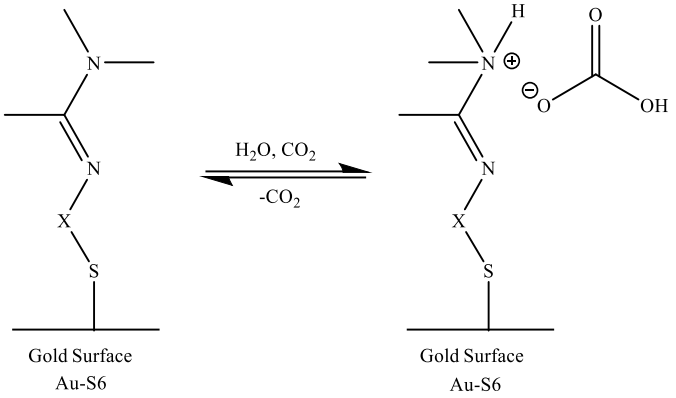

Scheme 5.3. A CO_2-responsive self-assembled monolayer on gold (Au-S6) where the functional thiol is N'-(6-mercaptohexyl)-N,N-dimethylacetimidamide and X is a hexylene linker.

Au-S6 was evaluated for CO_2-responsive behaviour as outlined in Section 5.2.1, and in detail in Section 5.4.10. WCA analysis was used to monitor changes in surface energy between the native state of Au-S6 (relatively hydrophobic), the state of Au-S6 when exposed to CO_2 (relatively hydrophilic), the state of Au-S6 after CO_2 had been removed from the system (relatively hydrophobic), and the state of Au-S6 during subsequent cycles of CO_2 exposure and removal (Figure 5.5).

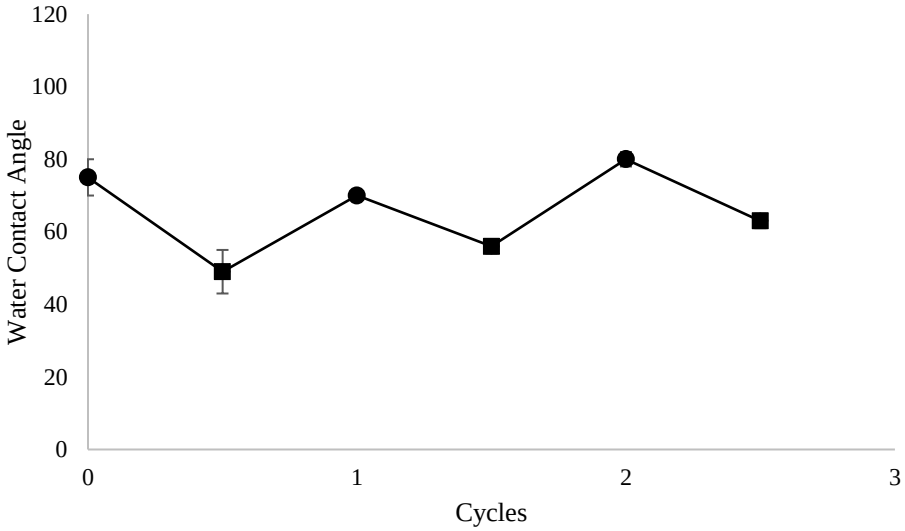

Figure 5.5. The CO_2-responsive behaviour of Au-S6 as measured by static water contact angle analysis over 2.5 cycles of switching from hydrophobic to hydrophilic and back to hydrophobic. Error bars represent the standard deviation for each data point. Au-S6 with CO_2 (■) and Au-S6 without CO_2 (●). Experimental procedure outlined in Section 5.4.10.

Observance of cyclic behaviour over a period of 2.5 cycles indicates successful switching between the relatively hydrophilic and relatively hydrophobic states of Au-S6. The average magnitude of change between CO_2 exposure and CO_2 removal was 19 $\pm$6°. The magnitude of change is not consistent over time (Figure 5.5). The relatively hydrophobic state could have been reduced by the incomplete removal of the bicarbonate species. The increased basicity of the amidine functionality, relative to amino-silanes S1-S4, would require a larger thermal input to reverse the reaction and evolve CO_2 from Au-S6; the persistence of bicarbonate salt after the thermal treatment would account of the reduced hydrophobicity noted in cycle 3. Au-S6 was cycled 2.5 times; however, by the 2nd cycle, a temperature increase was necessary to induce its hydrophobic form. Removal of CO_2 from Au-S6 in the hydrophilic state was unsuccessful at 60 ºC. Partial regeneration of hydrophobic surface character was observed at 70 ºC; full regeneration was not observed

until extended exposure at 80 ºC, which is sufficiently high to limit the energy savings offered by a CO_2-responsive system.

Additional analysis of Figure 5.5 shows an overall increase in the hydrophobicity of Au-S6**,** in both the charged and the neutral states. This upward trend is likely due to a combination of factors; the hydrophobicity of the surface could have been increased by contamination with dirt or oil, or by the loss of S6 from the gold surface. It was noted that the fragile mica substrate, onto which the Au layer was deposited, was easily damaged throughout the CO_2-switching process.

Importantly, Au-S6 was repeatedly able to switch between a hydrophilic and a hydrophobic state; the surface of Au-S6 does not contain silanols because it a gold substrate. Therefore, the switchable behaviour of Au-S6 supports the idea that interaction between free surface silanols and the CO_2-responsive amine functionalities was responsible for the persistent hydrophobic state that was observed with amino-silane functionalisation techniques on silicon and glass (Table 5.1 and Figure 5.4).

Furthermore, efficient use of SAMs currently requires Au surfaces, which are expensive and not practical for widespread use lining industrial pipelines or reaction vessels; also, tertiary amino-thiols are not readily available commercially, nor are amidine-thiols. Thus, amidino-functionalised thiol self-assembled monolayers on gold are not a readily viable means for accessing a switchable surface of current use.

5.2.4 CO_2-responsive silicon surfaces using 1,1'-carbonyldiimidazole as an acyl transfer reagent

The search for a robust method of functionalising a silicon surface with a variety of CO_2-switchable functionalities initially led to the use of 1,1'-carbonyldiimidazole (CDI). The Jessop and Cunningham research groups have had success with CDI based functionalisation methods in the past, when cellulose nanocrystals (CNCs) were modified through a one-step CDI-mediated coupling with 1-(3-aminopropyl)imidazole (API) to create CO_2-responsive cellulose nanocrystals.[38] Additional experimentation using CDI-mediated coupling for the synthesis of CO_2-responsive polysaccharide surfaces is discussed in Chapter 6.

In this section, the synthesis of CO_2-responsive silicon surfaces by CDI-mediated coupling is presented. CO_2-responsive silicon surfaces were created, but unfortunately, they could not be reliably reproduced. CDI-meditated reactions were explored and more reactive CDI-based carbamoylimidazolium salts were utilised in attempts to reproduce the successful results.

CDI-mediated reactions on silicon result in a silyl ester carbonate/carbamate linkage. The silyl ester carbonate/carbamate linkage was determined to be too unstable for the conditions at which the CO_2-switching processes occur. The envisioned CO_2-responsive surface as prepared by acyl transfer reagents is shown in Scheme 5.4.

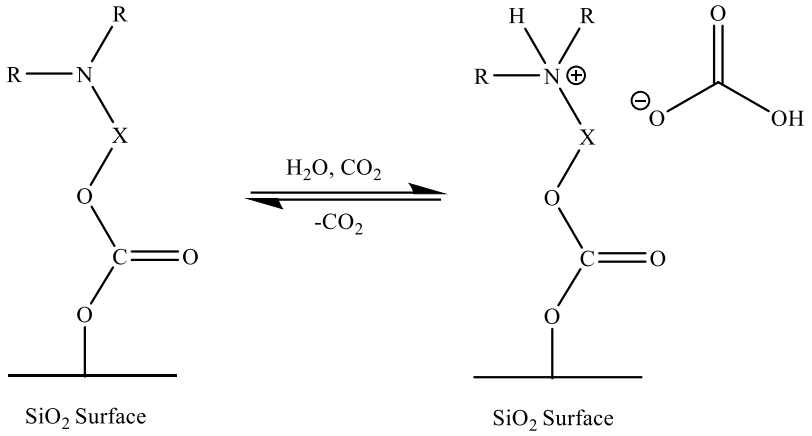

Scheme 5.4. A CO_2-responsive surface utilising a silyl ester carbonate linkage to the bulk substrate. X: ethylene or propylene, R: methyl, ethyl, isopropyl.

The synthesis of a CO_2-responsive surface via acyl transfer reagents contains three constituent parts: the silicon surface, the acyl transfer reagent, and the CO_2-responsive co-nucleophile. A variety of CO_2-responsive co-nucleophilic species were selected for their various pK_{aH} and log$\mathcal{P}$ values. The scope of CO_2-responsive co-nucleophilic species is shown in Figure 5.6. Highlights include species such as: 2-(diisopropylamino)ethanol, that is both basic and hydrophobic; 2-dimethylamino-1-ethanol, which is basic and relatively hydrophilic; and 1-(3-aminopropyl)imidazole, which is hydrophilic but a relatively weak base.

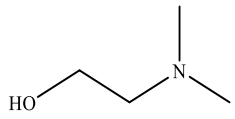

2-dimethylaminoethanol
pK_{aH}: 8.41
log$\mathcal{P}$: 0.56
LogD (pH 4.6): -2.77
LogD (pH 7.4): -0.49
S7

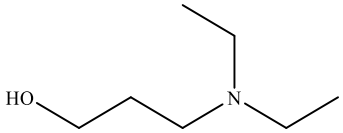

3-diethylamino-1-propanol
pK_{aH}: 10.00
log$\mathcal{P}$: 1.33
LogD (pH 4.6): -2.16
LogD (pH 7.4): -1.22
S8

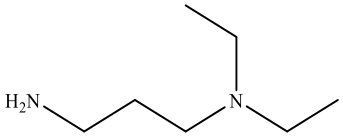

3-(diethylamino)propylamine
pK_{aH}: 9.84
log$\mathcal{P}$: 0.6
LogD (pH 4.6): -2.89
LogD (pH 7.4): -1.80
S9

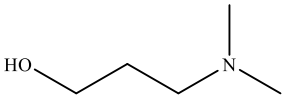

3-dimethylamino-1-propanol
pK_{aH}: 9.46
log$\mathcal{P}$: 0.62
LogD (pH 4.6): -2.86
LogD (pH 7.4): -1.42
S10

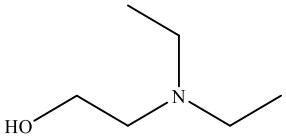

2-(diethylamino)ethanol
pK_{aH}: 8.96
log$\mathcal{P}$: 1.27
LogD (pH 4.6): -2.17
LogD (pH 7.4): -0.29
S11

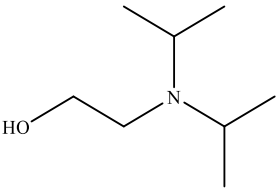

2-(diisopropylamino)ethanol
pK_{aH}: 9.52
log$\mathcal{P}$: 2.11
LogD (pH 4.6): -1.38
LogD (pH 7.4): 0.00
S12

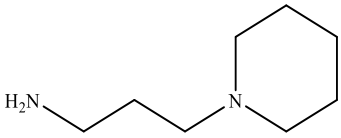

N-(3-aminopropyl)piperidine
pK_{aH}: 9.06
log$\mathcal{P}$: 0.74
LogD (pH 4.6): -2.17
LogD (pH 7.4): -0.92
S13

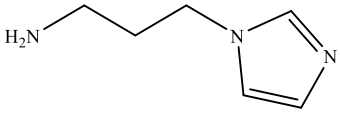

1-(3-aminopropyl)imidazole
pK_{aH}: 6.79
log$\mathcal{P}$: -0.22
LogD (pH 4.6): -0.80
LogD (pH 7.4): -0.29
S14

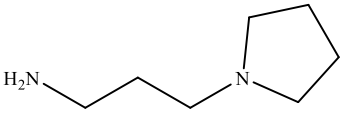

1-(3-aminopropyl)pyrrolidine
pK_{aH}: 9.19
log$\mathcal{P}$: 0.30
LogD (pH 4.6): -3.17
LogD (pH 7.4): -1.49
S15

Figure 5.6. Proposed CO_2-responsive co-nucleophilic species for acyl transfer group mediated coupling with a silicon substrate. All values were predicted using model compounds; model compounds are indicative of the compound when bound to a surface via a carbonate or carbamate bond (Appendix VII).[27]

In general, the CO_2-responsive surfaces were prepared in two ways. The first method involves mixing a solution of CDI and silicon substrate, then adding the CO_2-responsive co-nucleophilic species. The second method involves mixing CDI with the CO_2-responsive co-nucleophilic species first, and then transferring that solution over a silicon substrate. Owing to the difficulty of characterising a silicon surface, real-time analysis of the reaction could not happen. Therefore, the reactions were deemed successful if the resultant surface exhibited CO_2-responsive behaviour.

CO_2-responsive silicon surfaces using CDI-mediated coupling were not achieved using the methods that had been proven successful on polysaccharide surfaces.[2] CDI-mediated synthetic approaches result in the formation of imidazoline intermediates. When various acid catalysts are used, the imidazoline becomes a more reactive imidazolide. The addition of acid catalysts was met with varying success. CO_2 has been shown to increase the rate of CDI-mediated coupling (Scheme 5.5).[19] The application of CO_2 gas to the coupling reaction did not result in a CO_2-responsive surface.

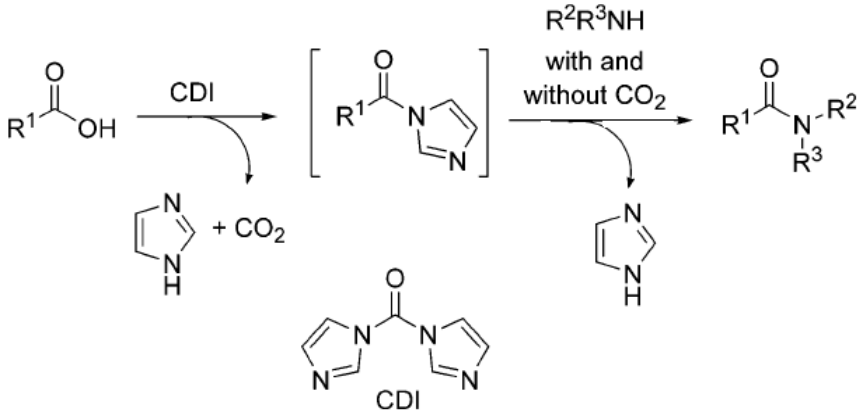

Scheme 5.5. General CDI-mediated coupling with and without CO_2. Image adapted from Vaidyanathan et al.[19]

In Scheme 5.5, R^1 is the silicon substrate resultant from initial coupling with CDI. The application of CO_2 was shown to facilitate the second coupling reaction through the mechanism shown in Scheme 5.6, where R^1 is the silicon substrate resultant from initial coupling with CDI and R^2NH_2 is a CO_2-responsive co-nucleophilic species such as S9 (Figure 5.6). The reactive intermediate, I, is expanded for clarity in Figure 5.7.

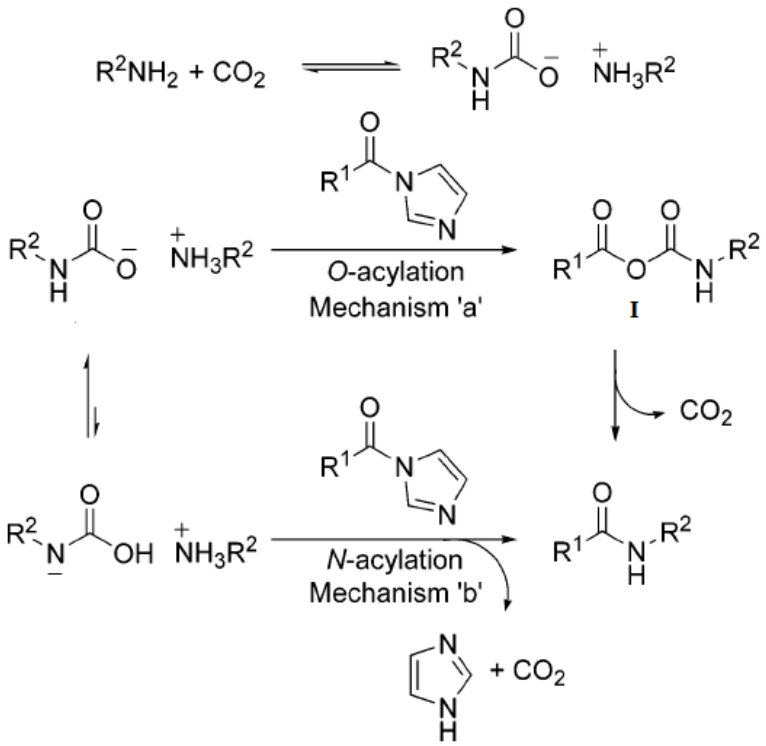

Scheme 5.6. Expanded CDI-mediated coupling with and without CO_2. Image adapted from Vaidyanathan et al.[19]

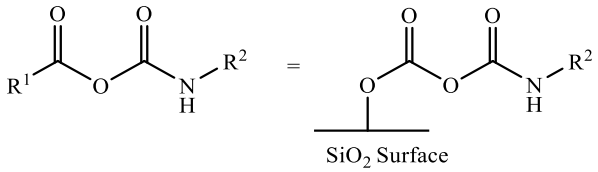

I **SiO_2-I**

Figure 5.7. Reactive intermediate, I, when envisioned for the synthesis of a CO_2-responsive surface, SiO_2-I.

The failure of the CO_2-promoted-CDI-mediated coupling reactions is postulated to occur when SiO_2-I is formed. This reactive intermediate is highly unstable and upon contact with a nucleophilic or protic species will likely degrade. A mechanism for the base catalysed degradation of SiO_2-I with residual water is proposed in Scheme 5.7. The base could be any number of species and probable candidates are shown; the most likely basic species involved in the catalytic degradation of SIO_2-I is the tertiary amine of the amino-functional group.

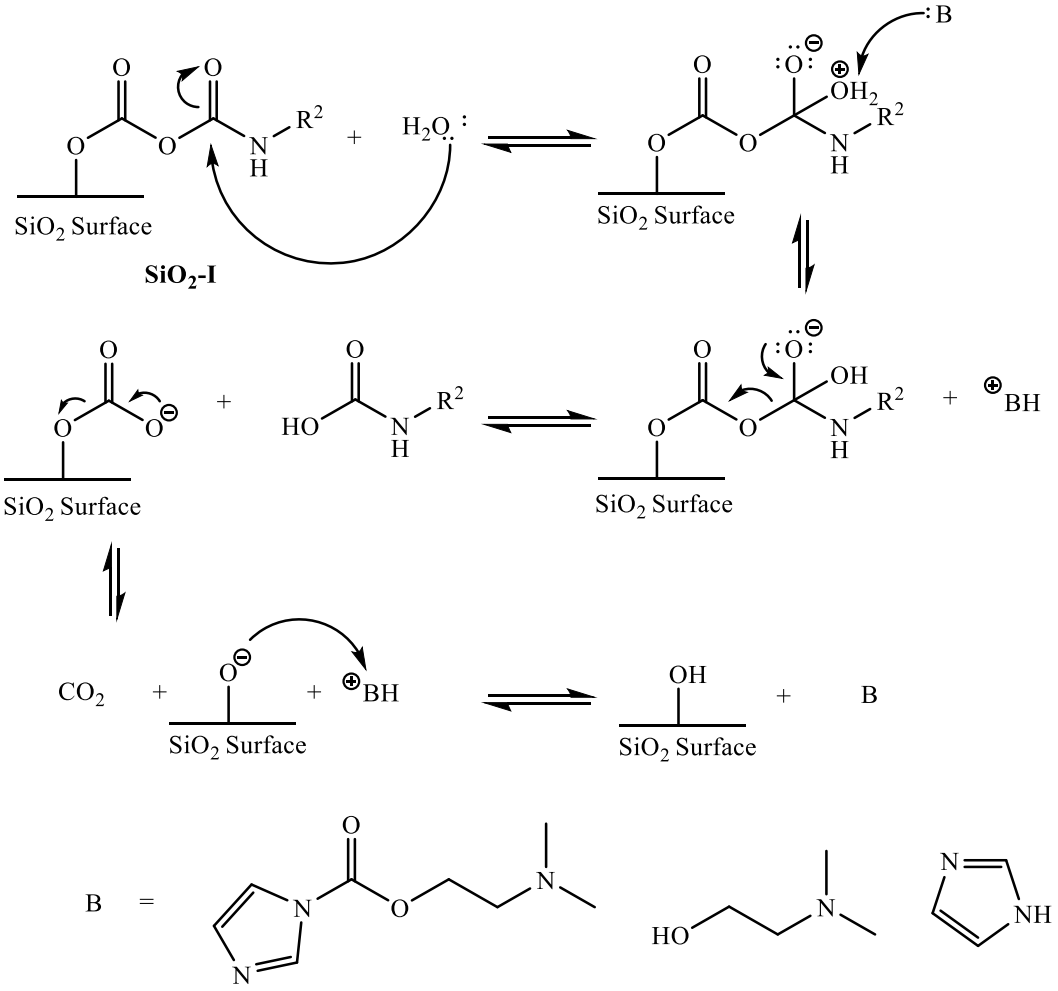

Scheme 5.7. Proposed mechanism for the base catalysed degradation of SiO_2-I with residual water.

Similarly, the final product is expected to be unstable owing to the silyl ester carbonate/carbamate bond. The base catalysed degradation of the final product (SiO_2-II) with residual water is shown in Scheme 5.8.

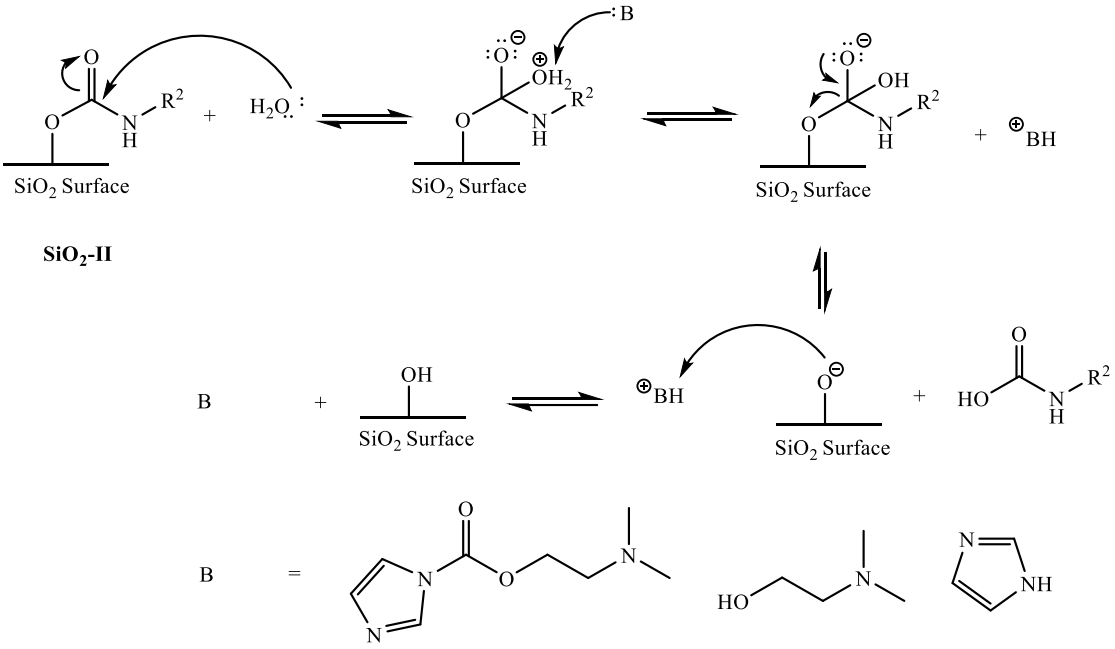

Scheme 5.8. Proposed mechanism for the base catalysed degradation of SiO_2-II with residual water. The bond to the surface could be a silyl ester carbamate (as shown) or silyl ester carbonate depending on which CO_2-responsive co-nucleophilic species is used.

Imidazole hydrochloride (ImHCl) has been shown to be a suitable alternative to using CO_2 as a promoting agent for CDI-mediated coupling reactions. ImHCl has been shown to promote the amidation of aromatic rings through CDI-mediated coupling by acting as a proton source for acid catalysis[39] (Scheme 5.9). The benefit of using ImHCl over CO_2 is that the reactive intermediate SiO_2-I is avoided.

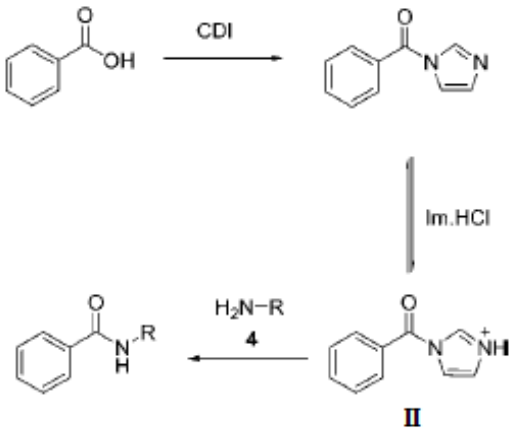

Scheme 5.9. CDI-mediated coupling the addition of imidazole hydrochloride (ImHCl) to form reactive intermediate II. Image adapted from Woodman et al.[39]

Protonation of the aromatic-bound imidazole group by imidazole hydrochloride increases the electron withdrawing properties of the bound imidazole. The resultant aromatic-bound imidazole-H^+ is a better leaving group and thus facilitates the subsequent nucleophilic attack, resulting in the formation of the desired product.

Both conjugate bases of the acid catalysed reactions using either CO_2 or ImHCl must be considered. CO_2 is evolved from the system after the initial coupling to form the reactive intermediate I (Scheme 5.6). Additionally, CO_2 is a byproduct of the final reaction. As such, CO_2 is present at each step of the reaction and can be easily removed when necessary. When ImHCl is used as the acid catalyst, the conjugate base byproduct is imidazole. Imidazole is already a byproduct that is produced throughout the coupling reaction. Additional imidazole is of little concern since its presence does not already inhibit product formation. Woodman et al. used an excess of ImHCl (1.5 eq.) and concluded that the addition of ImHCl significantly enhances the rate of the reaction.[39] Thus, in theory,

either acid catalyst (CO_2 or ImHCl) should not negatively affect the formation of the intended product.

In the literature, acid catalysis of CDI-mediated coupling reactions results in faster formation of reactive intermediates I and II. However, that enhancement did not translate to a silicon surface owing to the instability of the reactive intermediate SiO_2-I (when CO_2 is the additive) and the instability of the final product SiO_2-II (both CO_2 and ImHCl). No direct evidence for this conclusion is available since one cannot isolate SiO_2-I, or monitor the reactions when a silicon wafer is involved. Additionally, the surfaces tested did not exhibit obvious CO_2-responsive behaviour.

There are two discernable differences between the published methodologies and the methodologies that are proposed here (Scheme 5.5). Herein, the proposed method involves a silicon wafer and a CO_2-responsive functionality. Published methodologies do not contain either. Thus, it is likely that the wafer, the CO_2-responsive functionality, or the combination of the two are causing the failure of an otherwise robust reaction pathway. The remaining series of experiments in this chapter will fundamentally address one or both of these concerns.

The degradation pathway of the reactive intermediate SiO_2-I is proposed to be catalysed by the presence of a weak base (Scheme 5.7). Additionally, regardless of whether an acid catalyst is present, the product SiO_2-II is formed. SiO_2-II contains a silyl ester carbonate/carbamate that is hypothesised to degrade similarly to SiO_2-I. Given the stipulation that the silyl ester carbonate/carbamate species will exist and the reactive intermediate SiO_2-I is avoided, the only variable to manipulate is the base catalyst. CDI-mediated coupling is tolerant to the imidazole (pK_{aH}: 6.97) byproduct that is formed

in situ. However, there is no precedent for the stability of a silyl ester carbonate/carbamate in the presence of imidazole. One must presume that the silyl ester carbonate/carbamate is stable in the presence of imidazole. Otherwise, the CDI-meditated approach is fundamentally not suitable for silicon substrate. It is entirely possible that the CDI-mediated approach is not suitable for silicon substrates. However, for initial experiments that hypothesis must be rejected. Instead, we look to the most basic functional group that is present in the system, at the same time as the silyl ester carbonate/carbamate, being the CO_2-responsive tertiary amine.

To stop the base catalysed degradation of SiO_2-I or SiO_2-II the CO_2-responsive tertiary amine was protonated with HCl to form the hydrochloride salt. The remaining coupling steps were carried out in the presence of the hydrochloride salt and it was not until the material was fully prepared that the hydrochloride salt was removed with an excess of a non-nucleophilic base, tetramethylguanidine (TMG). SiO_2-S7, a dimethylamino-terminated CO_2-responsive surface was prepared in this manner (Scheme 5.10).

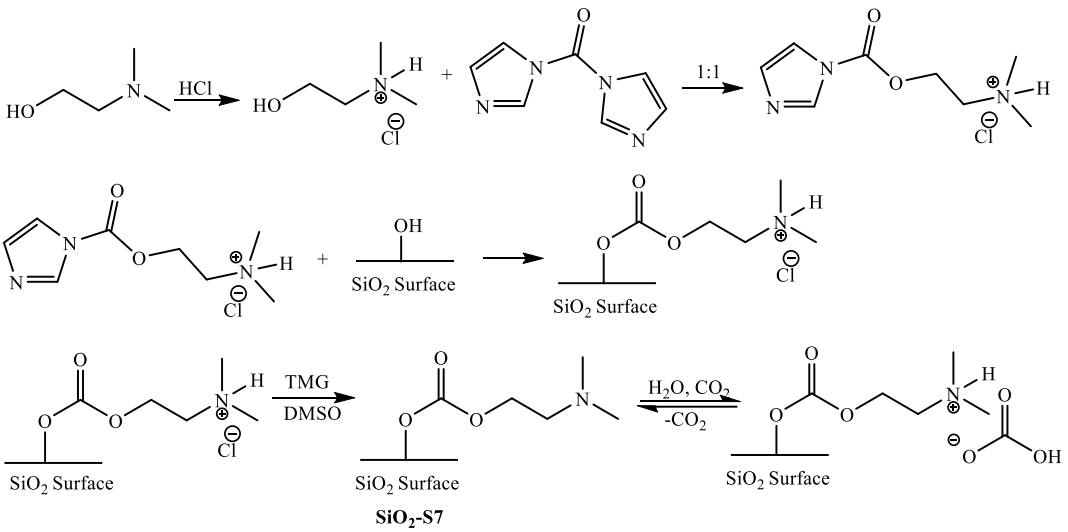

Scheme 5.10. Synthesis of a dimethylamino-terminated silicon surface, SiO_2-S7.

SiO_2-S7 exhibited CO_2-responsive behaviour over 4.5 cycles, switching from neutral and hydrophobic to charged and hydrophilic and back again (Figure 5.8).

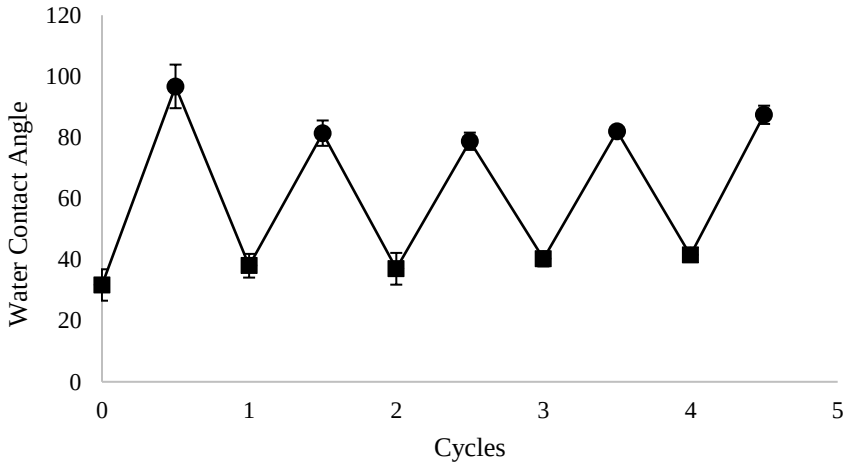

Figure 5.8. The CO_2-responsive behaviour of SiO_2-S7 as measured by static water contact angle analysis over 4.5 cycles of switching from hydrophilic to hydrophobic and back to hydrophilic. Error bars represent the standard deviation for each data point. SiO_2-S7 with CO_2 (■) and SiO_2-S7 without CO_2 (●). Experimental procedure outlined in Section 5.4.10.

The hydrophobic state of SiO_2-S7, as determined by WCA, was consistently >80° and the hydrophilic state was ca. 40°. The reproducibility of the CO_2-responsive behaviour declined after the 4th cycle, after which testing was concluded. The decline in the CO_2-responsive behaviour is hypothesised to be the result of a loss of CO_2-responsive functionality over time. It is plausible that when given enough time in solution, the final state of SiO_2-S7 degrades through the degradation pathway proposed in Scheme 5.8.

The results of this experiment could not be reproduced despite multiple efforts (e.g. sample CDI-14 and CDI-15). XPS analysis was conducted on those subsequent efforts; the nitrogen content was incredibly low and barely distinguishable from the baseline (0.6 At%). WCA of subsequent efforts showed no change in surface energy in response to CO_2 exposure. To increase the likelihood of achieving a result similar to that of SiO_2-S7, more reactive acyl transfer reagents were employed.

5.2.5 CO_2-responsive silicon surfaces using chloroformates as acyl transfer reagents

Acylations of silicon wafers and silica particles were carried out using methyl chloroformate (MCF), ethyl chloroformate (ECF), and phosgene in attempts to reproduce the results of SiO_2-S7.

The functionalisation of silica particles with MCF (KBB5PG39) was confirmed by XPS analysis. Subsequently, the MCF-functionalised particles were treated with S9 to produce a CO_2-responsive material (KBB5PG48**)**. XPS analysis of the S9-treated particles revealed a significant decrease in the At% of carbon and a negligible amount of nitrogen relative to the MCF-functionalised particles. The natural conclusion is that the MCF

functionality on silica is unstable in the presence of a nucleophile such as S9. It was hypothesised that the instability of the MCF functionality is due to the relative stability of the leaving groups (Scheme 5.11).

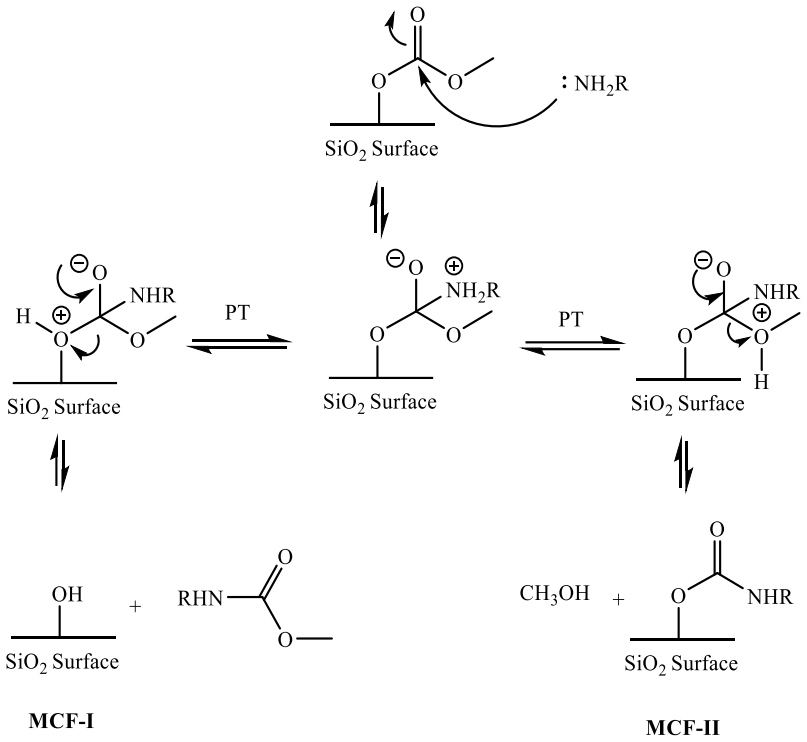

Scheme 5.11. MCF on a SiO_2 substrate. Applicable to either a silicon wafer or a silica particle. A proton transfer is indicated by PT.

The two elimination pathways are shown in Scheme 5.11. On the left, the surface silanol is eliminated and the resultant product is an unfunctionalised silicon wafer (MCF-I). On the right, the methoxy group is eliminated and the resultant product is the amine-functionalised silicon wafer (MCF-II). This reaction was applied to both a silicon wafer and silica particles, with the same results. The functionalised surfaces did not

demonstrate a response to CO_2. Thus, it is probable that the silanol is the preferred leaving group when MCF is used as an acyl transfer reagent, yielding MCF-I as the major product.

To increase the likelihood of silicon/silica functionalisation (i.e. formation of MCF-II) the leaving group needed to be improved. The methoxy group of MCF was changed to an ethoxy group, using ECF (Scheme 5.12).

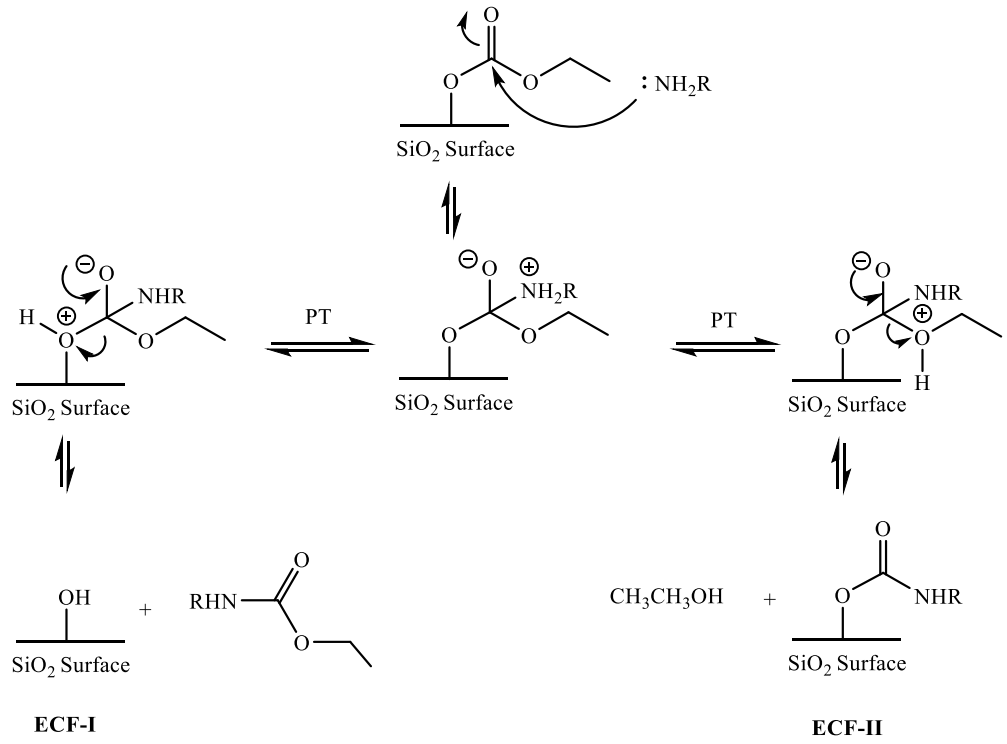

Scheme 5.12. ECF on a SiO_2 substrate. Applicable to either a silicon wafer or a silica particle. A proton transfer is indicated by PT.

The ethoxy group of ECF is a better leaving group than the methoxy group of MCF due to the increased ability of the longer alkyl chain to delocalize the charge that is formed on the oxygen of the leaving group. This increase in stability, however slight, proved enough to facilitate the functionalisation of the silicon wafer with a CO_2-responsive

functionality (ECF-II). XPS analysis of a silicon wafer treated with ECF and S14 showed significant nitrogen content (5.68 At%). Initial WCA analysis of SiO_2-S13 exhibited characteristic hydrophobic contact angles (>80°). Additionally, hexadecane contact angle analysis (HCA) was used to probe the oleophilic nature of the substrate. SiO_2-S13 was found to be superoleophilic, exhibiting an HCA of <10°. However, subsequent exposure to CO_2 and drying cycles reduced both the hydrophobic and oleophilic nature of the substrate. It is hypothesised that the silyl ester carbamate bond linking S14 to the silicon surface was not stable in the conditions associated with CO_2-switching over time.

A final effort to probe the stability of silyl ester carbonates/carbamates and CO_2-responsive functionalities was undertaken using phosgene as a coupling agent (Scheme 5.13). Phosgene is highly reactive and when handled appropriately is an efficient –albeit not green- method of acyl group transfer.

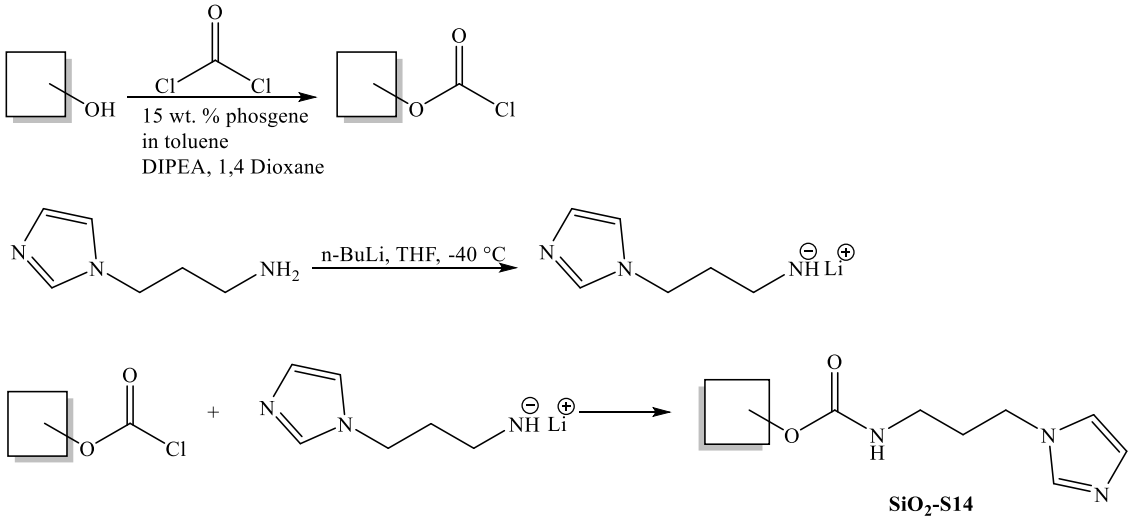

Scheme 5.13. Synthetic method for the synthesis of SiO_2-S14 via phosgene mediated acyl transfer.

Additional steps were taken to further increase the likelihood of the successful functionalisation of a silicon substrate with a CO_2-responsive functionality. The reactivity of the CO_2-responsive co-nucleophilic species was increased by activation with n-BuLi. S14 was chosen as the best CO_2-responsive co-nucleophilic species because the primary amine can be activated and the tertiary amine (i.e. the CO_2-responsive functionality) is less likely to promote a hydrolysis reaction in comparison to other CO_2-responsive groups. The imidazole of S14 is sterically hindered and a weaker base than other CO_2-responsive functionalities, therefore it is less likely to catalyse a hydrolysis reaction that would lead to the cleavage of the CO_2-responsive functionality from the silicon surface. The efforts were successful and CO_2-responsive behaviour over 4 cycles was recorded (Figure 5.9).

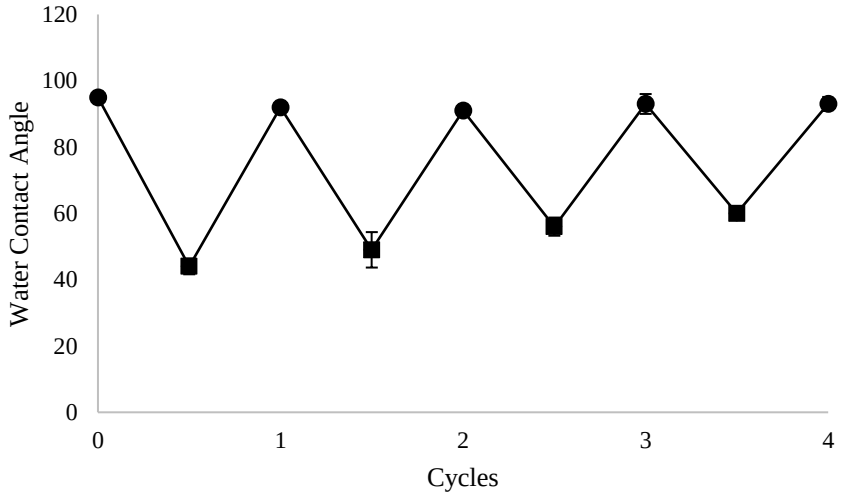

Figure 5.9. The CO_2-responsive behaviour of SiO_2-S14 as measured by static water contact angle analysis over 4 cycles of switching from hydrophobic to hydrophilic and back to hydrophobic. Error bars represent the standard deviation for each data point. SiO_2-S14 with CO_2 (■) and SiO_2-S14 without CO_2 (●). Experimental procedure outlined in Section 5.4.10.

Observance of cyclic behaviour over a period of 4 cycles indicates successful switching between hydrophilic and hydrophobic states of SiO_2-S14. The average magnitude of change between hydrophilic and hydrophobic states decreases over time. As seen in Figure 5.9, the hydrophobic nature of SiO_2-S14 is consistent whereas the hydrophilic nature of the surface gradually decreases. This observation could be explained by contamination of the surface with hydrophobic particles/oils or by the loss of CO_2-responsive functionalities. The CO_2-responsive functionalities could have been hydrolytically cleaved from the surface of SiO_2-S14 in the same manner in which SiO_2-II was proposed to degrade (Scheme 5.8). If a loss of CO_2-responsive functionality did occur, the resulting surface would consist of a free surface silanols. As previously discussed, the acid-base interactions between free surface silanols and CO_2-responsive functionalities are hypothesised to result in a persistent hydrophobic state. Thus, the loss of CO_2-responsive functionalities would result in an increase in the hydrophobicity of the surface when exposed to CO_2; thereby decreasing the average magnitude of change between hydrophilic and hydrophobic states as measured by the water contact angle.

In summary, CO_2-responsive surfaces have been created using a variety of acyl transfer reagents. Cyclic switching behaviour has been observed for multiple cycles. The lifetime of these CO_2-responsive surfaces is short, often under 5 cycles, with a measurable reduction in performance taking place as each cycle progresses.

Changes in both the hydrophilic state and the hydrophobic state of CO_2-responsive materials were observed over the course of experimentation. CO_2-responsive surfaces synthesised through the use of acyl transfer reagents are thought to be hydrolytically unstable. The silyl ester carbonate/carbamate linkage is not stable enough in an aqueous

environment to keep the CO_2-responsive functionality bound to the silicon or silica substrate. Multiple degradation pathways were proposed and discussed. The main degradation pathway is thought to be base catalysed hydrolysis.

5.2.6 CO_2-responsive smooth silicon surfaces using surface-initiated atom transfer radical polymerisation

Surface grafted-polymer brushes, functionalised with a tertiary ethyl amino group have been reported as a CO_2-responsive technology.[7] The authors of this report describe a PDEAEMA brush that can be switched between extended (hydrated) and collapsed (dehydrated) chain conformations, by passing CO_2 and an inert gas such as N_2 in solution. They use the CO_2-responsive surface for the reversible capture of proteins. With 5 consecutive switches being reported, cyclic CO_2-responsive behaviour has been demonstrated (Figure 5.10).

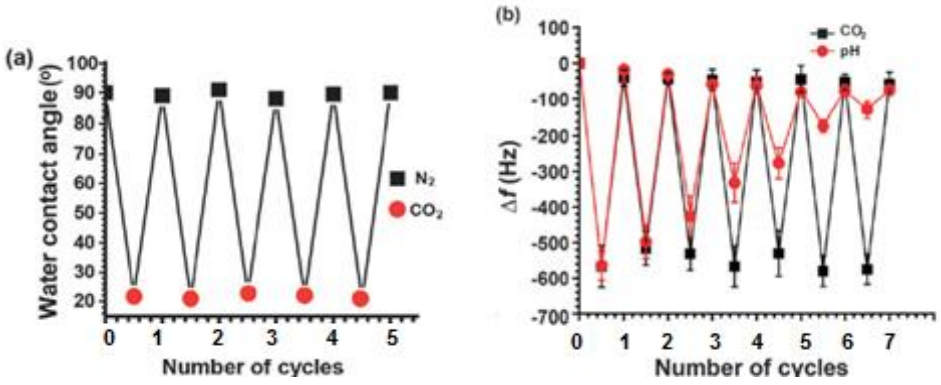

Figure 5.10. The CO_2-responsive behaviour of PDEAEMA brushes grafted from silicon wafers. (a) Image is denoting cyclic behaviour in response to CO_2. (b) Image is denoting the loss of cyclic behaviour in response to acid and base stimuli. Images adapted from Kumar et al.[7]

The CO_2-responsive polymer brush was characterised by ellipsometry and WCA. The authors did not report the molecular weight of the grafted polymer chain. Additionally, grafting density was modified but not reported in enough detail to facilitate reproduction and verification of their results.

Low-density surfaces result in a net reduction of steric repulsions and intermolecular interactions that can occur between neighbouring polymer brushes. Since changes in surface properties resulting from the use of polymer brushes are, in most cases, a consequence of morphological changes, a low-density surface would be expected to contribute to the ease at which this morphological change can occur. However, Kumar et al. do not specifically outline the exact ratios of reagents required to produce low-density surfaces within their described system.

Additionally, the method in which the polymerisation was conducted is not suitable for other CO_2-responsive polymers, such as PDiPAEMA, that may be of interest. For example, one could not produce near monodisperse PDiPAEMA chains at $M_n > \sim 10$ kDa, owing to the tendency of PDiPAEMA to precipitate out of polar solvents as M_n increases; methanol was used in their study. Their work can be improved upon with the CO_2-responsive polymerisation methods presented here.

Through the use of low initiator content, Kumar et al. were able to achieve an unprecedented increase the magnitude of change between the charged and hydrophilic state and the neutral and hydrophobic state of the polymer graft on a smooth surface. Since the exact ratio of reagents are not published, it is impossible to know for sure what the grafting density of the smart material was. However, a minor investigation into grafting density was conducted using a novel SI-AGET-ATRP approach developed here. The SI-AGET-

ATRP polymerisation method, when coupled with the synthetic outline for surface functionalisation that is presented within this chapter, has proven to be a viable tool to study these effects.

Another instance of a pH-responsive surface being achieved through the use of SI-ATRP was reported by Stratakis et al. (Figure 5.11).[21] The PDiPAEMA brushes were grafted from both smooth and roughened surfaces using traditional ATRP methods. The molecular weight and dispersity of the grafted polymer were not reported. Ultra-fast lasers in a reactive gas atmosphere were used to texture three dimensional micro-, nanostructured silicon surfaces, from which the PDiPAEMA chains were grafted This work highlights what can be achieved when the CO_2-responsive chemical response is coupled with cutting edge surface patterning techniques.

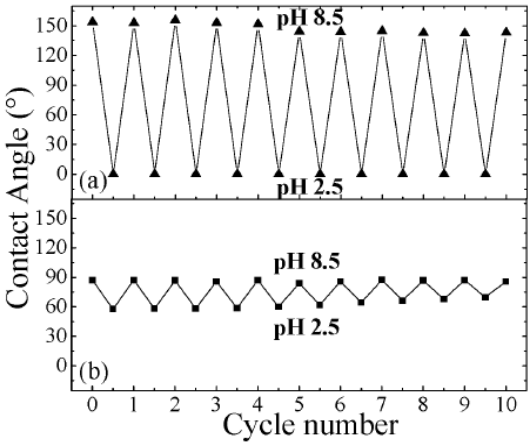

Figure 5.11. Average CA values of a water droplet residing on the PDiPAEMA functionalised hierarchically structured (a), and smooth (b) surfaces following successive immersions at pH 8.5 and pH 2.5. Reproduced from reference 21 with permission from The Royal Society of Chemistry.

Where Kumar et al. used CO_2 as a trigger, Stratakis et al. used HCl and NaOH solutions. As demonstrated by Kumar et al., the CO_2 system outperforms the acid-base system over continuous cycles when using a single solution to elicit a response from the material. The acid-base system as demonstrated by Stratakis et al. used multiple solutions where the acid never came in contact with the base, so the salt accumulation that Kumar et al. demonstrated did not happen.

When *grafting from* a smooth wafer, Kumar et al. established that low density PDEAEMA brushes switched reversibly from hydrophilic (WCA <10°) to hydrophobic (WCA ~90°). Stratakis et al. demonstrated a reversible switch from a hydrophilic state (WCA ~60°) to a hydrophobic state (WCA ~90°) when grafting PDiPAEMA from a smooth surface and from a hydrophilic state (WCA <10°) to a hydrophobic state (WCA ~150°) when grafting PDiPAEMA from a rough surface.

The two polymers, PDiPAEMA and PDEAEMA, are very similar and differ only at the alkyl substitution of the amine. Why is it then that Kumar et al. and Stratakis et al. observed very different results? The chosen polymer, grafting density, molecular weight, and anion effects could all probably explain the observed difference. The problem that lies herein is that these effects were not thoroughly investigated. Additionally, the polymerization methods used by Kumar et al. and Stratakis et al. are not conducive to studying these effects.

Kumar et al. and Stratakis et al. both used traditional SI-ATRP methods to graft CO_2-responsive polymers from a silicon surface. The shortcomings of traditional SI-ATRP methods on smooth surfaces are not as pronounced as they are with spherical surfaces. Regardless, the SI-AGET-ATRP methods presented within this work represent a step

forward in the design and understanding of CO_2-responsive materials. Efforts to reconcile the work of Stratakis et al. and Kumar et al. were undertaken using the SI-AGET-ATRP methodology developed in Chapter 4 and are presented herein. Methods to apply SI-AGET-ATRP across smooth and roughened surfaces are presented. Two methods were developed to graft PDiPAEMA on a smooth silicon wafer (Schemes 5.14 and 5.15). The molecular weight (M_n) and molecular weight dispersity (Đ) of grafted polymers is approximated by precise characterisation of the free polymer (FP) that is produced in-situ during the surface-initiated polymerization.

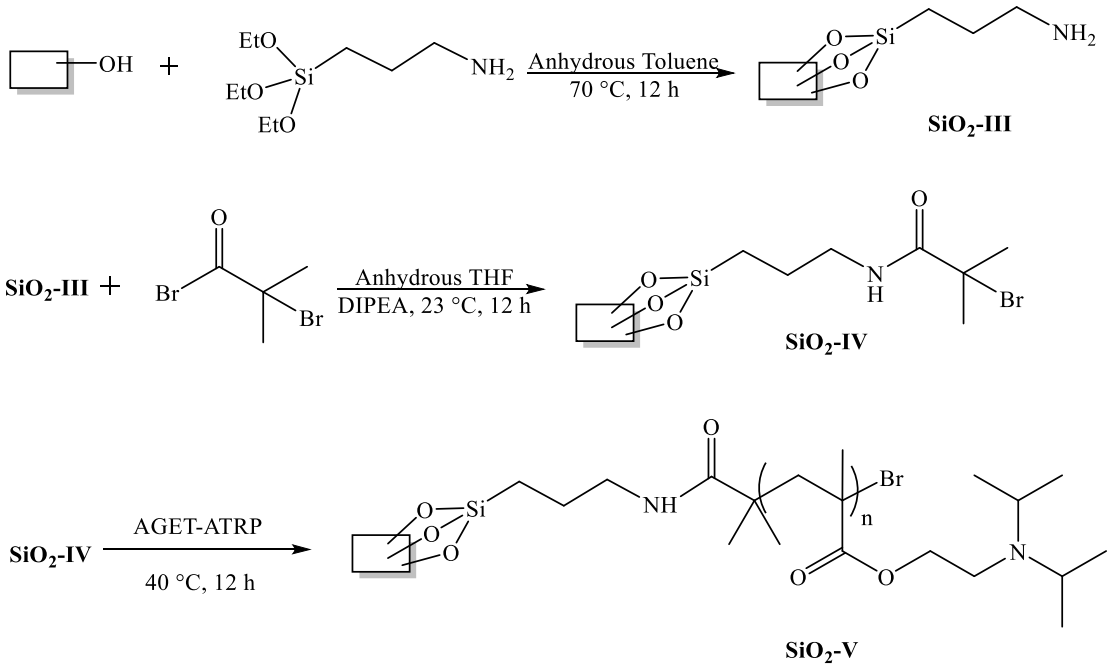

Scheme 5.14. SI-AGET-ATRP of PDiPAEMA from a silicon oxide surface, SiO_2-V.

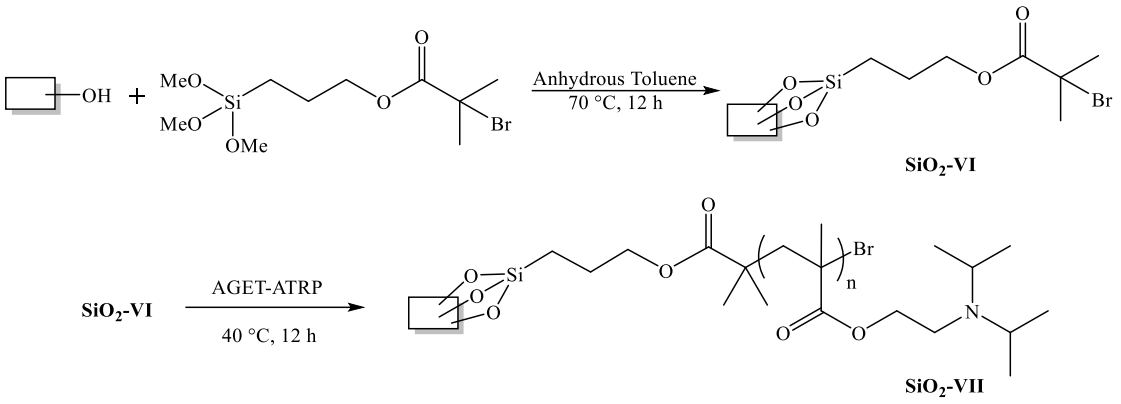

Scheme 5.15. SI-AGET-ATRP of PDiPAEMA from a silicon oxide surface, SiO_2-VII.

In both cases, the ATRP initiator is grafted using silane bonds to a silicon oxide surface. The first experiments use a two-step process to put the initiator on the silica surface (SiO_2-IV), whereas the latter method utilised a commercially available initiator-containing silane (SiO_2-VI). The results of both methods are the same. However, the use of a commercially available silane-based initiator simplifies the process. SiO_2-S15 was synthesised using the first method shown in (Scheme 5.14).

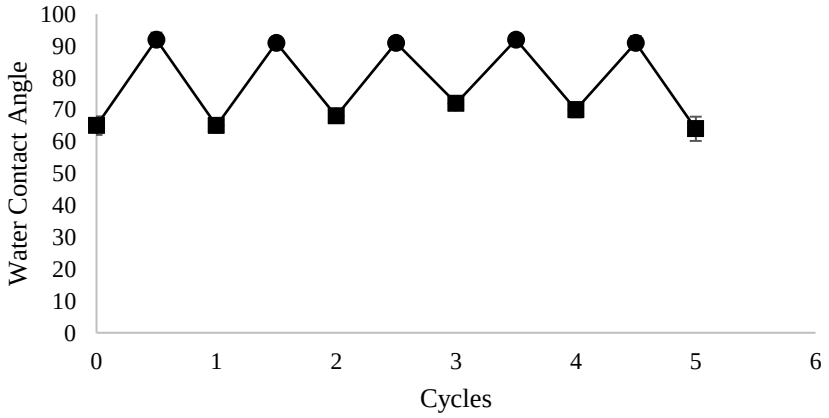

Figure 5.12. The CO_2-responsive behaviour of SiO_2-S15 as measured by static water contact angle analysis over 5 cycles of switching from hydrophilic to hydrophobic and back to hydrophilic. Error bars represent the standard deviation for each data point. SiO_2-S15 with CO_2 (■) and SiO_2-S15 without CO_2 (●). Experimental procedure outlined in Section 5.4.10.

The polymerisation for SiO_2-S15 reached 97% conversion in 24 h (FP M_n: 36.4 kDa, Đ: 1.35). Reproducible switching behaviour using CO_2 in water as the forward stimulus and waste heat as the reverse stimulus was observed. SiO_2-S15 demonstrated a reversible switch from a hydrophilic state (WCA~60°) to a hydrophobic state (WCA ~90°); this observation is in good agreement with the response observed by Stratakis et al.[21]

Similar CO_2-responsive behaviour was observed for SiO_2-S16. SiO_2-S16 was synthesised by the method shown in Scheme 5.15. The synthesis of SiO_2-S16 took a total of 3 steps: plasma cleaning of the substrate, initiator grafting, and polymerisation. The method outlined in Scheme 5.15 represents the shortest route in which a CO_2-responsive polymer can be *grafted from* a silicon surface. This experiment was conducted in tandem with another wafer that possessed a laser etched pattern (SiO_2-S17). The polymerisation of SiO_2-S16 reached 80% conversion and was stopped prematurely due to high viscosity (FP M_n: 41.1 kDa, Đ: 3.7). The molecular weight dispersity of the homopolymer produced in situ during the polymerisation SiO_2-S16 is poorly controlled. Experimental conditions were varied in subsequent polymerisations to increase the controlled nature of the polymerisation, thus lowering the dispersity of the molecular weight distribution. However, despite poor molecular weight dispersity SiO_2-S16 exhibited a reproducible response to CO_2 (Figure 5.13).

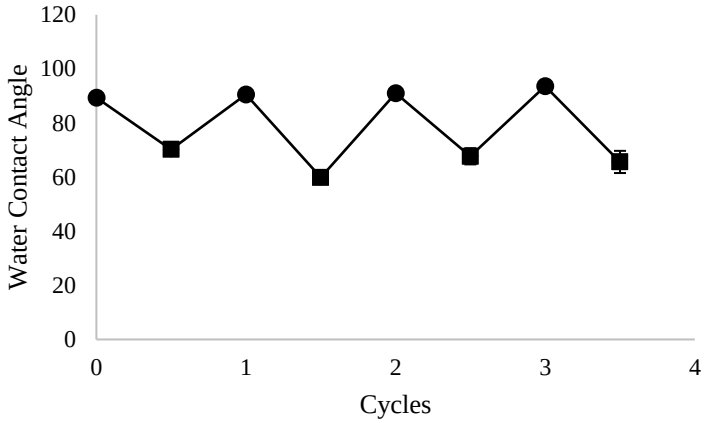

Figure 5.13. The CO_2-responsive behaviour of SiO_2-S16 as measured by static water contact angle analysis over 3.5 cycles of switching from hydrophobic to hydrophilic and back to hydrophobic. Error bars represent the standard deviation for each data point. SiO_2-S16 with CO_2 (■) and SiO_2-S16 without CO_2 (•). Experimental procedure outlined in Section 5.4.10.

The CO_2-responsive PDiPAEMA-grafted silicon surfaces produced to date are in good agreement with each other (Figures 5.12, 5.13) and with the work on smooth silicon surfaces reported by Stratakis et al. (Figure 5.11).[21] However, Kumar et al. report a much larger change in the magnitude of the response to CO_2, citing that their results were achieved by tailoring the grafting density of the polymer chains. Kumar et al. changed the initiator-grafting step such that a mixture of silanes was grafted to the surface; a silane containing no terminal functional group ("non-functional") was added in addition to the silane containing a functional group that facilitates SI-ATRP ("functional"). The details of this procedure are not reported.

SiO_2-S18 was created in an attempt to understand the work published by Kumar et al. (Figure 5.10).[7] SiO_2-S18 was polymerised from a surface that contained a mixture of silanes. The silane deposition solution consisted of 25 mol% functional silane

[(3-trimethoxysilyl)propyl-2-bromo-2-methylpropionate] and 75 mol% non-functional silane [n-propyltriethoxysilane] in anhydrous toluene.

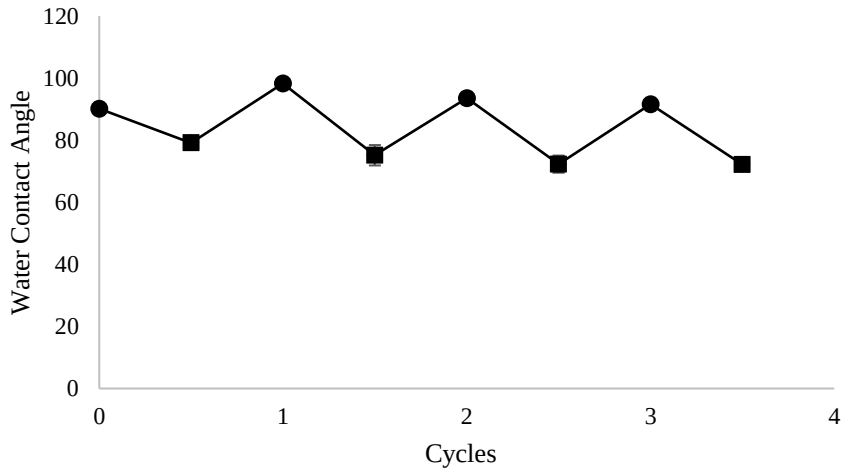

Figure 5.14. The CO_2-responsive behaviour of SiO_2-S18 as measured by static water contact angle analysis over 3.5 cycles of switching from hydrophobic to hydrophilic and back to hydrophobic. Error bars represent the standard deviation for each data point. SiO_2-S18 with CO_2 (■) and SiO_2-S18 without CO_2 (●). Experimental procedure outlined in Section 5.4.10.

The polymerisation of SiO_2-S18 reached 96% conversion in 24 h (FP M_n: 39.6 kDa, Đ: 1.17). SiO_2-S18 demonstrated a reversible switch from a hydrophilic state (WCA ~70°) to a hydrophobic state (WCA ~90°); this observation is in good agreement with the response observed by Stratakis et al. for a smooth silicon surface. However, it did not exhibit the larger switch as reported by Kumar et al. It is possible to infer a slight difference between SiO_2-S18 and previous examples, SiO_2-S16 for example. The hydrophilic state for SiO_2-S18 (WCA ~70°) appears to differ slightly from the hydrophilic states for

SiO_2-S15 and SiO_2-S16 (WCA ~60°). This is a small but potentially meaningful decrease, which could be correlated to the grafting density of PDiPAEMA on SiO_2.

5.2.7 CO_2-responsive rough silicon surfaces using surface-initiated atom transfer radical polymerisation

It has been demonstrated in the literature that a roughened surface is a necessary component for creating superhydrophobic materials.[21–23,40,41] Consequently, it has been considered that a surface's switchable properties may be enhanced if the surface is roughened before being functionalised: that a roughened surface functionalised with a switchable moiety may be able to switch between a superhydrophobic state and a superhydrophilic state. Multiple methods were evaluated for their ability to produce a roughened surface. The methods range from extremely accessible (i.e. physical abrasion with sand paper) to restricted access equipment (i.e. laser micromachining systems).

Physical abrasion methods, using a various grit sandpaper, failed to induce a hydrophobic state on a silicon wafer. Even the smallest grit that can be found at the local hardware store is much too big to create the nanoscale roughness that is required for hydrophobicity.

Wet etching methods, using various exposure times to aqueous solutions of hydrofluoric acid (HF), successfully modified the hydrophilic silicon surface to a hydrophobic state. The general procedure for wet chemical etching with HF on a silicon wafer is shown below, alongside relevant alternative wet treatments (Figure 5.15).

Silicon wafers (1 cm by 1 cm) were subjected to the following treatments:

A: Control silicon wafer, used as received from manufacturer.

B: Silicon wafer treated with acidic piranha solution (7:3 H_2SO_4: 30% H_2O_2).

C: Silicon wafer treated with acidic piranha solution (7:3 H_2SO_4: 30% H_2O_2), followed by treatment with basic piranha solution (5:1:1 Water: NH_4OH: 30% H_2O_2).

D: Silicon wafer treated with acidic piranha solution (7:3 H_2SO_4: 30% H_2O_2), followed by treatment with basic piranha solution (5:1:1 Water: NH_4OH: 30% H_2O_2) and treatment with HF (known etchant of silicon).

E: Silicon wafer treated with HF.

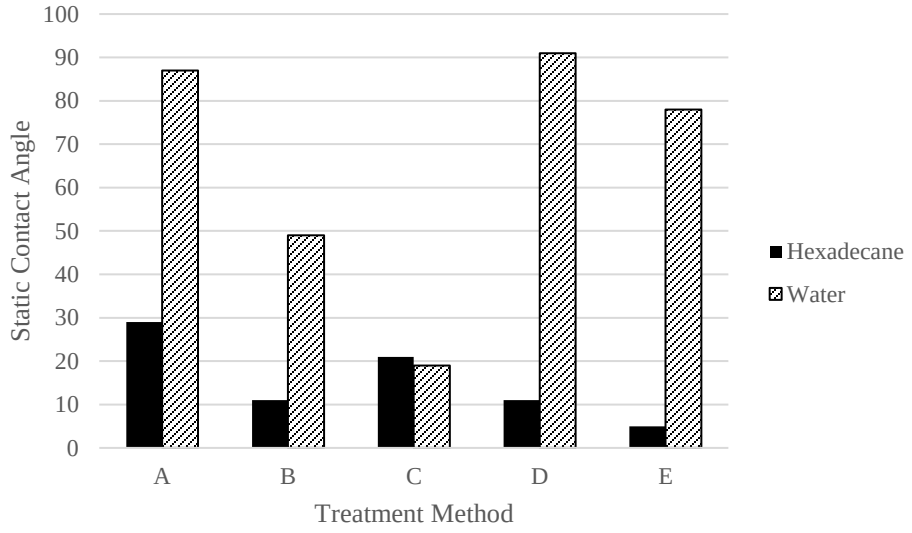

Figure 5.15. Wet chemical treatments for enhancing hydrophobicity through surface roughness.

Following treatment with piranha solutions and/or HF, each surface was analysed by WCA to measure its hydrophobicity. It was found that surfaces B and C were not

'roughened' by their treatment with acidic and/or basic piranha solution. In contrast, surfaces D and E were roughened by their treatment with HF, as evidenced by the observed contact angles; water's behaviour on a surface (i.e. contact angle) is indicative of a surface's texture (i.e. rough vs. smooth). Contact angles for hexadecane and water were measured for each surface (Figure 5.15). The high water contact angles observed for surfaces D and E suggest that roughening a surface by treatment with HF can enhance that surface's hydrophobicity.

Laser micromachining was accomplished at Nanofabrication Kingston (NFK) under the supervision of the lab manager, Dr. Graham Gibson. The laser micromachining was performed using an Oxford Lasers A Series Compact Micromachining System, equipped with a 355 nm solid-state diode-pumped picosecond pulsed laser. The system contains an integrated power meter, which indicates a laser power of 45.7 ± 4.5 mW, which is variably attenuated with motorised optics. The associated software uses G-code programs to manipulate an XY stage and laser optics (in Z) to perform the machining. Programs were created to mill grids in a silicon substrate with the ability to vary the size of the grid, laser power, pitch between laser passes and the speed at which the stage moves during the process.

The silicon substrate is placed inside the enclosure of the laser micromachining system and fixed onto the x/y stage a metal holster to prevent any movement while the stage is in motion. Once in place, using the system's software (Cimita), the substrate is brought into focus by adjusting the height of the laser optics (with mounted camera) and focusing using the on-screen optical image. When the substrate is in focus the G-code machining routine can be initiated, and the milling process begins.

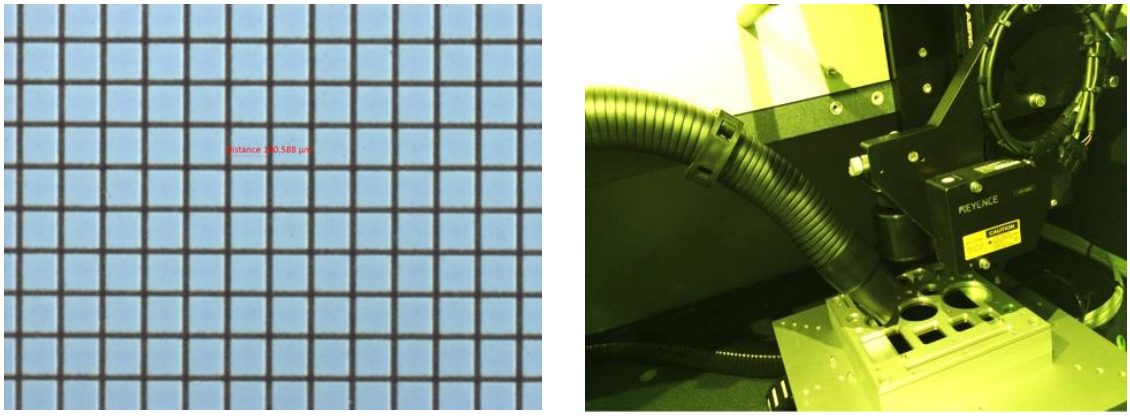

Figure 5.16. A silicon wafer with a laser patterned grid. Line spaces are 100 μm apart. Image was taken using a Carl Zeiss Axio Imager A1m optical microscope at NFK (left). A close up of the inside of the laser micromachining unit featuring the laser, substrate, and metal holster (right).

The laser patterned surfaces were cleaned with O_2 plasma. The oxidized-patterned-surfaces were determined to be hydrophilic, with a WCA of 20°. The oxidized-patterned-surfaces were then wet etched with HF to induce nanoscale roughness and hydrophobic surface character. The smooth parts of the silicon wafers were determined to have a WCA of 90°, confirming the results shown in Figure 5.16. The HF etched-patterned part of the surface was determined to be very hydrophobic, with a WCA of 160° (Figure 5.17).

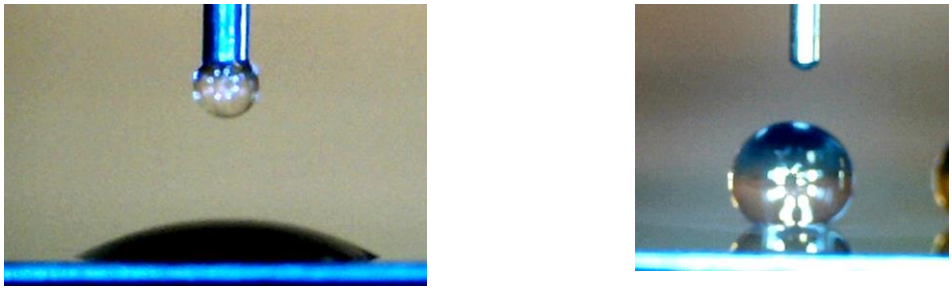

Figure 5.17. Oxidized and patterned silicon wafer (left) exhibiting a hydrophilic WCA of 20°. HF etched and patterned silicon wafer (right) exhibiting a hydrophobic WCA of 160°.

HF etching on a laser patterned grid was able to increase the WCA of the silicon wafer from 90° to 160°. This increase in the hydrophobicity of the silicon wafer is a significant improvement over that which can be achieved by chemical modification of the silicon wafer with a CO_2-responsive polymer (90°); wet etching a smooth substrate with HF (90°); grid laser patterning (20°). The working hypothesis was that when a CO_2-responsive polymer was grafted from a HF-etched-laser-patterned-surface, the resulting surface would be switchable between a hydrophilic state and a hydrophobic state that borders on the lines of superhydrophilic and superhydrophobic. The envisioned system for a smooth and a rough CO_2-responsive surface is shown in Figure 5.18.

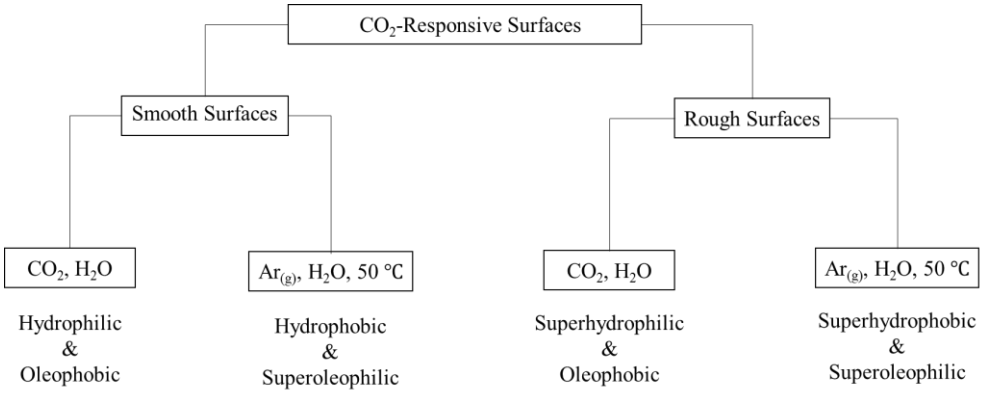

Figure 5.18. Hypothesized responses to various liquids of a given CO_2-responsive system as a function of exposure to a stimulus.

Roughened surfaces were grafted with a CO_2-responsive polymer (PDiPAEMA) in two ways. The synthetic method varies at the point of attachment to the silicon surface. One of the ways involves silane coupling chemistry; silane coupling chemistry relies on condensation of the silane silanols with free surface silanols on the silicon substrate. Therefore, the silicon substrate must be oxidized. Oxidation by O_2 plasma is an accessible method to ensure that organic contaminants have been removed from the silicon surface and that the silicon surface is oxidised. For methods using silane bonds to graft the initiator to the surface, plasma cleaning was the first step.

Oxidized-laser-patterned-surfaces (no HF treatment) were subjected to SI-AGET-ATRP to graft PDiPAEMA. A CO_2-responsive surface (SiO_2-S17) was created in this manner.

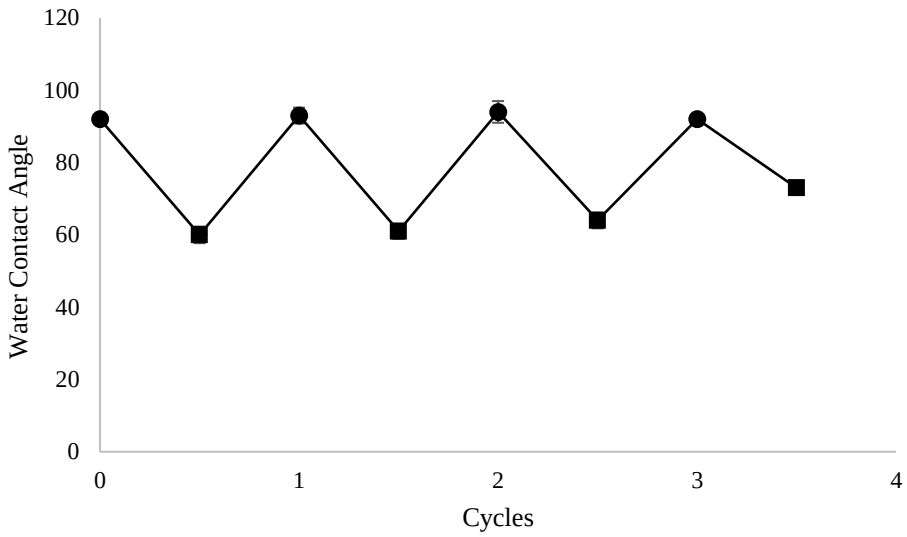

Figure 5.19. CO_2-responsive behavior of SiO_2-S17 as measured by static water contact angle analysis over 3.5 cycles of switching from hydrophobic to hydrophilic and back to hydrophobic. Error bars represent the standard deviation for each data point. SiO_2-S17 with CO_2 (■) and SiO_2-S17 without CO_2 (●). Experimental procedure outlined in Section 5.4.10.

SiO_2-S17 (Figure 5.19, laser patterned) was created in tandem with SiO_2-S16 (Figure 5.13, smooth surface) using the same polymerisation conditions. The polymerisation of SiO_2-S16 reached 80% conversion (FP M_n: 41.1 kDa, Đ: 3.7). The polymerisation of SiO_2-S17 reached 87% conversion (FP M_n: 47.0 kDa, Đ: 1.7). Both polymerisations were stopped early due to high viscosity, thus the molecular weight distribution of the resultant homopolymers is wider than expected. The CO_2-responsive behaviour of both surfaces have been overlayed and presented in Figure 5.20. The y-axis has been scaled down to 50-100 to better compare the two surfaces.

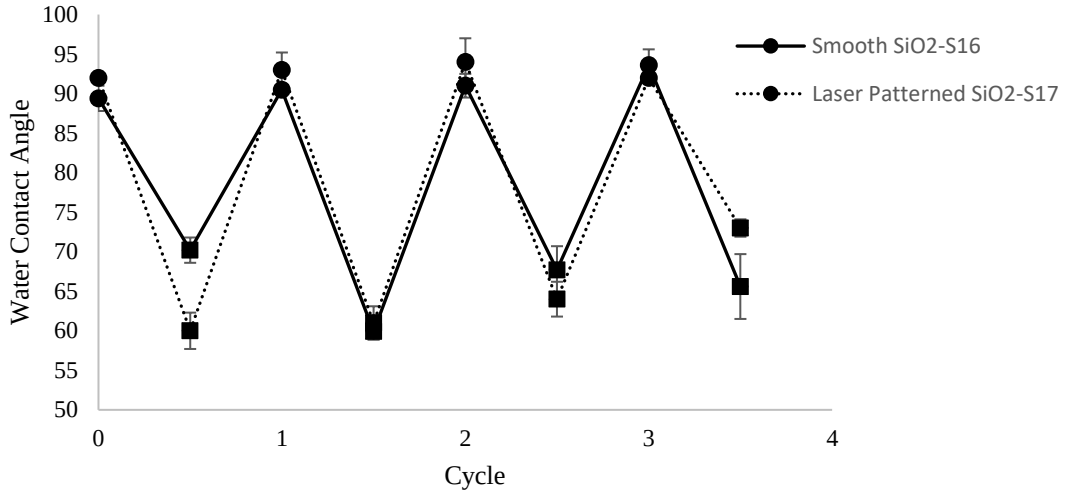

Figure 5.20. The CO_2-responsive behaviour of SiO_2-S16 and SiO_2-S17 as measured by static water contact angle analysis over 3.5 cycles of switching from hydrophobic to hydrophilic and back to hydrophobic. Error bars represent the standard deviation for each data point. SiO_2-S16/17 with CO_2 (■) and SiO_2-S16/17 without CO_2 (●). Experimental procedure outlined in Section 5.4.10.

The polymer-grafted "laser patterned" and "smooth" surfaces exhibit the same response to CO_2. The laser pattern did little to increase the hydrophilic or hydrophobic nature of the surface when in a charged or neutral state. It appears that the chemical response of the CO_2-responsive polymer is more of a factor in governing the surface properties of the silicon wafer than the laser patterned microstructure.

The laser patterned (microstructure) was etched with HF to further roughen the surface of the substrate by creating nanostructures within the microstructure. The effects of HF on a laser patterned surface were demonstrated previously in Figure 5.17. A silicon surface that has been treated with HF is terminated with silicon hydride (Si-H) species. The Si-H surface must then be oxidised (Si-OH) to allow for silane coupling. The oxidation process (Si-OH to Si-H) returns the silicon substrate to a hydrophilic state. Thus, to utilise

the hydrophobic character of the HF treatment the Si-H surface must be functionalised directly.

Subsequently, new synthetic methods were developed to functionalise silicon substrates that were terminated with Si-H bonds. Hydrosilylation of the silicon hydride surface was achieved by adaptation of the work reported by Boukherroub et al.[42] Boukherroub et al. reported that the thermal reaction of undecylenic acid with a hydrogen-terminated porous silicon surface takes place at 95 °C to yield an organic monolayer covalently attached to the surface through Si-C bonds. The acid terminal group remains intact and is not affected by the chemical process. The authors also reported further derivatization of the carboxylic acid with commonly employed peptide coupling techniques. For the purposes of this work peptide coupling conditions were adapted from MacMillan et al. where they demonstrated that HATU in dimethylformamide (DMF) was a suitable reagent system for coupling of an alkyl carboxylic acid and an amine.[43] The proposed reaction scheme is shown in Scheme 5.16.

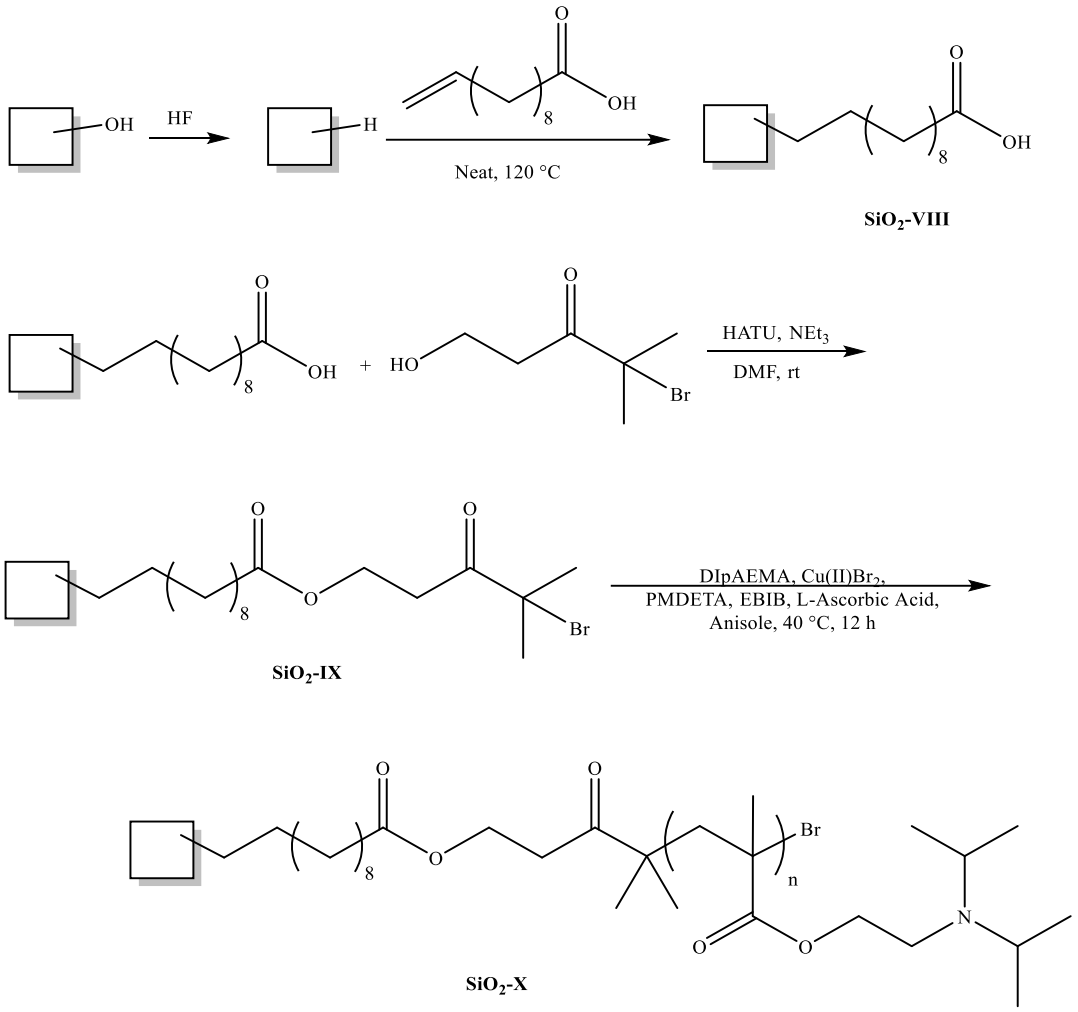

Scheme 5.16. SI-AGET-ATRP of PDiPAEMA from a silicon hydride surface, **SiO_2-X**.

A CO_2-responsive surface (SiO_2-S19) was created using the synthesis outlined in Scheme 5.16. The polymerisation of SiO_2-S19 reached 60% conversion (FP M_n: 30.2 kDa, Đ: 2.4). SiO_2-S19 (Figure 5.21) demonstrated a reversible switch from a hydrophilic state (WCA ~60°) to a hydrophobic state (WCA ~90°).

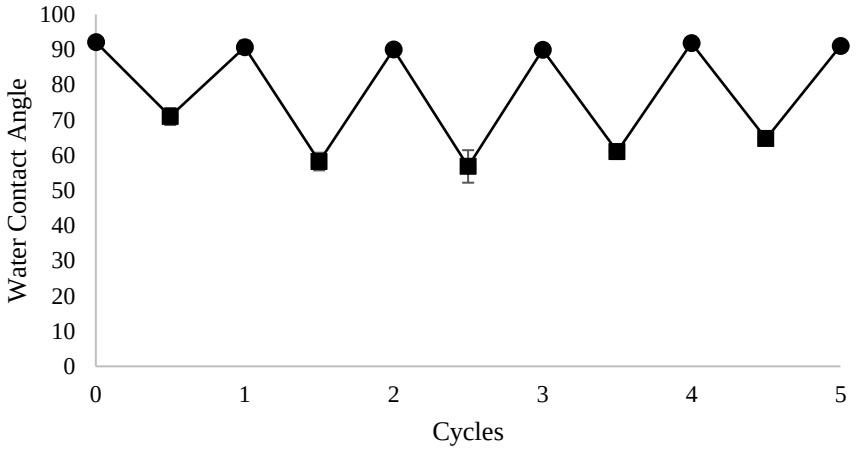

Figure 5.21. The CO_2-responsive behaviour of SiO_2-S19 as measured by static water contact angle analysis over 5 cycles of switching from hydrophobic to hydrophilic and back to hydrophobic. Error bars represent the standard deviation for each data point. SiO_2-S19 with CO_2 (■) and SiO_2-S19 without CO_2 (●). Experimental procedure outlined in Section 5.4.10.

The CO_2-responsive behaviour of SiO_2-S19 was very similar to each previous CO_2-responsive surface in which PDiPAEMA had been grafted from a silicon surface (Figure 5.22).

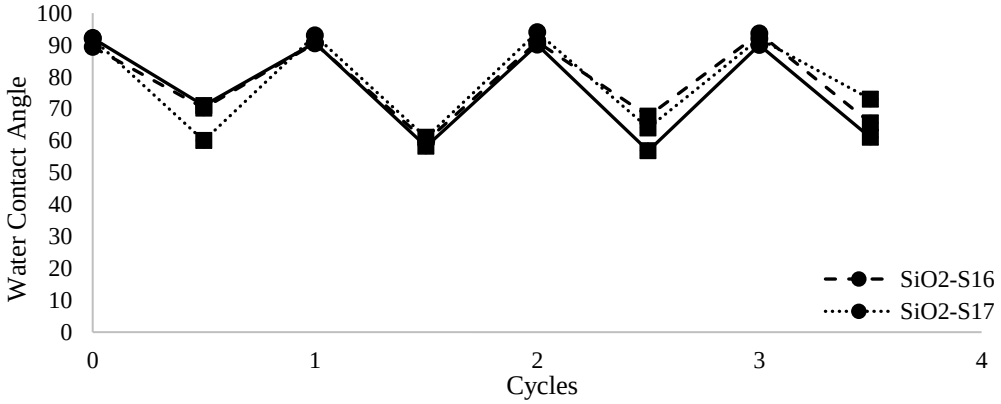

Figure 5.22. The CO_2-responsive behaviour of SiO_2-S16 (smooth), SiO_2-S17 (laser patterned), and SiO_2-S19 (HF etched) as measured by static water contact angle analysis over 3.5 cycles of switching from hydrophobic to hydrophilic and back to hydrophobic. Error bars represent the standard deviation for each data point. SiO_2-S16/17/19 with CO_2 (■) and SiO_2-S16/17/19 without CO_2 (●). Experimental procedure outlined in Section 5.4.10.

The natural conclusion from the analysis of this body of work is that the surface energy of the CO_2-responsive surfaces was controlled by the surface chemistry of the CO_2-responsive functionality and not the surface structures that were present on the substrate. A variety of surfaces were tested where microscale roughness was achieved through laser patterning and the end result was that the microscale roughness did not change the performance of the CO_2-responsive surface. Additionally, the HF etching failed to impart the expected additional hydrophobic character associated with nanoscale roughness in the CO_2-responsive surfaces. The polymer-grafted surface probably filled in the small nanoscale roughness created by the HF etch, thus the effect of the HF treatment was lost.

It is expected that HF treatment of a laser pattern, followed by functionalisation by hydrosilylation and SI-AGET-ATRP of PDiPAEMA would fail to produce a CO_2-responsive superhydrophobic surface. Larger more robust nanostructures such as the nanopillars employed by Stratakis et al. are most likely required to impart the hydrophobic effects that are associated with dual micro- and nanoscale roughness into the surface characteristics of the stimuli responsive material.

5.3 Conclusions

Single-unit functionalisation of a silicon surface has been demonstrated. Acyl transfer reagents were used to create CO_2-responsive surfaces. However, acyl transfer methods result in the formation of a silyl ester carbonate or a silyl ester carbamate linkage to the silicon surface. Silyl ester carbonates and silyl ester carbamates are not stable enough to achieve reproducible CO_2-responsive behaviour over multiple cycles in a CO_2-responsive system. For single-unit functionalisation methods to be commercially viable, alternative surface linkages need to be explored.

Additionally, the coordination of single-unit CO_2-responsive functionality to carbonyl moieties increases the likelihood of the single-unit CO_2-responsive functionality hydrolyzing from the surface. The alkylene chain between the carbonyl and the CO_2-responsive unit should be at least three methylene units long (i.e. propylene linker) to minimise the risk of hydrolysis and other unwanted coordination events. Steric bulk around the CO_2-responsive functionality (i.e. isopropyl>ethyl>methyl) decreases the risk of coordination events, thus decreasing the likelihood of the single-unit CO_2-responsive functionality hydrolyzing from the surface.

Polymeric functionalisation of a silicon surface was shown to produce CO_2-responsive surfaces that are stable in the CO_2-responsive system for numerous cycles (>10). The surface characteristic of a CO_2-responsive surface was determined to be dominated by the chemical nature of the CO_2-responsive functionality and not by the surface structure. Microscale roughness as achieved by laser patterning did not change the surface character of the polymer-grafted CO_2-responsive surfaces. Nanoscale roughness

as achieved by HF etching did not change the surface character of the polymer-grafted CO_2-responsive surfaces.

It has been demonstrated in the literature that exotic surface structures are able to impart additional hydrophobic and hydrophilic character to a silicon surface containing CO_2-responsive functionalities. However, the relatively simple methods for altering the surface structure of the silicon wafer that were employed in this study were unable to reproduce the effect.

Lastly, the grafting density of a CO_2-responsive polymer on a surface has been identified as an important parameter, which contributes to the overall surface energy of the polymer-grafted material and to the magnitude of the change between the native and neutral hydrophobic state and the CO_2-exposed and charged hydrophilic state. Preliminary results indicate that the SI-AGET-ATRP method presented here is a suitable technique to create and study CO_2-responsive surfaces with variable grafting densities.

5.4 Experimental methods

5.4.1 Materials

All aqueous solutions were prepared with deionized water (DIW) unless stated otherwise. All silica particles were purchased from Silicycle unless stated otherwise. 2,2′-Azobisisobutyronitrile (AIBN, Aldrich, 98%) was recrystallized from methanol. The following chemicals were used as received unless otherwise stated: VA-061 (Wako Chemicals), butyl methacrylate (BMA, Aldrich, contains 10 ppm MEHQ as inhibitor 99%), methyl methacrylate (MMA, Aldrich, contains <30 ppm MEHQ as inhibitor, 99%),

2-(diisopropylamino)ethyl methacrylate (DiPAEMA, Aldrich, 97%, contains ~100 ppm MEHQ as inhibitor), 2-(diethylamino)ethyl methacrylate (DEAEMA, Aldrich, contains 1500 ppm MEHQ as inhibitor, 99%), N,N-dimethylacetamide dimethyl acetal (TCI America, stabilized with 5-10% methanol*)*, 6-amino-1-hexanethiol hydrochloride (Aldrich), Amberlite-OH exchange resin (Aldrich), sodium borohydride (Aldrich, 99.99% trace metal basis), hydrofluoric acid (Aldrich, ACS reagent, 48%), magnesium sulfate (Aldrich, >99.999% trace metals basis), 3-(dimethylamino)propyl-functionalised silica (Aldrich), $CO_{2(g)}$ (Chromatography grade, Praxair), Argon (5.0, ultra-high purity, Praxair), hydrochloric acid (Fisher Scientific, concentrated, reagent grade), 1,1'-carbonyldiimidazole (CDI, Aldrich, reagent grade), N,N-dimethylacetamide (DMAc, EMD Millipore, anhydrous), dimethylsulfoxide (DMSO, Fisher Scientific), 1,1,3,3-tetramethylguanidine (TMG, Aldrich, 99%), silicon wafer (N type, P dope, 100 mm (wafer size), single side polish, 325 μm (thickness of thermally grown oxide layer), test grade from universitywafer.com), glass microscope slides (Fisher Scientific). epitaxial gold on mica (size 75x25 mm^2, with (111)-layer of gold, 300 nm thickness, from George Albert Physical Vapour Deposition Coatings, Germany), 4-(dimethylamino)pyridine (DMAP, Aldrich, ≥ 99%), dichloromethane (DCM, EMD Millipore, anhydrous, stabilised with an alkene, ≥98.5%), methanol (MeOH, EMD Millipore, anhydrous), dimethylformamide (DMF, Aldrich, 98%, anisole (Aldrich, anhydrous, 99.7%), toluene (Aldrich, anhydrous), tetrahydrofuran (Aldrich, anhydrous, contains 250 ppm BHT as inhibitor, ≥99.9%), copper(II) bromide (Aldrich, 99.999% trace metals basis), N,N,N`,N``,N``-pentamethyldiethylenetriamine (PMDETA, Aldrich, 99%), ethylenediaminetetraacetic acid (EDTA, Aldrich, purified grade, ≥98.5%), sodium

hydroxide (NaOH, Aldrich, ACS reagent, ≥97%), aluminium oxide (Aldrich, activated, basic, Brockmann I), (3-aminopropyl)triethoxysilane (APTES, Aldrich, 99%), L-ascorbic acid (AA, Aldrich, reagent grade), tin(II) 2-ethylhexanoate ($Sn(EH)_2$, Aldrich, 92.5-100%), ethanol (Commercial Alcohols, anhydrous), ethyl acetate (Aldrich, anhydrous, 99.8%), methyl chloroformate (MCF, Aldrich, 99%), ethyl chloroformate (ECF, Aldrich, 97%), 3-(diethylamino)propylamine (DEAPA, Aldrich, >99%), 2-dimethylaminoethanol (Aldrich, >99.5%), 3-diethylamino-1-propanol (Aldrich, 95%), 3-dimethylamino-1-propanol (Aldrich, 99%), 2-(diethylamino)ethanol (Aldrich, > 99.5%), 2-(diisopropylamino)ethanol (Aldrich, >99%), N-(3-aminopropyl)piperidine (Aldrich, 95%), 1-(3-aminopropyl)imidazole (Aldrich, >97%), 1-(3-aminopropyl)pyrrolidine (Aldrich^{CPR}), potassium *tert*-butoxide (Aldrich, reagent grade >98%), phosgene solution (Aldrich, 15 wt% in toluene), sodium bicarbonate (Aldrich, reagent grade ≥99.7%), n-butyllithium solution (Aldrich, 2.5 M in hexanes), (3-trimethoxysilyl)propyl-2-bromo-2-methylpropionate (Gelest), 10-undecenoic acid (Aldrich, 98%), N-[(dimethylamino)-1H-1,2,3-triazolo-[4,5-b]pyridin-1-ylmethylene]-N-methylmethanaminium hexafluorophosphate N-oxide (HATU, Aldrich, 97%), n-hexyltrimethoxysilane (Aldrich), (N,N-dimethylaminopropyl)trimethoxysilane (Gelest), (N,N-diethylaminomethyl)trimethoxysilane (Gelest), [3-(diethylamino)propyl]-trimethoxysilane (Gelest).

Piranha solutions were used to clean silicon substrates. Acidic piranha solution consists of a 7:3 (v/v) mixture of concentrated sulfuric acid and 30% hydrogen peroxide solution, commonly heated to 85 °C. Basic piranha solution consists of a 5:1:1 (v/v/v)

mixture of Millipore water, 30% hydrogen peroxide solution, and 40% ammonium hydroxide solution, commonly heated to 70 °C.

Warning: Piranha solution is highly dangerous and its use requires considerable care. Piranha solution is either strongly acidic or basic and a strong oxidizer. The mixing of piranha solution is very exothermic and should be done slowly; if the reagents are mixed too quickly, the temperature can easily exceed 100 °C, which will result in boiling and splashing of the piranha solution. Piranha solution will react violently with organic compounds; therefore, it should be used in a fume hood clear of organic solvents and waste. Make only as much Piranha solution as needed; when disposing of excess or used piranha solution do NOT cap the bottle. It commonly takes a day or two for the reagent to neutralize fully, during this time oxygen gas is produced. Refer to your institution's standard operating procedures before attempting to use or dispose of piranha solutions.

5.4.2 Surface preparation methods

An initial literature review was conducted to identify an appropriate method for preparing various surfaces for functionalization. The surfaces to be functionalised included test grade silicon wafers, glass microscope slides, and epitaxial gold on mica. The cleanliness of the substrates was judged by contact angle measurements and the quality of the SAM/functionalized surface that was produced. Shiral et al. did a thorough review of 18 methods for the pretreatment of glass filler for silane bonding.[30] Of the 18 methods reviewed, they concluded through XPS studies that placing the SiO_2 substrate in a boiling 5% sodium persulfate aqueous solution for 15 min followed by ultrasonic rinsing with

acetone for 15 min produced a contaminant free surface in a safe manner, within a short amount of time. Cras et al. tested 8 methods of pretreatment for glass substrates.[29] They took glass microscope slides and subjected them to a variety of pretreatments only to conclude that multiple methods were deemed suitable pretreatments.

Multiple other sources suggested using piranha solutions for the pretreatment of glass and silicon substrates. Piranha solutions are well known and widely used but considerably more dangerous. Piranha solutions were used for the majority of the work in this chapter; exceptions will be noted when applicable.

Silicon substrates, wafers and/or glass microscope slides, were cut into 1 cm x 1 cm pieces. The pieces were subjected to a three-part treatment to remove organic contaminants and promote a hydroxyl-rich surface. Firstly, the silicon substrates were stirred in acidic piranha solution for 1 h at 85 °C, followed by copious rinsing with Millipore water. Secondly, the silicon substrates were stirred in basic piranha solution for 20 min at 70 °C, followed by copious rinsing with Millipore water. Lastly, the silicon substrates were blown dry with Ar and dried in an oven overnight at 110 °C. The clean and hydroxyl-rich silicon substrates were used immediately or stored in a sealed vessel under an Ar atmosphere until further use.

In some instances; silicon wafers were cleaned by oxygen plasma for 5 min. The necessary equipment, a Plasmatic System Plasma-Preen microwave oven, was stationed at Nanofabrication Kingston (NFK).

Gold substrates were handled with great care. The mica supporting the gold is fragile and layers easily separate due to the shear stress resultant from handling the

substrate. The gold surfaces were rinsed with copious amounts of acetone and blown dry under a stream of Ar. Literature sources recommend ultrasonic rinsing in acetone, both pre and post functionalisation.[44] However, in practice, ultrasonic rinsing was found to destroy the mica support, rendering the gold unsupported and thus not suitable for functionalisation.

5.4.3 Synthesis of CO_2-responsive polymer thin films

Polymerisations took place in anisole, sparged with Ar for a minimum of 30 min. A switchable initiator VA-061 was used for each polymerisation. A solution of VA-061 was made in anisole and sparged with Ar before being cannula transferred into the reaction vessel. Approximately 100 mg of VA-061 was used in each synthesis. Polymers were isolated by precipitation in various solvents; commonly a mixture of water and acetone successfully precipitated the polymer.

The CO_2-responsive behaviour of DEAEMA was utilised for the workup of the P(MMA-co-BMA-co-DEAEMA). Specifically, the crude polymer was dissolved in 40 mL of methanol and diluted with 160 mL of water. CO_2 was bubbled through the solution to help solubilize the polymer. The cloudy solution was then heated to approximately 40 °C and Ar was sparged through the solution. After some time, the polymer completely separated from the water. The water was decanted, and the polymer frozen with liquid nitrogen. The frozen polymer was crushed up in a small blender and stored in a glass jar for future use.

Thin films were created on glass microscope slides by the use of a spin coating apparatus. Thin films of ~50 kDA poly(diethylamino)ethylmethacrylate (PDEAEMA) polymers and copolymers were spun onto clean glass microscope slides. Solutions of PDEAEMA in methanol having a concentration of 2 $mg \cdot mL^{-1}$ were spun at 5000 RPM. Coated slides were oven cured at 110 °C for 10 min.

5.4.4 Synthesis of CO_2-responsive amino-silane self-assembled monolayers

N,N-dimethyl-N'-(3-(trimethoxysilyl)propyl)acetimidamide was synthesised using a simple and effective synthesis based on "A synthesis of Acetamidines" by Harjani et al.[45] 3-(Aminopropyl)-triethoxysilane (APTES, 0.0269 mmol) was mixed with N,N-dimethylacetamide dimethyl acetal (0.038 mmol) in methanol and stirred at 60 °C for 2 h. The methanol byproduct was removed under vacuum and the intended product was formed in high yield (S5). The product was confirmed via ^{13}C and ^{1}H NMR spectroscopy.

Cleaned substrates were added to a 100 mL glass reaction vessel. The vessel was kept at a constant temperature of 70 °C. The atmosphere in the reaction vessel was removed under vacuum and replaced with Ar. To the sealed reaction vessel, a 1% v/v solution of silane in anhydrous toluene was added via cannula transfer. The reaction was left gently stirring at 70 °C overnight. The silane-grafted substrates were collected and washed multiple times with ethanol, followed by sonication in ethanol 3 times. The silane-grafted substrates were blown dry with Ar and stored in a sealed vessel under Ar until further use.

5.4.5 Synthesis of CO_2-responsive gold-thiol self-assembled monolayers

N'-(6-Mercaptohexyl)-N,N-dimethylacetimidamide was synthesised as follows:

6-Amino-1-hexanethiol hydrochloride ($0.1026x10^{-4}$ mol) was mixed with Amberlite-OH exchange resin (1.02 g), 3 Å molecular sieves (0.026 g), methanol (40 mL) and magnetically stirred for approximately 24 h. The mixture was then filtered into a new round bottom flask. To the new round bottom flask, N,N-dimethylacetamide dimethyl acetal (TCI America, stabilised with 5-10% methanol, 0.68 mmol) was added; the mixture was stirred at 60 °C for 3 h. Any volatile components (methanol and byproduct) were then removed under vacuum and the crude product was treated with $NaBH_4$ (30 mg in water) at 50 °C for 30 min. Any remaining $NaBH_4$ was neutralised and the crude product mixture was protonated with an acidic workup. Sodium chloride salts were filtered out of the mixture and the water was removed under vacuum. Isolated N'-(6-mercaptohexyl)-N,N-dimethyl acetimidamide was purified using a short silica column and a 40:60 v/v acetonitrile to ethanol mobile phase. The purified product, N'-(6-mercaptohexyl)-N,N-dimethylacetimidamide (30 mg, 0.15 mmol, 25% yield), was characterised via ^{13}C NMR and ^{1}H-^{13}C HSQC (Heteronuclear Single Quantum Correlation) NMR spectroscopy. The appearance of a quaternary carbon at approximately 180 ppm confirmed that the amidine functionality had been synthesised and high-resolution mass spectrometry confirmed an expected molecular weight of 202 g/mol.

Functionalisation of a cleaned gold substrate was performed as follows:

1. A select thiol compound (25 mg) was added to anhydrous ethanol (6.5 mL) and then further diluted (3.2 mL of thiol solution into 8.8 mL anhydrous ethanol) to yield a final concentration of 1-5 mM.
2. 1,1,3,3-Tetramethylguanidine (TMG) was added to the diluted thiol solution (ca. 1 mM)
3. Gold surfaces were added to a vial containing the thiol solution; the vial was backfilled with Ar and sealed and left for 48 h.
4. Functionalised gold surfaces were removed and rinsed with a 1 mM TMG in ethanol solution for 10-15 s. The surfaces were then rinsed thoroughly with anhydrous ethanol (50 mL) and blown dry under a stream of Ar for approximately 4 min.
5. Functionalised gold surfaces were stored in a sealed vial under Ar until further use.

5.4.6 Synthesis of CO_2-responsive silicon surfaces by carbonyldiimidazole-mediated acyl transfer

Synthesis of a dimethylamino-terminated silicon surface, SiO_2-S7:

2-Dimethylamino-1-ethanol was distilled under vacuum and dissolved in a minimum amount of ethyl acetate (1 eq., 2.50 mmol, in 30 mL). To this solution, 0.8 eq. of 38% hydrochloric acid (10.42 M) was added drop wise. A resulting aqueous layer was separated and the water removed under vacuum. An isolated hydrochloride salt of 2-dimethylamino-1-ethanol was added to a solution of 1.0 eq. carbonyldiimidazole (CDI, 0.42 g, 2.50 mmol) in a minimum of dimethylacetamide (DMAc). This mixture was allowed to react at room temperature (ca. 23 ℃) for 24 h, after which it was added to a vial containing a cleaned silicon oxide wafer. This mixture sat at room temperature for 48 h, after which the wafer was rinsed with a solution of dimethylsulfoxide (DMSO, 40 mL) and 1,1,3,3-tetramethylguanidine (TMG, 10 mL). The wafer was then rinsed with distilled water, dried under a stream of Ar and subjected to experimentation and water contact angle analysis.

Note: CDI-14 and CDI-15 were prepared in the same manner as SiO_2-S7.

5.4.7 Synthesis of CO_2-responsive silicon surfaces by chloroformate-mediated acyl transfer

KBB5PG33:

A silicon wafer was cleaned and dried as outlined previously. The wafer was placed into a 50 mL round bottom flask (RBF) containing a small stir bar; the RBF was fitted with a condenser and purged with Ar. Anhydrous tetrahydrofuran (THF, 16 mL) and triethylamine (TEA, 65 mmol) were injected into the RBF, which was subsequently cooled with an ice bath. Methyl chloroformate (MCF, 65 mmol) was added dropwise to the solution. The reaction was vigorous and a white precipitate was formed instantly. After addition of MCF, the solution was warmed slowly to the point of reflux (ca. 75 °C) and allowed to react for 12 h. The MCF functionalised wafer was removed from the solution and rinsed with THF, after which it was dried under a stream of Ar and placed into a clean, dry, 100 mL RBF for further functionalisation.

A solution of 3-(diethylamino)propylamine (DEAPA, 3.8 mmol) and potassium *tert*-butoxide (t-BuOK, 0.92 mmol) in 60 mL of anhydrous THF was prepared. The solution was mixed thoroughly and cannula transferred into the RBF containing the MCF functionalised silicon wafer. The solution was heated to 50 °C and stirred overnight under static Ar. The wafer was removed from the solution and rinsed with fresh THF, blown dry with Ar and subjected to WCA analysis.

KBB5PG39:

Silica particles (SiO_2 #5, SiliaFlash P60, 40-63 μm, 100 Å pore size) were subjected to a three-part treatment in order to remove organic contaminants and promote a hydroxyl-rich surface. Firstly, the particles were stirred in acidic piranha solution for 1 h at 85 ℃, followed by rinsing three times with Millipore water. Secondly, the particles were stirred in basic piranha solution for 20 min at 70 ℃, followed by rinsing three times with Millipore water. Lastly, the particles were vacuum filtered and dried in an oven overnight at 110 ℃. The clean and hydroxyl-rich particles were stored in a sealed vessel until further use

Warning: Piranha solution is very dangerous. Refer to Materials section

Clean and hydroxyl-rich particles (4 g) were added to a flame-dried 250 mL round bottom flask containing 140 mL of anhydrous dichloromethane (DCM) and mixed thoroughly by magnetic stirring. The flask was fitted with an addition funnel. The addition funnel was charged with 20 mL of anhydrous DCM and 9 mL of methyl chloroformate (MCF, 116 mmol). The contents of the addition funnel were discharged into the round bottom flask at a rate of 5 drops per second. Triethylamine (TEA, 11.8 mL, 87 mmol) was injected in the flask, the contents of which were stirred overnight at room temperature (ca. 27 ℃). The MCF functionalised silica particles were collected via vacuum filtration, washed thoroughly with DCM, methanol, water, and lastly once more with methanol. The MCF functionalised particles were dried under reduced pressure, at 100 ℃ for 48 h.

KBB5PG48:

MCF-functionalised particles (1 g) were added to a flame-dried 250 mL round bottom flask. A solution of 3-(diethylamino)propylamine (DEAPA, 54 mmol) and potassium *tert*-butoxide (t-BuOK, 54 mmol) in 125 mL of anhydrous THF was prepared. The solution was mixed thoroughly and cannula transferred into the RBF containing the MCF functionalised silica particles. The solution was heated to 50 ℃ and stirred overnight under static Ar. The silica particles were collected via vacuum filtration and rinsed with fresh THF. Only 0.22 g of silica particles were recovered. The functionalised particles were examined by XPS. This attempt was deemed unsuccessful as the XPS analysis showed no signs of nitrogen on the silica particles.

SiO_2-S13 KBB6PG40:

A silicon wafer was cleaned and dried as outlined previously. The wafer was placed into a 100 mL round bottom flask (RBF) containing a small stir bar; the RBF was fitted with a condenser and purged with Ar. Anhydrous dichloromethane (DCM, 60 mL) and diisopropylethylamine (DIPEA, 12.5 mmol) were injected into the RBF and subsequently cooled with an ice bath. Ethyl chloroformate (ECF, 12.5 mmol) was added dropwise to the solution. The reaction was vigorous and a white precipitate was formed instantly. After addition of ECF, the solution was warmed slowly to the point of reflux (ca. 75 ℃) and allowed to react for 12 h. The ECF functionalised wafer was removed from the solution and rinsed with DCM, after which it was dried under a stream of Ar and placed into a clean, dry, 100 mL RBF for further functionalisation.

A solution of 1-(3-aminopropyl)imidazole (API, 12.5 mmol), water (10.8 μL) and potassium *tert*-butoxide (t-BuOK, 25.1 mmol) in 72 mL of anhydrous THF was prepared. Water was added to THF to bring the overall water content of the solution up to 0.2%.[46] The solution was mixed thoroughly and cannula transferred into the RBF containing the MCF functionalised silicon wafer. The solution stirred overnight at room temperature (ca. 26 ℃) under static Ar. The wafer was removed from solution and rinsed with fresh THF, blown dry with Ar and subjected to WCA and XPS analysis.

SiO_2-S14 KBB7PG80:

The following experimental procedure is dangerous. The manipulation of these reagents requires great care and should not be undertaken without first reviewing the proper techniques for neutralizing phosgene and working with acid gases.

A silicon wafer was cleaned and dried as outlined previously. The wafer was placed in a 50 mL round bottom flask (RBF) containing a small stir bar; the RBF was purged with Ar. The following steps were undertaken using an inert environment. Anhydrous 1,4-dioxane was dried over molecular sieves. Diisopropylethylamine (DIPEA) was removed from a fresh bottle; its purity was checked by ^{1}H NMR spectroscopy and GC-FID and deemed satisfactory. A solution of DIPEA (1 mL, 5.8 mmol, 1 eq.) in 10 mL of dried 1,4-dioxane was cannula transferred over the silicon wafer. The solution was stirred gently (60 RPM) via magnetic stirring, the solution was cooled using an ice bath. Phosgene solution (1 mL, 15 wt% in toluene, 5.6 mmol) was charged to the RBF containing the silicon wafer. The reaction was left for 4 h, after which dried 1,4-dioxane was purged

through the RBF using a series of cannula needles. The purged solvent exited the RBF into a sodium bicarbonate solution. At no point was the wafer removed from RBF, the wafer was kept under an inert environment at all times. The wafer and RBF were purged with anhydrous THF. Excess solvent was removed from the RBF containing the wafer with dynamic Ar. The wafer was left under vacuum overnight

n-BuLi in hexanes was titrated and determined to be 0.98 M.[47] A solution of 1-(3-aminopropyl)imidazole (API, 10 mL, 84 mmol) in anhydrous THF (15 mL) was charged to a flame-dried 100 mL RBF. The solution was cooled using a dry ice/acetone bath. The solution was stirred vigorously as n-BuLi in hexanes was added dropwise (59 ml, 0.98 M). The mixture was stirred for 1 h, after which the API had been activated to form the lithium salt of the API anion, now referred to as active-API. Active-API solution (5 mL, ca. 4 mmol of Active-API) was charged to the reaction flask containing the functionalised silicon wafer. The solution transferred was enough to coat the wafer fully. The mixture was left overnight to react. The RBF was purged with anhydrous THF; purged solvent was neutralised with a sodium bicarbonate solution. The API-functionalised wafer was rinsed with THF and sonicated in water for 0.5 h. The API-functionalised wafer (SiO_2-S14) was dried in a vacuum over at 50 ℃ overnight. SiO_2-S14 was then tested for CO_2-responsiveness by WCA analysis.

5.4.8 Synthesis of CO_2-responsive smooth silicon surfaces by surface-initiated atom transfer radical polymerisation

SiO_2-S15 KBB9PG47:

A clean silicon wafer (diameter 5 cm) was added to a 500 mL glass reaction vessel. The glass reaction vessel was equipped with an overhead stirrer and an ethylene glycol heating unit. The vessel was kept at a constant temperature of 70 ℃. The atmosphere in the reaction vessel was removed under vacuum and replaced with Ar. To the sealed reaction vessel, 500 mL of anhydrous toluene was added via cannula transfer. After vigorous stirring, 5 mL of (3-aminopropyl)triethoxysilane (APTES) was added via syringe. The reaction was left stirring at 70 ℃ overnight. The APTES-grafted silicon wafer was removed from the reaction flask and washed multiple times with toluene, followed by sonication for 10 min in toluene, repeated 3 times. The APTES-grafted silicon wafer was blown dry with Ar and stored in a sealed vessel under Ar until further use.

SiO_2-S15 KBB9PG47:

An ATPES-grafted silicon wafer (diameter 5 cm) was added to a 500 mL glass reaction vessel. The glass reaction vessel was equipped with an overhead stirrer and an ethylene glycol heating unit. The vessel was kept at a constant temperature of 4 ℃. The atmosphere in the reaction vessel was removed under vacuum and replaced with Ar. Reactants were added using Schlenk techniques for inert conditions; diisopropylethylamine (1.1 eq., 23.0 mmol) and 200 mL of anhydrous tetrahydrofuran (THF) were added to the reaction vessel. The initiator, 2-bromo-2-methylpropionyl

bromide, (BIBB, 1 eq., 21.4 mmol) was added dropwise via syringe. The mixture was stirred for 20 min before the temperature control unit was turned off and the mixture was allowed to warm to room temperature (ca. 27 °C) and to react overnight. The BIBB-grafted silicon wafer was removed from the reaction flask and washed multiple times with toluene, followed by sonication for 10 min in toluene, repeated 3 times. The silane-grafted substrate was blown dry with Ar and stored in a sealed vessel under Ar until further use.

SI-AGET-ATRP PDiPAEMA on silicon, SiO_2-S15 KBB9PG47:

An initiator-grafted silicon wafer (diameter 5 cm) was placed into a 500 mL reaction vessel equipped with an overhead stirring device. 2-(Diisopropylamino)ethyl methacrylate (DiPAEMA, 235 eq., 210 mmol) was passed through an inhibitor remover column [Sigma-Aldrich, removing hydroquinone (HQ) or hydroquinone monomethyl ether (MEHQ, 4-methoxyphenol), or 4-*tert*-butylcatechol (TBC)] and charged to the 500 mL round bottom flask containing the initiator-functionalised silicon wafer. Anisole (100 mL), Cu(II)Br_2 (0.6 eq., 0.58 mmol), N,N,N′,N″,N″-pentamethyldiethylenetriamine (PMDETA, 3.2 eq., 2.9 mmol) and ethyl 2-bromo-2-methylpropionate (EBIB, 1 eq., 0.88 mmol) were added to the round bottom flask and the mixture was stirred vigorously while slowly being heated to 40 °C. Once the mixture reached the desired temperature, L-ascorbic acid (9.5 eq., 8.5 mmol) was added to the reaction flask, which was promptly sealed. No additional techniques were used to remove atmospheric or dissolved oxygen. The polymerisation solution changed colour from blue (oxidised copper) to colourless (ca. 2 h on average) and then to yellow/orange over the course of 16 h. The polymer-grafted silicon wafer was removed from the bulk solution and washed thoroughly with anisole,

followed by multiple washings with THF. The wafer was washed in basic EDTA solution before being dried at 110 ℃ for 1 h. The free polymer was collected as described in Section 4.3.5.

SiO_2-S16 KBB9PG60:

A clean silicon wafer (1 cm x 1 cm) was added to a 50 mL glass reaction vessel. The vessel was kept at a constant temperature of 80 ℃. The atmosphere in the reaction vessel was removed under vacuum and replaced with Ar. To the sealed reaction vessel, 25 mL of a 10 mM solution of (3-trimethoxysilyl)propyl-2-bromo-2-methylpropionate in anhydrous toluene was added via cannula transfer. The reaction was left gently stirring at 70 ℃ overnight. The silane-grafted substrate was collected and washed multiple times with ethanol, followed by sonication in ethanol 3 times. The silane-grafted substrate was blown dry with Ar and stored in a sealed vessel under Ar until further use.

SI-AGET-ATRP of PDiPAEMA on silicon, SiO_2-S16 KBB9PG73:

An initiator-grafted silicon wafer (1 cm x 1 cm) was added to a 100 mL glass reaction vessel. 2-(Diisopropylamino)ethyl methacrylate (DiPAEMA, 238 eq., 52 mmol) was passed through an inhibitor remover column [Sigma-Aldrich, removing hydroquinone (HQ) or hydroquinone monomethyl ether (MEHQ, 4-methoxyphenol), or 4-*tert*-butylcatechol (TBC)] and charged to the 100 mL round bottom flask containing the initiator-functionalised silicon wafer. Anisole (25 mL), Cu(II)Br_2 (0.65 eq., 0.15 mmol), N,N,N′,N″,N″-pentamethyldiethylenetriamine (PMDETA, 6.5 eq., 1.4 mmol) and

ethyl 2-bromo-2-methylpropionate (EBIB, 1 eq., 0.22 mmol) were added to the round bottom flask and the mixture was stirred gently to avoid breaking the silicon wafer (ca. 400 RPM), while slowly heating to 40 ℃. Once the mixture reached the desired temperature, tin(II) 2-ethylhexanoate (9.7 eq., 2.2 mmol) was added to the reaction flask, which was promptly sealed. No additional techniques were used to remove atmospheric or dissolved oxygen. The polymerisation solution changed colour from blue (oxidised copper) to colourless (ca. 2 h on average) and then to yellow/orange over the course of 16 h. The polymer-grafted silicon wafer was removed from the bulk solution and washed thoroughly with anisole, followed by multiple washings with THF. The wafer was washed in basic EDTA solution before being dried at 110 ℃ for 1 h. The free polymer was collected as described in Section 4.3.5.

SiO_2-S18 KBB9PG80:

A clean silicon wafer (1 cm x 1 cm) was added to a 50 mL glass reaction vessel. The vessel was kept at a constant temperature of 80 ℃. The atmosphere in the reaction vessel was removed under vacuum and replaced with Ar. To the sealed reaction vessel, 75 mL of a 10 mM solution consisting of 25 mol% (3-trimethoxysilyl)propyl-2-bromo-2-methylpropionate (0.18 mmol) and 75 mol% n-propyltriethoxysilane (0.56 mmol) in anhydrous toluene was added via cannula transfer. The reaction was left gently stirring at 80 ℃ overnight. The silane-grafted substrate was collected and washed multiple times with ethanol, followed by sonication in ethanol for 10 min, repeated 3 times. The silane-grafted substrate was blown dry with Ar and stored in a sealed vessel under Ar until further use.

SI-AGET-ATRP of PDiPAEMA on silicon, SiO_2-S18 KBB9PG82:

An initiator-grafted silicon wafer (1 cm x 1 cm) was added to a 100 mL glass reaction vessel. 2-(Diisopropylamino)ethyl methacrylate (DiPAEMA, 238 eq., 40 mmol) was passed through an inhibitor remover column [Sigma-Aldrich, removing hydroquinone (HQ) or hydroquinone monomethyl ether (MEHQ, 4-methoxyphenol), or 4-*tert*-butylcatechol (TBC)] and charged to the 100 mL round bottom flask containing the initiator-functionalised silicon wafer. Anisole (10 mL), Cu(II)Br_2 (0.65 eq., 0.11 mmol), N,N,N′,N″,N″-pentamethyldiethylenetriamine (PMDETA, 3.2 eq., 0.56 mmol) and ethyl 2-bromo-2-methylpropionate (EBIB, 1 eq., 0.17 mmol) were added to the round bottom flask and the mixture was stirred gently, to avoid breaking the silicon wafer (ca. 400 RPM), while slowly heating to 40 ℃. Once the mixture reached the desired temperature, L-ascorbic acid (9.8 eq., 1.7 mmol) was added to the reaction flask, which was promptly sealed. No additional techniques were used to remove atmospheric or dissolved oxygen. The polymerisation solution changed colour from blue (oxidised copper) to colourless (ca. 2 h on average) and then to yellow/orange over the course of 16 h. The polymer-grafted silicon wafer was removed from the bulk solution and washed thoroughly with anisole, followed by multiple washings with THF. The wafer was washed in basic EDTA solution before being dried at 110 ℃ for 1 h. The free polymer was collected as described in Section 4.3.5.

5.4.9 Synthesis of CO_2-responsive rough silicon surfaces by surface-initiated atom transfer radical polymerisation

SiO_2-S17 KBB9PG60:

A clean, laser-etched silicon wafer (1 cm x 1 cm) was added to a 50 mL glass reaction vessel. The vessel was kept at a constant temperature of 80 ℃. The atmosphere in the reaction vessel was removed under vacuum and replaced with Ar. To the sealed reaction vessel, 25 mL of a 10 mM solution of (3-trimethoxysilyl)propyl-2-bromo-2-methylpropionate in anhydrous toluene was added via cannula transfer. The reaction was left gently stirring at 70 ℃ overnight. The silane-grafted substrate was collected and washed multiple times with ethanol, followed by sonication in ethanol for 10 min, repeated 3 times. The silane-grafted substrate was blown dry with Ar and stored in a sealed vessel under Ar until further use.

SI-AGET-ATRP of PDiPAEMA on silicon, SiO_2-S17 KBB9PG73:

An initiator-grafted silicon wafer (1 cm x 1 cm) was added to a 100 mL glass reaction vessel. 2-(Diisopropylamino)ethyl methacrylate (DiPAEMA, 238 eq., 52 mmol) was passed over an inhibitor remover column [Sigma-Aldrich, removing hydroquinone (HQ) or hydroquinone monomethyl ether (MEHQ, 4-methoxyphenol), or 4-*tert*-butylcatechol (TBC)] and charged to the 100 mL round bottom flask containing the initiator-functionalised silicon wafer. Anisole (25 mL), Cu(II)Br_2 (0.65 eq., 0.15 mmol), N,N,N′,N″,N″-pentamethyldiethylenetriamine (PMDETA, 6.5 eq., 1.4 mmol) and ethyl 2-bromo-2-methylpropionate (EBIB, 1 eq., 0.22 mmol) were added to the round

bottom flask and the mixture was stirred gently, to avoid breaking the silicon wafer (ca. 400 RPM), while slowly heating to 40 °C. Once the mixture reached the desired temperature, tin(II) 2-ethylhexanoate (9.7 eq., 2.2 mmol) was added to the reaction flask, which was promptly sealed. No additional techniques were used to remove atmospheric or dissolved oxygen. The polymerisation solution changed colour from blue (oxidised copper) to colourless (ca. 2 h on average) and then to yellow/orange over the course of 16 h. The polymer-grafted silicon wafer was removed from the bulk solution and washed thoroughly with anisole, followed by multiple washings with THF. The wafer was washed in basic EDTA solution before being dried at 110 °C for 1 h. The free polymer was collected as described in Section 4.3.5.

SiO_2-S19 KBB9PG59:

A clean silicon wafer (4 cm x 1 cm) was subjected to wet etching with hydrofluoric acid (HF). The clean silicon wafer was added to a plastic centrifuge tube containing 10 mL of 48% $HF_{(aq)}$. The wafer was left in solution for 5 min to ensure the complete removal of the silicon oxide surface. The etched wafer was rinsed thoroughly with water and blown dry under a stream of Ar. The etched wafer was immediately added into a Schlenk tube containing 15 mL of neat 10-undecenoic acid that had been deoxygenated by two freeze pump thaw cycles. The wafer/undecenoic acid mixture was further deoxygenated by two more freeze pump thaw cycles. The mixture was heated to 120 °C under dynamic Ar, for 16 h. The resultant functionalised wafers were rinsed thoroughly with DMF, followed by sonication in DMF. At this point, the wafer was considered to be terminated with a carboxylic acid functionality.

A carboxylic acid functionalised wafer was further functionalised by HATU-mediated coupling with an ATRP initiator, 2-hydroxyethyl-2-bromoisobutyrate (HEBIB). The carboxylic acid functionalised wafer was added to a Schlenk tube containing solution of TEA (9 mmol) and HATU (1 mmol) in anhydrous DMF. The mixture was cooled with an ice bath and stirred for 30 min. The formation of an "active" ester is associated with a colour change; the solution changes colour from a light yellow to a deep orange/red when the "active" ester is formed. After 30 min, by which time the colour change had been observed, HEBIB (0.35 mmol) was added to the mixture. The ice bath was removed and the solution was allowed to warm to room temperature (ca. 23 ℃) as it reacted for 4 h. The ATRP-initiator grafted silicon wafer was rinsed thoroughly in DMF, followed by rinsing in anisole. The wafer was then subjected to SI-AGET-ATRP without further treatment.

SI-AGET-ATRP of PDiPAEMA on silicon, SiO_2-S19 KBB9PG59:

An initiator-grafted silicon wafer (4 cm x 1 cm) was added to a 50 mL Schlenk tube. 2-(Diisopropylamino)ethyl methacrylate (DiPAEMA, 235 eq., 16 mmol) was passed through an inhibitor remover column [Sigma-Aldrich, removing hydroquinone (HQ) or hydroquinone monomethyl ether (MEHQ, 4-methoxyphenol), or 4-*tert*-butylcatechol (TBC)] and charged to 50 mL Schlenk tube containing the initiator-functionalised silicon wafer. Anisole (10 mL), Cu(II)Br_2 (0.66 eq., 0.046 mmol), N,N,N′,N″,N″-pentamethyldiethylenetriamine (PMDETA, 3.3 eq., 0.22 mmol) and ethyl 2-bromo-2-methylpropionate (EBIB, 1 eq., 0.068 mmol) were added to the 50 mL Schlenk tube and the mixture was stirred gently, to avoid breaking the silicon wafer (ca. 400 RPM), while slowly heating to 40 ℃. Once the mixture reached the desired

temperature, tin(II) 2-ethylhexanoate (19 eq., 1.32 mmol) was added to the reaction flask, which was promptly sealed. No additional techniques were used to remove atmospheric or dissolved oxygen. The polymerisation solution changed colour from blue (oxidised copper) to colourless (ca. 2 h on average) and then to yellow/orange over the course of 16 h. The polymer-grafted silicon wafer was removed from the bulk solution and washed thoroughly with anisole, followed by multiple washings with THF. The wafer was washed in basic EDTA solution before being dried at 110 ℃ for 1 h. The free polymer was collected as described in Section 4.3.5.

5.4.10 Water contact angle analysis of CO_2-responsive inorganic surfaces

A surface's hydrophilicity or hydrophobicity can be measured by a quantitative analysis of a surface's free surface energy. A contact angle is the angle at which a liquid interface meets a solid surface, which can be measured via contact angle goniometry. A substrate of interest was placed onto a goniometer's observation deck. The goniometer then deposits a 0.75 μL droplet of probe liquid (commonly Millipore water) onto the wafer's surface and captured a high-resolution image of the droplet. A contact angle can be calculated using the goniometer's software. This procedure is commonly referred to as a sessile droplet method. Contact angles were measured using an AST Products VCA Optima Goniometer. The goniometer used for measuring contact angles was not equipped to accurately measure roll-off angles. The goniometer was used for CO_2-responsive amino-silane surfaces and gold-thiol surfaces.

To facilitate rapid assessment of static contact angles and sliding angles of functionalised surfaces the remaining contact angle analyses were carried out using a VehoVMS004D microscope. Images were processed using ImageJ and Dropsnake software.[48] Full instructions can be found online at: http://bigwww.epfl.ch/demo/dropanalysis/. Droplet volumes when using the USB microscope were ca. 5-10 μL.

A standardised method for the static contact angle analysis of surfaces is as follows:

1. CO_2 was bubbled through a gas dispersion tube into a beaker of Millipore water for 10 min.
2. A functionalised wafer was placed into the CO_2-sparged solution for a total of 30 min. The solution was continuously sparged with CO_2 over the course of the 30 min.
3. After 30 min, it was assumed the wafer had become protonated and thus hydrophilic. The wafer was removed and characterised by WCA analysis.
4. After water contact angle analysis, Ar was sparged through a beaker of Millipore water, which was heated to 60 ˚C.
5. The functionalised wafer was placed into the heated, Ar-sparged solution for a total of 30 min. The solution was continuously sparged with Ar over the course of the 30 min.
6. After 30 min, it was assumed the wafer had become deprotonated and thus hydrophobic. The wafer was removed and characterised by WCA analysis.

In some instances, user error can significantly change the outcome of the water contact angle analysis. Consequently, user error was recorded and monitored over time. User error or repeatability (i.e. the error associated with the author, Kyle J. Boniface, making the measurements on the same image was most recently recorded as $\pm$ 1.9°, where 8 measurements were recorded. Additionally, the instrument error as calculated by finding the average standard deviation from a population of 33, where those 33 standard deviations are resultant of over 100 individual measurements, was recorded as $\pm$ 1.8°. For reference, the interlaboratory (reproducibility) error is cited to be ca. $\pm$ 10°. The error associated with the reported contact angle is highly dependent on the user and the quality of the image.[49,50] The sessile drop method was used in all measurements for the contact angles reported in the entirety of this thesis. The sessile drop method is the most reproducible and has the greatest reproducibility owing to the simplicity of the method.[49] The surface structures in this chapter did not hinder contact angle analysis. However, the surface structures of polysaccharide substrates (Chapter 6) hinder contact angle analysis; the error associated with each measurement is inherently higher because the larger surface features interfere with capturing a clear image of the substrate-droplet interface.

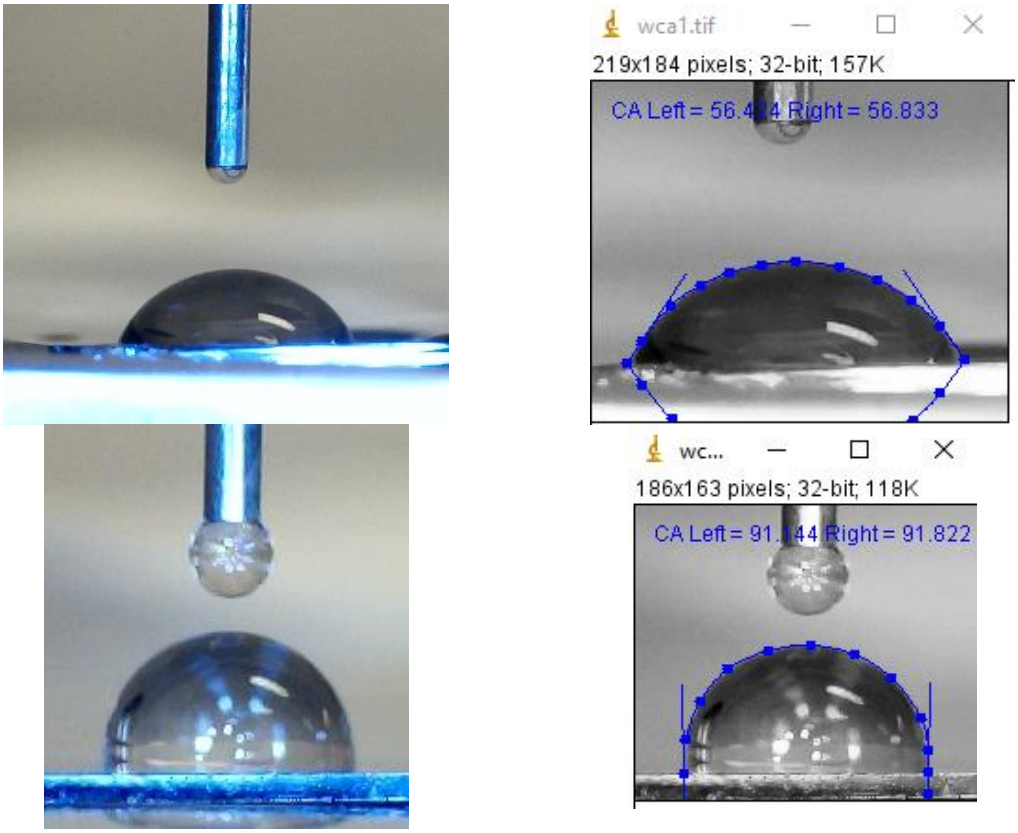

Figure 5.23. Sessile drop/static contact angle analysis for a CO_2-responsive surface (KBB9PG61, PDiPAEMA-grafted silicon wafer). Raw image of the surface when charged after exposure to CO_2 in water (upper left) and processed image (upper right). Raw image of the surface when neutral and dry (lower left) and processed image (lower right).

To ensure that the reported contact angle data is significant, the standard T-test was applied to each dataset. A representative T-test is shown below. The procedure for the T-test and instructions for its execution using Microsoft Excel™ were taken from a helpful book titled "Data analysis for chemistry, an introductory guide for students and laboratory scientists" written by D. Brynn Hibbert and J. Justin Gooding.

	WCA Measurements	
	Hydrophobic State	Hydrophilic State
	92	65
	91	65
	91	68
	92	72
	91	70
		64
Average	91.4	67.3
Standard Deviation	0.547	3.21
F-Statistic	34.22	
Degrees of freedom	5	6
p	0.0022	
T-statistic	18.08	
Degrees of freedom on T-statistic	5	
p	0.0000095	

If $p < 0.05$, reject null and conclude that the two data sets are significantly different

Probability of data sets being significantly different 99.99999

5.4.11 Gel permeation chromatography

Gel Permeation Chromatography (GPC) was performed with a Waters 2690 Separation Module and Waters 410 Differential Refractometer with THF as the eluent. The column bank consisted of Waters Styragel HR (4.6x300 mm) 4, 3, 1, and 0.5 separation columns operating at 40 ℃ and 0.3 mL min^{-1}. GPC data are reported as poly(methylmethacrylate) (PMMA) equivalents, based on a calibration curve of narrow molecular weight distribution PMMA standards purchased from Polymer Standards.

5.4.12 X-ray photoelectron spectroscopy of CO_2-responsive inorganic surfaces

Detailed accounts of the XPS studies conducted on CO_2-responsive inorganic surfaces can be found in Appendix V.

5.5 References

1. K. J. Boniface, T. J. Clark, M. F. Cunningham, P. G. Jessop, B. E. Mariampillai, S. M. Mercer, R. Resendes, T. Robert, WO. Pat., 039 247, 2015.

2. P. Champange, P. G. Jessop, K. J. Boniface, M. F. Cunningham, H. Wang, O. Garcia-Valdez, A. Cormier, S. Ge, J. Arrendondo-Luna, WO. Pat., 149 815, 2016.

3. K. J. Boniface, R. R. Dykeman, A. Cormier, H.-B. Wang, S. M. Mercer, G. Liu, M. F. Cunningham and P. G. Jessop, *Green Chem.*, 2015, **18**, 208–213.

4. A. Darabi, P. G. Jessop and M. F. Cunningham, *Chem. Soc. Rev.*, 2016, **45**, 4391–4436.

5. X. Yuan, E. G. Kim, C. A. Sanders, B. E. Richter, M. F. Cunningham, P. G.Jessop and R. D. Oleschuk, *Green Chem.*, 2017, **19**, 1757–1765.

6. S. Wang, K. Liu, X. Yao and L. Jiang, *Chem. Rev.*, 2015, **115**, 8230–8293.

7. S. Kumar, X. Tong, Y. L. Dory, M. Lepage and Y. Zhao, *Chem. Commun.*, 2012, **49**, 90–92.

8. D. Zhang, F. Chen, G. Fang, Q. Yang, D. Xie, G. Qiao, W. Li, J. Si and X. Hou, *J. Micromechanics Microengineering*, 2010, **20**, 075029.

9. C. Vericat, M. E. Vela, G. Benitez, P. Carro and R. C. Salvarezza, *Chem. Soc. Rev.*, 2010, **39**, 1805–1834.

10. R. G. Nuzzo and D. L. Allara, *J. Am. Chem. Soc.*, 1983, **105**, 4481–4483.

11. C. D. Bain, J. Evall and G. M. Whitesides, *J. Am. Chem. Soc.*, 1989, **111**, 7155–7164.

12. M. D. Porter, T. B. Bright, D. L. Allara and C. E. D. Chidsey, *J. Am. Chem. Soc.*, 1987, **109**, 3559–3568.

13. F. d. Osterholtz and E. r. Pohl, *J. Adhes. Sci. Technol.*, 1992, **6**, 127–149.

14. F. S. Mohammed, S. Wuttigul and C. L. Kitchens, *Ind. Eng. Chem. Res.*, 2011, **50**, 8034–8041.

15. Gelest silane coupling guide, https://www.gelest.com/wp-content/uploads/Goods-PDF-brochures-couplingagents.pdf, (accessed November 2017).

16. N. R. E. N. Impens, P. van der Voort and E. F. Vansant, *Microporous Mesoporous Mater.*, 1999, **28**, 217–232.

17. J. A. Grzyb, M. Shen, C. Yoshina-Ishii, W. Chi, R. S. Brown and R. A. Batey, *Tetrahedron*, 2005, **61**, 7153–7175.

18. R. Wolfenden and W. P. Jencks, *J. Am. Chem. Soc.*, 1961, **83**, 4390–4393.

19. R. Vaidyanathan, V. G. Kalthod, D. P. Ngo, J. M. Manley and S. P. Lapekas, *J. Org. Chem.*, 2004, **69**, 2565–2568.

20. J. O. Zoppe, N. C. Ataman, P. Mocny, J. Wang, J. Moraes and H.-A. Klok, *Chem. Rev.*, 2017, **117**, 1105–1318.

21. E. Stratakis, A. Mateescu, M. Barberoglou, M. Vamvakaki, C. Fotakis and S. H. Anastasiadis, *Chem. Commun.*, 2010, **46**, 4136–4138.

22. F. Chen, D. Zhang, Q. Yang, J. Yong, G. Du, J. Si, F. Yun and X. Hou, *ACS Appl. Mater. Interfaces*, 2013, **5**, 6777–6792.

23. B. N. Chichkov, C. Momma, S. Nolte, F. von Alvensleben and A. Tünnermann, *Appl. Phys. A*, 1996, **63**, 109–115.

24. Technical data brochure specialty monomers, http://www.specialty-monomers.basf.com/portal/streamer?fid=235727, (accessed November 2017).

25. Monomers product guide, http://www.polysciences.com/skin/frontend/default/polysciences/pdf/wb_2011_MONOmers%20Guide.pdf, (accessed November 2017).

26. R. J. Young and P. A. Lovell, Introduction to Polymers, Second Edition, Chapman and Hall, London, 1991.

27. Chemicalize, https://chemicalize.com/ (Accessed June 2017).

28. J. C. Wittmann and A. J. Kovacs, *J Polym. Sci C*, 1969, **16**, 4443.

29. J. J. Cras, C. A. Rowe-Taitt, D. A. Nivens and F. S. Ligler, *Biosens. Bioelectron.*, 1999, **14**, 683–688.

30. K. Shirai, Y. Yoshida, Y. Nakayama, M. Fujitani, H. Shintani, K. Wakasa, M. Okazaki, J. Snauwaert and B. Van Meerbeek, *J. Biomed. Mater. Res.*, 2000, **53**, 204–210.

31. R. Anwander, I. Nagl, M. Widenmeyer, G. Engelhardt, O. Groeger, C. Palm and T. Röser, *J. Phys. Chem. B*, 2000, **104**, 3532–3544.

32. D. R. Knapp, Handbook of Analytical Derivatization Reactions, Wiley, New Jersey, 1979.

33. K. Blau and J. M. Halket, Handbook of Derivatives for Chromatography, 2nd Edition, John Wiley & Sons, Ltd., Chichester, England, 1993.

34. M. L. Hair and W. Hertl, *J. Phys. Chem.*, 1971, **75**, 2181–2185.

35. M. C. Capel-Sanchez, L. Barrio, J. M. Campos-Martin and J. L. G. Fierro, *J. Colloid Interface Sci.*, 2004, **277**, 146–153.

36. W. H. Tallent and R. Kleiman, *J. Lipid Res.*, 1968, **9**, 146–148.

37. S. L. Hruby and B. H. Shanks, *J. Catal.*, 2009, **263**, 181–188.

38. H.-D. Wang, P. G. Jessop, J. Bouchard, P. Champagne and M. F. Cunningham, *Cellulose*, 2015, **22**, 3105–3116.

39. E. K. Woodman, J. G. K. Chaffey, P. A. Hopes, D. R. J. Hose and J. P. Gilday, *Org. Process Res. Dev.*, 2009, **13**, 106–113.

40. H. Zhao, K.-Y. Law and V. Sambhy, *Langmuir*, 2011, **27**, 5927–5935.

41. Y.-L. Zhang, H. Xia, E. Kim and H.-B. Sun, *Soft Matter*, 2012, **8**, 11217–11231.

42. R. Boukherroub, J. T. C. Wojtyk, D. D. M. Wayner and D. J. Lockwood, *J. Electrochem. Soc.*, 2002, **149**, H59–H63.

43. D. S. MacMillan, J. Murray, H. F. Sneddon, C. Jamieson and A. J. B. Watson, *Green Chem.*, 2013, **15**, 596–600.

44. Molecular self-assembly, http://www.sigmaaldrich.com/content/dam/sigma-aldrich/materials-science/material-matters/material_matters_v1n2.pdf, (accessed November 2017).

45. J. R. Harjani, C. Liang and P. G. Jessop, *J. Org. Chem.*, 2011, **76**, 1683–1691.

46. B. R. Kim, H.-G. Lee, S.-B. Kang, G. H. Sung, J.-J. Kim, J. K. Park, S.-G. Lee and Y.-J. Yoon, *Synthesis*, 2012, **44**, 42–50.

47. A. F. Burchat, J. M. Chong and N. Nielsen, *J. Organomet. Chem.*, 1997, **542**, 281–283.

48. A. F. Stalder, G. Kulik, D. Sage, L. Barbieri and P. Hoffmann, *Colloids Surf. Physicochem. Eng. Asp.*, 2006, **286**, 92–103.

49. Y. Yuan and T. R. Lee, in Surface Science Techniques, Springer, Berlin, Heidelberg, 2013, pp. 3–34.

50. Standard Test Method for Hydrophobic Contamination on Glass by Contact Angle Measurement, https://www.astm.org/Standards/C813.htm, (accessed November 2017).

Chapter 6

CO_2-Responsive Polysaccharides

6.1 Preface

Natural polysaccharide fibres, when utilised as substrates for CO_2-responsive systems, suffer from their inherent hydrophilicity. The native state of a polysaccharide surface is superhydrophilic and/or absorbent. To enable a stimulus-response, the surface of the polysaccharide must be sufficiently modified with a hydrophobic functionality that is capable of responding to a stimulus. When the polysaccharide surface area is large, or the degree of polymerisation of a fibre is high, the degree of modification must also be large to effectively modify the polysaccharide surface character. Unfortunately, this is quite difficult to achieve with single-unit modifiers, partly because the larger polysaccharides exist in a heterogeneous state when in solution and partly because the ratio of polysaccharide to hydrophobic modifier is so high. Polymeric modification allows for a greater amount of hydrophobic modifier relative to polysaccharide. Thus, polymeric modificiation was found to be more appropriate for modifying the surface character of larger polysaccharide materials such as membranes, filters, and cloth. Herein, both single-unit and polymeric modifications on various polysacharides of both low and high surface area are demonstrated.

6.1.1 Abstract

Functionalisation of polysaccharide fibres with CO_2-responsive single-unit and polymeric functionalities is presented herein. High surface area polysaccharides with single-unit modifications were evaluated as CO_2-switchable drying agents, similar to the polymer-grafted silica particles in Chapters 2 and 4. Low surface area polysaccharides with polymeric modifications were evaluated by contact angle analysis and by selective sorption tests using various oils and dyes, with or without CO_2 present.

The effects of single-unit CO_2-responsive functionalities on a polysaccharide fibre were minimal, owing to a low degree of substitution. The CO_2-responsive fibres, as made, remained considerably hydrophilic. This inherent hydrophilicity significantly reduces their ability to function as a CO_2-switchable drying agent, in which a significant change in hydrophilicity is required. In contrast, the effects of polymeric CO_2-responsive functionalities on a polysaccharide fibre are quite pronounced. The natural roughness of a woven cellulose surface enhanced the change in surface character that CO_2-responsive functionalities, when *grafted from* a surface, can achieve. The neutral and hydrophobic state of PDiPAEMA when *grafted from* a cotton fabric surface was determined to be ca. 150°, where previously the neutral and hydrophobic state of PDiPAEMA when *grafted from* a smooth silicon substrate was ca. 90°. The charged and hydrophilic state of PDiPAEMA, when grafted from a cotton fabric surface, was determined to be superhydrophilic, and absorbent, where previously the charged and hydrophilic state of PDiPAEMA when *grafted from* a smooth silicon substrate was ca. 60°. Thus, where the laser etching techniques presented in Chapter 5 failed, nature has provided a readily available and easily modifiable rough surface.

6.2 Introduction

Natural polysaccharides are biopolymers made of monosaccharide units bound by glycosidic linkages. A few examples of common natural polysaccharides are alginate, cellulose, chitin, chitosan, dextran, and starch. These biopolymers are produced in nature by a variety of living organisms such as plants and fungi. These biopolymers are abundant, renewable, and low-cost materials. Furthermore, they typically exhibit non-toxicity, biocompatibility and biodegradability.

Increasing environmental awareness has driven research efforts to replace petroleum-based polymeric materials with materials from renewable resources. However, the application of biopolymers in traditional industries is limited by their incompatibility with petroleum-based polymeric materials and the associated processing techniques. Chemical modification of biopolymers is often employed to overcome these issues.[1,2]

Cellulose is an abundant, inexpensive, biodegradable and a renewable resource that possesses several attributes such as high strength, durability, the ability to absorb moisture, high thermal stability, good biocompatibility, relatively low cost, and good mechanical properties at a low density. Cellulose and various other polysaccharides are therefore used as fillers or additives in composites. However, cellulose has some inherent drawbacks such as poor solubility in common solvents, poor dimensional stability, lack of thermoplasticity, high hydrophilicity, and a lack of antimicrobial properties. The hydrophilicity of cellulose can either be an advantage or a disadvantage depending on the intended application. To overcome such drawbacks, chemical modification of the polysaccharide surface is often applied.[1]

Surface modification of cellulose and other polysaccharides by graft-polymerisation has been widely studied for several decades.[1–15] Early work on polysaccharide modification sought to modify the hydrophilic nature of the polysaccharide with graft and block copolymers.[16] Dimensional stability, resistance to abrasion, wrinkle recovery, oil and water repellency, heat resistance, and antimicrobial activity are examples of properties that can be improved by graft-copolymerisation of cellulose.[2] When cellulose fibres are used as reinforcing agents in composites it is crucial, and often difficult, to obtain a sufficient fibre-to-matrix adhesion. Grafting of hydrophobic polymers to the fibre surface greatly enhances the hydrophobicity of the polysaccharide fibres, thus improving their adhesion to a polymer matrix.[2]

Recently a class of higher-ordered cellulose known as cellulose nanocrystals (CNC) has become readily available. CNC have been receiving increasing attention in recent years due to their high specific strength and modulus, high surface area (dimensions of ca. 100 nm by 10 nm), and unique optical properties.[13,17] CNC are only dispersible in polar/hydrophilic systems, which greatly restricts their use in common nonpolar/hydrophobic systems such as hydrophobic polymer matrices. Additionally, once CNC are dry, their subsequent redispersion is challenging.[13,18] Due to their properties, CNC have been considered for use as nanofillers in composites and as absorbents/flocculants.

In 2015, Wang et al. demonstrated that modification of a CNC surface with CO_2-responsive functionalities could control the ability of the functionalised CNC to disperse in aqueous solutions. The prepared CO_2-responsive CNC showed fast and reversible dispersion behaviour without requiring sonication, vortexing, or stirring.[17] In

2017, Garcia et al. demonstrated similar CO_2-responsive behaviour when grafting CO_2-responsive polymers to the surface of CNC.[12] The CO_2-responsive polymer-grafted CNC displayed more stable aqueous dispersions in their protonated state than in their neutral state. It was determined that the critical properties of CNC were preserved when the CO_2-responsive polymers were grafted to their surface. Modification of polysaccharides with CO_2-responsive functionalities has the ability to address some of the challenges of using polysaccharides, specifically their lack of solubility and poor ability to disperse in most solvents. Therefore, CO_2-responsive technology for polysaccharides might be useful at the industrial scale.

In addition to their use as fillers or additives in composites, cellulose and various other polysaccharides fibres can be woven into larger materials; common examples are various forms of paper, filters, membranes, and textiles. These woven cellulosic substrates are the focus of a sub-set of research on superhydrophobic surfaces, which focuses on developing superhydrophobic character on renewable substrates. The fabrication of superhydrophobic cellulose surfaces could extend the use of cellulose and its derivatives into new areas such as self-cleaning textiles, water repellent packaging materials, coatings with improved barrier properties, and membrane technology.[5]

One of the most common cellulosic substrates that is studied is filter paper. Filter paper is commonly available and easy to handle. Nystrom et al. reported a graft on graft method of functionalising filter paper to induce self-cleaning and superhydrophobic properties.[3,5] Wang et al. demonstrated that polymeric coatings on cotton fabric could be used to create a novel bifunctional Janus membrane that could separate oil from oil-in-water emulsions.[19]

As previously discussed in Chapter 5, the wetting characteristics of a surface can be greatly enhanced by physical modification of the surface (i.e. creating surface roughness) or by chemical modification by modifying a surface (rough or smooth) with hydrophobic coatings. The rough surface structure of the cellulosic substrate inherently lends itself to the creation of superhydrophobic or "very-hydrophobic" surfaces. Thus, graft modification of cellulose substrates is a viable method for the creation of smart surfaces.

Cellulose is inherently more reactive and easier to work with than the inorganic substrates like the silicon wafers that were used in Chapter 5. Understanding the molecular structure of cellulose is the key to its modification. The repeating β-D-anhydroglucopyranose units are held together by β-1,4-glycosidic bonds (Figure 6.1).

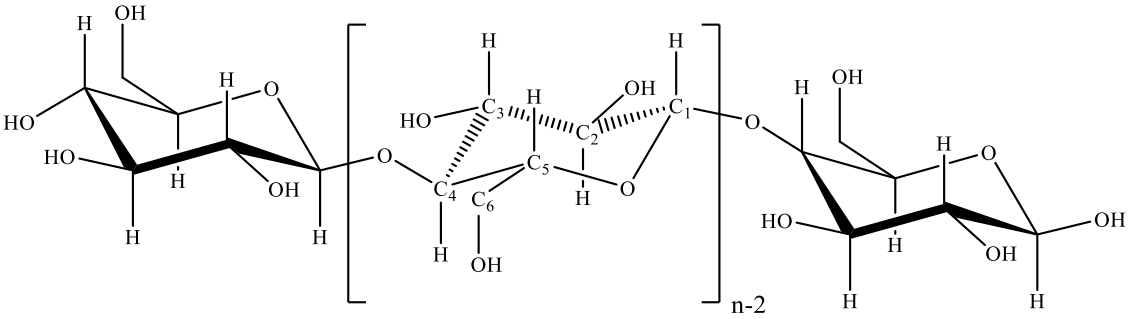

Figure 6.1. The molecular structure of cellulose (n=DP, degree of polymerisation).

The degree of polymerisation (DP) of cellulose varies with its source and extraction techniques. In the case of cotton and other plant fibres, DP values range from 800-10,000. Regenerated or highly processed cellulose fibres have DP values that range from 20-300.[1] Cellulose fibres form larger aggregates and sheets through extended hydrogen bonding networks; when these networks are disrupted, or a given cellulose fibre is at the surface of

the bulk aggregate it can be chemically modified by either of the three hydroxyl groups in the glucose repeat unit (Figure 6.1).

In glucose, the equatorial hydroxyl groups at C_2 and C_3 have reactivity typical of secondary alcohols and the hydroxyl group at C_6 has reactivity typical of a primary alcohol. However, the reactivity of cellulose cannot be simplified to that of a trihydric alcohol that is similar in its chemistry to a simple sugar containing three alcohols. The heterogeneity of the cellulose substrate in solution, combined with the polymeric nature of the cellulose substrate greatly influences the reactivity of each hydroxyl group.[1]

Studies involving the esterification of cellulose found that the hydroxyl group at C_6 can react ten times faster than the other hydroxyl groups.[20,21] Additionally, the hydroxyl group at C_2 was observed to react twice as fast in etherification reactions as the hydroxyl group at C_3.[21] Thus, the primary hydroxyl group is often the most reactive and the first of the three to participate in a substitution reaction.

Starch, a structurally-related polysaccharide, was also investigated in the present study. Plants store glucose as starch; there are two forms of starch, amylose and amylopectin. Amylose consists typically of more than 1000 D-glucopyranoside units connected by α-1,4 linkages (recall cellulose has β linkages). Amylopectin is similar to amylose except that amylopectin has α-1,6 branching points that occur at intervals of 20-25 glucose units. The chemical reactivity of starch fibres is very similar to that of cellulose fibres. Any noticeable differences in chemical properties is thus due to the larger supramolecular structures of either polysaccharide fibre.

Herein, both cellulose and starch fibres were modified with CO_2-responsive functionalities using the synthetic methods outlined in Chapter 5 (Scheme 6.1).

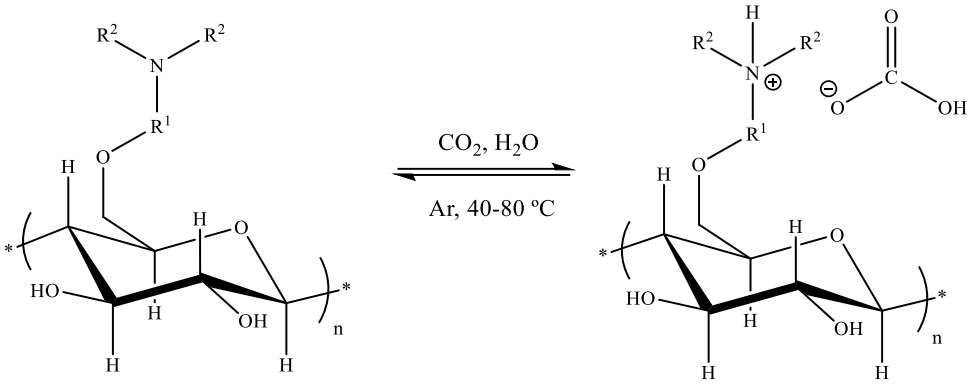

Scheme 6.1. A generic CO_2-responsive polysaccharide, where R^1= ethylene, propylene; R^2= alkyl group.

CO_2-responsive polysaccharides were evaluated as CO_2-responsive drying agents for the removal of water from wet isobutanol. Additionally, SI-AGET-ATRP was applied to cellulosic substrates to create CO_2-responsive cotton fabric that could reversibly switch between superhydrophilic and "very-hydrophobic". To the best of my knowledge, a superhydrophilic/superhydrophobic or superhydrophilic/"very-hydrophobic" CO_2-responsive cellulosic surface has not been reported.

6.3 Results and discussion

6.3.1 CO_2-responsive cellulose fibres

As described in Chapter 5, acyl transfer reagents were applied, with limited success, to the synthesis of CO_2-responsive silicon surfaces. The stability of the silyl ester carbamate/carbonate linkage was hypothesised to be low, which resulted in a high rate of hydrolysis for the single-unit functionalised CO_2-responsive silicon materials. The synthetic methods presented herein are the same as those from Chapter 5, with some minor modifications. When these synthetic methods are applied to a polysaccharide surface, the resulting linkage is a carbonate/carbamate ester (Scheme 6.2). Carbonate/carbamate esters are considerably more stable than their silyl counter parts; thus, a high degree of polysaccharide functionalisation with CO_2-responsive functional groups was expected. Two synthetic methods were examined for the functionalisation of cellulose fibres with CO_2-responsive functional groups (Scheme 6.2 and 6.3).

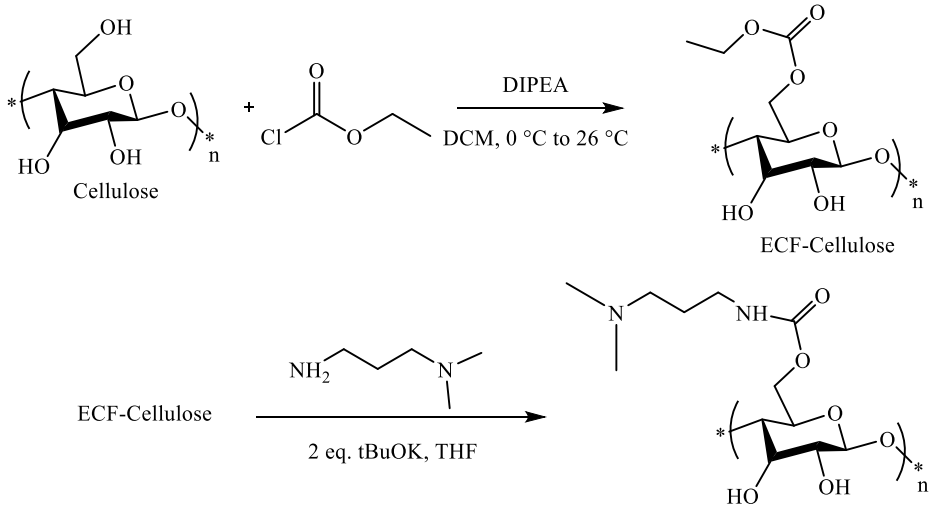

Scheme 6.2. Synthetic method 1 for the functionalisation of cellulose fibres with CO_2-responsive functional groups. Method adapted from Kim et al.[22]

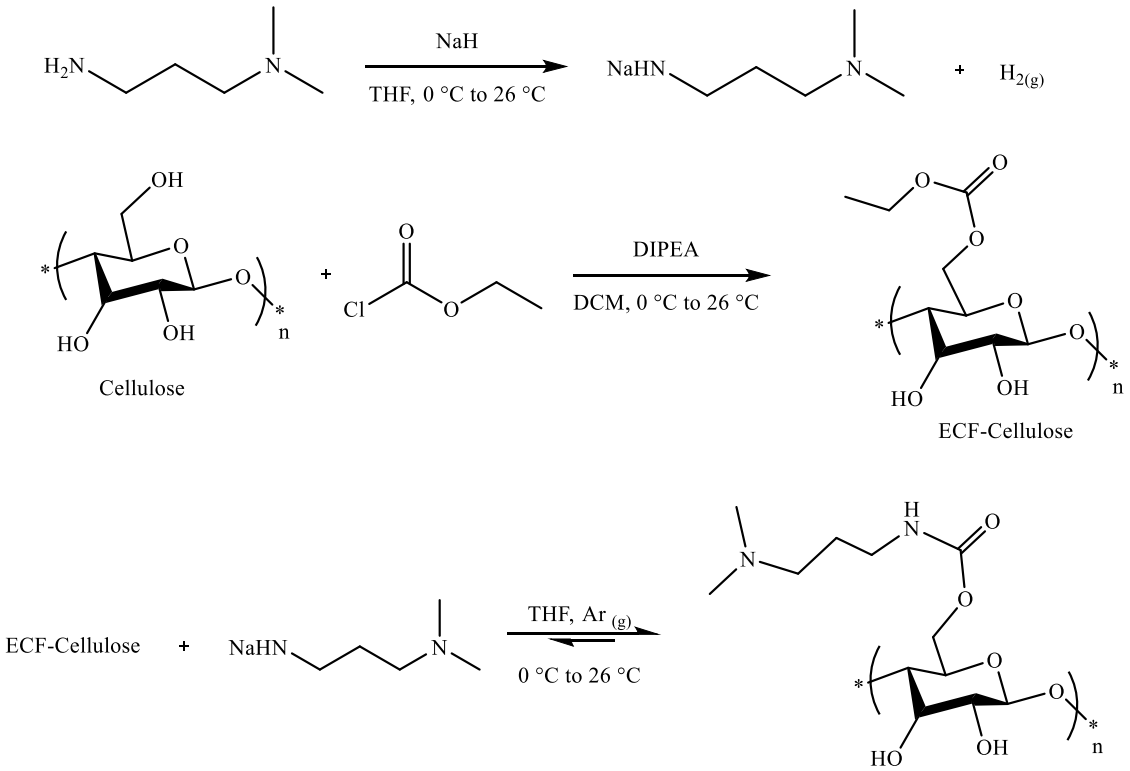

Scheme 6.3. Synthetic method 2 for the functionalisation of cellulose fibres with CO_2-responsive functional groups.

Native cellulose fibres were treated with ethyl chloroformate (ECF). ECF-cellulose fibres were modified with a variety of CO_2-responsive functionalities (Figure 6.2). Cellulose based drying agents are more robust than their silica counterparts; as such, mechanical stirring causing degradation is not a concern. The ease of use of both materials is comparable. The cellulose fibres are a white powder and are considerably less prone to static charging than the silica based drying agents.

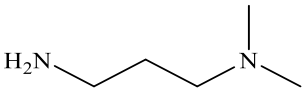

3-(dimethylamino)propylamine
pK_{aH}: 9.3
log$\mathcal{P}$: -0.11
LogD (pH 4.6): -3.58
LogD (pH 7.4): -2.00
A1

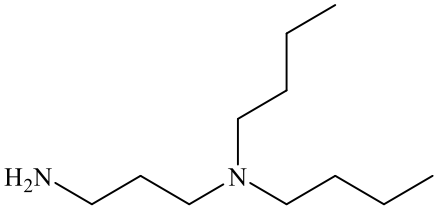

3-(dibutylamino)-1-propylamine
pK_{aH}: 10.35
log$\mathcal{P}$: 2.54
LogD (pH 4.6): -0.96
LogD (pH 7.4): -0.31
A2

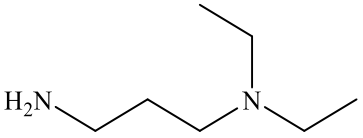

3-(diethylamino)propylamine
pK_{aH}: 9.84
log$\mathcal{P}$: 0.6
LogD (pH 4.6): -2.89
LogD (pH 7.4): -1.80
A3

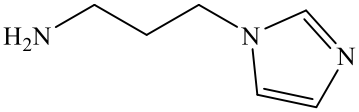

1-(3-aminopropyl)imidazole
pK_{aH}: 6.79
log$\mathcal{P}$: -0.22
LogD (pH 4.6): -0.80
LogD (pH 7.4): -0.29
A4

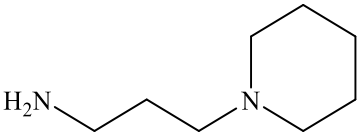

N-(3-aminopropyl)piperidine
pK_{aH}: 9.06
log$\mathcal{P}$: 0.74
LogD (pH 4.6): -2.17
LogD (pH 7.4): -0.92
A5

Figure 6.2. Proposed CO_2-responsive co-nucleophilic species for acyl transfer group mediated coupling with a polysaccharide substrate. All values were predicted using model compounds; model compounds are indicative of the compound when bound to a surface via a carbonate or carbamate bond. As such, the pK_{aH} values correspond to the tertiary amine and not the primary amine (Appendix VII).[23]

Functionalisation was confirmed by FT-IR and solid-state NMR spectroscopy. In one example, FT-IR spectroscopy of A1 (method 2) suggests that functionalisation of cellulose with 3-(dimethylamino)-1-propylamine was successful. The IR spectrum of A1-cellulose was different from the FT-IR spectrum of non-functionalised cellulose, in that the peak at ~1600 cm^{-1} was broader for A1 than non-functionalised cellulose, and thus indicative of functionalisation. Additionally, the broadening of the ^{13}C cellulose peaks and

the appearance of new ^{13}C peaks at 168 ppm and 38 ppm suggest that functionalisation had occurred.

Characterisation of the CO_2-responsive cellulose fibres was difficult owing to the relatively low surface area and the degree of substitution that likely occurred. In comparison, the characterisation of CO_2-responsive CNC, which has a relatively high surface area, was straightforward.[17] The reactions with polysaccharides, specifically larger fibres like cellulose, are heterogeneous. Fibres form aggregates in solution, which further reduces the accessibility of the reactive primary hydroxyl site. This problem is compounded after each step in the synthesis; low ECF-grafting will result in an even lower amine-grafting.

The CO_2-responsive cellulose fibres were investigated for their ability to act as CO_2-responsive drying agents (DA). The solvent chosen to compare the utility of switchable cellulose materials as drying agents was isobutanol, which was doped with 5 wt% H_2O. The CO_2-responsive cellulose and 'wet' isobutanol solution were added to a vial, and CO_2 was sparged through the solution for 1 h. The vial was then sealed and stirred for 15 h. The CO_2-responsive cellulose fibres were separated from the wet isobutanol solution via vacuum filtration; water content remaining in the isobutanol solution after filtration was analyzed via gas chromatography thermal conductivity detector (GC-TCD). The results are reported in Table 6.1.

Table 6.1. The removal of water from wet isobutanol using CO_2-responsive cellulose fibres.

Cellulose	Water removed[a,b] (mg H_2O/gDA)			
	Cycle 1	Cycle 2	Cycle 3	Without CO_2
Control[f]	170 ± 11	-	-	-
Cellulose 1[c]	440 ± 1	300 ± 4	430 ± 5	-
Cellulose 2[d]	460 ± 5	300 ± 4	130 ± 6	-
ECF-Cellulose	430 ± 4	-	-	110 ± 5
A1-Cellulose	230 ± 1	340 ± 2	480 ± 3	-
A2-Cellulose	330 ± 6	-	-	190 ± 5
A3-Cellulose	320 ± 1	-	-	380 ± 9
A4-Cellulose	380 ± 3	-	-	270 ± 4
A5-Cellulose	460 ± 5	-	-	260 ± 4
A1-Cellulose[e]	450 ± 2	-	-	340 ± 10
A2-Cellulose[e]	500 ± 1	-	-	-

[a]Reaction conditions: 10 g isobutanol with water at a concentration of 5 wt%, 0.5 g drying agent added, 1 h mixing with CO_2 bubbling through solution then continued mixing in a sealed vial for 15 h, water content analysed by GC-TCD. [b]Drying agent regeneration was performed at 50 °C for 4 h. [b] Water removed with respect to drying agent used. [c]Cellulose (as received) with CO_2 bubbling. [d]Cellulose (as received) without CO_2 bubbling. [e]Synthesised by synthetic method 2. [f]No drying agent was added to the control experiment. Water removed is a result of CO_2 sparging. Reported error is associated with measuring in triplicate; all values are representative of a single experiment. Each cycle used fresh isobutanol with 5 wt% water.

Untreated cellulose fibres are hydrophilic and perform well as drying agents in the presence of CO_2 (Table 6.1 row 1). However, the performance of untreated cellulose fibres, without CO_2, declines over three cycles (Table 6.1, row 2). It is plausible that the addition of CO_2 aids in the dispersion of the untreated cellulose fibres by disrupting the extended intermolecular hydrogen bonding network of the cellulose fibres. Further dispersion of the cellulose fibres would result in a higher surface area to which water could be bound and removed from the isobutanol solution. Thus, it is likely that the performance fluctuations for untreated cellulose fibres are a result of how well the fibres are dispersed in solution and not a direct result of whether CO_2 is present.

Modification of the cellulose fibres with CO_2-responsive functionalities did little to increase performance as a drying agent. In most instances, the CO_2-responsive cellulose fibres performed worse in the 1st cycle than untreated cellulose. The data might suggest that CO_2-responsive cellulose fibres (Table 6.1 rows 4-10, column 1) perform better in the presence of CO_2 than without CO_2 (Table 6.1 column 5). It is plausible that CO_2-responsive functionalities in their neutral state would aid aggregate formation by participating in hydrogen bonding, thereby reducing the surface area accessible for the removal of water, thus reducing performance as a drying agent. It is also plausible that the CO_2-responsive functionality would aid in the redispersion of the aggregate material when CO_2 is present, thus increasing the performance of the drying agent. This type of behaviour was demonstrated with high surface area CO_2-responsive CNC in aqueous solutions.[17] However, the drying experiments presented here were not conducted in an aqueous environment; they were conducted in isobutanol with 5 wt% water. Therefore, the CO_2-induced redispersion effect would be severely limited by the polarity of the solvent and the availability of water.

As evident from the performance of untreated cellulose, the availability of water in the organic solvent is not the limiting factor. Untreated cellulose (ca. 440 mg H_2O/g DA) performed similarly to the 1st generation of polymer-grafted silica particles (Chapter 2, 490 mg H_2O/g DA) but not as well as the 2nd generation of polymer-grafted silica particles (Chapter 4, 1053 mg H_2O/g DA).

It is more likely that drying performance is a function of CO_2 exposure and the relative amount of exposed surface area of the drying agent. The relative exposed surface area of a polysaccharide could be increased by reducing the overall size of the

polysaccharide (e.g. CNC instead of cellulose fibres) and by increasing the amount of grafted CO_2-responsive functionality. Due to the increased stability of single-unit CO_2-responsive functionalities on polysaccharides, it is possible that single-unit CO_2-responsive polysaccharides could be effective drying agents whereas single-unit CO_2-responsive silica particles were not. Additionally, polymer grafting methods are another way in which the relative surface area of a CO_2-responsive drying agent could be increased. Grafting polymer chains from a polysaccharide essentially results in a branched copolymer and it is well documented that branched polymers are less likely to aggregate in solution than their linear counterparts due to a reduction in intermolecular attractive forces. Thus, CO_2-responsive polymer-grafted polysaccharides would experience less aggregation due to branching effects and greater dispersion in polar solvents when CO_2 is present due to the formation of the amine-bicarbonate salt complexes.

6.3.2 CO_2-responsive starch fibres

Starch fibres were investigated briefly as a polysaccharide based support for single-unit functionalisation with CO_2-responsive functional groups. It was hypothesised that the branched nature of starch would allow for a higher degree of substitution with CO_2-responsive functional groups; the relative surface area of starch would be higher that than of cellulose fibres of similar size.

It was observed that unfunctionalised starch was not soluble in water at room temperature, but that it could be solubilised by boiling water for a short period. Once solubilised into hot water, the resultant starch solution could be cooled and stored for a

moderate period, though it was observed that the starch would eventually aggregate and precipitate out of the water.

Synthesis of a switchable starch, involving surface functionalisation to comprise switchable moieties as defined above, was initially investigated to provide means for solubilising starch without the use of excessive heat. Starch was functionalised with CO_2-responsive functional groups using a CDI-mediated coupling approach. Similar challenges were encountered with starch that were encountered with cellulose fibres; characterisation was difficult and it was hard to extrapolate what effect the CO_2-responsive functionalities were having. A quantifiable increase, relatively to native starch, in the solubility of single-unit functionalised CO_2-responsive starch fibres in aqueous solutions with CO_2 present was not observed. Therefore, work related to CO_2-responsive starch fibres was ceased. The same conclusions that were drawn for cellulose fibres apply to starch fibres. Detailed synthesis can be found in Appendix VI.

6.3.3 CO_2-responsive single-unit functionalised filter paper

Single-unit functionalisation of cellulose surfaces with CO_2-responsive functionalities was achieved using CDI-mediated coupling. Initial experiments used Whatman type 1 filter paper as the cellulose substrate. As a proof of concept, CDI-mediated coupling was demonstrated using a long chain "waxy" carboxylic acid to the surface of the filter paper. The functionalized filter paper was observed to be hydrophobic, with no discernable changes in surface energy as a result of exposure to CO_2. Various CDI-mediated coupling methods were evaluated with CO_2-resposinve

functionalities on filter paper. Detailed schemes and discussion can be found in Appendix VI. However, in every case, these methods failed to produce a CO_2-responsive polysaccharide surface. Further work on single-unit functionalisation method development was abandoned for more promising polymeric functionalisation techniques

6.3.4 CO_2-responsive polymer-grafted filter paper

CO_2-responsive polymers were *grafted from* cellulosic substrates and tested for their ability to modify the surface energy of the substrate under a variety of external triggers. The traditional ATRP polymer grafting methods that were presented in Chapter 2 were applied to polysaccharide substrates. At the time, the SI-ARGET-ATRP method presented in Chapter 4 was not developed. Known CO_2-responsive polymers were grafted to Whatman type 1 filter paper. The first attempt at grafting PDMAPMAm to filter paper (PGFP-1) utilised the same strategy that was employed for grafting PDMAPMAm to silica particles (PGS-7). The filter paper was analysed by ATR-FTIR spectroscopy and WCA; PGFP-1 failed to exhibit CO_2-responsive behaviour and grafted-PDMAPMAm could not be identified in the IR spectrum. It was hypothesised that the surface-initiated grafting reaction failed due to poor initiator loading. Various techniques are suggested in the literature that would enable the initiator-grafting step. The suggestions aim to disrupt the hydrogen bonding network in cellulose, thus making the hydroxyl functional groups more accessible. The suggestions include soaking the filter paper in THF or $NaOH_{(aq)}$, the addition of auxiliary bases, the addition of salts, and the use of polar aprotic solvents such

as DMSO or DMAc.[1–3,24] Additionally, it was recommended that thermal pretreatments or refluxing with solvent should be avoided to prevent heat-treating the cellulose fibres.[25]

A second attempt at grafting PDMAPMAm to filter paper (PGFP-2) was undertaken with the specific goal of avoiding any and all applications of heat to the filter paper surface.[25] WCA analysis and IR spectroscopy determined that the grafting reaction was unsuccessful. This reaction was carried out without the presence of a free initiator in solution. It was hypothesised that the addition of free initiator to the polymerisation solution in tandem with avoiding heat treatment of the fibres would result in a successful grafting reaction. Thus, a third attempt of grafting PDMAPMAm to the cellulose surface was conducted. IR spectroscopy indicated the presence of polymer on the surface, but the surface energy of the cellulose surface was not modified substantially. Either the grafting density of PDMAPMAm was too low, or PDMAPMAm was not hydrophobic enough to modify the surface energy of the cellulose surface. Thus, CO_2-responsive polymers with higher hydrophobic character were used in place of PDMAPMAm.

A fourth polymer grafting experiment was conducted using PDEAEMA (PGFP-4), which is more hydrophobic than PDMAPMAm. Heat treatment of the fibres was avoided and free initiator was added to the polymerisation solution. IR spectroscopy confirmed the presence of grafted PDEAEMA. Initial WCA analysis indicated that the modified cellulose substrate was hydrophobic (Figure 6.3). The modified surface remained hydrophobic for 10-20 s, after which the water droplet was slowly absorbed into the cellulose substrate. This behaviour is common of polymer-grafted filter paper substrates that have low polymer loadings.[25] PGFP-4 exhibited CO_2-responsive behaviour; PGFP-4 when exposed to CO_2 and water was superhydrophilic, PGFP-4 when dried, was hydrophobic for a short period.

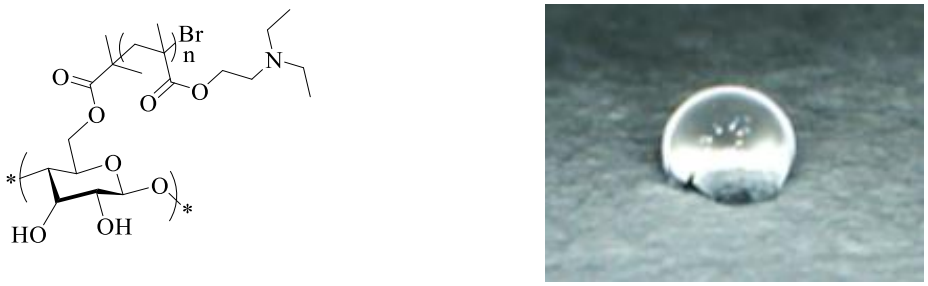

Figure 6.3. PDEAEMA grafted filter paper, PGFP-4 (left). WCA analysis of PGFP-4 in the neutral and hydrophobic state (right). Experimental procedure outlined in Section 5.4.10.

A fifth polymer grafting experiment was conducted using PDiPAEMA (PGFP-5), which is more hydrophobic than PDMAPMAm or PDEAEMA. Heat treatment of the fibres was avoided and free initiator was added to the polymerisation solution. IR spectroscopy confirmed the presence of grafted PDiPAEMA. Initial WCA analysis indicated that the modified cellulose substrate was hydrophobic (Figure 6.4). Surface characterisation of a rough filter paper is not straightforward; contact angle measurements are complicated by both the surface roughness and the absorbing nature of the filter paper. Therefore, the contact angle measurements presented here, as measured from a rough cellulose surface, can only be considered as estimates of the surface properties. PGFP-5 exhibited CO_2-responsive behaviour; PGFP-5 when exposed to CO_2 and water, was superhydrophilic; PGFP-5 when dried, was hydrophobic for an extended period. PGFP-5 did not show a loss of hydrophobic character as a function of exposure to water. It is possible that this behaviour is a result of the increased hydrophobic character of PDiPAEMA in comparison to PDEAEMA or PDMAPMAm. Additionally, the prolonged

hydrophobic character of PGFP-5 could be due to a higher polymer loading as a result of a better polymerisation.

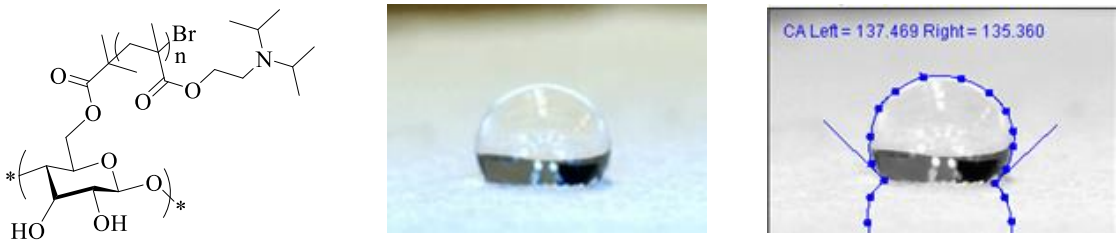

Figure 6.4. PDiPAEMA grafted filter paper, PGFP-5 (left). WCA analysis of PGFP-5 in the neutral and hydrophobic state (centre and right). Experimental procedure outlined in Section 5.4.10.

The free polymer produced in situ during the SI-ATRP of PGFP-5 was collected and analysed. The molecular weight of the grafted chains was approximated through the characterisation of the free polymer produced in situ. The molecular weight and dispersity of free PDiPAEMA were determined to be M_n: 42.5 kDa, Đ: 1.38. As a result of these experiments, it became apparent that PDiPAEMA was CO_2-responsive and hydrophobic enough to exhibit prolonged hydrophobic surface character when grafted from a polysaccharide surface.

Filter paper, while hydrophobic, was tear-resistant and could be manipulated easily. However, prolonged exposure to CO_2 and water, in tandem with subsequent characterisation, destroyed the polymer-grafted filter paper. To continue testing, a more robust substrate was required. Woven cotton swatches were used for the remainder of these experiments. At no point did the woven cotton substrate show signs of degradation.

6.3.5 CO_2-responsive polymer-grafted cotton fabric

CO_2-responsive polymer-grafted cotton fabric was synthesised using the SI-AGET-ATRP method presented in Chapter 4. The naturally rough surface of the cotton fabric proved to be a suitable support for CO_2-responsive polymers. CO_2-responsive polymer-grafted cotton fabric exhibited very-hydrophobic behaviour when neutral, and superhydrophilic behaviour when charged (Scheme 6.4).

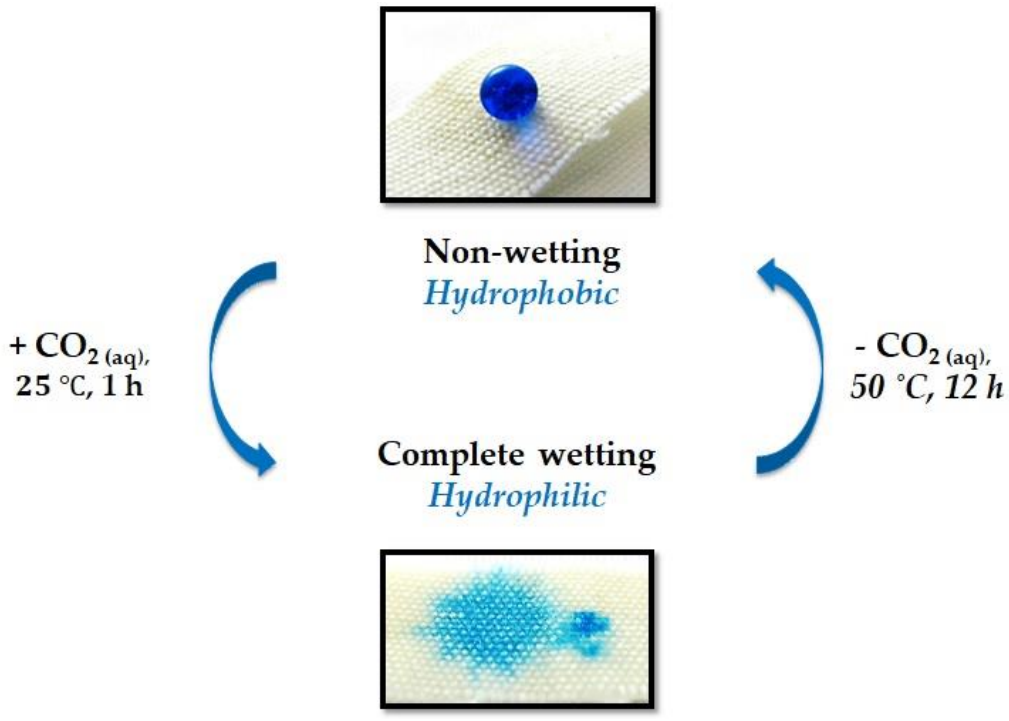

Scheme 6.4. The CO_2-responsive polymer-grafted cotton fabric system. The probe liquid was a solution of blue food colouring in water. The surface shown is PGC-1. Experimental procedure outlined in Section 5.4.10.

Polymer-grafted surfaces were analysed by WCA, IR spectroscopy, XPS, and SEM. Free PDiPAEMA was characterised by GPC; for PGC-1 the free polymer was determined to be M_n: 55.6 kDa, Đ: 1.25. CO_2-responsive behaviour was demonstrated over

multiple cycles, no deterioration in performance was observed (Figure 6.5). The hydrophobic state was persistent; any change in contact angle over time was due to evaporation of the water droplet and not absorption of the water droplet. When exposed to CO_2 and water, PGC-1 remained superhydrophilic for upwards of 1 h when left exposed to the laboratory atmosphere. The superhydrophilic nature of the charged surface was lost slowly over the course of 2 h; extended exposure of the charged surface to the laboratory atmosphere fully restored PGC-1 to its neutral and hydrophobic state.

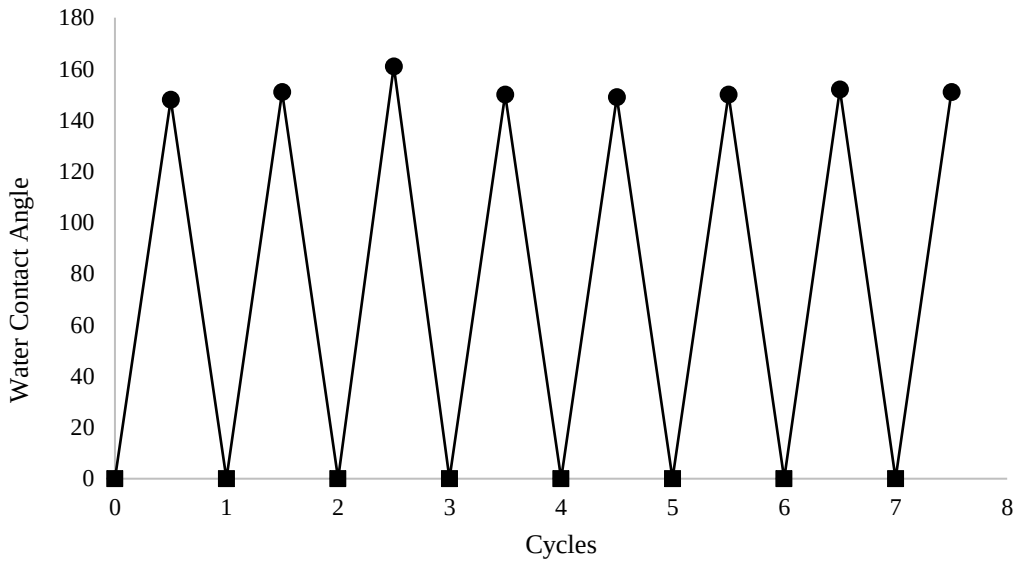

Figure 6.5. The CO_2-responsive behaviour of PGC-1 as measured by static water contact angle analysis over 7.5 cycles of switching from hydrophilic to hydrophobic and back to hydrophilic. PGC-1 with CO_2 (■) and PGC-1 without CO_2 (●). Experimental procedure outlined in Section 5.4.10.

Further contact angle analysis of PGC-1 in the neutral state showed the polymer-grafted cotton fabric to be very hydrophobic (WCA ca. 150°) and adhesive. The surface is thus very hydrophobic and not superhydrophobic (Figure 6.6).

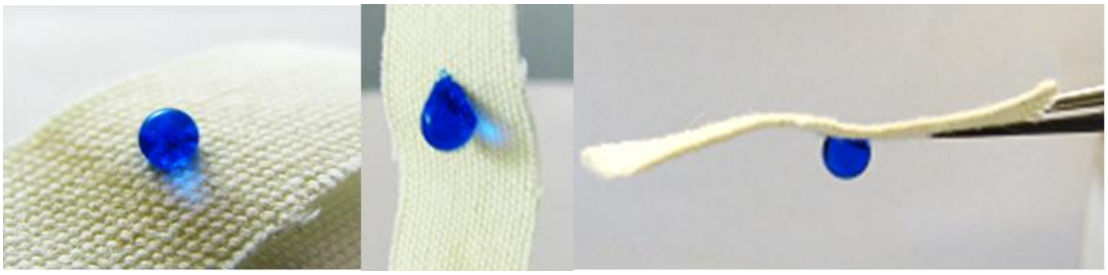

Figure 6.6. WCA analysis of PGC-1 at various inclinations. Parallel to the ground (left), 90° rotation from the ground (middle), 180° inversion-parallel to the ground, suspended with tweezers (right). The probe liquid was a solution of blue food colouring in water.

Further contact angle analysis of PGC-1 was conducted after exposure to CO_2 in water for 1 h. PGC-1 was determined to be superhydrophilic and absorbent. Figure 6.7 shows full adsorption of a water droplet coloured with blue food colouring.

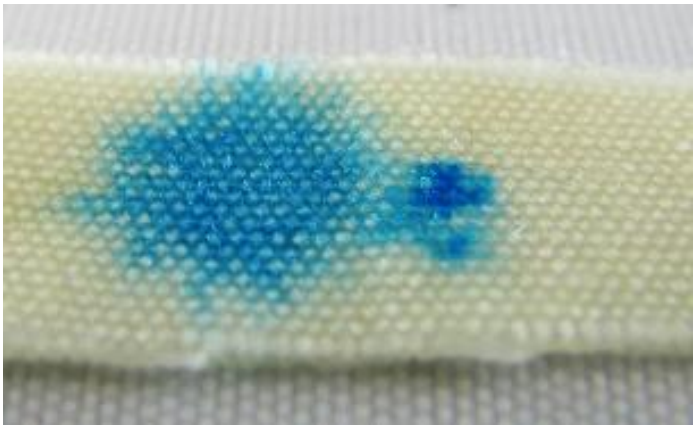

Figure 6.7. WCA analysis of PGC-1 after exposure to CO_2 in water for 1 h. The probe liquid was a solution of blue food colouring in water.

SEM analysis of the polymer-grafted cotton surface reveals polymer globules grafted along the cellulose fibres. Attempts to map the nitrogen content using various X-ray techniques were unsuccessful as the high-energy electron beam charred the cotton surface and reliable data was not collected. Nonetheless, the SEM images are a clear

indication of the grafted-PDiPAEMA chains and provide a striking visual representation of the actual nature of PGC-1 and the grafted-PDiPAEMA chains.

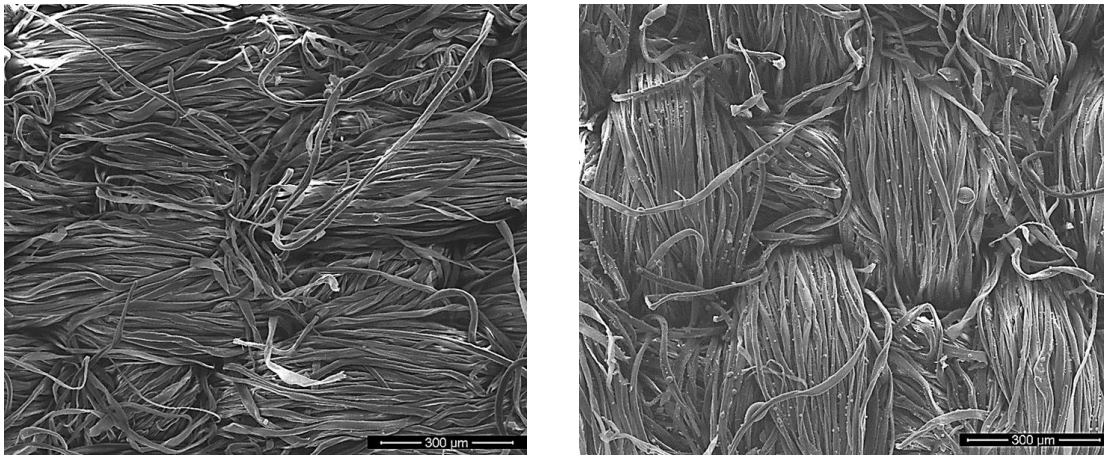

Figure 6.8. SEM images of a washed cotton swatch (left) and a PDiPAEMA-grafted cotton swatch, PGC-1 (right). 300 μm scale bar.

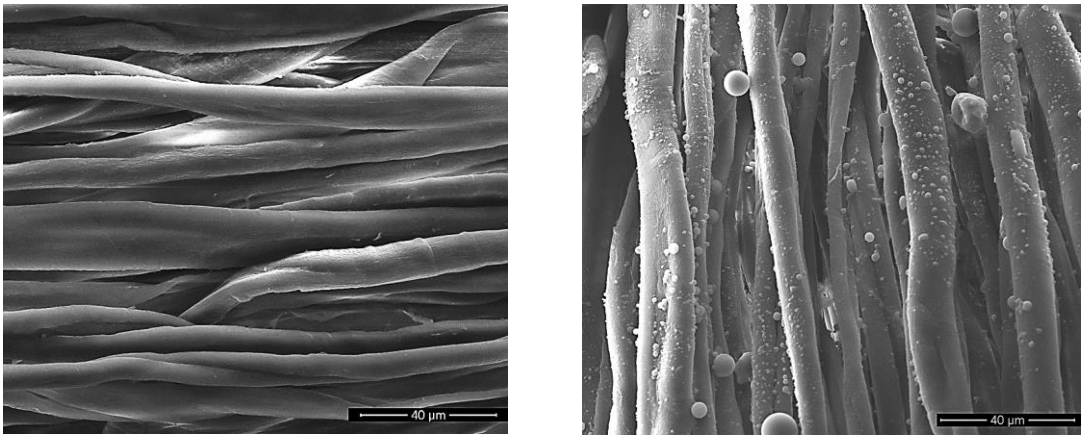

Figure 6.9. SEM images of a washed cotton swatch (left) and a PDiPAEMA-grafted cotton swatch, PGC-1 (right). 40 μm scale bar.

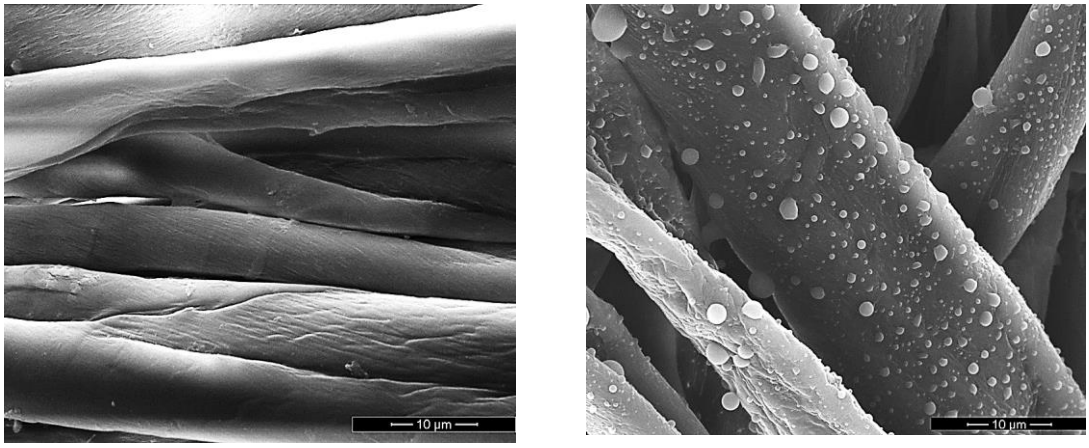

Figure 6.10. SEM images of a washed cotton swatch (left) and a PDiPAEMA-grafted cotton swatch, PGC-1 (right). 10 μm scale bar.

One envisioned application of a CO_2-responsive cotton membrane/filter is that it could be used as a recyclable filter for wastewater remediation. Additionally, it could be used as a recyclable osmosis membrane. It was enivsioned that contaminants could be captured from wastewater and subsequently released during a regeneration treatment; the filter could be reused in this manner multiple times. Alternatively, a CO_2-responsive membrane would be ideally suited for CO_2-switchable forward osmosis, a technology that has been developed by Forward Water Technologies and one that remains a point of interest in the Jessop group. Lastly, this technology could be used for the separation of oil from oil-in-water emulsions, similar to Janus membranes reported by Wang et al.[19] For PGC-1 to be considered in these applications, it would have to be able to capture contaminants, maintain its CO_2-responsive behaviour while "dirty" and be able to be cleaned without suffering subsequent loss in performance. Whether the CO_2 induced changes in surface energy would be enough to expel contaminants was of particular interest.

Various dyes were used to test the hypothesis that a CO_2-responsive polysaccharide surface could selectively capture and release hydrophobic or hydrophilic compounds. The hydrophilic probe liquid was blue food colouring in water and the hydrophobic probe liquids were Oil Red O in both hexadecane and soybean oil. The CO_2-responsive system, in the presence of various probe liquids was tested using PGC-1 (Figure 6.11).

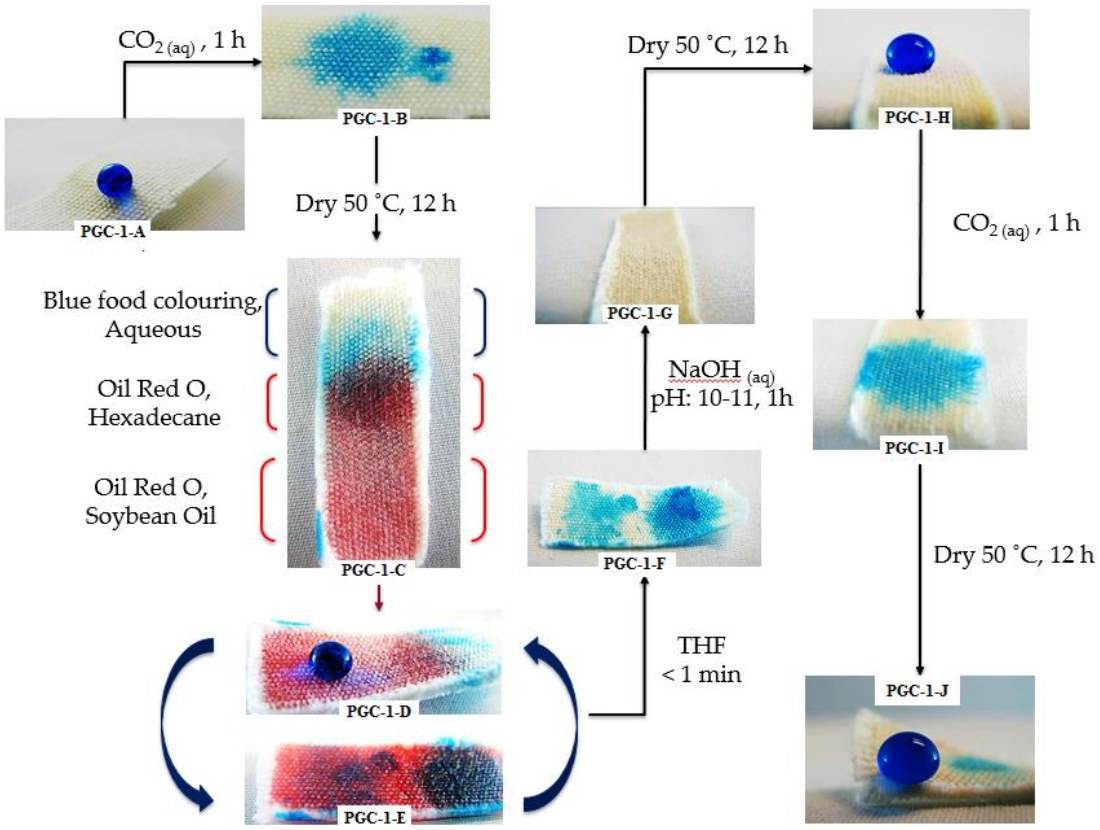

Figure 6.11. PGC-1, a CO_2-responsive polysaccharide, exhibiting selective capture and release of hydrophilic and hydrophobic probe liquids.

In the hydrophobic state, PGC-1 repels the blue hydrophilic probe liquid (PGC-1-A). Upon exposure to CO_2 in water, PGC-1 adsorbs the blue hydrophilic probe liquid (PGC-1-B). Subsequent drying of PGC-1 returns the surface to its hydrophobic form.

Hydrophobic probe liquids (red) were introduced to the dried surface and were subsequently absorbed by the surface (PGC-1-C). The oil-saturated surface was then further tested with the hydrophilic probe liquid (blue) and shown to be hydrophobic, despite being saturated with hexadecane and soybean oil (PGC-1-D). The CO_2-responsive behaviour of PGC-1 was not lost despite being saturated with oils. PGC-1 when exposed to CO_2 in water became hydrophilic and subsequently absorbed the blue hydrophilic probe liquid (PGC-1-E). Cycling of the CO_2-responsive system, as outlined in Scheme 6.4 and illustrated by the large arrows in Figure 6.11, was carried out over numerous cycles with no loss in hydrophobic or hydrophilic character. It was observed that bulk oil was expelled from PGC-1 during the carbonation step; however, the red and blue dyes remained adhered to the polymer-grafted cotton fabric. Removal of the red dye was achieved by quickly dipping PGC-1 into THF. Within seconds of being exposed to THF the red dye was removed from PGC-1 (PGC-1-F). Removal of residual blue dye was slightly more challenging; PGC-1 had to be treated with $NaOH_{(aq)}$ for 1 h to remove all traces of the blue food colouring. There was a concern that the $NaOH_{(aq)}$ treatment might degrade PGC-1 by cleaving the polymer from the surface, however subsequent exposure to the CO_2-responsive system conditions showed no loss in performance (PGC-1-H, -I, -J).

6.4 Conclusions

CO_2-responsive chemistry was investigated for polysaccharides surfaces. Both single-unit and polymeric functionalisation techniques were presented. Single-unit functionalisation techniques were successful in modifying the polysaccharide surface with CO_2-responsive functionalities. However, single-unit functionalised materials failed to show any promise in applications that would be of current use. Single-unit functionalisation techniques could be improved by achieving homogeneous reaction conditions and by using higher surface area substrates such as CNC or cellulose fibres with low degrees of polymerisation.

Polymeric functionalisation techniques provided, for the first time, a CO_2-responsive very-hydrophobic/superhydrophilic polysaccharide surface. The natural roughness of a woven cellulose surface was able to increase the change in surface character that CO_2-responsive functionalities, when *grafted from* a surface, can achieve. The neutral and hydrophobic state of PDiPAEMA when *grafted from* a cotton fabric surface was determined to be ca. 150°, where previously the neutral and hydrophobic state of PDiPAEMA when *grafted from* a smooth silicon substrate was ca. 90°. The charged and hydrophilic state of PDiPAEMA, when grafted from a cotton fabric surface, was determined to be superhydrophilic and absorbent, where previously the charged and hydrophilic state of PDiPAEMA when *grafted from* a smooth silicon substrate was ca. 60°. Thus, where the laser etching techniques presented in Chapter 5 failed, nature has provided a readily available and easily modifiable rough surface.

For the first time, a CO_2-responsive polysaccharide filter has been used to capture and release various dyes and oils selectively. CO_2-responsive chemistry was able to remove bulk oil from the surface of the CO_2-responsive cotton fabric. However, a hydrophobic dye could not be released with CO_2 and had to be removed with THF, an organic solvent. Proof of concept that a CO_2-responsive membrane can selectively capture and release oil from water without suffering a loss in performance was demonstrated.

6.5 Experimental methods

6.5.1 Materials

All aqueous solutions were prepared with deionized water (DIW) unless stated otherwise. The following chemicals were used as received unless otherwise stated: water (Millipore, type 1, 18.2 MΩ·cm @ 25 ℃), hydrogen peroxide (Aldrich, 30 wt% in H_2O), 2-bromo-2-methylpropionyl bromide (BIBB, Aldrich, 98%), diisopropylethylamine (DIPEA, Aldrich, ≥99.9%), 4-(dimethylamino)pyridine (DMAP, Aldrich, ≥99%), dichloromethane (DCM, EMD Millipore, anhydrous, ≥98.5%), tetrahydrofuran (Aldrich, anhydrous, contains 250 ppm BHT as inhibitor, ≥99.9%), methanol (MeOH, EMD Millipore, anhydrous), dimethylacetamide (DMAc, EMD Millipore, anhydrous), ethanol (Commercial Alcohols, anhydrous), dimethylsulfoxide (DMSO, Fisher Scientific), ethyl acetate (Aldrich, anhydrous, 99.8%), copper(I) bromide (Aldrich, 99.999% trace metals basis), copper(II) bromide (Aldrich, 99.999% trace metals basis), N-[3-(dimethylamino)propyl]methacrylamide (DMAPMAm, Aldrich, contains MEHQ as inhibitor, 99%), 2-(diisopropylamino)ethyl methacrylate (DiPAEMA, Aldrich, 97%,

contains ~100 ppm MEHQ as inhibitor), 2-(diethylamino)ethyl methacrylate (DEAEMA, Aldrich, contains 1500 ppm MEHQ as inhibitor, 99%), N,N,N`,N``,N``-pentamethyldiethylenetriamine (PMDETA, Aldrich, 99%), ethylenediaminetetraacetic acid (EDTA, Aldrich, purified grade, ≥98.5%), L-ascorbic acid (AA, Aldrich, reagent grade), sodium hydroxide (NaOH, Aldrich, ACS reagent, ≥97%), aluminium oxide (Aldrich, activated, basic, Brockmann I), nonanoic acid (Aldrich, 96%), 1,1'-carbonyldiimidazole (CDI, Aldrich, reagent grade), 1,1,3,3-tetramethylguanidine (TMG, Aldrich, 99%, N,N-dimethylformamide (DMF, Aldrich, 98%), anisole (Aldrich, anhydrous, 99.7%), potassium *tert*-butoxide (Aldrich, reagent grade >98%), methyl chloroformate (MCF, Aldrich, 99%), ethyl chloroformate (ECF, Aldrich, 97%), sodium hydride (Aldrich, 95% trace metal basis), 3-(dimethylamino)propylamine (DMAPA, Aldrich, >99%), 3-(dibutylamino)propylamine (DBAPA, Aldrich, >99%), 3-(diethylamino)propylamine (DEAPA, Aldrich, >99%), N-(3-aminopropyl)piperidine (Aldrich, 95%), 1-(3-aminopropyl)imidazole (Aldrich, >97%), cellulose fibres (Aldrich, Sigmacell cellulose type 101), starch (J.T. Baker, CAS 9005-84-9), hexadecane (Aldrich), Oil Red O (Aldrich), soybean oil (Presidents Choice), Whatman type 1 filter paper, 42.5 mm (Fisher Scientific), cotton fabric (provided by Dr. Guojun Liu of Queen's University, Kingston, Ontario, Canada), 3-(dimethylamino)propionic acid hydrochloride (Aldrich, 97%), imidazole hydrochloride (Aldrich, ACS reagent grade >99%), methyliodide (Aldrich, >99.5%), $CO_{2(g)}$ (Praxair), Argon (5.0, ultra-high purity, Praxair).

6.5.2 Synthesis of CO_2-responsive cellulose fibres

Synthetic method 1:

Cellulose fibres (Aldrich, Sigmacell cellulose type 101) were dried overnight at 110 ℃ in an oven. Dried cellulose was then used as is, with no other pretreatments. Dried cellulose fibres (6.5 g) were added to a 250 mL round bottom flask and flame dried under vacuum. Reactants were added using Schlenk techniques for inert conditions; diisopropylethylamine (1.6 eq., 0.19 mol) and anhydrous dichloromethane (150 mL, alkene stabilised) were added to the round bottom flask using Schlenk techniques for inert conditions. The round bottom flask was cooled in an ice bath for approximately 30 min, after which ethyl chloroformate (ECF, 1.5 eq., 0.18 mol) was added dropwise via an addition funnel to the cooled mixture. The mixture was warmed to room temperature and allowed to react for 12 h. The cellulose fibres were recovered by vacuum filtration and washed thoroughly with ethanol, followed by multiple washings with distilled water. The washed particles were dried at 110 ℃ overnight, then stored under Ar until further use.

ECF-functionalised cellulose (1 g) was added to a 150 mL round bottom flask. Following a procedure reported by Kim et al.,[22] tetrahydrofuran (THF, 80 mL) with 0.2% water was added to the round bottom flask and stirred for 30 min. Potassium *tert*-butoxide (2.2 eq.) was added, turning the clear solution a cloudy light yellow. A select amine (1.1 eq.) was added to the reaction mixture, which was then left stirring overnight at room temperature (ca. 26 ℃) exposed to air. The amine-functionalised cellulose fibres were recovered by vacuum filtration and washed thoroughly with THF, followed by multiple

washings with distilled water. The washed particles were dried at 110 ℃ overnight, then stored under Ar until further use.

Synthetic method 2:

Cellulose fibres (Aldrich, Sigmacell cellulose type 101) were dried overnight at 110 ℃ in an oven. Dried cellulose was then used as is, with no other pretreatments. Dried cellulose fibre (6.5 g) was added to a 250 mL round bottom flask and flame dried under vacuum. Diisopropylethylamine (1.6 eq., 0.19 mol) and anhydrous dichloromethane (150 mL, alkene stabilised) were added to the round bottom flask using Schlenk techniques for inert conditions. The round bottom flask was cooled in an ice bath for approximately 30 min, after which ethyl chloroformate (1.5 eq., 0.18 mol) was added dropwise via addition funnel to the cooled mixture. The mixture was allowed to warm to room temperature, ca. 27 ℃, and allowed to react for 12 h. The cellulose fibres were recovered by vacuum filtration and washed thoroughly with ethanol, followed by multiple washings with distilled water. The washed particles were dried at 110 ℃ overnight, then stored under Ar until further use.

3-(Dimethylamino)-1-propylamine (DMAPA, 1 eq. 75.2 mmol) was added dropwise under inert conditions to a cooled (ice bath, ca. 1 ℃) suspension of sodium hydride (1 eq., 75.2 mmol) in tetrahydrofuran (40 mL). The ice bath was removed and the mixture was stirred rapidly while being allowed to warm to room temperature (ca. 26 ℃) over the course of ca. 3 h. In a separate round bottom flask, the ethyl formate-functionalised cellulose was dried at 110 ℃ for 3 h and then stored temporarily

under dynamic Ar. The mixture of 3-(dimethylamino)propyl-1-amine and sodium hydride (comprising sodium (3-aminopropyl)dimethylamine) was then transferred via cannula into the round bottom containing the ethyl formate-functionalised cellulose after 3 h had passed. The resultant mixture was stirred rapidly at room temperature, overnight. The reaction was neutralised using an excess of ammonium chloride solution (ca. 1.3 eq.) in water. Functionalised cellulose was recovered using vacuum filtration. To deprotonate any of the cellulose that had been protonated by the excess ammonium chloride, it was mixed overnight in a solution of tetramethylguanidine/tetrahydrofuran (1:4 v/v). The functionalised cellulose was then rinsed with copious amounts of ethanol, followed by sonication for 20 min in 50 mL of ethanol (repeated three times). The functionalised cellulose was then dried in an oven at 110 ℃ for 4 h, after which it was characterised by ATR-FTIR spectroscopy.

Synthetic method 3:

3-(Dibutylamino)-1-propylamine (DBAPA, 1 eq. 75.2 mmol) was added drop-wise under inert conditions to a cooled (ice bath, ca. 1 ℃) suspension of sodium hydride (1 eq., 75.2 mmol) in tetrahydrofuran (40 mL). The ice bath was removed and the mixture was stirred rapidly while being allowed to warm to room temperature (ca. 26 ℃) over ca. 3 h. In a separate round bottom flask, ethyl formate-functionalised cellulose was dried at 110˚C for 3 h and then stored temporarily under dynamic Ar. The mixture of 3-(dibutylamino)propyl-1-amine and sodium hydride (comprising sodium (3-aminopropyl)dibutylamine) was then transferred via cannula under inert conditions into the round bottom flask containing the ethyl formate-functionalised cellulose after 3 h had

passed. The resultant mixture was stirred rapidly at room temperature overnight to yield a butyl-amine functionalised cellulose. The reaction was neutralised using an excess of ammonium chloride solution (ca. 1.3 eq.) in water. Functionalised cellulose was recovered using vacuum filtration.

To deprotonate any of the functionalised cellulose protonated by excess ammonium chloride, it was stirred overnight in a solution of tetramethylguanidine/tetrahydrofuran (1:4 v/v). The functionalised cellulose was then rinsed with copious amounts of ethanol, followed by sonication for 20 min in 50 mL of ethanol (repeated three times). The functionalised cellulose was then dried in an oven at 110 ℃ for 4 h, after which it was characterised by ATR-FTIR spectroscopy.

6.5.3 Synthesis of CO_2-responsive polymer-grafted filter paper

Various methods were evaluated for the synthesis of CO_2-responsive polymer-grafted filter paper. For illustrative purposes, method 5 for the synthesis of PGDP-5 is presented below. Detailed accounts of the synthesis of PGFP-1 to PGFP-4 can be found in Appendix VI.

Method 5 (PGFP-5):

A cellulosic substrate (Whatman type 1 filter paper, 42.5 mm) was rinsed thoroughly in acetone, followed by THF. The cellulosic substrate was then sonicated in acetone for 30 min, followed by sonication in THF for 30 min. The cellulosic substrate was then left in fresh THF to soak for 4 h. In a 100 mL 2-neck round bottom flask, a solution of triethylamine (TEA, 2.2 eq., 1.375 mmol, 0.1916 mL), 2-bromo-2-methylpropionyl bromide (BIBB, 2 eq., 1.25 mmol, 0.154 mL), and a catalytic amount of 4-dimethylaminopyridine (DMAP, 0.01 eq., 0.0625 mmol, 7.6 mg) was prepared in 40 mL of tetrahydrofuran, at room temperature (ca. 26 ℃), under Ar. The cellulosic substrate was immersed into the solution and left overnight at room temperature (ca. 26 ℃) to react. The resultant functionalised substrate was then rinsed and sonicated in tetrahydrofuran, followed by sonication in methanol. The functionalised substrate was left in dry methanol until it was ready to be polymerised.

The BIBB-functionalised filter paper was placed in a 250 mL round bottom flask, the flask was charged with 2-(diisopropylamino)ethyl methacrylate (DiPAEMA, 300 eq.

186 mmol, 34 mL), ethyl 2-bromo-2-methylpropionate (EBIB, 1 eq., 0.62 mmol) and 100 mL of anhydrous methanol under Ar. Ethyl 2-bromo-2-methylpropionate was used as an ATRP initiator and served as a sacrificial initiator. A stir bar was added to the round bottom flask and the flask was sparged with Ar via needle for 1 h. The radical inhibitor MEHQ was removed from DiPAEMA by passing the monomer through a basic alumina column. In a separate flask, the catalyst was prepared by mixing N,N,N′,N″,N″-pentamethyldiethylenetriamine (PMDETA, 2 eq., 1.2 mmol, 0.22 mL) with copper(I)bromide (1 eq., 0.62 mmol, 90 mg) in 15 mL of anhydrous methanol. The catalyst solution was sparged with Ar for 0.5 h. The solution containing monomer and BIBB-functionalised filter paper was heated to 45 ℃, at which point the catalyst solution added via cannula. The polymerisation was left to occur, with stirring under Ar, over the course of 34 h. The resultant polymer-grafted filter paper was sonicated for 20 min in fresh methanol (three times) to remove physisorbed polymer, excess monomer, ligand and catalyst. It was observed that the filter paper appeared white, with no colour from residual copper. The presence of polymer was confirmed by ATR-FTIR spectroscopy and subsequent CO_2-responsive behaviour was observed as determined by WCA analysis.

6.5.4 Synthesis of CO_2-responsive polymer-grafted cotton fabric

Method 1(PGC-1):

A swatch of cotton fabric (ca. 4 x 4 cm, 0.3301 g, 1 eq., @ 1 mmol·g^{-1}) was soaked in THF overnight to remove residual organic contaminants. The cotton swatch was sonicated in fresh THF for 20 min, after which it was rinsed thoroughly and left to soak in fresh THF until further use was required. The decontaminated cotton swatch was added to a flame dried 250 mL round bottom flask. Diisopropylethylamine (2.5 eq., 0.7525 mmol), 4-dimethylaminopyridine (DMAP, 0.2 eq., 0.065 mmol) and 150 mL of anhydrous THF were added to the round bottom flask using Schlenk techniques for inert conditions. The round bottom flask was cooled in an ice bath for approximately 30 min, after which the initiator, 2-bromo-2-methylpropionyl bromide, (BIBB, 1.5 eq., 0.495 mmol) was added dropwise via syringe. The mixture was stirred for 20 min before the ice bath was removed and the mixture was allowed to warm to room temperature, ca. 27 ℃, and allowed to react overnight. The initiator-grafted cotton fabric was collected by vacuum filtration, washed multiple times with THF, and then soaked in anisole for 30 min, at which point the solvent was exchanged for fresh anisole in preparation for the polymerisation step.

The initiator-grafted cotton swatch was placed into a 250 mL reaction vessel. 2-(Diisopropylamino)ethyl methacrylate (DiPAEMA, 258 eq., 219 mmol) was passed through an inhibitor remover column [Sigma-Aldrich, removing hydroquinone (HQ) or hydroquinone monomethyl ether (MEHQ, 4-methoxyphenol), or 4-*tert*-butylcatechol (TBC)] and charged to the 250 mL round bottom flask containing the initiator-grafted cotton swatch. Anisole (50 mL), Cu(II)Br_2 (0.7 eq., 0.58 mmol),

N,N,N′,N″,N″-pentamethyldiethylenetriamine (PMDETA, 3.3 eq., 2.8 mmol) and ethyl 2-bromo-2-methylpropionate (EBIB, 1 eq., 0.85 mmol) were added to the round bottom flask and the mixture was stirred vigorously while slowly heating to 40 ℃. Once the mixture reached the desired temperature L-ascorbic acid (10 eq., 8.5 mmol) was added to the reaction flask, which was promptly sealed. No additional techniques were used to remove atmospheric or dissolved oxygen. The polymerisation changed colour from blue (oxidised copper) to colourless (ca. 2 h on average) and then to yellow/orange over the course of 12 h. The polymer-grafted cotton swatch (PGC-1) was removed from the bulk solution and washed thoroughly with anisole, followed by multiple washings with THF. PGC-1 was washed in a basic EDTA solution (pH>10) before being dried at 110 ℃ for 1 h. The free polymer was collected as described in Section 4.3.5

6.5.5 Infrared spectroscopy of CO_2-responsive polysaccharides

Fourier Transform Infrared (FTIR) spectroscopy was conducted on a Bruker Alpha spectrometer using an Attenuated Total Reflectance (ATR) accessory. The substrate that provided the most reproducible response to CO_2 in water was PGC-1. Therefore, selected spectra that illustrate the polymer-grafting process for PGC-1 are provided as a reference. The IR signals for PDiPAEMA and the native cotton swatch are expected to be similar and in most cases, they are overlapping. To illustrate the IR peaks associated with only the grafted PDiPAEMA chains (Figure 6.14), the IR spectrum of a washed native cotton swatch (Figure 6.13) was subtracted from the IR spectrum of a PDiPAEMA-grafted cotton swatch (Figure 6.15). Characteristic IR peaks associated to PDiPAEMA are 1728 cm^{-1} (s, sh) and 1583 cm^{-1} (w, sh). Where: m=medium, w=weak, s=strong, n=narrow, b=broad, sh=sharp. Additional IR spectroscopy data for various single-unit functionalized substrates can be found in Appendix VI.

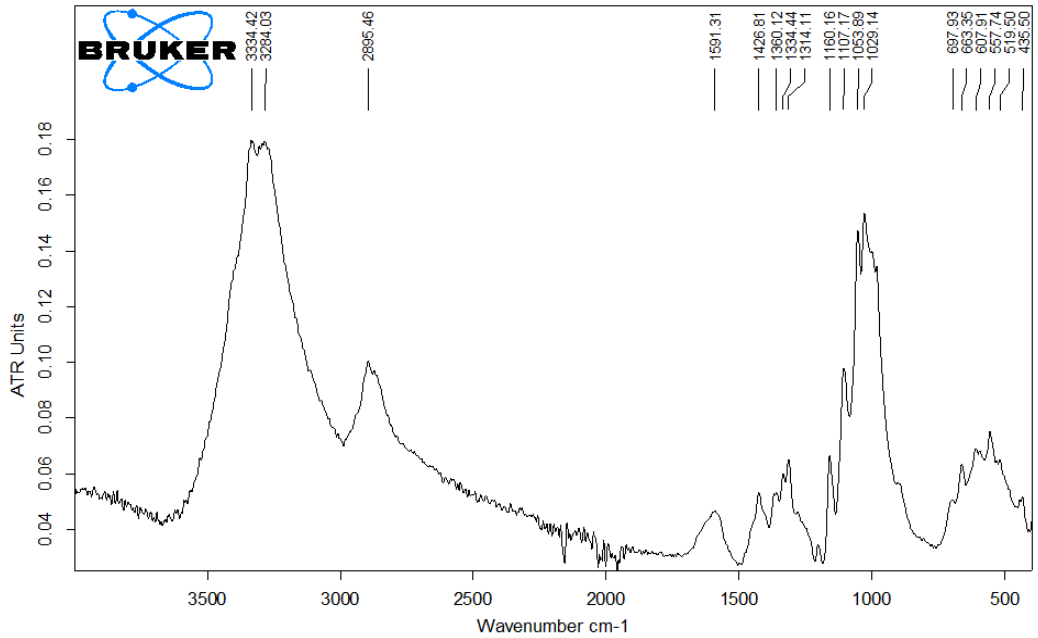

Figure 6.12. ATR-FTIR spectrum of a washed native cotton swatch.

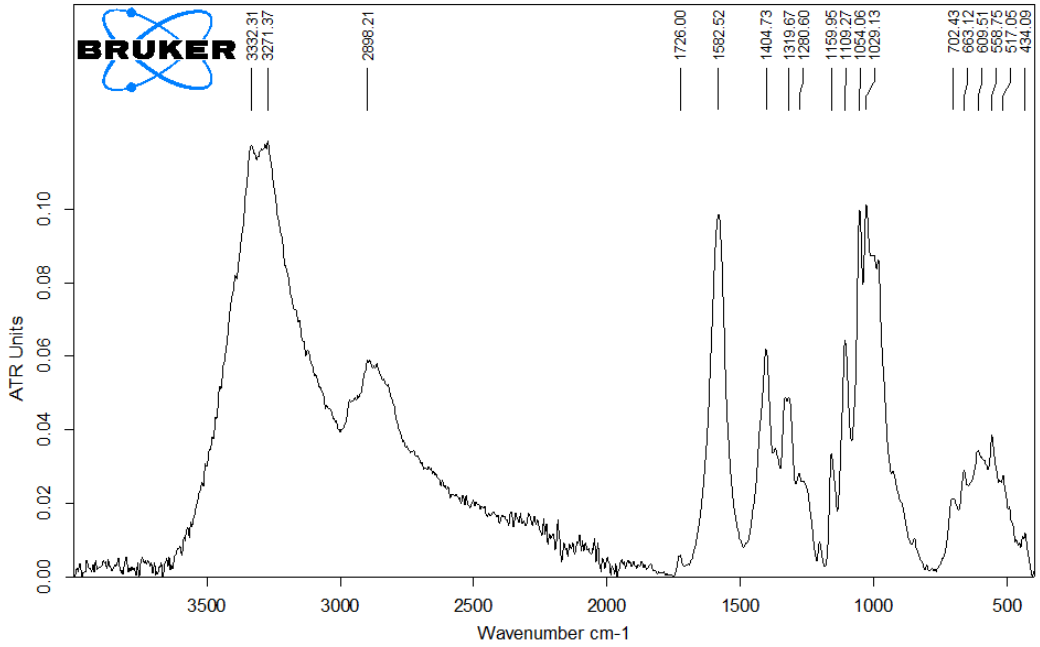

Figure 6.13. ATR-FTIR spectrum of a PDiPAEMA-grafted cotton swatch (PGC-1).

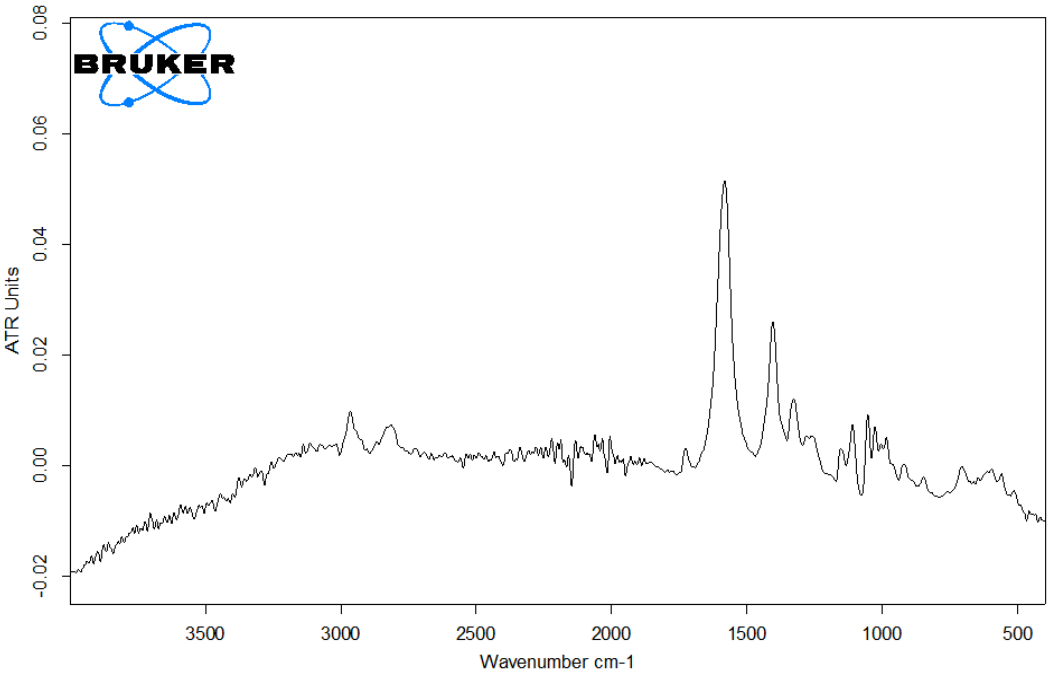

Figure 6.14. The resultant IR spectrum when the IR spectrum of native, washed cotton is subtracted from the IR spectrum of PGC-1.

6.5.6 X-ray photoelectron spectroscopy of CO_2-responsive polymer-grafted cotton fabric

XPS measurements were conducted and interpreted by Dr. Gabriele Schatte of Queen's University, Kingston, Ontario, Canada. The XPS spectra were measured on a Microlab 310-F spectrometer equipped with an XR-4 twin anode (Al/Mg). The manufacturer of this system is VG Scientific. The samples were mounted on a stub-type stainless steel holder using double-sided adhesive Cu tape. The samples were kept under high vacuum (10^{-8} mbar) overnight inside the preparation chamber before they were transferred into the analysis chamber (10^{-9} mbar) of the spectrometer. The XPS data were collected using MgK_{α} radiation at 1253.6 eV (280 W, 14 kV) and a spherical sector analyser (SSA) operating in CAE (constant analyser energy) mode. Binding energies are referenced to the C1s peak at 285 eV. Survey spectra were recorded from -5 to 1000 eV at a pass energy of 40 eV (number of scans: 5) using an energy step size of 2 eV. High-resolution spectra were measured for C1s, O1s, N1s and Br3d in the appropriate regions at a pass energy of 20 eV and an energy step size of 0.05 eV. The analysed area on the specimens is about 5×2 mm^2.

PGC-1 was found to contain 4.37 At% nitrogen. Additionally, PGC-1 showed a small contamination with silicon (2.87 At%). While cross contamination of samples within the vacuum is possible, the silicon on PGC-1 is most likely from the silicon grease that was used to help create an inert atmosphere within the reaction vessel in which PGC-1 was synthesised.

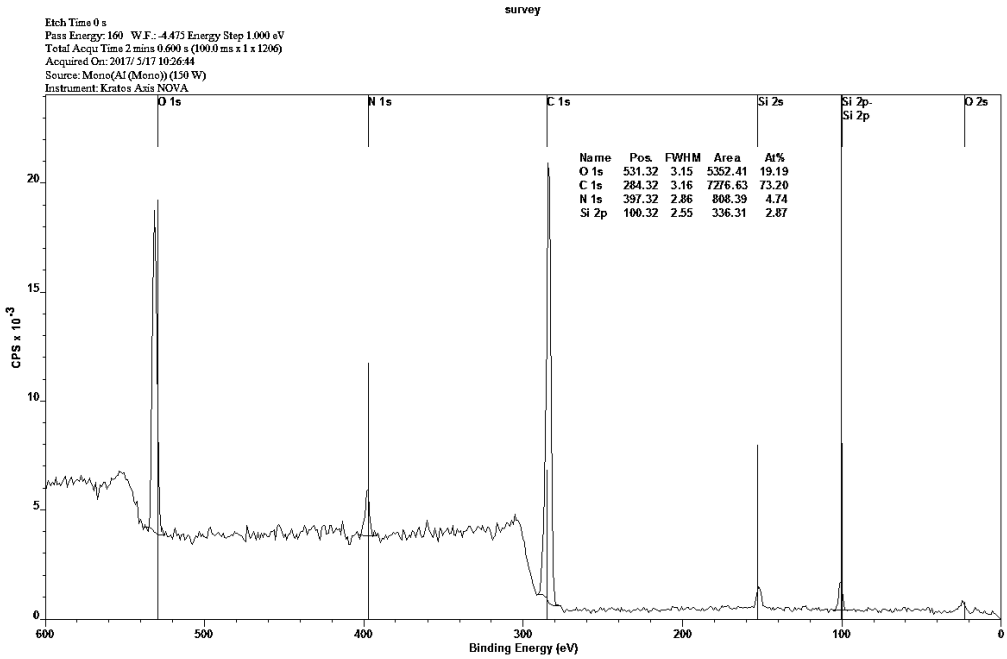

Figure 6.15. Survey spectrum of PGC-1.

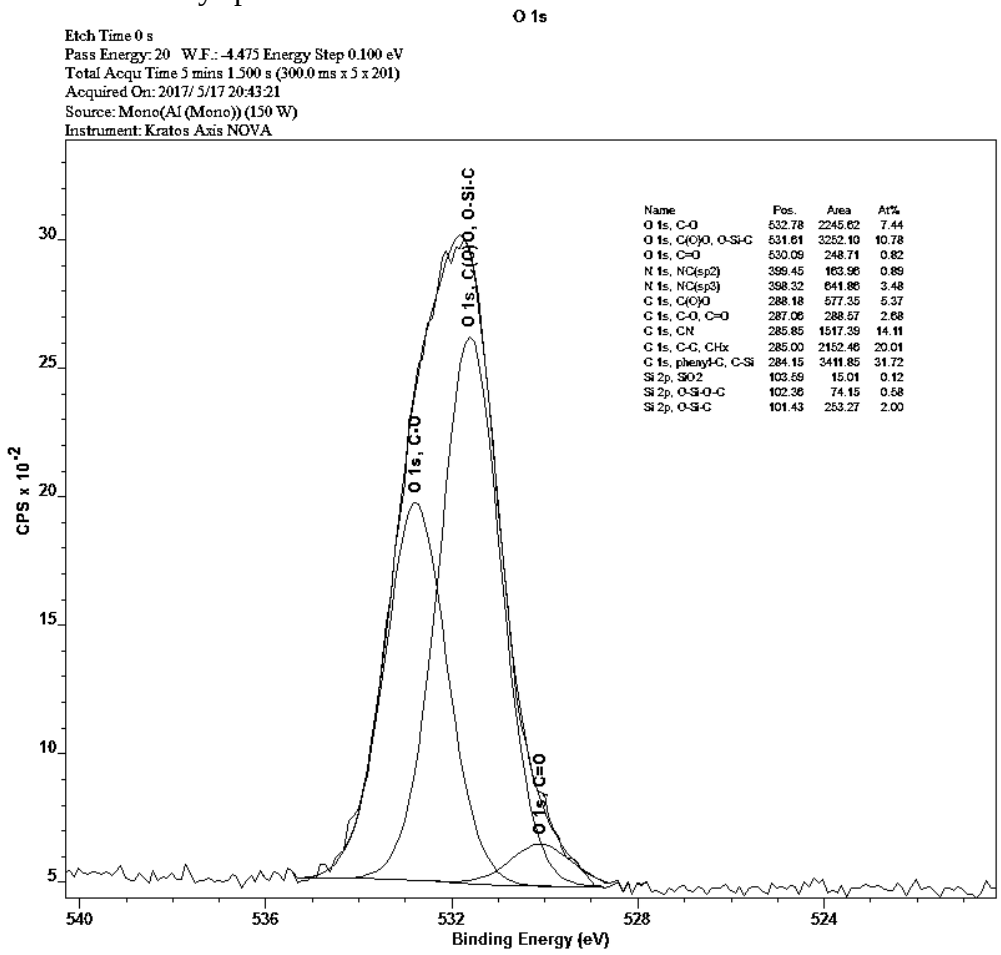

Figure 6.16. High-resolution O1s core-level spectrum of PGC-1.

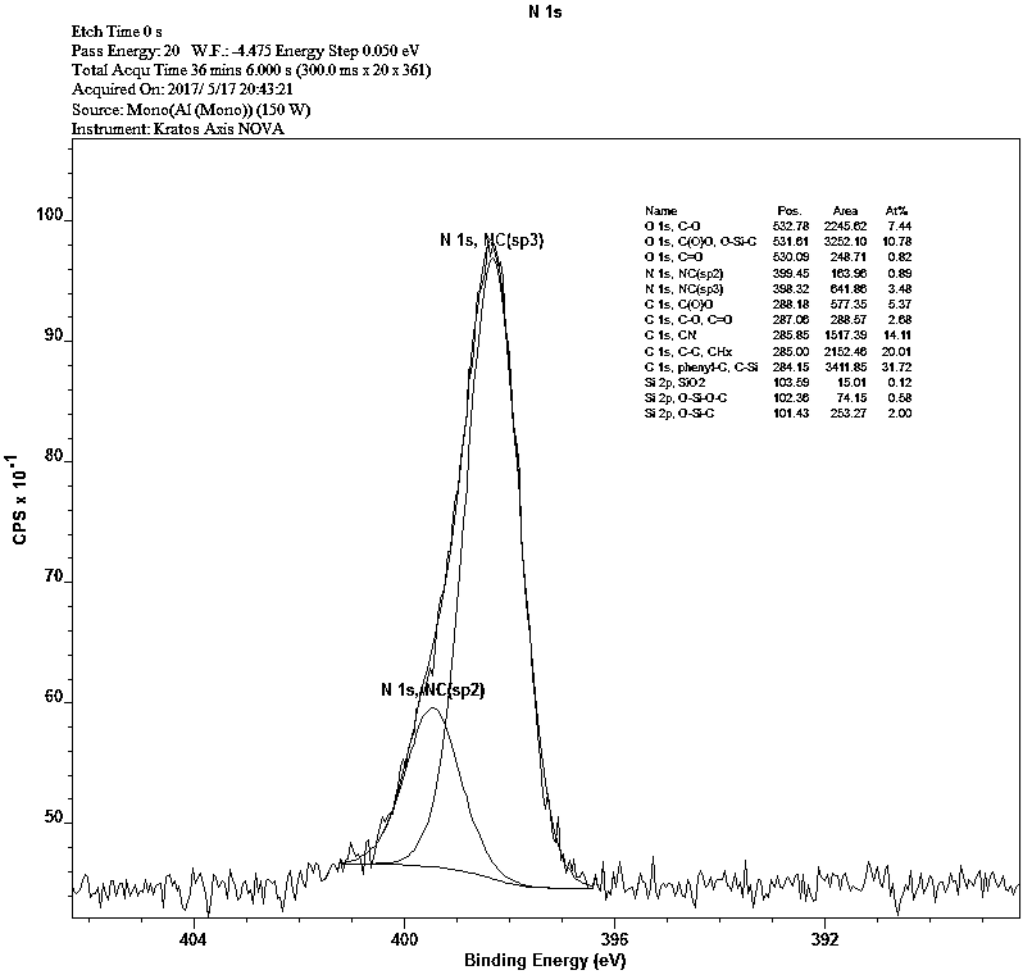

Figure 6.17. High-resolution N1s core-level spectrum of PGC-1.

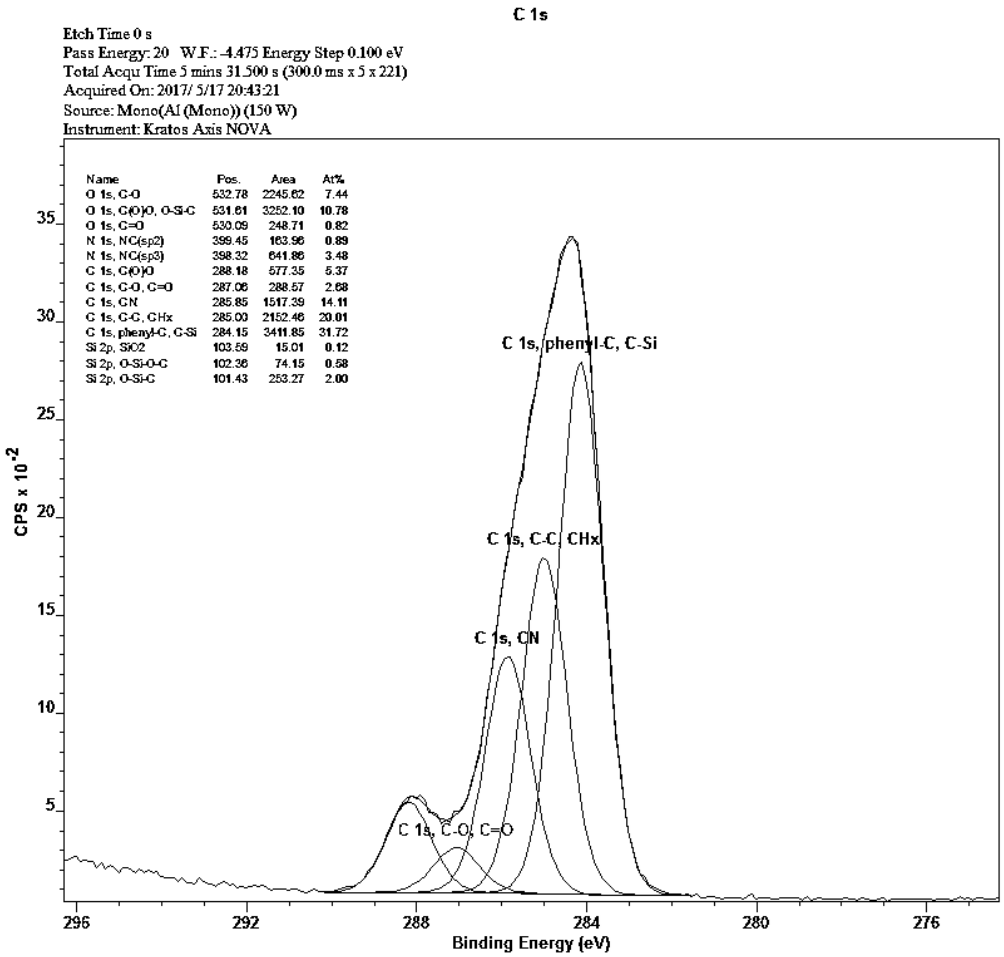

Figure 6.18. High-resolution C1s core-level spectrum of PGC-1.

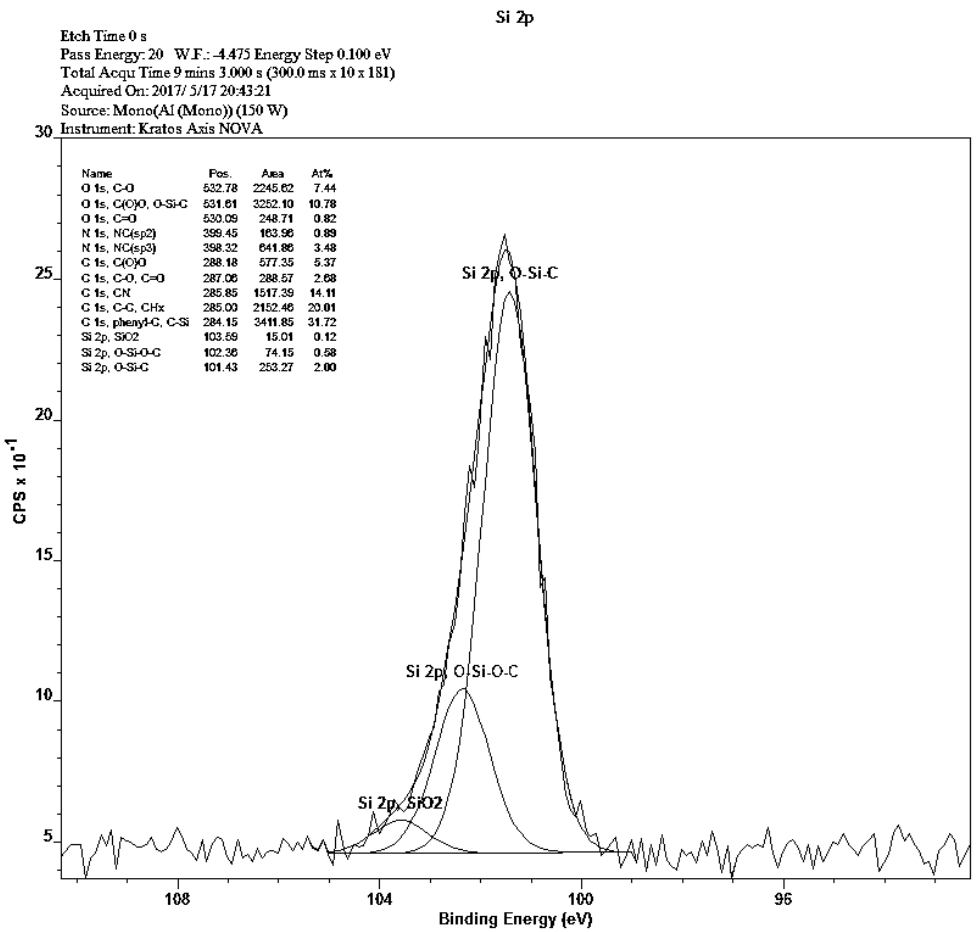

Figure 6.19. High-resolution Si2p core-level spectrum of PGC-1.

6.5.7 Gel permeation chromatography

Gel Permeation Chromatography (GPC) analysis was performed with a Waters 2690 Separation Module and Waters 410 Differential Refractometer with THF as the eluent. The column bank consisted of Waters Styragel HR (4.6x300 mm) 4, 3, 1, and 0.5 separation columns operating at 40 °C and 0.3 mL min^{-1}. GPC data are reported as poly(methylmethacrylate) (PMMA) equivalents, based on a calibration curve of narrow molecular weight distribution PMMA standards purchased from Polymer Standards.

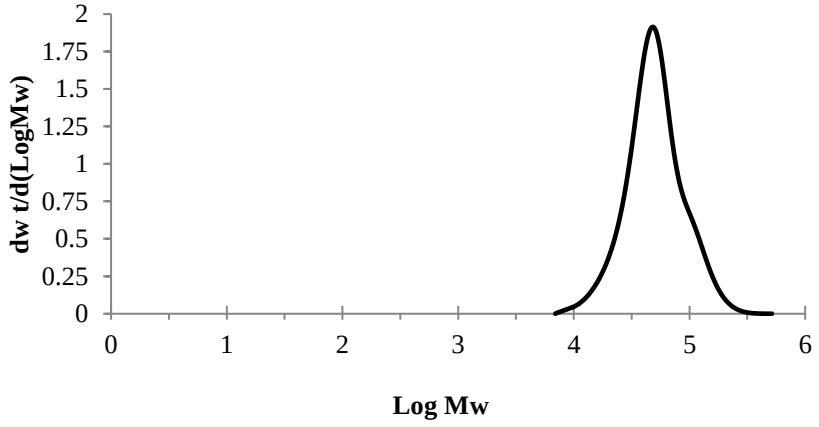

Figure 6.20. GPC trace of PDiPAEMA free polymer (PGFP-5, M_n: 42.5 kDa, Đ: 1.38).

6.6 References

1. D. Roy, M. Semsarilar, J. T. Guthrie and S. Perrier, *Chem. Soc. Rev.*, 2009, **38**, 2046–2064.

2. J. Lindqvist and E. Malmström, *J. Appl. Polym. Sci.*, 2006, **100**, 4155–4162.

3. D. Nyström, J. Lindqvist, E. Östmark, A. Hult and E. Malmström, *Chem. Commun.*, 2006, **0**, 3594–3596.

4. J. Lindqvist, D. Nyström, E. Östmark, P. Antoni, A. Carlmark, M. Johansson, A. Hult and E. Malmström, *Biomacromolecules*, 2008, **9**, 2139–2145.

5. D. Nyström, J. Lindqvist, E. Östmark, P. Antoni, A. Carlmark, A. Hult and E. Malmström, *ACS Appl. Mater. Interfaces*, 2009, **1**, 816–823.

6. O. García-Valdez, R. Champagne-Hartley, E. Saldívar-Guerra, P. Champagne and M. F. Cunningham, *Polym. Chem.*, 2015, **6**, 2827–2836.

7. V. Kapishon, R. A. Whitney, P. Champagne, M. F. Cunningham and R. J. Neufeld, *Biomacromolecules*, 2015, **16**, 2040–2048.

8. H.-D. Wang, R. D. Roeder, R. A. Whitney, P. Champagne and M. F. Cunningham, *J. Polym. Sci. Part Polym. Chem.*, 2015, **53**, 2800–2808.

9. A. Darabi, O. García-Valdez, P. Champagne and M. F. Cunningham, *Macromol. React. Eng.*, 2016, **10**, 82–89.

10. R. D. Roeder, O. Garcia-Valdez, R. A. Whitney, P. Champagne and M. F. Cunningham, *Polym. Chem.*, 2016, **7**, 6383–6390.

11. J. Arredondo, P. G. Jessop, P. Champagne, J. Bouchard and M. F. Cunningham, *Green Chem.*, 2017, **19**, 4141–4152.

12. O. Garcia-Valdez, T. Brescacin, J. Arredondo, J. Bouchard, P. G. Jessop, P. Champagne and M. F. Cunningham, *Polym. Chem.*, 2017, **8**, 4124–4131.

13. O. Garcia-Valdez, P. Champagne and M. F. Cunningham, *Prog. Polym. Sci.*, in press, DOI:10.1016/j.progpolymsci.2017.08.001.

14. M. Morits, J. R. McKee, J. Majoinen, J.-M. Malho, N. Houbenov, J. Seitsonen, J. Laine, A. H. Gröschel and O. Ikkala, *ACS Sustainable Chem. Eng.*, 2017, **5**, 7642–7650.

15. J. Glasing, J. Bouchard, P. G. Jessop, P. Champagne and M. F. Cunningham, *Polym. Chem.*, in press, DOI:10.1039/C7PY01258F.

16. V. E. H. Immergut and H. Mark, *Makromol. Chem.*, 1956, **18**, 322–341.

17. H.-D. Wang, P. G. Jessop, J. Bouchard, P. Champagne and M. F. Cunningham, *Cellulose*, 2015, **22**, 3105–3116.

18. S. Beck, J. Bouchard and R. Berry, *Biomacromolecules*, 2012, **13**, 1486–1494.

19. Z. Wang, Y. Wang and G. Liu, *Angew. Chem. Int. Ed.*, 2016, **55**, 1291–1294.

19. P.J. Wakelyn, in Handbook of Fiber Chemistry, ed. M.Lewin and E. M. Pearce, Marcel Dekker, New York, 1988, pp. 642-654.

20. A. Hebeish and J. T. Guthrie, The Chemistry and Technology of Cellulosic Copolymers, Springer-Verlag, Berlin, 1981.

22. B. R. Kim, H.-G. Lee, S.-B. Kang, G. H. Sung, J.-J. Kim, J. K. Park, S.-G. Lee and Y.-J. Yoon, *Synthesis*, 2012, **44**, 42–50.

22. Chemicalize, https://chemicalize.com/ (Accessed June 2017).

24. E. Bianchi, A. Bonazza, E. Marsano and S. Russo, *Carbohydr. Polym.*, 2000, **41**, 47–53.

25. A. Carlmark and E. Malmström, *J. Am. Chem. Soc.*, 2002, **124**, 900–901.

Chapter 7

Conclusions and Recommendations

7.1 Conclusions

A variety of CO_2-responsive smart surfaces have been developed for green applications. CO_2-switchable drying agents, as described in chapters 2 and 4, have been created for the first time and were evaluated in the drying of wet organic solvents such as isobutanol. CO_2-responsive polymer-grafted silica particles were superior to other amine-containing drying agents in drying ability and hydrolytic stability at low pH. Additionally, the 2nd generation of CO_2-responsive polymer-grafted silica particles considerably outperformed all previous drying agents including traditional drying agents such as inorganic oxides and molecular sieves.

Chapter 3 demonstrated that CO_2-responsive particles are relevant to more than just removing water from organic solvents. CO_2-responsive particles, when used as a functional support for ruthenium nanoparticles, can influence the selectivity of the hydrogenation of furfuralacetone in the presence of CO_2.

Chapter 4 presented the development of a robust and substrate friendly method that has considerably improved the synthesis, characterisation, and substrate scope for CO_2-responsive materials. A SI-AGET-ATRP methodology was developed for the production of CO_2-responsive materials. This method can produce high molecular weight PDiPAEMA, with low dispersity, as a homopolymer (M_n>100 kDa, Đ: 1.17) or from a surface (FP, M_n>40 kDa, Đ: 1.17). The control provided by this method adds confidence to the overall characterisation of CO_2-responsive materials.

Various single-unit functionalisation techniques were evaluated for the synthesis of CO_2-responsive surfaces on inorganic and organic substrates. Chapter 5 demonstrated that a silyl ester carbonate/carbamate surface linkage is not sufficiently stable to achieve reproducible CO_2-responsive behaviour over multiple cycles in a CO_2-responsive system. Additionally, coordination of a single-unit CO_2-responsive functionality to a carbonyl moiety increases the likelihood of the single-unit CO_2-responsive functionality being hydrolysed from the surface. Therefore, the alkylene chain between the carbonyl and the CO_2-responsive unit should be at least three methylene units long (i.e. propylene linker). Additionally, steric bulk around the CO_2-responsive functionality (i.e. isopropyl>ethyl>methyl) should be present to minimise the risk of hydrolysis and other unwanted coordination events that would ultimately decrease the number of available amines on the CO_2-responsive surface.

In Chapter 6, similar single-unit functionalisation techniques were applied to the creation of CO_2-responsive surfaces on organic surfaces such as cellulose, starch, and cotton. Single-unit functionalisation techniques failed to noticeably modify the hydrophilicity of the native substrate when CO_2 was either added or removed. Thus, single-unit functionalisation of these materials with CO_2-responsive functionalities failed to show any promise in applications that would be of current use. However, single-unit functionalisation techniques could be improved by achieving homogeneous reaction conditions and by using higher surface area substrates such as CNC or cellulose fibres with low degrees of polymerisation. The ester carbamate/carbonate linkage between a polysaccharide surface and the CO_2-responsive functionality was stable to a variety of conditions such as those pertaining to CO_2-switching, additional heat treatments (>100 ℃),

and exposure to $NaOH_{(aq)}$. Despite the surface linker having increased stability, the conclusions regarding alkylene linker length and steric bulk surrounding the CO_2-responsive amine-moiety apply to all CO_2-responsive surfaces containing a carbonyl moiety and a CO_2-responsive amine-moiety.

Various polymeric functionalisation techniques were evaluated for the synthesis of CO_2-responsive surfaces on inorganic and organic substrates. Chapter 5 demonstrated that polymeric functionalisation of a silicon surface produced CO_2-responsive surfaces that are stable in the CO_2-responsive system for numerous cycles (>10). The surface behaviour of a CO_2-responsive surface was determined to be dominated by the chemical nature of the CO_2-responsive functionality and not by the surface structure of the silicon substrate. Microscale roughness as achieved by laser patterning did not change the surface character of the polymer-grafted CO_2-responsive surfaces. Nanoscale roughness as achieved by HF etching did not change the surface character of the polymer-grafted CO_2-responsive surfaces. In Chapter 6, polymeric functionalisation techniques provided, for the first time, a CO_2-responsive very-hydrophobic/superhydrophilic polysaccharide surface. The natural roughness of a cotton fabric was able to increase the change in surface character that CO_2-responsive functionalities, when *grafted from* a surface, can achieve. The neutral and hydrophobic state of PDiPAEMA when *grafted from* a cotton fabric surface was determined to be ca. 150°, where previously the neutral and hydrophobic state of PDiPAEMA when *grafted from* a smooth silicon substrate was ca. 90°. The charged and hydrophilic state of PDiPAEMA, when grafted from a cotton fabric surface, was determined to be superhydrophilic and absorbent, where previously the charged and hydrophilic state of PDiPAEMA when *grafted from* a smooth silicon substrate was ca. 60°.

Thus, where the laser etching techniques presented in Chapter 5 failed, nature has provided a readily available and easily modifiable rough surface. Additionally, for the first time, a CO_2-responsive cotton fabric has been used to capture and release various dyes and oils selectively. Proof of concept that a CO_2-responsive membrane can selectively capture and release oil from water without suffering a loss in performance was demonstrated.

The newly developed SI-AGET-ATRP method allows for the controlled polymerisation of CO_2-responsive polymers from a variety of substrates. The increased performance of the 2nd generation CO_2-responsive polymer surfaces in industrially applicable scenarios validates the use of the SI-AGET-ATRP method as well as the use of CO_2-responsive technology to address challenges in the chemical industries.

7.2 Future work

Important questions regarding the development and performance of CO_2-responsive materials remain. Polymer loading, polymer molecular weight, and polymer grafting density are three critical variables that directly affect the performance of CO_2-responsive materials. The SI-AGET-ATRP methodology, while not perfect, is well suited to investigate these variables. Using a proven and well-studied polymer (PDiPAEMA), future research can systematically vary the molecular weight of the grafted polymer and monitor the performance of the CO_2-responsive material. For studies involving polymer-grafted silica particles, the proven and well-studied drying agent platform is a suitable standard test to monitor the changes in material performance as a function of molecular weight. For studies involving polymer-grafted surfaces, whether

smooth or rough, contact angle analysis is a suitable platform for monitoring changes in surface energy.

Additionally, the study of grafting density and its effect on material performance is quickly moving to the forefront of stimuli-responsive surface research. It is common knowledge that low grafting densities allow for a variety of polymer conformations to occur. Moreover, low grafting densities permit grafted polymers to transition from one conformation to another as a result of an external stimulus. What is not common knowledge is whether it is the transitions between conformations that allow for reversible changes in surface energy or it is a single conformation that best responds to an external stimulus. As demonstrated in Chapter 5, smooth silicon surfaces are best suited for identifying the role of grafting density and surface energy as a function of an external stimulus, such as CO_2. Techniques such as contact angle analysis, X-ray photoelectron spectroscopy and variable angle ellipsometry will allow researchers to determine surface energy, grafting density, and film thickness. Additionally, surface energy and film thickness should be monitored as a function of exposure to a stimulus, e.g. CO_2, to determine at which grafting density does the stimulus have the most significant effect. Furthermore, these techniques will also allow researchers to monitor the conformational changes of the grafted polymers as a function of temperature. Since one of the means for the removal of CO_2 is hypothesised to be facilitated by temperature-dependent conformational changes in the graft polymer layer, monitoring film thickness as a function of temperature, for known grafting density and molecular weight, will provide valuable insight into the mechanism of CO_2-responsive behaviour.

An additional variable that warrants further investigation is the effect of stirring on the grafted polymer layer. Recent research suggested that stirring a SI-ATRP results in a higher rate of termination between grafted polymer chains.[1,2] The study proposes that the increased termination is due to an increased mobility of grafted-chains as a result of stirring the reaction solution. The authors suggest that linear substrates (i.e. silicon wafer, cotton swatch) should be deposited at an angle, acute from normal, and left in solution undisturbed. Additionally, when grafting from a particulate surface, the authors found that polymer brush growth is affected by the curvature of the particle; when the particle had a diameter of less than 450 nm, the growth of the polymer brush was significantly increased. The authors suggest that above a diameter of 450 nm the grafted chains are in an environment similar to that of a smooth surface and that polymer brush growth is effectively independent of surface curvature. In summary; the authors concluded that "These findings will be of broad interest to anyone conducting surface-initiated polymerisation because they demonstrate that polymerisations conducted under the same reaction conditions with the same reaction time do not produce equivalent brushes; rather, they are dependent on the substrate geometry."[2] Importantly, stir rate must remain high enough, when grafting from particulate surfaces, to keep the particulate substrates well dispersed in solution.

Furthermore, moving towards smaller particle sizes would have multiple advantages for applications requiring a high polymer to substrate ratio. Investigations centred around the synthesis of sub 450 nm silica particles and their subsequent functionalisation with CO_2-responsive polymers could prove very fruitful. Unfortunately, the benefits of using sub 450 nm silica particles are not applicable to applications such as

chromatography or SPE, since the backpressure that would be associated with their use would be too high for current technology (ca. 1030 bar). Currently, spherical silica particles of ca. 2 μm diameter are the smallest particle size that is commercially available for use in ultra performance liquid chromatography (UPLC). It is recommended that CO_2-responsive polymer-grafted silica particles, having a diameter of ca. 2 μm, be evaluated for CO_2-responsive UPLC applications in the near future.

The work presented in this thesis has focused on the "neutral to cationic" subset of CO_2-switchable materials. Additionally, within that subset, this work has focused solely on tertiary amines. In Chapter 3, proof of concept that a CO_2-responsive polymer-grafted support could influence the activity of a deposited heterogeneous catalyst was presented. One limitation of the subset studied here is that water must be present; it is common knowledge that water is often incompatible with traditional catalysts. The "neutral to cationic" subset consisting of primary amines and non-bulky secondary amines, thus forming carbamic acid and carbamate salts with CO_2, does not require water to be responsive. Therefore, the work demonstrated in Chapter 3, which requires minute amounts of water to elicit a response to CO_2, could be extended to water sensitive catalysis if primary or non-bulky secondary amines were used instead of tertiary amines.

Additionally, the work presented in this thesis has focused on CO_2-responsive behaviour at room temperature. If the operational temperature range of a CO_2-responsive material needed to be tailored, e.g. to modify the selectivity of a heterogeneous catalyst as a function of CO_2 at slightly elevated temperatures, a stronger bond to CO_2 would be required. Increasing the basicity of the CO_2-responsive amine or using CO_2-responsive

amines that are selective to carbamate salt formation, are two ways in which a CO_2-responsive material could remain cationic at slightly elevated temperatures.

Lastly, the work presented in this thesis and the literature has identified surface roughness to essential factor for the creation of superhydrophobic, superhydrophilic, and superamphiphobic materials.[3] Future research should continue to examine various organic and inorganic substrates with unique roughness in the pursuit of creating robust CO_2-responsive superamphiphobic surfaces.

7.3 References

1. D. Xiao and M. J. Wirth, *Macromolecules*, 2002, **35**, 2919–2925.
2. B. T. Cheesman, A. J. G. Neilson, J. D. Willott, G. B. Webber, S. Edmondson and E. J. Wanless, *Langmuir*, 2013, **29**, 6131–6140.
3. Z. Chu and S. Seeger, *Chem. Soc. Rev*., 2014, **43**, 2784–2798.

Appendix I

Synthesis and characterization of initiator-grafted silica particles

Elemental analysis of initiator-grafted silica particles

A series of experiments were undertaken, in which various initiators and conditions were screened, to identify the grafting density of the initiator functionality on the silica particle. Initial grafting experiments utilised the most abundant silica source available at the time, which was SiliaFlash P60. SiliaFlash P60, ordered in bulk, is commonly used throughout the Chemistry Department for flash chromatography. SiliaFlash P60 (SiO_2 #5, see Appendix VII for more details) is an irregular silica particle, varying in size from 40-63 μm (100 Å pore size).

Table A.1. Elemental analysis of Nitrogen (N), Carbon (C), and Hydrogen (H) for initiator-functionalised silica particles as achieved by various grafting methods.

Method	N (%)	C (%)	H (%)	Carbon content $mmol \cdot g^{-1}$	Initiator content $mmol \cdot g^{-1}$
Control SiO_2	0.082	0.028	0.913	0.023	-
5-MAC	0.083	0.757	0.735	0.630	0.158
6-MAC	0.031	0.271	0.413	0.226	-
7-MAC	0.028	0.513	0.415	0.427	-
3-BIBB	0.050	0.736	0.483	0.613	0.153
4-BIBB	0.086	0.250	0.385	0.208	-
8-BIBB	0.065	0.272	0.459	0.226	-

Experimental error was ±0.4%, which equates to ±0.333 $mmol \cdot g^{-1}$ for carbon, ±0.285 $mmol \cdot g^{-1}$ for nitrogen, and ±3.97 $mmol \cdot g^{-1}$ for hydrogen.
BIBB on SiO_2 is C_4H_6OBr.
MAC on SiO_2 is C_4H_5O.

Examination of the EA data in Table A.1 shows that "method 3-BIBB" and "method 5-MAC" have the highest overall carbon content with ca. 0.7 $mmol \cdot g^{-1}$ of carbon each. These two methods involve different initiators, but the same auxiliary base (DIPEA) and solvent (DCM) was used in both reactions. Additional reagents, such as 4-(dimethylamino)pyridine (DMAP), were not used in either reaction. Further examination of the EA data presents multiple problems; firstly, the experimental error is greater than the majority of the recorded data. Secondly, the hydrogen content reported for the control sample is greater than the experimental error. The control sample should not contain hydrogen. Thus, the control sample or the EA instrument must have been contaminated. The conclusion is thus that EA is not a suitable instrument for the determination of initiator loading on silica particles using the aforementioned synthetic methods.

CP-MAS-NMR spectroscopy of initiator-grafted silica particles

Cross polarization-magic angle spinning (CP-MAS) NMR spectroscopy was used to examine the possibility of residual nitrogen, hydrogen, and carbon being bound to the silica particles post-functionalisation (Figures AI.1, AI.2, and AI.3) by means other than the initiator. Silica particles were stirred in a flask containing an auxiliary base, DIPEA or TEA, and DCM.

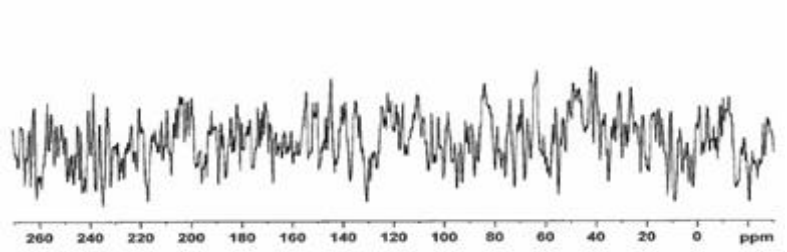

Figure A1.1. ^{13}C CP-MAS NMR spectrum of clean SiO_2 #5.

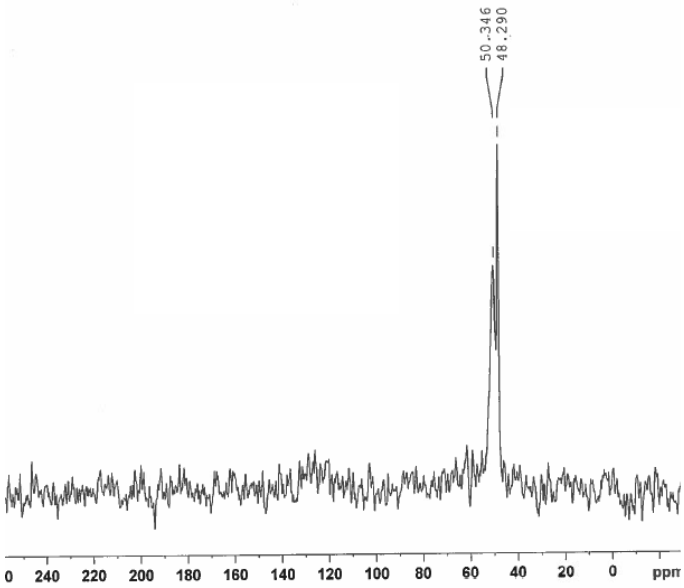

Figure A1.2. ^{13}C CP-MAS NMR spectrum of SiO_2 #5 treated with TEA.

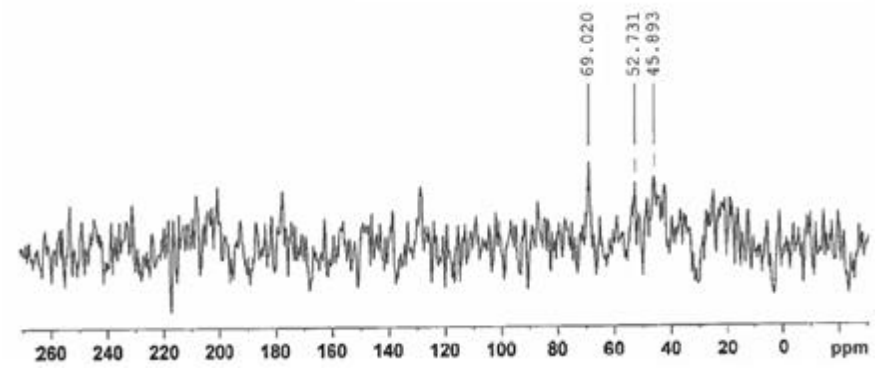

Figure A1.3. ^{13}C CP-MAS NMR spectrum of SiO_2 #5 treated with DIPEA.

As seen from a comparison of the ^{13}C peaks in Figures AI.1, AI.2, and AI.3, the silica particles were contaminated as a result of exposure to an auxiliary base and DCM. The resultant contamination of the silica particles with an auxiliary base was considerably

lower when DIPEA was used instead of TEA. The reduced degree of contamination seen when DIPEA was used is likely due to the compound's increased steric bulk which reduces its ability to participate in an acid-base reaction with the slightly acidic silica particle. Therefore, all subsequent reactions that call for the use of an auxiliary base in the presence of silica particles utilise DIPEA.

Initiator grafting method 1:

Clean and hydroxyl-rich silica particles (5 g) were added to a 100 mL round bottom flask containing solution of potassium carbonate (4.6 mmol) in 50 mL of acetone. To that mixture, the initiator, 2-bromo-2-methylpropionyl bromide (BIBB, 18 mmol), was added dropwise via an addition funnel at room temperature (ca. 27 ℃). The contents of the round bottom flask were heated at a continuous reflux for 12 h. The silica particles were recovered by vacuum filtration and washed thoroughly with methanol, followed by multiple washings with distilled water. The washed particles were dried at 110 ℃ for 20 min, then stored under Ar until further use.

Initiator grafting method 2:

Clean and hydroxyl-rich silica particles (5 g) were added to a 100 mL round bottom flask containing solution of triethylamine (80.9 mmol) in 50 mL of tetrahydrofuran. The mixture was continuously stirred via a magnetic stir bar while being cooled to 0 ℃. After 1 h, a solution of the initiator, 2-bromo-2-methylpropionyl bromide (BIBB, 18 mmol) in 10 mL tetrahydrofuran, was added dropwise via addition funnel to the cooled mixture. The mixture was stirred for 20 min, the ice bath removed, and the mixture was allowed to warm

to room temperature (ca. 27 ℃). The reaction was stirred vigorously (via magnetic stir bar) overnight for approximately 16 h. The silica particles were recovered by vacuum filtration and washed thoroughly with methanol, followed by multiple washings with distilled water. The washed particles were dried at 110 ℃ for 20 min, then stored under Ar until further use.

Initiator grafting method 3:

Clean and hydroxyl-rich silica particles (2 g) were added to a 250 mL round bottom flask and flame dried under vacuum. Reactants were added using Schlenk techniques for inert conditions; diisopropylethylamine (1 eq., 4.09 mmol) and 150 mL of anhydrous dichloromethane were added to the round bottom flask. The round bottom flask was cooled in an ice bath for approximately 30 min, after which the initiator, 2-bromo-2-methylpropionyl bromide (BIBB, 1 eq., 4.04 mmol), was added dropwise via syringe. The mixture was stirred for 20 min, the ice bath removed, and the mixture was allowed to warm to room temperature (ca. 27 ℃). The reaction was stirred vigorously (via magnetic stir bar) overnight for approximately 16 h. The silica particles were recovered by vacuum filtration and washed thoroughly with methanol, followed by multiple washings with distilled water. The washed particles were dried at 110 ℃ for 20 min, then stored under Ar until further use.

Initiator grafting method 4:

Clean and hydroxyl-rich silica particles (2 g) were added to a 250 mL round bottom flask and flame dried under vacuum. Reactants were added using Schlenk techniques for inert conditions; 4-dimethylaminopyridine (DMAP, 0.015 eq., 0.06 mmol), diisopropylethylamine (DIPEA, 1 eq., 4.09 mmol), and 150 mL of anhydrous dichloromethane were added to the round bottom flask. The round bottom flask was cooled in an ice bath for approximately 30 min, after which the initiator, 2-bromo-2-methylpropionyl bromide (BIBB, 1 eq., 4.04 mmol), was added dropwise via syringe. The mixture was stirred for 20 min, the ice bath removed, and the mixture was allowed to warm to room temperature (ca. 27 ℃). The reaction was stirred vigorously (via magnetic stir bar) overnight for approximately 16 h. The silica particles were recovered by vacuum filtration and washed thoroughly with methanol, followed by multiple washings with distilled water. The washed particles were dried at 110 ℃ for 20 min, then stored under Ar until further use.

Initiator grafting method 5:

Clean and hydroxyl-rich silica particles (2 g) were added to a 250 mL round bottom flask and flame dried under vacuum. Reactants were added using Schlenk techniques for inert conditions; diisopropylethylamine (1 eq., 4.0 mmol) and 150 mL of anhydrous dichloromethane were added to the round bottom flask. The round bottom flask was cooled in an ice bath for approximately 30 min, after which the initiator, methacryloyl chloride (MAC, 1 eq., 4.0 mmol), was added dropwise via syringe. The mixture was stirred for 20

min, the ice bath removed, and the mixture was allowed to warm to room temperature (ca. 27 ℃). The reaction was stirred vigorously (via magnetic stir bar) overnight for approximately 16 h. The silica particles were recovered by vacuum filtration and washed thoroughly with methanol, followed by multiple washings with distilled water. The washed particles were dried at 110 ℃ for 20 min, then stored under Ar until further use.

Initiator grafting method 6:

Clean and hydroxyl-rich silica particles (2 g) were added to a 250 mL round bottom flask and flame dried under vacuum. Reactants were added using Schlenk techniques for inert conditions; 4-dimethylaminopyridine (DMAP, 0.015 eq., 0.06 mmol), diisopropylethylamine (1 eq., 4.09 mmol), and 150 mL of anhydrous dichloromethane were added to the round bottom flask. The round bottom flask was cooled in an ice bath for approximately 30 min, after which the initiator, methacryloyl chloride (MAC, 1 eq., 4.0 mmol), was added dropwise via syringe. The mixture was stirred for 20 min, the ice bath removed, and the mixture was allowed to warm to room temperature (ca. 27 ℃). The reaction was stirred vigorously (via magnetic stir bar) overnight for approximately 16 h. The silica particles were recovered by vacuum filtration and washed thoroughly with methanol, followed by multiple washings with distilled water. The washed particles were dried at 110 ℃ for 20 min, then stored under Ar until further use.

Initiator grafting method 7:

Clean and hydroxyl-rich silica particles (2 g) were added to a 250 mL round bottom flask and flame dried under vacuum. Reactants were added using Schlenk techniques for inert conditions; diisopropylethylamine (DIPEA, 1 eq., 4.0 mmol) and 200 mL of anhydrous tetrahydrofuran were added to the round bottom flask. The round bottom flask was cooled in an ice bath for approximately 30 min, after which the initiator, methacryloyl chloride (MAC, 1 eq., 4.0 mmol), was added dropwise via syringe. The mixture was stirred for 20 min before the ice bath was removed and the mixture was allowed to warm to room temperature (ca. 27 ℃). The reaction was then heated to a continuous reflux (ca. 90 ℃) and stirred vigorously (via magnetic stir bar) overnight for approximately 16 h. The silica particles were recovered by vacuum filtration and washed thoroughly with methanol, followed by multiple washings with distilled water. The washed particles were dried at 110 ℃ for 20 min, then stored under Ar until further use.

Initiator grafting method 8:

Clean and hydroxyl-rich silica particles (2 g) were added to a 250 mL round bottom flask and flame dried under vacuum. Reactants were added using Schlenk techniques for inert conditions; diisopropylethylamine (DIPEA, 1 eq., 4.0 mmol) and 200 mL of anhydrous tetrahydrofuran were added to the round bottom flask. The round bottom flask was cooled in an ice bath for approximately 30 min, after which the initiator, 2-bromo-2-methylpropionyl bromide (BIBB, 1 eq., 4.04 mmol), was added dropwise via syringe. The mixture was stirred for 20 min, the ice bath removed, and the mixture was

allowed to warm to room temperature (ca. 27 ℃). The reaction was then heated to a continuous reflux (ca. 90 ℃) and stirred vigorously (via magnetic stir bar) overnight for approximately 16 h. The silica particles were recovered by vacuum filtration and washed thoroughly with methanol, followed by multiple washings with distilled water. The washed particles were dried at 110 ℃ for 20 min, then stored under Ar until further use

Appendix II

Titration procedure and sample calculations concerning polymer-grafted silica particles containing amine functionalities.

Titrations of amine-functionalized particles

Extra caution was used to prepare precise pH solutions. All containers/vessels were plastic; they were purchased brand new and rinsed thoroughly with Millipore water (18.2 MΩ·cm). The vessels were filled with Millipore water and the pH was measured. If the pH of the solution was <6, the vessel was rinsed once more and a new pH reading was taken. This process was repeated until the pH was >6. A pH of 7.5 ±0.3 was achieved on most occasions. In some instances, it was hard to remove dissolved $CO_{2(g)}$; as a result of the dissolved $CO_{2(g)}$, the pH of the water was >6 but <7. Stock solutions of NaOH (9.006 mM) and HCl (10.5 mM) were prepared. In some instances, the stock solutions were diluted to either 5.25 mM (HCl) or 0.9006 mM (NaOH) to achieve better accuracy. In a typical experiment, ca. 10 mg of drying agent was added to 20 mL of Millipore (18.2 MΩ·cm) in a 50 mL centrifuge vial. 10.5 mM HCl was added in 0.1 mL aliquots to the centrifuge vial; between each addition, the vial was capped and vigorously shaken for 20-30 s. The pH was recorded after each addition and the titration was stopped ca. pH 4 or pH 2, depending on the nature of the titration. Acidified samples were then centrifuged for 30 min at 3000 RPM. 15 mL of the supernatant was removed and placed into a freshly washed centrifuge vial. The acidified supernatant was back-titrated with NaOH until neutral, ca. pH 7.

The pH of ultrapure Millipore water, which should be 7, when measured in a glass vial was >8 owing to the basic nature of the glass vial. Multiple purification systems were tested in both the Department of Chemistry and the Department of Chemical Engineering at Queen's University, and the effect of the glass vials on pH was consistent.

Sample calculation for the titration of accessible amines (i.e. protonatable sites) on a CO_2-responsive silica particle (PGS-1, sample D)

Moles of HCl added – Moles HCl left in supernatant = Moles of Accessible Amines

$$\frac{Moles\ of\ Accessible\ amines}{mg\ of\ sample\ used} * \frac{1000\ mmol}{1\ mol} * \frac{1000\ mg}{1\ g} = \frac{mmol}{g}$$

$pH_i = 9.02$
$pH_A = 4.07$
$pH_B = 7.04$
$V_{H_2O} = 20\ mL$
$m_{PGS-1} = 9.37\ mg$
$V_{HCl} = 1\ mL$
$C_{HCl} = 5.25\ mM$
$V_{NaOH} = 1.8\ mL$
$C_{NaOH} = 0.9006\ mM$
$V_{supernatant} = V_{HCl} + V_{H_2O}$
$V_{supernatant} = 21\ mL$
$V_{supernatant\ extract} = 15\ mL$

$n_{HCl} = 5.25\times10^{-6}$ mol
$n_{NaOH} = 1.62108\times10^{-6}$ mol
$C_{supernatant} = 1.62108\times10^{-6}$ mol / 0.015 L
$C_{supernatant} = 1.08072\times10^{-4}$ M
$n_{supernatant} = 1.08072\times10^{-4}$ M * 0.021 mL
$n_{supernatant} = 2.26951\times10^{-6}$ mol
$n_{accesible\ amines} = n_{HCl} - n_{supernatant}$
$n_{accesible\ amines} = 2.98049\times10^{-6}$ mol
$Accessible\ amines = \frac{n_{accessible\ amines}}{m_{PGS-1}}$
$Accessible\ amines = 2.98049\times10^{-3}$ mmol / 0.00937 g
$Accessible\ amines = 0.31808\ mmol/g$
$Accessible\ amines \cong 0.3\ mmol/g$

Sample calculation for Molar Hydration Value (MHV):

Sample ID: DMA-S.
Where: Accessible amines (aa); Drying agent (DA).
DMA-S_{aa}: 1.1 $mmol_{aa}/g_{DA}$, as determined by titration.
DMA-S removed 180 mgH_2O/g_{DA}, as determined by drying wet isobutanol test.

$$\frac{180\,\frac{mg_{H_2O}}{g_{DA}}}{18.02\,\frac{g_{H_2O}}{mol_{H_2O}}} = 10\,\frac{mg_{H_2O}}{g_{DA}} * \frac{mol_{H_2O}}{g_{H_2O}}$$

$$10\,\frac{mg_{H_2O}}{g_{DA}} * \frac{mol_{H_2O}}{g_{H_2O}} * \frac{1g}{1000mg} = 0.01\,\frac{mol_{H_2O}}{g_{DA}}$$

$$0.01\frac{mol_{H_2O}}{g_{DA}} * \frac{1000\ mmol}{1\ mol} = 10\,\frac{mmol_{H_2O}}{g_{DA}}$$

$$\frac{10\,\frac{mmol_{H_2O}}{g_{DA}}}{1.1\,\frac{mmol_{aa}}{g_{DA}}} = 9.09\,\frac{mmol_{H_2O}}{g_{DA}} * \frac{g_{DA}}{mmol_{aa}}$$

$$= 9.09\,\frac{mmol_{H_2O}}{mmol_{aa}}$$

Therefore the Molar Hydration Value for DMA-S is $9.09\,\frac{mmol_{H_2O}}{mmol_{aa}}$.

Polymer extension calculations

The following calculations are provided as a reference for the discussions regarding polymer length and pore size compatibility in Section 2.2.3. Herein, the maximum extension and ideal length of a PDiPAEMA homopolymer are calculated.

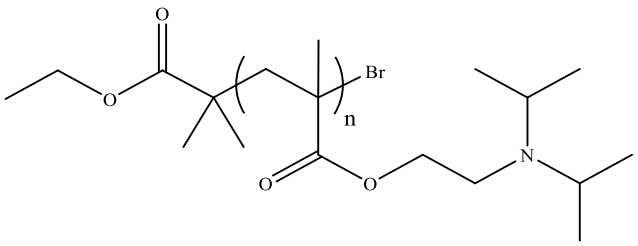

Figure AII.1. PDiPAEMA homopolymer of n repeat units, where the repeat unit is enclosed within the parenthesis.

Firstly, the repeat unit length must be determined. The repeat unit, as denoted with parenthesis in Figure AII.1, consists of one full C-C bond and two half C-C bonds. The repeat unit therefore consists of two full C-C bonds; since all three carbons are sp^3 hybridized, the individual bond lengths are 1.54 Å, thus, the repeat unit length is 3.08 Å. The bond angle for each sp^3 hybridized carbon is 109.5°.

The maximum extension of a polymer is then calculated by multiplying repeat unit length by the number of repeat units (Equation AII.1)

$$L_P = nb \qquad \text{(AII.1)}$$

where L_P =length of polymer, n =number of repeat units, b =length of repeat unit.

For example, a given sample of PDiPAEMA was determined to be 30 kDa relative to PMMA standards. Since the molecular weight of DiPAEMA is 213.32 g/mol, the number of repeat units in a 30 kDa sample of PDiPAEMA is roughly 140. Using Equation AII.1, the maximum extension of a 30 kDa sample of PDiPAEMA is then calculated to be ca. 430 Å. The maximum extension of a polymer is useful for theoretical comparison, however, to fully stretch a polymer to the point where each bond was linear, thus fully extended, is thermodynamically highly improbable.

A more precise measure of a polymers length, when extended and bond angles remain constant (i.e. not linear), is given by Equation AII.2.

$$L_P = Nl\cos(\theta/2) \qquad \text{(AII.2)}$$

where L_P =length of polymer, N =number of bonds, l =bond length, θ =bond angle, 109.5°.

The number of bonds can be determined by multiplying the repeat unit (2 bonds) by the number of repeat units in the polymer (ca. 140 repeat units in a 30 kDa sample). Thus, the 30 kDa sample of PDiPAEMA consists of ca. 280 C-C bonds. Using Equation AII.2, the length of a 30 kDa sample of PDiPAEMA is then calculated to be ca. 250 Å.

The radius of gyration of an ideal polymer, R_g, is a meaningful calculation because it provides a measure for size of a polymer coil (Equation AII.3).

$$R_g^2 = Nl^2/6 \quad \text{(AII.3)}$$

Where: *N*= number of bonds and l=bond length.

For example, a 30 kDa freely jointed PDiPAEMA chain would have a radius of gyration of ~10.5 Å.

Appendix III

Investigations of SI-ARGET and SI-AGET-ATRP of DIpAEMA

Solvent screening from PDiPAEMA

Various solvents were screened for their ability to dissolve a sample of PDiPAEMA (M_n: 15.3 kDa, Đ: 1.19, Table AIII.1) and eventually replace methanol as a polymerisation solvent. Anisole and toluene readily dissolved the polymer, as did THF. Acetone dissolves small amounts of PDiPAEMA but at higher loadings failed to dissolve the PDiPAEMA sample. As a general statement, solvents that have a polarity greater than or equal to that of acetone are bad solvents for PDiPAEMA.

Table AIII.1. Good and bad solvents for PDiPAEMA (M_n: 15 kDa, Đ: 1.19) at 2 mg/mL.

Good Solvent	Anisole	Toluene	Tetrahydrofuran	Acetone		
Bad Solvent	Methanol	Ethanol	Isobutyl alcohol	Isopropyl alcohol	Water	Acetonitrile

Observations regarding the selective binding of TPMA to silica particles

The following is provided as a detailed reference for the discussion regarding the analysis of PGS-11 and the binding of TPMA to silica particles in Section 4.3.2.

TPMA proved to be a suitable ligand for ARGET-ATRP of PDIpAEMA when in solution. However, when conducting a SI-ARGET-ATRP (PGS-10 and PGS-11) from silica particles TPMA was observed to be selectively binding to the silica particles. Bound

TPMA not only hinders the growth of polymer brushes through steric interactions but it reduces the amount of active catalyst in solution, thus slowing the rate of propagation.

An initial visual inspection of both PGS-10 and PGS-11 concluded that both samples were coloured. The colour of these materials was unexpected since neither the polymer nor the substrate contain chromophores. Figure AIII.1 shows the colours of PGS-11 over the various stages of synthesis. At all stages, the material is expected to be white. The sample second from the left is PGS-11 as it was first collected, it has a slight green colour to it. A green colour could easily be attributed to residual copper left in the polymer or stuck on the silica particle itself. Further washing to remove copper resulted in the removal of the majority of the green colour but the sample remained off-white and slightly brown. Oven drying of PGS-11 turned the green sample into a dark red/brown sample (shown furthest to the right).

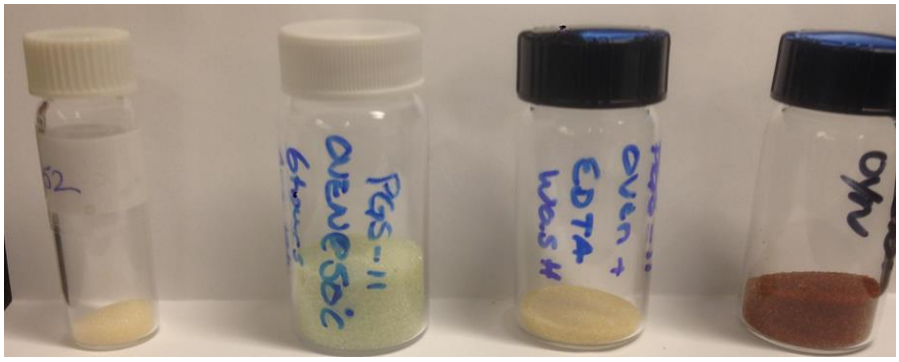

Figure AIII.1. The colours of PGS-11 at various stages of synthesis. From left: initiator-grafted SiO_2; PGS-11 as collected; PGS-11 rinsed then dried followed by a wash with an EDTA solution; PGS-11 left overnight in the oven at 110 °C.

TGA of each sample of PGS-11 was found to have two significant mass loss regimes. The onset of mass loss occurred at ca. 250 °C (Figure AIII.2). This observation

is in contrast to every other TGA run on a polymer-grafted substrate in which the onset of major mass loss occurs at 300 °C. The TGA of PGS-17, which was a successful SI-AGET-ATRP of DiPAEMA, is provided for comparison (Figure AIII.3)

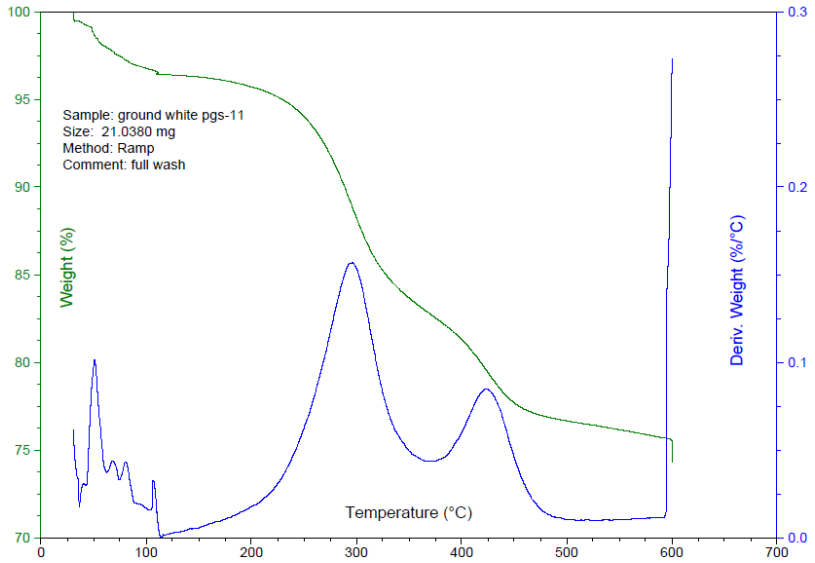

Figure AIII.2. TGA of PGS-11 (grafted PDiPAEMA) after washing the sample with a basic EDTA solution followed by multiple washes with DI water

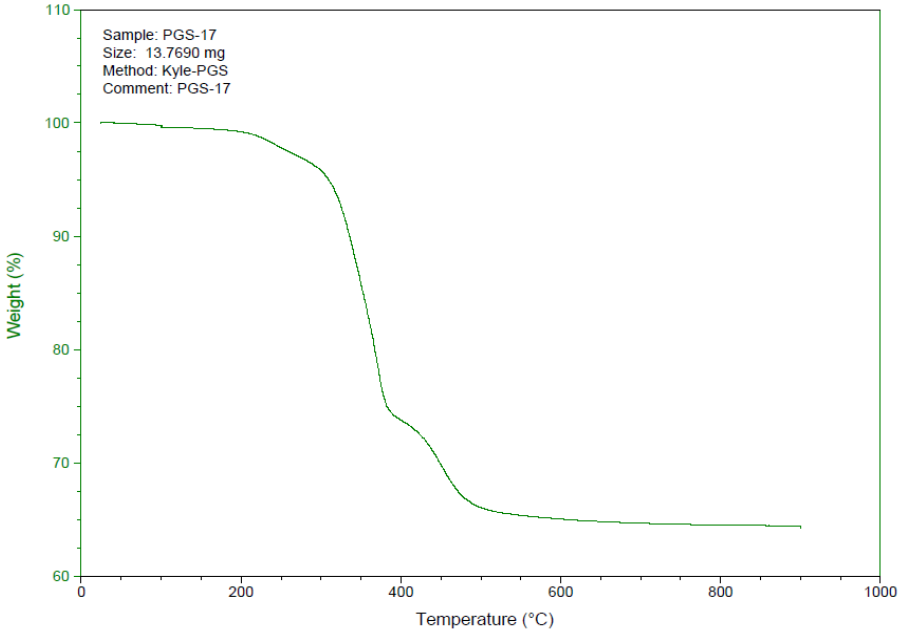

Figure AIII.3. TGA of PGS-17 (PDiPAEMA-grafted silica particles).

X-ray photoelectron spectroscopy data for PGS-11

XPS measurements were conducted and interpreted by Dr. Gabriele Schatte of Queen's University, Kingston, Ontario, Canada. The XPS spectra were measured on a Microlab 310-F spectrometer equipped with an XR-4 twin anode (Al/Mg). The manufacturer of this system is VG Scientific. The samples were mounted on a stub-type stainless steel holder using double-sided adhesive Cu tape. The samples were kept under high vacuum (10^{-8} mbar) overnight inside the preparation chamber before they were transferred into the analysis chamber (10^{-9} mbar) of the spectrometer. The XPS data were collected using MgK_{α} radiation at 1253.6 eV (280 W, 14 kV) and a spherical sector analyser (SSA) operating in CAE (constant analyser energy) mode. Binding energies are referenced to the C1s peak at 285 eV. Survey spectra were recorded from -5 to 1000 eV at a pass energy of 40 eV (number of scans: 5) using an energy step size of 2 eV. High-resolution spectra were measured for C1s, O1s, N1s and Br3d in the appropriate regions at a pass energy of 20 eV and an energy step size of 0.05 eV. The analysed area on the specimens is about 5×2 mm^2.

XPS analysis of each sample of PGS-11, regardless of colour, showed a bimodal distribution for the peak area in the high-resolution N1s core-level spectrum (Figure AIII.4). The high-resolution N1s core-level spectrum for PGS-7 (Figure AIII.5) is provided as an example of what an XPS spectrum is expected to look like for a polymer-grafted substrate containing PDMAPMAm or PDiPAEMA. The dual peak assignment in PGS-7, centred around 402 eV, can be attributed to the tertiary amine and the amide of PDMAPMAm. The dual peaks in PGS-11 cannot be accounted for by PDiPAEMA since it contains only one source of nitrogen which is the tertiary amine. The tertiary amine of

PDiPAEMA should show up at 402 eV, similar to that of PDMAPMAm in PGS-7. The second unknown peak in the N1s core-level spectrum for PGS-11 appears to be centred around 405 eV. The binding energy for this peak is shifted considerably from that of a sp^3 hybridised tertiary amine, suggesting that the nitrogen is significantly more electropositive and possibly sp or sp^2 hybridised, or positively charged. Cumulatively, the TGA and XPS data indicate that an additional nitrogen source (other than PDiPAEMA) is present on PGS-11. The only nitrogen source other than DiPAEMA was TPMA, which is the ligand used for ATRP (Figure AIII.6). The XPS results for PGS-11 could be explained by a cationic TPMA-H^+, with the silica substrate (Si-O^-) forming the anion. Alternatively, a cationic nitrogen species could be explained by the reduction mechanism proposed in Scheme 4.5 or by the formation of an amine oxide.

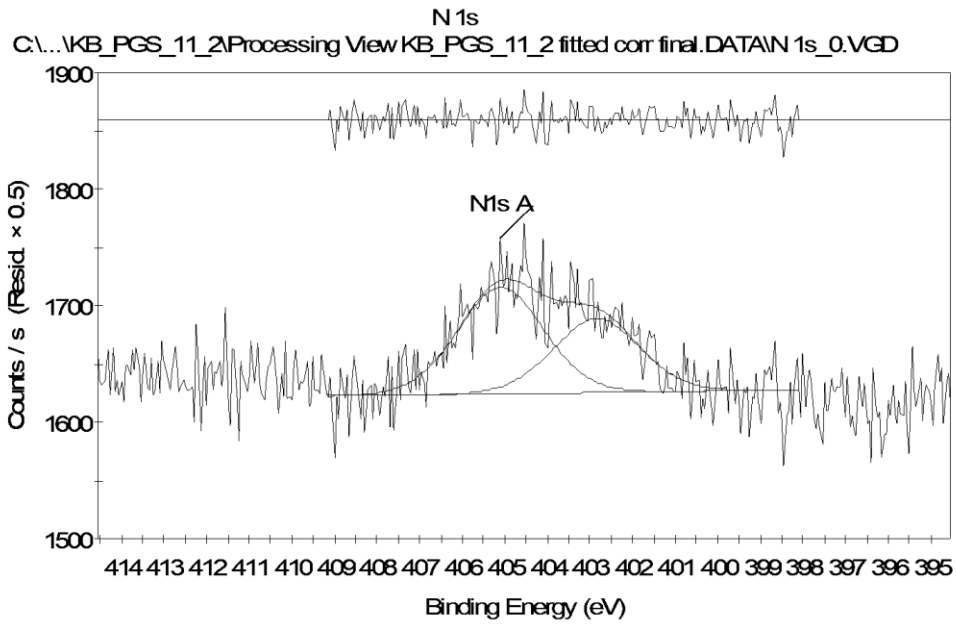

Figure AIII.4 High-resolution N1s core-level spectrum of PGS-11.

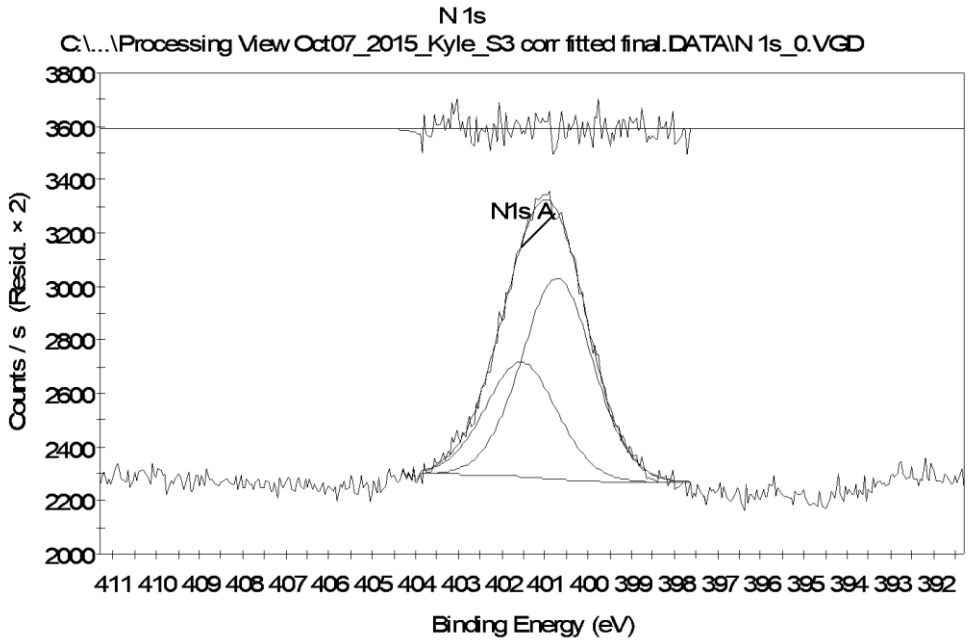

Figure AIII.5. High-resolution N1s core-level spectrum of PGS-7.

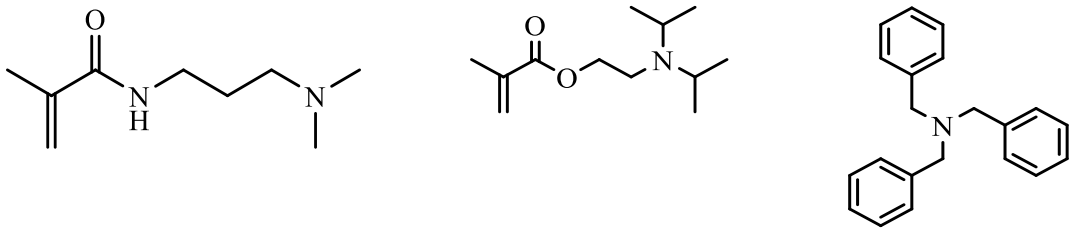

Figure AIII.6. Amine-containing species used in the synthesis of polymer-grafted silica particles. From left to right: DMAPMAm (used in PGS-7); DiPAEMA (used in PGS-11); TPMA (used in PGS-11).

In addition to XPS studies, a qualitative assessment was undertaken in efforts to elucidate the source of nitrogen contamination on PGS-10 and PGS-11. As shown in Figure AIII.1, the PGS-11 sample turned reddish-brown when left in the oven - a characteristic not associated with other PGS samples. Similarly, a sample of TPMA (white powder) turned reddish-brown after being left in the oven overnight (110 °C). With all factors considered, the source of nitrogen contamination and the unwanted colour was

determined to be due to TPMA, which was bound to the silica substrate. TPMA coordinating to the silica substrate poses more than just a cosmetic problem. If TPMA is coordinated to the silica particle, it is not coordinated to the metal, and the catalyst is not formed. If the catalyst is not being formed, the rate of polymerisation is retarded. Additionally, if TPMA coordinates to the silica particles in a high degree, it is plausible that steric effects will make polymer brush growth less favourable. Steric effects could cause the grafting density and amount of polymer-grafted to the silica substrate to be reduced. The intensity of the nitrogen signal in the survey spectrum of PGS-11 (Figure AIII.7) is considerably lower than that of PGS-7 (Figure AIII.8); lending support to the hypothesis that bound TPMA contributes to a reduction of polymer-grafted to the silica substrate.

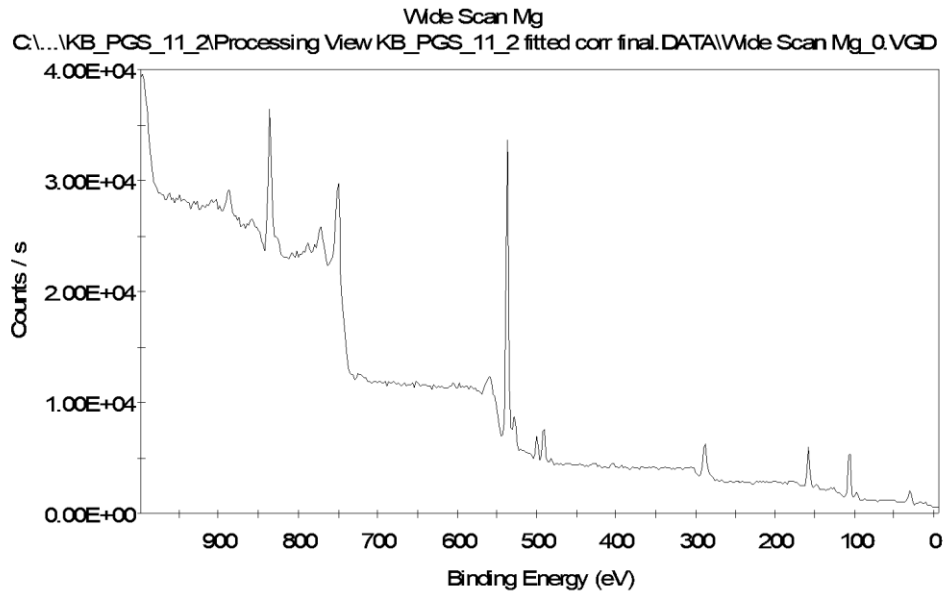

Figure AIII.7. Survey spectrum of PGS-11.

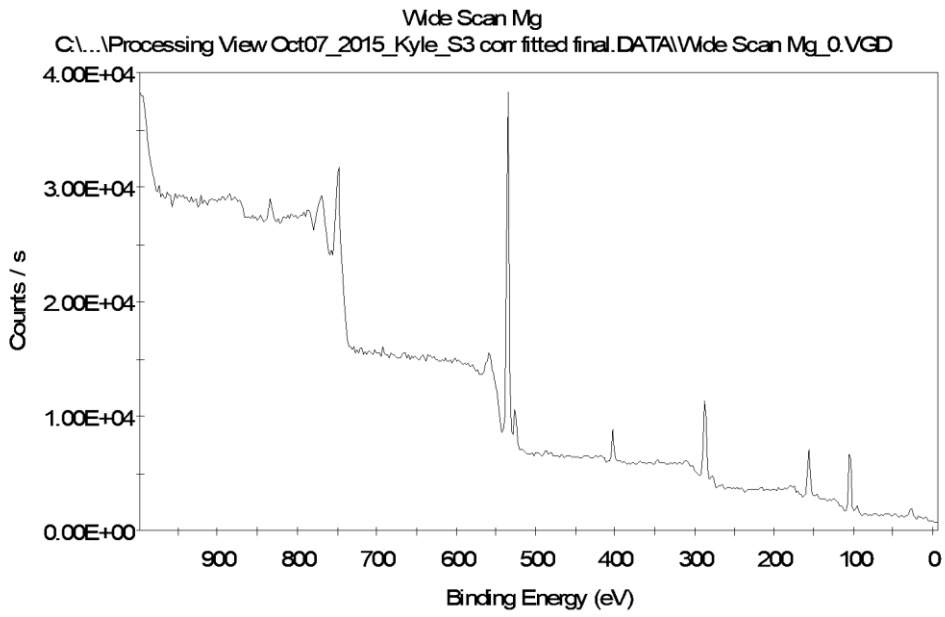

Figure AIII.8. Survey spectrum of PGS-7.

Table AIII.2. XPS peak analysis for PGS-11, atomic percent reported as a function of the normalised peak area.

Peak	Start BE	Peak BE	End BE	Area KE^0.6	Atom %
Si2p	110.19	104.99	102.05	9.11	2.47
Si2p A	110.19	106.34	102.05	53.53	14.5
Si2p B	110.19	107.33	102.05	23.84	6.46
C1s	293.89	285.08	281.4	6.95	1.88
C1s A	293.89	286.94	281.4	21.16	5.73
C1s B	293.89	288.51	281.4	28.61	7.75
C1s C	293.89	290.04	281.4	15.39	4.17
C1s D	293.89	291.98	281.4	4.25	1.15
O1s	539.3	534.47	532.27	21.8	5.9
O1s A	539.3	535.96	532.27	136.78	37.05
O1s B	539.3	536.95	532.27	43.82	11.87
N1s	409.15	402.84	398.1	1.6	0.43
N1s A	409.15	405.1	398.1	2.3	0.62

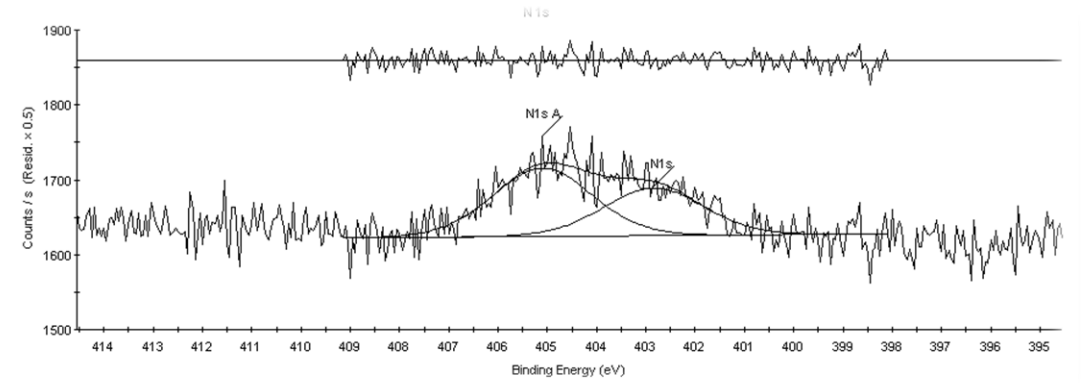

Figure AIII.9. High-resolution N1s core-level XPS spectrum of PGS-11.

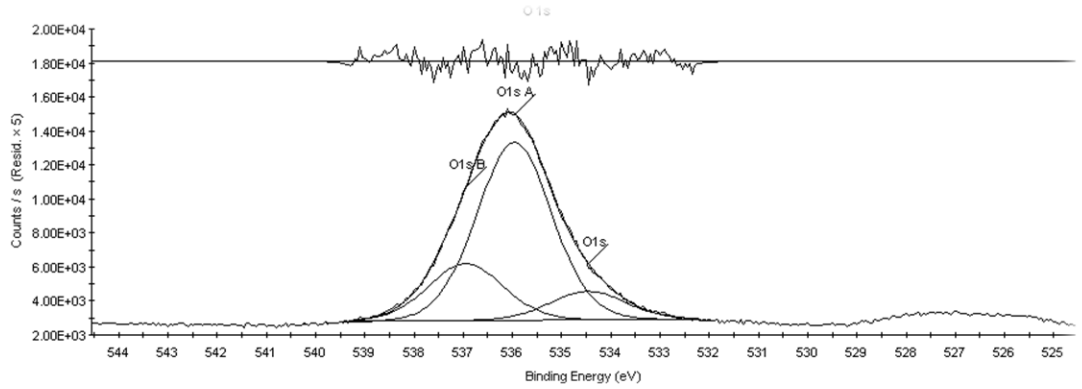

Figure AIII.10. High-resolution O1s core-level XPS spectrum of PGS-11.

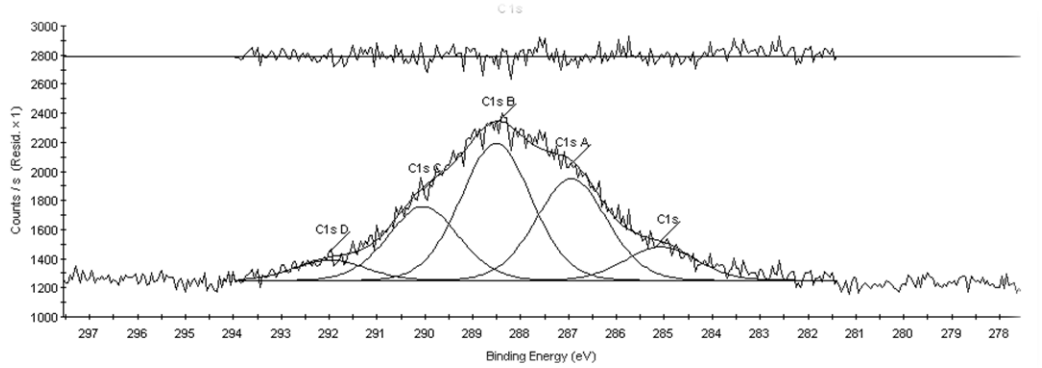

Figure AIII.11. High-resolution C1s core-level XPS spectrum of PGS-11.

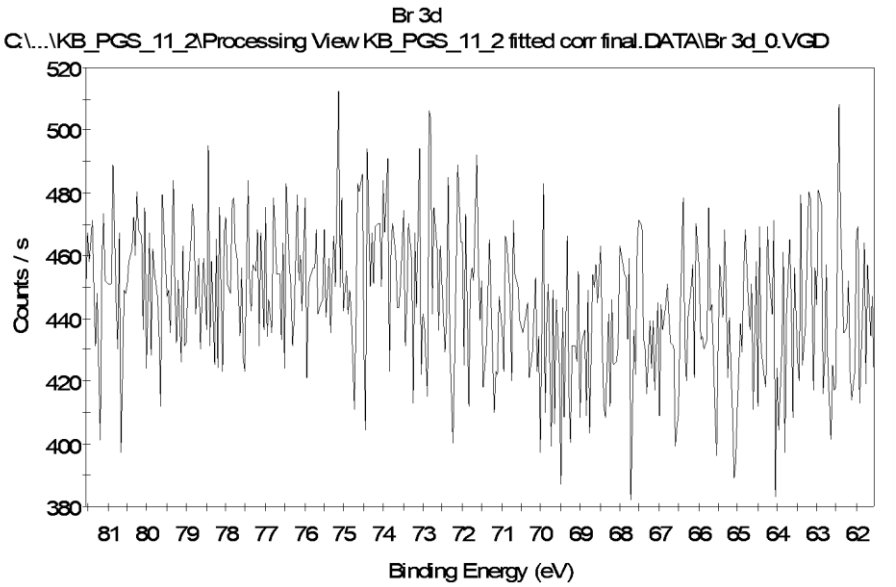

Figure AIII.12. High-resolution Br3d core-level XPS spectrum of PGS-11.

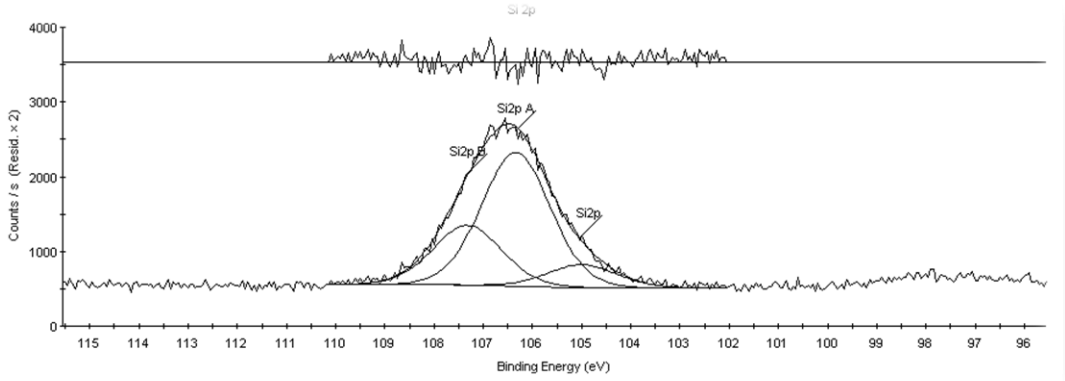

Figure AIII.13. High-resolution Si2p core-level XPS spectrum of PGS-11.

Appendix IV

Synthesis and characterization of polymer-grafted silica particles

Synthesis of PGS-8

Initiator grafting method (KBB7PG22):

Clean and hydroxyl-rich silica particles particles (SiO_2 #1, Silicycle, 200-500 μm particle size, 100 Å pore size, 20 g, 1 eq. assumption 1 $mmol \cdot g^{-1}$) were added to a 250 mL flame dried round bottom flask, to which a condenser was fixed. Reactants were added using Schlenk techniques for inert conditions; diisopropylethylamine (5 eq., 100.0 mmol) and 150 mL of anhydrous dichloromethane (DCM) were added to the round bottom flask. The round bottom flask was cooled in an ice bath for approximately 30 min, after which the initiator, 2-bromo-2-methylpropionyl bromide (BIBB, 4 eq., 80 mmol), was added dropwise via syringe. The mixture was stirred with a magnetic stir bar (1200 RPM) for 20 min before the ice bath was removed and the mixture was allowed to warm to room temperature, ca. 27 ℃ and allowed to react overnight. The BIBB-grafted silica was then collected by vacuum filtration and washed multiple times with DCM. The washed particles were dried at 110 ℃ for 20 min, then stored under Ar until further use.

SI-AGET-ATRP of PDMAPMAm from silica, PGS-8, (KBB7PG25):

Initiator-functionalised silica (SiO_2 #1, Silicycle, 200-500 μm particle size, 100 Å pore size, 4.2 g) were added to a 500 mL 3-neck round bottom flask containing 150 mL of anhydrous methanol. The mixture was sparged with Ar for 1 h. The monomer, N-[3-(dimethylamino)propyl]methacrylamide (DMAPMAm 0.67 mol, 80 eq.), was passed through a basic alumina column, followed by sparging with Ar for 30 min. The catalyst was prepared by mixing copper(I) bromide (8.4 mmol, 1 eq.) with N,N,N′,N″,N″-pentamethyldiethylenetriamine (PMDETA, 16.8 mmol, 2 eq.) in 25 mL anhydrous methanol. The mixture was sparged with Ar for 1 h. The sparged components were added to the 3-neck flask under Ar, heated to 50 ℃, and stirred with a magnetic stir bar (900 RPM) overnight. The polymer-grafted silica particles were recovered via vacuum filtration and washed thoroughly with an aqueous solution of ethylenediaminetetraacetic acid (EDTA), followed by multiple washings with distilled water. The particles were dried at 110 °C overnight, then stored under Ar until further use.

Synthesis of PGS-9

Initiator grafting method (KBB7PG22):

Refer to PGS-8. The same batch of silica used in PGS-8 was used for PGS-9

SI-AGET-ATRP of PDMAPMAm from silica, PGS-9, (KBB7PG41):

Initiator-functionalised silica (SiO_2 #1, Silicycle, 200-500 μm particle size, 100 Å pore size, 14.6 g) were added to a 1 L 3-neck round bottom flask containing 300 mL of anhydrous methanol. The mixture was sparged with Ar for 1 h. The monomer, N-[3-(dimethylamino)propyl]methacrylamide (DMAPMAm 2.3 mol, 80 eq.), was passed through a basic alumina column, followed by sparging with Ar sparging for 30 min. The catalyst was prepared by mixing copper(I) bromide (29 mmol, 1 eq.) with N,N,N′,N″,N″-pentamethyldiethylenetriamine (PMDETA, 58 mmol, 2 eq.) in 25 mL anhydrous methanol. The mixture was sparged with Ar for 1 h. The sparged components were added to the 3-neck flask under Ar, heated to 50 ℃, and stirred with a magnetic stir bar (900 RPM) overnight. The polymer-grafted silica particles were recovered via vacuum filtration and washed thoroughly with an aqueous solution of ethylenediaminetetraacetic acid (EDTA), followed by multiple washings with distilled water. The particles were dried at 110 ℃ overnight, then stored under Ar until further use.

Synthesis of PGS-10

Initiator grafting method (KBB8PG35):

Clean and hydroxyl-rich silica particles particles (SiO_2 #2, Silicycle, 200-500 μm particle size, 60 Å pore size, 10 g ,1 eq. assumption 1 $mmol \cdot g^{-1}$) were added to a 500 mL glass reaction vessel that was equipped with an overhead stirrer and an ethylene glycol temperature control unit. Diisopropylethylamine (6 eq., 60.0 mmol), 4-(dimethylamino)pyridine (1 eq., 10 mmol) and 300 mL of anhydrous dimethylformamide (DMF) were added to the reaction flask under dynamic Ar. The reaction flask was cooled to 4 ℃, at which point the initiator, 2-bromo-2-methylpropionyl bromide (BIBB, 1 eq., 10 mmol), was added dropwise via syringe. The mixture was stirred with an overhead stirring device for 20 min before the temperature was raised to room temperature, ca. 22 ℃. The mixture was stirred overnight. The BIBB-grafted silica was then collected by vacuum filtration and washed multiple times with DMF, followed by THF. The washed particles were dried at 110 ℃ for 20 min, then stored under Ar until further use.

SI-ARGET-ATRP PDiPAEMA from silica, PGS-10, (KBB8PG50):

Initiator-functionalised silica particles (SiO_2 #2, Silicycle, 200-500 μm particle size, 60 Å pore size, 10 g) were added to a 250 mL round bottom flask equipped with an overhead stirring device. 2-(Diisopropylamino)ethyl methacrylate (DiPAEMA, 117 eq., 295 mmol) was passed through an inhibitor remover column [Sigma-Aldrich, removing hydroquinone (HQ) or hydroquinone monomethyl ether (MEHQ, 4-methoxyphenol), or 4-*tert*-butylcatechol (TBC)] and charged to the 250 mL round bottom flask containing the

initiator-functionalised silica. Anisole (142 mL), Cu(II)Cl_2 (0.05 eq., 0.126 mmol), tris(2-pyridylmethyl)amine (TPMA, 0.25 eq., 0.6 mmol) and ethyl 2-bromo-2-methylpropionate (EBIB, 1 eq., 2.5 mmol) were added to the round bottom flask. The mixture was stirred vigorously while being slowly heated to 40 ℃. Once the mixture reached the desired temperature, tin(II) 2-ethylhexanoate (5 eq., 12 mmol) was added to the round bottom flask; which was promptly sealed. No additional techniques were used to remove atmospheric or dissolved oxygen. The polymerisation solution changed colour from blue (oxidised copper) to colourless (ca. 2 h on average) and then to yellow/orange over the course of 72 h. The polymer-grafted silica particles were recovered via vacuum filtration and washed thoroughly with anisole, followed by multiple washings with THF. The particles were dried at 110 ℃ overnight, then stored under Ar until further use. The free polymer was collected via precipitation in basic water (pH>10).

Synthesis of PGS-11

Initiator grafting method (KBB8PG35):

Diisopropylethylamine (DIPEA, 2 eq., 56.0 mmol) and 100 mL of anhydrous dichloromethane (DCM) were added to a 500 mL glass reaction vessel that was equipped with an overhead stirrer and an ethylene glycol temperature control unit. The reaction flask was cooled to 2 ℃, at which point the initiator, 2-bromo-2-methylpropionyl bromide (BIBB, 1.5 eq., 42 mmol), was added dropwise via syringe, under dynamic Ar. The mixture was stirred at 2 ℃ for 20 min before the silica particles were added.

Clean and hydroxyl-rich silica particles particles (SiO_2 #2, Silicycle, 200-500 μm particle size, 60 Å pore size, 12.7 g, 1 eq. assumption 1 $mmol \cdot g^{-1}$) were heated in a calcination over for 2 h at 200 ℃. The particles were removed from the calcination oven and immediately added to the 500 mL glass reaction vessel containing a solution of BIBB and DIPEA in DCM. The mixture was stirred for 20 min, after which an additional 200 mL of anhydrous DCM was added under Ar. The temperature control unit was set to 25 ℃ and the solution was stirred overnight. The BIBB-grafted silica was then collected by vacuum filtration and washed multiple times with DCM, followed by THF. The excess solvent was removed for the particles under reduced pressure and the particles were stored for future use.

SI-ARGET-ATRP PDiPAEMA from silica, PGS-11, (KBB8PG54):

Initiator-functionalised silica particles (SiO_2 #2, Silicycle, 200-500 μm particle size, 60 Å pore size, 10 g) were added to a 250 mL round bottom flask equipped with an overhead stirring device. 2-(Diisopropylamino)ethyl methacrylate (DiPAEMA, 117 eq., 295 mmol) was passed through an inhibitor remover column [Sigma-Aldrich, removing hydroquinone (HQ) or hydroquinone monomethyl ether (MEHQ, 4-methoxyphenol), or 4-*tert*-butylcatechol (TBC)] and charged to the 250 mL round bottom flask containing the initiator-functionalised silica. Anisole (70 mL), $Cu(II)Cl_2$ (0.05 eq., 0.126 mmol), tris(2-pyridylmethyl)amine (TPMA, 0.25 eq., 0.6 mmol) and ethyl 2-bromo-2-methylpropionate (EBIB, 1 eq., 2.5 mmol) were added to the round bottom flask. The mixture was stirred vigorously while being slowly heated to 40 ℃. Once the mixture reached the desired temperature, tin(II) 2-ethylhexanoate (5 eq., 12 mmol) was added to the round bottom flask; which was promptly sealed. No additional techniques were used to remove atmospheric or dissolved oxygen. The polymerisation solution changed colour from blue (oxidised copper) to colourless (ca. 2 h on average) and then to yellow/orange over the course of 67 h. The polymer-grafted silica particles were recovered via vacuum filtration and washed thoroughly with anisole, followed by multiple washings with THF. The particles were dried at 110 ℃ overnight, then stored under Ar until further use. The free polymer was collected via precipitation in basic water (pH>10).

Synthesis of PGS-12

PGS-12 was a control experiment, there was no initiator grafted to the silica particles.

SI-AGET-ATRP PDiPAEMA from silica, PGS-12 (KBB8PG76):

Silica particles (SiO_2 #5, SiliaFlash P60, 40-63 μm, 100 Å pore size, 5 g) were added to a 250 mL round bottom flask equipped with an overhead stirring device. 2-(Diisopropylamino)ethyl methacrylate (DiPAEMA, 114 eq., 164 mmol) was passed through an inhibitor remover column [Sigma-Aldrich, removing hydroquinone (HQ) or hydroquinone monomethyl ether (MEHQ, 4-methoxyphenol), or 4-*tert*-butylcatechol (TBC)] and charged to the 250 mL round bottom flask containing the initiator-functionalised silica. Anisole (150 mL), Cu(II)Br_2 (0.78 eq., 1.1 mmol), N,N,N′,N″,N″-pentamethyldiethylenetriamine (PMDETA, 4 eq., 5.7 mmol) and ethyl 2-bromo-2-methylpropionate (EBIB, 1 eq., 1.4 mmol) were added to the round bottom flask and the mixture was stirred vigorously while slowly heating to 40 ℃. Once the mixture reached the desired temperature, tin(II) 2-ethylhexanoate (77 eq., 111 mmol) was added to the round bottom flask; which was promptly sealed. No additional techniques were used to remove atmospheric or dissolved oxygen. The polymerisation solution changed colour from blue (oxidized copper) to colourless (ca. 2 h on average) and then to yellow/orange over the course of 20 h. The silica particles were recovered via vacuum filtration and washed thoroughly with anisole, followed by multiple washings with THF. The particles were dried at 110 ℃ overnight, then stored under Ar until further use. The free polymer was collected via precipitation in basic water (pH>10).

Synthesis of PGS-13

Initiator grafting method (KBB8PG69):

Diisopropylethylamine (DIPEA, 1 eq., 15 mmol) and 200 mL of anhydrous dichloromethane (DCM) were added to a 250 mL round bottom flask that was equipped with an overhead stirrer. The reaction flask was cooled to 4 ℃ using an ice bath. After which, the initiator, 2-bromo-2-methylpropionyl bromide (BIBB, 3 eq., 45 mmol), was added dropwise via syringe, under dynamic Ar. The mixture was stirred at 4 ℃ for 20 min before the silica particles were added.

Clean and hydroxyl-rich silica particles particles (SiO_2 #2, Silicycle, 200-500 μm particle size, 60 Å pore size, 12.7 g, 1 eq. assumption 1 $mmol \cdot g^{-1}$) were heated in a calcination over for 2 h at 200 ℃. The particles were removed from the calcination oven and immediately added to the 250 mL round bottom flask containing a solution of BIBB and DIPEA in DCM. The mixture was stirred overnight. Significant solvent loss occurred and the majority of the solvent had evaporated. BIBB-functionalised silica was not damaged as a result of the loss of solvent. The BIBB-grafted silica was collected by vacuum filtration and washed multiple times with DCM, followed by THF. The excess solvent was removed for the particles in vacuo, the particles were then stored for future use.

SI-AGET-ATRP PDiPAEMA from silica, PGS-13 (KBB8PG77):

Initiator-functionalised silica particles (SiO_2 #2, Silicycle, 200-500 μm particle size, 60 Å pore size, 5 g) were added to a 250 mL round bottom flask equipped with an overhead stirring device. 2-(Diisopropylamino)ethyl methacrylate (DiPAEMA, 114 eq., 164 mmol) was passed through an inhibitor remover column [Sigma-Aldrich, removing hydroquinone (HQ) or hydroquinone monomethyl ether (MEHQ, 4-methoxyphenol), or 4-tert-butylcatechol (TBC)] and charged to the 250 mL round bottom flask containing the initiator-functionalised silica. Anisole (150 mL), Cu(II)Br_2 (0.78 eq., 1.1 mmol), N,N,N′,N″,N″-pentamethyldiethylenetriamine (PMDETA, 4 eq., 5.7 mmol) and ethyl 2-bromo-2-methylpropionate (EBIB, 1 eq., 1.4 mmol) were added to the round bottom flask and the mixture was stirred vigorously while slowly heating to 40 ℃. Once the mixture reached the desired temperature, tin(II) 2-ethylhexanoate (77 eq., 111 mmol) was added to the round bottom flask; which was promptly sealed. No additional techniques were used to remove atmospheric or dissolved oxygen. The polymerisation solution changed colour from blue (oxidized copper) to colourless (ca. 2 h on average) and then to yellow/orange over the course of 16 h. The polymer-grafted silica particles were recovered via vacuum filtration and washed thoroughly with anisole, followed by multiple washings with THF. The particles were dried at 110 ℃ overnight, then stored under Ar until further use. The free polymer was collected via precipitation in basic water (pH>10).

Synthesis of PGS-16

Initiator grafting method part 1, (KBB9PG19):

Clean, hydroxyl-rich silica particles (SiO_2 #3, Silicycle, 200-500 μm particle size, 500 Å pore size, 15 g) were added to a 500 mL glass reaction vessel. The glass reaction vessel was equipped with an overhead stirrer and an ethylene glycol heating unit. The vessel was kept at a constant temperature of 70 ℃. The atmosphere in the reaction vessel was removed under vacuum and replaced with Ar. To the sealed reaction vessel, 500 mL of anhydrous toluene was added via cannula transfer. After vigorous stirring, 5 mL of (3-aminopropyl)triethoxysilane (APTES) was added via syringe. The reaction was left stirring at 70 ℃ overnight. The APTES-grafted silica was collected by vacuum filtration and washed multiple times with ethanol before being stored under Ar until further use.

Initiator grafting method part 2, (KBB9PG19):

APTES-functionalised silica particles (SiO_2 #3, Silicycle, 200-500 μm particle size, 500 Å pore size, 15 g) were added to a flame dried 250 mL round bottom flask. The round bottom flask was equipped with an overhead stirring device. Reactants were added using Schlenk techniques for inert conditions; diisopropylethylamine (1 eq., 4.0 mmol) and 200 mL of anhydrous tetrahydrofuran (THF) were added to the round bottom flask. The round bottom flask was cooled in an ice bath for approximately 30 min, after which the initiator, 2-bromo-2-methylpropionyl bromide (BIBB, 1 eq., 4.04 mmol), was added dropwise via syringe. The mixture was stirred for 20 min before the ice bath was removed and the mixture was allowed to warm to room temperature (ca. 27 ℃) and to react overnight. The

BIBB-grafted silica was then collected by vacuum filtration and washed multiple times with THF before being stored under Ar until further use.

SI-AGET-ATRP PDiPAEMA from silica, PGS-16, (KBB9PG19):

Initiator-functionalised silica particles (SiO_2 #3, Silicycle, 200-500 μm particle size, 500 Å pore size, 15 g) were added to a 250 mL round bottom flask equipped with an overhead stirring device. 2-(Diisopropylamino)ethyl methacrylate (DiPAEMA, 247 eq., 210 mmol) was passed through an inhibitor remover column [Sigma-Aldrich, removing hydroquinone (HQ) or hydroquinone monomethyl ether (MEHQ, 4-methoxyphenol), or 4-*tert*-butylcatechol (TBC)] and charged to the 250 mL round bottom flask containing the initiator-functionalised silica. Anisole (50 mL), Cu(II)Br2 (0.68 eq., 0.58 mmol), N,N,N′,N″,N″-pentamethyldiethylenetriamine (PMDETA, 3.26 eq., 2.77 mmol) and ethyl 2-bromo-2-methylpropionate (EBIB, 1 eq., 1.7 mmol) were added to the round bottom flask. The mixture was stirred vigorously while being slowly heated to 40 ℃. Once the mixture reached the desired temperature, L-ascorbic acid (10 eq., 8.5 mmol) was added to the round bottom flask, which was promptly sealed. No additional techniques were used to remove atmospheric or dissolved oxygen. The polymerisation solution changed colour from blue (oxidised copper) to colourless (ca. 2 h on average) and then to yellow/orange over the course of 16 h.

Isolation of free polymer and polymer-grafted silica:

Refer to Section 4.3.5.

Additional IR spectroscopy data collected from PGS samples

Table AIV.1. CP-MAS NMR data from selected spectra.

PDiPAEMA (KBB9PG47):	2963 cm^{-1}, 2927 cm^{-1}, 2873 cm^{-1}, 2715 cm^{-1}, 2609 cm^{-1}, 1725 cm^{-1}, 1601 cm^{-1}, 1577 cm^{-1}, 1541 cm^{-1}, 1465 cm^{-1}, 1390 cm^{-1}, 1361 cm^{-1}, 1333 cm^{-1}, 1256 cm^{-1}, 1243 cm^{-1}, 1143 cm^{-1}, 1066 cm^{-1}, 1029 cm^{-1}, 981 cm^{-1}, 860 cm^{-1}, 750 cm^{-1}, 691 cm^{-1}, 572 cm^{-1}, 546 cm^{-1}, 515 cm^{-1}, 487 cm^{-1}.
PGS-8:	3649 cm^{-1}, 3369 cm^{-1}, 2961 cm^{-1}, 2828 cm^{-1}, 2537 cm^{-1}, 1991 cm^{-1}, 1875 cm^{-1}, 1637 cm^{-1}, 1529 cm^{-1}, 1476 cm^{-1}, 1394 cm^{-1}, 1090 cm^{-1}, 971 cm^{-1}, 802 cm^{-1}.
PGS-9:	3399 cm^{-1}, 3068 cm^{-1}, 2961 cm^{-1}, 2884 cm^{-1}, 2733 cm^{-1}, 2532 cm^{-1}, 2011 cm^{-1}, 1870 cm^{-1}, 1712 cm^{-1}, 1632 cm^{-1}, 1534 cm^{-1}, 1483 cm^{-1}, 1394 cm^{-1}, 1316 cm^{-1}, 1090 cm^{-1}, 981 cm^{-1}, 915 cm^{-1}, 796 cm^{-1}.
PGS-10:	3423 cm^{-1}, 2995 cm^{-1}, 2940 cm^{-1}, 2882 cm^{-1}, 1992 cm^{-1}, 1872 cm^{-1}, 1805 cm^{-1}, 1760 cm^{-1}, 1649 cm^{-1},1468 cm^{-1}, 1388 cm^{-1}, 1098 cm^{-1}, 967 cm^{-1}, 808 cm^{-1}.
PGS-11 EDTA washed:	3458 cm^{-1}, 2971 cm^{-1}, 2631 cm^{-1}, 2379 cm^{-1}, 2346 cm^{-1}, 2005 cm^{-1}, 1871 cm^{-1}, 1725 cm^{-1}, 1655 cm^{-1}, 1647 cm^{-1}, 1629 cm^{-1}, 1476 cm^{-1}, 1466 cm^{-1}, 1449 cm^{-1}, 1389 cm^{-1}, 1364 cm^{-1}, 1123 cm^{-1}, 1098 cm^{-1}, 964 cm^{-1}, 197 cm^{-1}.
PGS-11 Brown:	3449 cm^{-1}, 2993 cm^{-1}, 2372 cm^{-1}, 2346 cm^{-1}, 1994 cm^{-1}, 1870 cm^{-1}, 1803 cm^{-1}, 1702 cm^{-1}, 1686 cm^{-1}, 1663 cm^{-1}, 1638 cm^{-1}, 1544 cm^{-1}, 1475 cm^{-1}, 1459 cm^{-1}, 1389 cm^{-1}, 1099 cm^{-1}, 969 cm^{-1}, 808 cm^{-1}, 796 cm^{-1}.
PGS-12 Insoluble species:	3419 cm^{-1}, 2964 cm^{-1}, 2935 cm^{-1}, 2872 cm^{-1}, 2472 cm^{-1}, 1727 cm^{-1}, 1639 cm^{-1}, 1628 cm^{-1}, 1466 cm^{-1}, 1389 cm^{-1}, 1361 cm^{-1}, 1238 cm^{-1}, 1148 cm^{-1}, 1065 cm^{-1}, 1029 cm^{-1}, 983 cm^{-1}, 676 cm^{-1}, 667 cm^{-1}, 650 cm^{-1}.
PGS-12:	1871 cm^{-1}, 1627 cm^{-1}, 1121 cm^{-1}, 1070 cm^{-1}, 963 cm^{-1}, 807 cm^{-1}.
PGS-13 Insoluble species:	3419 cm^{-1}, 2964 cm^{-1}, 2935 cm^{-1}, 2872 cm^{-1}, 2472 cm^{-1}, 1727 cm^{-1}, 1639 cm^{-1}, 1628 cm^{-1}, 1466 cm^{-1}, 1389 cm^{-1}, 1361 cm^{-1}, 1238 cm^{-1}, 1148 cm^{-1}, 1065 cm^{-1}, 1029 cm^{-1}, 983 cm^{-1}, 676 cm^{-1}, 667 cm^{-1}, 650 cm^{-1}.
PGS-13:	3485 cm^{-1}, 1995 cm^{-1}, 1873 cm^{-1}, 1630 cm^{-1}, 1173 cm^{-1}, 1062 cm^{-1}, 971 cm^{-1}, 803 cm^{-1}
PGS-15:	3646 cm^{-1}, 3366 cm^{-1}, 2966 cm^{-1}, 2933 cm^{-1}, 2875 cm^{-1}, 2827 cm^{-1}, 2719 cm^{-1}, 2608 cm^{-1}, 1994 cm^{-1}, 1871 cm^{-1}, 1729 cm^{-1}, 1649 cm^{-1}, 1535 cm^{-1}, 1462 cm^{-1}, 1390 cm^{-1}, 1361 cm^{-1}, 1333 cm^{-1}.

PGS-17: 3657 cm^{-1}, 2966 cm^{-1}, 2933 cm^{-1}, 2875 cm^{-1}, 2819 cm^{-1}, 2731 cm^{-1}, 2607 cm^{-1}, 1991 cm^{-1}, 1871 cm^{-1}, 1729 cm^{-1}, 1467 cm^{-1}, 1390 cm^{-1}, 1361 cm^{-1}, 1114 cm^{-1}, 1100 cm^{-1}, 983 cm^{-1}, 803 cm^{-1}, 793 cm^{-1}, 749 cm^{-1}.

Additional CP-MAS-NMR data collected from PGS samples

Table AIV.2. ^{29}Si and ^{13}C CP-MAS NMR data from selected spectra.

Clean SiO_2 #3……	-106 ppm.
Clean SiO_2 #3:……...	No peaks detected.
PGS-1 ^{29}Si:……	-107 ppm, -118 ppm.
PGS-1 ^{13}C:……	53 ppm, 41 ppm. 34 ppm.
PGS-2 ^{13}C:……	179 ppm, 122 ppm, 76 ppm, 65 ppm, 61 ppm, 54 ppm, 42 ppm.
PGS-2 ^{29}Si:……...	-106 ppm, -114 ppm
PGS-7 ^{13}C:……	177 ppm, 56 ppm, 47 ppm, 43 ppm, 23 ppm, 16 ppm.
PGS-7 ^{29}Si:……...	-106 ppm, -117 ppm.
PGS-8 ^{13}C:……	177 ppm, 56 ppm, 43 ppm, 23 ppm, 15 ppm.
PGS-10 ^{13}C:……..	170 ppm, 44 ppm, 29 ppm, 21 ppm, 18 ppm, 11 ppm.
PGS-10 ^{29}Si:……	-97 ppm, -106 ppm.
PGS-11 ^{13}C:……..	176 ppm, 65 ppm, 55ppm, 48 ppm, 44 ppm, 19 ppm.
PGS-12 ^{29}Si: ……	-107 ppm, -115 ppm.
PGS-12 ^{13}C:……..	46 ppm, 35 ppm, 18 ppm, 15 ppm, 9 ppm.
PGS-13 ^{29}Si:……	-108 ppm, -117 ppm.
PGS-13 ^{13}C:……..	46 ppm, 42 ppm, 35 ppm, 29 ppm, 25 ppm, 16 ppm, 14 ppm.
PGS-15 ^{13}C:……...	176 ppm, 65 ppm, 55 ppm, 48 ppm, 44 ppm, 31 ppm, 20 ppm, 9 ppm.
PGS-15 ^{29}Si:……..	-64 ppm, -69 ppm, -107 ppm, -116 ppm.
PGS-15-EXT-PS ^{13}C:……	176 ppm, 127 ppm, 64 ppm, 55 ppm, 48 ppm, 44 ppm, 31 ppm, 20 ppm.
PGS-15-EXT-PS ^{29}Si:……...	-65 ppm, -72 ppm, -96 ppm, -107 ppm, -116 ppm.
SiO_2 #3-APTES ^{13}C:……..	56 ppm, 43 ppm, 20 ppm, 15 ppm, 8 ppm
SiO_2 #3-APTES ^{29}Si:……	-107 ppm, -118 ppm.
SiO_2 #3-APTES-BIBB ^{13}C:……...	173 ppm, 58 ppm, 41 ppm, 30 ppm, 21 ppm, 15 ppm, 9 ppm.
SiO_2 #3-APTES-BIBB ^{29}Si:……..	-107 ppm, -116 ppm.
PGS-16 ^{29}Si:……..	-108 ppm, -115 ppm.
PGS-16 ^{13}C:……...	176 ppm, 64 ppm, 55 ppm, 48 ppm, 44 ppm, 20 ppm, 15 ppm.
PGS-17 ^{13}C:……...	176 ppm. 65 ppm, 55 ppm, 48 ppm, 44 ppm, 20 ppm, 15 ppm.

PGS-17 ^{29}Si:……..	-107 ppm, 111 ppm, -117 ppm.
SiO_2#5-APTES ^{13}C:……..	56 ppm, 43 ppm, 24 ppm, 15 ppm, 8 ppm
SiO_2#5-APTES ^{29}Si:……..	-64 ppm, -65 ppm, -67 ppm, -106 ppm, -117 ppm.
SiO_2#5-APTES-BIBB ^{13}C:……	171 ppm, 58 ppm, 42 ppm, 30 ppm, 22 ppm, 17 ppm, 9 ppm.
SiO_2#5-APTES-BIBB ^{29}Si:……...	-64 ppm, -107 ppm, -116 ppm.
PGS-13-Insoluble species ^{13}C:…..	182 ppm, 176 ppm, 99 ppm, 65 ppm, 62 ppm, 55 ppm, 48 ppm, 44 ppm, 29 ppm, 22 ppm, 20 ppm, 13 ppm, 7 ppm.
DMA-S (3-(dimethylamino)propylsilane, Silicycle) ^{15}N:……	No peaks detected.
DMA-S (3-(dimethylamino)propylsilane, Silicycle) ^{29}Si:……	-65 ppm, -74 ppm, -107 ppm, -116 ppm.
DMA-S (3-(dimethylamino)propylsilane, Silicycle) ^{13}C:……	61 ppm. 43 ppm, 20 ppm, 10 ppm.
SiO_2 #5 treated with triethylamine (TEA) ^{13}C:…….	55 ppm, 47 ppm, 5 ppm. Note: Peaks are well defined.
SiO_2 #5 treated with diisopropylethylamine DIPEA ^{13}C:…….....	69 ppm, 52 ppm, 45 ppm. Note: Peaks barely distinguishable from baseline

Appendix V

X-ray photoelectron spectroscopy data collected for various CO_2-responsive inorganic surfaces as presented in Chapter 5.

XPS measurements were conducted and interpreted by Dr. Gabriele Schatte of Queen's University, Kingston, Ontario, Canada. The XPS spectra were measured on a Microlab 310-F spectrometer equipped with an XR-4 twin anode (Al/Mg). The manufacturer of this system is VG Scientific. The samples were mounted on a stub-type stainless steel holder using double-sided adhesive Cu tape. The samples were kept under high vacuum (10^{-8} mbar) overnight inside the preparation chamber before they were transferred into the analysis chamber (10^{-9} mbar) of the spectrometer. The XPS data were collected using MgK_{α} radiation at 1253.6 eV (280 W, 14 kV) and a spherical sector analyser (SSA) operating in CAE (constant analyser energy) mode. Binding energies are referenced to the C1s peak at 285 eV. Survey spectra were recorded from -5 to 1000 eV at a pass energy of 40 eV (number of scans: 5) using an energy step size of 2 eV. High-resolution spectra were measured for C1s, O1s, N1s, Si2p and Br3d in the appropriate regions at a pass energy of 20 eV and an energy step size of 0.05 eV. The analysed area on the specimens is about 5×2 mm^2. At% reported as a function of the normalised peak area.

The following XPS data are provided as a detailed reference for the discussion regarding the analysis of amino-silane CO_2-responsive surfaces (SiO_2-S4) in Section 5.4.4.

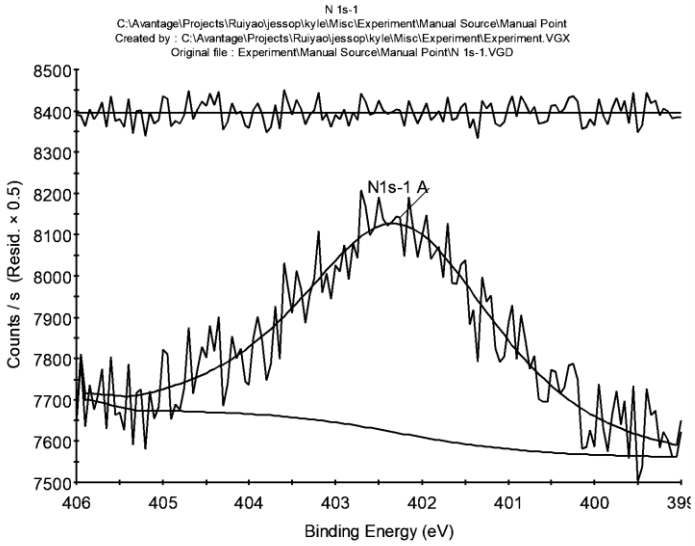

Figure AV.1. High-resolution N1s core-level XPS spectrum of an amino-silane functionalised wafer before the persistent hydrophobic phase was observed.

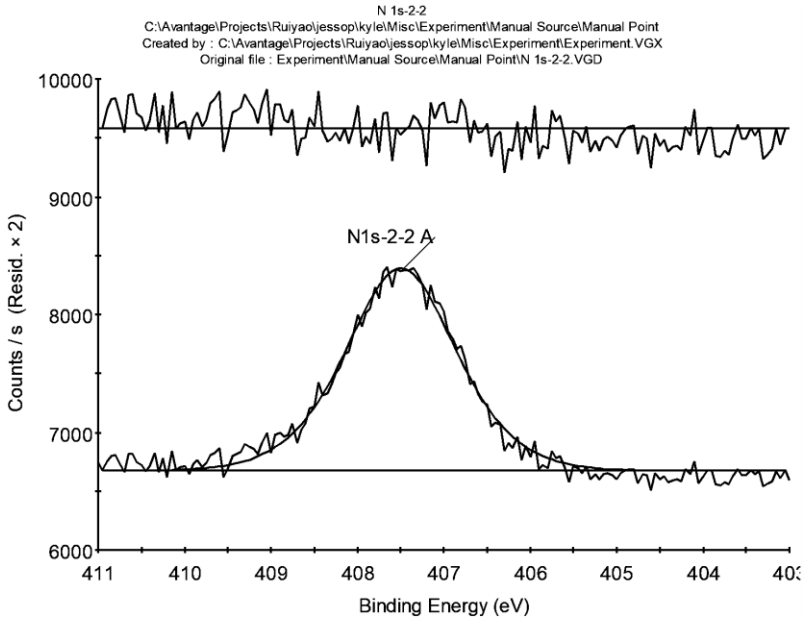

Figure AV.2. High-resolution N1s core-level XPS spectrum of an amino-silane functionalised wafer after the persistent hydrophobic phase was observed.

The following XPS data are provided as a detailed reference for the discussion regarding the analysis of CDI-mediated CO_2-responsive surfaces (SiO_2-S7) in Section 5.4.6.

Table AV.1. XPS peak analysis for CDI-14.

Peak	Peak BE	At%	Overall At%
C1s	284.92	73.26	
C1s A	286.23	14.69	21.39
C1s B	287.54	6.22	
C1s C	289.32	5.83	
N1s	402.75	47.68	
N1s A	400.82	39.19	0.63
N1s B	399.04	13.13	
O1s	532.74	88.10	
O1s A	531.36	6.41	45.64
O1s B	534.14	5.50	
Si2p3	102.51	17.54	
Si2p1	103.12	17.19	32.34
Si2p3 A	103.63	32.96	
Si2p1 A	104.24	32.31	

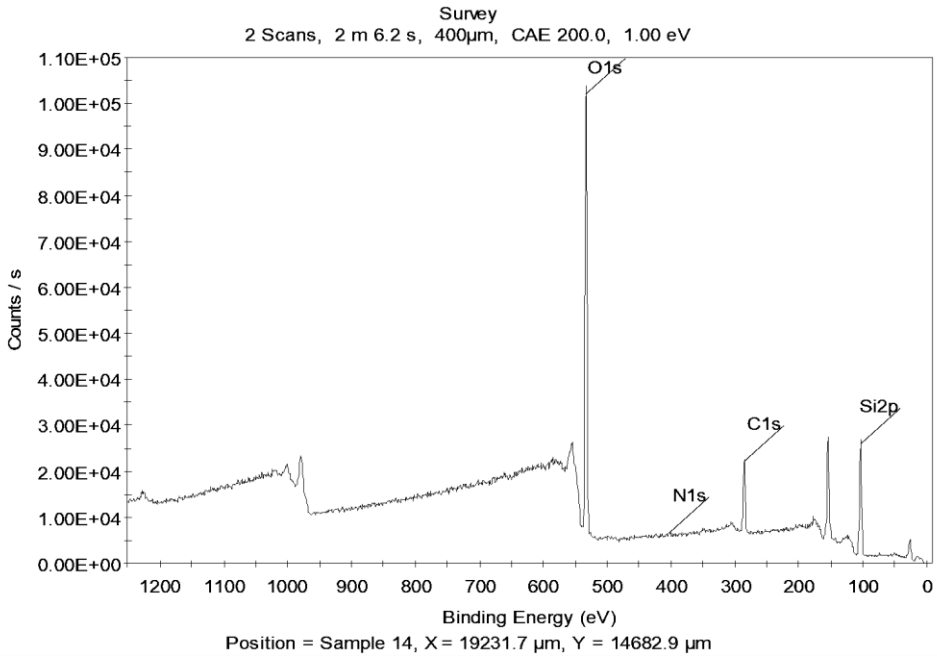

Figure AV.3. Survey spectrum of CDI-14.

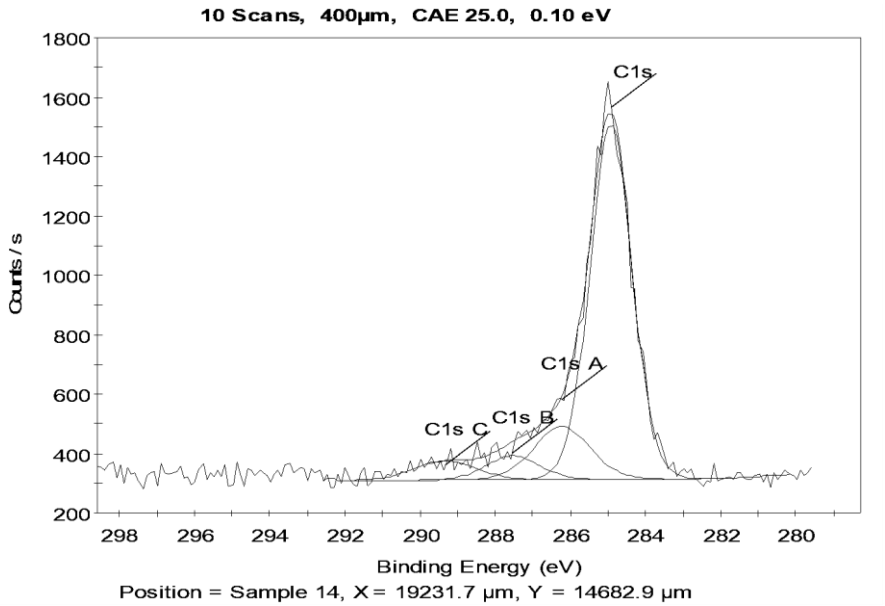

Figure AV.4. High-resolution C1s core-level XPS spectrum of CDI-14.

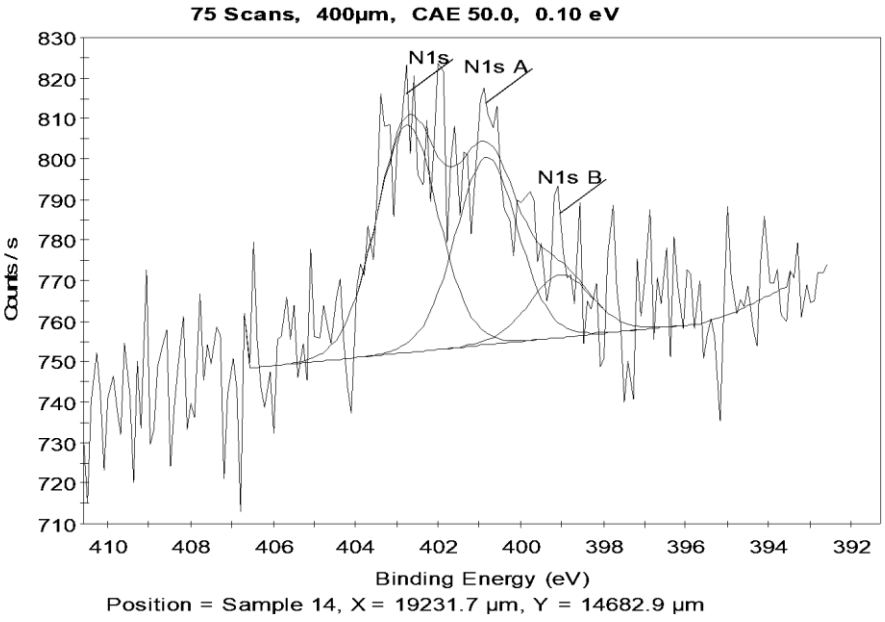

Figure AV.5. High-resolution N1s core-level XPS spectrum of CDI-14.

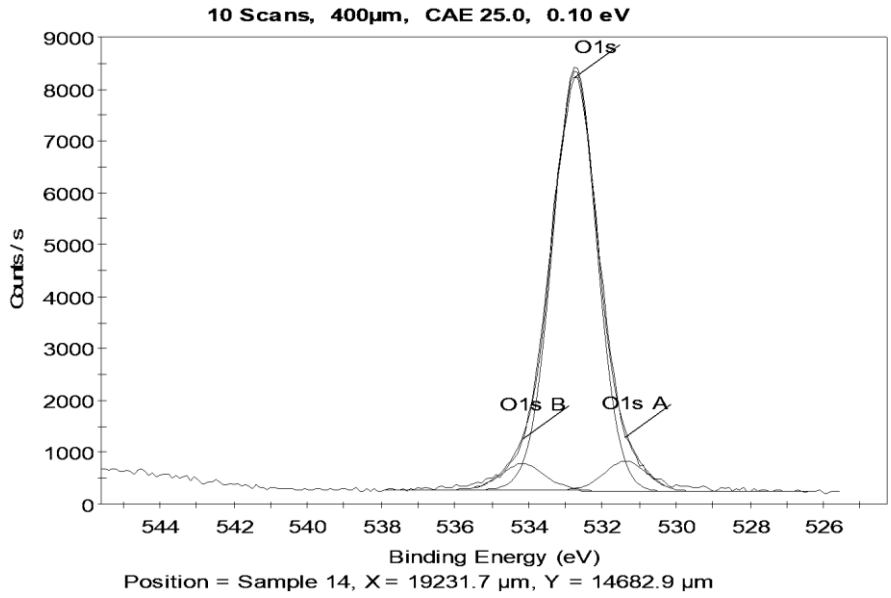

Figure AV.6. High-resolution O1s core-level XPS spectrum of CDI-14.

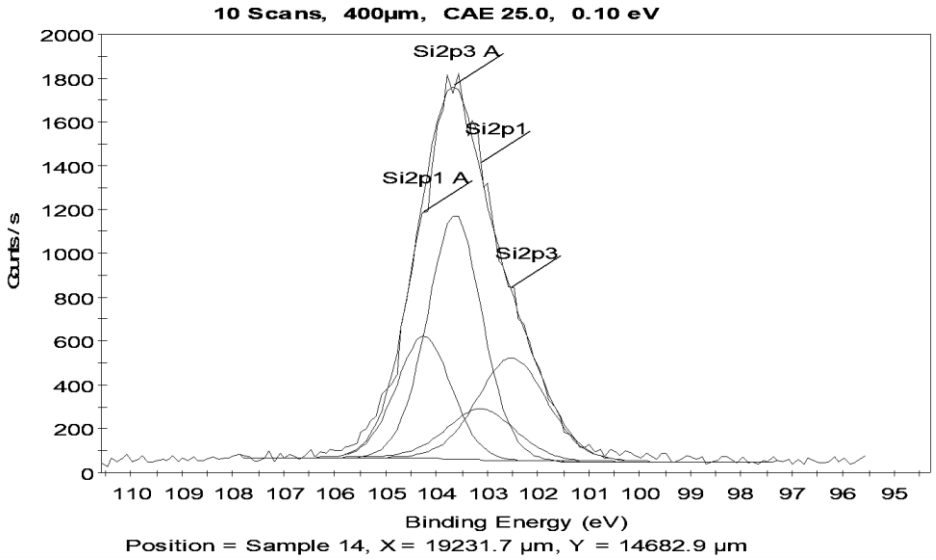

Figure AV.7. High-resolution Si2p core-level XPS spectrum of CDI-14.

Table AV.2. XPS peak analysis for CDI-15.

Peak	Peak BE	At%	Overall At%
C1s	285.01	82.06	
C1s A	286.61	9.79	24.19
C1s B	287.42	4.03	
C1s C	289.39	4.12	
N1s	402.56	37.67	
N1s A	400.60	38.69	0.53
N1s B	398.97	23.64	
O1s	532.71	86.83	
O1s A	531.21	5.36	43.52
O1s B	533.85	7.80	
Si2p3	102.42	14.05	
Si2p1	103.03	13.78	31.76
Si2p3 A	103.57	36.44	
Si2p1 A	104.18	35.73	

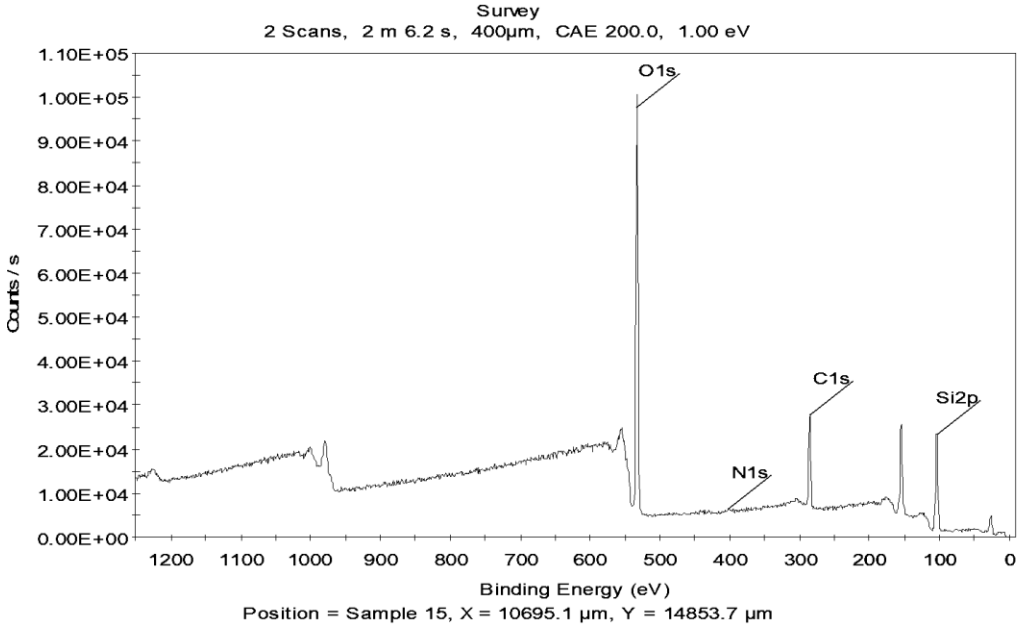

Figure AV.8. Survey spectrum of CDI-15.

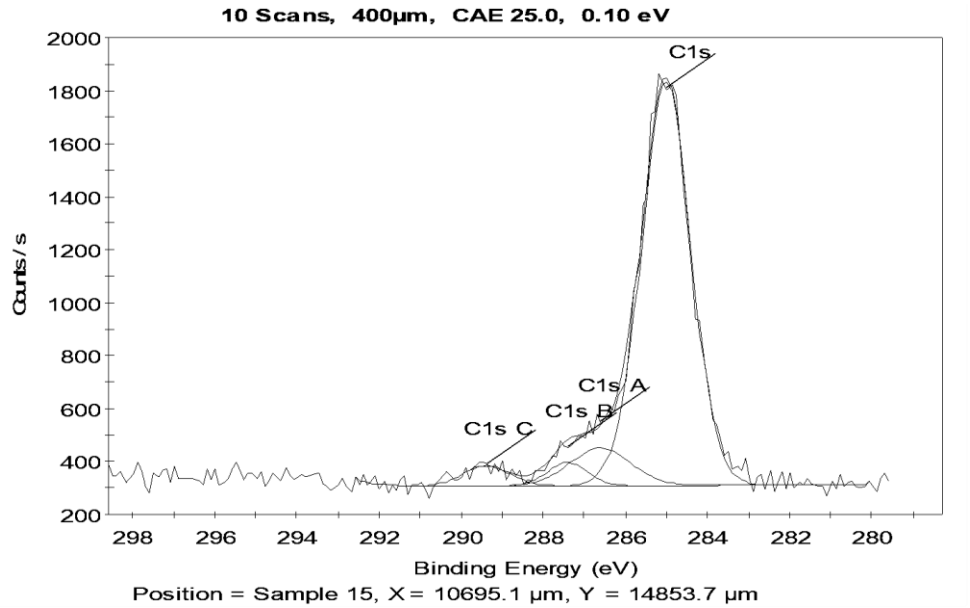

Figure AV.9. High-resolution C1s core-level XPS spectrum of CDI-15.

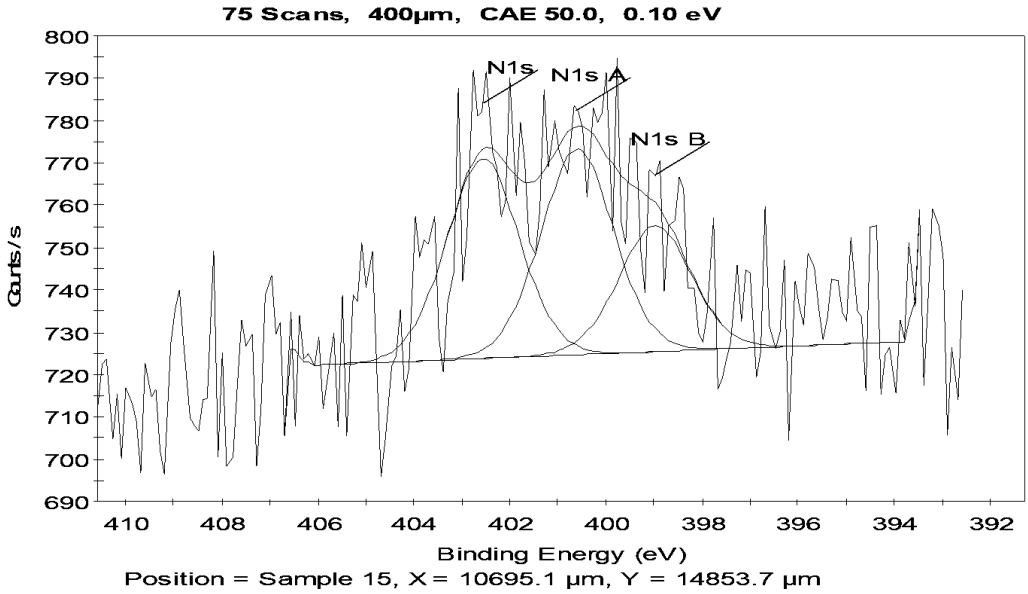

Figure AV.10. High-resolution N1s core-level XPS spectrum of CDI-15.

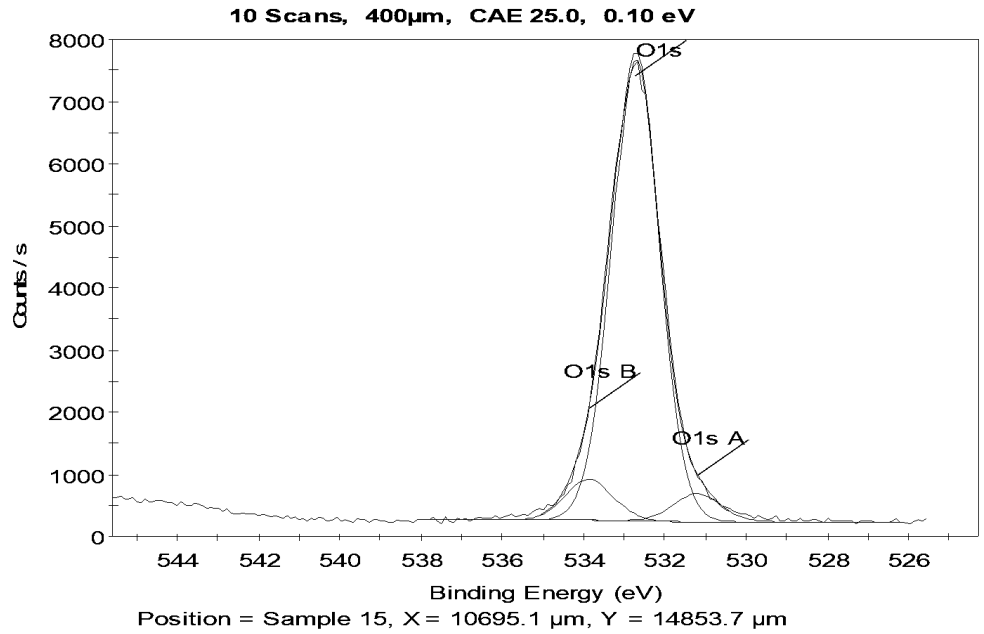

Figure AV.11. High-resolution O1s core-level XPS spectrum of CDI-15.

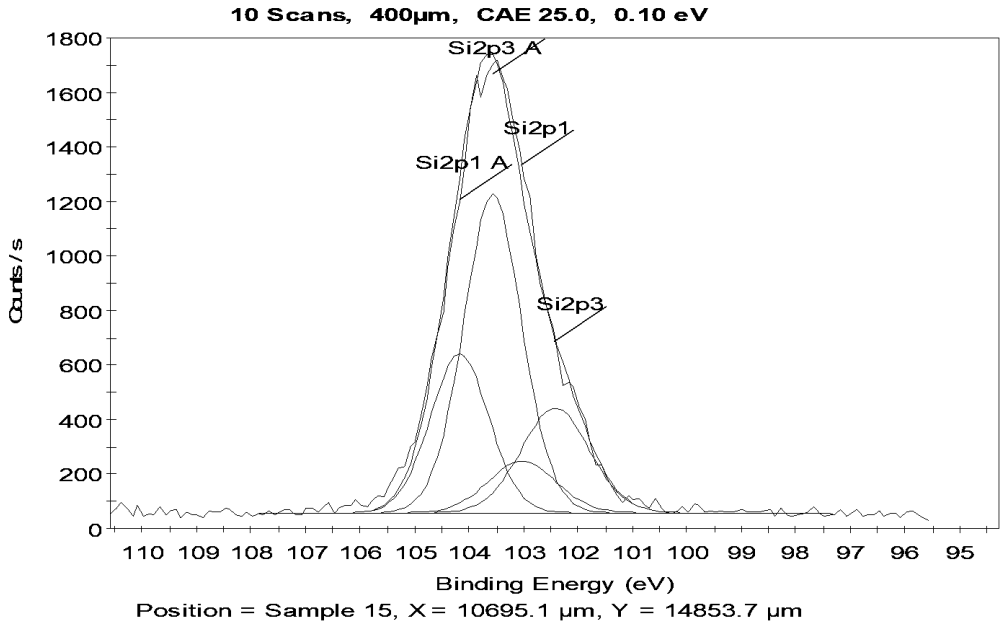

Figure AV.12. High-resolution Si2p core-level XPS spectrum of CDI-15.

The following XPS data are provided as a detailed reference for the discussion regarding the analysis of methyl chloroformate-mediated CO_2-responsive surfaces in Section 5.4.7.

The following analysis is specific to KBB5PG33:

Table AV.3. XPS peak analysis for sample KBB5PG33.

Peak	Sample A	Sample B	Sample C
Si2p	33.23	17.37	35.64
C1s	6.37	32.39	6.96
O1s	60.08	49.83	56.85
N1s	0.33	0.41	0.55

Sample A: Clean wafer, non-functionalised
Sample B: Wafer treated with MCF
Sample C: Wafer treated with MCF and DMAPA.

The following analysis is specific to KBB5PG48:

Table AV.4. XPS peak analysis for sample KBB5PG48.

Peak	Peak BE	At%
C1s	284.45	21.35
C1s A	285.7	2.64
C1s A	288.62	4.1
C1s B	290.03	2.68
N1s	-	0
O1s	533.04	28.97
O1s A	531.01	21.16
Si2p3	103.22	19.1

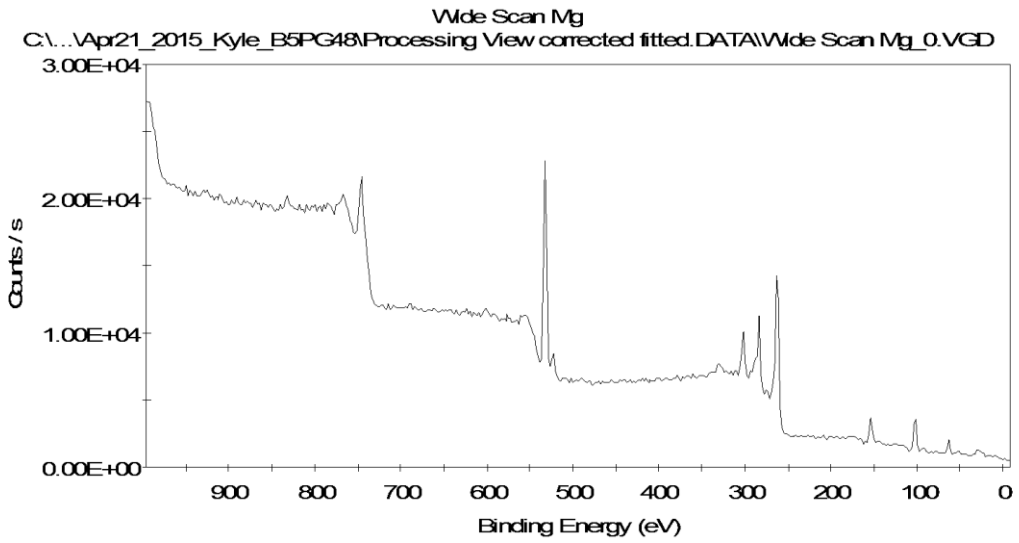

Figure AV.13. Survey spectrum of sample KBB5PG48.

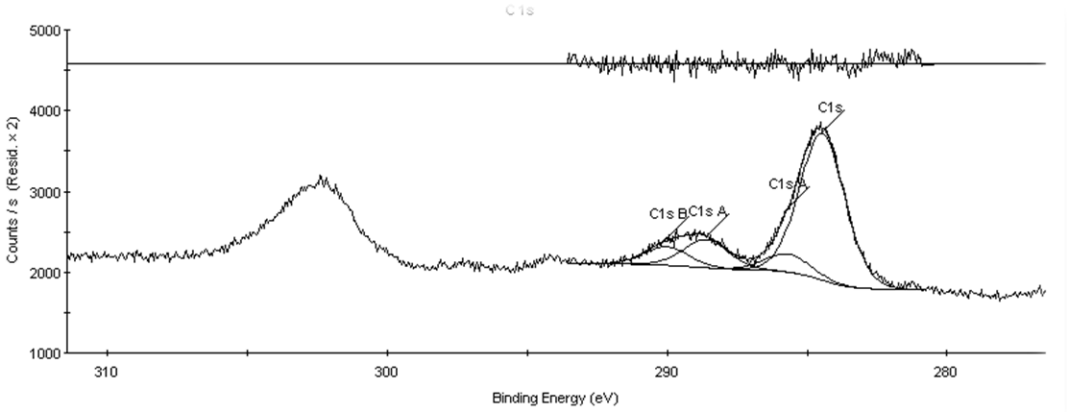

Figure AV.14. High-resolution C1s core-level XPS spectrum of sample KBB5PG48.

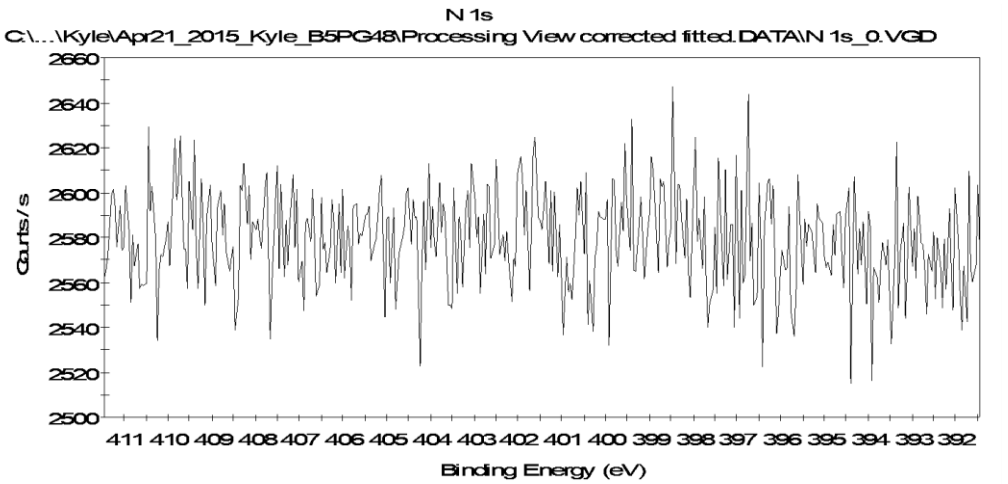

Figure AV.15. High-resolution N1s core-level XPS spectrum of sample KBB5PG48.

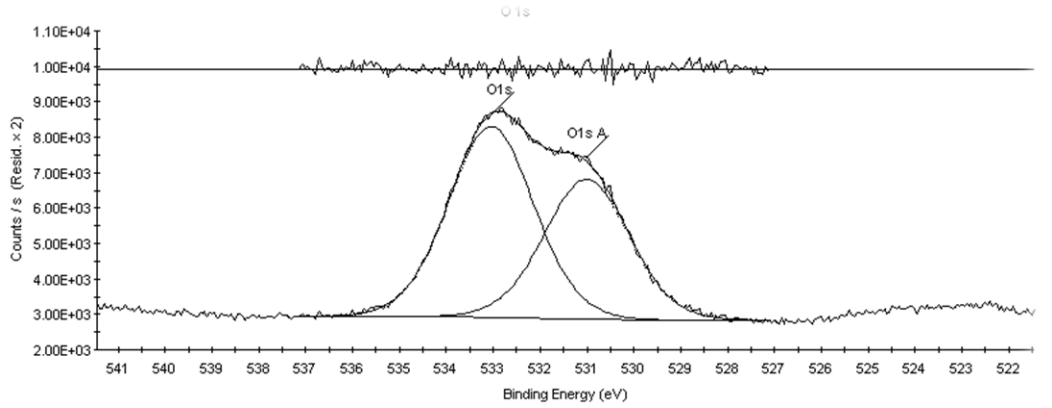

Figure AV.16. High-resolution O1s core-level XPS spectrum of sample KBB5PG48.

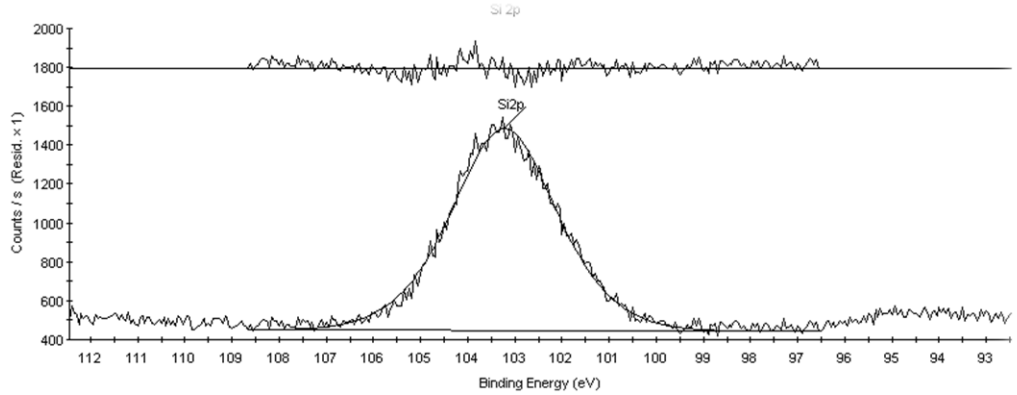

Figure AV.17. High-resolution Si2p core-level XPS spectrum of sample KBB5PG48.

The following XPS data were collected and interpreted by Dr. Rana Sodhi of Surface Interface Ontario, located at the University of Toronto, Ontario, Canada. The data was collected using a Thermo Scientific K-Alpha spectrometer. The following XPS data are provided as a detailed reference for the discussion regarding the analysis of ethyl chloroformate-mediated CO_2-responsive surfaces in Section 5.4.7.

The following analysis is from KBB6PG41:

Table AV.5. XPS peak analysis for sample KBB6PG41.

Peak	Sample A	Sample B	Sample C
Si2p	31.98	31.38	12.97
C1s	8.86	11.09	44.92
O1s	58.56	56.93	30.68
N1s	0.56	0.57	5.68

Sample A: Clean wafer, non-functionalised.
Sample B: Wafer treated with ECF Wafer treated with ECF and API
Sample C: Wafer treated with ECF and API

The following XPS measurements were conducted and interpreted by Dr. Gabriele Schatte of Queen's University, Kingston, Ontario, Canada. The XPS spectra were measured on a Kratos Nova AXIS spectrometer equipped with an Al X-ray source. The samples were mounted on a coated aluminium plate using double-sided adhesive Cu tape and were kept under high vacuum (10^{-8} Torr) overnight inside the preparation chamber before they were transferred into the analysis chamber (ultra-high vacuum, 10^{-9} Torr) of the spectrometer. The XPS data were collected using AlK_{α} radiation at 1486.69 eV (150 W, 15 kV), charge neutralizer and a delay-line detector (DLD) consisting of three multi-channel plates. Binding energies are referenced to the C1s peak at 285 eV. Survey spectra were recorded from -5 to 1200 eV at a pass energy of 160 eV (number of sweeps: 1) using an energy step size of 1 eV and a dwell time of 100 ms. High resolution spectra for O1s, N1s, C1s and Si2p were recorded in the appropriate regions at a pass energy of 20 eV (number of sweeps: O1s, 5; N1s, 20; C1s, 5; Si2p, 10) using a dwell time of 300 s and energy step sizes of 0.1 eV and 0.05 eV (N1s), respectively. The analysed area on the specimens was about 300 × 700 μm^2 (lens mode: FOV 1) at this position.

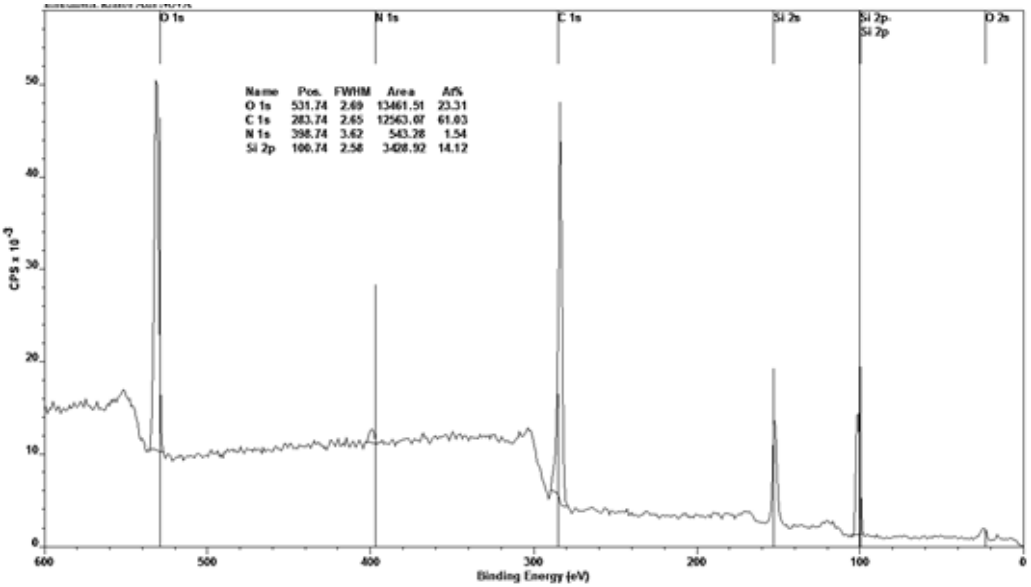

Figure AV.18. Survey spectrum of SiO_2-S15.

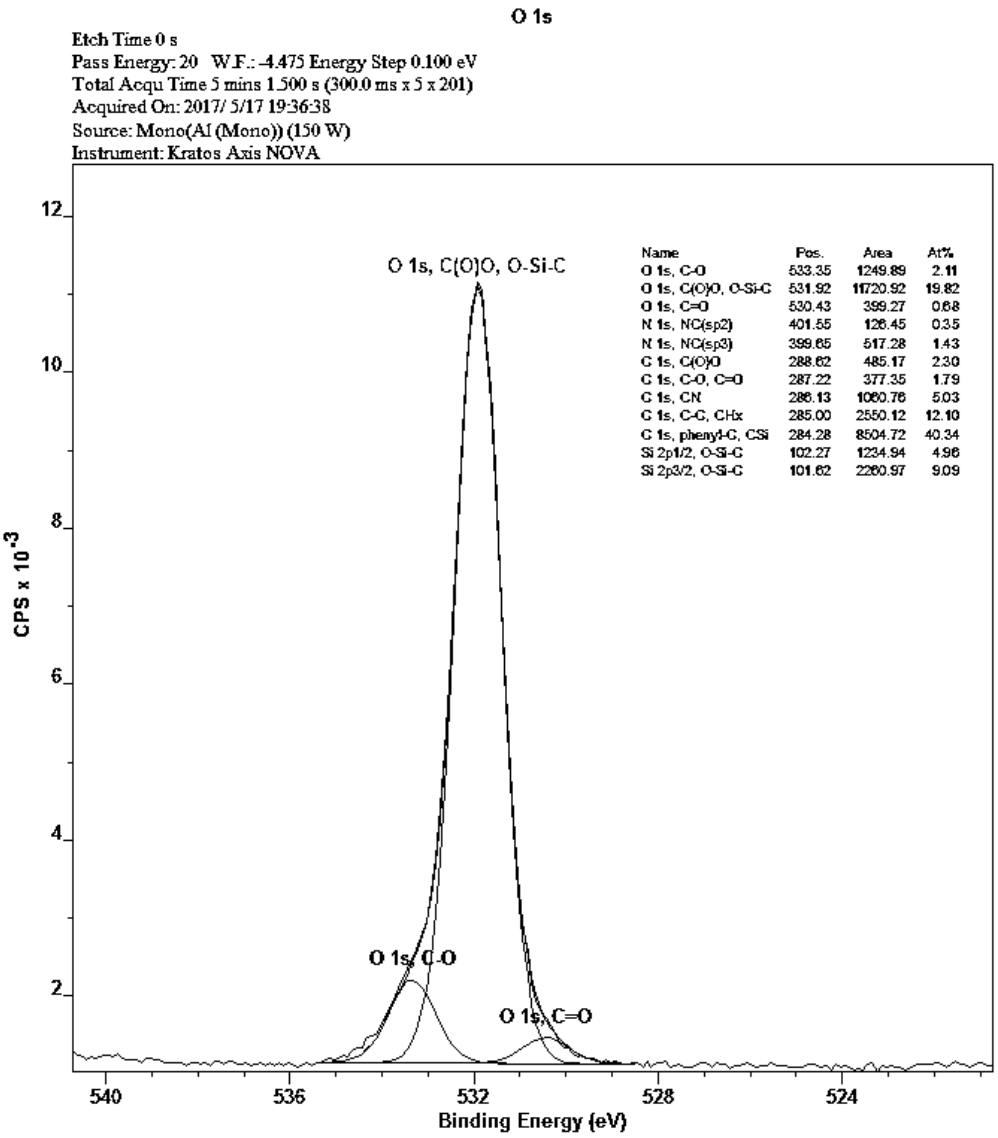

Figure AV.19. High-resolution O1s core-level XPS spectrum of SiO_2-S15.

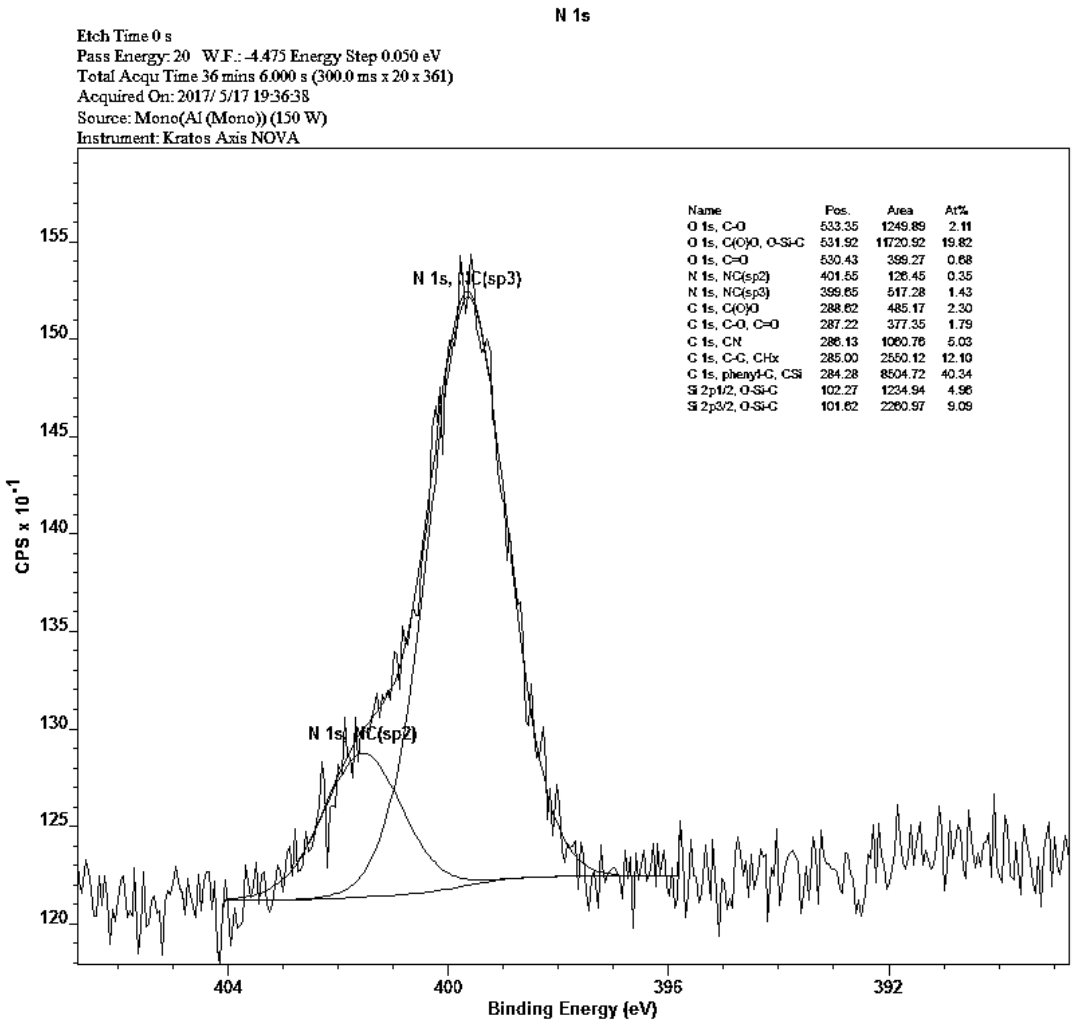

Figure AV.20. High-resolution N1s core-level XPS spectrum of SiO_2-S15.

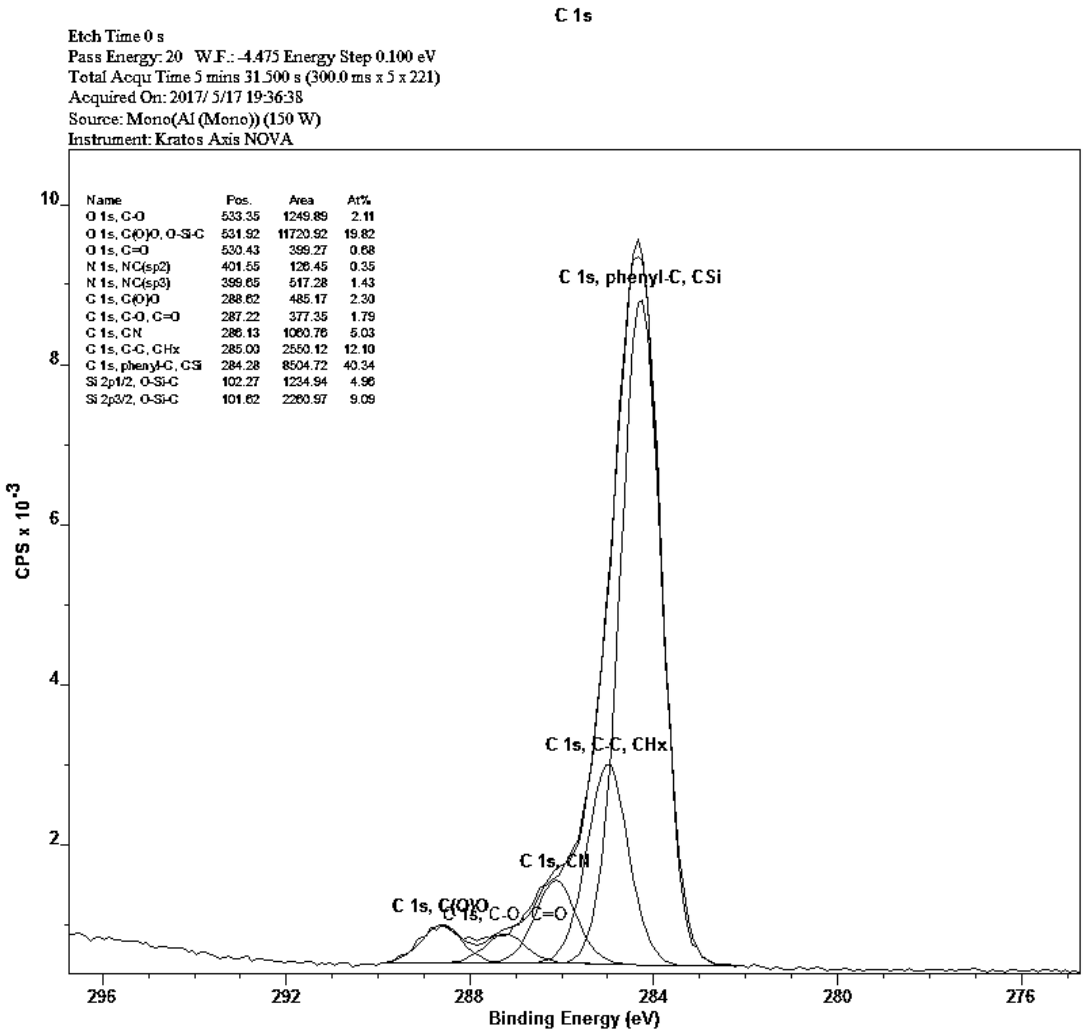

Figure AV.21. High-resolution C1s core-level XPS spectrum of SiO_2-S15.

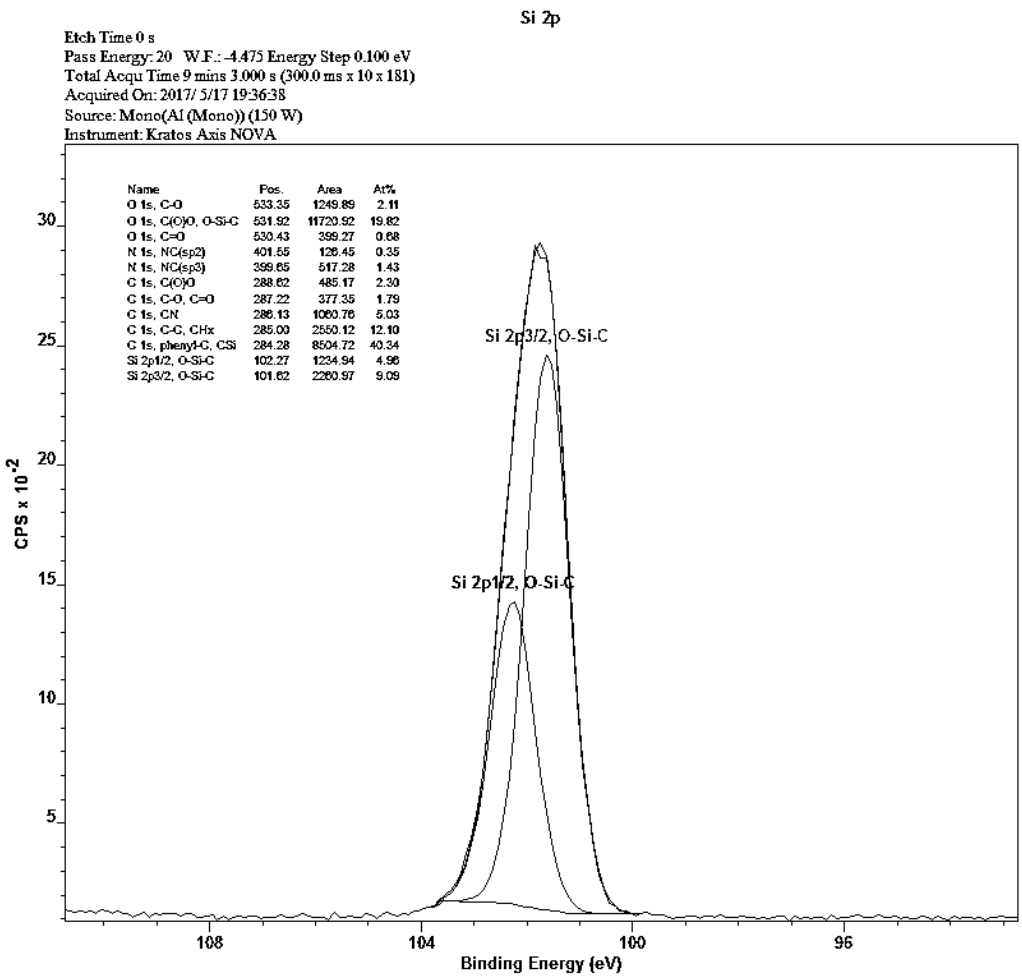

Figure AV.22. High-resolution Si2p core-level XPS spectrum of SiO_2-S15.

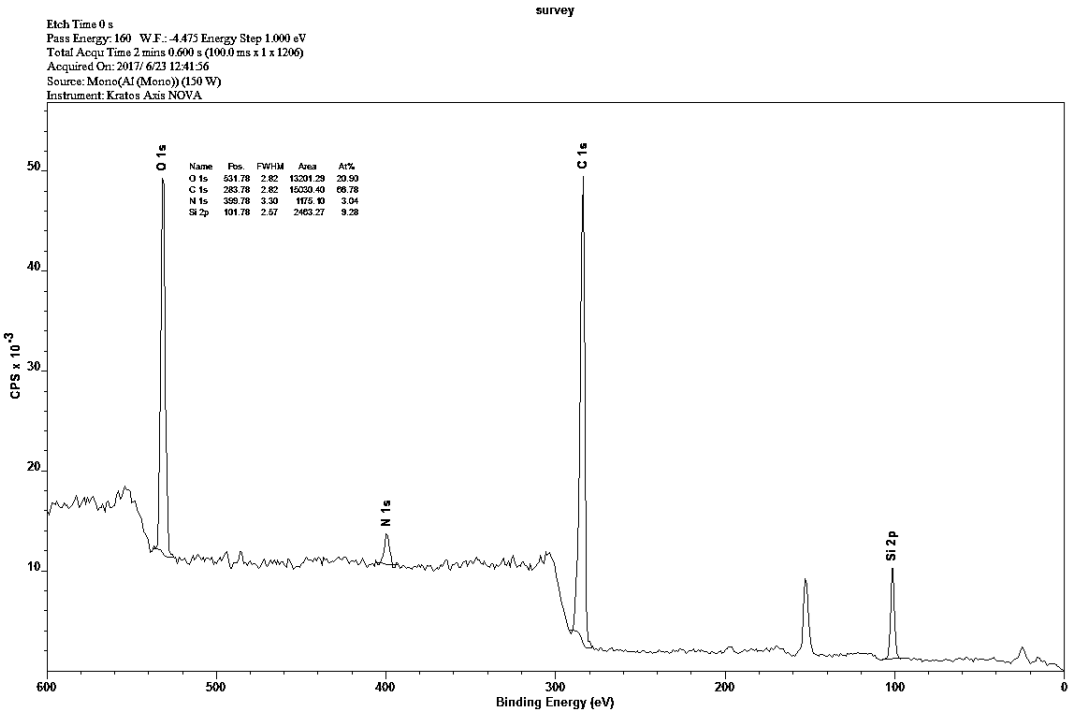

Figure AV.23. Survey spectrum of SiO_2-S16.

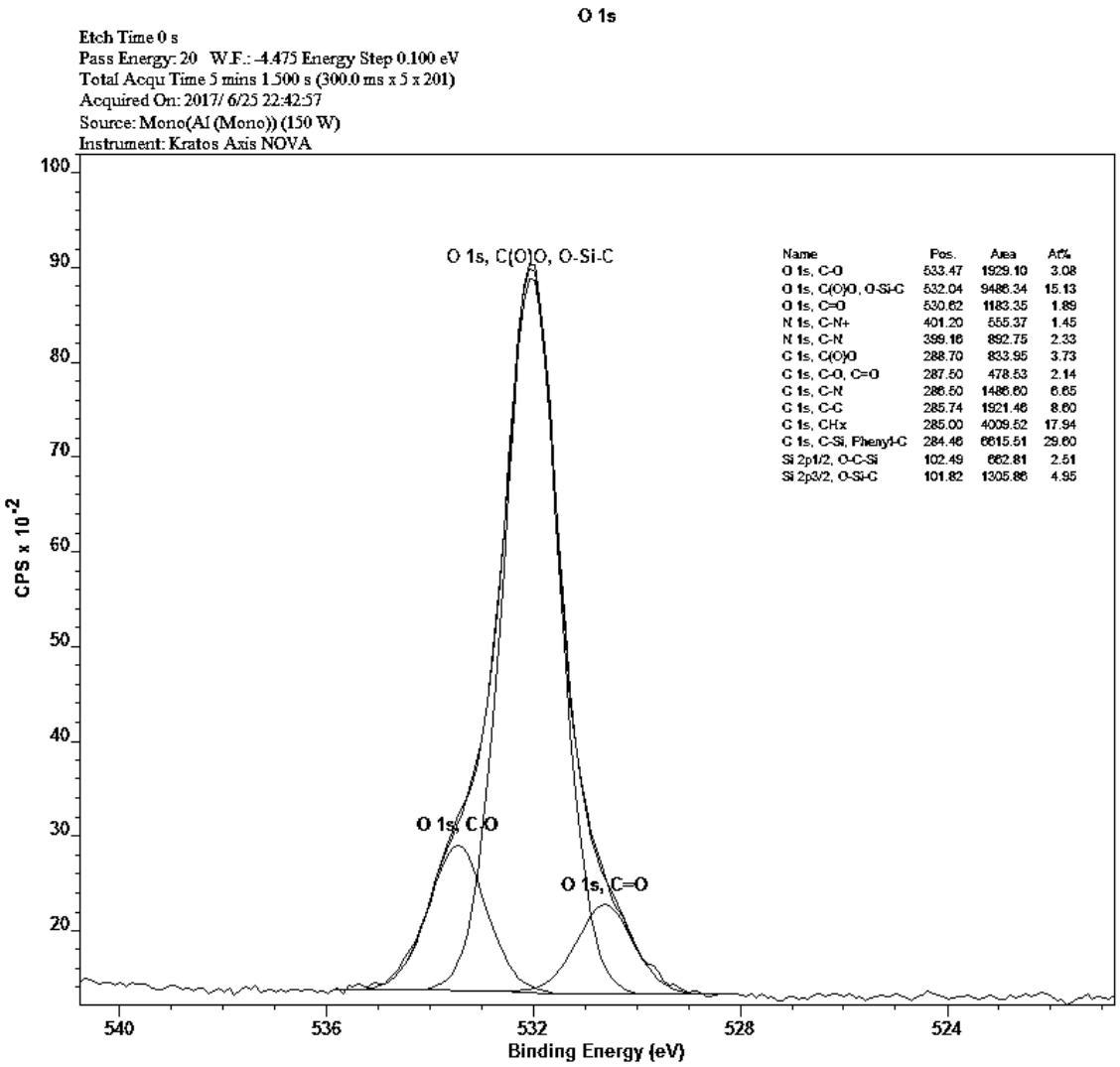

Figure AV.24. High-resolution O1s core-level XPS spectrum of SiO_2-S16.

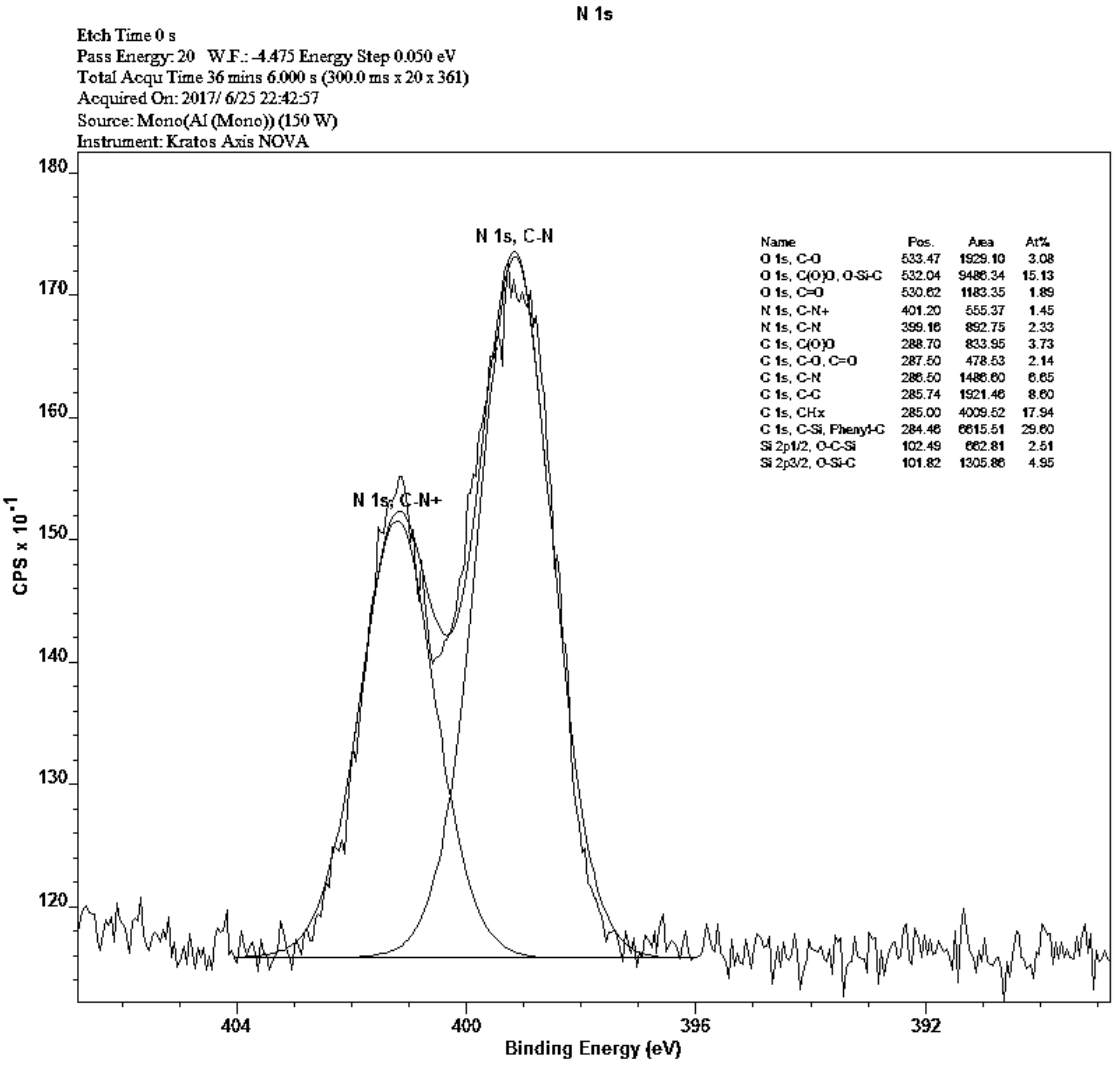

Figure AV.25. High-resolution N1s core-level XPS spectrum of SiO_2-S16.

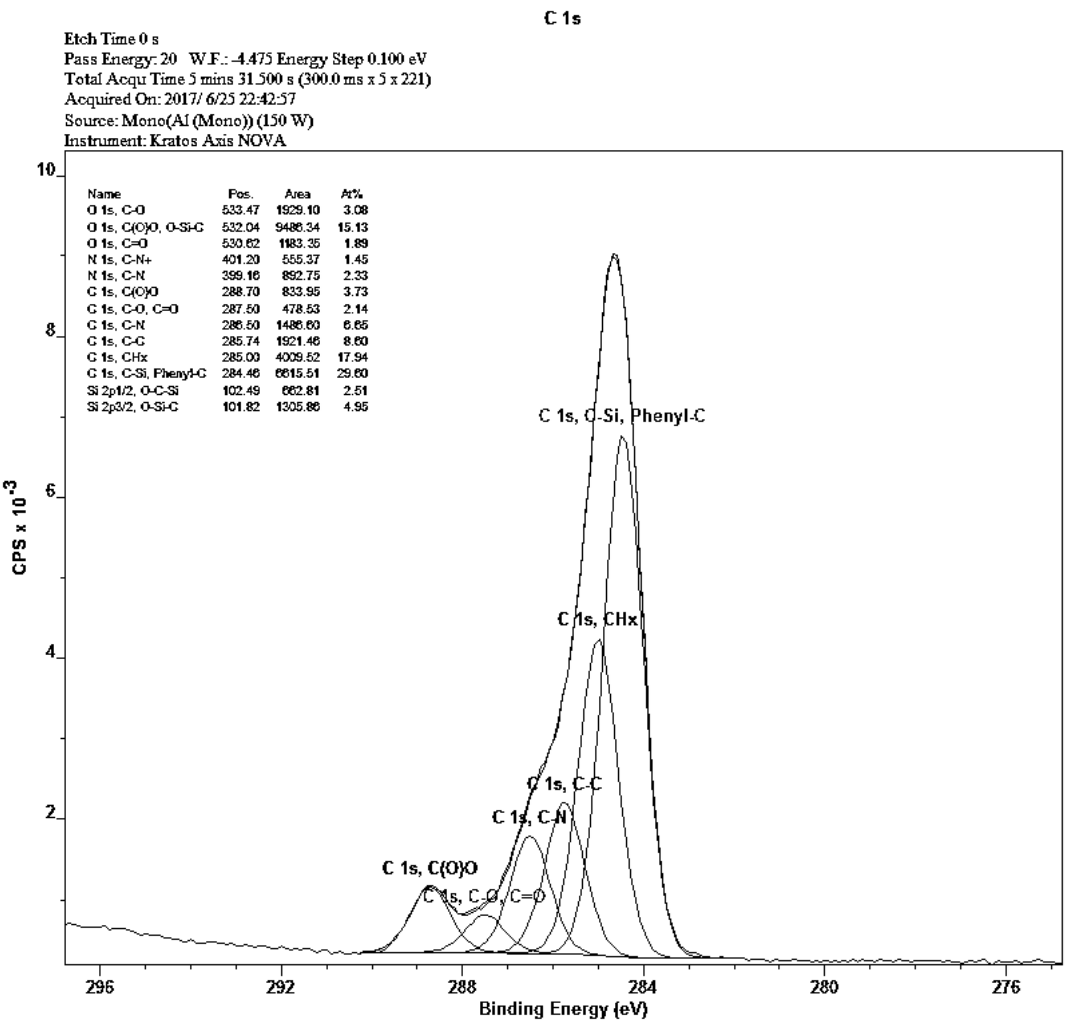

Figure AV.26. High-resolution C1s core-level XPS spectrum of SiO_2-S16.

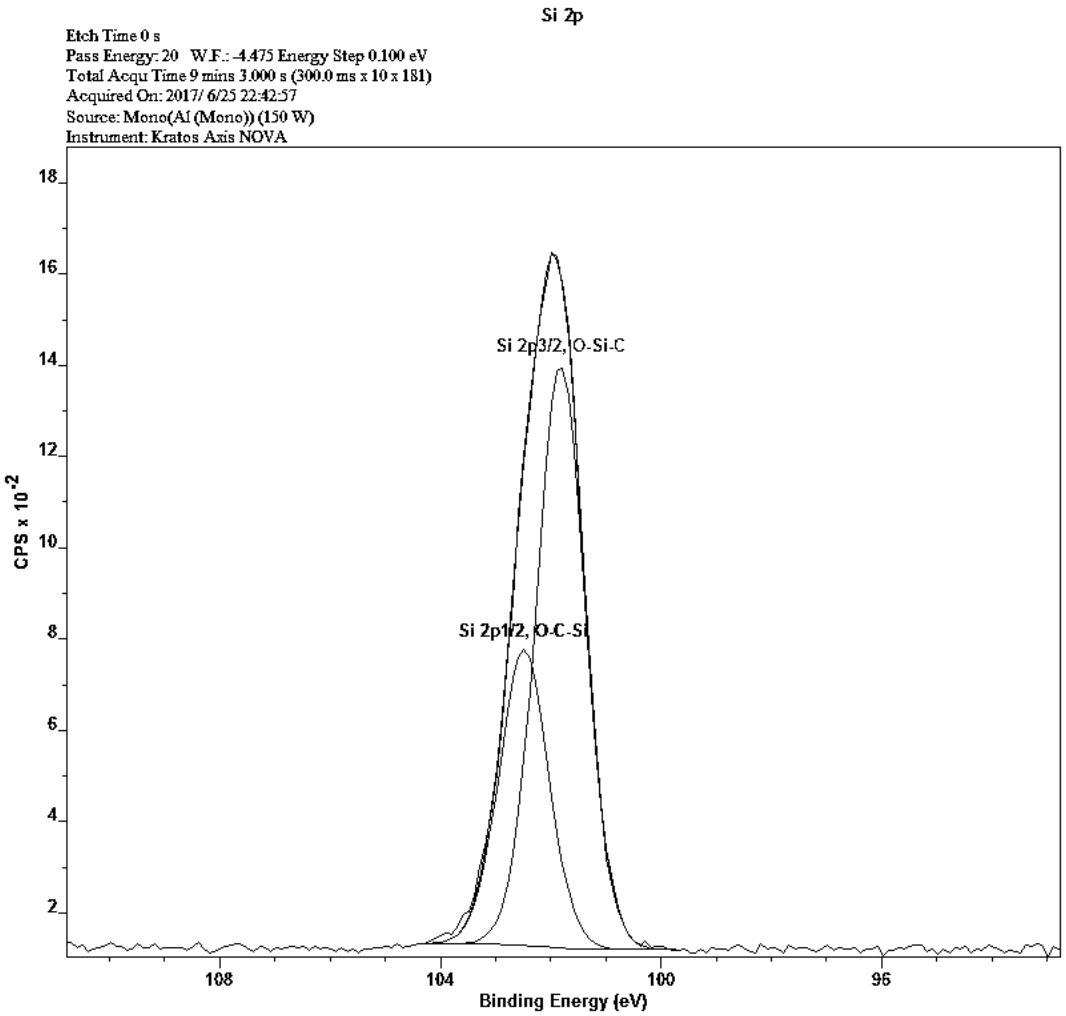

Figure AV.27. High-resolution Si2p core-level XPS spectrum of SiO_2-S16.

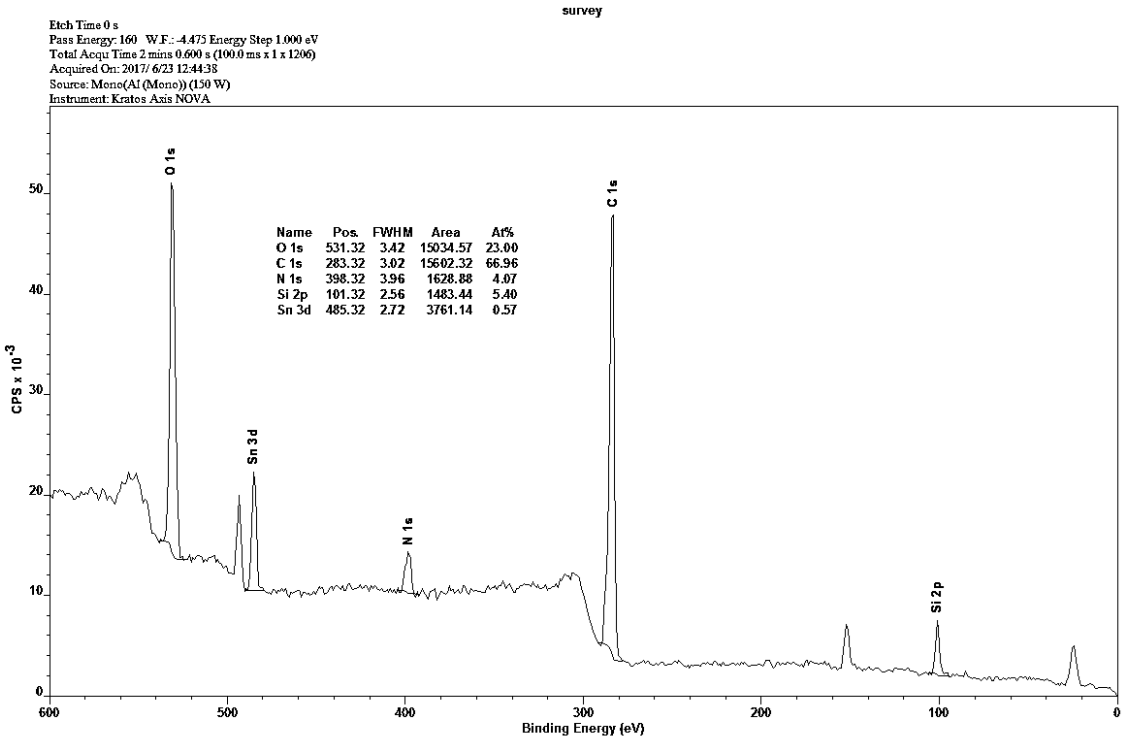

Figure AV.28. Survey spectrum of SiO_2-S17.

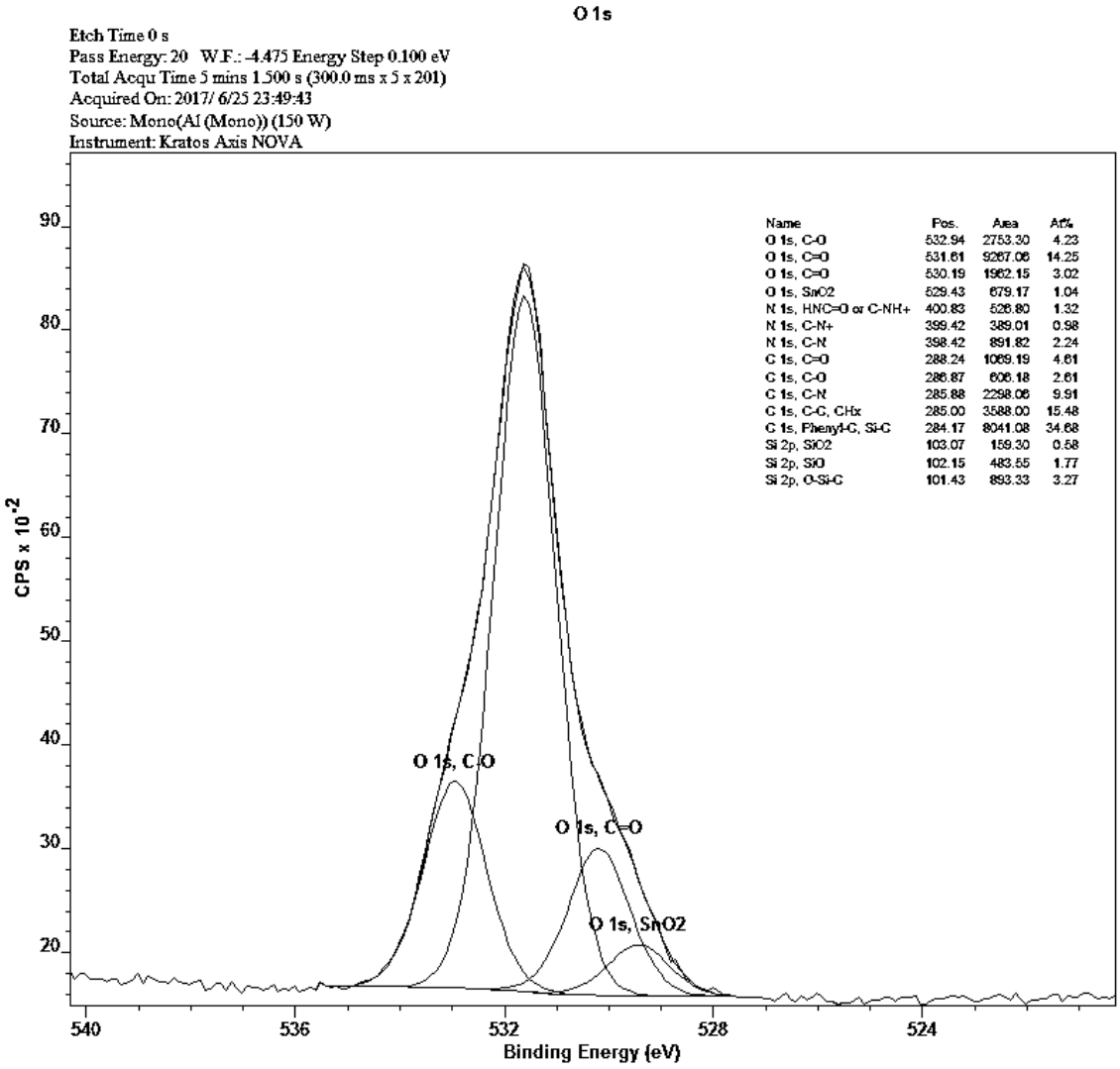

Figure AV.29. High-resolution O1s core-level XPS spectrum of SiO_2-S17.

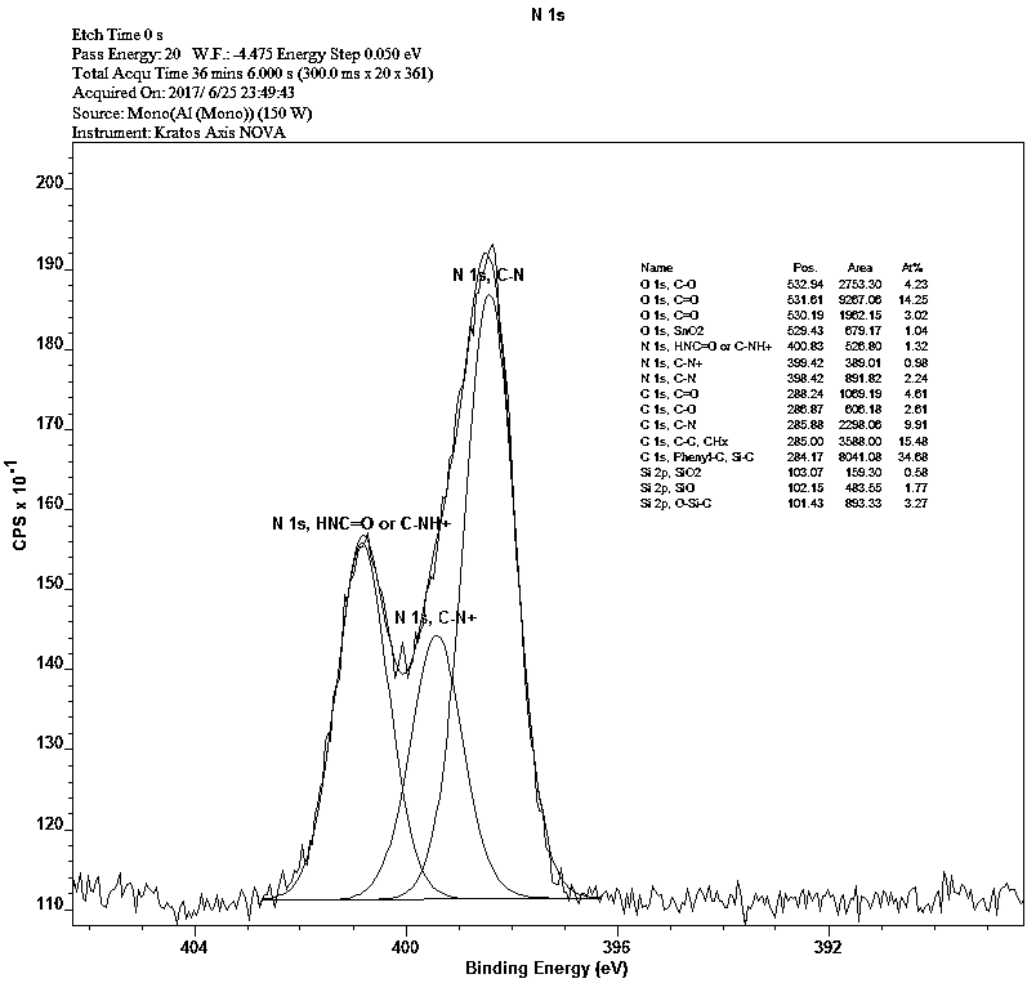

Figure AV.30. High-resolution N1s core-level XPS spectrum of SiO_2-S17.

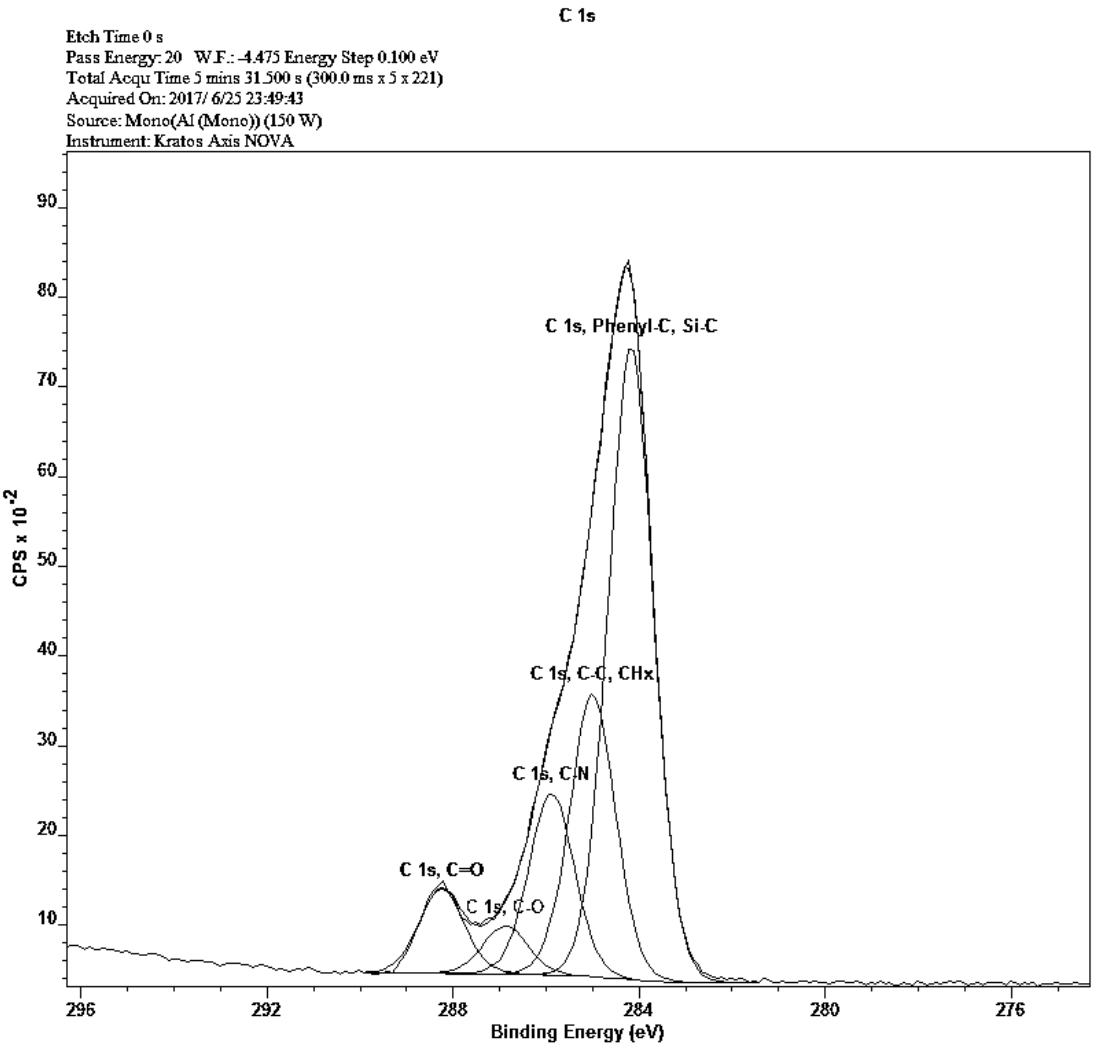

Figure AV.31. High-resolution C1s core-level XPS spectrum of SiO_2-S17.

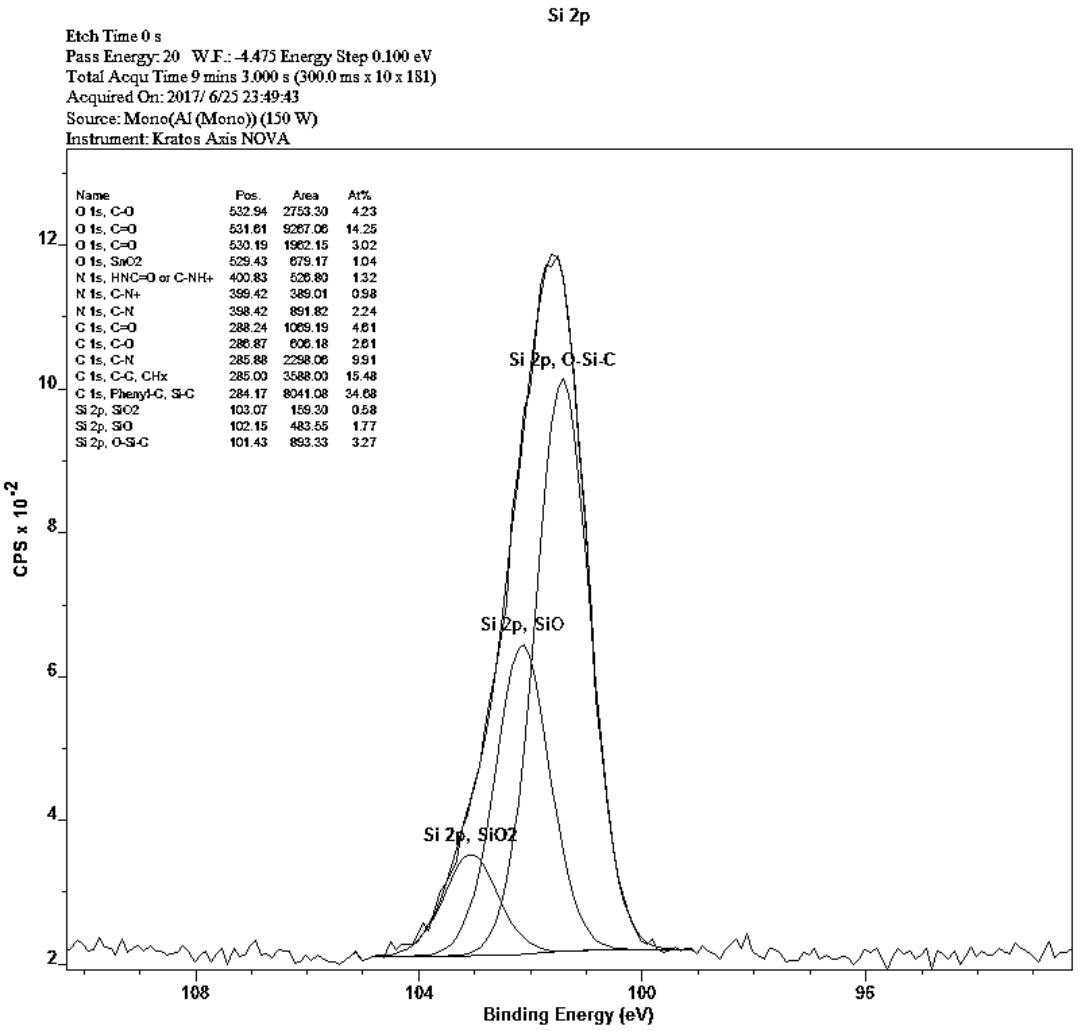

Figure AV.32. High-resolution Si2p core-level XPS spectrum of SiO_2-S17.

Appendix VI

Investigations of CO_2-responsive polysaccharide surfaces

CO_2-responsive single-unit functionalized filter paper

Two methods were evaluated using CDI-mediated coupling for nonanoic acid and the filter paper surface (Schemes AVI.1 and AVI.2). It was observed that the order in which reagents were coupled was vital to the formation of a waxy-surface. The waxy-surface (FP-I) was formed when CDI was combined with nonanoic acid first, then subsequently introduced to the filter paper. When CDI was combined with the filter paper first, FP-II was formed. Subsequent treatment of FP-II with nonanoic acid failed to produce a waxy surface (FP-I).

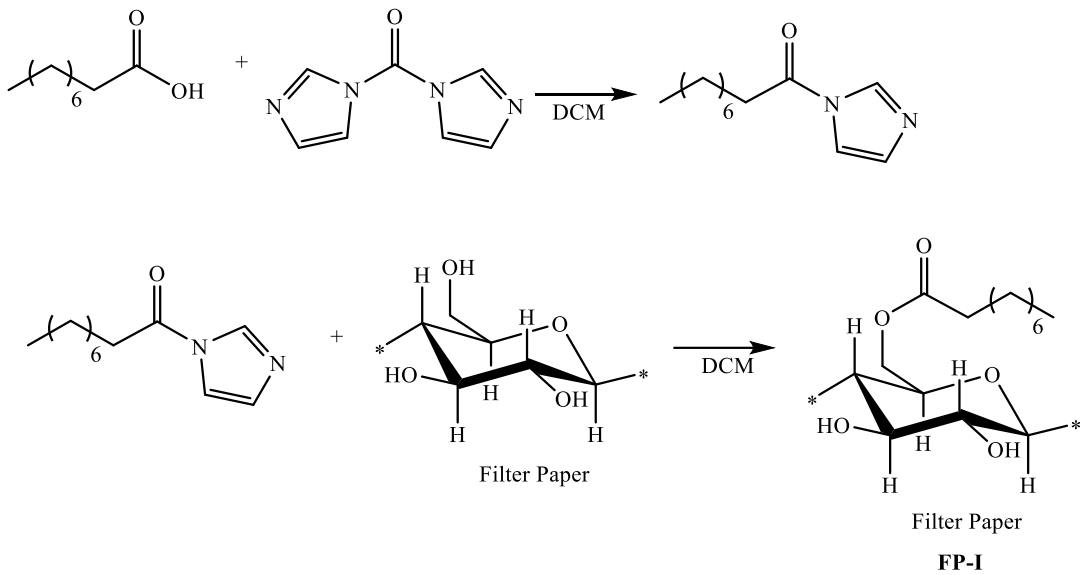

Scheme AVI.1. Hydrophobic functionalisation of filter paper via CDI-mediated coupling with nonanoic acid.

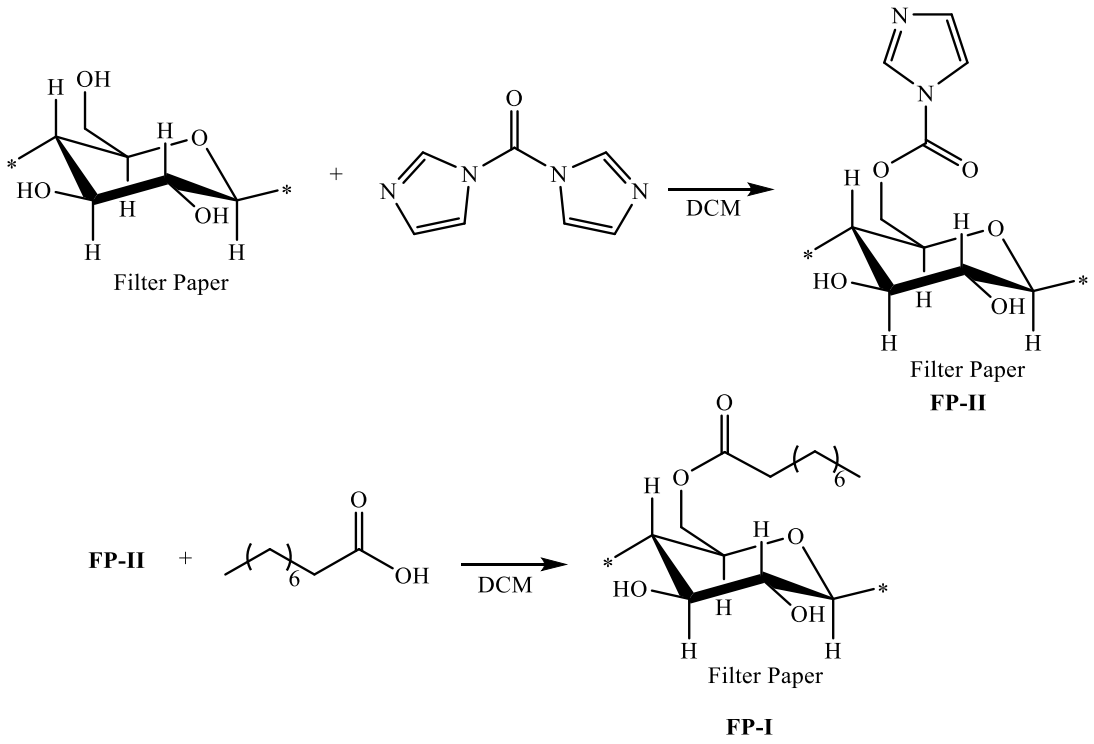

Scheme AVI.2. Failed hydrophobic functionalisation of filter paper via CDI-mediated coupling with nonanoic acid.

WCA analysis of the functionalised filter paper (FP-I) indicated that the waxy surface was hydrophobic and oleophilic, whereas the untreated filter paper was hydrophilic and oleophilic (Table AVI.1). A hydrophobic water contact angle of 117° was observed. This experiment served as a proof of concept that CDI-mediated coupling was compatible with filter paper when coupling to the filter paper surface was performed last (Scheme AVI.3).

Table AVI.1. Contact angle analysis of hydrophobic filter paper (FP-I) and native filter paper.

	Probe Liquid for Contact Angle Analysis	
	Water Droplet	Hexadecane Droplet
Native Filter Paper	 Superhydrophilic	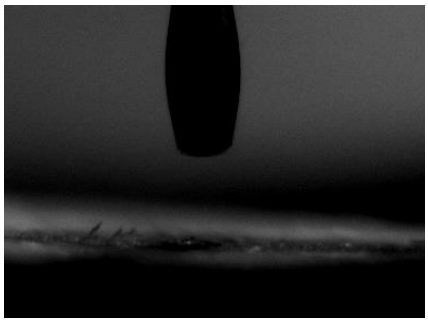 Superoleophilic
Waxy Filter Paper	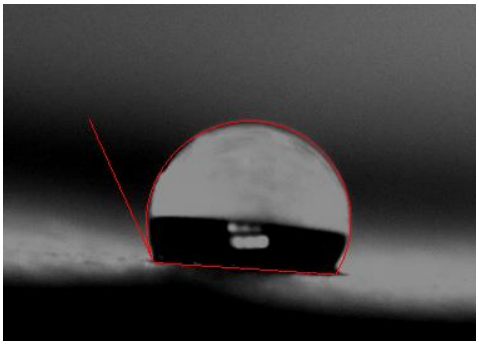 117˚ Hydrophobic	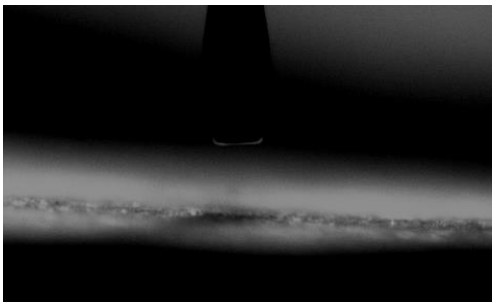 Superoleophilic

Variations on CDI-mediated coupling were applied to the synthesis of CO_2-responsive single-unit functionalised polysaccharide surfaces (Schemes AVI.4 to AVI.6). Functionalised filter paper surfaces failed to exhibit a response to CO_2. WCA analysis of the functionalised filter paper surfaces revealed hydrophilic and oleophilic behaviour that is consistent with native cellulose. It is possible that functionalisation failed; attenuated total reflectance Fourier transform infrared (ATR-FTIR) spectroscopy was not helpful in determining whether functionalisation occurred. The expected IR peaks associated with the CO_2-responsive functionalities are not that different from native

cellulose. It is possible that ATR-FTIR spectroscopy would fail to differentiate native cellulose from functionalised cellulose (FP-IV, -V, -VI) owing to the low degree of substitution that is expected. Additionally, it is possible that the functionalised surfaces remained charged and were thus hydrophilic. It is unknown whether the charged surface, at a low degree of substitution, would exhibit oleophilic properties. Thus, CA analysis with hexadecane was not helpful in determining whether functionalisation occurred.

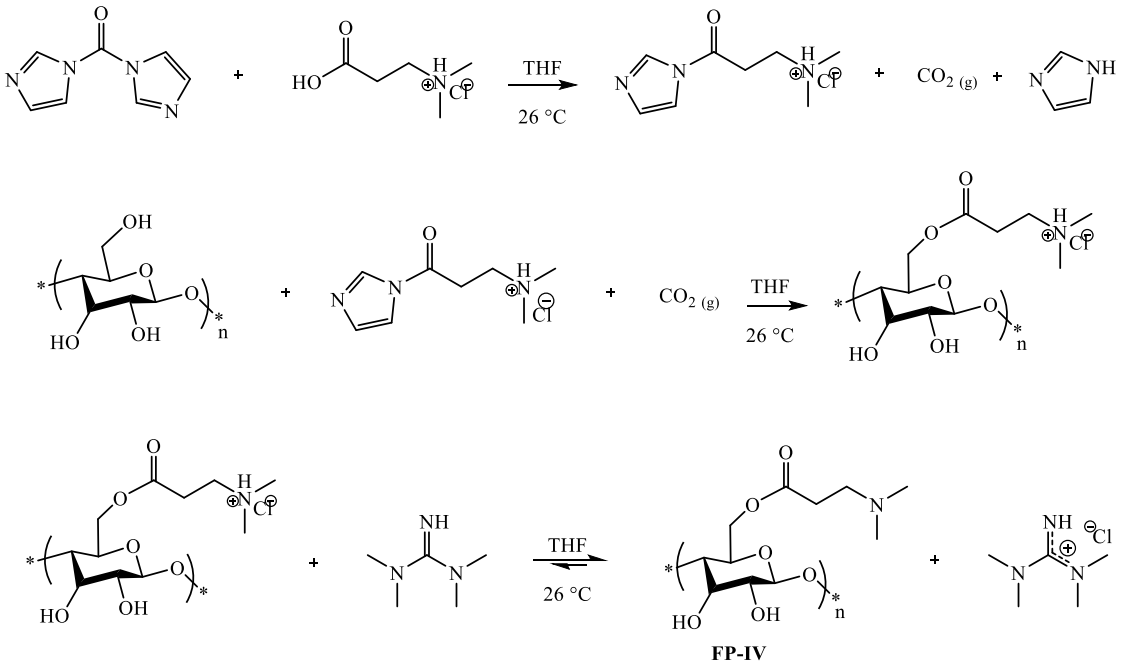

Scheme AVI.4. CDI-mediated coupling method 1.

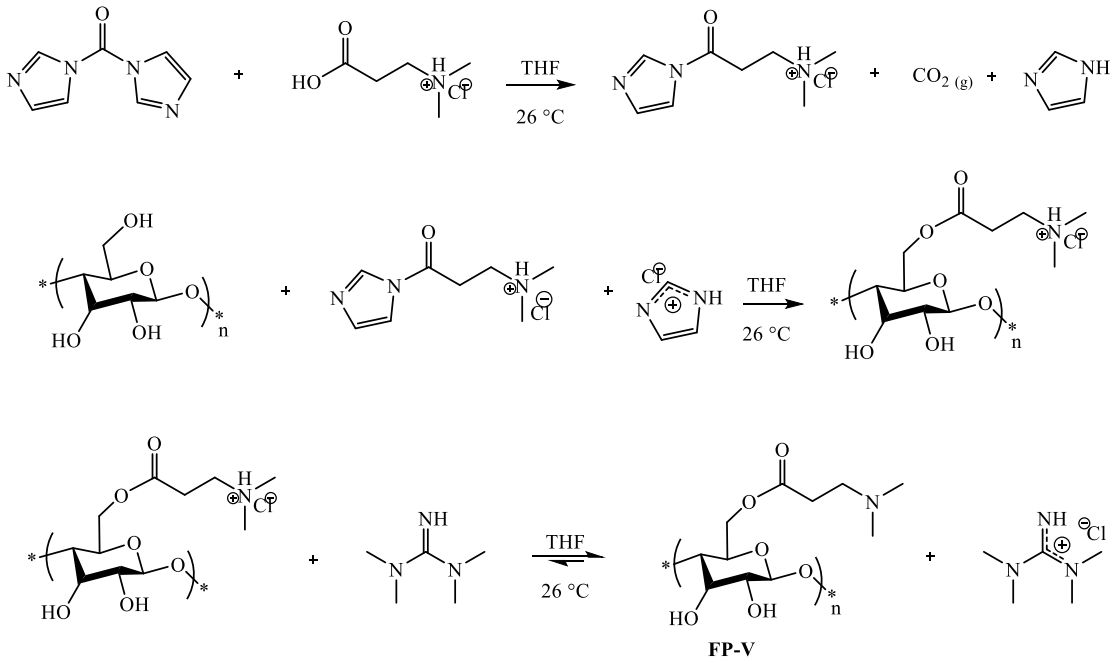

Scheme AVI.5. CDI-mediated coupling method 2.

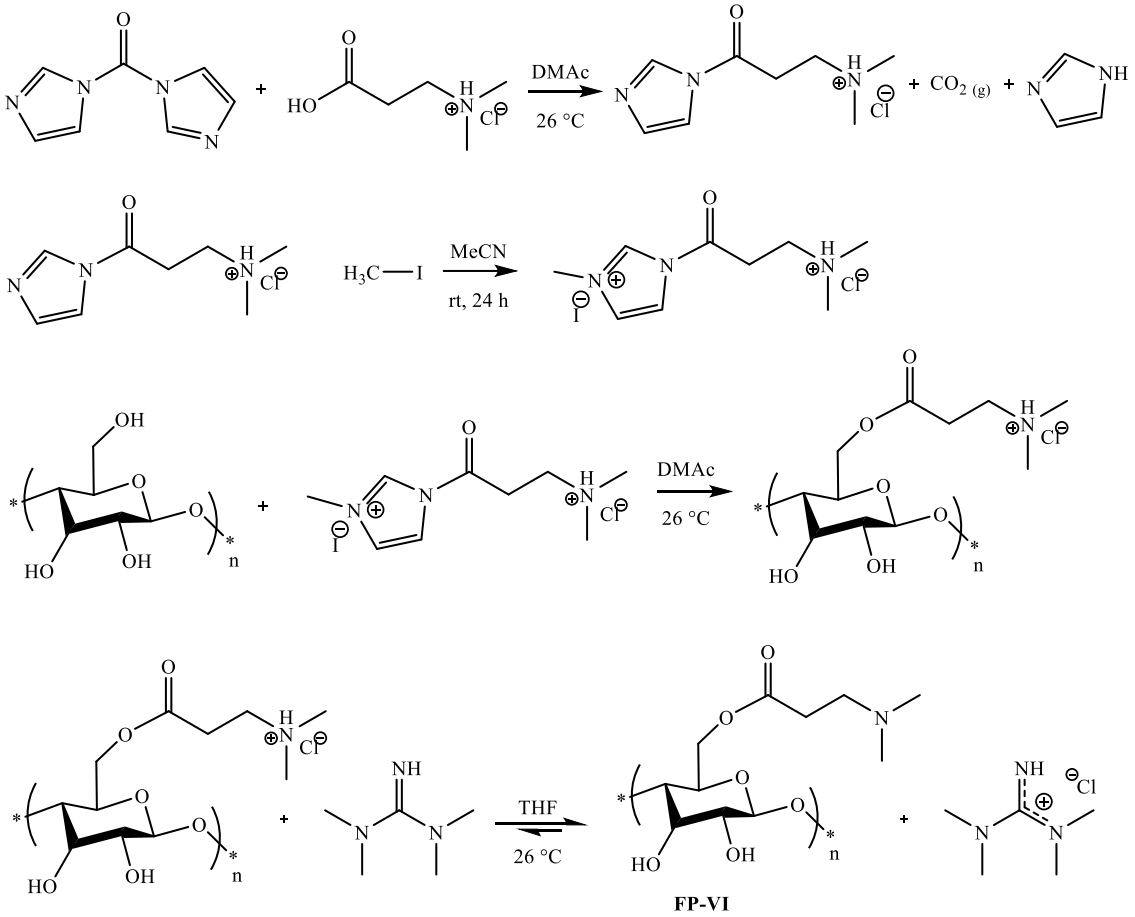

Scheme AVI.6. CDI-mediated coupling method 3.

The CDI-mediated coupling methods in Schemes AVI.4 to AVI.6 failed to produce a CO_2-responsive polysaccharide surface. Further work on single-unit functionalisation method development was abandoned for more promising polymeric functionalisation techniques.

Synthesis of CO_2-responsive single-unit functionalized starch fibers

Synthetic method 1:

Starch (CAS 9005-84-9, J.T. Baker, 2 g, 36.6 mmol, 1 eq.) was added to a round bottom flask containing dimethylformamide (DMF, 50 mL) and heated until it dissolved. In a separate round bottom flask, carbonyldiimidazole (5.8 g, 36.6 mmol, 1eq.), imidazole hydrochloride (9.6 g, 91.5 mmol, 2.5 eq.), and 3-diethylaminopropylamine (6.4 mL, 40 mmol, 1.1 eq.) were added to DMF (100 mL). The solution was heated to 60 ℃ and magnetically stirred for 2 h. After 2 h, the dissolved starch was added to the round bottom flask containing the carbonyldiimidazole, imidazole hydrochloride, and 3-(diethylamino)-1-propylamine. At this point, more imidazole hydrochloride (5.7 g, 55 mmol, 1.5 eq.) was added. The solution was heated to 80 ℃ for approximately 72 h. The reaction was allowed to cool and the starch was recovered via vacuum filtration. The starch was rinsed thoroughly with DMF (three times), followed by rinsing with methanol (three times). Functionalised starch (1.6919 g) was recovered and used as is for further experimentation.

Synthetic method 2:

Starch (CAS 9005-84-9, J.T. Baker, 0.4 g, 7.3 mmol, 1 eq.) was added to a round bottom flask containing dimethylsulfoxide (DMSO, 40 mL) and heated to 110 ℃. In a separate round bottom flask, carbonyldiimidazole (1.4 g, 8.6 mmol, 1.2 eq.), imidazole hydrochloride (1.35 g, 13 mmol, 1.5 eq.), and 3-(diethylamino)-1-propylamine (1.3 mL, 8.6 mmol, 1.2 eq.) were added to DMSO (50 mL). The solution was heated to 100 ℃ and stirred rapidly for 1 h. After 1 h, the hot dissolved starch was added to the round bottom

flask containing the carbonyldiimidazole, imidazole hydrochloride, and 3-(diethylamino)-1-propylamine. The solution was heated at a constant at 110 ℃ for approximately 16 h. The reaction was allowed to cool and the starch was recovered via vacuum filtration. The starch was rinsed thoroughly with DMF (three times), followed by rinsing with methanol (three times). Functionalised starch (0.12 g) was recovered and used as is for further experimentation.

Synthesis of CO_2-responsive single-unit functionalized filter paper by 1,1'carbonyldiimaidazole-mediate acyl transfer

Synthetic method 1 (Scheme AVI.4):

A cellulosic substrate (Whatman type 1 filter paper, 42.5 mm) was dried at 110 ℃overnight, placed into a 250 mL round bottom flask, and stored under Ar. In a separate round bottom flask, a solution of carbonyldiimidazole (5.14 mmol, 1 eq.) and 3-(dimethylamino)propionic acid hydrochloride (5.14 mmol, 1 eq.) in tetrahydrofuran (ca. 50 mL) was mixed rapidly for 4 h. After which, the solution was transferred to the round bottom flask containing the cellulosic substrate; the resultant mixture was left stirring under a dynamic flow of CO_2 overnight at room temperature (ca. 26 ℃). The substrate was rinsed with copious amounts of ethanol, followed by sonication for 20 min in 50 mL of ethanol (repeated three times). The hydrochloride salt of the functionalised cellulose substrate was removed by mixing the substrate overnight in a solution of tetramethylguanidine/tetrahydrofuran (1:4 v/v). The cellulosic substrate was then rinsed with copious amounts of ethanol, followed by sonication for 20 min in 50 mL of ethanol (three times). The functionalised substrate was then dried in an oven at 110 ℃ for 4 h.

Synthetic method 2 (Scheme AVI.5):

A cellulosic substrate (Whatman type 1 filter paper, 42.5 mm) was stirred in THF overnight to remove hydrophobic organic residues. The filter paper was sonicated in fresh THF (twice) and then dried at 110 ℃ overnight, placed into a 250 mL round bottom flask and stored under Ar. In a separate round bottom flask, a solution of carbonyldiimidazole (5.14 mmol, 1 eq.) and 3-(dimethylamino)propionic acid hydrochloride (5.14 mmol, 1 eq.) in tetrahydrofuran (50 mL) was mixed rapidly for 4 h. The solution, as well as imidazole hydrochloride (mild acid catalyst, 25.7 mmol, 5 eq.), were added to the round bottom flask containing the cellulosic substrate. The resultant mixture was left mixing overnight at room temperature (26 ℃). The substrate was rinsed with copious amounts of ethanol, followed by sonication for 20 min in 50 mL of ethanol (three times). The hydrochloride salt of the functionalised cellulose substrate was removed by mixing the substrate overnight in a solution of tetramethylguanidine/tetrahydrofuran (1:4 v/v). The cellulosic substrate was then rinsed with copious amounts of ethanol, followed by sonication for 20 min in 50 mL of ethanol (repeated three times). The functionalised substrate was then dried in an oven at 110 ℃ for 4 h

Synthetic method 3 (Scheme AVI.6):

A cellulosic substrate (Whatman type 1 filter paper, 42.5 mm) was dried at 110 ℃ overnight, placed into a 250 mL round bottom flask and stored under Ar. In a separate round bottom flask, a solution of carbonyldiimidazole (5.14 mmol, 1 eq.) and 3-(dimethylamino)propionic acid hydrochloride (5.14 mmol, 1 eq.) in tetrahydrofuran (ca.

50 mL) was mixed rapidly overnight. The solvent was removed and the solids were then dissolved in acetonitrile (ca. 40 mL), treated with methyl iodide (4 eq.) at room temperature (ca. 26 ℃) and stirred for 24 h. The solvent was removed under vacuum to yield solids. The solids were then added to a round bottom flask containing the dried filter paper and triethylamine (1 eq.); the solution was stirred at room temperature (ca. 26 ℃) for 24 h. The substrate was removed and rinsed with copious amounts of ethanol, followed by sonication for 20 min in 50 mL of ethanol (repeated three times). The hydrochloride salt of the functionalised cellulose substrate was removed by mixing the substrate overnight in a solution of tetramethylguanidine/tetrahydrofuran (1:4 v/v). The cellulosic substrate was then rinsed with copious amounts of ethanol, followed by sonication for 20 min in 50 mL of ethanol (repeated three times). The functionalised substrate was then dried in an oven at 110 ℃ for 4 h.

Synthesis of CO_2-responsive polymer-grafted filter paper

Method 1 (PGFP-1):

A cellulosic substrate (Fisherbrand filter paper, 9 cm diameter, type P8) was dried at 110 ℃ overnight, torn into six pieces, placed into a 500 mL round bottom flask and stored under Ar. The round bottom flask containing the cellulosic substrate was charged with a solution of diisopropylethylamine (46 mmol) in tetrahydrofuran (THF, ca. 50 mL). The solution was cooled to approximately 0 ℃ with an ice bath. To the cooled solution, 2-bromo-2-methylpropionyl bromide (BIBB, 46 mmol) was added dropwise. Once dropwise addition had completed, the solution remained in the ice bath for approximately

20 min, after which the ice bath was removed and the solution was left to equilibrate to room temperature, ca. 26 ˚C. This reaction was left overnight and ran for a total of 18 h. The resultant BIBB-functionalised filter paper was rinsed thoroughly with THF, followed by rinsing with methanol and then dried at 110 ˚C overnight before subsequent usage.

The BIBB-functionalised filter paper was placed in a 100 mL round bottom flask, the flask was charged with a stir bar, N,N-[(dimethylamino)propyl]methacrylamide (DMAPMAm, 205 mmol, 200 eq.) and N-(1-naphthyl)-N-phenylmethacrylamide (NPMAm, 0.35 mmol, 1.2 eq.) under Ar. NPMAm is a UV active monomer and if incorporated, the resultant copolymer was expected to fluoresce under UV light (λ_{MAX} 220 nm). DMAPMAm was passed through a basic alumina column to remove monomethyl ether of hydroquinone (MEHQ), a radical inhibitor. MEHQ was removed from DMAPMAm but not from NPMAm because it was considered that the amount of NPMAm used did not contain enough inhibitor to warrant removal (500-1000 ppm MEHQ in 100 mg NPMAm). It was understood that MEHQ would not prevent the ATRP, only slightly retard the rate of propagation. The flask was charged with 50 mL of anhydrous methanol and sparged with Ar via a needle for 1 h. In a separate round bottom flask, the catalyst was prepared: copper(I)bromide (0.30 mmol, 1 eq.) was mixed with N,N,N′,N″,N″-pentamethyldiethylenetriamine (PMDETA, 0.60 mmol, 2 eq.) in 15 mL of anhydrous methanol under Ar. The catalyst solution was sparged with Ar for 0.5 h. The solution containing monomer and the BIBB-functionalised filter paper was heated to 50 ℃, at which point the catalyst solution added via cannula. The polymerisation was left to occur, with stirring under Ar, over the course of 3 days. The polymer-grafted filter paper

was rinsed first with methanol to remove physisorbed compounds, followed by a 0.1 M solution of EDTA in water to remove the residual copper catalyst. The washed polymer-grafted filter paper was then dried in a vacuum oven at 100 ℃ for 4 h.

Subsequent analysis by ATR-FTIR spectroscopy did not detect a difference between the polymerised filter paper and the native substrate. The filter paper was not found to be hydrophobic, as it absorbed water. The BIBB reaction may have in part because of overheating of the fibres before functionalisation.

Method 2 (PGFP-2):

A cellulosic substrate (Whatman type 1 filter paper, 42.5 mm) was rinsed thoroughly with acetone, followed by THF. The cellulosic substrate was then sonicated in acetone for 30 min, followed by sonication in THF for 30 min. The cellulosic substrate was then left in fresh THF to soak for 4 h. In a 100 mL 2-neck round bottom flask, a solution of triethylamine (TEA, 2.2 eq., 1.375 mmol, 0.1916 mL), 2-bromo-2-methylpropionyl bromide (BIBB, 2 eq., 1.25 mmol, 0.154 mL) and a catalytic amount of 4-dimethylaminopyridine (DMAP, 0.01 eq., 0.0625 mmol, 7.6 mg) was prepared in 40 mL of THF, at room temperature (ca. 26 ℃). The cellulosic substrate was immersed into the solution and left overnight at room temperature (ca. 26 ℃) to react under Ar. The functionalised substrate was then rinsed and sonicated in THF, followed by sonication in methanol. The functionalised substrate was left in dry methanol until it was ready to be used further.

The resultant BIBB-functionalised filter paper was placed in a 250 mL round bottom flask, this flask was charged with N,N-[(dimethylamino)propyl]methacrylamide (DMAPMAm, 300 eq. 186 mmol, 34 mL) and 100 mL of anhydrous methanol. A stir bar was added and the flask was sparged with Ar via needle for 1 h. The radical inhibitor MEHQ was removed from DMAPMAm by passing the monomer through a basic alumina column. In a separate flask, the catalyst was prepared: copper(I)bromide (1 eq., 0.625 mmol, 90 mg) was mixed with N,N,N′,N″,N″-pentamethyldiethylenetriamine (PMDETA, 2 eq., 1.2 mmol, 0.22 mL) in 15 mL of anhydrous methanol. The catalyst solution was sparged with Ar for 0.5 h. The solution containing monomer and BIBB-functionalised filter paper was heated to 45 ℃, at which point the catalyst solution was added via cannula. The polymerisation was left to occur, with stirring under Ar, over the course of 34 h. The resultant polymer-grafted filter paper was sonicated for 20 min in fresh methanol (three times) to remove physisorbed polymer, excess monomer, ligand, and catalyst. The filter paper was sonicated in 0.1 M EDTA solution to remove the residual copper.

Subsequent analysis via ATR-FTIR spectroscopy, relative to native cellulose, suggested the presence of polymer on the filter paper, with an amide peak at ~1640 cm^{-1}. Two different spots on the above-described polymer-grafted filter paper were analysed by ATR-FTIR spectroscopy. A varying amide peak height at ~1640 cm^{-1} was observed, suggesting that the polymer grafting may not have occurred equally across the filter paper.

Method 3 (PGFP-3):

A cellulosic substrate (Whatman type 1 filter paper, 42.5 mm) was rinsed thoroughly in acetone, followed by THF. The cellulosic substrate was then sonicated in acetone for 30 min, followed by sonication in THF for 30 min. The cellulosic substrate was then left in fresh THF to soak for 4 h. In a 100 mL 2-neck round bottom flask, a solution of triethylamine (TEA, 2.2 eq., 1.375 mmol, 0.1916 mL), 2-bromo-2-methylpropionyl bromide (BIBB, 2 eq., 1.25 mmol, 0.154 mL), and a catalytic amount of 4-dimethylaminopyridine (DMAP, 0.01 eq., 0.0625 mmol, 7.6 mg) was prepared in 40 mL of THF, at room temperature (ca. 26 ℃), under Ar. The cellulosic substrate was immersed into the solution and left overnight at room temperature (ca. 26 ℃) to react. The resultant functionalised substrate was then rinsed and sonicated in THF, followed by sonication in methanol. The functionalised substrate was left in dry methanol until it was ready to be polymerised.

The BIBB-functionalised filter paper was placed in a 250 mL round bottom flask, the flask was charged with N,N-[(dimethylamino)propyl]methacrylamide (DMAPMAm, 300 eq. 186 mmol, 34 mL), ethyl 2-bromo-2-methylpropionate (EBIB, 0.005 eq., 0.0031 mmol) and 100 mL of anhydrous methanol under Ar. Ethyl 2-bromo-2-methylpropionate was used as an ATRP initiator and served as a sacrificial initiator. A stir bar was added to the round bottom flask and the flask was sparged with Ar via needle for 1 h. The radical inhibitor MEHQ was removed from DMAPMAm by passing the monomer through a basic alumina column. In a separate flask, the catalyst was prepared by mixing N,N,N′,N″,N″-pentamethyldiethylenetriamine (PMDETA, 2 eq., 1.2 mmol, 0.22 mL) with

copper(I)bromide (1 eq., 0.625 mmol, 90 mg) in 15 mL of anhydrous methanol. The catalyst solution was sparged with Ar for 0.5 h. The solution containing monomer and filter paper bound initiator was heated to 45 ℃, at which point the catalyst solution was added via cannula. The polymerisation was left to occur, with stirring under Ar, over the course of 34 h. The resultant polymer-grafted filter paper was sonicated for 20 min in fresh methanol (three times) to remove physisorbed polymer, excess monomer, ligand and catalyst. It was observed that the filter paper appeared white, with no colour from residual copper. Subsequent analysis via ATR-FTIR spectroscopy, relative to native cellulose, suggested the presence of polymer on the filter paper, with an amide peak at ~1640 $cm^{-1.}$ Two different spots on the above-described polymer-grafted filter paper were analysed by ATR-FTIR spectroscopy. A varying amide peak height at ~1640 cm^{-1} was observed, suggesting that the polymer-grafting may not have occurred equally across the filter paper.

Method 4 (PGFP-4):

A cellulosic substrate (Whatman type 1 filter paper, 42.5 mm) was rinsed thoroughly in acetone, followed by THF. The cellulosic substrate was then sonicated in acetone for 30 min, followed by sonication in THF for 30 min. The cellulosic substrate was then left in fresh THF to soak for 4 h. In a 100 mL 2-neck round bottom flask, a solution of triethylamine (TEA, 2.2 eq., 1.375 mmol, 0.1916 mL), 2-bromo-2-methylpropionyl bromide (BIBB, 2 eq., 1.25 mmol, 0.154 mL), and a catalytic amount of 4-dimethylaminopyridine (DMAP, 0.01 eq., 0.0625 mmol, 7.6 mg) was prepared in 40 mL of tetrahydrofuran, at room temperature (ca. 26 ℃), under Ar. The cellulosic substrate was immersed into the solution and left overnight at room temperature

(ca. 26 °C) to react. The resultant functionalised substrate was then rinsed and sonicated in tetrahydrofuran, followed by sonication in methanol. The functionalised substrate was left in dry methanol until it was ready to be polymerised.

The BIBB-functionalised filter paper was placed in a 250 mL round bottom flask, the flask was charged with 2-(diethylamino)ethyl methacrylate (DEAEMA, 300 eq. 186 mmol, 34 mL), ethyl 2-bromo-2-methylpropionate (EBIB, 1 eq., 0.62 mmol) and 100 mL of anhydrous methanol under Ar. Ethyl 2-bromo-2-methylpropionate was used as an ATRP initiator and served as a sacrificial initiator. A stir bar was added to the round bottom flask and the flask was sparged with Ar via needle for 1 h. The radical inhibitor MEHQ was removed from DEAEMA by passing the monomer through a basic alumina column. In a separate flask, the catalyst was prepared by mixing N,N,N′,N″,N″-pentamethyldiethylenetriamine (PMDETA, 2 eq., 1.2 mmol, 0.22 mL) with copper(I)bromide (1 eq., 0.62 mmol, 90 mg) in 15 mL of anhydrous methanol. The catalyst solution was sparged with Ar for 0.5 h. The solution containing monomer and BIBB-functionalised filter paper was heated to 45 °C, at which point the catalyst solution was added via cannula. The polymerisation was left to occur, with stirring under Ar, over the course of 34 h. The resultant polymer-grafted filter paper was sonicated for 20 min in fresh methanol (three times) to remove physisorbed polymer, excess monomer, ligand and catalyst. It was observed that the filter paper appeared white, with no colour from residual copper. The presence of polymer was confirmed by ATR-FTIR spectroscopy and subsequent CO_2-responsive behaviour was observed as determined by WCA analysis.

Additional IR spectroscopy data for single-unit functionalized polysaccharides

Single-unit CO_2-responsive cellulose fibres were examined by ATR-FTIR spectroscopy. Had the DRIFT accessory been available at the time it would have been used instead, since DRIFT analysis is better suited to analysing powdered samples. In general, functionalised cellulose exhibited an increased intensity in broad shifts in the following ranges: 1000-1200 cm^{-1} (C-N stretch), 2800-3000 cm^{-1} (potential carbamate ester N-H) and 3300-3500 cm^{-1} (potential carbamate ester N-H).

Native cellulose exhibited the following IR peaks: 3242 cm^{-1} (*s*, *b*), 2899 cm^{-1} (*m*, *b*), 1651 cm^{-1} (*w*, *b*), 1433-1261 cm^{-1} (*m*, *b*), 1162-1059 cm^{-1} (*s*, *b*), 896 cm^{-1} (*w*, *sh*).

3-(Dimethylamino)-1-propylamine (A1) functionalised cellulose (A1, method 2) exhibited the following IR peaks: 3241 cm^{-1} (*s*, *b*), 2921 cm^{-1} (*m*, *b*),1616 cm^{-1} (*m*, *b*), 1433-1261 cm^{-1} (*m*, *b*), 1162-1059 cm^{-1} (*s*, *b*), 896 cm^{-1} (*w*, *sh*), 750-850 (*w*, *sh*).

3-(Dibutylamino)-1-propylamine functionalised cellulose (A2, method 3) exhibited the following IR peaks: 3241 cm^{-1} (*s*, *b*), 2921 cm^{-1} (*m*, *b*),1616 cm^{-1} (*m*, *b*), 1433-1261 cm^{-1} (*m*, *b*), 1162-1059 cm^{-1} (*s*, *b*), 896 cm^{-1} (*w*, *sh*), 750-850 cm^{-1} (*w*, *sh*).

Appendix VII

Supplemental information

Internal referencing system

References to physical lab notebooks are provided in the format KB B__PG__.

Where: KB refers to the author, Kyle Boniface; B refers to the book number; PG refers to the page number within that book.

For example: KBB6PG8, would be Kyle Boniface, book 6, page 8.

Silica particle designations

Table AVII.1. Silica particle type and designations

Type of Silica	Particle Size (μm)	Pore Size (Å)	Internal Designation (SiO_2-x)
Spherical Silica Gel (Silicycle)	200-500	100	1
SiliaFlash B60 (Silicycle) "Irregular silica"	200-500	60	2
Spherical Silica Gel (Silicycle)	200-500	500	3
Silica Gel (Alfa Aesar) "Irregular silica"	60-200	60	4
SiliaFlash P60 (Silicycle) "Irregular silica"	40-63	60	5
Spherical Silica Gel (Silicycle)	5	100	6

Particle and pore sizes are reported from the manufacturer.

Software predictions for Figures 5.6 and 6.2.

Table AVII.2. Proposed CO_2-responsive co-nucleophilic species and their corresponding model compounds used to predict surface activity when bound to a substrate. The pK_{aH} values correspond to the basic tertiary amine.

Commercial Compound	Model Compound for Predictions
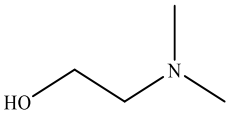	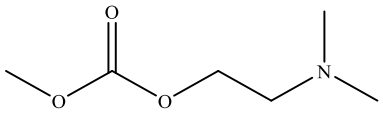
2-dimethylaminoethanol	2-(dimethylamino)ethyl methyl carbonate
pK_{aH}: 8.92	pK_{aH}: 8.41
log$\mathcal{P}$: 1.04	log$\mathcal{P}$: 0.56
S7	LogD (pH 4.6): -2.77
	LogD (pH 7.4): -0.49
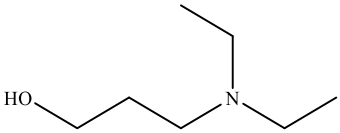	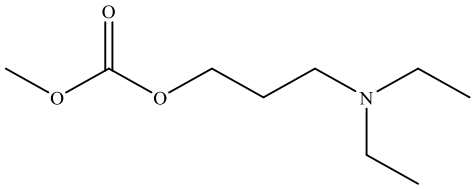
3-diethylamino-1-propanol	3-(diethylamino)propyl methyl carbonate
pK_{aH}: 9.71	pK_{aH}: 10.00
log$\mathcal{P}$: 0.27	log$\mathcal{P}$: 1.33
S8	LogD (pH 4.6): -2.16
	LogD (pH 7.4): -1.22
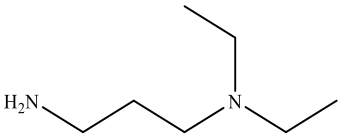	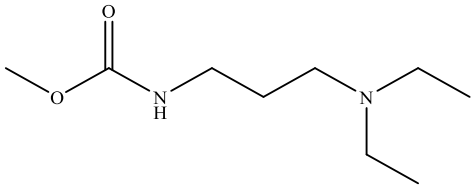
3-(diethylamino)propylamine	methyl N-[3-(diethylamino)propyl]carbamate
pK_{aH}: 10.21	pK_{aH}: 9.84
log$\mathcal{P}$: 0.17	log$\mathcal{P}$: 0.6
S9	LogD (pH 4.6): -2.89
A3	LogD (pH 7.4): -1.80

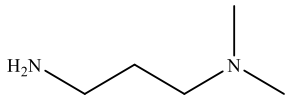	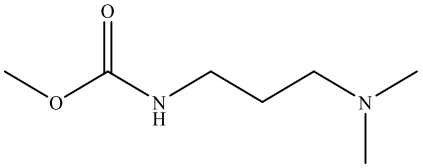
3-(dimethylamino)propylamine pK_{aH}: 8.13 log$\mathcal{P}$: -0.55 **A1**	methyl N-[3-(dimethylamino)propyl]carbamate pK_{aH}: 9.3 log$\mathcal{P}$: -0.11 LogD (pH 4.6): -3.58 LogD (pH 7.4): -2.00
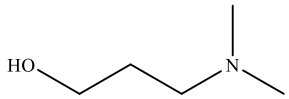	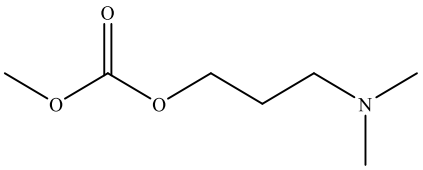
3-dimethylamino-1-propanol pK_{aH}: 9.16 log$\mathcal{P}$: -0.44 **S10**	3-(dimethylamino)propyl methyl carbonate pK_{aH}: 9.46 log$\mathcal{P}$: 0.62 LogD (pH 4.6): -2.86 LogD (pH 7.4): -1.42
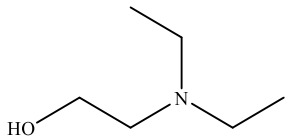	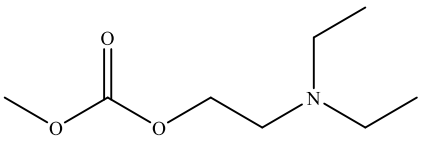
2-(diethylamino)ethanol pK_{aH}: 9.55 log$\mathcal{P}$: 0.21 **S11**	2-(diethylamino)ethyl methyl carbonate pK_{aH}: 8.96 log$\mathcal{P}$: 1.27 LogD (pH 4.6): -2.17 LogD (pH 7.4): -0.29

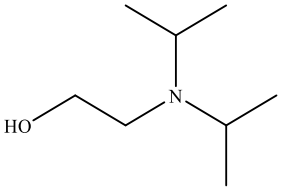	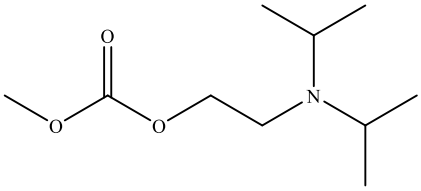
2-(diisopropylamino)ethanol pK_{aH}: 10.11 log$\mathcal{P}$: 1.05 **S12**	2-(diisopropylamino)ethyl methyl carbonate pK_{aH}: 9.52 log$\mathcal{P}$: 2.11 LogD (pH 4.6): -1.38 LogD (pH 7.4): 0.00
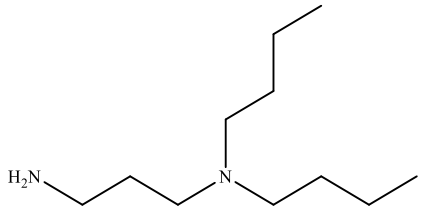	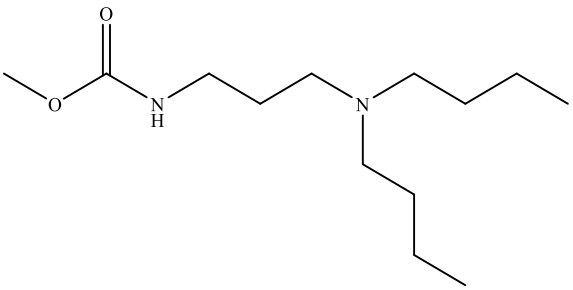
3-(dibutylamino)-1-propylamine pK_{aH}: 10.55 log$\mathcal{P}$: 2.10 **A2**	methyl N-[3-(dibutylamino)propyl]carbamate pK_{aH}: 10.35 log$\mathcal{P}$: 2.54 LogD (pH 4.6): -0.96 LogD (pH 7.4): -0.31
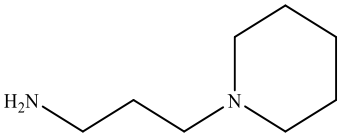	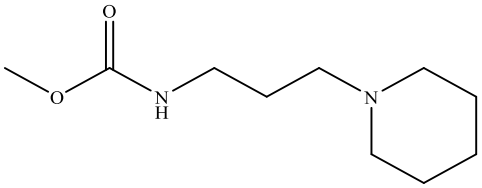
N-(3-aminopropyl)piperidine pK_{aH}: 10.18 log$\mathcal{P}$: 0.30 **S13** **A5**	methyl N-[3-(piperidin-1-yl)propyl]carbamate pK_{aH}: 9.06 log$\mathcal{P}$: 0.74 LogD (pH 4.6): -2.17 LogD (pH 7.4): -0.92

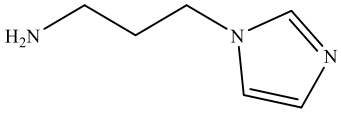

1-(3-aminopropyl)imidazole

pK_{aH}: 6.53

log$\mathcal{P}$: -0.66

S14

A4

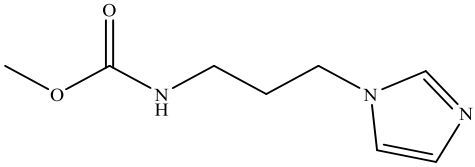

methyl N-[3-(imidazol-1-yl)propyl]carbamate

pK_{aH}: 6.79

log$\mathcal{P}$: -0.22

LogD (pH 4.6): -0.80

LogD (pH 7.4): -0.29

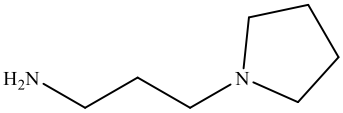

1-(3-aminopropyl)pyrrolidine

pK_{aH}: 10.29

log$\mathcal{P}$: -0.14

S15

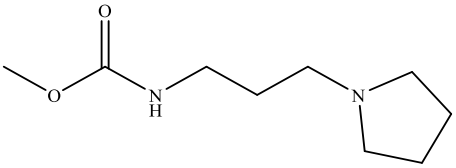

methyl N-[3-(pyrrolidin-1-yl)propyl]carbamate

pK_{aH}: 9.19

log$\mathcal{P}$: 0.30

LogD (pH 4.6): -3.17

LogD (pH 7.4): -1.49